APRIL 2026
VOLUME 85
ISSUE
4

ANNALS OF THE RHEUMATIC DISEASES

THE EULAR JOURNAL

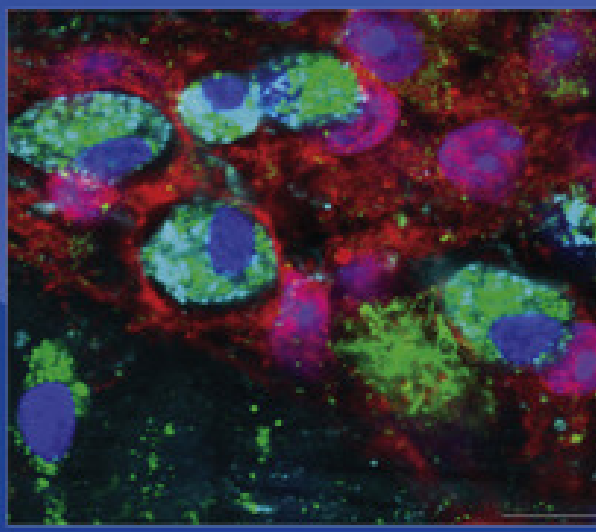

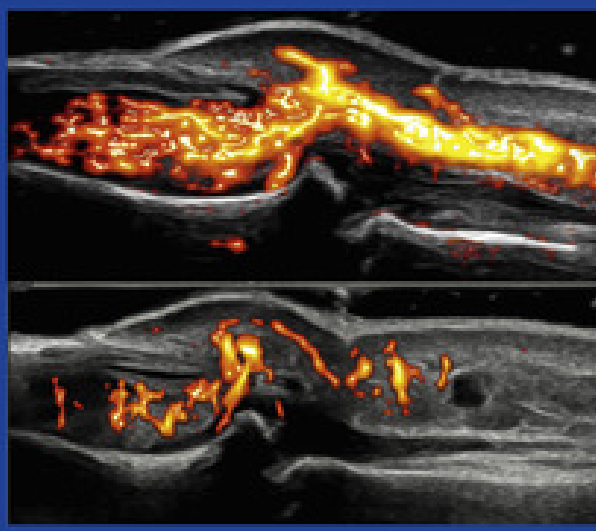

ELSEVIER

eular
EUROPEAN ALLIANCE OF ASSOCIATIONS FOR RHEUMATOLOGY

The home of innovative rheumatology research

Ann Rheum Dis 85 (2026) 585–587

Contents lists available at ScienceDirect

Annals of the Rheumatic Diseases

journal homepage: https://www.sciencedirect.com/journal/annals-of-the-rheumatic-diseases

Editorial

Immune endotypes and treatment response in psoriatic arthritis

Psoriatic arthritis (PsA) remains a clinically heterogeneous disease in which advances in targeted therapies have not yet translated into uniformly successful outcomes. Despite the availability of multiple biologic and targeted synthetic disease-modifying antirheumatic drugs, fewer than half of patients appear to achieve sustained low disease activity, and a substantial proportion progress to a 'difficult-to-treat' phenotype, even when managed according to current treat-to-target strategies [1,2]. This gap between mechanistic insight and clinical control highlights a fundamental challenge in PsA, reflecting both 'difficult-to-manage' and 'treatment-refractory' PsA patients. While therapies are increasingly pathway-specific, the biological networks and disease complexity of individual patients remain poorly defined and are likely not dependent on a single cytokine signalling pathway [3].

In this context, a new study by Eder et al [4] in this journal represents an important conceptual shift. Rather than comparing PsA patients with healthy individuals or focusing on individual immune populations, the authors apply unsupervised clustering to circulating CD3+ T-cell subsets within a clinically heterogeneous PsA population followed over time. They identify distinct immune endotypes associated with imaging-defined inflammation, structural damage, and responses to advanced therapies [4]. By further integrating mass cytometry, musculoskeletal ultrasound, longitudinal clinical outcomes, and serum proteomics, the study moves beyond immune description towards a new concept of biologically anchored patient stratification.

Among the 3 immune endotypes identified, a CD4+ memory T-cell–dominant profile emerged as clinically and biologically distinct. Patients within this endotype had higher sonographic synovitis and enthesitis scores, greater periarticular and entheseal new bone formation, and a markedly reduced likelihood of achieving meaningful clinical improvement with treatment [4]. Importantly, this immune profile remained stable over time despite treatment and was progressively enriched for 'difficult-to-treat' PsA over 2 years of follow-up. These observations are consistent with immune memory reflecting a durable, persistent PsA disease state rather than a transient marker of inflammatory activity at a given time point.

The prominence of immune memory is particularly relevant in PsA, where discordance among clinical assessment, laboratory markers, and imaging findings is common in daily clinical practice. Memory T cells are long-lived, rapidly responsive, and capable of sustaining inflammation through polyfunctional cytokine production [5]. The stability of the identified immune endotypes despite therapy implies that current targeted treatments may suppress downstream inflammatory pathways without fundamentally altering the underlying immune architecture in a subset of patients with PsA. Targeting the latter may be a step towards a cure rather than a treatment aimed at achieving disease control. This model aligns closely with long-standing clinical experience, in which domain changes, persistent imaging activity, and progressive structural damage coexist with apparent biochemical quiescence and may even help explain the limited utility of C-reactive protein in many patients with PsA [6,7].

The study has limitations. The association observed by Eder et al [4] between the CD4+ memory T-cell endotype and older age warrants careful interpretation. Ageing is accompanied by predictable immune system changes, including contraction of the naïve T-cell pool and expansion of memory subsets, as well as features of chronic low-grade inflammation [8]. In PsA, older age has been linked to greater structural damage [9,10]. Whether immune memory only tracks with age or actively mediates age-associated disease severity cannot be resolved in the present study. Importantly, age should not be viewed solely as a statistical confounder but as a biological process reflecting cumulative immune exposure and remodelling, which may be partially captured by immune endotyping in the study by Eder et al [4].

A central conceptual challenge of the study lies in integrating CD3+ T-cell–restricted immune endotyping with global serum proteomics. Serum proteins originate from multiple cellular and tissue sources and cannot, therefore, be interpreted as direct molecular messengers of T cells alone. Hence, the proteomics analysis is mostly informative and likely reflects only a partial image of the integrated serum-level consequences of immune endotypes operating within a much more complex immune-stromal-vascular environment. Some caution is therefore warranted in interpreting the proteomic analysis.

Nevertheless, among the enriched pathways associated with the CD4+ memory T-cell endotype, dysregulation of WNT signalling was particularly prominent. WNT-related proteins correlated with imaging-defined enthesitis and periarticular new bone formation, while showing little association with systemic inflammatory markers [4]. WNT signalling has established roles in pathological bone formation and tissue repair [11], and also contributes to T-cell differentiation and memory stability [12]. The convergence of immune persistence, aberrant tissue remodelling, and osteoproliferation, as suggested by this study, provides a plausible biological framework for a better understanding of a biologically active, structurally progressive disease in the CD4+ memory T-cell endotype.

The enrichment of 'difficult-to-treat' PsA in the CD4+ memory T-cell endotype should also be interpreted with nuance.

https://doi.org/10.1016/j.ard.2026.01.017
Received 23 December 2025; Accepted 23 January 2026

'Difficult-to-treat' disease reflects a complex interplay of biological, clinical, and patient-related factors, including comorbidities, pain amplification, treatment adherence, and disease perception [2]. Immune endotyping represents only one layer of this complexity, but it is increasingly controllable from a therapeutic point of view. From a clinical perspective, the current findings suggest that a subset of patients labelled as 'difficult-to-treat' may share a common biological substrate characterised by durable immune memory and maladaptive tissue responses, raising the possibility of earlier identification and more tailored management strategies.

Taken together, the work discussed supports a shift from pathway-centric thinking to biologically informed stratification in PsA. In the near future, immune endotyping may help refine prognosis and contextualise incomplete treatment responses. In the longer term, it raises critical research questions: can immune memory be reprogrammed, and if so, at what stage of disease? Are there therapeutic windows in which altering immune architecture may prevent progression to treatment resistance? While validation in independent cohorts is essential, the study by Eder et al [4] provides a novel framework for integrating immune biology, imaging, and longitudinal outcomes. Highlighting immune memory as a potential driver of persistent disease invites a re-examination of how heterogeneity in PsA is defined, monitored, and ultimately treated.

Finally, the paper highlighted here illustrates how to integrate advanced analytical technologies, such as extensive immunophenotyping and proteomics, into clinical questions. The seemingly limitless amount of data that such technological approaches can generate often exceeds the number of patients included in study cohorts, thereby increasing the risk of false-positive findings due to multiple testing. The approach used in this paper avoids focusing on single-molecule-level discovery by using clustering after immunophenotyping and pathway integration after proteomics. Translational research questions are best explored through this type of strategy to advance the field and to avoid unjustified claims of insights into disease mechanisms based on a single technology and a focus on single genes, proteins, or cell types. Nevertheless, further biological validation and direct mechanistic studies will be required to validate the newly proposed endotypes and pathway associations and to guide more effective therapeutic strategies.

Competing interests

Leuven R&D, KU Leuven's tech transfer office, has received lecture or consultancy fees on behalf of RL from AbbVie, J&J, Lily, Novartis, and UCB. RL is coholder of the Alfasigma Chair for research in Rheumatoid Arthritis. SM has received lecture or consultancy fees from AbbVie, Sandoz, Boehringer Ingelheim, AstraZeneca, Berlin Chemie, and Fresenius Kabi.

Contributors

Conceptualisation: SM and RL. Writing—original draft: RL. Writing—review and editing: SM and RL.

Funding

This editorial did not receive any specific grant from funding agencies in the public, commercial, or not-for-profit sectors.

Patient consent for publication

Not applicable.

Ethics approval

Not applicable.

Provenance and peer review

Commissioned by Editor-in-Chief.

Declaration of generative AI and AI-assisted technologies in the writing process

During the preparation of this work the authors used ChatGPT v5.2 in order to edit language and edit grammar. The scientific content, data interpretation, and conclusions were entirely generated and validated by the authors. After using this tool/service, the authors reviewed and edited the content as needed and take full responsibility for the content of the publication.

Orcid

Rik Lories: http://orcid.org/0000-0002-5986-3092

Sandra Meisalu[1], Rik Lories[2,3,*]

[1] *Department of Rheumatology, East Tallinn Central Hospital, Tallinn, Estonia*

[2] *Division of Rheumatology, UZ Leuven, Leuven, Belgium*

[3] *Skeletal Biology and Engineering Research Centre, KU Leuven, Leuven, Belgium*

*__Correspondence to__ Dr. Rik Lories, Division of Rheumatology, UZ Leuven, Leuven, Belgium.

E-mail address: Rik.Lories@kuleuven.be (R. Lories).

REFERENCES

[1] Gossec L, Kerschbaumer A, Ferreira RJO, Aletaha D, Baraliakos X, Bertheussen H, et al. EULAR recommendations for the management of psoriatic arthritis with pharmacological therapies: 2023 update. Ann Rheum Dis 2024;83(6):706–19. doi: 10.1136/ard-2024-225531.

[2] Marzo-Ortega H, Harrison SR, Fragoulis GE, Michelena X, Macía-Villa C, Aydin SZ, et al. EULAR points to consider and consensus definitions for difficult-to-manage and treatment-refractory psoriatic arthritis. Ann Rheum Dis 2026;85(1):61–74. doi: 10.1016/j.ard.2025.10.002.

[3] Veale DJ, Fearon U. The pathogenesis of psoriatic arthritis. Lancet 2018;391(10136):2273–84. doi: 10.1016/S0140-6736(18)30830-4.

[4] Eder L, Dang S, Caucheteux SM, Li X, Thib S, Ganatra D, et al. CD3+ immune cell endotypes are associated with PsA disease phenotype and response to advanced therapy: an integrated mass cytometry and proteomics cohort study. Ann Rheum Dis 2026;85(3):457–66. doi: 10.1016/j.ard.2025.10.011.

[5] McKinstry KK, Strutt TM, Swain SL. The potential of CD4 T-cell memory. Immunology 2010;130(1):1–9. doi: 10.1111/j.1365-2567.2010.03259.x.

[6] Houttekiet C, de Vlam K, Neerinckx B, Lories R. Systematic review of the use of CRP in clinical trials for psoriatic arthritis: a concern for clinical practice? RMD Open 2022;8(1):e001756. doi: 10.1136/rmdopen-2021-001756.

[7] Ogdie A, Tillett W, Booth N, Howell O, Schubert A, Peterson S, et al. Usage of C-reactive protein testing in the diagnosis and monitoring of psoriatic arthritis (PsA): results from a real-world survey in the USA and Europe. Rheumatol Ther 2022;9(1):285–93. doi: 10.1007/s40744-021-00420-x.

[8] Nikolich-Žugich J. The twilight of immunity: emerging concepts in aging of the immune system. Nat Immunol 2018;19(1):10–9. doi: 10.1038/s41590-017-0006-x.
[9] Koc GH, Kok MR, do Rosario Y, Luime JJ, Tchetverikov I, Kasiem FR, et al. Determinants of radiographic progression in early psoriatic arthritis: insights from a real-world cohort. RMD Open 2024;10(2):e004080. doi: 10.1136/rmdopen-2024-004080.
[10] Ozdemir Isik O, Gokcen N, Temiz Karadag D, Yazici A, Cefle A. Radiological progression and predictive factors in psoriatic arthritis: insights from a decade-long retrospective cohort study. Clin Rheumatol 2024;43(1):259–67. doi: 10.1007/s10067-023-06839-7.
[11] Lories RJ, Schett G. Pathophysiology of new bone formation and ankylosis in spondyloarthritis. Rheum Dis Clin North Am 2012;38(3):555–67. doi: 10.1016/j.rdc.2012.08.003.
[12] Sung BY, Lin YH, Kong Q, Shah PD, Glick Bieler J, Palmer S, et al. Wnt activation promotes memory T cell polyfunctionality via epigenetic regulator PRMT1. J Clin Invest 2022;132(2):e140508. doi: 10.1172/JCI140508.

Ann Rheum Dis 85 (2026) 588–602

Contents lists available at ScienceDirect

Annals of the Rheumatic Diseases

journal homepage: https://www.sciencedirect.com/journal/annals-of-the-rheumatic-diseases

Review

Recent pathogenetic insights and therapeutic advances in ANCA-associated vasculitis

Iftach Sagy[1,*], David R W Jayne[1,2]

[1] *Cambridge University Hospitals NHS Foundation Trust, Cambridge, UK*
[2] *Department of Medicine, University of Cambridge, Cambridge, UK*

ARTICLE INFO

Article history:
Received 30 September 2025
Received in revised form 26 November 2025
Accepted 27 November 2025

ABSTRACT

Advances in the understanding of antineutrophil cytoplasmic antibody (ANCA)-associated vasculitis have influenced both treatment strategies and approaches to disease monitoring. While conventional therapies remain the foundation of care, introducing targeted biologics, complement pathway inhibitors, and emerging cellular treatments have broadened therapeutic options to minimise adverse effects, reduce glucocorticoid requirements, and enhance disease control. Nevertheless, many patients still face frequent relapses, progressive tissue damage, and chronic impairments in quality of life. Existing definitions of remission underestimate ongoing disease activity and impact, and interpretation of residual symptoms can be challenging, especially in the absence of overt inflammation. There is a growing interest in personalised management to address these limitations, using biomarkers to better predict relapse risk, differentiate between active disease and residual damage, and guide treatment intensity. Effective long-term care now requires suppression of disease activity and careful management of treatment-related complications, comorbidity risks, and patient-experienced outcomes. Optimising care in ANCA-associated vasculitis will depend on integrating therapeutic innovation with a sustained focus on outcomes that matter most to patients, including durable remission, functional recovery, and improved day-to-day well-being.

INTRODUCTION

Antineutrophil cytoplasmic antibody (ANCA)-associated vasculitis (AAV) is an autoimmune inflammatory disorder that primarily affects small blood vessels. In addition to being diagnostic, classification, and monitoring tools, the ANCA subtypes proteinase (PR)3-ANCA and myeloperoxidase (MPO)-ANCA contribute to pathogenesis through activation of perivascular neutrophils, leading to necrotising vasculitis and, ultimately, end-organ damage.

AAV commonly involves the sinonasal tract, lungs, kidneys, skin, and nervous system and encompasses 3 subtypes: granulomatosis with polyangiitis (GPA), microscopic polyangiitis (MPA), and eosinophilic granulomatosis with polyangiitis (EGPA).

The identification of the 3 AAV forms was historically based on distinct clinical features and pathological findings from autopsies conducted in the 1930s through to the 1950s. Early research distinguished between patients with systemic arteritic lung lesions and widespread necrotising glomerulonephritis and those with systemic arteritis without major glomerular or pulmonary involvement, corresponding to what is now diagnosed as polyarteritis nodosa (PAN) [1]. The current definitions of GPA, MPA, and EGPA as pauci-immune small vessel vasculitides were established and revised by the 1993 and 2012 Chapel Hill Consensus Conferences (CHCC) [2]. The more recent American College of Rheumatology (ACR) and European Alliance of Associations for Rheumatology (EULAR) data-driven classification criteria for GPA/MPA and EGPA were published in 2022 [3–5]. In addition, the European Medicines Agency developed an algorithm for primary systemic vasculitis based on the previous ACR criteria and CHCC definitions to facilitate data-driven classification criteria [6]. Although the 2022 classification criteria demonstrated high specificity and

*Correspondence to Dr. Iftach Sagy.
E-mail address: iftachsagy@gmail.com (I. Sagy).
Handling editor Josef S. Smolen.

https://doi.org/10.1016/j.ard.2025.11.024

sensitivity, diagnostic criteria have not been developed, and the timely diagnosis of AAV remains challenging. A recent analysis incorporating data from 3868 patients with AAV across 6 European countries showed that these subclassifications of AAV offer high predictive value for accurate diagnosis and patient outcomes regardless of which specific criteria are used [7]. Genome-wide association studies (GWASs) have found a closer association of genetic variants with ANCA subtype (PR3 or MPO-ANCA) than with clinical phenotype (GPA or MPA). Using ANCA serotype alone results in close agreement with the 2022 ACR/EULAR criteria for both GPA and MPA, but through a much simpler process [8]. The development and widespread testing of diagnostic criteria is an important component of the research agenda.

PATHOGENESIS

Genetics

The breakdown of immune tolerance lies at the core of AAV pathogenesis, with genetic, epigenetic, and environmental factors all potentially contributing to this process. Candidate-gene association studies, followed by GWASs, have identified specific loci associated with the onset of disease. Lyons et al [8] demonstrated that the strongest genetic associations in AAV were with ANCA specificity rather than clinical phenotype, with PR3-ANCA linked to the human leukocyte antigen (HLA)-DP, SERPINA1 (gene for the protease inhibitor, α1 antitrypsin), and PRTN3 (the gene for the autoantigen proteinase 3) genes, and MPO-ANCA to the human leukocyte antigen-DQ (HLA-DQ) gene. Furthermore, HLA alleles were associated with the severity (HLA-DRB1*04:02), prognosis (HLA-DRB1*04:05), and relapse (DPB1*04:01) of AAV [9]. Further genetic associations have been reported in candidate studies for genes related to T cell activation, PTPN22 and cytotoxic T-lymphocyte–associated antigen 4 (CTLA4), and complement activation. In EGPA, a GWAS identified 11 associated loci and, more importantly, revealed genetic and clinical differences between ANCA-positive and ANCA-negative disease, particularly in HLA-DQ associations [10]. ANCA-positive EGPA is an eosinophilic autoimmune disease that shares clinical features and an HLA-DQ association with MPO-ANCA MPA and GPA, whereas ANCA-negative EGPA may originate from mucosal or barrier dysfunction with shared associations with eosinophilic asthma. The shared HLA-DQ association between MPO-ANCA EGPA and MPA suggests a possible common genetic origin, yet the genetic and pathogenic complexity of these conditions extends beyond this overlap [11].

B cells

Loss of immune tolerance to MPO or PR3 antigens, resulting in the autoreactivation of T and B lymphocytes, is a central pathogenic mechanism in AAV. The detection of ANCA before the clinical symptoms of AAV become apparent suggests that the loss of immune tolerance occurs in the early stages of disease development [12]. Several hypotheses have been proposed to explain the loss of immune tolerance to PR3 and MPO. These include impaired clearance of apoptotic neutrophils, dysfunction of regulatory B cells, and chronic infections that lead to the excessive release of neutrophil extracellular traps (NETs) and molecular mimicry [13,14]. The pathogenic role of ANCA in the development of AAV has been supported by the development of crescentic glomerulonephritis in MPO-knockout mice immunised with MPO [15]; the localisation of ANCA within areas of fibrinoid necrosis alongside their target antigens; and, clinically, a few reported cases of neonates who developed pulmonary-renal syndrome born to mothers positive for MPO-ANCA [16].

T cells

T-lymphocyte responses in AAV involve distinct pathways: Th1 cells, producing interferon gamma, tumour necrosis factor-α, and interleukin (IL)-2, drive proinflammatory activity and contribute to granuloma formation in GPA, whereas T helper type 2 (Th2) cells, through IL-4 and IL-13 production, promote ANCA generation by B cells [17]. Additionally, decreased circulating regulatory T cells (Tregs) contribute to the immune response against self-antigens, such as MPO and PR3. Th17 cells stimulate the recruitment of neutrophils to inflamed sites, further amplifying tissue damage [18]. Effector $CD4^+$ cell depletion in a mouse model of attenuated crescentic glomerulonephritis and effector cell influx without altering ANCA titres, while B cell–deficient mice without ANCA still developed severe crescentic glomerulonephritis, highlighting the importance of $CD4^+$ cells in promoting AAV [19]. In clinical settings, the important role of T cells in AAV has been demonstrated in several case reports of patients treated with immune checkpoint inhibitors to treat underlying malignancies [20]. By blocking PD-1 and CTLA-4, these inhibitors remove inhibitory signals from T cells, leading to enhanced T cell activation. Consequently, some patients subsequently developed AAV after undergoing this therapy.

Complement and neutrophils

Complement system activation, particularly via the alternative pathway and C5a receptor (C5aR) signalling, is a major driver of inflammation in AAV. In murine models, complement depletion with cobra venom factor or the administration of anti-C5 antibodies prevented the development of ANCA-associated glomerulonephritis following the transfer of anti-MPO immunoglobulin (Ig)G, and mice deficient in the C5aR were similarly protected from necrotising glomerulonephritis [21]. Moreover, mice deficient in factors B and C5, but not factor C4, did not develop crescentic glomerulonephritis, emphasising the importance of the alternative complement pathway over the classical/lectin pathways in AAV [22]. Priming of neutrophils by C5a induces the translocation of ANCA antigens to the cell membrane, which facilitates ANCA binding and, after crosslinkage with Fc receptors, neutrophil activation, a respiratory burst, and degranulation, with release of tissue factor, cytokines, properdin, and NETs with microparticles. This process results in endothelial cell injury, activation of the coagulation system, and positive feedback activation of the alternative complement pathway [23]. Recent findings suggest that complement activation may play a role in EGPA. In a recent study, anti-C5aR antibody levels were lower in patients with EGPA than those in healthy controls, and reduced anti-C5aR levels were linked to a higher likelihood of relapse within 1 year [24]. There is also evidence from clinical studies of classical pathway activation with deposition of C4 and the C5b-9 terminal attack complex in glomeruli and vessel walls, and a combination of low serum C3 and C4 levels was identified in 92% of patients with AAV who required renal replacement therapy or died [25]. These findings emphasise a rationale for broader targeting of the complement system beyond the alternative pathway in future therapies.

Eosinophils

EGPA exhibits unique pathogenic and clinical characteristics that distinguish it from GPA and MPA. The primary driver of inflammation in EGPA is hypereosinophilia, which results from the dominant activation of Th2 cells through the production of cytokines, including IL-4, IL-5, and IL-13. IL-5 promotes eosinophil maturation in the bone marrow, facilitates migration, and enhances their survival in peripheral tissues by binding to the IL-5 receptor on eosinophils [26]. An increased Th17/Treg ratio has also been observed in EGPA, which contributes to the secretion of IL-5 [27]. Additionally, $CD4^+$ T cells inhibit eosinophil apoptosis, whereas Th1 activation increases interferon secretion and promotes granuloma formation [18]. Increased peripheral blood type 2 innate lymphoid cells and serum IL-33 concentrations were associated with disease activity in EGPA, implying that elevated serum IL-33 levels may serve as a marker of active vasculitis in EGPA [28]. Eosinophils can secrete several mediators that contribute to tissue damage, including eosinophil cationic protein, eosinophil-derived neurotoxin, and major basic protein, as well as fibrogenic cytokines [29]. Lastly, the humoral immune system also plays an important role in EGPA, as evidenced not only by high titres of anti-MPO antibodies observed in 40% to 50% of patients with EGPA but also by elevated levels of IgE- and IgG4-rich plasma cells [30].

CLINICAL FEATURES

Epidemiology

The incidence of all 3 subgroups of AAV has increased over the past decade, along with a rise in the mean age of affected patients. A recent analysis showed that the incidence of MPA and GPA in European countries and the United States rose from 1.5 to 2.7 per million in the 1980s to 24.7 to 33.0 per million in the last decade [31]. This change may be attributed to improved awareness of these conditions, especially in the elderly, driven by the better dissemination of guidelines, as well as the broader use of ANCA testing. MPA is much more common than GPA in China and Japan, while EGPA remains the rarest of the 3 conditions overall [31].

The clinical presentation

The clinical presentation of AAV is extremely varied, ranging from localised disease affecting 1 organ to life-threatening diffuse alveolar haemorrhage or rapidly progressive glomerulonephritis. GPA is characterised by granulomatous inflammation in addition to vasculitis, almost always involving the upper and lower respiratory tract, while MPA lacks granulomata. Kidney involvement is more frequent in MPA, but similar kidney histology between syndromes, although chronicity/fibrosis is usually more advanced in MPA [32]. EGPA follows a distinct clinical course, defined by a triad of poorly controlled asthma, peripheral eosinophilia, and systemic inflammation [33]. AAV is characterised by the production of antibodies targeting components of neutrophil cytoplasm: PR3-ANCA are found in over 90% of patients with GPA, whereas MPO-ANCA antibodies are detected in 60% to 80% of MPA cases and approximately 40% of EGPA cases. Clinical manifestations of AAV by disease subtype over time are shown in Figure 1 [34].

Activity

Clinical assessment instruments used in published trials for AAV are listed in Table 1 [35–43]. The Birmingham Vasculitis Activity Score (BVAS) is the most widely recognised and validated tool for assessing disease activity in patients with AAV, particularly in clinical trials [35]. First developed in 1994 and later validated in 1997 and 2008, BVAS evaluates 56 clinical items across 9 organ systems—including general; cutaneous; mucous membranes/eyes; ear, nose, and throat (ENT); chest; and cardiovascular, abdominal, renal, and nervous systems—based on symptoms attributable to active vasculitis within the previous 4 weeks. Items are scored based on whether they are new or persistent, with higher scores indicating more severe or active disease.

BVAS has demonstrated strong correlations with physician global assessments, decisions around treatment escalation, quality-of-life metrics, inflammatory markers (eg, C-reactive protein), the 5-factor score (FFS), the vasculitis damage index (VDI), and both short- and long-term mortality [44]. The score is central to defining both remission and relapse in clinical trials. Remission is typically defined as a BVAS of 0 to 1 (no major organ involvement and limited minor activity), although some studies incorporate additional factors such as a reduction in glucocorticoid (GC) dose or improvements in kidney function or inflammatory markers.

A modified version, BVAS for Wegener granulomatosis (BVAS/WG), was developed specifically for GPA and refines certain organ-specific assessments relevant to GPA [36]. Although both BVAS and BVAS/WG remain essential tools for standardised disease assessment in AAV research and offer comprehensive frameworks for clinical evaluation, they require appropriate training and experience to ensure reliable and validated use. In addition, the BVAS/WG may not correlate closely with biomarkers, can be confounded by symptoms related to chronic damage, and demonstrates variable performance across AAV subtypes and organ systems [45]. A paediatric version (PVAS) is also available [46].

Damage

The chronic inflammatory nature of AAV, along with treatment-related toxicity and comorbidities, can lead to irreversible long-term damage. The VDI is the most widely used tool to assess such damage [40]. It includes 64 nonweighted items across 11 organ systems, recorded only if they persist for more than 3 months, regardless of whether the cause is disease or treatment related. A higher VDI score early in the disease course, particularly >5 within the first 3 months, has been linked to increased mortality risk [47]. However, VDI has limitations: it does not distinguish between types or severity of damage, such as the difference between conductive and sensorineural hearing loss or degrees of cardiac dysfunction.

The GC toxicity index (GTI) was developed through multidisciplinary efforts to capture the cumulative damage resulting from long-term GC use [42]. Although not specific to AAV, it provides a comprehensive measure of GC-related toxicity over time. It has been adopted as a key secondary outcome in many randomised controlled trials (RCTs) in rheumatology, including the ADVOCATE trial [48].

Prognosis

In terms of prognosis, the most widely used tool is the FFS, initially developed for PAN and EGPA and later expanded to include

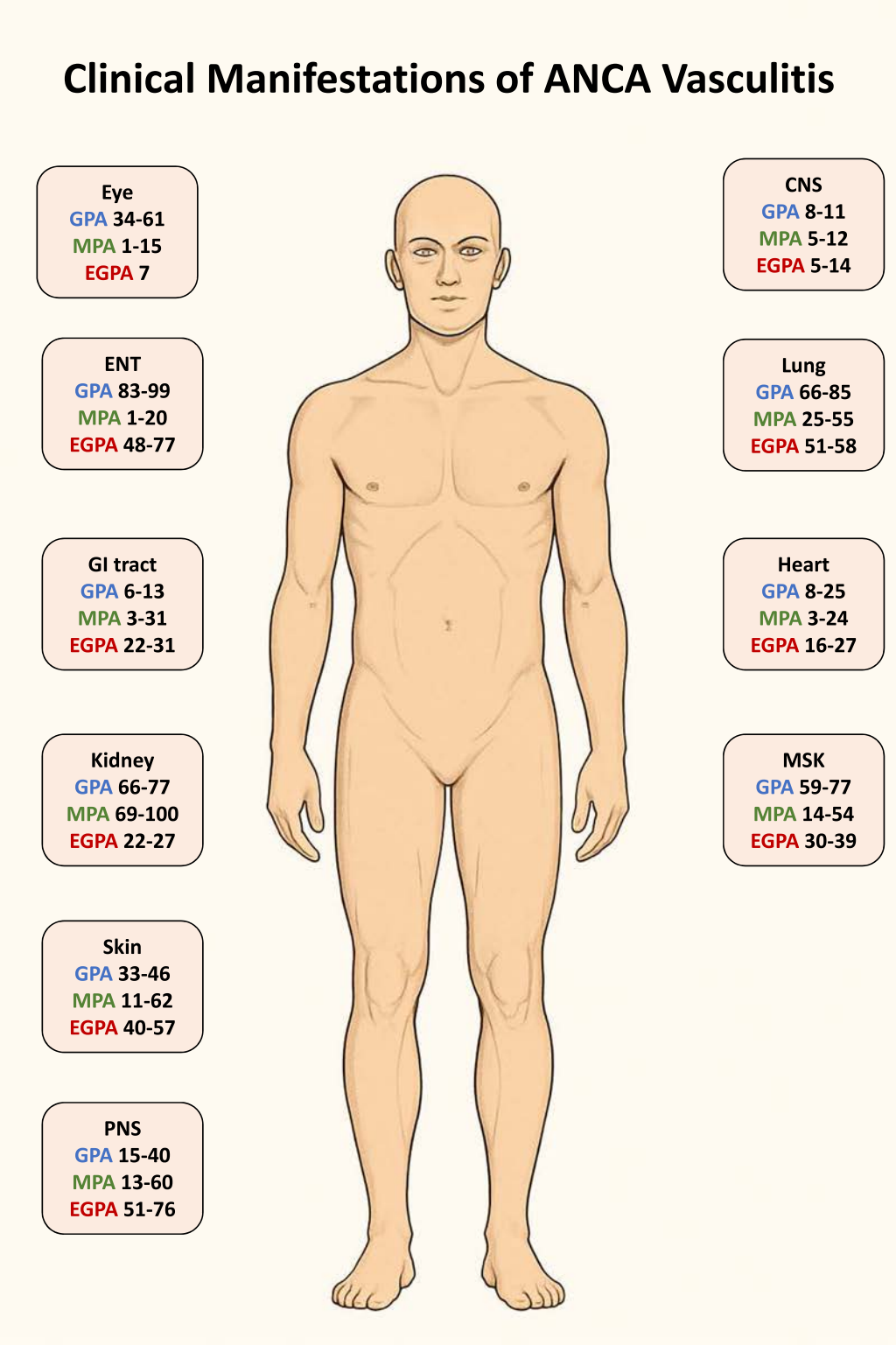

Figure 1. Clinical manifestations of AAV by disease subtype over time. Data with permission from Reference [34]. AAV, ANCA-associated vasculitis; ANCA, antineutrophil cytoplasmic antibody; CNS, central nervous system; EGPA, eosinophilic granulomatosis with polyangiitis; ENT, ear, nose, and throat; GI, gastrointestinal; GPA, granulomatosis with polyangiitis; MPA, microscopic polyangiitis; MSK, musculoskeletal; PNS, peripheral nervous system.

GPA and MPA [43]. Factors such as age over 65, cardiac or gastrointestinal involvement, renal insufficiency, and absence of ENT disease are associated with higher 5-year mortality, ranging from 9% (FFS = 0) to 40% (FFS ≥2). For renal outcomes, the ANCA Kidney Risk Score combines histological features with baseline estimated glomerular filtration rate (eGFR) to predict the 36-month risk of end-stage kidney disease, offering a validated and practical tool for long-term renal prognosis in AAV [49].

Patient-reported outcomes

Assessing patient-reported outcomes is essential for understanding the full impact of AAV, as patients' perspectives often differ from those of physicians. Most tools used in AAV studies are not disease specific, such as Patient-Reported Outcomes Measurement Information System (PROMIS), Short form (SF)-36, PtGA, MFI-20, Health Assessment Questionnaire–Disability Index (HAQ-DI), EuroQol 5-Dimension (EQ-

Table 1
Clinical assessment instruments used for ANCA-associated vasculitis patients in published clinical trials

Instrument name	Assessment focus	Clinical trials used in	Type of disease	Remarks
Activity				
BVAS (v.1-3) [35]	Assesses disease activity, relapse, and remission using 56 items (categorised as minor and major) over the previous 28 d	6 vs 12 CYC, ADVOCATE, AZA ANCA, BREVAS, CORTAGE, CHUSPAN, CHUSPAN2, CYCAZAREM, CYCLOPS, 6 vs 12 CYC, LEF vs MTX, MMF vs CYC, IMPROVE, MAINRITSAN, MANDARA, MTX vs CYC, Mizoribine, MEPEX, MIRRA, MYCYC, RITUXVAS, NORAM, REMAIN, RITUXVAS, CYC vs MMF, WEGNET, MMF vs CYC	Validated and specific to all forms of AAV	Some trials combined BVAS with CRP, ESR, and minimal GCs dose or cessation
BVAS/WG [36]	Assesses disease activity, relapse, and remission using 34 items (categorised as minor and major) over the previous 28 d	ALEVIATE, PEXIVAS, RAVE, RITAZAREM, MAINTANCAVAS, CO-TRIMOXAZOLE	Validated specifically for GPA, but also used in other forms of AAV	The ALEVIATE trial also included BD
SNOT-22 [37]	Assess the severity and impact of symptoms across multiple domains relevant to chronic rhinosinusitis and related ENT conditions	MIRRA, MANDARA	Not specific to AAV	
DEI [38]	Disease activity in 11 items	LEF vs MTX, NORAM, CO-TRIMOXAZOLE	Validated only in GPA	
ACQ-6 [39]	Measure the adequacy of asthma control in the previous week by 6 items	MIRRA, MANDARA	Not specific to AAV	Evaluated in EGPA
Damage				
VDI [40]	Chronic manifestations: 64 items required, covering the past 3 mo	ADVOCATE, CHUSPAN, CHUSPAN2, BREVAS, CYCAZAREM, CYCLOPS, IMPROVE, LoVAS, MAINRITSAN, REMAIN MANDARA, MEPEX, MIRRA, MYCYC, NORAM, RAVE, RITUXVAS, CYC vs MMF, MAINTANCAVAS	Validated and specific to all forms of AAV	Higher scores are associated with a greater risk of mortality
CDA [41]	Includes 135 items, derived from the AVID	ALEVIATE, PEXIVAS, RITAZAREM	Validated specifically for GPA, but also used in other forms of AAV	
GTI [42]	Includes 31 items assessed at a minimum of a 3-mo interval	ADVOCATE	Not specific to AAV	
Prognostic				
FFS, FFS-2009 [43]	Assess involvement of age, ENT, cardiac, GI, and renal systems	6 vs 12 CYC	Validated in AAV and PAN	The FFS-2009 version has not been validated in clinical trials
Patient-reported outcomes				
SF-36	Health-related quality of life measured using 36 items	ADVOCAT, CHUSPAN, CYCAZAREM, LEF vs MTX, LoVAS, MAINRITSAN, MANDARA, MEPEX, NORAM, PEXIVAS, RAVE, RITAZAREM, RITUXVAS, WEGNET	Not specific to AAV	
HAQ-DI	Evaluates the ability to perform activities of daily living using 20 questions	CHUSPAN, MAINRITSAN	Not specific to AAV	
EQ-5D-5L	Assessment of health status in 5 dimensions	ADVOCATE, PEXIVAS	Not specific to AAV	
PtGP	Score 0-10 by patients	LoVAS	Not specific to AAV	

AAV, ANCA-associated vasculitis; ACQ-6, Asthma Control Questionnaire, 6-item version; ANCA, antineutrophil cytoplasmic antibody; BD, Behçet disease; BVAS, Birmingham Vasculitis Activity Score; BVAS/WG, BVAS for Wegener granulomatosis; CDA, combined damage assessment; CRP, C-reactive protein; DEI, Disease Extent Index; EGPA, eosinophilic granulomatosis with polyangiitis; ENT, ear, nose, and throat; EQ-5D-5L, EuroQol 5-Dimension 5-Level Questionnaire; ESR, erythrocyte sedimentation rate; FFS, 5-factor score; GC, glucocorticoid; GPA, granulomatosis with polyangiitis; GTI, glucocorticoid toxicity index; HAQ-DI, Health Assessment Questionnaire–Disability Index; PAN, polyarteritis nodosa; PtGP, patient global perspective; SF-36, Short Form-36; SNOT-22, 22-item Sinonasal Outcome Test; VDI, vasculitis damage index. Please refer to the clinical trial references provided in the table for full trial names and detail.

5D), and COMPASS31. Of these, only the SF-36 and, to a lesser extent, the HAQ-DI and EQ-5D, have been evaluated in AAV trials. Recently, the AAV Patient-Reported Outcome (AAV-PRO) was developed specifically for AAV, assessing symptoms, impact on daily life, and well-being across 29 items and 6 domains [50]. AAV-PRO correlates with patient-focused measures, such as the SF-36 and depression scores, but not with clinician-based tools like the BVAS or VDI, highlighting its value in complementing traditional clinical end points [51].

Comorbidities

Patients with AAV are at increased risk for a range of complications, including myocardial infarction, myocarditis, and subsequent heart failure, stroke, chronic kidney disease (CKD), osteoporosis, malignancies, and serious infections. These risks stem from the direct effects of the autoimmune process, causing endothelial damage and accelerating atherosclerosis; comorbid conditions such as diabetes and hypertension; and long-term damage caused by both the vasculitis itself and the use of immunosuppressive therapies. Serious infections are the major cause of death in the first year of therapy, and recurrent infection due to secondary immunodeficiency is now a common complication of B cell depletion therapy in AAV [52]. Patients with AAV have a 65% higher risk of developing cardiovascular events and up to an 8.5-fold increased risk of stroke, with both risks being most pronounced during the first year after diagnosis [53]. Moreover, traditional cardiovascular risk factors such as diabetes, hypertension, dyslipidaemia, and obesity are 10 times more common in patients with AAV than those in the general population. These comorbidities contribute to a vicious cycle, further increasing the risk of both cardiovascular and CKD [53]. Not surprisingly, the recent EULAR and Kidney Disease Improving Global Outcomes (KDIGO) guidelines for AAV highlight the critical importance of actively monitoring and managing comorbid conditions in these patients, including annual urine surveillance for those treated with cyclophosphamide, considering avacopan in cases with a high GC burden, and more aggressive management of traditional metabolic syndrome risk factors [54,55].

Table 2
Recommended induction and maintenance therapies for ANCA-associated vasculitis

	Induction of remission	Maintenance of remission
Treatment	Rituximab 1000 mg at week 0 and 2 (alternatively: cyclophosphamide 15 mg/kg at weeks 0, 2, 4, 7, 10, and 13)[a] Glucocorticoids dosing according to the PEXIVAS study (alternatively: avacopan 30 mg twice daily)	Rituximab 500-1000 mg every 6 mo for 24-48 mo[b] (alternatively: azathioprine, mycophenolate, or methotrexate) Glucocorticoids dosing according to the PEXIVAS study (alternatively: avacopan 30 mg twice daily)

ANCA, antineutrophil cytoplasmic antibody. Please refer to the clinical trial references provided in the table for full trial names and details.
[a] Consider an extended treatment period if required, with dose adjustments based on glomerular filtration rate and age.
[b] A longer treatment duration, a 1000-mg dose, or shorter dosing intervals should be considered for relapsing patients or those at higher risk of relapse.

MONITORING

Clinical

BVAS, as described earlier, remains the most widely used tool for assessing disease activity in AAV trials. Clinically, up to 90% of patients with GPA or MPA are positive for ANCA. The achievement of ANCA negativity after induction therapy reduces long-term relapse risk [56]. Among 57 PR3-positive patients treated with rituximab for 2 years, achieving PR3 negativity or at least a 50% reduction in PR3 titres from baseline was associated with a longer relapse-free survival [57]. Persistently positive or rising ANCA levels, PR3-ANCA subtype at diagnosis, the presence of ENT disease, and better kidney function are associated with increased relapse risk, although the predictive value remains limited [58]. A meta-analysis evaluating the diagnostic utility of ANCA titres in predicting AAV relapse found that using either enzyme-linked immunosorbent assay (ELISA) or indirect immunofluorescence assays yielded a sensitivity of 0.70 and a specificity of 0.66, with slightly better performance observed for ELISA [59]. Despite the associations of relapse risk with ANCA, this is an insensitive biomarker, and the utility of serial ANCA testing in guiding treatment remains debated.

Biomarkers

Increasing attention has been given to non-invasive markers that reflect disease activity and may improve the prediction of flares, particularly renal. Several studies have evaluated the role of various B cell subsets (eg, $CD5^+$ and $IgD^-CD27^-CD38^-$ B cells) in AAV disease activity and renal involvement [60,61]. The use of B cells as biomarkers in AAV was examined in 2 clinical trials of rituximab for remission maintenance. In the MAINRITSAN2 (Maintenance of Remission Using Rituximab in Systemic ANCA-Associated Vasculitis) trial, relapse rates were similar between patients who received rituximab tailored according to $CD19^+$ B cell counts and those who received fixed-schedule dosing [62].

In contrast, the MAINTANCAVAS trial found that tailoring rituximab dosing based on $CD20^+$ B cell repopulation was associated with fewer relapses compared with ANCA-guided treatment [63]. Complement components C3a and C5a, central to the alternative complement pathway, are elevated in active AAV and drive neutrophil activation and recruitment. Elevated serum C5a, C5b-9, and factor B levels are seen during active disease, while urinary C5a can increase up to 19-fold compared with that in remission [64]. Lower baseline serum C3 levels associate with worse long-term renal and overall outcomes [65]. Urinary soluble CD163 (sCD163), a marker of M2 macrophage activation, is associated with active renal vasculitis and can be detected even in glomeruli that appear unaffected on histology [66]. Similarly, urinary monocyte chemoattractant protein (MCP)-1, a chemokine involved in monocyte recruitment, correlates with both disease activity and chronic kidney injury [67]. The combination of sCD163 and MCP-1 improves sensitivity for detecting early or mild renal flares [68]. Additionally, urinary $CD4^+$ T cells have emerged as a promising predictor of renal relapse, with high specificity and potential clinical utility in guiding monitoring strategies [69].

STANDARD OF CARE

The treatment of AAV is based on 2 phases: induction of remission and maintenance of remission (Table 2). The former typically includes GCs combined with cyclophosphamide, rituximab, or both, with the optional addition of avacopan. Remission maintenance involves long-term therapy with either rituximab or azathioprine to prevent relapse. The effective use of cyclophosphamide and rituximab in patients with AAV supports the crucial role of B cells in the disease's pathogenesis. Multiple guidelines recommend both agents as first-line treatment [54]. Rapid depletion of circulating B cells is associated with achieving remission in AAV. In contrast, persistently positive ANCA and elevated levels of plasmablasts during remission may indicate an increased risk of relapse [70]. Supplementary Table S1 presents ongoing clinical trials evaluating emerging therapeutic agents in AAV. Current controversies in the management of AAV are presented in Table 3.

Cyclophosphamide

The beneficial use of cyclophosphamide, an alkylating agent with inhibitory effects on B cells, has been demonstrated in both phases of therapy induction of remission and maintenance of remission, when administered as intermittent pulses for 3 to 6 months, or less frequently, orally. Higher cumulative doses of cyclophosphamide associate with reduced relapse rates and a survival benefit lasting up to 5 years from the initiation of treatment [71]. Moreover, pulse cyclophosphamide induced remission at a similar rate to daily oral administration but with a reduced cumulative dose and fewer side effects [72]. Compared with other agents such as methotrexate and azathioprine, cyclophosphamide was at least as effective in the remission phase and showed an advantage over mycophenolate in the induction phase with fewer subsequent relapses, especially in the PR3-ANCA subgroup [73–75]. As the greatest concern with cyclophosphamide is its relatively high rate of adverse effects, long-term cancer risk, and infertility, the use of 6 fixed 500 mg intravenous (IV) doses was associated with a similar remission rate but fewer side effects than standard therapy in patients ≥65 years old [76].

Rituximab

The efficacy of rituximab was comparable with that of cyclophosphamide in the RAVE (Rituximab in ANCA-Associated

Table 3
Current controversies in the management of AAV

Research agenda	Cons	Pros	RCT data	The controversy	Topic
Evaluate different GC dosing strategies according to specific AAV subtypes, disease severity, and baseline comorbidities	Use of the lower dose was associated with increased risk for a composite of death, ESKD, and AAV progression in a large retrospective analysis	Lower cumulative GCs doses and lower GC-related toxicity Similar remission rates in 6 and 12 mo with GC-induced toxicity	Use of oral GC 0.5 mg/kg was noninferior to 1 mg/kg in the PEXIVAS and LoVAS trials	Newer studies use a lower initial dosage of GCs	GC dosing for induction remission
Repeating early GC withdrawal studies in additional regional, clinical, and serological settings	Low generalisability: data come from a single trial of Japanese patients with MPA treated only with RTX, where GPA and PR3+ are both risk factors for relapse, not included in this study	Similar remission rates with lower SAE	Use of GC for 5 mo after induction was evaluated at 24 mo (LoVAS)	When is the exact time to stop GC treatment	GC withdraw timing
Compare RTX and CYC according to AAV severity, organ system involvement, and the risk of treatment-related adverse effects	Favoured remission rate for RTX in relapsing AAV, regardless of disease subgroup Observational data from the French Vasculitis Study Group Registry found a higher remission rate for RTX among GPA CYC is associated with a higher risk of malignancy and infertility	Similar remission rates in 6 and 12 mo	The RAVE and RITUXVAS trial compared RTX vs CYC for induction	Which one is the drug of choice for the initial induction of remission	RTX vs CYC for induction remission
Study the effect of long-term remission maintenance therapy on mortality and ESKD, stratified by treatment type	Similar relapse-free survival and remission rates for extended vs standard AZA treatment Mortality or ESKD effect was not reported in those trials	Lower major relapse rates and relapse-free survival with extended treatment with RTX An extended period of treatment was not associated with a higher risk of SAE	The MAINRITSAN3, RITAZAREM, and the AZA-ANCA trials evaluated an extended period of RTX/AZA maintenance treatment (up to 4 y)	What is the ideal remission maintenance length of treatment	Duration of maintenance
Evaluate the safety and efficacy of combined RTX and CYC induction therapy for severe AAV manifestations	Prospective data of RTX combined with a full course of CYC is lacking Potential for high infection risk	Potentially higher remission rates for severe AAV manifestations with lower GC exposure	The RITUXVAS trial combined 2 CYC doses with RTX for induction. The ENDURRANCE-1 trial will compare RTX plus low-dose CYC (500 mg every 2 wk for 6 doses) to RTX alone	Should RTX and CYC be used together?	RTX/CYC combined treatment
Investigating the role of plasma exchange in the treatment of life-threatening AAV, stratified by organ involvement and patients' baseline risk of infection	Higher infection risk Mortality or beneficial effect on alveolar haemorrhage was not demonstrated in a post hoc analysis of the PEXIVAS trial Low availability of the treatment	Both MEPEX and a later meta-analysis found a reduction in the risk of ESKD at 12 mo The effect was more prominent when serum creatinine of >3.4 mg/dL	The MEPEX and PEXIVAS trials evaluated plasma exchange in AAV with impaired kidney disease or alveolar haemorrhage	What is the place of plasma exchange in the post-PEXIVAS era	Plasma exchange
Determine whether avacopan should be used for longer than 12 mo or in patients with advanced CKD or paediatric AAV	Lack of robust data to support the use in these indications Potential adverse effects due to drug toxicity	Small-scale and postmarketing data support avacopan efficacy and safety in ESKD/advanced patients with CKD and paediatric patients A phase 3 trial is recruiting paediatric patients (NCT06321601)	The ADVOCAT trial included only adult patients with GFR >15 mL/min who were treated for 12 mo	Should it be used to treat patients with advanced CKD? Paediatric AAV patients? What is the optimal duration of time?	Avacopan indications
Evaluate whether IL-5 inhibitors should be used in patients with EGPA with organ-threatening manifestations	There is no robust evidence supporting their use as monotherapy in organ- or life-threatening EGPA	Most published real-world series and observational studies of mepolizumab/benralizumab in EGPA have focused on patients with relapsing or refractory disease, often with nonorgan-threatening manifestations, and typically as add-on therapy to other immunosuppressants	Both MIRRA and MANDARA excluded patients with severe EGPA manifestations	Should IL-5 inhibitors be used in organ-threatening EGPA?	Use of IL-5 inhibitors in severe EGPA

AAV, ANCA-associated vasculitis; ANCA, antineutrophil cytoplasmic antibody; AZA, azathioprine; CKD, chronic kidney disease; CYC, cyclophosphamide; EGPA, eosinophilic granulomatosis with polyangiitis; ESKD, end-stage kidney disease; GBM, glomerular basement membrane; GC, glucocorticoids; GFR, glomerular filtration rate; GPA, granulomatosis with polyangiitis; IL, interleukin; MPA, microscopic polyangiitis; PR3+, proteinase 3-positive; RCT, randomised controlled trial; RTX, rituximab; SAE, serious adverse event. Please refer to the clinical trial references provided in the table for full trial names and details.

Vasculitis) trial, which directly compared the 2 treatments for induction of remission, with greater benefit observed in patients with relapsing AAV [77]. The RITUXVAS (Rituximab versus Cyclophosphamide in ANCA-Associated Vasculitis) trial focused on patients with more severe kidney disease and compared the combination of rituximab with low-dose IV cyclophosphamide to conventionally dosed cyclophosphamide and found no differences in efficacy or safety [78]. The impact of fixed interval, repeat dose rituximab on relapse risk was assessed in the MAINRITSAN and RITAZAREM (Rituximab versus Azathioprine for Maintenance of Remission in ANCA-Associated Vasculitis) studies [79]. Both trials found a lower relapse rate with rituximab than with azathioprine over 2 years, but observed increases in relapse risk in the rituximab treatment groups after drug

withdrawal. Current guidelines suggest a duration of rituximab of 2 to 4 years, depending on perceived relapse risk, but because relapse risk returns whenever rituximab is stopped and there are increasing risks of multiple infections and humoral immunodeficiency, an approach is emerging to personalise remission therapy by estimation of relapse risk and the consequences of relapse and by close monitoring to minimise rituximab exposure.

As rituximab has become the default immunosuppressive for induction, there is a continued debate as to the additional value of low-dose cyclophosphamide, especially when there is nephritis with acute kidney injury. While this combination was tested in RITUXVAS, it was not compared with rituximab. Observational studies have suggested a high rate of efficacy for the combination and its use to reduce GC exposure [80]. The ENDURRANCE-1 (Exploring Durable Remission With Rituximab in Antineutrophil Cytoplasmic Antibody(ANCA)-Associated Vasculitis) trial will compare the combination to rituximab alone, both treatment groups followed by maintenance rituximab, tailored according to B cell and ANCA status (NCT03942887). A large retrospective survey found rituximab to cause more infections and more repeated infections than nonrituximab regimens, and this information, coupled with concerns about hypogammaglobulinaemia and relapse, is driving the development of alternative remission maintenance strategies [52].

While rituximab has been extensively investigated in MPA and GPA, high-quality data from RCTs of rituximab in EGPA are lacking. Treatment with rituximab in a retrospective cohort of 41 patients was associated with high rates of clinical improvement and a reduced requirement for prednisolone [81]. A systematic literature review that included 171 rituximab-treated patients reported similar results, along with the finding that ANCA-positive patients tended to respond better to rituximab than ANCA-negative patients [82]. Of note, most patients in both studies had refractory or relapsing disease. The REOVAS (Rituximab in Eosinophilic Granulomatosis with Polyangiitis –associated Vasculitis) study was the first randomised, controlled, double-blind trial to evaluate rituximab vs cyclophosphamide as induction therapy in patients with EGPA [83]. Participants were stratified according to their FFS and received either 2 g of rituximab over 14 days or nine 500- to 600-mg cyclophosphamide pulses. The results showed that relapse rates and average daily GC doses were comparable between the 2 groups. However, Health Assessment Questionnaire scores on days 180 and 360 and VDI scores on day 360 tended to be better in the rituximab group. Long-term results, with a median follow-up of 45 months, from the REOVAS study showed similar efficacy. However, in ANCA-positive patients, rituximab was associated with better relapse-free survival [84].

Avacopan

Avacopan, an orally administered small-molecule antagonist of C5aR 1 (CD88), has been approved for the treatment of severe active AAV in combination with rituximab or cyclophosphamide. This approval was supported by results from the phase 2 CLASSIC (Clinical ANCA Vasculitis Safety and Efficacy Study of Inhibitor of C5aR) and CLEAR (C5a Receptor Inhibitor in ANCA-Associated Vasculitis) studies and the phase 3 ADVOCATE trial [48,85,86]. This showed that the avacopan treatment group, when compared with a standard GC taper, had similar remission rates at week 26 and higher sustained remission rates at week 52, without any specific safety concerns. Avacopan development has focused on replacing GCs, but secondary end point analysis of ADVOCATE showed reduced relapse rates, better kidney function recovery, and better quality of life with avacopan. Of note, the superiority of avacopan over GCs at week 52 was observed only in the subgroup of patients who received rituximab for induction and did not receive maintenance therapy beyond week 4. Additionally, the infection rate was similar between the groups. A post hoc analysis of the ADVOCATE trial found that mean GC use over 26 weeks was lower in the avacopan group than that in the GC group (1374 vs 3364 mg). Additionally, patients in the avacopan group experienced less GC-related toxicity, particularly in the domains of body mass index, glucose tolerance, lipid metabolism, and skin toxicity, as measured by the GTI [87].

Mepolizumab

Considering the important function of IL-5 in EGPA, it was not surprising that the first Food and Drug Administration (FDA)-approved drug exclusively for EGPA was mepolizumab, a humanised monoclonal antibody (mAb) specific for the α-subunit of IL-5. The MIRRA study was a multicentre, double-blind, phase 3 trial that included patients with relapsing or refractory non–organ-threatening EGPA who received either 300 mg of mepolizumab or placebo for 52 weeks [88]. Patients treated with mepolizumab had higher remission rates and fewer relapses and required a lower average daily dose of GCs compared with those receiving placebo, regardless of their MPO status or disease phenotype [89]. The efficacy of mepolizumab was replicated by the IL-5 receptor inhibitor, benralizumab, 30 mg every 4 weeks in the MANDARA trial, which found no differences between mepolizumab and benralizumab groups apart from greater eosinophil reduction and a higher rate of complete oral GC withdrawal at week 48 with benralizumab [39]. Longer-term exposure studies for both MIRRA and MANDARA have confirmed continued benefit with these medications after 12 months [90]. MIRRA and MANDARA focused on prevalent patients with EGPA and nonsevere disease activity, and there is an absence of data with these drugs in severe, active disease. The E-Merge Study is an ongoing randomised, controlled, double-blind phase 3 trial evaluating mepolizumab vs cyclophosphamide/azathiopine in EGPA regardless of disease severity (NCT05030155).

Benralizumab

In addition to mepolizumab, 2 other FDA-approved IL-5 –based treatments for eosinophilic asthma are currently being investigated in EGPA. Reslizumab, an intravenous IL-5 mAb, was associated with a significant reduction in daily oral corticosteroid use in a small, open-label study involving 10 patients with EGPA [91]. Benralizumab, a mAb targeting the IL-5α receptor, was evaluated in a double-blind, phase 3, randomised, noninferiority trial compared with mepolizumab in patients with non–organ-threatening EGPA [39]. The results of the MANDARA study demonstrated that, after 52 weeks, benralizumab was noninferior to mepolizumab in remission induction in patients with relapsing or refractory EGPA. Similar findings were observed in the 2-year extension phase of the trial [90]. Of special note, unlike the ACR/EULAR 2022 classification criteria for EGPA, patients enrolled in the published clinical trials of IL-5 inhibitors were not required to have evidence of vasculitis before their recruitment.

NEWER THERAPIES

B cell/CAR-T targeted

Obinutuzumab, a type II anti-CD20 humanised mAb with high affinity for tissue CD20$^+$ cells, is being evaluated in the phase 2 OBIVAS (Obinutuzumab in ANCA-Associated Vasculitis) clinical trial vs rituximab (NCT05376319) [92]. Treatment with obinutuzumab has demonstrated superiority over rituximab in follicular lymphoma, and its efficacy over standard therapy was confirmed in a phase 3 trial for lupus nephritis [93]. Obinutuzumab has been used successfully in 2 small cohorts comprising patients with AAV who either developed rituximab intolerance or had an inadequate response to standard therapy (Figure 2) [94,95].

B cell lymphocyte stimulator (BLyS) and a proliferation-inducing ligand (APRIL) are 2 important cytokines that promote B cell maturation, survival, and antibody secretion. The BLyS cytokine is successfully targeted by belimumab, an FDA-approved therapy for systemic lupus erythematosus (SLE) and lupus nephritis. The use of belimumab in AAV was evaluated in the BREVAS (Belimumab in Remission of ANCA-Associated Vasculitis) trial, which compared belimumab with placebo, both on an azathioprine background, for maintenance of remission. Although belimumab did not reduce the risk of relapse in combination with azathioprine, both study arms experienced a low number of events, which may have affected the assessment of belimumab's efficacy [96]. Interestingly, none of the patients receiving rituximab induction and subsequent belimumab experienced a relapse in this trial. This observation led to the investigation of a combined approach using rituximab and belimumab in the ongoing COMBIVAS trial (NCT03967925) [97].

The transmembrane activator and calcium-modulating cyclophilin ligand interactor (TACI) is a receptor that binds BLyS and APRIL. Increased expression of TACI on CD19$^+$ cells and immature B cells has been observed in patients with AAV, even during the remission phase, compared with healthy controls [98]. Telitacicept, which binds to BLyS and APRIL, preventing them from interacting with their transmembrane receptors, including TACI, has been approved in China for treating lupus based on a phase 2b study. It is also being evaluated in an ongoing study, TTCAZAREM, in China to assess its potential for remission maintenance in AAV, with telitacicept being compared with azathioprine (NCT05965284). Povetacicept is an enhanced dual APRIL and B-cell activating factor (BAFF) inhibitor that has demonstrated greater suppression of B cell populations than other TACI-Fc fusion proteins and CD20-, APRIL-, or BAFF-selective agents [99]. It is currently being evaluated in an open-label RUBY-3 (Povetacicept in Autoantibody-Associated Glomerular Diseases) study investigating its use in autoantibody-associated glomerular diseases, but not in patients with AAV nephritis (NCT05732402). RCT-18 and atacicept are fusion proteins that neutralise both BLyS and APRIL. They have been evaluated in various conditions, including lupus and rheumatoid arthritis, but have yet to be tested in clinical trials for AAV.

Chimeric antigen receptor (CAR) T cell therapy, unlike rituximab, which mainly depletes circulating CD20$^+$ cells, targets autoreactive B cells within lymphoid tissue and inflamed organs in AAV, offering potential for deeper and more durable remission, with next-generation CAR-T approaches (eg, Treg and fibrosis directed) further expanding therapeutic opportunities [100].

In a mouse model of MPO-ANCA vasculitis, treatment with CD19 CAR-T cells prevented glomerulonephritis and led to a decline in MPO-ANCA levels [101]. There have been at least 2 case reports of successful CAR-T treatment in treatment-resistant

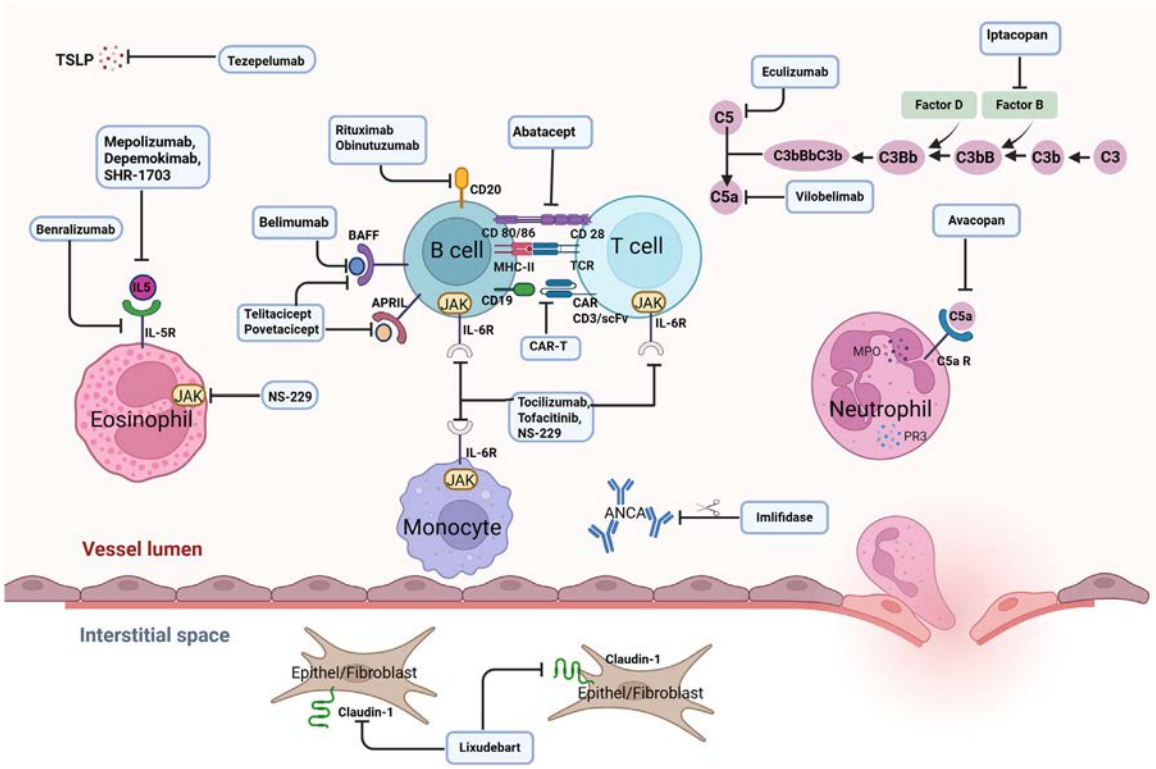

Figure 2. Treatments under evaluation in ongoing or recently completed clinical trials for AAV. ANCA, antineutrophil cytoplasmic antibody; APRIL, a proliferation-inducing ligand; BAFF, B cell–activating factor; CAR-T, chimeric antigen receptor T cell therapy; C5aR, C5a receptor; IL, interleukin; IL-6R, interleukin-6 receptor; JAK, Janus kinase; MHC, major histocompatibility complex; TSLP, thymic stromal lymphopoietin.

GPA [102,103]. Although several CAR-T trials are ongoing, published data on the long-term efficacy and safety of CAR-T in autoimmune diseases remain limited, largely based on small cohorts [104]. Most clinical experience comes from lupus, with minimal data in AAV. Concerns include comparison with newer anti-CD20 agents, the need for lymphodepletion, and uncertainties around long-term outcomes [103].

Complement targeted

In addition to avacopan, several other complement-targeted treatments are under clinical investigation in the AAV treatment pipeline. Iptacopan is an oral inhibitor of complement factor B, targeting the alternative complement pathway, and has been approved for treating paroxysmal nocturnal hemoglobinuria and IgA nephropathy. Similar to avacopan, iptacopan is currently being evaluated in an ongoing phase 2 study investigating its use in combination with rituximab for both induction and maintenance of remission in patients with AAV (NCT06388941). Tarperprumig is an oral properdin inhibitor, a cofactor for alternative pathway activation. A phase II trial of tarperprumig in AAV has recently been launched (NCT07160608). The use of vilobelimab (IFX-1), a chimeric IgG4κ antibody targeting C5a that was approved for the treatment of COVID-19–induced acute respiratory distress syndrome, was evaluated in 2 phase 2 studies, the largest of which enrolled 57 participants, with results pending publication (NCT03895801). Notably, eculizumab, a recombinant humanised mAb targeting the complement component C5, is used in various indications, including atypical hemolytic uremic syndrome and catastrophic antiphospholipid syndrome. It was evaluated in a phase 2 clinical trial, which was subsequently withdrawn (NCT01275287).

T cells

Although T cell dysfunction contributes to the break in immune tolerance and ANCA B cell activation and is a direct cause of tissue damage, there has been limited development of T cell–targeted therapeutics. In a preliminary study involving 20 patients with nonsevere relapsing GPA treated with abatacept (CTLA4-Ig), 90% showed disease improvement, and 80% achieved remission within 2 months [105]. The ABROGATE trial was a phase 3 clinical study that enrolled 65 patients with relapsing GPA and similar clinical features to receive abatacept or placebo for 12 months. The results suggested that treatment failure occurred in 62% of abatacept-treated patients and 68% of those given a placebo [106].

The role of the Th17 axis in AAV was demonstrated through a single-cell transcriptome analysis of kidney biopsies from 34 patients with AAV, identifying proinflammatory, cytokine-producing $CD4^+$ and $CD8^+$ T cells as key pathogenic signatures. This finding subsequently led to the successful treatment of 4 patients from the cohort with ustekinumab, a mAb targeting IL-12/23, over 24 weeks [107]. Serum levels of IL-17A and IL-23 were significantly elevated in 28 patients with acute AAV compared with those in healthy controls. Patients with higher levels of IL-23 had more active disease, as measured by BVAS, than those with lower IL-23 levels [108]. These findings suggest that the Th17 axis, specifically IL-23, plays a role in mediating AAV severity; however, their clinical implications should be evaluated in randomised trials.

The pan-lymphocyte depleting anti-CD52 antibody alemtuzumab induces a long-term reduction in $CD4^+$ T cells and is approved for the treatment of multiple sclerosis. One dose ranging trial demonstrated limited efficacy in patients with refractory AAV [109].

Eosinophils

In addition to the expanding use of IL-5 inhibitors in EGPA, several long-acting mAbs are under investigation. Depemokimab is a twice-yearly IL-5 inhibitor treatment that has been shown to reduce the annualised rate of exacerbations in patients with severe eosinophilic asthma, as well as the burden of chronic rhinosinusitis with nasal polyps [110]. In healthy subjects, a single 400-mg dose of the investigational drug SHR-1703 resulted in a substantial reduction in peripheral blood eosinophils, with effects lasting up to 6 months [111]. Both depemokimab and SHR-1703 are being evaluated in phase 3 trials for patients with nonsevere EGPA (NCT05979051). Notably, depemokimab is being compared with mepolizumab in the OCEAN (Efficacy and Safety of Depemokimab Compared With Mepolizumab in Adults With Relapsing or Refractory EGPA) trial (NCT05263934).

Tezepelumab is a human IgG2λ mAb that inhibits thymic stromal lymphopoietin, leading to downstream suppression of type 2 (Th2) inflammation, including reductions in airway submucosal eosinophils, fractional exhaled nitric oxide, and concentrations of IL-5 and IL-13 [112]. Approved for use in patients 12 years and older, this treatment serves as an add-on maintenance option for managing severe asthma, regardless of phenotype (eosinophilic or allergic) [113]. Based on its efficacy in asthma, the RACE-MATE (Randomised Trial to Explore the efficacy and Mechanism of Action of Tezepelumab in EGPA) study is an ongoing phase 2 randomised, double-blind, placebo-controlled trial evaluating the effectiveness of tezepelumab compared with placebo over a 24-week treatment period in patients with active (nonsevere) EGPA (NCT06230354). NS-229, a selective Janus kinase (JAK)1 inhibitor, is being evaluated in a phase 2 randomised, double-blind trial (NCT06046222) enrolling patients with EGPA, with or without background mepolizumab or benralizumab therapy.

Neutrophil- and fibrosis-targeted therapies

Cathepsins are a protease family whose role in disease pathogenesis has been identified in various conditions. Cathepsin C, an enzyme regulating the maturation of neutrophil serine proteases and neutrophil activation, has emerged as a therapeutic target. Inhibition of cathepsin C dose dependently ameliorated vasculitis and reduced NETs in a rat model of MPO-AAV [114].

Claudin-1 is a component of tight junction strands, primarily maintaining the integrity of epithelial and endothelial surfaces. Claudin-1 downregulation has been associated with impaired barrier function in the blood-brain barrier, skin, and gut. Notably, in the healthy kidney, claudin-1 plays a crucial role in maintaining the integrity of the permeability barrier, thereby preventing plasma protein leakage into Bowman capsule [115]. Claudin-1 has been identified as a potential therapeutic target for CKD, particularly in crescentic glomerulonephritis, and its involvement in chronic fibrosis may underlie its anti-inflammatory effects [116]. Two clinical trials of lixudebart, a fully humanised antihuman claudin-1 mAb targeting nonjunctional claudin-1, are currently ongoing, including a phase 2 trial in patients with AAV with rapidly progressive glomerulonephritis (NCT06047171).

Imlifidase is a protease derived from the IgG-degrading enzyme of *Streptococcus pyogenes*. It has been shown to inhibit anti-HLA antibody–mediated natural killer cell activation and antibody-dependent cellular cytotoxicity. Imlifidase was originally developed to desensitise highly HLA-sensitised patients

and enable kidney transplantation. It was later evaluated in a phase 2 trial involving 15 adults with circulating anti-GBM antibodies and an eGFR of <15 mL/min/1.73 m^2; notably, 6 of these patients were also positive for ANCA. At 6 months, 67% of participants were dialysis independent, a rate substantially higher than that reported in previous anti-GBM disease cohorts [117]. Notably, 2 hours after the infusion, ANCA titres were undetectable in the serum of all patients; however, 50% showed a rebound by day 15. These encouraging results are expected to be further evaluated in a larger phase 3 trial in anti-GBM disease (NCT05679401), which is planned to begin recruitment soon. In addition, a smaller, single-centre, open-label pilot study will include 10 patients with severe AAV and pulmonary haemorrhage (EUCT 2024-516727-13-00).

Finally, serum IL-6 is another interesting target because it promotes the differentiation of B and T cells, activates macrophages, and supports plasma cell survival. Higher levels of IL-6 were noted in patients with AAV than those in healthy controls. These levels correlated with PR3 titres and elevated IL-6 levels during complete remission predicted subsequent relapse [118]. Tocilizumab, a recombinant humanised mAb of the IgG1 subclass against the I>-6 receptor, and tofacitinib, a JAK1 and JAK3 inhibitor indirectly involved in the IL-6 pathway, have both been reported to be effective in refractory relapses in selected cases of patients with AAV [119,120]. The SATELITE (NCT04871191) study is a phase 3 trial enrolling patients with active or relapsing GPA to receive rituximab, tocilizumab, or tofacitinib as induction therapy for remission. One of the major advantages of this study is its comparison of biologics targeting 3 distinct pathways; its results may enhance our understanding of the immunological aspects of AAV and potentially expand the therapeutic arsenal.

Emerging-targeted immunotherapies

Chimeric autoantibody receptor (CAAR)-T cell therapy is a specialised form of CAR-T treatment that targets autoreactive B cells with high specificity. Unlike standard CAR-T cells, CAAR-T cells display an autoantigen rather than an scFv region, allowing them to bind directly to B cell receptors on pathogenic autoreactive B cells. This interaction activates T cells and eliminates disease-causing B cells while largely sparing healthy B cells. CAAR-T cells have shown encouraging results in mouse models of myasthenia gravis and pemphigus vulgaris, and phase 1 trials in myasthenia gravis are ongoing [121]. Tregs are also a promising cellular therapy, as patients with AAV have reduced and dysfunctional Tregs. In a humanised mouse model of SLE, a single infusion of CAR Tregs lowered autoantibody production and delayed lymphopenia [122]. CAR Tregs are now being tested in a phase 1 and 2 study in kidney transplant recipients. Bispecific T cell engagers (BiTEs) bring a T cell into close contact with a target cell by binding to CD3 on the T cell and a second molecule, such as CD19 or CD20, on the target cell. Several BiTEs are in early trials for lupus and rheumatoid arthritis, although no studies in AAV are planned [123]. Bispecific autoantigen T cell engagers use the same concept but include an autoantigen arm to remove autoreactive cells, a strategy that may be relevant for MPO- or PR3-directed disease. Another approach is Siglec-engaging tolerance-inducing antigenic liposomes (STALs), which codeliver an autoantigen and a Siglec ligand to inhibit or remove autoreactive B cells [124]. STALs may induce immune tolerance, although this has not yet been investigated in AAV. A schematic overview of emerging-targeted immunotherapies for AAV is presented in Figure 3, and further research topics are outlined in Table 4.

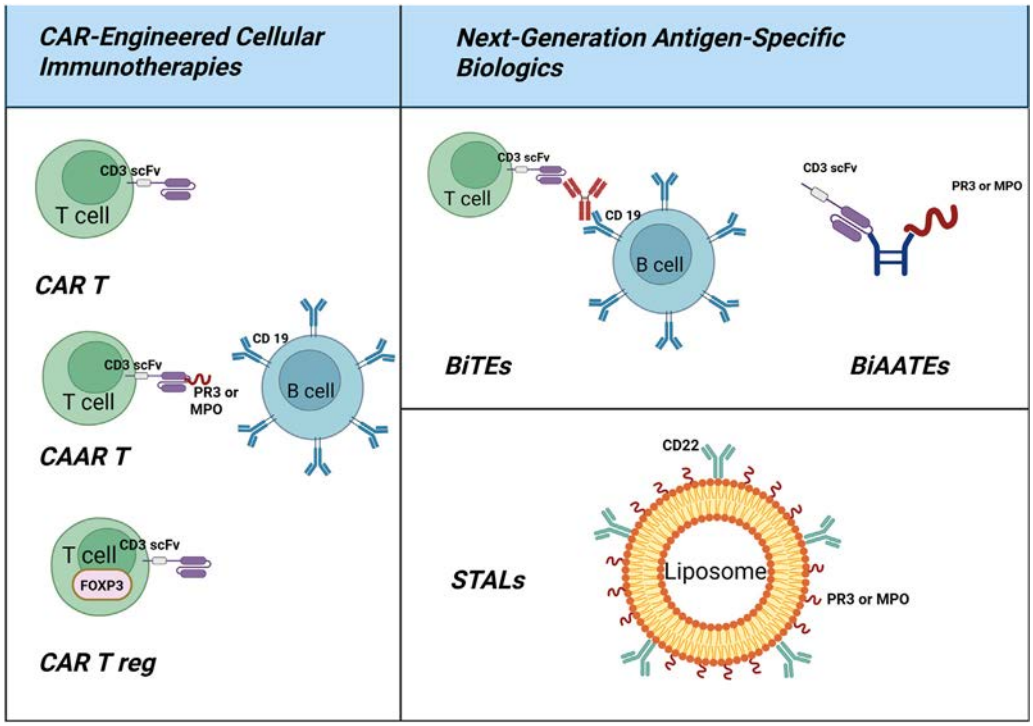

Figure 3. Schematic overview of emerging-targeted immunotherapies for antineutrophil cytoplasmic antibody (ANCA)-associated vasculitis. CAR-engineered cellular therapies, including chimeric antigen receptor T cells (CAR-T), chimeric autoantibody receptor T cells (CAAR-T), and regulatory T cells (CAR-Treg), bispecific T cell engagers (BiTEs), bispecific autoantigen T cell engagers (BiAATEs), and Siglec-engaging tolerance-inducing antigenic liposomes (STALs). MPO, myeloperoxidase; PR, proteinase.

Table 4
Research agenda

Topic
Diagnosis
• Develop data-driven diagnostic criteria (current ones are classification-focused)
• Define disease subtypes (eg, severe vs nonsevere, organ-threatening vs not)
• Refine ANCA-based classification (PR3 vs MPO) for better risk stratification
• Improve early diagnosis to prevent irreversible organ damage
Disease activity
• Standardise data-driven definitions of remission, response, and relapse; align outcome measures and patient-reported outcomes across trials
• Identify biomarkers and risk factors for relapse, remission, and damage
• Validate imaging, biopsy, and urine biomarkers (eg, usCD163 and MCP-1) for subclinical activity and treatment response
• Clarify whether persistent haematuria/proteinuria reflects active disease vs damage
• Develop biomarkers to predict drug toxicity
Advanced treatments
• Optimise glucocorticoid use (dose, pulse use, duration, and potential replacement by avacopan)
• Advance B cell therapies: deeper depletion (eg, obinutuzumab), cytokine inhibition (eg, belimumab and telitacicept), and antigen-specific approaches (eg, STALs and CAAR-T)
• Evaluate cell-based therapies (CAR-T, BiTEs) to induce durable remissions via Treg restoration
• Expand complement inhibition beyond C5aR1 (eg, iptacopan and vilobelimab)
• Target neutrophil activation (NET, Syk, and PAD4 inhibitors) and fibrosis (eg, claudin-1)

ANCA, antineutrophil cytoplasmic antibody; BiTE, bispecific T cell engager; CAAR-T, chimeric autoantibody receptor T cell therapy; CAR-T, chimeric antigen receptor T cell therapy; C5aR1, C5a receptor 1; MCP, monocyte chemoattractant protein; MPO, myeloperoxidase; NET, neutrophil extracellular trap; PAD, peptidylarginine deiminase; PR3, proteinase 3; STAL, Siglec-engaging tolerance-inducing antigenic liposome; Syk, spleen tyrosine kinase; Treg, regulatory T cell; usCD163, urinary soluble CD163.

CONCLUSION

Notwithstanding these challenges, our understanding of AAV has evolved significantly, including the development of internationally collaborative classification criteria, expanded monitoring options such as biomarker- and pathology-driven analyses, and a broadened therapeutic arsenal, some of which will hopefully become available in the near future. By reducing the time from symptom onset to accurate diagnosis and initiating rapid, tailored treatment, our aim is not only to minimise disease burden but also to improve our patients' quality of life.

FUNDING

This research did not receive any specific grant from funding agencies in the public, commercial, or not-for-profit sectors.

Competing interests

DRWJ reports a relationship of consulting or advisory with Alentis Therapeutics AG, Amgen Inc, AstraZeneca, Aurinia Pharmaceuticals Inc, Boehringer Ingelheim Ltd, Chinook Therapeutics Inc, Fate Therapeutics Inc, GSK, Novartis Pharmaceuticals Corporation, Otsuka Pharmaceutical Co Ltd, Roche, Takeda Pharmaceutical Company Limited, and Vifor Pharma Inc and reports a relationship of speaking and lecture fees with Amgen Inc, GSK, and Vifor Pharma Inc The other author declares no competing financial interests.

CRediT authorship contribution statement

Iftach Sagy: Writing – review & editing, Writing – original draft, Conceptualization. **David R W Jayne:** Writing – review & editing, Writing – original draft, Conceptualization.

Patient consent for publication

Not applicables.

Ethics approval

Not applicable.

Provenance and peer review

Not commissioned; externally peer reviewed.

Supplementary materials

Supplementary material associated with this article can be found in the online version at doi:10.1016/j.ard.2025.11.024.

Orcid

Iftach Sagy: http://orcid.org/0000-0002-2720-9934

REFERENCES

[1] Ball GV. The history of ANCA-associated vasculitis. Rheum Dis Clin North Am 2010 Aug;36(3):439–46.
[2] Jennette JC, Falk RJ, Bacon PA, Basu N, Cid MC, Ferrario F, et al. 2012 revised International Chapel Hill Consensus Conference Nomenclature of Vasculitides. Arthritis Rheum 2013;65(1):1–11 Jan.
[3] Suppiah R, Robson JC, Grayson PC, Ponte C, Craven A, Khalid S, et al. 2022 American College of Rheumatology/European Alliance of Associations for Rheumatology Classification criteria for microscopic polyangiitis. Arthritis Rheumatol 2022;74(3):400–6.
[4] Robson JC, Grayson PC, Ponte C, Suppiah R, Craven A, Judge A, et al. 2022 American College of Rheumatology/European Alliance of Associations for Rheumatology Classification criteria for granulomatosis with polyangiitis. Arthritis Rheumatol 2022;74(3):393–9.
[5] Grayson PC, Ponte C, Suppiah R, Robson JC, Craven A, Judge A, et al. 2022 American College of Rheumatology/European Alliance of Associations for Rheumatology Classification criteria for eosinophilic granulomatosis with polyangiitis. Arthritis Rheumatol 2022;74(3):386–92.
[6] Watts R, Lane S, Hanslik T, Hauser T, Hellmich B, Koldingsnes W, et al. Development and validation of a consensus methodology for the classification of the ANCA-associated vasculitides and polyarteritis nodosa for epidemiological studies. Ann Rheum Dis 2007 Feb;66(2):222–7.
[7] Gisslander K, White A, Aslett L, Hrušková Z, Lamprecht P, Musiał J, et al. Data-driven subclassification of ANCA-associated vasculitis: model-based clustering of a federated international cohort. Lancet Rheumatol 2024 Nov 1;6(11):e762–70.

[8] Lyons PA, Rayner TF, Trivedi S, Holle JU, Watts RA, Jayne DRW, et al. Genetically distinct subsets within ANCA-associated vasculitis. N Engl J Med 2012 Jul 19;367(3):214–23.
[9] Li W, Huang H, Cai M, Yuan T, Sheng Y. Antineutrophil cytoplasmic antibody-associated vasculitis update: genetic pathogenesis. Front Immunol 2021 Mar 26;12:624848.
[10] Lyons PA, Peters JE, Alberici F, Liley J, Coulson RMR, Astle W, et al. Genome-wide association study of eosinophilic granulomatosis with polyangiitis reveals genomic loci stratified by ANCA status. Nat Commun 2019 Nov 12;10(1):5120.
[11] Trivioli G, Marquez A, Martorana D, Tesi M, Kronbichler A, Lyons PA, et al. Genetics of ANCA-associated vasculitis: role in pathogenesis, classification and management. Nat Rev Rheumatol 2022 Oct;18(10):559–74.
[12] Olson SW, Arbogast CB, Baker TP, Owshalimpur D, Oliver DK, Abbott KC, et al. Asymptomatic autoantibodies associate with future anti-glomerular basement membrane disease. J Am Soc Nephrol 2011 Oct;22(10):1946–52.
[13] Wilde B, Thewissen M, Damoiseaux J, Knippenberg S, Hilhorst M, van Paassen P, et al. Regulatory B cells in ANCA-associated vasculitis. Ann Rheum Dis 2013 Aug 1;72(8):1416–9.
[14] Nakazawa D, Shida H, Tomaru U, Yoshida M, Nishio S, Atsumi T, et al. Enhanced formation and disordered regulation of NETs in myeloperoxidase-ANCA-associated microscopic polyangiitis. J Am Soc Nephrol 2014 May;25(5):990–7.
[15] Xiao H, Heeringa P, Hu P, Liu Z, Zhao M, Aratani Y, et al. Antineutrophil cytoplasmic autoantibodies specific for myeloperoxidase cause glomerulonephritis and vasculitis in mice. J Clin Invest 2002 Oct 1;110(7):955–63.
[16] Schlieben DJ, Korbet SM, Kimura RE, Schwartz MM, Lewis EJ. Pulmonary-renal syndrome in a newborn with placental transmission of ANCAs. Am J Kidney Dis 2005 Apr 1;45(4):758–61.
[17] Wang C, He R, Bai X, Zhang Y, Li J, Zhao J, et al. Immune cell crosstalk between ANCA-associated vasculitis and IgG4-related disease: an unresolved pathogenic link. Front Immunol 2025 Oct 16;16:1660956.
[18] Paroli M, Gioia C, Accapezzato D. New insights into pathogenesis and treatment of ANCA-associated vasculitis: autoantibodies and beyond. Antibodies (Basel) 2023 Mar 21;12(1):25.
[19] Ruth AJ, Kitching AR, Kwan RYQ, Odobasic D, Ooi JDK, Timoshanko JR, et al. Anti-neutrophil cytoplasmic antibodies and effector CD4+ cells play nonredundant roles in anti-myeloperoxidase crescentic glomerulonephritis. J Am Soc Nephrol 2006 Jul;17(7):1940–9.
[20] Pan M, Zhao H, Jin R, Leung PSC, Shuai Z. Targeting immune checkpoints in anti-neutrophil cytoplasmic antibodies associated vasculitis: the potential therapeutic targets in the future. Front Immunol 2023;14:1156212.
[21] Schreiber A, Xiao H, Jennette JC, Schneider W, Luft FC, Kettritz R. C5a receptor mediates neutrophil activation and ANCA-induced glomerulonephritis. J Am Soc Nephrol 2009 Feb;20(2):289–98.
[22] Xiao H, Schreiber A, Heeringa P, Falk RJ, Jennette JC. Alternative complement pathway in the pathogenesis of disease mediated by anti-neutrophil cytoplasmic autoantibodies. Am J Pathol 2007 Jan;170(1):52–64.
[23] Chen M, Jayne DRW, Zhao MH. Complement in ANCA-associated vasculitis: mechanisms and implications for management. Nat Rev Nephrol 2017 Jun;13(6):359–67.
[24] Klapa S, Müller A, Arnold S, Koch A, Staehle A, Kaehler W, et al. Decreased concentrations of C5a complement receptor antibodies are associated with relapse in eosinophilic granulomatosis with polyangiitis (EGPA). RMD Open 2025 Mar 6;11(1):e005323.
[25] Tampe D, Baier E, Hakroush S, Tampe B. Comparative analysis of complement C3 and C4 serum levels for outcome prediction in ANCA-associated renal vasculitis. J Nephrol 2023 Jan;36(1):125–32.
[26] Pelaia C, Paoletti G, Puggioni F, Racca F, Pelaia G, Canonica GW, et al. Interleukin-5 in the pathophysiology of severe asthma. Front Physiol 2019;10:1514.
[27] Mo C, Zeng Z, Deng Q, Ding Y, Xiao R. Imbalance between T helper 17 and regulatory T cell subsets plays a significant role in the pathogenesis of systemic sclerosis. Biomed Pharmacother 2018 Dec;108:177–83.
[28] Tsurikisawa N, Oshikata C, Watanabe M, Tsuburai T, Kaneko T, Saito H. Innate immune response reflects disease activity in eosinophilic granulomatosis with polyangiitis. Clin Exp Allergy 2018 Oct;48(10):1305–16.
[29] Matucci A, Vivarelli E, Perlato M, Mecheri V, Accinno M, Cosmi L, et al. EGPA Phenotyping: not only ANCA, but also eosinophils. Biomedicines 2023 Mar;11(3):776.
[30] Hua L, Xie M. Heterogeneity and individualized therapy for eosinophilic granulomatosis with polyangiitis. Ther Adv Respir Dis 2025 May 1;19:17534666251318615.
[31] Watts RA, Hatemi G, Burns JC, Mohammad AJ. Global epidemiology of vasculitis. Nat Rev Rheumatol 2022 Jan;18(1):22–34.
[32] Kronbichler A, Bajema IM, Bruchfeld A, Mastroianni Kirsztajn G, Stone JH. Diagnosis and management of ANCA-associated vasculitis. Lancet 2024 Feb;403(10427):683–98.
[33] White J, Dubey S. Eosinophilic granulomatosis with polyangiitis: a review. Autoimmun Rev 2023 Jan 1;22(1):103219.
[34] Paul A, Monach SAC. Anti-neutrophil cytoplasmic antibody-associated vasculitis. In: Firestein GS, Budd RC, Gabriel SE, McInnes IB, Koretzky GA, O'Dell JR, editors. Firestein & Kelley's Textbook of Rheumatology. 12th ed. Elsevier Health Sciences; 2024. p. 1616–34.
[35] Luqmani RA, Exley AR, Kitas GD, Bacon PA. Disease assessment and management of the vasculitides. Baillieres Clin Rheumatol 1997 May;11(2):423–46.
[36] Stone JH, Hoffman GS, Merkel PA, Min YI, Uhlfelder ML, Hellmann DB, et al. A disease-specific activity index for Wegener's granulomatosis: modification of the Birmingham Vasculitis Activity Score. International Network for the Study of the Systemic Vasculitides (INSSYS). Arthritis Rheum 2001 Apr;44(4):912–20.
[37] Hopkins C, Gillett S, Slack R, Lund VJ, Browne JP. Psychometric validity of the 22-item Sinonasal Outcome Test. Clin Otolaryngol 2009;34(5):447–54.
[38] de Groot K, Gross WL, Herlyn K, Reinhold-Keller E. Development and validation of a disease extent index for Wegener's granulomatosis. Clin Nephrol 2001 Jan;55(1):31–8.
[39] Wechsler ME, Nair P, Terrier B, Walz B, Bourdin A, Jayne DRW, et al. Benralizumab versus mepolizumab for eosinophilic granulomatosis with polyangiitis. N Engl J Med 2024 Mar 7;390(10):911–21.
[40] Exley AR, Bacon PA, Luqmani RA, Kitas GD, Gordon C, Savage CO, et al. Development and initial validation of the Vasculitis Damage Index for the standardized clinical assessment of damage in the systemic vasculitides. Arthritis Rheum 1997 Feb;40(2):371–80.
[41] Suppiah R, Flossman O, Mukhtyar C, Alberici F, Baslund B, Brown D, et al. Measurement of damage in systemic vasculitis: a comparison of the Vasculitis Damage Index with the Combined Damage Assessment Index. Ann Rheum Dis 2011 Jan;70(1):80–5.
[42] Stone JH, McDowell PJ, Jayne DRW, Merkel PA, Robson J, Patel NJ, et al. The glucocorticoid toxicity index: measuring change in glucocorticoid toxicity over time. Semin Arthritis Rheum 2022 Aug 1;55:152010.
[43] Guillevin L, Pagnoux C, Seror R, Mahr A, Mouthon L, Toumelin PL, et al. The Five-Factor Score revisited: assessment of prognoses of systemic necrotizing vasculitides based on the French Vasculitis Study Group (FVSG) cohort. Medicine (Baltimore) 2011 Jan;90(1):19–27.
[44] Berti A, Boleto G, Merkel PA, Tómasson G, Monti S, Quinn KA, et al. Psychometric properties of outcome measurement instruments for ANCA-associated vasculitis: a systematic literature review. Rheumatology (Oxford) 2022 Nov 28;61(12):4603–18.
[45] Ahn SS, Ha JW, Park YB, Lee SW. BVAS version 3 and BVAS/GPA: standing on the same line? Clin Rheumatol 2022 Nov 1;41(11):3429–37.
[46] Dolezalova P, Price-Kuehne FE, Özen S, Benseler SM, Cabral DA, Anton J, et al. Disease activity assessment in childhood vasculitis: development and preliminary validation of the Paediatric Vasculitis Activity Score (PVAS). Ann Rheum Dis 2013 Oct;72(10):1628–33.
[47] Kamali S, Erer B, Artim-Esen B, Gul A, Ocal L, Konice M, et al. Predictors of damage and survival in patients with Wegener's granulomatosis: analysis of 50 patients. J Rheumatol 2010 Feb;37(2):374–8.
[48] Jayne DRW, Merkel PA, Schall TJ, Bekker P, Study Group ADVOCATE. Avacopan for the treatment of ANCA-associated vasculitis. N Engl J Med 2021 Feb 18;384(7):599–609.
[49] Bate S, McGovern D, Costigliolo F, Tan PG, Kratky V, Scott J, et al. The improved kidney risk score in ANCA-associated vasculitis for clinical practice and trials. J Am Soc Nephrol 2024 Mar 1;35(3):335–46.
[50] Robson JC, Dawson J, Doll H, Cronholm PF, Milman N, Kellom K, et al. Validation of the ANCA-associated vasculitis patient-reported outcomes (AAV-PRO) questionnaire. Ann Rheum Dis 2018 Aug;77(8):1157–64.
[51] Maunz A, Jacoby J, Henes J, Robson JC, Hellmich B, Löffler C. Association of the AAV-PRO questionnaire with established outcome measures in AAV. Rheumatology (Oxford) 2024 Jan 1;63(1):174–80.
[52] Uchida L, Jones RB, Smith RM, Nodale M, Bond S, Loechel C, et al. Long-term surveillance study of rituximab originator treated patients with granulomatosis with polyangiitis (GPA) or microscopic polyangiitis (MPA). Rheumatol Adv Pract 2024;8(3):rkae090.
[53] Mercuzot C, Letertre S, Daien CI, Zerkowski L, Guilpain P, Terrier B, et al. Comorbidities and health-related quality of life in patients with antineutrophil cytoplasmic antibody (ANCA) —associated vasculitis. Autoimmun Rev 2021 Jan;20(1):102708.
[54] Hellmich B, Sanchez-Alamo B, Schirmer JH, Berti A, Blockmans D, Cid MC, et al. EULAR recommendations for the management of ANCA-associated vasculitis: 2022 update. Ann Rheum Dis 2024 Jan 1;83(1):30–47.
[55] Cheung AK, Chang TI, Cushman WC, Furth SL, Hou FF, Ix JH, et al. KDIGO 2021 Clinical practice guideline for the management of blood pressure in chronic kidney disease. Kidney Int 2021 Mar;99(3):S1–87.

[56] Casal Moura M, Falde S, Sethi S, Fervenza FC, Specks U, Baqir M. Granulomatosis with polyangiitis with and without antineutrophil cytoplasmic antibodies: a case-control study. Rheumatology (Oxford) 2024 Dec 1;63(12):3279–88.
[57] McClure ME, Wason J, Gopaluni S, Tieu J, Smith RM, Jayne DR, et al. Evaluation of PR3-ANCA status after rituximab for ANCA-associated vasculitis. J Clin Rheumatol 2019 Aug 1;25(5):217–23.
[58] Junek ML, Merkel PA, Vilayur E, Wald R, Khalidi N, Jayne D, et al. Risk of relapse of antineutrophil cytoplasmic antibody-associated vasculitis in a randomized controlled trial of plasma exchange and glucocorticoids. Arthritis Rheumatol 2024;76(9):1431–8.
[59] Mehta P, Balakrishnan A, Phatak S, Pathak M, Ahmed S. Diagnostic accuracy of antineutrophil cytoplasmic antibodies (ANCA) in predicting relapses of ANCA-associated vasculitis: systematic review and meta-analysis. Rheumatol Int 2023 Mar 1;43(3):437–48.
[60] Wang C, Li ZY, Gong Y, You R, Ming-Hui Zhao, Chen M. Increased frequency of IgD-CD27hiCD38hi B cells and its association with the renal involvement in ANCA-associated vasculitis. Arthritis Res Ther 2022 May 14;24(1):109.
[61] Unizony S, Lim N, Phippard DJ, Carey VJ, Miloslavsky EM, Tchao NK, et al. Peripheral CD5+ B cells in antineutrophil cytoplasmic antibody-associated vasculitis. Arthritis Rheumatol 2015 Feb;67(2):535–44.
[62] Charles P, Terrier B, Perrodeau É, Cohen P, Faguer S, Huart A, et al. Comparison of individually tailored versus fixed-schedule rituximab regimen to maintain ANCA-associated vasculitis remission: results of a multicentre, randomised controlled, phase III trial (MAINRITSAN2). Ann Rheum Dis 2018 Aug;77(8):1143–9.
[63] Zonozi R, Cortazar FB, Jeyabalan A, Sauvage G, Nithagon P, Huizenga NR, et al. Maintenance of remission of ANCA vasculitis by rituximab based on B cell repopulation versus serological flare: a randomised trial. Ann Rheum Dis 2024 Feb 15;83(3):351–9.
[64] Moiseev S, Lee JM, Zykova A, Bulanov N, Novikov P, Gitel E, et al. The alternative complement pathway in ANCA-associated vasculitis: further evidence and a meta-analysis. Clin Exp Immunol 2020 Dec;202(3):394–402.
[65] Crnogorac M, Horvatic I, Kacinari P, Ljubanovic DG, Galesic K. Serum C3 complement levels in ANCA associated vasculitis at diagnosis is a predictor of patient and renal outcome. J Nephrol 2018 Apr;31(2):257–62.
[66] O'Reilly VP, Wong L, Kennedy C, Elliot LA, O'Meachair S, Coughlan AM, et al. Urinary soluble CD163 in active renal vasculitis. J Am Soc Nephrol 2016 Sep;27(9):2906–16.
[67] Jönsson N, Erlandsson E, Gunnarsson L, Pettersson Å, Ohlsson S. Monocyte chemoattractant protein-1 in antineutrophil cytoplasmic autoantibody-associated vasculitis: biomarker potential and association with polymorphisms in the MCP-1 and the CC chemokine receptor-2 gene. Mediators Inflamm 2018;2018:6861257.
[68] Moran SM, Monach PA, Zgaga L, Cuthbertson D, Carette S, Khalidi NA, et al. Urinary soluble CD163 and monocyte chemoattractant protein-1 in the identification of subtle renal flare in anti-neutrophil cytoplasmic antibody-associated vasculitis. Nephrol Dial Transplant 2020 Feb 1;35(2):283–91.
[69] Prskalo L, Skopnik CM, Goerlich N, Freund P, Wagner L, Grothgar E, et al. Urinary CD4 + T cells predict renal relapse in ANCA-associated vasculitis. J Am Soc Nephrol 2024 Apr;35(4):483–94.
[70] Al-Soudi A, Vegting Y, Klarenbeek PL, Hilhorst ML. Do relapses follow ANCA rises? A systematic review and meta-analysis on the value of serial ANCA level evaluation. Front Med (Lausanne) 2022 Jul 4;9:844112.
[71] De Groot K, Rasmussen N, Bacon PA, Tervaert JWC, Feighery C, Gregorini G, et al. Randomized trial of cyclophosphamide versus methotrexate for induction of remission in early systemic antineutrophil cytoplasmic antibody-associated vasculitis. Arthritis Rheum 2005 Aug;52(8):2461–9.
[72] de Groot K, Harper L, Jayne DRW, Flores Suarez LF, Gregorini G, Gross WL, et al. Pulse versus daily oral cyclophosphamide for induction of remission in antineutrophil cytoplasmic antibody-associated vasculitis: a randomized trial. Ann Intern Med 2009 May 19;150(10):670–80.
[73] Jayne D, Rasmussen N, Andrassy K, Bacon P, Tervaert JWC, Dadoniené J, et al. A randomized trial of maintenance therapy for vasculitis associated with antineutrophil cytoplasmic autoantibodies. N Engl J Med 2003 Jul 3;349(1):36–44.
[74] Maritati F, Alberici F, Oliva E, Urban ML, Palmisano A, Santarsia F, et al. Methotrexate versus cyclophosphamide for remission maintenance in ANCA-associated vasculitis: a randomised trial. PLoS One 2017 Oct 10;12(10):e0185880.
[75] Jones RB, Hiemstra TF, Ballarin J, Blockmans DE, Brogan P, Bruchfeld A, et al. Mycophenolate mofetil versus cyclophosphamide for remission induction in ANCA-associated vasculitis: a randomised, non-inferiority trial. Ann Rheum Dis 2019 Mar;78(3):399–405.
[76] Pagnoux C, Quéméneur T, Ninet J, Diot E, Kyndt X, de Wazières B, et al. Treatment of systemic necrotizing vasculitides in patients aged sixty-five years or older: results of a multicenter, open-label, randomized controlled trial of corticosteroid and cyclophosphamide-based induction therapy. Arthritis Rheumatol 2015;67(4):1117–27.
[77] Stone JH, Merkel PA, Spiera R, Seo P, Langford CA, Hoffman GS, et al. Rituximab versus cyclophosphamide for ANCA-associated vasculitis. N Engl J Med 2010 Jul 15;363(3):221–32.
[78] Jones RB, Tervaert JWC, Hauser T, Luqmani R, Morgan MD, Peh CA, et al. Rituximab versus cyclophosphamide in ANCA-associated renal vasculitis. N Engl J Med 2010 Jul 15;363(3):211–20.
[79] Smith RM, Jones RB, Specks U, Bond S, Nodale M, Al-Jayyousi R, et al. Rituximab versus azathioprine for maintenance of remission for patients with ANCA-associated vasculitis and relapsing disease: an international randomised controlled trial. Ann Rheum Dis 2023 Jul;82(7):937–44.
[80] Salehi T, Chapman GB, Farrah TE, Chapman FA, Pugh D, Hunter RW, et al. Combination cyclophosphamide and rituximab to minimize glucocorticoid use in antineutrophil cytoplasm antibody-associated vasculitis. Kidney Int Rep 2025 Jul;10(7):2334–43.
[81] Mohammad AJ, Hot A, Arndt F, Moosig F, Guerry MJ, Amudala N, et al. Rituximab for the treatment of eosinophilic granulomatosis with polyangiitis (Churg-Strauss). Ann Rheum Dis 2016 Feb;75(2):396–401.
[82] Akiyama M, Kaneko Y, Takeuchi T. Rituximab for the treatment of eosinophilic granulomatosis with polyangiitis: a systematic literature review. Autoimmun Rev 2021 Feb;20(2):102737.
[83] Terrier B, Pugnet G, De Moreuil C, Bonnotte B, Benhamou Y, Chauveau D, et al. Rituximab versus conventional therapy for remission induction in eosinophilic granulomatosis with polyangiitis: a randomized controlled trial. Ann Intern Med 2025 Sep;178(9):1249–57.
[84] Long-term efficacy of remission-induction regimens for eosinophilic granulomatosis with polyangiitis—ACR Meeting Abstracts [Internet]. [cited 2025 May 15]. Available from: https://acrabstracts.org/abstract/long-term-efficacy-of-remission-induction-regimens-for-eosinophilic-granulomatosis-with-polyangiitis/?utm_source=chatgpt.com
[85] Jayne DRW, Bruchfeld AN, Harper L, Schaier M, Venning MC, Hamilton P, et al. Randomized trial of C5a receptor inhibitor avacopan in ANCA-associated vasculitis. J Am Soc Nephrol 2017 Sep;28(9):2756–67.
[86] Merkel PA, Niles J, Jimenez R, Spiera RF, Rovin BH, Bomback A, et al. Adjunctive treatment with avacopan, an oral C5a receptor inhibitor, in patients with antineutrophil cytoplasmic antibody-associated vasculitis. ACR Open Rheumatol 2020 Nov;2(11):662–71.
[87] Patel NJ, Jayne DRW, Merkel PA, Bekker P, Zhang Y, Yue H, et al. Glucocorticoid Toxicity Index scores by domain in patients with antineutrophil cytoplasmic antibody-associated vasculitis treated with avacopan versus standard prednisone taper: post-hoc analysis of data from the ADVOCATE trial. Lancet Rheumatol 2023 Mar;5(3):e130–8.
[88] Wechsler ME, Akuthota P, Jayne D, Khoury P, Klion A, Langford CA, et al. Mepolizumab or placebo for eosinophilic granulomatosis with polyangiitis. N Engl J Med 2017 May 18;376(20):1921–32.
[89] Terrier B, Jayne DRW, Hellmich B, Bentley JH, Steinfeld J, Yancey SW, et al. Clinical benefit of mepolizumab in eosinophilic granulomatosis with polyangiitis for patients with and without a vasculitic phenotype. ACR Open Rheumatol 2023 Jul;5(7):354–63.
[90] Merkel PA, Nair PK, Khalidi N, Terrier B, Hellmich B, Bourdin A, et al. Two-year efficacy and safety of anti-interleukin-5/receptor therapy for eosinophilic granulomatosis with polyangiitis. Ann Rheum Dis 2025 Nov;84(11):1888–99.
[91] Manka LA, Guntur VP, Denson JL, Dunn RM, Dollin YT, Strand MJ, et al. Efficacy and safety of reslizumab in the treatment of eosinophilic granulomatosis with polyangiitis. Ann Allergy Asthma Immunol 2021 Jun;126(6):696–701 .e1.
[92] McGovern DP, McClure ME, Coates M, Bond S, Martinez Del Pero M, Mynard K, et al. Study protocol for a randomised, phase II, double-blind, experimental medicine study of obinutuzumab versus rituximab in ANCA-associated vasculitis: ObiVas. BMJ Open 2024 Jul 17;14(7):e083277.
[93] Furie RA, Rovin BH, Garg JP, Santiago MB, Aroca-Martínez G, Zuta Santillán AE, et al. Efficacy and safety of obinutuzumab in active lupus nephritis. N Engl J Med 2025 Apr 17;392(15):1471–83.
[94] van Leeuwen JR, Bredewold OW, Rabelink TJ, Teng YKO. Obinutuzumab in rituximab-intolerant antineutrophil cytoplasmic antibody-associated vasculitis patients. Kidney Int Rep 2025 Apr 1;10(4):1288–91.
[95] Wu W, Wang J, Chen S. Reduced-dose obinutuzumab induces remission in refractory ANCA-associated vasculitis: a report of 16 cases. Front Immunol 2025 Aug 29;16:1624234.
[96] Jayne D, Blockmans D, Luqmani R, Moiseev S, Ji B, Green Y, et al. Efficacy and safety of belimumab and azathioprine for maintenance of remission in antineutrophil cytoplasmic antibody-associated vasculitis: a randomized controlled study. Arthritis Rheumatol 2019;71(6):952–63.
[97] McClure ME, Gopaluni S, Wason J, Henderson RB, Van Maurik A, Savage CCO, et al. A randomised study of rituximab and belimumab sequential therapy in PR3 ANCA-associated vasculitis (COMBIVAS): design of the study protocol. Trials 2023 Mar 11;24(1):180.

[98] Shimojima Y, Kishida D, Ichikawa T, Takamatsu R, Nomura S, Sekijima Y. Features of BAFF and APRIL receptors on circulating B cells in antineutrophil cytoplasmic antibody-associated vasculitis. Clin Exp Immunol 2023 Jul 5;213(1):125–37.
[99] Evans LS, Lewis KE, DeMonte D, Bhandari JG, Garrett LB, Kuijper JL, et al. Povetacicept, an enhanced dual APRIL/BAFF antagonist that modulates B lymphocytes and pathogenic autoantibodies for the treatment of lupus and other B cell-related autoimmune diseases. Arthritis Rheumatol 2023;75(7):1187–202.
[100] Aghajanian H, Kimura T, Rurik JG, Hancock AS, Leibowitz MS, Li L, et al. Targeting cardiac fibrosis with engineered T cells. Nature 2019 Sep;573 (7774):430–3.
[101] Lodka D, Zschummel M, Bunse M, Rousselle A, Sonnemann J, Kettritz R, et al. CD19-targeting CAR T cells protect from ANCA-induced acute kidney injury. Ann Rheum Dis 2024 Apr 1;83(4):499–507.
[102] Uhlmann L, Pierer M, Krasselt M, Franke G, Zeidler R, Sabri O, et al. Effective use of anti-CD19 chimeric antigen receptor T cells in a case of treatment-resistant granulomatosis with polyangiitis. Ann Rheum Dis 2025 Jul 1;84(7):1280–3.
[103] Minopoulou I, Wilhelm A, Albach F, Kleyer A, Wiebe E, Schallenberg S, et al. Anti-CD19 CAR T cell therapy induces antibody seroconversion and complete B cell depletion in the bone marrow of a therapy-refractory patient with ANCA-associated vasculitis. Ann Rheum Dis 2025 Mar 1;84(3):e4–7.
[104] Müller F, Taubmann J, Bucci L, Wilhelm A, Bergmann C, Völkl S, et al. CD19 CAR T-cell therapy in autoimmune disease—a case series with follow-up. N Engl J Med 2024 Feb 21;390(8):687–700.
[105] Langford CA, Monach PA, Specks U, Seo P, Cuthbertson D, McAlear CA, et al. An open-label trial of abatacept (CTLA4-IG) in non-severe relapsing granulomatosis with polyangiitis (Wegener's). Ann Rheum Dis 2014 Jul;73 (7):1376–9.
[106] Langford CA, Khalidi N, Springer J, Friedman M, Hellmich B, Pagnoux C, et al. A randomized, double-blind, placebo-controlled trial of abatacept for the treatment of relapsing, nonsevere, granulomatosis with polyangiitis. Arthritis Rheumatol 2025 Online ahead of print. doi: 10.1002/art.43272.
[107] Engesser J, Khatri R, Schaub DP, Zhao Y, Paust HJ, Sultana Z, et al. Immune profiling-based targeting of pathogenic T cells with ustekinumab in ANCA-associated glomerulonephritis. Nat Commun 2024 Sep 19;15(1):8220.
[108] Nogueira E, Hamour S, Sawant D, Henderson S, Mansfield N, Chavele KM, et al. Serum IL-17 and IL-23 levels and autoantigen-specific Th17 cells are elevated in patients with ANCA-associated vasculitis. Nephrol Dial Transplant 2010 Jul;25(7):2209–17.
[109] Gopaluni S, Smith R, Goymer D, Cahill H, Broadhurst E, Wallin E, et al. Alemtuzumab for refractory primary systemic vasculitis-a randomised controlled dose ranging clinical trial of efficacy and safety (ALEVIATE). Arthritis Res Ther 2022 Apr 1;24(1):81.
[110] Jackson DJ, Wechsler ME, Jackson DJ, Bernstein D, Korn S, Pfeffer PE, et al. Twice-yearly depemokimab in severe asthma with an eosinophilic phenotype. N Engl J Med 2024 Dec 19;391(24):2337–49.
[111] Yang L, Fang Y, Luo Y, Fu M, Shen K, Luo Z. Safety, pharmacokinetics and pharmacodynamics of SHR-1703, an innovative long-acting anti-interleukin-5 monoclonal antibody, in healthy subjects: a randomized, double-blind, dose-escalation, placebo-controlled phase I study. Expert Opin Investig Drugs 2024 Jul 2;33(7):741–52.
[112] Diver S, Khalfaoui L, Emson C, Wenzel SE, Menzies-Gow A, Wechsler ME, et al. Effect of tezepelumab on airway inflammatory cells, remodelling, and hyperresponsiveness in patients with moderate-to-severe uncontrolled asthma (CASCADE): a double-blind, randomised, placebo-controlled, phase 2 trial. Lancet Respir Med 2021 Nov;9(11):1299–312.
[113] Corren J, Parnes JR, Wang L, Mo M, Roseti SL, Griffiths JM, et al. Tezepelumab in adults with uncontrolled asthma. N Engl J Med 2017 Sep 7;377 (10):936–46.
[114] Nishibata Y, Arai S, Taniguchi M, Nakade I, Ogawa H, Kitano S, et al. Cathepsin C inhibition reduces neutrophil serine protease activity and improves activated neutrophil-mediated disorders. Nat Commun 2024 Aug 22;15(1):6519.
[115] Jayne D, Herbert C, Anquetil V, Teixeira G. Exploring the critical role of tight junction proteins in kidney disease pathogenesis. Nephron 2025;149 (4):240–50.
[116] Teixeira G, Delbet JD, Anquetil V, Toso A, Toovey S, Manenti L, et al. Claudin-1 is a therapeutic target for crescentic glomerulonephritis: TH-PO531. J Am Soc Nephrol 2023 Nov;34(11S):238.
[117] Uhlin F, Szpirt W, Kronbichler A, Bruchfeld A, Soveri I, Rostaing L, et al. Endopeptidase cleavage of anti-glomerular basement membrane antibodies in vivo in severe kidney disease: an open-label phase 2a study. J Am Soc Nephrol 2022 Apr;33(4):829–38.
[118] Berti A, Warner R, Johnson K, Cornec D, Schroeder DR, Kabat BF, et al. The association of serum interleukin-6 levels with clinical outcomes in antineutrophil cytoplasmic antibody-associated vasculitis. J Autoimmun 2019 Dec;105:102302.
[119] Sakai R, Kondo T, Kurasawa T, Nishi E, Okuyama A, Chino K, et al. Current clinical evidence of tocilizumab for the treatment of ANCA-associated vasculitis: a prospective case series for microscopic polyangiitis in a combination with corticosteroids and literature review. Clin Rheumatol 2017 Oct;36(10):2383–92.
[120] Linde L, Faurschou M, Krintel SB, Baslund B. Response to treatment with tofacitinib in 11 patients with refractory granulomatosis with polyangiitis. J Rheumatol 2023 Aug;50(8):1088–9.
[121] Cheever A, Kang CC, O'Neill KL, Weber KS. Application of novel CAR technologies to improve treatment of autoimmune disease. Front Immunol 2024;15:1465191.
[122] Doglio M, Ugolini A, Bercher-Brayer C, Camisa B, Toma C, Norata R, et al. Regulatory T cells expressing CD19-targeted chimeric antigen receptor restore homeostasis in systemic lupus erythematosus. Nat Commun 2024 Mar 27;15(1):2542.
[123] Robinson WH, Fiorentino D, Chung L, Moreland LW, Deodhar M, Harler MB, et al. Cutting-edge approaches to B-cell depletion in autoimmune diseases. Front Immunol 2024 Oct 9;15:1454747.
[124] Free ME. Emerging cell therapies in the vasculitis field. Rheumatology (Oxford) 2025 Mar 1;64(supplement_1):i11–4.

Ann Rheum Dis 85 (2026) 603–608

Contents lists available at ScienceDirect

Annals of the Rheumatic Diseases

journal homepage: https://www.sciencedirect.com/journal/annals-of-the-rheumatic-diseases

Viewpoint

The positive perspective paradigm: proposal of a model to mitigate the impact of chronic inflammatory arthritis through comprehensive and early intervention

Michaël Doumen[1,2,*], Laure Gossec[3,4], Mwidimi Ndosi[5], Peter C. Taylor[6], Marc Thelissen[7], René Westhovens[1,2], Patrick Verschueren[1,2]

[1] *Department of Development and Regeneration, KU Leuven, Leuven, Belgium*
[2] *Rheumatology, University Hospitals Leuven, Leuven, Belgium*
[3] *INSERM, Institut Pierre Louis d'Epidémiologie et de Santé Publique, Team Pepites, Sorbonne Université, Paris, France*
[4] *Rheumatology, AP-HP, Pitié-Salpêtrière Hospital, Paris, France*
[5] *School of Health and Social Wellbeing, University of the West of England, Bristol, UK*
[6] *Botnar Research Centre, Nuffield Department of Orthopaedics, Rheumatology and Musculoskeletal Sciences, University of Oxford, Headington, Oxford, UK*
[7] *Patient Research Partner, ReumaNet VZW, Zaventem, Belgium*

ARTICLE INFO

Article history:
Received 2 July 2025
Received in revised form 23 December 2025
Accepted 2 January 2026

ABSTRACT

Many people with chronic inflammatory arthritis (IA) experience significant disease impact, even with well-controlled disease activity. For rheumatoid arthritis (RA), 20% to 50% of patients in remission still report pain, disability, fatigue, or negative illness perceptions, leading to poorer long-term outcomes. However, evidence shows that long-term patient-reported outcomes improve when remission is achieved early, and that this is at least partly explained by a positive influence on psychological factors like illness perceptions. Based on these insights and a narrative literature review, we propose a conceptual framework to support clinical practice and further research in the prevention of the long-term impact of chronic IA, using the example of RA. Building on Leventhal's Model of Self-Regulation, the 'positive perspective paradigm' postulates that the early stages of a chronic inflammatory disease present an optimal time window where appropriate intervention might positively influence one's health perspective, in turn contributing to reduced long-term disease impact. Through the model, we discuss how pharmacological control of inflammation can be integrated with patient education and psychosocial support, emphasising early intervention and positive communication whenever possible. We hypothesise that these interventions have both direct effects on the long-term impact of chronic IA and indirect effects through a positive influence on the patient's health perspective. Fostering a positive perspective is thus the focal point of the model. By proposing this paradigm, we aim to provide a foundation for further validation in independent cohorts or other chronic inflammatory conditions, with the ultimate goal of implementing it to reduce long-term disease impact and promote well-being.

*Correspondence to Dr. Michaël Doumen, Rheumatology, KU Leuven University Hospitals, Leuven, Belgium.
E-mail address: michael.doumen@uzleuven.be (M. Doumen).
Handling editor Josef S. Smolen.

https://doi.org/10.1016/j.ard.2026.01.001

INTRODUCTION

Major advances have been made in the management of chronic inflammatory arthritis (IA). However, this does not always translate into less disease impact from the patient's perspective. For rheumatoid arthritis (RA), which we will use as a primary example, 20% to 50% of patients in remission experience persisting pain and disability, and fatigue appears even more common [1–3]. Similarly, 1-in-5 patients with RA fail to achieve (Boolean) remission because of an elevated patient global assessment, mainly driven by residual symptoms [4]. In the Care in early RA (CareRA) strategy trial, 20% of patients in remission still experienced negative illness perceptions and suboptimal psychosocial well-being [5], and this group of patients was subsequently less likely to sustain remission. Finally, less than 1-in-4 patients in CareRA achieved a sustained improvement in fatigue despite appropriate disease-modifying antirheumatic drugs (DMARDs) [6].

All of the preceding findings are particularly relevant because the first priority for people suffering from RA is symptom relief and a return to normal life [7]. The question is thus what can be done to prevent persistent disease impact in IA. We start from a narrative literature review to propose a theoretical model, with strong patient involvement, that could support this goal in clinical practice and research. The search was conducted in PubMed on 28 April 2025, based on free-text search terms and—when available—MeSH terms related to 'inflammatory arthritis', 'rheumatoid arthritis', 'remission', 'illness perceptions', 'patient-reported outcomes', and 'disease impact'. With our proposed model, the 'positive perspective paradigm', we aim to provide a foundation for clinical implementation and validation in independent cohorts or other chronic inflammatory conditions.

Adjustment to chronic disease

Even today, RA remains a chronic disease impacting many aspects of life. It requires individuals to adjust to a 'new normal', including the disease's physical, emotional, and social impact. This process has been conceptualised in Leventhal's Model of Self-Regulation [8]. This model postulates that when confronted with a health threat, such as a chronic illness, people develop cognitive and emotional representations about this illness, so-called illness perceptions, which influence how they cope with it. Coping is often defined as one's intentional efforts to minimise the negative impact of the illness on their well-being [9]. Adjustment according to Leventhal is iterative, with illness perceptions influenced by one's personal and sociocultural background, by the evolution over time and by the perceived impact of coping procedures. For example, early after diagnosis, patients with chronic IA are already more likely to report negative illness perceptions when they are younger, have lower socioeconomic status, or report a higher symptom burden [10]. However, these illness perceptions are not static personality traits, but can evolve over time [11]. In addition to pharmacological management, these insights are crucial to achieving well-being, given the influence of illness perceptions, psychological factors, and coping procedures on patient outcomes [12–14]. How one can prevent persistent disease impact, thus, partly depends on how we can positively influence patients' adjustment to their diagnosis.

Early control of inflammation

When managing RA, it is well established that prompt initiation of DMARDs is key [15]. The critical time in early disease when its progression might be more effectively modified is known as the 'window of opportunity'. However, recent evidence suggests that within this time window, rather than merely initiating treatment, we should also strive for a clinically meaningful treatment response. Table [5,6,11,16–24] provides a nonexhaustive overview of relevant studies that illustrate this concept. Early remission has long been associated with better clinical outcomes, including more sustained remission and reduced radiographic progression [25,26]. However, recent studies have also shown an association between early treatment response and improved long-term patient-reported outcomes (PROs) like physical functioning, fatigue, and work participation [6,16,17,19,27]. Notably, this also seems to apply to other rheumatic diseases, including juvenile idiopathic arthritis [28] and psoriatic arthritis [20].

Regarding potential mechanisms through which prompt control of inflammation might exert these positive effects, psychosocial factors seem crucial. In the CareRA trial, the beneficial impact of early remission on long-term PROs appeared primarily driven by psychological factors, including more positive illness perceptions, rather than by direct effects on inflammation [18]. Similarly, people with clinically suspect arthralgia, a potential preclinical stage of RA, who received methotrexate in the TREAT-EARLIER trial experienced more symptom relief and developed more optimistic illness perceptions than those who received a placebo, and this persisted after stopping methotrexate [22]. However, offering DMARDs at this early stage conjointly led to more pessimistic perceptions regarding the disease's emotional and physical consequences, perhaps because a need for treatment implies a more serious diagnosis.

Psychosocial support and patient education

Together, these findings illustrate the importance of emphasising a positive message throughout patient education, from the early diagnostic phase onwards. The European Alliance of Associations for Rheumatology (EULAR) defines patient education as a planned interactive learning process to support and enable people to manage their life with chronic IA and optimise their health and well-being [29]. Incorporating positive communication in this process, both verbally and nonverbally, is central to the paradigm we propose. Although it is challenging to define what such 'positive communication' precisely entails, evidence shows modest but consistent beneficial effects on outcomes like pain when healthcare provider-patient communication is more empathic or more strongly promotes positive expectations about health outcomes [30,31].

Indeed, although RA might traditionally have been described as a destructive disease, recent developments imply that patient education can now reflect a more positive outlook. For example, even today, the drug information sheets available to patients are generally dominated by adverse events without emphasising the much greater likelihood of treatment benefit. As needs-based patient education can improve self-efficacy and treat-to-target implementation [21,23,24], positive communication may help people with RA develop a more hopeful perspective on their health, particularly early in the disease.

The positive perspective paradigm

Building on the aforementioned insights (summarised in Table), we propose a conceptual framework (Fig) to describe how pharmacological treatment, as well as patient education and psychosocial support, could be strategically integrated to reduce the long-term impact of chronic inflammatory diseases, using RA as a model. Our

Table
Data supporting the principles of the positive perspective paradigm

Principle	Supporting data
1. Early and optimal control of inflammation reduces long-term patient-reported disease impact.	- IMPROVED trial (RA): early remission (<4 mo) was associated with lower HAQ scores after 5 y [16]. - ARCTIC trial (RA): early remission (<6 mo) was associated with lower odds of clinically relevant fatigue after 2 y [17]. - CareRA trial (RA): early remission (<4 mo) was associated with higher self-efficacy after 2 y and with less fatigue over 5 y, assessed longitudinally [6,18]. - CareRA2020 trial (RA): early responders (wk 8-32) to initial remission-induction DMARDs reported lower RAID scores over 2 y, assessed longitudinally [19]. - DEPAR cohort (PsA): early Minimal Disease Activity (<1 y) was associated with improved HR-QoL, fatigue, pain, HAQ, anxiety and depression scores over 2 y, assessed longitudinally [20].
2. The beneficial effects of early control of inflammation on long-term disease impact are partly explained by a positive influence on patients' health perspective.	- RAMS cohort (RA): illness perceptions improved in around 20% of patients over the first year of methotrexate treatment, and negative illness perceptions were associated with worse scores for HAQ, pain and fatigue, assessed longitudinally [11]. - CareRA trial (RA): ○ The beneficial effect of early remission on 2-y self-efficacy was fully mediated by psychosocial factors, including more positive illness perceptions [18]. ○ The longitudinal relationship between disease activity and fatigue was fully mediated by psychosocial factors, including mental health [6]. ○ The longitudinal relationship between disease activity and psychosocial well-being was complex and bidirectional [5]. - TREAT-EARLIER trial (CSA): patients treated with methotrexate (vs placebo) experienced more symptom relief and hence developed more optimistic illness perceptions regarding symptoms, consequences, disease duration, and treatment efficacy, which were sustained after treatment cessation [22].
3. Patients should be offered psychosocial support and patient education as soon as the diagnosis is made, with a focus on positive communication.	- Needs-based patient education, either digitally or face-to-face, improves self-efficacy both in established and newly diagnosed RA [21,23]. - Various educational interventions can improve T2T implementation in RA management [24]. - TREAT-EARLIER trial & Rotterdam CSA cohort (CSA): despite its positive effects (see above), offering treatment to patients with CSA resulted in more perceived emotional and physical consequences of the disease [22], illustrating that a positive message is key.

ARCTIC, Aiming for Remission in Rheumatoid Arthritis: a Randomised Trial Examining the Benefit of Ultrasound in a Clinical Tight Control Regime; CareRA, Care in early RA; CSA, clinically suspect arthralgia; DEPAR, Dutch southwest Early Psoriatic Arthritis cohort; HAQ, Health Assessment Questionnaire; HR-QoL, health-related quality of life; IMPROVED, induction therapy with MTX and prednisone in rheumatoid or very early arthritic disease; RA, rheumatoid arthritis; PsA, psoriatic arthritis; DMARD, disease-modifying antirheumatic drug; MTX, methotrexate; RAID, rheumatoid arthritis impact of disease; RAMS, Rheumatoid Arthritis Medication Study.
The supporting data listed here are the result of a narrative literature review conducted on April 28, 2025, and represent a nonexhaustive overview of evidence to inform the positive perspective paradigm.

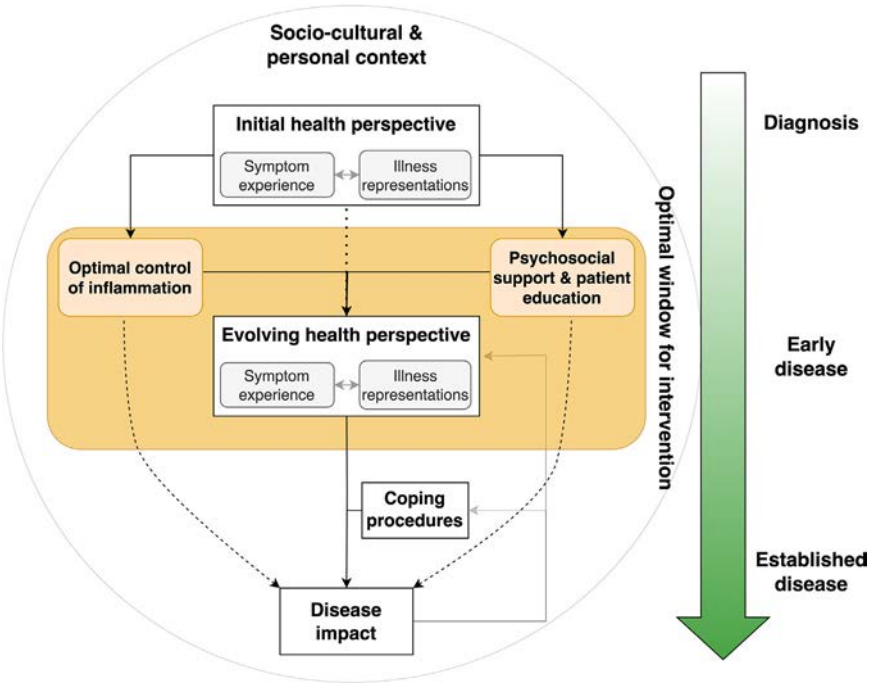

Figure. Schematic overview of the positive perspective paradigm. The positive perspective paradigm postulates that the early stages of a chronic inflammatory disease present an optimal time window where appropriate intervention might positively influence one's health perspective, in turn contributing to reduced long-term disease impact. Specifically, we propose that such an intervention should involve the prompt control of inflammation with appropriate pharmacotherapy, as well as tailored patient education and psychosocial support with a focus on positive communication from the time of diagnosis. The main hypothesis of the model is that both these types of interventions will lead to less patient-experienced disease impact both directly and through positive effects on patients' health perspective.

'positive perspective paradigm' builds on the foundations of Leventhal's model but adds a focus on how timely intervention could positively affect a person's evolving health perspective. In this context, we consider one's health perspective to encompass both cognitive and emotional illness representations and the way a person experiences their symptoms. As in Leventhal's model, this perspective is influenced by a personal and sociocultural context, and might evolve through changes in this context, the disease, or the results of coping. Given the evidence discussed above, we postulate that the early stages of a chronic inflammatory disease present an optimal time window where appropriate intervention might positively influence one's health perspective, in turn contributing to reduced long-term disease impact. In keeping with RA treatment recommendations [15], clinicians should aim to promptly achieve control of inflammation with pharmacotherapy. In parallel, we propose that patients should be offered psychosocial support and patient education from diagnosis, while emphasising positive communication whenever possible. Although both these interventions also have direct effects on disease impact, the aforementioned research suggests that these effects are at least partly explained by positively influencing the patient's health perspective. For instance, the experience of prompt symptom control appears to reinforce optimistic illness perceptions that in turn are essential for attenuating long-term disease impact. Fostering a positive perspective is therefore the focal point of our model.

Towards the future

The positive perspective paradigm aims to offer a novel viewpoint on how early interventions, both pharmacological and non-pharmacological, can help shape a patient's long-term experience of chronic disease. The model intends to provide a foundation for further validation in independent cohorts or other chronic inflammatory conditions beyond RA. Longitudinal and interventional studies should further investigate how a patient's evolving health perspective can be positively influenced by both timely pharmacological treatment and patient education or psychosocial support. Ideally, future studies should aim to further disentangle how both these interventions affect long-term disease impact, both directly and through their impact on patients' health perspective, for instance via mediation analyses. In addition, the role of positive communication in this process warrants further investigation. For example, this could be approached by studying how fostering positive expectations for treatment efficacy affects illness perceptions in chronic inflammatory conditions, similarly to what has been reported in the context of pain relief [32]. In parallel, we believe the ongoing evolution around preclinical RA and similar conditions warrants further research into the potential negative effects of earlier diagnosis and treatment on illness perceptions.

In clinical practice, we encourage the use of PROs to facilitate identification of the aspects of life that are most impacted for individuals living with IA. By using such information, the positive perspective paradigm might serve as a guiding framework for healthcare providers to contextualise a patient's evolving health perspective through the biological, psychological, and social factors that shape it. When applied consistently across the multidisciplinary team, this model can strengthen shared understanding, promote continuity of care, and ensure that psychosocial needs are addressed alongside biomedical priorities.

Moreover, as medicine increasingly incorporates algorithm-driven decision-making and artificial intelligence to optimise treatment strategies, a conceptual model centred on the patient's personal experience of illness provides both a counterpart and a complement to this evolution. The positive perspective paradigm might help to balance biomedical advances in precision medicine with a patient-centred approach and to ensure that these aspects continue to play a role in the personalised medicine of the future. In this regard, we consider it essential that our model was developed in strong collaboration with a patient research partner. By providing a basis for validation and clinical implementation, the positive perspective paradigm aims to contribute to a more holistic vision of chronic disease management, addressing not just how we treat disease, but how we support patients in living well with it.

Competing interests

MD reports a relationship with Research Foundation Flanders that includes: funding grants. LG reports a relationship with AbbVie Inc that includes: funding grants. LG reports a relationship with Eli Lilly and Company that includes: funding grants. LG reports a relationship with Novartis that includes: funding grants. LG reports a relationship with AbbVie Inc that includes: consulting or advisory. LG reports a relationship with Alfasigma SpA that includes: consulting or advisory. LG reports a relationship with Amgen Inc that includes: consulting or advisory. LG reports a relationship with Bristol-Myers Squibb Company that includes: consulting or advisory. LG reports a relationship with Celltrion Pharm, Inc that includes: consulting or advisory. LG reports a relationship with Janssen Pharmaceuticals Inc that includes: consulting or advisory. LG reports a relationship with Eli Lilly and Company that includes: consulting or advisory. LG reports a relationship with MoonLake Immunotherapeutics Ltd that includes: consulting or advisory. LG reports a relationship with Novartis that includes: consulting or advisory. LG reports a relationship with Pfizer that includes: consulting or advisory. LG reports a relationship with STADA Arzneimittel AG that includes: consulting or advisory. LG reports a relationship with UCB Pharma SpA that includes: consulting or advisory. PCT reports a relationship with Alfasigma SpA that includes: funding grants. MN reports a relationship with Vifor Pharma Inc that includes: funding grants. MN reports a relationship with Sanofi that includes: funding grants. MN reports a relationship with Pfizer that includes: consulting or advisory. PCT reports a relationship with AbbVie Inc that includes: consulting or advisory. PCT reports a relationship with Eli Lilly and Company that includes: consulting or advisory. PCT reports a relationship with UCB Pharma SpA that includes: consulting or advisory. PCT reports a relationship with Roche that includes: consulting or advisory. PCT reports a relationship with Biogen Inc that includes: consulting or advisory. PCT reports a relationship with Janssen Pharmaceuticals Inc that includes: consulting or advisory. PCT reports a relationship with Fresenius Kabi USA LLC that includes: consulting or advisory. PCT reports a relationship with Alfasigma SpA that includes: consulting or advisory. PCT reports a relationship with Gilead Sciences Inc that includes: consulting or advisory. PCT reports a relationship with Nordic Pharma Ltd that includes: consulting or advisory. PCT reports a relationship with Takeda UK Ltd that includes: consulting or advisory. PCT reports a relationship with AnaptysBio Inc that includes: consulting or advisory. PCT reports a relationship with ACELYRIN Inc that includes: consulting or advisory. PCT reports a relationship with Immunovant Inc that includes: advisory board membership. PCT reports a relationship with MoonLake Immunotherapeutics Ltd that includes: advisory board membership. PCT reports a relationship with Sanofi that includes: advisory board membership. PV reports a relationship with Alfasigma SpA that includes: funding grants. PV reports a

relationship with AbbVie Inc that includes: speaking and lecture fees. PV reports a relationship with Fresenius Kabi USA LLC that includes: consulting or advisory. PV reports a relationship with Eli Lilly and Company that includes: consulting or advisory. PV reports a relationship with Boehringer Ingelheim Ltd that includes: consulting or advisory. PV reports a relationship with Citryll BV that includes: consulting or advisory. All other authors declare they have no competing interests.

Acknowledgements

The authors thank Delphine Bertrand, Elias De Meyst, Sarah Marent, and Sofia Pazmino for their participation in the discussions that gave rise to the model.

Contributors

MD was responsible for conceptualisation, methodology, and writing—original draft. LG was responsible for conceptualisation and writing—review and editing. MN was responsible for conceptualisation and writing—review and editing. PCT was responsible for conceptualisation and writing—review and editing. MT was responsible for conceptualisation and writing—review and editing. RW was responsible for conceptualisation and writing—review and editing. PV was responsible for conceptualisation and writing—review and editing.

Funding

This work did not receive any specific grant from funding agencies in the public, commercial, or not-for-profit sectors.

Patient consent for publication

Not applicable.

Ethics approval

Not applicable.

Provenance and peer review

Not commissioned; externally peer reviewed.

Patient and public involvement

A patient research partner (MT) contributed to the conceptualisation of the model and reviewed the manuscript as co-author.

Orcid

Michaël Doumen: http://orcid.org/0000-0001-6073-7635

REFERENCES

[1] Gwinnutt JM, Norton S, Hyrich KL, Lunt M, Combe B, Rincheval N, et al. Exploring the disparity between inflammation and disability in the 10-year outcomes of people with rheumatoid arthritis. Rheumatology (Oxford) 2022;61:4687–701.

[2] Druce KL, Bhattacharya Y, Jones GT, Macfarlane GJ, Basu N. Most patients who reach disease remission following anti-TNF therapy continue to report fatigue: results from the British Society for Rheumatology Biologics Register for Rheumatoid Arthritis. Rheumatology (Oxford). 2016;55(10):1786–90.

[3] Michaud K, Pope J, van de Laar M, Curtis JR, Kannowski C, Mitchell S, et al. Systematic literature review of residual symptoms and an unmet need in patients with rheumatoid arthritis. Arthritis Care Res (Hoboken) 2021;73(11):1606–16.

[4] Ferreira RJO, Welsing PMJ, Jacobs JWG, Gossec L, Ndosi M, MacHado PM, et al. Revisiting the use of remission criteria for rheumatoid arthritis by excluding patient global assessment: an individual meta-analysis of 5792 patients. Ann Rheum Dis 2021;80(3):293–303.

[5] Doumen M, De Cock D, Pazmino S, Bertrand D, Joly J, Westhovens R, et al. Psychosocial burden predicts sustained remission in early rheumatoid arthritis: unraveling the complex interplay of well-being and disease activity. Arthritis Care Res (Hoboken) 2023;75(4):758–67.

[6] Doumen M, Pazmino S, Bertrand D, De Cock D, Joly J, Westhovens R, et al. Longitudinal trajectories of fatigue in early RA: the role of inflammation, perceived disease impact and early treatment response. Ann Rheum Dis 2022;81(10):1385–91.

[7] Van der Elst K, Mathijssen EGE, Landgren E, Bremander A, De Groef A, Lindqvist E, et al. What do patients prefer? A multinational, longitudinal, qualitative study on patient-preferred treatment outcomes in early rheumatoid arthritis. RMD Open 2020;6:e001339.

[8] Leventhal H, Phillips LA, Burns E. The Common-Sense Model of Self-Regulation (CSM): a dynamic framework for understanding illness self-management. J Behav Med 2016;39(6):935–46.

[9] Gellman MD, Turner JR. Encyclopedia of Behavioral Medicine [Internet]. New York, NY: Springer New York; 2013. [cited 2025 Nov 18]. Available from: http://link.springer.com/10.1007/978-1-4419-1005-9.

[10] Lindgren LH, de Thurah A, Thomsen T, Hetland ML, Aadahl M, Vestergaard SB, et al. Sociodemographic and clinical variables associated with negative illness perception in patients newly diagnosed with rheumatoid arthritis, axial spondyloarthritis, or psoriatic arthritis-a survey based cross-sectional study. Rheumatol Int 2024 June 1;44(6):1119–31.

[11] Gwinnutt JM, Norton S, Hyrich KL, Lunt M, Barton A, Cordingley L, et al. Changes in the illness perceptions of patients with rheumatoid arthritis over the first year of methotrexate therapy. Rheumatology (Oxford) 2021;60(5):2355–65.

[12] Groarke A, Curtis R, Coughlan R, Gsel A. The role of perceived and actual disease status in adjustment to rheumatoid arthritis. Rheumatology (Oxford) 2004;43(9):1142–9.

[13] Matcham F, Norton S, Scott DL, Steer S, Hotopf M. Symptoms of depression and anxiety predict treatment response and long-term physical health outcomes in rheumatoid arthritis: secondary analysis of a randomized controlled trial. Rheumatology (Oxford) 2016;55(2):268–78.

[14] Folkman S, Moskowitz JT. Coping: pitfalls and Promise. Annu Rev Psychol 2004 Feb 1;55(1):745–74.

[15] Smolen JS, Landewé RBM, Bergstra SA, Kerschbaumer A, Sepriano A, Aletaha D, et al. EULAR recommendations for the management of rheumatoid arthritis with synthetic and biological disease-modifying antirheumatic drugs: 2022 update. Ann Rheum Dis 2023;82(1):3–18.

[16] Akdemir G, Heimans L, Bergstra SA, Goekoop RJ, Van Oosterhout M, Van Groenendael JHLM, et al. Clinical and radiological outcomes of 5-year drug-free remission-steered treatment in patients with early arthritis: IMPROVED study. Ann Rheum Dis 2018;77(1):111–8.

[17] Holten K, Paulshus Sundlisater N, Lillegraven S, Sexton J, Nordberg LB, Moholt E, et al. Fatigue in patients with early rheumatoid arthritis undergoing treat-to-target therapy: predictors and response to treatment. Ann Rheum Dis 2022;81(3):344–50.

[18] Doumen M, De Cock D, Pazmino S, Bertrand D, Joly J, Westhovens R, et al. Treatment response and several patient-reported outcomes are early determinants of future self-efficacy in rheumatoid arthritis. Arthritis Res Ther 2021;23:269.

[19] Doumen M, Bertrand D, Joly J, De Meyst E, Pazmino S, Westhovens R, et al. AB0525 Early responders to remission-induction treatment with methotrexate and bridging glucocorticoids report lower Rheumatoid Arthritis Impact of Disease (RAID) over 2 years: secondary analysis of the CareRA2020 trial. Ann Rheum Dis 2024;83(Suppl 1):1537.

[20] Snoeck Henkemans SVJ, de Jong PHP, Luime JJ, Kok MR, Tchetverikov I, Kasiem FR, et al. Importance of quick attainment of minimal disease activity for a positive impact on lives of patients with psoriatic arthritis. RMD Open 2022;8:e002706.

[21] Ndosi M, Johnson D, Young T, Hardware B, Hill J, Hale C, et al. Effects of needs-based patient education on self-efficacy and health outcomes in people with rheumatoid arthritis: a multicentre, single blind, randomised controlled trial. Ann Rheum Dis 2016;75(6):1126–32.

[22] Van Griethuysen SRG, Dumoulin QA, Van Mulligen E, Van Der, Helm-van Mil AHM. Can treatment expectations or treatment itself in patients with arthralgia suspicious for progression to rheumatoid arthritis improve illness perceptions? Rheumatology (Oxford) 2025;64(6):3444–50.

[23] Knudsen LR, Ndosi M, Hauge EM, Lomborg K, Dreyer L, Aaboe S, et al. Effectiveness of a novel digital patient education programme to support self-management of early rheumatoid arthritis: a randomized controlled trial. Rheumatology (Oxford) 2024;63(9):2547–56.

[24] Gossec L, Bessette L, Xavier RM, Favalli EG, Östör A, Buch MH. Barriers to, facilitators of, and interventions to support treat-to-target implementation in rheumatoid arthritis: a systematic review. Arthritis Care Res (Hoboken) 2024;76(12):1626–36.
[25] Verstappen M, Niemantsverdriet E, Matthijssen XME, le Cessie S, van der Helm-van Mil AHM. Early DAS response after DMARD-start increases probability of achieving sustained DMARD-free remission in rheumatoid arthritis. Arthritis Res Ther 2020;22:276.
[26] Kedra J, Lafourcade A, Combe B, Dougados M, Hajage D, Fautrel B. Positive impact on 10-year outcome of the window of opportunity for conventional synthetic DMARDs in rheumatoid arthritis: results from the ESPOIR cohort. RMD Open 2022;8:e002040.
[27] Verschueren P, Esselens G, Westhovens R. Predictors of remission, normalized physical function, and changes in the working situation during follow-up of patients with early rheumatoid arthritis: an observational study. Scand J Rheumatol 2009;38(3):166–72.
[28] Ong MS, Ringold S, Kimura Y, Schanberg LE, Tomlinson GA, Natter MD, et al. Improved disease course associated with early initiation of biologics in polyarticular juvenile idiopathic arthritis: trajectory analysis of a childhood arthritis and rheumatology research alliance consensus treatment plans study. Arthritis Rheumatol 2021;73(10):1910–20.
[29] Zangi HA, Ndosi M, Adams J, Andersen L, Bode C, Boström C, et al. EULAR recommendations for patient education for people with inflammatory arthritis. Ann Rheum Dis 2015;74(6):954–62.
[30] Di Blasi Z, Harkness E, Ernst E, Georgiou A, Kleijnen J. Influence of context effects on health outcomes: a systematic review. Lancet 2001 Mar 10;357(9258):757–62.
[31] Howick J, Moscrop A, Mebius A, Fanshawe TR, Lewith G, Bishop FL, et al. Effects of empathic and positive communication in healthcare consultations: a systematic review and meta-analysis. J R Soc Med 2018 July 1;111(7):240–52.
[32] Peerdeman KJ, van Laarhoven AIM, Keij SM, Vase L, Rovers MM, Peters ML, et al. Relieving patients' pain with expectation interventions: a meta-analysis. Pain 2016 June;157(6):1179–91.

Ann Rheum Dis 85 (2026) 609–619

Contents lists available at ScienceDirect

Annals of the Rheumatic Diseases

journal homepage: https://www.sciencedirect.com/journal/annals-of-the-rheumatic-diseases

Rheumatoid arthritis

Spacing of a TNF inhibitor or dose reduction of methotrexate vs continued treatment in patients with rheumatoid arthritis in remission or low disease activity: a randomised, controlled trial (SORAIRO trial)

Yuki Imai[1], Michihito Kono[2], Tomonori Ishii[3], Toshihisa Kojima[4], Shintaro Hirata[5], Yoshiya Tanaka[6,7], Eiichi Tanaka[8], Koichiro Ohmura[9], Shunsuke Okamoto[10], Rumiko Matsumoto[10], Yuri Sato[10], Takashi Yamamura[10], Tsutomu Takeuchi[1,11], Yuko Kaneko[1,*]

[1] *Division of Rheumatology, Department of Internal Medicine, Keio University School of Medicine, Tokyo, Japan*
[2] *Department of Rheumatology, Endocrinology and Nephrology, Faculty of Medicine and Graduate School of Medicine, Hokkaido University, Sapporo, Japan*
[3] *Department of Haematology and Rheumatology, Tohoku Medical and Pharmaceutical University Hospital, Sendai, Japan*
[4] *Department of Orthopaedic Surgery, National Hospital Organization Nagoya Medical Centre, Nagoya, Japan*
[5] *Department of Clinical Immunology and Rheumatology, Hiroshima University Hospital, Hiroshima, Japan*
[6] *The First Department of Internal Medicine, University of Occupational and Environmental Health, Kitakyushu, Japan*
[7] *Department of Molecular Targeted Therapeutics, School of Medicine, University of Occupational and Environmental Health, Kitakyushu, Japan*
[8] *Department of Rheumatology, Tokyo Women's Medical University School of Medicine, Tokyo, Japan*
[9] *Department of Rheumatology, Kobe City Medical Centre General Hospital, Kobe, Japan*
[10] *Taisho Pharmaceutical Co., Ltd., Tokyo, Japan*
[11] *Saitama Medical University, Saitama, Japan*

ARTICLE INFO

Article history:
Received 10 November 2025
Received in revised form 3 February 2026
Accepted 5 February 2026

ABSTRACT

Objectives: This study aimed to assess the noninferiority of spacing a tumour necrosis factor (TNF) inhibitor or reducing the methotrexate dose with continued treatment in patients with rheumatoid arthritis.

Methods: The SORAIRO trial was a multicentre, open-label, randomised, noninferiority study. Patients who had been in remission or low disease activity based on the Clinical Disease Activity Index (CDAI) in the preceding phase III trial of ozoralizumab, a next-generation TNF inhibitor, were enrolled. The precalculated sample size was 141. Patients were randomised into continued treatment, ozoralizumab spacing, or methotrexate dose reduction groups. The primary endpoint was a noninferiority of low disease activity maintenance at week 48 with a prespecified noninferiority margin of −18%.

Results: A total of 144 patients were analysed. The mean age was 58.2 years, 75.0% were female, and the mean CDAI was 2.70 with 61.8% in remission. The low disease activity at week 48 was 97.9% in the continued treatment group, 79.2% in the ozoralizumab spacing

*Correspondence to Dr Yuko Kaneko, Division of Rheumatology, Department of Internal Medicine, Keio University School of Medicine, Tokyo, Japan.
E-mail address: ykaneko.z6@keio.jp (Y. Kaneko).
Handling editor Josef S Smolen

https://doi.org/10.1016/j.ard.2026.02.004

group (difference, −21.6; 95% CI, −39.9 to −5.7), and 72.7% in the methotrexate dose reduction group (difference, −30.4; 95% CI, −54.0 to −10.5). In the baseline remission subgroup, remission maintenance rates were comparable in the 3 groups (77.4%, 76.7%, 79.2%, respectively). No significant differences were demonstrated in changes in the Health Assessment Questionnaire Disability Index and modified total Sharp score. Adverse events occurred in 68.0%, 59.2%, and 58.0%, respectively.

Conclusions: Treatment tapering may not be feasible in patients with low disease activity, whereas both extending the TNF inhibitor interval and reducing the methotrexate dose may be reasonable options for patients in remission.

WHAT IS ALREADY KNOWN ON THIS TOPIC

- Rheumatoid arthritis is a chronic condition requiring long-term therapy. Medication tapering should be considered after achieving treatment targets. However, standardised strategies for tapering tumour necrosis factor (TNF) inhibitors and methotrexate remain unestablished.
- Ozoralizumab is a uniquely structured anti-TNFα biological agent, composed of 3 humanised, camelid-derived single-domain antibodies. Its small size and lack of an Fc domain allows rapid efficacy. Its efficacy and safety have been demonstrated in 2 phase III trials, and it has been approved for the treatment of rheumatoid arthritis at a dose of 30 mg subcutaneously every 4 weeks in Japan.

WHAT THIS STUDY ADDS

- This randomised controlled trial provides new evidence on the efficacy and safety of medication tapering with a TNF inhibitor and methotrexate in patients who have achieved remission or low disease activity by directly comparing continued treatment, ozoralizumab spacing, and methotrexate dose reduction strategies.
- At week 48, low disease activity was maintained in 97.9% of patients in the continued treatment group, 79.2% in the ozoralizumab spacing group, and 72.7% in the methotrexate dose reduction group, falling short of the prespecified noninferiority margin. However, among patients in remission at baseline, the remission maintenance rates were comparable across the groups (77%-79%).
- Rescue therapy, ie, returning to the original ozoralizumab treatment interval or methotrexate dose, effectively restored low disease activity in most patients who experienced disease flares. The tapering groups also showed a slightly lower incidence of adverse events than the continued treatment group.

HOW THIS STUDY MIGHT AFFECT RESEARCH, PRACTICE OR POLICY

- In patients who have achieved remission with TNF inhibitor plus methotrexate therapy, extending the TNF inhibitor dosing interval or reducing the methotrexate dose is feasible and favourable under careful clinical monitoring. However, tapering of medications for patients with low disease activity is challenging.

INTRODUCTION

Rheumatoid arthritis is a systemic autoimmune disease characterised by synovitis as the central pathological feature that leads to joint destruction and impaired physical function. Over the past quarter-century, rheumatoid arthritis management has advanced dramatically with the establishment of early and optimal methotrexate-based treatment strategies and the development of biologic and targeted synthetic disease-modifying antirheumatic drugs [1]. The current treatment standard for rheumatoid arthritis is prompt initiation of methotrexate after diagnosis, followed by the addition of a drug that targets specific pathophysiological molecules when the initial treatment goals are not achieved [2,3].

Therapeutic strategies after achieving treatment goals have long been discussed. Recent international guidelines recommend not discontinuing antirheumatic drugs but tapering them to minimise adverse events (AEs) and reduce healthcare costs while maintaining a remission status [2,3]. Although several studies have been conducted on such tapering strategies [4–12], a standardised approach for combining methotrexate and a tumour necrosis factor (TNF) inhibitor is yet to be established.

Ozoralizumab is a next-generation TNF inhibitor based on the heavy-chain variable domains of heavy-chain antibodies, known as NANOBODY. It consists of a trivalent structure with 2 anti-human TNFα NANOBODY molecules and 1 anti-human serum albumin NANOBODY molecule, resulting in a low total molecular weight of approximately 38 kDa [13]. The efficacy and safety of ozoralizumab have been demonstrated with and without methotrexate coadministration in clinical trials [14–16]. In patients with an inadequate response to methotrexate, ozoralizumab plus methotrexate achieved American College of Rheumatology (ACR) 20/50/70 response rates of 92.3%, 79.7%, and 60.8% at week 52 [15], whereas ozoralizumab without methotrexate achieved response rates of 72.3%, 51.1%, and 30.9% at week 52, respectively [16]. Owing to its small molecular weight and serum albumin-binding ability, ozoralizumab demonstrates rapid clinical efficacy, with significant improvements observed as early as 3 days after initiation. Its half-life is approximately 18 days [17], and neutralising antibodies were detected in 7.5% to 27.7% of patients [15,16]. Ozoralizumab was approved for rheumatoid arthritis treatment at a dose of 30 mg subcutaneously administered every 4 weeks in Japan in 2022 [13]. We used this TNF inhibitor to establish evidence for the optimal tapering strategy for TNF inhibitors and methotrexate in patients who achieved treatment targets.

METHODS

Study participants

The SORAIRO trial (jRCTs031220406) is a multicentre, open-label, randomised, parallel-group noninferiority study following a long-term extension (HOSHIZORA trial, jRCT2080224848) of the preceding pivotal phase III trial (OHZORA trial, jRCT2080223971) (Fig 1A). In the previous OHZORA trial, patients aged 20-75 years who were diagnosed with rheumatoid arthritis, fulfilling the 2010 classification criteria of the European Alliance of Association for Rheumatology (EULAR)/ACR

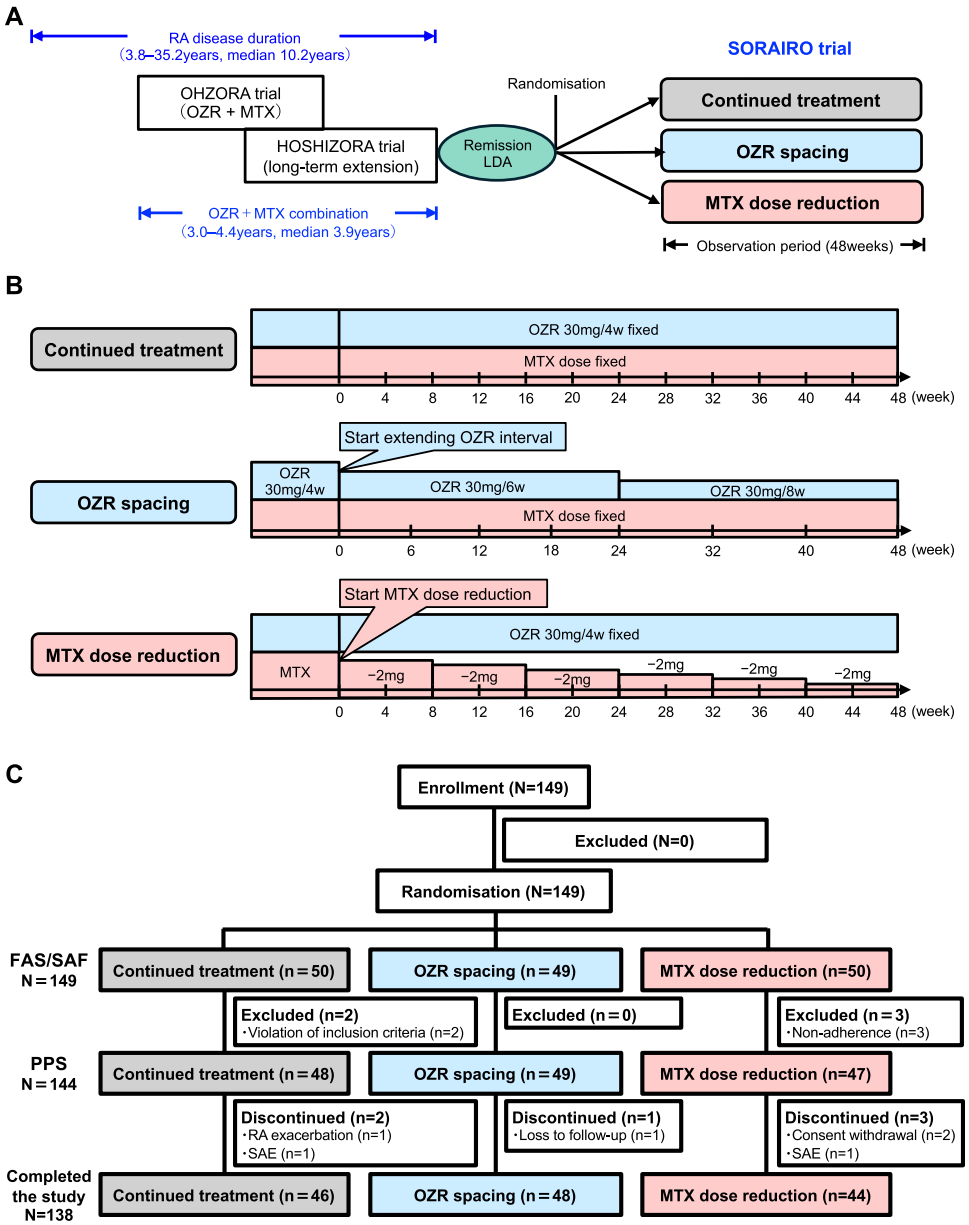

Figure 1. Study design and patient flow. (A) Patients with RA and an inadequate response to MTX were enrolled in the phase III OHZORA trial and subsequently in the long-term extension HOSHIZORA trial. From this cohort, patients in sustained remission or LDA entered the SORAIRO trial and were randomised into 3 groups. (B) In the continued treatment group, patients received OZR 30 mg subcutaneously every 4 weeks along with a fixed dose of MTX. In the OZR spacing group, the dosing interval was extended to every 6 weeks during the first 24 weeks and to every 8 weeks during the subsequent 24 weeks. In the MTX dose reduction group, the MTX dose was decreased by 2 mg every 8 weeks. (C) A total of 149 patients were enrolled and randomised into 3 groups. FAS, full analysis set; LDA, low disease activity; MTX, methotrexate; OZR, ozoralizumab; PPS, per-protocol set; RA, rheumatoid arthritis; SAE, serious adverse event; SAF, safety analysis set.

and showed an inadequate response to methotrexate, were enrolled, and ozoralizumab or placebo plus methotrexate were compared [14,15,18,19]. Patients who had achieved remission and were stable or those with a low disease activity based on the Clinical Disease Activity Index (CDAI ≤ 10) [20] for at least 4 weeks before enrolling in the study were eligible for the current SORAIRO trial. As patients had been receiving an unchanged treatment regimen of ozoralizumab plus methotrexate for a median duration of 3.9 years, stable disease activity status was assumed by confirming low disease activity or remission at 2 consecutive visits before enrolment. Patients were required to be on the same dose of methotrexate for at least 4 weeks and to have been receiving ozoralizumab 30 mg every 4 weeks at the time of randomisation. The detailed eligibility criteria are shown in Supplementary Table.

The study was approved by the Certified Review Board of Keio, and was conducted with permission at each site, and conformed to the Declaration of Helsinki and good clinical practice guidelines, and was reported in accordance with the CONSORT recommendations.

Study design

Patients were randomised through an electronic data capture system using a minimisation method stratified by baseline CDAI (remission or low disease activity) and methotrexate dose (<10 mg/wk or ≥10 mg/wk) in a 1:1:1 ratio to the continued treatment, ozoralizumab spacing, or methotrexate dose reduction groups. The allocation sequence was automated, and the allocated treatment was open to patients and treating physicians.

Figure 1B shows the treatment scheme for each group. In the continued treatment group, patients continued receiving subcutaneous ozoralizumab 30 mg every 4 weeks with a fixed dose of methotrexate. In the ozoralizumab spacing group, ozoralizumab 30 mg was administered every 6 weeks for the first 24 weeks and every 8 weeks for the subsequent 24 weeks, with a fixed dose of methotrexate. This was determined based on the estimated trough concentrations of ozoralizumab, which were 2.7, 1.2, and 0.6 μg/mL with a 4-, 6-, and 8-week intervals, whereas the previous trial showed an efficacy-associated trough concentration of 1.15 μg/mL at week 16; however, this threshold concentration decreased at week 24, and no clear threshold was observed at week 52 [17]. For the methotrexate dose-tapering schedule, we aimed to reduce the methotrexate dose and preferably discontinue it through a practical stepwise approach by avoiding acute dose tapering or withdrawal of methotrexate. Accordingly, the methotrexate dose was reduced by 2 mg/wk every 8 weeks, with the option to discontinue, and ozoralizumab was administered at a fixed dose of 30 mg every 4 weeks. In the group in which the ozoralizumab treatment was spaced or the methotrexate dose was reduced, medication tapering was mandatory according to a predefined schedule unless the CDAI exceeded 10. The concomitant use of glucocorticoids equivalent to prednisolone at less than 10 mg/d was permitted, whereas the use of conventional synthetic disease-modifying antirheumatic drugs other than methotrexate and other biological or targeted disease-modifying antirheumatic drugs was prohibited during the study.

In the case of flares, defined as CDAI > 10, the treatment was reversed to the previous ozoralizumab treatment regimen or methotrexate dose, followed by a stepwise escalation back to the original baseline regimen as the first rescue. If the flare remained unresolved after the first rescue, further rescue treatments, including the initiation of or increase in glucocorticoid dose via any route, the use of analgesics, or the use of intra-articular glucocorticoid injections, were permitted. If low disease activity cannot be achieved with rescue treatments, alternative treatments can be attempted by the attending physician. If continuing ozoralizumab therapy was deemed difficult, the patient was withdrawn from the study. No tapering was attempted after the rescue treatment.

Assessment

Vital signs, laboratory findings, disease activity of rheumatoid arthritis, and safety data were collected every 6 weeks during the first half and every 8 weeks during the second half in the ozoralizumab spacing group, and every 4 or 8 weeks in the other 2 groups. Disease activity was assessed using the CDAI [20], Simplified Disease Activity Index (SDAI) [21], disease activity score using 28 joints with C-reactive protein (DAS28-CRP) [22], DAS28 with erythrocyte sedimentation rate (DAS28-ESR) [23], and Boolean remission [24,25]. Physical function was assessed using the Health Assessment Questionnaire Disability Index (HAQ-DI) [26]. Radiographs of the hands and feet at baseline and week 48 were evaluated and calculated by 2 independent experienced readers using the van der Heijde-modified total Sharp score (mTSS) [27].

Outcomes

The primary endpoint was the proportion of patients maintaining low disease activity (CDAI ≤ 10) at week 48. Secondary endpoints included remission rates based on CDAI remission, low disease activity and remission based on SDAI, DAS28-CRP, DAS28-ESR, Boolean remission rates, flare rates, and changes from baseline CDAI, SDAI, DAS28-CRP, DAS28-ESR, mTSS, C-reactive protein (CRP), erythrocyte sedimentation rate (ESR), matrix metalloproteinase-3 (MMP-3), and rheumatoid factor (RF) levels. Exploratory analyses included a subgroup analysis based on baseline CDAI, as well as evaluations of functional remission, defined as HAQ-DI ≤0.5 [26], structural remission, defined as a change in mTSS (ΔmTSS) of ≤0.5 [24], and methotrexate-free achievement, defined as discontinuation of methotrexate by week 44 without resumption afterwards. Post hoc analyses included the assessment of transitions in oral glucocorticoid dose and comparison of CDAI components at the baseline and flare. Safety was monitored for 48 weeks, and all AEs were reported. Serious AEs were defined as those that led to death, life-threatening events, hospitalisation, disability, birth defects, or other medically important conditions.

Statistical analysis

This trial was designed to demonstrate the noninferiority of ozoralizumab spacing and methotrexate dose reduction to continued treatment regarding maintaining low disease activity according to CDAI, with a noninferiority margin of −18%. The margin was hypothesised based on approximately half of the placebo-adjusted effect size of ozoralizumab (37.8%) observed in the previous OHZORA trial [7,8]. Assuming a CDAI ≤10 maintenance rate at week 48 of 92%, a one-sided significance level of 2.5% and a power of 80% with a noninferiority margin of 18% required a sample size of 47 patients per group (a total of 141). Considering a possible dropout rate of 20%, the target sample size was determined to be 177 patients. Efficacy analyses were performed using the predefined full analysis set (FAS) and per-protocol set (PPS), with the PPS prespecified for the primary analysis and the FAS for sensitivity analyses. The FAS population was defined as patients who received at least 1 dose of methotrexate or ozoralizumab with at least 1 follow-up assessment, and the PPS population was defined as patients who received at least 1 dose of methotrexate or ozoralizumab treatment with at least 1 follow-up assessment without major protocol violations of the eligibility criteria or treatment adherence. Safety was assessed in patients who received at least 1 dose of methotrexate or ozoralizumab treatment. Noninferiority of the ozoralizumab spacing or methotrexate dose reduction groups was concluded if the lower bound of the 95% CIs of the difference in maintenance rates of low disease activity or remission at week 48 exceeded −18%. The difference and corresponding 95% CI between the 2 groups were calculated using the Newcombe method, adjusted for allocation factors (baseline CDAI status and methotrexate dose). Comparisons of continuous variables between the 3 groups were conducted using analysis of variance. Categorical variables were compared using the chi-squared test. Patients who required rescue treatment were considered to have failed to maintain low disease activity. Although no imputation was performed for missing data, a sensitivity analysis using the last observation carried forward method was conducted for the efficacy outcomes.

RESULTS

Patient disposition and demographics

Between October 2022 and March 2023, 179 patients who completed the preceding HOSHIZORA trial while receiving ozoralizumab at a 4-week interval plus methotrexate were invited, and 149 patients across 58 sites in Japan participated in the trial. Figure 1C shows the flow diagram of the patients. Patients were

randomised into the continued treatment (n = 50), ozoralizumab spacing (n = 49), and methotrexate dose reduction groups (n = 50). All patients received at least 1 dose of the study medication and were included in the FAS and safety analyses. Five patients were excluded from the FAS because of major protocol violations of the eligibility criteria due to miscalculated CDAI (n = 2) or an unscheduled methotrexate dose increase (n = 3). Consequently, 144 patients were included in the PPS group (48, 49, and 47 in the continued treatment, ozoralizumab spacing, and methotrexate dose reduction groups, respectively). The number of patients with PPS reached a predefined value.

The baseline characteristics of patients with PPS are presented in Table 1; 75.0% were females, and the mean age, disease duration, and methotrexate dose were 58.2 years, 10.5 years, and 8.7 mg/wk, respectively. The mean baseline CDAI was 2.7, with a CDAI remission rate of 61.8%. These characteristics were well balanced across the 3 groups.

Maintenance of remission and low disease activity

Figure 2A shows the proportion of patients with low disease activity or remission at week 48. The primary endpoint, the proportion of patients maintaining CDAI ≤10 at week 48, was 97.9% (46/47) in the continued treatment group, 79.2% (38/48) in the ozoralizumab spacing group (difference from the continued treatment group, −21.6%; 95% CI, −39.9 to −5.7), and 72.7% (32/44) in the methotrexate dose reduction group (difference, −30.4%; 95% CI, −54.0 to −10.5). Neither the ozoralizumab spacing nor the methotrexate dose reduction groups met the noninferiority criterion for the continued treatment group. Sensitivity analyses with the last observation carried forward method confirmed similar results (95.8%, 79.2%, and 68.1%, respectively), as well as for the FAS population (97.9%, 79.2%, and 70.2%, respectively) and the FAS population with the last observation carried forward method (92.0%, 79.2%, and 66.0%, respectively). The proportions of patients who maintained remission at week 48 were 68.1% (32/47), 54.2% (26/48), and 54.5% (24/44), respectively. Figure 2B shows the time-course changes in the mean CDAI. The mean CDAI in the continued treatment group was consistently lower than those in the other 2 groups, with mean CDAI values at week 48 of 2.1, 3.2, and 3.6, respectively (P = .066). Supplementary Figure S1A-E shows the remission and low disease activity rates assessed using CDAI, SDAI, DAS28-CRP, DAS28-ESR, and Boolean remission definition at each time point. The Boolean remission rates at week 48 were 57.4% (27/47), 39.6% (19/48), and 38.6% (17/44) in the continued treatment, ozoralizumab spacing, and methotrexate dose reduction groups, respectively.

In the subgroup of patients with baseline remission (CDAI ≤ 2.8, Fig 2C), the CDAI ≤10 maintenance rates at week 48 were 100% (31/31) in the continued treatment group, 93.3% (28/30) in the ozoralizumab spacing group (difference, −7.1%; 95% CI, −17.9 to 2.6), and 91.7% (22/24) in the methotrexate dose reduction group (difference, −9.1%; 95% CI, −23.2 to 3.3), demonstrating that the ozoralizumab spacing group met the noninferiority criterion. The maintenance rates of remission at week 48 in this baseline remission subgroup were comparable: 77.4% (24/31), 76.7% (23/30), and 79.2% (19/24), respectively. Time-course changes in CDAI were also comparable throughout the study (Fig 2D).

The transition of CDAI categories for all patients is shown in Figure 2E. As patients who received rescue therapy when a flare occurred were regarded as having failed to maintain remission or low disease activity after rescue, Figure 2E does not reflect the effect of rescue therapy.

Changes in CRP, ESR, MMP-3, and RF

Time-course changes in CRP, ESR, MMP-3, and RF levels were all stable in the 3 groups (Supplementary Fig S2A-D).

Table 1
Baseline characteristics (per-protocol set)

Characteristics	All, N = 144	Continued treatment, n = 48	OZR spacing, n = 49	MTX dose reduction, n = 47
Age (y)	58.2 (10.7)	57.7 (10.2)	59.0 (11.2)	57.7 (10.8)
Female	108 (75.0)	32 (66.7)	40 (81.6)	36 (76.6)
Body weight (kg)	58.8 (11.9)	60.6 (11.7)	56.7 (11.8)	59.3 (12.3)
Disease duration (y)	10.5 (6.2)	9.4 (5.5)	11.0 (7.0)	11.2 (5.9)
CRP (mg/dL)	0.18 (0.47)	0.11 (0.26)	0.32 (0.72)	0.11 (0.22)
ESR (mm/h)	19.7 (19.1)	15.0 (13.2)	25.0 (21.7)	18.9 (20.3)
MMP-3 (ng/mL)	70.0 (77.4)	77.4 (78.9)	75.0 (86.2)	57.3 (40.5)
Positivity for rheumatoid factor	87 (60.4)	23 (47.9)	36 (73.5)	28 (59.6)
Positivity for anti-CCP antibody[a]	112 (81.8)	33 (71.7)	43 (89.5)	36 (83.7)
Tender joint count in 68 joints	0.6 (1.1)	0.6 (1.2)	0.8 (1.1)	0.5 (0.9)
Swollen joint count in 68 joints	0.6 (1.3)	0.5 (1.0)	0.8 (1.4)	0.6 (1.4)
CDAI	2.70 (2.57)	2.60 (2.78)	3.01 (2.81)	2.49 (2.06)
CDAI ≤2.8	89 (61.8)	32 (66.7)	30 (61.2)	27 (57.4)
SDAI	2.88 (2.72)	2.70 (2.80)	3.33 (3.13)	2.60 (2.11)
DAS28-CRP	1.68 (0.61)	1.61 (0.57)	1.82 (0.73)	1.62 (0.49)
DAS28-ESR	2.29 (0.89)	2.11 (0.92)	2.53 (0.97)	2.24 (0.73)
Boolean remission	72 (50.0)	28 (58.3)	22 (44.9)	22 (46.8)
HAQ-DI score	0.21 (0.37)	0.20 (0.36)	0.24 (0.40)	0.19 (0.36)
MTX dose (mg/wk)	8.7 (2.8)	8.8 (2.8)	8.4 (2.6)	8.9 (3.0)
Glucocorticoid use	32 (22.2)	15 (31.3)	7 (14.3)	10 (21.3)
Prednisolone dose (mg/d)	3.8 (2.9)	4.0 (2.0)	3.3 (1.7)	4.0 (4.5)
Biologic-naïve before OZR initiation	89 (61.8)	35 (72.9)	29 (59.2)	25 (53.2)

CCP, cyclic citrullinated peptide; CDAI, Clinical Disease Activity Index; CRP, C-reactive protein; DAS28-CRP, disease activity score using 28 joints with CRP; DAS28-ESR, disease activity score using 28 joints with ESR; ESR, erythrocyte sedimentation rate; HAQ-DI, Health Assessment Questionnaire Disability Index; MMP-3, matrix metalloproteinase-3; MTX, methotrexate; OZR, ozoralizumab; SDAI, Simplified Disease Activity Index.

Continuous variables are presented as mean (SD). Categorical variables are presented as number (percentage).

[a] Anti-CCP antibody was measured at week 48 in 137 patients: 46 in the continued treatment group, 48 in the OZR spacing group, and 43 in the MTX dose reduction group.

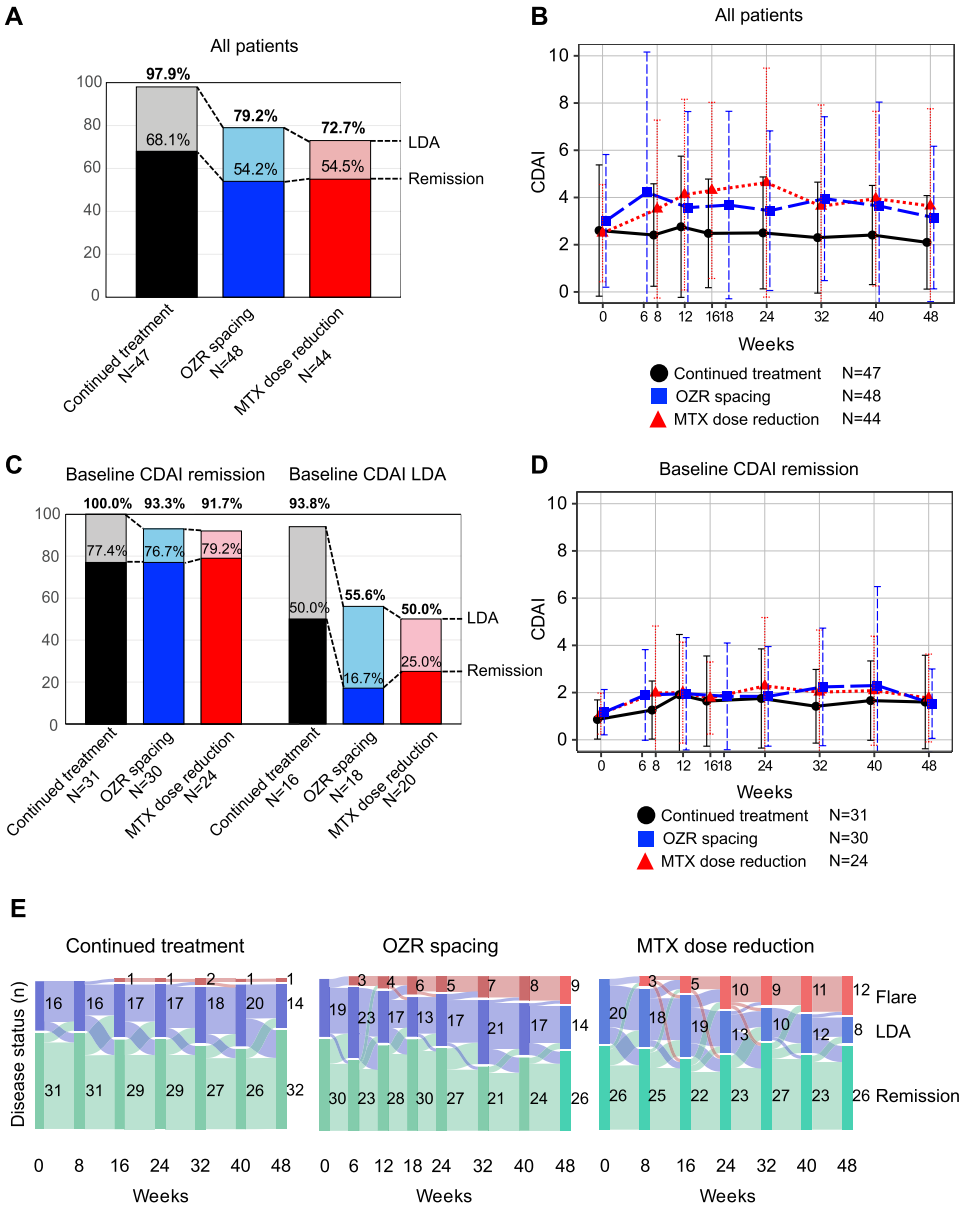

Figure 2. Disease activity based on the CDAI status. (A) The upper bars indicate the proportion of patients in low disease activity, and the lower bars indicate those in remission, both based on CDAI at week 48. (B) Time-course changes in the mean CDAI values during the study period with SD bars. A black circle with a solid line indicates the continued treatment group, a blue square with a dashed line indicates the ozoralizumab spacing group, and a red triangle with a dotted line indicates the methotrexate dose reduction group. (C) The proportion of patients achieving low disease activity or remission, stratified by the baseline CDAI status. (D) The mean CDAI values for patients in remission at baseline. (E) The Sankey diagrams illustrate CDAI status at every 6 to 8 weeks. Missing values were imputed using the last observation carried forward method. After rescue therapy, patients were categorised as having a flare. CDAI, Clinical Disease Activity Index; LDA, low disease activity; MTX, methotrexate; OZR, ozoralizumab.

Changes in RF positivity from baseline to week 48 were −2.4% in the continued treatment group, −2.7% in the ozoralizumab spacing group, and 8.6% in the methotrexate dose reduction group (Supplementary Fig S2A-E).

Physical function and patient global assessment scores

Time-course changes in HAQ-DI scores are shown in Figure 3A, and those in the subgroup with baseline CDAI remission are shown in Figure 3B. The HAQ-DI scores remained low and stable throughout the study (approximately 0.2 in all groups). At week 48, no significant difference was observed between the groups (P = .653). Functional remission rates (HAQ-DI ≤ 0.5) at week 48 were 83.0% (39/47) in the continued treatment group, 87.5% (42/48) in the ozoralizumab spacing group, and 81.8% (36/44) in the methotrexate dose reduction group. Patient global assessment throughout the study period is shown in Supplementary Figure S2F. The continued treatment group consistently showed lower values than the other 2 groups; however, most of the differences between the groups were <5 mm on a 100 mm scale.

Glucocorticoids usage

At baseline, concomitant glucocorticoids were used in 15 (31.3%), 7 (14.3%), and 10 (21.3%) patients in the continued treatment, ozoralizumab spacing, and methotrexate dose reduction groups, respectively. The mean prednisolone dose changed from 3.8 to 3.5 mg/d, 2.9 to 2.1 mg/d, and 2.7 to 2.6 mg/d at week 48

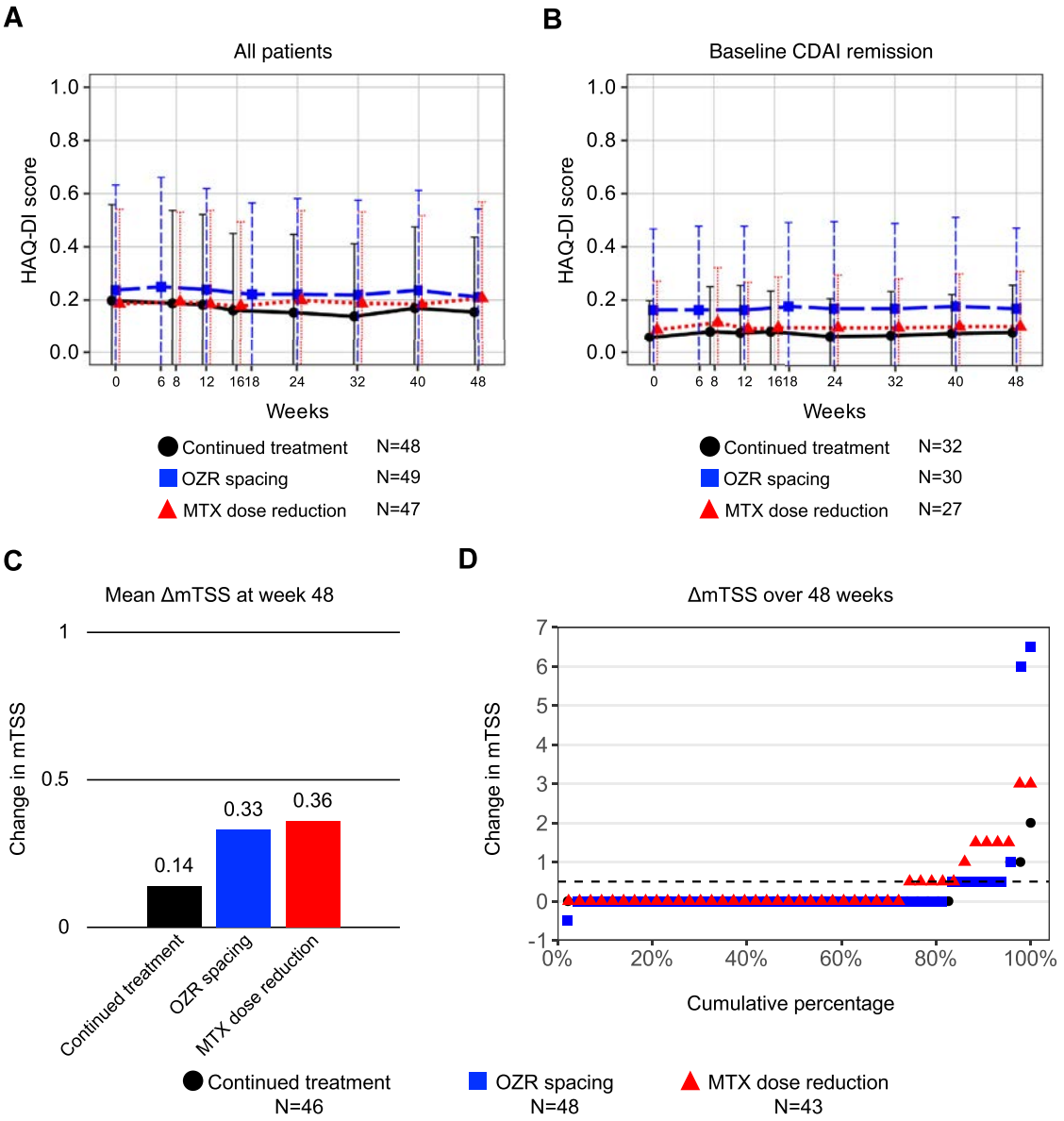

Figure 3. Physical function and radiological progression. (A) Transition of HAQ-DI scores with SD bars. A black circle with a solid line indicates the continued treatment group, a blue square with a dashed line indicates the ozoralizumab spacing group, and a red triangle with a dotted line indicates the methotrexate dose reduction group. (B) Subgroup analysis among patients in baseline remission is shown on the right. (C) Mean changes in the mTSS, and (D) cumulative probability plots of radiological progression over 48 weeks. A horizontal dashed line represents the functional remission threshold of HAQ-DI (0.5). CDAI, Clinical Disease Activity Index; HAQ-DI, Health Assessment Questionnaire Disability Index; mTSS, modified Total Sharp Score; ΔmTSS, change in mTSS; MTX, methotrexate; OZR, ozoralizumab.

in the groups, respectively (Supplementary Fig S3). No significant changes were observed throughout the study period in any group.

Radiological progression

The mean changes in mTSS from baseline to week 48 were 0.14 in the continued treatment group, 0.33 in the ozoralizumab spacing group, and 0.36 in the methotrexate dose reduction group (P = .441, Fig 3C). Structural remission rates were 93.5% (43/46), 93.8% (45/48), and 83.7% (36/43), respectively. Cumulative probability plots showed that most patients did not experience radiographic progression during the study period (Fig 3D).

Flare and rescue

Among the 11 patients who had flares in the ozoralizumab spacing group, 7 (63.6%) had flares during the first phase (6-week interval) of ozoralizumab administration (between 0 and 24 weeks) and 4 (36.4%) had flares during the second phase (8-week interval) (between 24 and 48 weeks). Among the 15 patients who had flares in the methotrexate group, the median change in the methotrexate dose at flares was −4.0 mg/wk. All 4 CDAI components, swollen joint count, tender joint count, patient global assessment, and evaluator global assessment at baseline and flares, are shown in Supplementary Figure S4A. All of them increased at flares in all groups.

At flares (Fig 2E), rescue therapy was performed in 21 patients (9 in the ozoralizumab spacing group and 12 in the methotrexate dose reduction group). All rescue therapy was the first regimen: a reverse to the previous ozoralizumab treatment interval or methotrexate dose, with 17 patients receiving a 1-step reverse and 4 patients (2 for each group) requiring a 2-step reverse. Low disease activity and remission were achieved in 88.9% (8/9) and 22.2% (2/9) of patients in the ozoralizumab spacing group and in 83.3% (10/12) and 8.3% (1/12) of patients in the methotrexate dose reduction group (Supplementary Fig S4B).

Table 2
Safety results (safety analysis set)

Adverse events	All, N = 149	Continued treatment, n = 50	OZR spacing, n = 49	MTX dose reduction, n = 50
All AEs	92 (61.7)	34 (68.0)	29 (59.2)	29 (58.0)
AE leading to death	0 (0.0)	0 (0.0)	0 (0.0)	0 (0.0)
Serious AEs	6 (4.0)	2 (4.0)	2 (4.1)	2 (4.0)
Tumours[a]	4 (2.7)	1 (2.0)	1 (2.0)	2 (4.0)
Submandibular abscess	1 (0.7)	1 (2.0)	0 (0.0)	0 (0.0)
Radius fracture	1 (0.7)	0 (0.0)	1 (2.0)	0 (0.0)
AEs observed ≥3				
SARS-CoV-2 infection	18 (12.1)	8 (16.0)	7 (14.3)	3 (6.0)
Nasopharyngitis	14 (9.4)	4 (8.0)	3 (6.1)	7 (14.0)
Cystitis	6 (4.0)	5 (10.0)	0 (0.0)	1 (2.0)
Bronchitis	4 (2.7)	1 (2.0)	1 (2.0)	2 (4.0)
Herpes zoster	4 (2.7)	1 (2.0)	2 (4.1)	1 (2.0)
Sinusitis	4 (2.7)	3 (6.0)	0 (0.0)	1 (2.0)
Fever	4 (2.7)	3 (6.0)	0 (0.0)	1 (2.0)
Back pain	4 (2.7)	1 (2.0)	1 (2.0)	2 (4.0)
Conjunctivitis	3 (2.0)	1 (2.0)	0 (0.0)	2 (4.0)
Pharyngitis	3 (2.0)	0 (0.0)	1 (2.0)	2 (4.0)
Stomatitis	3 (2.0)	1 (2.0)	2 (4.1)	0 (0.0)
Iron deficiency anaemia	3 (2.0)	0 (0.0)	3 (6.1)	0 (0.0)
Asthma	3 (2.0)	2 (4.0)	1 (2.0)	0 (0.0)
Allergic rhinitis	3 (2.0)	1 (2.0)	1 (2.0)	1 (2.0)
Caries	3 (2.0)	0 (0.0)	1 (2.0)	2 (4.0)
Contact dermatitis	3 (2.0)	0 (0.0)	1 (2.0)	2 (4.0)
Eczema	3 (2.0)	0 (0.0)	1 (2.0)	2 (4.0)
Ureteral calculi	3 (2.0)	2 (4.0)	1 (2.0)	0 (0.0)

AE, adverse event; MTX, methotrexate; OZR, ozoralizumab.
Variables are presented as number (percentage).
[a] Tumours included bladder cancer (continued treatment group), neuroendocrine tumour (OZR spacing group), and oral and lung cancers (MTX dose reduction group).

Methotrexate withdrawal

By week 48, 23 patients in the methotrexate dose reduction group achieved methotrexate-free status. After excluding 4 patients whose baseline methotrexate dose was >12 mg/wk, which meant that they could not reach methotrexate-free status under the protocol, the rate of methotrexate-free status was 53.5% (23/43).

Safety

AEs are summarised in Table 2. The overall AE rate was 68.0% (34/50) in the continued treatment group, 59.2% (29/49) in the ozoralizumab spacing group, and 58.0% (29/50) in the methotrexate dose reduction group (P = .532). Six serious AEs occurred, 2 in each group, including radial fracture, submandibular abscess, and 4 tumours (neuroendocrine tumour, oral cancer, lung cancer, and bladder cancer). The most frequently observed AEs were SARS-CoV-2 infection (12.1%), followed by nasopharyngitis (9.4%), and cystitis (4.0%).

DISCUSSION

The SORAIRO trial demonstrated that in patients with rheumatoid arthritis in remission or with low disease activity, neither ozoralizumab spacing nor methotrexate dose reduction showed noninferiority to continued treatment for maintaining low disease activity. In contrast, in patients in remission, both the ozoralizumab spacing and methotrexate dose reduction strategies showed a similar remission maintenance rate to that of the continued treatment strategy. The incidence of AEs was slightly lower in the treatment tapering groups than in the continued treatment group.

Our study showed that spacing TNF inhibitor administration was not noninferior to continued treatment in patients with low disease activity. Dose reduction and spacing of TNF inhibitors have been investigated in several trials. Although the overall study design was different, the PRESERVE trial demonstrated that reducing etanercept from 50 to 25 mg/wk in combination with methotrexate showed comparable rates of maintaining low disease activity with continued treatment with etanercept at 50 mg/wk [7]. This difference may be ascribed to the different kinds of TNF inhibitors (etanercept vs ozoralizumab), concomitant doses of methotrexate (15-25 mg/wk vs 8.7 mg/wk), or strategies (dose reduction or spacing). Indeed, the STRASS trial, in which the primary endpoint was the DAS28 slope, demonstrated that extending the etanercept or adalimumab dosing interval was not equivalent to continuing the treatment [28]. Although the DRESS study demonstrated the noninferiority of spacing etanercept or adalimumab compared with maintenance treatment in terms of major flare occurrence, defined as a persistent increase in DAS28-CRP for more than 3 months [24], transient flares occurred significantly more frequently in the spacing group. However, in our study, it should be noted that patients in remission based on the CDAI could maintain remission similarly with all strategies. As the RRR and HONOR trials revealed, deep remission achievement is the key to successful discontinuation of TNF inhibitors [4,9]. Also, EULAR 2023 recommendations include dose reduction or gradual discontinuation after achieving remission [2]. Collectively, these findings and the results of our study suggest that spacing the administration of TNF inhibitors is feasible for patients in stable remission.

The methotrexate dose reduction was not noninferior to the continued treatment, whereas approximately half of the patients in the methotrexate dose reduction group achieved a methotrexate-free status. Previous studies have assessed the feasibility of methotrexate dose reduction during TNF inhibitor initiation. The

MIRACLE trial demonstrated that a reduced methotrexate dose (7.6 mg/wk) was noninferior to a continued maximum tolerated methotrexate dose (13.2 mg/wk) when starting adalimumab concomitantly [5]. However, the MIRACLE trial targeted methotrexate-naïve patients and reduced the dose of methotrexate by approximately half. In contrast, the MUSICA trial failed to show the noninferiority of low-dose methotrexate (7.5 mg/wk) with adalimumab administration compared with high-dose methotrexate (20 mg/wk) in patients with an inadequate response to methotrexate [6]. Our study differs from these studies in that the methotrexate dose was gradually tapered at inactive status during the concomitant use of a TNF inhibitor. The ARCTIC REWIND trial also did not demonstrate the noninferiority of reducing the methotrexate dose (from 19.5 to 11.7 mg/wk) to maintaining its dose (19.0 mg/wk) in patients in remission for 12 months with methotrexate monotherapy [29]. In this trial, even in patients with sustained remission for >1 year, decreasing the methotrexate dose was associated with an increased risk of disease flares, suggesting that methotrexate monotherapy may offer limited flexibility for dose reduction. Interestingly, although our study showed that methotrexate dose reduction led to more frequent flares than continued treatment, almost half of the patients achieved a methotrexate-free status, suggesting that the response to methotrexate tapering varies substantially among patients. Indeed, the DREAM registry reported that successful tapering or discontinuation of concomitant methotrexate in patients treated with TNF inhibitors was frequently observed without affecting the disease activity in clinical practice [30]. Notably, the methotrexate dose used in this study was relatively low. However, a low methotrexate dose in Japanese population does not necessarily indicate low methotrexate exposure, because the levels of erythrocyte methotrexate polyglutamate, active methotrexate metabolites, are similar between Japanese patients with relatively low-dose methotrexate and Caucasian patients with high-dose methotrexate. For example, 1 study reported that the erythrocyte methotrexate polyglutamate level was 65 nmol/L with methotrexate 13.4 mg/wk in North American patients, and 94 nmol/L with 10.3 mg/wk in Japanese patients [31]. However, the generalisability of the results to populations of other ethnicities should be carefully discussed. Taken together, tapering of the methotrexate dose is possible but should be performed cautiously while monitoring disease activity and adjusting the tapering schedule.

Increases in CDAI values and flares were observed mainly early after tapering initiation. As this was not the case in patients in remission at baseline, this further indicates that treatment tapering is not feasible in patients with low disease activity, although it is also possible that this was partly related to nocebo effects, because this study was conducted in an open-label manner or because of the diversity of the necessary doses of medication among individual patients.

Another important factor for the successful tapering of treatment is the duration of remission. Both EULAR and ACR recommend maintaining target disease activity for at least 6 months before medication tapering [2,3], whereas our inclusion criteria were the remission or low disease activity status at 2 consecutive visits only 4 weeks apart before enrolment. However, the study population consisted of relatively homogeneous patients who remained on ozoralizumab and methotrexate for a median duration of 3.9 years, with little treatment modification, indicating that their disease activity was stable. Indeed, low disease activity was maintained in all the patients in remission at baseline in the continued treatment group. Nevertheless, the short period of disease activity confirmation and possible selection bias may necessitate careful interpretation of the results. Moreover, the patients in the study could be referred to as healthy survivors, as inclusion in this study was only offered to those who were doing well on the combined administration of ozoralizumab and methotrexate for a long time. This finding adds another point to the interpretation of the results.

In our study, most patients who experienced a flare after tapering regained low disease activity or remission after the reversal to the previous ozoralizumab treatment regimen or methotrexate doses. Many previous studies have shown that 80% to 100% of patients who experienced disease flares following medication tapering regained low disease activity, and 70% to 100% of patients achieved remission within a few weeks to several months after restarting or reverting to biological agents or methotrexate [4,8–10,32]. These consistent findings provide reassurance to rheumatologists and patients when considering tapering medications in clinical practice.

Regarding safety, the incidence of AEs was slightly higher in the continued treatment group, although this difference was not statistically significant. As both the EULAR and ACR recommend [2,3], we should keep the challenge of establishing optimal tapering strategies to minimise AEs and reduce healthcare costs while maintaining remission status.

This study has some limitations. First, this was an open-label trial, and knowledge of treatment allocation may have influenced patient or physician assessments. Second, the sample size was relatively small, even though the number of patients reached the predefined plan. Third, ozoralizumab is a TNF inhibitor with unique structures that use variable domains of heavy-chain antibodies, which may reduce the generalisability of the results. In particular, the relatively long half-life of approximately 18 days and absence of an Fc region should be considered when interpreting the results. However, previous evidence has shown that treatment spacing or dose tapering is common among monoclonal and fusion types of TNF inhibitors. Fourth, the 48-week follow-up period after reaching the final dose may not have been adequate for capturing late-onset flares. Although flares were frequently observed during the early phases of tapering, a longer observation period is necessary to confirm the long-term stability and safety of these de-escalation strategies. Fifth, to our regret, the exact duration of remission or low disease activity in our trial could not be evaluated, as these trial data were originally collected for the preceding study, and the use of these data requires further approval. Further integrated analyses that combine previous and current trials are warranted. Finally, the tapering protocols used in this study may not represent optimal regimens. Notably, patients in the methotrexate dose reduction group discontinued methotrexate at different time points, which introduced heterogeneity in methotrexate exposure. Although this approach reflects real-world clinical practice, further investigations are required to determine the optimal strategy for tapering TNF inhibitors or methotrexate.

In conclusion, the spacing of a TNF inhibitor or methotrexate dose reduction in patients in remission treated with a TNF inhibitor plus methotrexate may be a feasible strategy under careful monitoring. Tapering strategies should be adjusted based on careful monitoring.

Competing interests

MK reports grants and/or speaking fees from AbbVie, Asahi Kasei, Astellas, AstraZeneca, Ayumi, Bristol Myers Squibb, Chugai, Daiichi Sankyo, Eisai, Eli Lilly, Gilead Sciences, GlaxoSmithKline, Janssen, Kowa, Kyocera, Lotte, Nippon Boehringer

Ingelheim, Nippon Shinyaku, Mitsubishi Tanabe, Mochida, Pfizer, Sandoz, Taiju Life Social Welfare Foundation, Taisho, Takeda, Terumo, UCB Japan and Yamazaki Baking, outside the submitted work. TI has received speaking fees from Asahi Kasei, Chugai, Eli Lilly, GSK, Pfizer, Boehringer Ingelheim, and AstraZeneca. SH has received speaker's fee, consultancy fee, or research grant from AbbVie, Asahi Kasei Pharma, Astellas, AstraZeneca, Ayumi, Bristol Myers Squibb, Boehringer Ingelheim, Chugai, Daiichi Sankyo, Eisai, Eli Lilly, Gilead Sciences, Glaxo SmithKline, Janssen, Nihon-Shinyaku, Novartis, Otsuka, Pfizer, Sandoz, Taisho, Tanabe-Mitsubishi, UCB. YT has received speaking fees and/or honoraria from Chugai, UCB, AbbVie, AstraZeneca, Eli Lilly, Behringer Ingelheim, GlaxoSmithKline, Eisai, IQVIA, Daiichi Sankyo, Otsuka, Taisho, Gilead Sciences, and Bristol Myers. ET has received lecture fees or consulting fees from AbbVie, Asahi Kasei, Astellas, Ayumi, Boehringer Ingelheim, Bristol Myers, Chugai, Eisai, Eli Lilly, Gilead Sciences, GlaxoSmithKline, Mikasa Seiyaku, Nichi-Iko, Nippon Kayaku, Pfizer, Sandoz, Taisho, Takeda, Towa, Mitsubishi Tanabe, UCB Japan, and Viatris and has received research funding from Pfizer. SO, RM, YS, and TY are employees of Taisho Pharmaceutical Co., Ltd. KO has received grants from AbbVie, Asahi Kasei, Chugai, Mitsubishi Tanabe, and has received speaker's fee from AbbVie, Asahi Kasei, Astellas Pharma, AstraZeneca, Ayumi, Boehringer Ingelheim, Bristol Myers, Chugai, Eisai, Eli Lilly, Gilead Sciences, GlaxoSmithKline, Mitsubishi Tanabe, Novartis Pharma, Otsuka, Taisho, Janssen, UCB. TT has received speaking fees from AbbVie, Chugai, Eli Lilly, Eisai, Gilead Sciences, Pfizer, Taisho, and has received consultant fees from AbbVie, Eli Lilly, Gilead Sciences, Mitsubishi Tanabe, and Taisho. YK has received research grants from AbbVie, Eisai, Sanofi, Chugai, Mitsubishi Tanabe, Taisho, and has received scholarship grant from Asahi Kasei, Eisai, Boehringer Ingelheim, Taisho, and has received speaking fees from AbbVie, Asahi Kasei, Astellas, Ayumi, Boehringer Ingelheim, Bristol Myers, Chugai, Eisai, Eli Lilly, GlaxoSmithKline, Janssen, Novartis, Pfizer, UCB, and Gilead Sciences. All other authors declare they have no competing interests.

Acknowledgements

The authors would like to express their sincere gratitude to all participants in this study. NANOBODY is a registered trademark of Ablynx NV, an affiliate of Sanofi. Ablynx NV originally discovered and performed initial development of the NANOBODY compound ozoralizumab. A portion of this work was previously presented at the European Congress of Rheumatology 2025 (abstract number LB0006) and at the 27th Asia-Pacific League of Associations for Rheumatology Congress and the 40th Annual meeting of the Japanese Society for Clinical Rheumatology and Related Research as an encore presentation.

Contributors

YI drafted the initial version of the manuscript. MK, TI, TK, SH, YT, ET, KO, TT, and YK were responsible for participant recruitment and data collection. SO, RM, YS, and TY, employees of the Taisho Pharmaceutical Co., Ltd., contributed to the study plan, result review, and provision of study-related information. YK takes full responsibility for the overall content of the manuscript. All authors revised the manuscript, contributed to the discussion, and approved the final version.

Funding

This research was funded by Taisho Pharmaceutical Co., Ltd. Taisho Pharmaceutical Co., Ltd was not involved in the conduct, data collection, or interpretation of the study.

Patient consent for publication

Written informed consent was obtained from all participants.

Ethics approval

The study was approved by the Keio University certified clinical research review board and registered in the Japan Registry of Clinical Trials (jRCTs031220406). The conduction of this study was permitted at each participating site.

Provenance and peer review

Not commissioned; externally peer reviewed.

Data availability statement

The data underlying this article cannot be shared publicly due to the privacy of individuals who participated in the study. The data will be shared on reasonable request to the corresponding author.

Patient and public involvement

Patients and/or the public were not involved in the design, conduct, reporting, or dissemination plans of this research.

Supplementary materials

Supplementary material associated with this article can be found, in the online version, at doi:10.1016/j.ard.2026.02.004.

Orcid

Yuki Imai: http://orcid.org/0000-0003-0729-9810
Yuko Kaneko: http://orcid.org/0000-0003-2646-5765

REFERENCES

[1] Smolen JS, Aletaha D, Barton A, Burmester GR, Emery P, Firestein GS, et al. Rheumatoid arthritis. Nat Rev Dis Primers 2018;4:18001. doi: 10.1038/nrdp.2018.1.
[2] Smolen JS, Landewé RBM, Bergstra SA, Kerschbaumer A, Sepriano A, Aletaha D, et al. EULAR recommendations for the management of rheumatoid arthritis with synthetic and biological disease-modifying antirheumatic drugs: 2022 update. Ann Rheum Dis 2022;82:3–18. doi: 10.1136/ard-2022-223356.
[3] Fraenkel L, Bathon JM, England BR, St Clair EW, Arayssi T, Carandang K, et al. 2021 American College of Rheumatology guideline for the treatment of rheumatoid arthritis. Arthritis Rheumatol 2021;73:1108–23. doi: 10.1002/art.41752.
[4] Tanaka Y, Takeuchi T, Mimori T, Saito K, Nawata M, Kameda H, et al. Discontinuation of infliximab after attaining low disease activity in patients with rheumatoid arthritis: RRR (remission induction by Remicade in RA) study. Ann Rheum Dis 2010;69:1286–91. doi: 10.1136/ard.2009.121491.
[5] Tamai H, Ikeda K, Miyamoto T, Taguchi H, Kuo CF, Shin K, et al. Reduced versus maximum tolerated methotrexate dose concomitant with adalimumab in patients with rheumatoid arthritis (MIRACLE): a randomised, open-label, non-inferiority trial. Lancet Rheumatol 2023;5:e215–24. doi: 10.1016/S2665-9913(23)00070-X.
[6] Kaeley GS, Evangelisto AM, Nishio MJ, Goss SL, Liu S, Kalabic J, et al. Methotrexate dosage reduction upon adalimumab initiation: clinical and

ultrasonographic outcomes from the randomized noninferiority MUSICA trial. J Rheumatol 2016;43:1480–9. doi: 10.3899/jrheum.151009.
[7] Smolen JS, Nash P, Durez P, Hall S, Ilivanova E, Irazoque-Palazuelos F, et al. Maintenance, reduction, or withdrawal of etanercept after treatment with etanercept and methotrexate in patients with moderate rheumatoid arthritis (PRESERVE): a randomised controlled trial. Lancet 2013;381:918–29. doi: 10.1016/S0140-6736(12)61811-X.
[8] Curtis JR, Emery P, Karis E, Haraoui B, Bykerk V, Yen PK, et al. Etanercept or methotrexate withdrawal in rheumatoid arthritis patients in sustained remission. Arthritis Rheumatol 2021;73:759–68. doi: 10.1002/art.41589.
[9] Hirata S, Saito K, Kubo S, Fukuyo S, Mizuno Y, Iwata S, et al. Discontinuation of adalimumab after attaining disease activity score 28-erythrocyte sedimentation rate remission in patients with rheumatoid arthritis (HONOR study): an observational study. Arthritis Res Ther 2013;15:R135. doi: 10.1186/ar4315.
[10] Kaneko Y, Kato M, Tanaka Y, Inoo M, Kobayashi-Haraoka H, Amano K, et al. Tocilizumab discontinuation after attaining remission in patients with rheumatoid arthritis who were treated with tocilizumab alone or in combination with methotrexate: results from a prospective randomised controlled study (the second year of the SURPRISE study). Ann Rheum Dis 2018;77:1268–75. doi: 10.1136/annrheumdis-2018-213416.
[11] Edwards CJ, Östör AJK, Naisbett-Groet B, Kiely P. Tapering versus steady-state methotrexate in combination with tocilizumab for rheumatoid arthritis: a randomized, double-blind trial. Rheumatology (Oxford) 2018;57:84–91. doi: 10.1093/rheumatology/kex358.
[12] Emery P, Burmester GR, Bykerk VP, Combe BG, Furst DE, Barré E, et al. Evaluating drug-free remission with abatacept in early rheumatoid arthritis: results from the phase 3b, multicentre, randomised, active-controlled AVERT study of 24 months, with a 12-month, double-blind treatment period. Ann Rheum Dis 2015;74:19–26. doi: 10.1136/annrheumdis-2014-206106.
[13] Takeuchi T. Structural, nonclinical, and clinical features of ozoralizumab: a novel tumour necrosis factor inhibitor. Mod Rheumatol 2023;33:1059–67. doi: 10.1093/mr/road038.
[14] Takeuchi T, Kawanishi M, Nakanishi M, Yamasaki H, Tanaka Y. Phase II/III results of a trial of anti−tumor necrosis factor multivalent NANOBODY compound ozoralizumab in patients with rheumatoid arthritis. Arthritis Rheumatol 2022;74:1776–85. doi: 10.1002/art.42273.
[15] Tanaka Y, Kawanishi M, Nakanishi M, Yamasaki H, Takeuchi T. Efficacy and safety of the anti-TNF multivalent NANOBODY® compound ozoralizumab in patients with rheumatoid arthritis and an inadequate response to methotrexate: a 52-week result of a Phase II/III study (OHZORA trial). Mod Rheumatol 2023;33:883–90. doi: 10.1093/mr/roac119.
[16] Tanaka Y, Kawanishi M, Nakanishi M, Yamasaki H, Takeuchi T. Efficacy and safety of anti-TNF multivalent NANOBODY® compound 'ozoralizumab' without methotrexate co-administration in patients with active rheumatoid arthritis: a 52-week result of phase III, randomised, open-label trial (NATSUZORA trial). Mod Rheumatol 2023;33:875–82. doi: 10.1093/mr/roac126.
[17] Takeuchi T, Chino Y, Kawanishi M, Nakanishi M, Watase H, Mano Y, et al. Efficacy and pharmacokinetics of ozoralizumab, an anti-TNFα NANOBODY® compound, in patients with rheumatoid arthritis: 52-week results from the OHZORA and NATSUZORA trials. Arthritis Res Ther 2023;25:60. doi: 10.1186/s13075-023-03036-4.
[18] Takeuchi T, Nakanishi M, Kawanishi M, Yamasaki H, Tanaka Y. Effect of the extended dosing interval of anti-TNF-α NANOBODY® compound ozoralizumab in patients with low disease activity rheumatoid arthritis. Mod Rheumatol 2024;34:678–85. doi: 10.1093/mr/road097.
[19] Tanaka Y, Miyazaki Y, Kawanishi M, Yamasaki H, Takeuchi T. Long-term safety and efficacy of anti-TNF multivalent VHH antibodies ozoralizumab in patients with rheumatoid arthritis. RMD Open 2024;10:e004480. doi: 10.1136/rmdopen-2024-004480.
[20] Aletaha D, Nell VPK, Stamm T, Uffmann M, Pflugbeil S, Machold K, et al. Acute phase reactants add little to composite disease activity indices for rheumatoid arthritis: validation of a clinical activity score. Arthritis Res Ther 2005;7:R796–806. doi: 10.1186/ar1740.
[21] Smolen JS, Breedveld FC, Schiff MH, Kalden JR, Emery P, Eberl G, et al. A simplified disease activity index for rheumatoid arthritis for use in clinical practice. Rheumatology (Oxford) 2003;42:244–57. doi: 10.1093/rheumatology/keg072.
[22] Wells G, Becker JC, Teng J, Dougados M, Schiff M, Smolen J, et al. Validation of the 28-joint Disease Activity Score (DAS28) and European League Against Rheumatism response criteria based on C-reactive protein against disease progression in patients with rheumatoid arthritis, and comparison with the DAS28 based on erythrocyte sedimentation rate. Ann Rheum Dis 2009;68:954–60. doi: 10.1136/ard.2007.084459.
[23] Prevoo ML, Van't Hof MA, Kuper HH, van Leeuwen MA, van de Putte LB, van Riel PL. Modified disease activity scores that include twenty-eight-joint counts. Development and validation in a prospective longitudinal study of patients with rheumatoid arthritis. Arthritis Rheum 1995;38:44–8. doi: 10.1002/art.1780380107.
[24] Felson DT, Smolen JS, Wells G, Zhang B, van Tuyl LH, Funovits J, et al. American College of Rheumatology/European League Against Rheumatism provisional definition of remission in rheumatoid arthritis for clinical trials. Arthritis Rheum 2011;63:573–86. doi: 10.1002/art.30129.
[25] Felson DT, Smolen JS, Wells G, Zhang B, van Tuyl LH, Funovits J, et al. American College of Rheumatology/European League Against Rheumatism provisional definition of remission in rheumatoid arthritis for clinical trials. Ann Rheum Dis 2011;70:404–13. doi: 10.1136/ard.2011.149765.
[26] Bruce B, Fries JF. The Stanford Health Assessment Questionnaire: a review of its history, issues, progress, and documentation. J Rheumatol 2003;30:167–78.
[27] van der Heijde D. How to read radiographs according to the Sharp/van der Heijde method. J Rheumatol 2000;27:261–3.
[28] Fautrel B, Pham T, Alfaiate T, Gandjbakhch F, Foltz V, Morel J, et al. Step-down strategy of spacing TNF-blocker injections for established rheumatoid arthritis in remission: results of the multicentre non-inferiority randomised open-label controlled trial (STRASS: Spacing of TNF-blocker injections in Rheumatoid ArthritiS Study). Ann Rheum Dis 2016;75:59–67. doi: 10.1136/annrheumdis-2014-206696.
[29] Lillegraven S, Paulshus Sundlisæter N, Aga AB, Sexton J, Olsen IC, Fremstad H, et al. Effect of half-dose vs stable-dose conventional synthetic disease-modifying antirheumatic drugs on disease flares in patients with rheumatoid arthritis in remission: the ARCTIC REWIND randomized clinical trial. JAMA 2021;325:1755–64. doi: 10.1001/jama.2021.4542.
[30] Manders SHM, Van De Laar MAFJ, Rongen-Van Dartel SAA, Bos R, Visser H, Brus HL, et al. Tapering and discontinuation of methotrexate in patients with RA treated with TNF inhibitors: data from the DREAM registry. RMD Open 2015;1:e000147. doi: 10.1136/rmdopen-2015-000147.
[31] Takahashi C, Kaneko Y, Okano Y, Taguchi H, Oshima H, Izumi K, et al. Association of erythrocyte methotrexate-polyglutamate levels with the efficacy and hepatotoxicity of methotrexate in patients with rheumatoid arthritis: a 76-week prospective study. RMD Open 2017;3:e000363. doi: 10.1136/rmdopen-2016-000363.
[32] Brocq O, Millasseau E, Albert C, Grisot C, Flory P, Roux CH, et al. Effect of discontinuing TNFα antagonist therapy in patients with remission of rheumatoid arthritis. Joint Bone Spine 2009;76:350–5. doi: 10.1016/j.jbspin.2008.11.009.

Ann Rheum Dis 85 (2026) 620–629

Contents lists available at ScienceDirect

Annals of the Rheumatic Diseases

journal homepage: https://www.sciencedirect.com/journal/annals-of-the-rheumatic-diseases

Rheumatoid arthritis

Development and validation of a model to predict the disease activity score: towards a remote treat-to-target approach for rheumatoid arthritis

Agnes E. M. Looijen[1,*], Paco M. J. Welsing[2], Sytske Anne Bergstra[3], Annette H. M. van der Helm-van Mil[1,3], Pascal H. P. de Jong[1]

[1] *Department of Rheumatology, Erasmus MC, Rotterdam, The Netherlands*
[2] *Department of Rheumatology & Clinical Immunology, University Medical Centre Utrecht, Utrecht, The Netherlands*
[3] *Department of Rheumatology, Leiden University Medical Center, Leiden, The Netherlands*

ARTICLE INFO

Article history:
Received 30 September 2025
Received in revised form 17 November 2025
Accepted 22 November 2025

ABSTRACT

Objectives: Remote monitoring of disease activity in patients with rheumatoid arthritis (RA) offers a promising solution to increasing healthcare demands. This study aimed to develop and validate a model using selected clinical and patient-reported outcome measure (PROM) items that efficiently and accurately reflect the original disease activity score (DAS).

Methods: Data from 5802 visits of 612 patients with RA from the treatment in the Rotterdam Early Arthritis Cohort and TApering strategies in RA trials were randomly split (1:1) into derivation and internal validation sets. An external validation was performed using 4404 visits from 1554 patients with RA from the Early Arthritis Cohort. A model was developed using Least Absolute Shrinkage and Selection Operator (LASSO) regression that incorporated age, sex, disease duration, autoantibody status, and individual PROM items, including visual analogue scale (VAS) general health, all Health Assessment Questionnaire-Disability Index (HAQ-DI) items, VAS pain, and VAS fatigue, to predict the DAS. The model's ability to detect active disease (DAS >2.4) and remission (DAS <1.6) was evaluated using the area under the receiver operating characteristic curve (AUC-ROC), along with sensitivity and specificity across predefined thresholds.

Results: The final model included 12 out of 28 predictors: age, sex, disease duration, VAS general health, 7 HAQ-DI items, and VAS pain. It showed excellent discriminative ability for detecting active disease with AUC-ROC values of 0.89 in both the development and internal validation sets, and 0.82 in the external validation set. For detecting remission, the AUC-ROC values were 0.86, 0.85, and 0.82, respectively. Test characteristics were provided for different thresholds.

Conclusions: The proposed DAS intended for digital remote assessment combines clinical and PROM items and can accurately and efficiently distinguish between disease activity states in RA, supporting its potential use in remote monitoring in the future.

*Correspondence to Agnes E. M. Looijen, Department of Rheumatology, Erasmus MC, Rotterdam, The Netherlands.
E-mail address: a.e.m.looijen@erasmusmc.nl (A.E.M. Looijen).
Handling editor Josef S. Smolen.

https://doi.org/10.1016/j.ard.2025.11.019

WHAT IS ALREADY KNOWN ON THIS TOPIC

- With rising demands on our healthcare system, remote monitoring can help sustain the quality of rheumatologic care by facilitating home-based detection of active disease and remission, which is essential for the recommended treat-to-target approach.
- The use of patient-reported outcome measures (PROMs) could help facilitate remote monitoring.
- However, current PROMs do not optimally align with the disease activity score, highlighting the need for improvement before they can be used to facilitate remote monitoring.

WHAT THIS STUDY ADDS

- A combination of age, sex, disease duration, visual analogue scale (VAS) general health, 7 Health Assessment Questionnaire-Disability Index items, and VAS pain can adequately differentiate between well-controlled and active disease with excellent diagnostic accuracy in an independent real-world cohort.

HOW THIS STUDY MIGHT AFFECT RESEARCH, PRACTICE OR POLICY

- The digital disease activity score (digital DAS) combines 9 individual PROM items, thereby reducing questionnaire burden, which is sufficient for effectively detecting active disease and remission according to the DAS.
- These results may facilitate remote monitoring of patients with rheumatoid arthritis and aid in maintaining the quality of rheumatic care in the future.

INTRODUCTION

Current guidelines for rheumatoid arthritis (RA) recommend a treat-to-target (T2T) approach, which involves modifying treatment until remission or low disease activity (LDA) is achieved [1–3]. Moreover, if patients are in sustained remission, tapering of treatment can be considered [2,3]. For a T2T approach, it is essential to monitor disease activity using validated disease activity indices such as the disease activity score (DAS), which necessitates a physical examination. These assessments are recommended every 1-6 months depending on the disease activity level [1]. However, regular in-clinic assessments are increasingly challenging due to the growing demands on our healthcare system [4,5]. For example, previous literature showed that only 34% of patients with RA with active disease were assessed within the recommended 3-month timeframe [2,4,6]. Therefore, alternative methods to assess disease activity are necessary to uphold the quality of rheumatic care [5,7].

One option is remote monitoring using patient-reported outcome measures (PROMs) [4,5]. PROM usage is already recommended for daily practice as they help quantify disease impact [8–10]. When PROMs are used as a screening tool to identify disease activity, they may also help reduce the number of outpatient clinic visits [4,5]. Several studies have examined the use of PROMs to monitor disease activity, including PRO-CLinical ARthritis Activity (PRO-CLARA) and routine assessment of patient index data 3 (RAPID3), which are also recommended by the American College of Rheumatology for use in daily practice [11–14]. Although informative during clinic visits, their ability to accurately align with DAS scores remains moderate as the reported Spearman correlation coefficients between the DAS28-erythrocyte sedimentation rate (ESR) and the PRO-CLARA and RAPID3 were 0.57 and 0.66, respectively [15]. A combination of multiple dichotomised PROMs resulted in a moderate diagnostic accuracy (area under the receiver operating characteristic curve [AUC-ROC] of 0.76) for detecting active disease [16]. However, total PROM questionnaires may contain items unrelated to disease activity, limiting their discriminative ability. From the patient's perspective, answering a large number of questions can be burdensome and may negatively affect compliance [17]. Moreover, the aforementioned model lacks external validation, which is crucial for assessing its generalisability and clinical applicability.

Therefore, we aimed to identify and validate a subset of clinical and independent PROM items that most effectively reflect the DAS, enabling efficient and accurate discrimination between disease activity states in RA. This could be a step towards remote monitoring of RA.

METHODS

Patients and study data

For model development and internal validation, we included patients who participated in the 'treatment in the Rotterdam Early Arthritis Cohort' trial (tREACH, ISRCTN26791028) and the 'TApering strategies in Rheumatoid Arthritis' trial' (TARA, NTR2754). For external validation of the model, patients from the 'Early Arthritis Cohort' (EAC) were included. All study protocols were approved by ethics committees at each participating centre, and all patients provided written informed consent before inclusion in accordance with the Declaration of Helsinki.

The tREACH trial was a single-blinded randomised controlled trial (RCT) conducted across 8 rheumatology centres in the Netherlands. Patients were recruited between July 2007 and April 2011. Disease-modifying antirheumatic drug (DMARD)-naïve early undifferentiated arthritis and patients with RA, who had arthritis in ≥1 joint(s) and a symptom duration of <1 year, were included. RA diagnosis was based on fulfilment of the 1987 or 2010 classification criteria [18,19]. The trial compared multiple initial treatment strategies and had a T2T management approach that aimed for LDA, defined as a DAS ≤2.4. Treatment was intensified until LDA was achieved and tapered if patients were in sustained remission, defined as a DAS <1.6 at 2 consecutive visits. If a flare occurred, defined as a DAS >2.4, full treatment was restarted according to the stage of the protocol. Visits occurred every 3 months for 3 years and thereafter annually up to 5 years. More information on the tREACH trial can be found elsewhere [20,21].

The TARA trial was a single-blinded RCT conducted across 12 rheumatology centres in the Netherlands. Patients were included between September 2011 and July 2016. RA-patients with well-controlled disease, defined as a DAS ≤2.4 and swollen joint count (SJC) ≤1 at 2 consecutive visits, who used both ≥1 conventional synthetic (cs)DMARDs and a tumour necrosis factor (TNF) inhibitor, were included. RA diagnosis was based on fulfilment of the 1987 or 2010 classification criteria [18,19]. The trial compared 2 tapering strategies: tapering csDMARDs in year 1 followed by TNF-inhibitors in year 2, or vice versa. If a disease flare occurred, defined as DAS >2.4 or SJC >1, the last effective treatment was restarted and intensified until well-controlled disease was re-established. Patients were followed for 2 years, with scheduled visits occurring every 3 months. Extensive information on the TARA trial can be found elsewhere [22].

The EAC is an ongoing population-based inception cohort in Leiden, The Netherlands. In the EAC, consecutive patients with recent-onset arthritis (symptom duration <2 years) have been

included since 1993. RA diagnosis was based on fulfilment of the 1987 or 2010 classification criteria [18,19]. Treatment of included patients follows current (inter)national guidelines and is determined by the treating rheumatologist. Follow-up visits take place biannually in the first year and annually thereafter. Further details on the EAC are available elsewhere [23]. For this study, only patients with RA enrolled from January 2006 onwards were included as they were treated according to the currently recommended T2T principles [24]. The most recent dataset entry is from October 2023.

Included data for this analysis

In all cohorts, the DAS and its components were collected at each visit by a trained research nurse. PROMs were completed at home using paper or digital questionnaires before the scheduled appointment. For model development and internal validation, we included patients from the tREACH and TARA cohorts who met the 1987 or 2010 RA criteria and had ≥1 variable of interest and a concurrent DAS measurement. For external validation, all EAC visits meeting the RA criteria were included if all variables of the developed model, as well as the DAS, were available at the same visit. Due to the scope of the initial study cohorts, measurements of the outcome and predictors were not blinded from each other.

Outcome variable—disease activity

Disease activity was assessed with the DAS that includes a 44-SJC, a tender joint count measured with the Ritchie Articular Index in 53 joints, ESR, and general health (visual analogue scale [VAS], 0-100 mm) or patient global assessment (PGA) (VAS, 0-100 mm) [25].

Patient characteristics and clinical outcomes

At baseline, sex, age, symptom duration, disease duration, anticitrullinated protein antibody (ACPA), and rheumatoid factor (RF) status were documented. C-reactive protein and ESR were measured at each visit. Sex, age, disease duration, and autoantibody status (ACPA and RF) were included as explanatory variables in our analyses because evidence suggests that these variables may influence disease activity in patients with RA [26–29].

PROMs

For our analyses, we selected PROMs that (i) aligned with the International Consortium for Health Outcome Measurement (ICHOM)–recommended domains, (ii) were available in the tREACH, TARA, and EAC cohorts, and (iii) were applicable to all patients, excluding, eg, work-related questionnaires [10]. Based on the aforementioned criteria, the following PROMs were selected: general health/PGA, Health Assessment Questionnaire-Disability Index (HAQ-DI), pain, and fatigue. Table 1 shows the collected PROMs per ICHOM outcome domain and cohort [10].

General health/PGA (VAS, 0-100 mm) was included as a PROM to capture the disease activity component as well as the health impact domain. Higher scores indicate a poorer perceived general health. Activity limitation was measured with the HAQ-DI, with a total score ranging from 0 to 3, and higher scores indicating more functional impairment [30–32]. Pain was measured with a numeric rating scale (NRS, 0-10) in the tREACH and TARA trial, whereas in the EAC, a VAS (0-100 mm) was used. Higher scores indicate greater pain severity. Lastly, fatigue was measured using a VAS (0-100 mm) in the tREACH and EAC. In the TARA, an NRS (0-10) was used. Higher scores represent more severe fatigue [33]. For comparability, all NRS were transformed to a 0 to 100 scale.

Statistical analysis

To account for differences in RA stage (early vs established RA), baseline DAS, and treatment protocols between the tREACH (n = 425) and TARA (n = 187) cohorts, all visits from both cohorts were merged into 1 dataset and thereafter randomly split (1:1) into development and internal validation sets. This ensured a balanced representation of early and established RA visits with an equal range in disease activity levels across both sets. It also accounted for patients who participated in both the tREACH and, thereafter, the TARA trial. Visits from the included patients with EAC (n = 1554) served as an external validation set.

Model development

A 'Least Absolute Shrinkage and Selection Operator' (LASSO) regression was used to develop the DAS intended for digital remote assessment (digital DAS hereafter). LASSO selects the most relevant variables from a set of potential predictor variables and thereby decreases overfitting, resulting in a more generalisable model. Potential predictors to estimate the DAS included age, sex, disease duration, ACPA, RF, and all individual PROM items from the following questionnaires: VAS general health/PGA (1 item), HAQ-DI (20 items), VAS pain (1 item), and VAS fatigue (1 item). For this analysis, the use of aids or help from others was not considered for individual HAQ-DI items. All items were treated as linear continuous variables to maintain an evenly distributed weight between different levels within 1 item. Age and disease duration were defined at the time of visit. ACPA and RF status were assessed at baseline and were then carried forward to subsequent visits. If general health or PGA values were missing in the tREACH or TARA datasets, the 3-item DAS was used to impute the DAS. This occurred in 46 of 5802 RA visits. Missing predictors were not imputed, and the final model included only visits with complete data for all selected variables.

Several methods for selecting λ were evaluated for goodness of fit, including cross-validation (CV), adaptive lasso–which

Table 1
PROMs per ICHOM-recommended outcome domain and cohort

Outcome domains [10]	tREACH	TARA	EAC
Disease activity component and health impact	VAS general health, 0-100 mm	VAS PGA,0-100 mm	VAS general health, 0-100 mm
Activity limitations	HAQ-DI	HAQ-DI	HAQ-DI
Pain	NRS, 0-10	NRS, 0-10	VAS, 0-100 mm
Fatigue	VAS, 0-100 mm	NRS, 0-10	VAS, 0-100 mm

EAC, Early Arthritis Cohort; HAQ-DI, Health Assessment Questionnaire-Disability Index; ICHOM, International Consortium for Health Outcome Measurement; NRS, numeric rating scale; PGA, patient global assessment of disease activity; PROM, patient-reported outcome measure; TARA, TApering strategies in Rheumatoid Arthritis; tREACH, treatment in the Rotterdam Early Arthritis Cohort; VAS, visual analogue scale.

iteratively applies lasso with CV, removing variables with zero coefficients and reweighting the remaining ones in each step—and selection of λ based on the Bayesian Information Criterion (BIC) [34]. The BIC method was chosen for its optimal balance of model simplicity, lowest mean squared error, and highest R-squared. The selected items and their penalised coefficients were combined into the digital DAS as follows:

$$digital\ DAS = \beta_0 + \beta_1 \cdot item_1 + \beta_2 \cdot item_2 + \beta_3 \cdot item_3 + \ldots \beta_n \cdot item_n$$

Model fit evaluation and recalibration

Agreement between the digital DAS and DAS was evaluated using Bland-Altman plots [35,36]. Model calibration was evaluated by comparing the predicted probabilities for active disease (DAS >2.4) and remission (DAS <1.6) against the actual outcome (active disease or remission) [37,38]. Calibration plots were generated using logistic regression with an intercept of 0 and an offset coefficient for the digital DAS score as a predictive variable. Based on the calibration plot of active disease, the model was recalibrated using a regression-derived intercept and coefficient. The recalibrated digital DAS was re-evaluated in the development set using Bland-Altman and calibration plots.

Evaluation of discriminative ability

The digital DAS was evaluated for its ability to discriminate between well-controlled disease vs active disease and remission vs no remission using the AUC-ROC [38]. An AUC-ROC of 0.5 to 0.6 indicates no discriminative ability, 0.6 to 0.7 is considered poor, 0.7 to 0.8 is acceptable, 0.8 to 0.9 is excellent, and an AUC-ROC greater than 0.9 is considered outstanding [39,40]. Additionally, sensitivity and specificity were evaluated using thresholds based upon (i) the Youden index, which balances the sensitivity and specificity; and (ii-iii) 95% sensitivity and specificity in the development set. To identify misclassification patterns, patient characteristics of the external validation visits were shown for each cell of the confusion matrix (ie, correct and misclassified visits), stratified for the aforementioned thresholds.

Sensitivity analysis

A sensitivity analysis was conducted to compare the performance of the digital DAS with an alternative model that incorporated its complete PROM scores. This alternative model, referred to as the 'full digital DAS', included the total scores of each PROM selected in the digital DAS instead of the individual items. For instance, if multiple individual items from the HAQ-DI were selected, the overall HAQ-DI score was used in the full digital DAS as 1 single predictor. In the full digital DAS, the PROM scores—along with other selected clinical variables such as age and sex—were included as explanatory variables in a ridge regression model to estimate the DAS. The resulting penalised coefficients and variables were combined into a single formula. The evaluation of the model fit, recalibration, and assessment of the discriminative ability was done in the same manner as the main analysis.

RESULTS

Patient characteristics

The patient selection flowchart and baseline characteristics of the initial cohorts are shown in Supplementary Figure S1 and Supplementary Table S1, respectively. Patient characteristics of the visits used in the development, internal, and external validation sets are shown in Table 2. The development set included 2901 visits, and active disease was present in 564 (19%) of these visits. The median (IQR) disease duration was 2.0 (0.8-4) years, and the mean DAS (SD) was 1.6 (1.0). In 59% of the visits, ACPA was present, whereas RF was present in 57% of them.

The internal validation set included 2901 visits, and active disease was present in 576 (20%) of these visits. The median (IQR) disease duration was 1.8 (0.8-4.0) years. The mean DAS (SD) was 1.7 (1.0). In 58% and 59% of the visits, ACPA and/or RF were present, respectively.

The external validation set included 4404 visits. Active disease was present in 1599 (36%) of these visits. The median (IQR) disease duration was 2.0 (0.3-5.0) years, and mean (SD) DAS was 2.0 (1.3). ACPA and patients with RF positive were evaluated in 46% and 45% of the visits, respectively.

Model development, evaluation, and recalibration

The number of missing values in the development and internal validation set varied from no missingness to 27% of missing values (Supplementary Table S2). Ranges of the items were comparable between all 3 datasets (Supplementary Table S2). The selected model included 12 of the 28 items: age, sex, disease

Table 2
Characteristics at the visits of the development, internal, and external validation sets

Patient characteristics	Development (2901 visits)		Internal validation (2901 visits)		External validation (4404 visits)	
Sex, female, visits (%)	1914	(67)	1888	(65)	2735	(62)
Age (y), mean (SD)	56	(13)	56	(14)	60	(14)
ACPA positive,[a] visits (%)	1712	(59)	1695	(58)	1970	(46)
RF positive,[a] visits (%)	1667	(57)	1710	(59)	792	(45)
Disease duration (y)	2.0	(0.8-4.0)	1.8	(0.8-4.0)	2.0	(0.3-5.0)
DAS, mean (SD)	1.6	(1.0)	1.7	(1.0)	2.0	(1.3)
44 swollen joint count	0	(0-2)	0	(0-2)	0	(0-3)
53 tender joint count	1	(0-4)	1	(0-4)	2	(0-7)
ESR (mm/h)	11	(5-20)	11	(5-20)	11	(6-28)
CRP (mg/L)	4	(1-9)	4	(1-8)	3	(3-8)
VAS general health/PGA (0-100 mm)	23	(10-42)	23	(10-43)	30	(20-50)

ACPA, anticitrullinated protein antibody; CRP, C-reactive protein; DAS, disease activity score (measured in 44 joints); ESR, erythrocyte sedimentation rate; PGA, patient global assessment; RF, rheumatoid factor; VAS, visual analogue scale.
One patient can have multiple visits that are randomly split across the development and internal validation sets. This table shows the patient characteristics at the visits per set. Baseline characteristics of each initial cohort are shown in Supplementary Table S1. All results are presented as medians (IQR) unless indicated otherwise.
[a] Measured at baseline.

Table 3
Selected items and penalised coefficients for the digital DAS, before and after recalibration

Variable	Weight	Recalibrated weight
Age (y)[a]	0.002	0.006
Sex (male = 0, female = 1)	0.116	0.335
Diagnosis duration (y)[a]	−0.054	−0.155
VAS general health/patient global assessment (0-100 mm)	0.018	0.053
VAS pain (0-100 mm)	0.005	0.015
HAQ-DI rising: ability to get in and out of bed (0-3)	0.065	0.188
HAQ-DI eating: ability to cut your meat (0-3)	0.035	0.102
HAQ-DI eating: ability to open a new carton of milk (0-3)	0.017	0.049
HAQ-DI walking: ability to climb up 5 stairs (0-3)	0.007	0.021
HAQ-DI reach: ability to reach and get down a 5-lb object (0-3)	0.034	0.098
HAQ-DI grip: ability to open jars which have been previously opened (0-3)	0.056	0.160
HAQ-DI grip: ability to turn taps on and off (0-3)	0.017	0.048
Constant	0.814	−4.480

HAQ-DI, Health Assessment Questionnaire-Disability Index; digital DAS, disease activity score intended for digital remote assessment; VAS, visual analogue scale.
[a] Diagnosis duration and age were defined at the time of the visit.

duration, VAS general health/PGA, 7 HAQ-DI items, and VAS pain. Table 3 shows the selected items with their penalised coefficients. The selected HAQ-DI items covered the following categories: rising, eating, walking, reach, and grip.

After recalibration, the mean difference (95% limits of agreement) between the digital DAS and DAS was 3.8 (1.2, 6.4). In general, the DAS is higher compared to the digital DAS across all values (Supplementary Fig S2). The recalibrated model showed a good calibration for active disease, and moderate calibration for remission, with an overestimation of patients in remission (DAS <1.6, Supplementary Fig S3).

Discriminative ability

Across all datasets, the model demonstrated excellent discriminative ability in distinguishing between well-controlled vs active disease and remission vs no remission (Fig 1). In the development set, the AUC-ROC was 0.89 for well-controlled vs active disease and 0.86 for remission vs no remission. These findings were consistent in the internal validation set, with AUC-ROCs of 0.89 and 0.85, respectively. In the external validation set, the model maintained excellent discriminative ability, achieving an AUC-ROC of 0.82 for both comparisons.

Thresholds

Different thresholds can be chosen, depending on whether a sensitive or specific measure would be preferred, or a balance herein. To investigate the effect of different thresholds on sensitivity and specificity, 3 thresholds were determined based on data from the development set: (i) the Youden index, which equally balances sensitivity and specificity; and (ii-iii) thresholds achieving 95% sensitivity and specificity, respectively. As shown in Figure 2, the sensitivity and specificity of all 3 thresholds are highest in the development set and show a slight decline when the same thresholds are applied in the internal and external

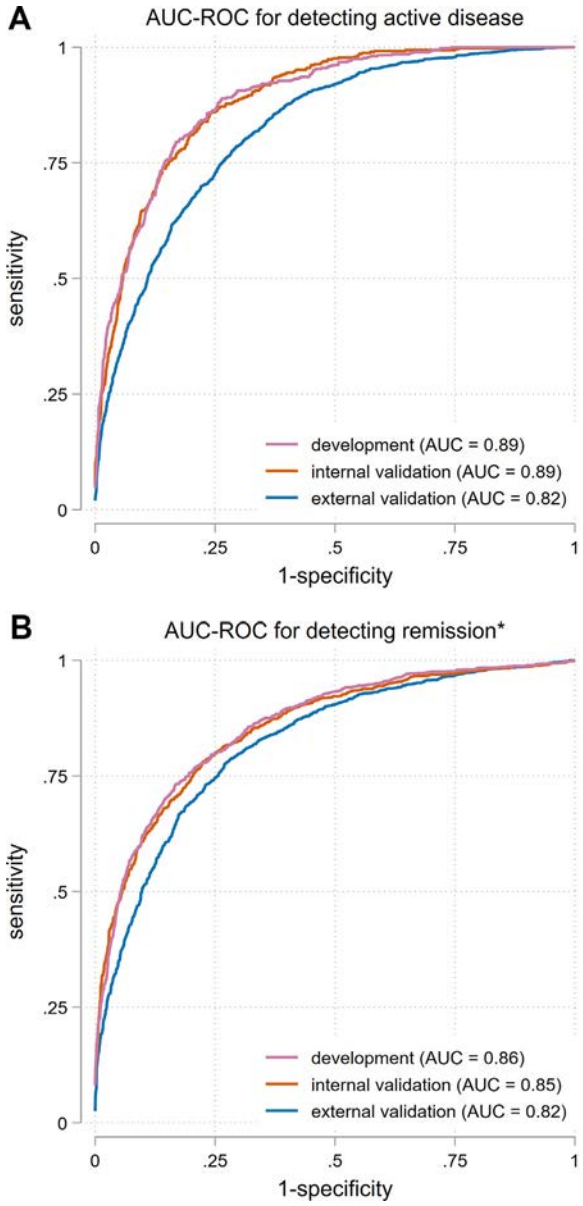

Figure 1. Receiver operating characteristic curve for detecting active disease (A) and remission (B) in the development, internal, and external validation set. *The graph shows the ability of the digital DAS to differentiate between a DAS <1.6 and ≥1.6. AUC, area under the curve; AUC-ROC, area under the receiver operating characteristic curve; DAS, disease activity score; digital DAS, disease activity score intended for digital remote assessment.

validation sets. Using the Youden index (threshold ≥ −1.27), the external validation yields a sensitivity of 66% and specificity of 81% for detecting active disease (Fig 2A). When applying the threshold that achieves 95% sensitivity (≥ −2.77) in the development set, then the sensitivity and specificity in the external validation set are 91% and 51%, respectively. Conversely, the threshold optimised for 95% specificity (≥0.15) yields 34% sensitivity and 95% specificity in the external validation set. The same interpretation can be applied for remission (Fig 2B).

Remote monitoring is useful when it leads to a substantial reduction in patient visits, whereas patients with active disease are not overlooked. In practice, the number of patients with active and well-controlled disease can vary, which can impact the benefit of the digital DAS. To illustrate this, we evaluated the correct and incorrect classifications in the real-world cohort (external validation cohort). As shown in Figure 3A, in 36% of

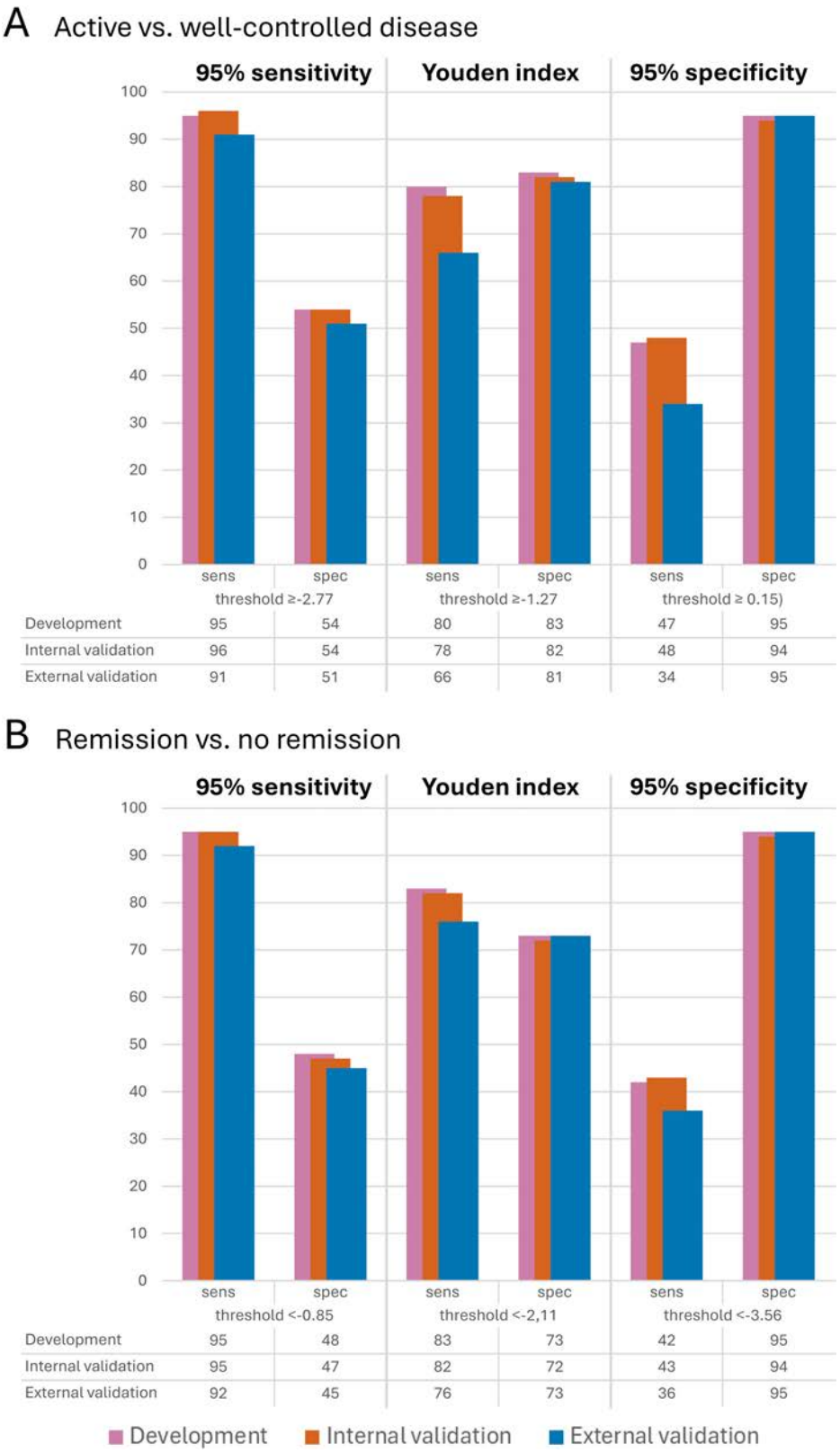

Figure 2. Sensitivity and specificity for different thresholds of the digital DAS in the development, internal, and external validation set for active disease (A) and remission (B). The thresholds are determined in the development set and are thereafter applied to all 3 datasets. Digital DAS, disease activity score intended for digital remote assessment.

the visits, patients had active disease. Using the Youden index (≥ −1.27), 24% of visits were correctly classified as active disease, 12% actually had active disease and were misclassified as well-controlled disease, 12% actually had well-controlled disease and were misclassified as active disease, and 51% were correctly classified as well-controlled disease. The same was done applying a 95%-sensitivity threshold (≥ −2.77). In this case, 33% of the visits were correctly identified as active disease, only 3% of visits with active disease were misclassified as well-controlled disease, 31% of the visits were false positives, and 33% of the visits were correctly classified as well-controlled disease. Conversely, using a 95%-specificity threshold (≥0.15) resulted in 60% of visits being correctly classified as well-controlled disease, but 24% of active disease visits were missed. For remission,

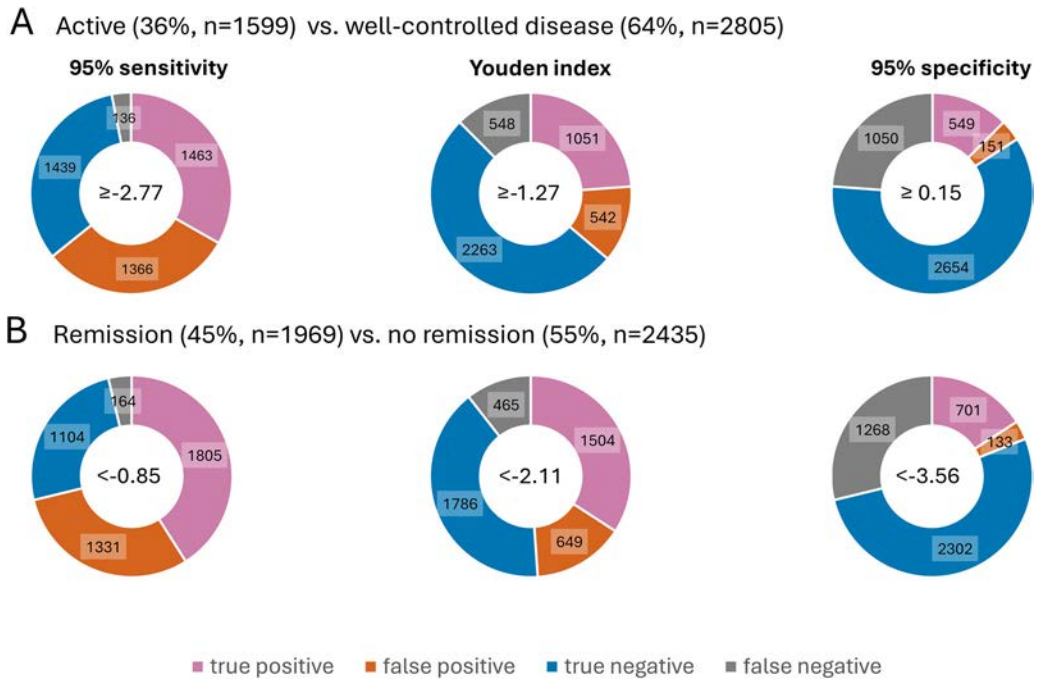

Figure 3. Distribution of visits in the external validation set across each cell of the confusion matrix based on the predefined thresholds for active disease (A) and remission (B). The figure shows the number of visits in the external validation set, classified by the model as follows: (i) correctly identified as active disease (A) or remission (B)—true positives (pink); (ii) incorrectly identified as active disease (A) or remission (B)—false positives (orange); (iii) correctly identified as well-controlled disease (A) or no remission (B)—true negatives (blue); or (iv) incorrectly identified as well-controlled disease (A) or no remission (B)—false negatives (grey).

the same interpretation applies, and its classification distribution is illustrated in Figure 3B.

Thus, inherent to the chosen threshold, choosing a sensitive definition results in very few visits with active disease that were missed, but at the cost of more false positives (patients with well-controlled disease that were identified as having active disease). The opposite was the case when choosing a very specific threshold. When using the Youden index as threshold, the percentage of visits with false-positive and false-negative DAS classifications was balanced (both 12%).

Characteristics of the visits per (mis)classification

To better understand the consequences of misclassifications, we studied the patient characteristics of the correct and misclassified visits. Supplementary Table S3 provides the patient characteristics for true-positive, true-negative, false-positive, and false-negative visits. In general, misclassified patients show a discordance of their VAS general health/PGA with their SJC and ESR. For example, in the case of active disease, patients with a false-negative test result had a lower VAS general health/PGA compared to the true positives, whereas no strong differences in SJC or ESR were observed between true positives and false negatives. Conversely, patients with a false-positive test result had a higher VAS general health/PGA compared to the true negatives, with no big observed differences in SJC or ESR between both groups. Thus, digital DAS misclassifications were often explained by discordance within the DAS between patient-reported components such as VAS general health/PGA and the more inflammation-based components, such as SJC and ESR.

Sensitivity analysis

A sensitivity analysis was conducted to evaluate the difference between a model composed of full PROM scores using a total of 27 individual items compared to the digital DAS using 12 individual items. Supplementary Table S4 and Supplementary Figs S4 and S5 show the coefficients, model fit and calibration plots of the full digital DAS. The ability to discriminate between well-controlled disease and active disease was similar for the full digital DAS compared to the digital DAS (AUC-ROC 0.84 vs 0.82 in the external validation set, Supplementary Fig S6A). Similar results were also found for remission vs no remission (AUC-ROC 0.84 vs 0.82 in the external validation set, Supplementary Fig S6B). Supplementary Figure S7 shows the sensitivity and specificity across different thresholds.

DISCUSSION

As demands on our healthcare system continue to rise, the implementation of remote monitoring using PROMs could help sustain the quality of our rheumatic care, including its T2T approach. Therefore, we assessed whether a model based on several clinical characteristics and selected PROM items could accurately reflect the DAS and its disease activity states in RA. Using LASSO regression, 12 of 28 possible explanatory items were combined. This resulted in a proposed DAS intended for digital remote assessment (digital DAS), which showed excellent discriminative ability with an externally validated AUC-ROC of 0.82 for both active disease and remission. Sensitivity and specificity varied depending on predefined thresholds. These results could be a step towards efficient remote monitoring with PROMs.

We have not chosen 1 specific threshold, allowing potential users to select thresholds based on their preference for high sensitivity, high specificity, or a balanced trade-off between the 2. To demonstrate the impact of these choices, we evaluated true and false classifications within a real-world RA cohort, where 36% of the visits entailed active disease and 64% well-controlled disease. A high-sensitivity threshold correctly identified 91% of

these active disease visits. Additionally, 51% of visits with well-controlled disease were correctly classified as such. If remote monitoring was used to reduce the need for patients with well-controlled disease to come to the rheumatology clinic, these patients could skip their physical outpatient visit. In our real-world cohort, this would result in a reduction of 36% of visits. A threshold with a balance between sensitivity and specificity correctly specified 66% of visits with active disease and enabled a 63% reduction in total visits. A high-specificity threshold correctly identified only 34% of active disease visits, but allowed for an 84% reduction in total visits.

The choice of threshold not only affects the number of correctly classified active or well-controlled patients but also results in a different percentage of patients with active disease being missed or patients with well-controlled disease being classified as active. For example, although a high-sensitivity threshold misclassifies only 9% of active disease visits, a balanced or high-specificity threshold misses 34% and 66%, respectively. Patients who were misclassified by the digital DAS often had a discordance between patient-reported components of the DAS (eg, general health/PGA) and more inflammatory-based components (eg, SJC and ESR). This indicates a misalignment in patients' perceived disease burden and inflammatory activity. To reduce this misalignment, the model could be extended with other home measurements that are a proxy for joint inflammation, such as hand function or finger fold measurements [41,42]. It is also worth noting that the identification of patients with a high disease burden, even without objective inflammatory activity, may not be undesirable, as these individuals still require additional care. This is consistent with the proposed dual T2T strategy in which both disease activity and disease impact are addressed [9].

In addition to diagnostic accuracy, the burden on patients to complete questionnaires is an important consideration when implementing models for remote monitoring. Therefore, we aimed to develop a parsimonious model using as few PROM items as possible. The proposed digital DAS, which integrates 9 PROM items with 3 clinical variables (not patient reported), demonstrated comparable performance to a model using the full PROM scores, which used 24 PROM items. This substantial reduction in items contributes to a more user-friendly and feasible tool for clinical applicability.

Alongside diagnostic accuracy and lowering questionnaire burden, several other factors should be considered when implementing a PROM-based measure for remote monitoring, including health literacy and compliance to complete the questionnaires. [17]. Additionally, some patients may still prefer the traditional outpatient clinic visits. Nevertheless, remote monitoring has the potential and flexibility to accommodate and facilitate patients' health care needs, as it may lead to a significant reduction in the frequency of outpatient clinical visits for the entire RA population.

This is not the first publication on remote monitoring using PROMs. However, the here developed digital DAS outperformed our earlier model in distinguishing well-controlled from active disease in RA (AUC-ROC = 0.76) [16]. Compared to the RAPID3, the digital DAS had a similar AUC-ROC and sensitivity (AUC-ROC = 0.80 and sensitivity = 93% vs AUC-ROC = 0.82 and sensitivity = 91%, respectively), but the digital DAS has a higher specificity (39% vs 51%) [43]. As the prevalence of active disease is generally lower due to improved treatment strategies, the increase in specificity will significantly reduce the number of outpatient clinic visits, whereas most patients with active disease are detected [44].

Other questionnaires, such as the Rheumatoid Arthritis Flare Questionnaire, also have a good discriminative ability for detecting disease flares [45]. However, these questionnaires are based on a different flare definition, which integrates aspects from both the physician's and patient's point of view [45,46]. In contrast, the digital DAS aligns with DAS-defined disease states commonly used in daily practice. Thus, the digital DAS serves a different purpose in comparison to the aforementioned tools.

The strengths of our study include the inclusion of both patients with early and established RA from 2 RCTs, with a protocolised T2T management approach, for model development and internal validation. Additionally, a real-world, independent cohort was used for external validation, further enhancing the robustness and applicability of our findings. All 3 datasets also included a large sample size of patients and visits.

There are also several issues that warrant consideration. Although the digital DAS showed strong discriminative ability across disease activity states, it initially overestimated scores at low DAS levels and underestimated them at higher DAS levels Supplementary Fig S1A. Overestimation could be caused by a higher perceived disease burden without objective inflammation or lasting functional impairment due to joint damage [47]. Underestimation at higher DAS levels may be caused by a disbalance in active vs nonactive disease visits in the development set. Recalibration improved the predicted probability of active disease, but led to an overestimation of predicted probability at lower DAS levels, limiting optimal prediction of remission probability. This trade-off was considered acceptable given the clinical priority of detecting active disease.

It should also be noted that PROMs may be sensitive to the time period in which they are completed. Additionally, PROMs, such as the HAQ-DI, were not designed for single item-level extraction or for application in contemporary remote monitoring settings, but rather primarily for scientific research purposes. This may limit the model's applicability in current patient populations. To mitigate this limitation, we prioritised the inclusion of patients who were treated according to the currently recommended T2T approach and had early as well as established disease to ensure that the model remains as representative as possible, despite the temporal gap of the study population.

Lastly, minor cohort differences, such as different HAQ-DI versions and use of VAS general health or VAS PGA, may have affected model performance. Nonetheless, the digital DAS maintained excellent discriminative ability during external validation, affirming its robustness and potential applicability in broader settings.

Future research should focus on investigating other measurement properties, such as responsiveness over time within 1 individual [48]. The model should also be tested in a fully remote setting using 1 universal set of questions to confirm that its discriminative ability remains intact in this environment. Additionally, updating the model with more modern questions, along with incorporating variables that specifically reflect joint inflammation, could further improve the model.

In conclusion, the digital DAS, incorporating age, sex, disease duration, VAS general health/PGA, 7 HAQ-DI items, and VAS pain, showed excellent diagnostic accuracy in identifying active disease and remission, even after external validation in an independent, real-world cohort. Although further validation and optimisation are preferred in future research, these findings support its potential for efficient remote monitoring of patients with RA.

Statements

The manuscript was prepared following the Transparent Reporting of a multivariable prediction model for Individual Prognosis or Diagnosis (TRIPOD) statement [49,50] (see also Supplementary Table S5 for the completed checklist).

Acknowledgements

We gratefully thank all participating patients, rheumatologists, and research nurses.

Contributors

AEML performed the statistical analysis and drafted the first version of the manuscript. PMJW and PHPdJ contributed to the analysis. SAB supplied the EAC data. All authors contributed to the design, revised the manuscript, and read and approved the final manuscript. PHPdJ is the guarantor.

Funding

This study was supported by an unrestricted grant from ZonMW (grant number 1711 + 02014), Pfizer (grant number WI229707) and AbbVie B.V. (grant number SA-003854).

Competing interests

SAB received an ASPIRE grant from Pfizer and speaker fees from Benecke and reports a relationship with Leiden University Medical Center that includes funding grants and speaking and lecture fees. The other authors have declared no conflicts of interest.

Patient consent for publication

Not applicable.

Ethics approval

Written informed consent was obtained from all participants according to the Declaration of Helsinki. The tREACH and TARA studies were approved by the ethics committee of the Erasmus MC (MEC-2006-252 for tREACH and MEC-2011-141 for TARA). The EAC was approved by the Local Medical Ethics Committee, named 'Commissie Medische Ethiek' (B19.008).

Provenance and peer review

Not commissioned; externally peer reviewed.

Patient and public involvement

Patients and/or the public were involved in the design and conduct of this research.

Data availability statement

The data underlying this article will be shared on reasonable request to the corresponding author.

Declaration of generative AI and AI-assisted technologies in the manuscript preparation process

During the preparation of this work the first author used Microsoft Copilot in order to assist with spelling, punctuation, and grammar. After using this tool, the authors reviewed and edited the content as needed and take full responsibility for the content of the published article.

Supplementary materials

Supplementary material associated with this article can be found in the online version at doi:10.1016/j.ard.2025.11.019.

Orcid

Agnes E. M. Looijen: http://orcid.org/0000-0002-5280-2182
Paco M. J. Welsing: http://orcid.org/0000-0003-2361-2803
Sytske Anne Bergstra: http://orcid.org/0000-0002-7136-5248
Annette H. M. van der Helm-van Mil: http://orcid.org/0000-0001-8572-1437
Pascal H. P. de Jong: http://orcid.org/0000-0001-6628-6222

REFERENCES

[1] Smolen JS, Breedveld FC, Burmester GR, Bykerk V, Dougados M, Emery P, et al. Treating rheumatoid arthritis to target: 2014 update of the recommendations of an international task force. Ann Rheum Dis 2016;75(1):3–15.
[2] Smolen JS, Landewé RBM, Bergstra SA, Kerschbaumer A, Sepriano A, Aletaha D, et al. EULAR recommendations for the management of rheumatoid arthritis with synthetic and biological disease-modifying antirheumatic drugs: 2022 update. Ann Rheum Dis 2023;82(1):3–18.
[3] Fraenkel L, Bathon JM, England BR, St Clair EW, Arayssi T, Carandang K, et al. 2021 American College of Rheumatology guideline for the treatment of rheumatoid arthritis. Arthritis Care Res 2021;73(7):924–39.
[4] Dejaco C, Landewé RBM. Controversies in rheumatology: telemedicine-friend or foe? Rheumatology (Oxford) 2023;62:2661–4.
[5] Knitza J, Gupta L, Hügle T. Rheumatology in the digital health era: status quo and quo vadis? Nat Rev Rheumatol 2024;20(12):747–59.
[6] Barber CEH, Mosher D, Dowling S, Bohm V, Solbak NM, Macmullan P, et al. Implementation and evaluation of audit and feedback for monitoring treat-to-target (T2T) strategies in rheumatoid arthritis using performance measures. Rheumatol Ther 2020;7(4):909–25.
[7] De Thurah A, Bosch P, Marques A, Meissner Y, Mukhtyar CB, Knitza J, et al. 2022 EULAR points to consider for remote care in rheumatic and musculoskeletal diseases. Ann Rheum Dis 2022;81(8):1065–71.
[8] Black N. Patient reported outcome measures could help transform healthcare. BMJ 2013;346:f167.
[9] Ferreira RJO, Ndosi M, de Wit M, Santos EJF, Duarte C, Jacobs JWG, et al. Dual target strategy: a proposal to mitigate the risk of overtreatment and enhance patient satisfaction in rheumatoid arthritis. Ann Rheum Dis 2019;78(10):e109.
[10] Oude Voshaar MAH, Das Gupta Z, Bijlsma JWJ, Boonen A, Chau J, Courvoisier DS, et al. International consortium for health outcome measurement set of outcomes that matter to people living with inflammatory arthritis: consensus from an international working group. Arthritis Care Res 2019;71(12):1556–65.
[11] Pickles T, Macefield R, Aiyegbusi OL, Beecher C, Horton M, Christensen KB, et al. Patient reported outcome measures for rheumatoid arthritis disease activity: a systematic review following COSMIN guidelines. RMD Open 2022;8(1):e002093.
[12] Hendrikx J, de Jonge MJ, Fransen J, Kievit W, van Riel PL. Systematic review of patient-reported outcome measures (PROMs) for assessing disease activity in rheumatoid arthritis. RMD Open 2016;2(2):e000202.
[13] England BR, Tiong BK, Bergman MJ, Curtis JR, Kazi S, Mikuls TR, et al. 2019 Update of the American College of Rheumatology recommended rheumatoid arthritis disease activity measures. Arthritis Care Res 2019;71(12):1540–55.
[14] Salaffi F, Migliore A, Scarpellini M, Corsaro SM, Laganà B, Mozzani F, et al. Psychometric properties of an index of three patient reported outcome (PRO)

measures, termed the CLinical ARthritis Activity (PRO-CLARA) in patients with rheumatoid arthritis. The NEW INDICES study. Clin Exp Rheumatol 2010;28(2):186–200.
[15] Salaffi F, Di Carlo M, Farah S, Marotto D, Atzeni F, Sarzi-Puttini P. Rheumatoid arthritis disease activity assessment in routine care: performance of the most widely used composite disease activity indices and patient-reported outcome measures. Acta Biomed 2021;92(4):e2021238.
[16] Looijen AEM, Snoeck Henkemans SVJ, Van Der Helm-Van Mil AHM, Welsing PMJ, Koc GH, Luime JJ, et al. Combining patient-reported outcome measures to screen for active disease in rheumatoid arthritis and psoriatic arthritis. RMD Open 2024;10(4):e004687.
[17] Glenwright BG, Simmich J, Cottrell M, O'Leary SP, Sullivan C, Pole JD, Russell T. Facilitators and barriers to implementing electronic patient-reported outcome and experience measures in a health care setting: a systematic review. J Patient Rep Outcomes 2023;7(1):13.
[18] Arnett FC, Edworthy SM, Bloch DA, McShane DJ, Fries JF, Cooper NS, et al. The American Rheumatism Association 1987 revised criteria for the classification of rheumatoid arthritis. Arthritis Rheum 1988;31(3):315–24.
[19] Aletaha D, Neogi T, Silman AJ, Funovits J, Felson DT, Bingham 3rd CO, et al. 2010 Rheumatoid arthritis classification criteria: an American College of Rheumatology/European League Against Rheumatism collaborative initiative. Arthritis Rheum 2010;62(9):2569–81.
[20] Claessen SJ, Hazes JM, Huisman MA, van Zeben D, Luime JJ, Weel AE. Use of risk stratification to target therapies in patients with recent onset arthritis; design of a prospective randomized multicenter controlled trial. BMC Musculoskelet Disord 2009;10:71.
[21] de Jong PH, Hazes JM, Han HK, Huisman M, van Zeben D, van der Lubbe PA, et al. Randomised comparison of initial triple DMARD therapy with methotrexate monotherapy in combination with low-dose glucocorticoid bridging therapy; 1-year data of the tREACH trial. Ann Rheum Dis 2014;73(7):1331–9.
[22] van Mulligen E, de Jong PHP, Kuijper TM, van der Ven M, Appels C, Bijkerk C, et al. Gradual tapering TNF inhibitors versus conventional synthetic DMARDs after achieving controlled disease in patients with rheumatoid arthritis: first-year results of the randomised controlled TARA study. Ann Rheum Dis 2019;78(6):746–53.
[23] de Rooy DP, van der Linden MP, Knevel R, Huizinga TW, van der Helm-van Mil AH. Predicting arthritis outcomes—what can be learned from the Leiden Early Arthritis Clinic? Rheumatology (Oxford) 2011;50(1):93–100.
[24] Matthijssen XME, Niemantsverdriet E, Huizinga TWJ, Van Der, Helm-Van Mil AHM. Enhanced treatment strategies and distinct disease outcomes among autoantibody-positive and -negative rheumatoid arthritis patients over 25 years: a longitudinal cohort study in the Netherlands. PLOS Med 2020;17(9):e1003296.
[25] Fransen J, van Riel PL. The Disease Activity Score and the EULAR response criteria. Rheum Dis Clin North Am 2009;35(4):745–57 vii-viii.
[26] Koc GH, Looijen AEM, Van Der Horst-Bruinsma IE, De Jong PHP. Sex differences in rheumatoid arthritis: new insights from clinical and patient-reported outcome perspectives. J Rheumatol 2025;52(6):553–62.
[27] Movahedi M, Cesta A, Li X, Bombardier C, investigators OBRI. Disease activity trajectories for early and established rheumatoid arthritis: real-world data from a rheumatoid arthritis cohort. PLoS One 2022;17(9):e0274264.
[28] Katchamart W, Koolvisoot A, Aromdee E, Chiowchanwesawakit P, Muengchan C. Associations of rheumatoid factor and anti-citrullinated peptide antibody with disease progression and treatment outcomes in patients with rheumatoid arthritis. Rheumatol Int 2015;35(10):1693–9.
[29] Innala L, Berglin E, Möller B, Ljung L, Smedby T, Södergren A, et al. Age at onset determines severity and choice of treatment in early rheumatoid arthritis: a prospective study. Arthritis Res Ther 2014;16(2):R94.
[30] Bruce B, Fries JF. The Health Assessment Questionnaire (HAQ). Clin Exp Rheumatol 2005;23(5 Suppl 39):S14–8.
[31] Boers M, Jacobs JW, van Vliet, Vlieland TP, van Riel PL. Consensus Dutch health assessment questionnaire. Ann Rheum Dis 2007;66(1):132–3.
[32] Fries JF, Spitz P, Kraines RG, Holman HR. Measurement of patient outcome in arthritis. Arthritis Rheum 1980;23(2):137–45.
[33] Strand V, Boers M, Idzerda L, Kirwan JR, Kvien TK, Tugwell PS, et al. It's good to feel better but it's better to feel good and even better to feel good as soon as possible for as long as possible. Response criteria and the importance of change at OMERACT 10. J Rheumatol 2011;38(8):1720–7.
[34] StataCorp. STATA LASSO reference manual. Texas: Stata Press; 2021.
[35] Giavarina D. Understanding Bland Altman analysis. Biochem Med 2015;25(2):141–51.
[36] Bland JM, Altman DG. Measuring agreement in method comparison studies. Stat Methods Med Res 1999;8(2):135–60.
[37] Dougados M, Aletaha D, van Riel P. Disease activity measures for rheumatoid arthritis. Clin Exp Rheumatol 2007;25(5 Suppl 46):S22–9.
[38] Dankers F.J.W.M., Traverso A., Wee L., et al. Prediction modeling methodology. 2018. In: Kubben P., Dumontier M., Dekker A., editors. Fundamentals of Clinical Data Science [Internet]. Cham (CH): Springer; 2019. Chapter 8. Available from: https://www.ncbi.nlm.nih.gov/books/NBK543534/
[39] Hosmer Jr. DW, Lemeshow S, Sturdivant RX. Applied logistic regression. Hoboken: John Wiley & Sons; 2013.
[40] Hoo ZH, Candlish J, Teare D. What is an ROC curve? Emerg Med J 2017;34(6):357–9.
[41] Krijbolder DI, Khidir SJH, Matthijssen XME, Ten Brinck RM, van Aken J, Speyer I, et al. Hand function is already reduced before RA development and reflects subclinical tenosynovitis. RMD Open 2023;9(1):e002885.
[42] Venerito V, Manigold T, Capodiferro M, Markham D, Blanchard M, Iannone F, et al. Single-camera motion capture of finger joint mobility as a digital biomarker for disease activity in rheumatoid arthritis. Rheumatol Adv Pract 2025;9(2):rkae143.
[43] Wiegel J, Seppen BF, Ter Wee MM, Nurmohamed MT, Boers M, Bos WH. The RAPID3 questionnaire as a screening tool to reduce the number of outpatient clinic visits: a retrospective cohort study. Clin Rheumatol 2022;41(8):2525–31.
[44] Scott IC, Ibrahim F, Panayi G, Cope AP, Garrood T, Vincent A, et al. The frequency of remission and low disease activity in patients with rheumatoid arthritis, and their ability to identify people with low disability and normal quality of life. Semin Arthritis Rheum 2019;49(1):20–6.
[45] Bingham CO, Alten R, Bartlett SJ, Bykerk VP, Brooks PM, Choy E, et al. Identifying preliminary domains to detect and measure rheumatoid arthritis flares: report of the OMERACT 10 RA Flare Workshop. J Rheumatol 2011;38(8):1751–8.
[46] Alten R, Pohl C, Choy EH, Christensen R, Furst DE, Hewlett SE, et al. Developing a construct to evaluate flares in rheumatoid arthritis: a conceptual report of the OMERACT RA Flare Definition Working Group. J Rheumatol 2011;38(8):1745–50.
[47] Bombardier C, Barbieri M, Parthan A, Zack DJ, Walker V, Macarios D, et al. The relationship between joint damage and functional disability in rheumatoid arthritis: a systematic review. Ann Rheum Dis 2012;71(6):836–44.
[48] Mokkink LB, Terwee CB, Knol DL, Stratford PW, Alonso J, Patrick DL, et al. The COSMIN checklist for evaluating the methodological quality of studies on measurement properties: a clarification of its content. BMC Med Res Methodol 2010;10(1):22.
[49] Collins GS, Reitsma JB, Altman DG, Moons KG. Transparent reporting of a multivariable prediction model for individual prognosis or diagnosis (TRIPOD): the TRIPOD statement. Ann Intern Med 2015;162(1):55–63.
[50] Moons KG, Altman DG, Reitsma JB, Ioannidis JP, Macaskill P, Steyerberg EW, et al. Transparent Reporting of a multivariable prediction model for Individual Prognosis or Diagnosis (TRIPOD): explanation and elaboration. Ann Intern Med 2015;162(1):W1–73.

Ann Rheum Dis 85 (2026) 630–639

Contents lists available at ScienceDirect

Annals of the Rheumatic Diseases

journal homepage: https://www.sciencedirect.com/journal/annals-of-the-rheumatic-diseases

Psoriatic arthritis

Inadequate response to anti-TNFα therapy is associated with a gain-of-function TNFR2-R polymorphic variant in patients with psoriatic arthritis

James K. Sullivan[1], Vandana Rai[2], Jennifer Harvey[2], Vincent Del Signore[2], Shashank Cheemalavagu[3], Jean Lin[3], Sujay S. Ithychanda[2], Jun Qin[1,2], Unnikrishnan M. Chandrasekharan[1,2], M. Elaine Husni[1,2,3,*]

[1] *Cleveland Clinic Lerner College of Medicine of Case Western Reserve School of Medicine, Cleveland, Ohio, USA*
[2] *Department of Cardiovascular & Metabolic Sciences, Lerner Research Institute, Cleveland Clinic, Cleveland, Ohio, USA*
[3] *Department of Rheumatic and Immunologic Diseases, Cleveland Clinic, Orthopaedic and Rheumatologic Institute, Cleveland, Ohio, USA*

ARTICLE INFO

Article history:
Received 21 January 2025
Received in revised form 18 July 2025
Accepted 13 October 2025

ABSTRACT

Objectives: Front-line treatment for psoriatic arthritis (PsA) often involves the use of tumour necrosis factor alpha (TNFα) blocking medications (tumour necrosis factor alpha inhibition [TNFi]). However, more than 40% of patients exhibit inadequate responses, and there is no predictive clinical test available. Our goal is to investigate whether the response to TNFi treatment is associated with TNFα receptor 2 (TNFR2) rs1061622 polymorphic variants, TNFR2-M or TNFR2-R, in PsA. Furthermore, to elucidate the underlying mechanisms, differences in cell signalling and gene expression conferred by TNFR2-M vs TNFR2-R were examined.

Methods: TNFR2 rs1061622 polymorphism status of 164 patients was assessed using restriction fragment length polymorphisms analysis. Discontinuation of the TNFi agents <12 months due to inadequate efficacy determined by chart review was the primary outcome. Human endothelial cells expressing endogenous or recombinant TNFR2-M or TNFR2-R and Jurkat T cells expressing recombinant TNFR2-M or TNFR2-R were utilised to investigate differences in cell signalling and gene expression.

Results: Patients with PsA with TNFR2-R variant had a ~5-fold increased likelihood of discontinuing TNFi therapy <12 months, vs TNFR2-M carriers (95% CI 1.98-12.78). The cells with TNFR2-R alleles showed higher levels of proinflammatory gene expression in the absence of TNFa stimulation ($P < .01$). This activity of TNFR2-R was unaffected by a TNFα-neutralising antibody, whereas blocked by a Rho kinase (ROCK)-specific inhibitor.

Conclusions: TNFR2 rs1061622 polymorphism significantly influences TNFi therapy responsiveness in PsA. The TNFα-independent, but ROCK activity-dependent gain-of-function activity conferred by TNFR2-R variant potentially serves as a mechanism underlying inadequate responses to TNFi in a subset of patients with PsA.

*Correspondence to Dr M. Elaine Husni, Cleveland Clinic, Cleveland, Ohio, USA.
E-mail address: husnie@ccf.org (M.E. Husni).
Handling editor Josef S. Smolen.

https://doi.org/10.1016/j.ard.2025.10.014

WHAT IS ALREADY KNOWN ON THIS TOPIC

- Tumour necrosis factor alpha (TNFα) receptor 2 (TNFR2) polymorphisms rs1061622 have been associated with disease activity and response to tumour necrosis factor alpha inhibition (TNFi) in multiple immune-mediated diseases, including psoriasis, ankylosing spondylitis, and ulcerative colitis, but underlying mechanisms are elusive.
- TNFR2 is capable of activating signalling pathways such as Mitogen-activated protein kinase (MAPK), Nuclear Factor-kappa B (NF-kB), and Rho kinase (ROCK) and these pathways, independently or in combination, are involved in TNFα induction of proinflammatory genes.

WHAT THIS STUDY ADDS

- TNFR2 rs1061622 polymorphisms are associated with TNFi therapy responsiveness in patients with psoriatic arthritis.
- Ligand-independent, gain-of-function of TNFR2-R allele as a mechanism underlying inadequate responses to TNFi.
- The ligand-independent proinflammatory function of TNFR2-R variant is ROCK activity dependent.

HOW THIS STUDY MIGHT AFFECT RESEARCH, PRACTICE OR POLICY

- The utility of single-nucleotide polymorphisms to predict treatment response in rheumatic disease has long been discussed but never implemented clinically. Additionally, there are currently no clinical tests to predict response to TNFi. This study provides testing of TNFR2 rs1061622 polymorphisms status as a plausible tool for personalised medicine for patients with psoriatic arthritis and potentially other immune-mediated inflammatory diseases.

INTRODUCTION

Tumour necrosis factor alpha (TNFα) inhibition (TNFi) therapies have revolutionised the treatment paradigm for several immune-mediated diseases, including rheumatoid arthritis, psoriatic arthritis (PsA), inflammatory bowel disease, and ankylosing spondylitis [1]. However, in several of these diseases, inadequate response is common, and mechanisms of TNFi resistance are incompletely understood. For example, PsA poses a formidable challenge as a seronegative inflammatory arthritis impacting as many as 30% of patients with psoriasis and 0.25% of the United States population [2,3]. The first-line treatment for PsA after initially failing non-steroidal anti-inflammatory medications is the use of TNFα-blocking agents [4], but over 40% experience inadequate response to these medications [5]. The mechanistic basis of this heterogeneity in responsiveness remains largely unknown, and currently, there is no reliable clinical test to predict responsiveness available, which further complicates therapeutic decision-making.

Pharmacogenetics, the variability of drug response due to genetic heterogeneity [6], has been considered as a contributory mechanism to treatment nonresponse in a number of rheumatic diseases [7,8]. Within this context, TNFα receptor 2 (TNFR2) rs1061622 polymorphisms have been implicated in TNFi response in chronic inflammatory diseases including rheumatoid arthritis [9], inflammatory bowel disease [10], ankylosing spondylitis [11], and psoriasis [12]. The association of these TNFR2 polymorphisms to drug responsiveness in patients with PsA is limited. One study explored various TNFR2 polymorphisms including rs1061622, for their association with TNFi response in patients with PsA [13]. However, this study, with a relatively small cohort (20 patients), was unable to reach a definite conclusion on the relationships between TNFi response and rs1061622 polymorphisms in patients with PsA.

TNFR2 has 4 extracellular cysteine-rich domains (CRD domains). TNFα makes physical contacts with the middle 2 CRD domains of TNF receptors. The rs1061622 is a single-nucleotide polymorphism (SNP) occurring as either a T or G variant on chromosome 1 within the TNF receptor superfamily member 1B gene (TNFRSF1B) [14], which encodes TNFR2. This SNP results in either methionine or arginine (TNFR2-M or TNFR2-R, respectively) at amino acid position 196 at the 4th CRD domain, which is not involved in TNFa binding. Although these polymorphisms have been implicated in immune-mediated disease severity and TNFi response, the functional difference induced by this M → R substitution is not clear. One group showed a moderate decrease in the soluble extracellular region of TNFR2 in the serum of people with the TNFR2-R variant [15]. Soluble TNFR2 inactivates circulating TNFa; therefore, a decrease in soluble TNFR2-R can increase circulating TNFa and augment TNFR signalling. However, a subsequent study did not find such an association [16]. It has also been reported that HeLa cells expressing recombinant TNFR2-R were more sensitive to TNFR1-mediated apoptosis with a concomitant reduction in anti-apoptotic gene expression [16], but this study did not address the mechanisms of enhanced inflammatory activity gained by TNFR2-R.

Our clinical data analysis conducted in a cohort of 164 patients, coupled with *in vitro* mechanistic functional studies, revealed novel insights on the basis for varied responses to TNFi.

MATERIALS AND METHODS

The institutional review board at the Cleveland Clinic approved this study (IRB# 07-623, PI: Husni). All patients provided written informed consent. For race and ethnicity, participants answered a fixed set of categories.

Study population

Participants with a confirmed diagnosis of PsA by a board-certified rheumatologist were enrolled in the Cleveland Clinic Psoriatic Disease Biorepository, which provided access to linked clinical, demographic, and biospecimen data for this study. The inclusion criteria consisted of individuals diagnosed with PsA who had ongoing or past exposure to TNFi therapy as documented in the registry or the Cleveland Clinic electronic medical record. The exclusion criteria comprised individuals diagnosed with any other additional inflammatory arthritis/arthropathy and those who discontinued anti-TNFi therapy due to reasons unrelated to efficacy, such as insurance coverage concerns or comorbidities.

Retrospective chart review of TNFi use

The Cleveland Clinic Psoriatic Disease Biorepository captures the pertinent variables related to TNFi therapy, including the therapeutic agent's name, duration of use, and reasons for discontinuation (classified as lack of skin efficacy alone, lack of joint efficacy alone, lack of skin and joint efficacy, side effect/adverse event, cost/insurance issues, or other reasons). In cases of incomplete data, a chart review was conducted in the Cleveland Clinic electronic medical record. This review involved assessing rheumatology provider notes and prescription history to determine the duration of TNFi use and the reason for

discontinuation. Adverse events and discontinuation due to lack of efficacy were only classified if explicitly documented by a rheumatologist or pharmacist note. Reasons for discontinuation due to lack of efficacy were determined by chart review of board-certified rheumatologists' notes for the following: (i) documentation verifying lack of efficacy, (ii) worsening joint involvement by physical exam and/or imaging, and (iii) documentation of worsening psoriasis. This was based on the ACR/NPF treatment recommendations [4]. In the event that the prescription history differed from the rheumatologist documentation, the latter was prioritised. For participants with the use of multiple anti-TNFα agents, the first agent prescribed was considered for the primary outcome. A secondary analysis was performed with TNFi discontinuation at 3 years of continuous use.

Assessment of the status of TNFR2 rs1061622 polymorphisms

The eligible participant's buffy coat underwent genotyping for TNFR2 rs1061622 polymorphisms using a restriction fragment length polymorphism (RFLP) analysis, as previously described [17]. Briefly, genomic DNA was extracted using the NucleoSpin Blood DNA extraction kit (Macherey-Nagel). Polymerase chain reaction (PCR) using TNFR2-specific primers encompassing the polymorphic region (forward: ACTCTCCTATCCTGCCTGCT; reverse: TTCTGGAGTTGGCTGCGTGT) was performed (PCRBio Systems). The PCR product was incubated overnight with NlAIII, a type II restriction enzyme at 37°C, and the resulting DNA fragments were developed on a 4% agarose gel. Genotypes were classified as follows: M/M genotype for 2 copies of TNFR2 M alleles, M/R genotype for 1 TNFR2-R and 1 TNFR2-M allele, and R/R genotype for 2 copies of TNFR2-R alleles.

Statistical approach

The aim of this analysis was to evaluate the correlation between TNFR2 rs1061622 polymorphisms status and use of TNFi exceeding 12 months, representing responsiveness to TNFi therapy. We assessed the unadjusted association between the primary outcome and TNFR2 rs1061622 polymorphism status using Pearson's Chi-Squared test. Multivariable logistic regression modelling was used to examine the association between the presence of TNFR2-R variant alleles and the likelihood of discontinuing the first prescribed TNFi agent before 12 months due to inadequate efficacy. The covariates included were age at PsA diagnosis and body mass index (BMI), selected based on established clinical relevance and previous literature in PsA identifying these as potential confounders of treatment response [18,19]. Reported odds ratios, *P* values, and confidence intervals are Wald-based calculations. All analyses were performed using JMP Pro 15.1.0 software (SAS Institute). The data supporting this article are available upon reasonable request to the corresponding author.

Sample size considerations were guided by the estimated prevalence of TNFi nonresponse in PsA, which is approximately 40% [20]. Assuming 2 degrees of freedom (based on 3 genotype groups for rs1061622), we estimated that a minimum of 20 nonresponder patients would be required to explore genotype–response associations with sufficient stability in an exploratory model.

Expression of recombinant TNFR2-M or TNFR2-R by lentivirus

Endothelial cells (EC) were isolated from unidentified discarded umbilical cords. Jurkat T cell line was purchased from American Type Culture Collection (ATCC) (Manassas, VA) (catalogue number TIB-152). ATCC routinely performs quality control on their cells and provides a certificate of analysis. The cells were expanded in culture and stored in frozen vials in liquid nitrogen. Cultured cells were infected with lentivirus with Myc-tagged TNFR2-R cDNA or TNFR2-M cDNA and a puromycin resistance gene. Following incubation with lentivirus for 8 hours in complete media, cells were subjected to a media change incorporating puromycin (1 μg/mL) and cultured for an additional 72 hours in the presence or absence of TNFα (2 ng/mL TNFα for 2 hours). The cells were harvested for ribonucleic acid (RNA) isolation or Western blot analysis.

Isolation of EC expressing endogenous TNFR2-M or TNFR2-R

Before EC isolation, umbilical cords were genotyped for TNFR2 rs1061622 polymorphisms status was then determined using the RFLP PCR technique described above. Once the genotype of each cord was known, EC were batch isolated and pooled as previously described [21] into 3 cultures with known genotype: TNFR2-M/TNFR2-M (M/M), TNFR2-M/TNFR2-R (M/R), and TNFR2-R/TNFR2-R (R/R). Total RNA of confluent EC cultures of the aforementioned genotypes was then harvested for quantitative PCR to quantify mRNA reflecting the gene expression using specific primers (Supplementary Table S1).

RNA interference (siRNA)

The sources and product identification of the small interfering RNAs (siRNAs) used in this study are as follows: Tnfr1-specific siRNA (ie, TNFR1si-1) (identification number 42862) and TNFR2-specific siRNA (identification number 110832) (Ambion, Life Technologies).

Transfections of EC with siRNA, along with TNFR2-M or TNFR2-R expressing cDNA, were performed with Targefect (Targeting Systems) according to the manufacturer's instructions. At 48 hours after transfection, cells were harvested, and an immunoblot was performed to determine TNFR1 and TNFR2 using antibodies B10920 (LifeSpan BioSciences) and MA5-32618 (Invitrogen), respectively.

Measurement of soluble ICAM-1 in human serum

Soluble Intercellular adhesion molecule 1 (ICAM-1) in the serum of PsA and healthy subjects were measured by Enzyme-linked immunosorbent assay (ELISA) using Human ICAM-1/CD54 Duo set sELISA kit from R&D Systems.

ROCK1 activity assay

ROCK1 enzyme was immunoprecipitated from recombinant TNFR2-M- or TNFR2-R-reconstituted EC using ROCK1-specific antibody (Cell Signalling, # 4035). Kinase activity of the immunoprecipitated ROCK1 was determined using ROCK1 substrate myosin phosphatase target subunit 1 (MYPT-1) as described previously [22].

ROCK, IKK, and p38 inhibitor treatment

Confluent cultures of EC with known rs1061622 polymorphisms status were treated with ROCK inhibitor Y27632 (20 μM, Sigma-Aldrich), Inhibitory kappa B kinase - 16 (IkK-16) inhibitor (10 μM, Selleck Chemicals LLC), or p38 inhibitor SB203580 (10 μM, Sigma-Aldrich) for 3 hours. Cultures were then harvested, and total RNA was prepared (NucleoSpin RNA Tissue, Macherey-Nagel) for real-time quantitative PCR (RTqPCR).

Table
Demographics of the 164 participants stratified by rs1061622 polymorphisms status

Demographics	Overall cohort (N = 164)	TNFi use >12 mo	TNFi use ≤12 mo	M/M (N = 91)	M/R (N = 67)	R/R (N = 6)
Mean age (SD)	49.3 (12.3)	48.8 (12.5)	51.1 (11.3)	50.4 (12.2)	47.5 (12.7)	52.5 (4.76)
Mean age at PsA dx (SD)	42.0 (15.2)	41.4 (15.5)	44.8 (13.0)	42.2 (15.5)	41.7 (15.2)	42.7 (7.9)
Female	89 (55%)	70 (54%)	18 (58%)	55 (62%)	31 (47%)	3 (50%)
Current smoker	13 (8%)	9 (7%)	4 (15%)	8 (9%)	5 (7%)	0 (0%)
Diabetes	18 (12%)	14 (12%)	4 (15%)	11 (12%)	6 (9%)	1 (17%)
Mean BMI (SD)	32.2 (7.9)	32.5 (6.7)	32.2 (8.1)	32.7 (8.6)	31.8 (7.2)	30.4 (4.2)
Concomitant oral DMARDs	80 (48%)	70 (53%)	10 (32%)	44 (48%)	33 (49%)	3 (50%)

BMI, body mass index; dx, diagnosis; DMARD, disease-modifying anti-rheumatic drug; TNFi, tumour necrosis factor alpha inhibition.

Real-time quantitative PCR

For RTqPCR, total RNA was harvested from cultured EC using NucleoSpin RNA Tissue (Macherey-Nagel) according to manufacturer specifications. cDNA was then synthesised using Perfect Real Time RT Reagent Kit (Takara Bio). Quantitative PCR was then performed using Fast Sybr (Thermo Fischer) according to manufacturer specifications, using relevant primer sets.

Patient and public involvement statement

Patients and/or the public were not involved in the design, or conduct, or reporting, or dissemination plans of this research.

RESULTS

Study population

There were 175 participants. Among them, 11 participants were excluded due to discontinuation of TNFi for reasons other than efficacy, before 12 months of use. Therefore, the final cohort eligible for the study consisted of 164 participants (Fig 1), with 133 participants using TNFi for more than 12 months and 31 (~ 19%) discontinuing the medication within 12 months due to lack of TNFi efficacy.

In our cohort, the majority of patients with PsA initiated therapy with adalimumab (104/175), followed by etanercept (53/175), infliximab (13/175), and either golimumab or certolizumab pegol (5/175). We did not observe significant baseline differences across users of different TNFi agents.

Table details demographic and pertinent clinical information regarding the final cohort of 164 individuals, stratified on duration of TNFi use and rs1061622 polymorphisms status. Within the 164 participants, 91 were M/M genotype, 67 were M/R genotype, and 6 were R/R genotypes. There were no substantial differences in mean age, gender, mean age at the time of PsA diagnosis, BMI, or prevalence of comorbid diabetes. There were observed baseline differences in the use of conventional Disease-modifying anti-rheumatic drugs (DMARDs) and prevalence of smoking between those who used TNFi for more or less than 12 months.

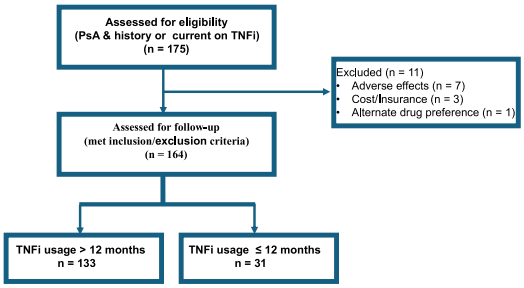

Figure 1. Flow diagram of participant selection. This illustrates the process of participants meeting inclusion and exclusion criteria for the primary outcome, which is discontinuation of TNFi use due to inefficiency, within 12 months. TNFi, tumour necrosis factor alpha inhibition; PsA, psoriatic arthritis.

Among the 164 participants, 156 (95%) were self-reported white, and 163 (99%) were self-reported non-Hispanic (Supplementary Table S2), which we acknowledge limits our study from extrapolating our findings to a general population.

Association of TNFR2-R polymorphic variant with TNFi discontinuation

Among the patients discontinued TNFi in less than 12 months, the prevalence of genotypes was as follows: 8 of 91 M/M genotype (9%), 20 of 67 M/R genotype (30%), and 3 of 6 R/R genotype (50%). Our analyses showed that patients carrying TNFR2-R alleles discontinued TNFi early (P value M/M vs M/R = 0.0006, M/M vs R/R = 0.002, M/R vs R/R = 0.31; Fig 2A). After adjusting for covariates, we found the presence of 1 R allele was significantly associated with our primary outcome, ie, the discontinuation of TNFi within 12 months [adjusted OR 5.03 (95% CI 1.98-12.78)]. Covariates included were BMI >30 and duration of PsA disease >5 years (Supplementary Table S3).

A total of 48 patients discontinued TNFi within the 36-month study period. Figure 2B illustrates the proportion of patients with M/M, M/R, and R/R genotypes who discontinued TNFi at 12 and 36 months. By the 12-month mark, 31 of 48 patients (65%) had discontinued TNFi. Among them, 17% (8/48) were M/M, 42% (20/48) were M/R, and 6% (3/48) were R/R. Patients carrying at least 1 R allele showed the highest percentage (26/48 = 54%) of TNFi discontinuation (chi-square P = .01). The sensitivity, specificity, and accuracy of having a single TNFR2-R allele for the inadequate response to TNF inhibitors up to 12 months in this cohort were 74%, 62% and 65%, respectively (Supplementary Table S4). These values indicate that the presence of at least 1 R allele has moderate predictive value for identifying nonresponders to TNFi therapy.

Similarly, at the 36-month mark, more patients carrying at least 1 R allele had discontinued TNFi (chi-square P = .01). Specifically, 40% (19/48) of those who discontinued were M/M, while 60% (29/48) had at least 1 R allele. These findings together support our hypothesis that TNFi responsiveness is associated with TNFR2 rs1061622 polymorphisms in patients with PsA.

Our analysis of baseline pretreatment disease activity scores (disease activity score-28) and inflammatory markers (C-reactive protein and erythrocyte sedimentation rate [ESR]) revealed no statistically significant differences across genotype groups (Fig 2C). This suggests that the R allele does not appear to

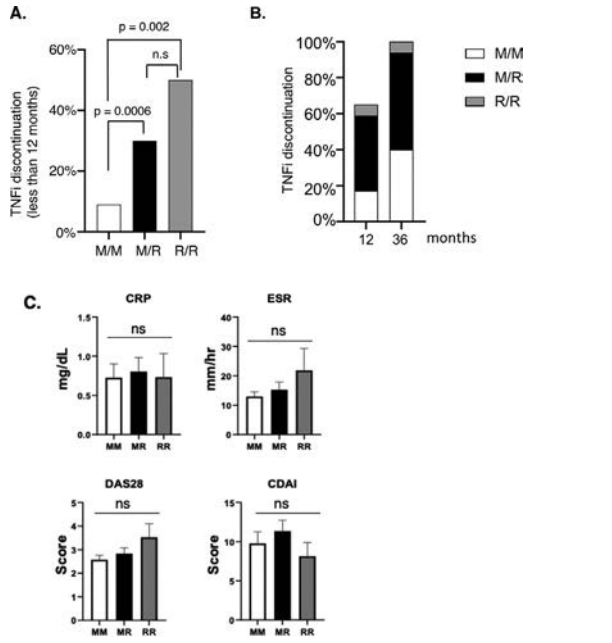

Figure 2. Early discontinuation of TNFi therapy with TNFR2-R variant. (A) Percentage of participants with TNFR2-M or TNFR2-R who discontinued TNFi therapy within 12 mo. Genotypes are categorised as M/M (2 copies of TNFR2-M alleles), M/R (1 copy each of TNFR2-M and TNFR2-R alleles) and R/R (2 copies of TNFR2-R alleles). (B) Proportion of patients with M/M, M/R, and R/R genotypes who discontinued TNFi therapy due to lack of efficacy within 12 or 36 mo. (C) Disease activity indices before initiation of anti-TNFα therapy expressed as mean ± SE. Serum levels of C-reactive protein (CRP), erythrocyte sedimentation rate (ESR), disease activity score-28 (DAS28) and clinical disease activity index (CDAI scores). Number of patients for CRP, ESR, and DAS28: MM: 64; MR: 40; RR: 6. For CDAI scores MM: 56; MR: 36; RR: 5. Significance determined by Kruskal-Wallis test, $P < .05$ considered significant. (D) Representative restriction fragment length polymorphism (RFLP) analysis of TNFR2 rs1061622 polymorphisms. PCR amplicon encompassing the SNP digested with NlaIII restriction enzyme, a type II restriction enzyme. The 133bp and 109bp, NlaIII fragments correspond to 2 copies of TNFR2-M (M/M). The 242bp (uncut) along with 133 bp and 109 bp fragments correspond to 1 copy each of TNFR2-M and TNFR2-R (M/R). The 242 bp fragment alone (uncut) corresponds to 2 copies of TNFR2-R (R/R). ns, not significant; PsA, psoriatic arthritis; SNP single-nucleotide polymorphism; TNFα, tumour necrosis factor alpha; TNFi, tumour necrosis factor alpha inhibition; TNFR2, TNFα receptor 2.

predispose individuals to a more inflammatory phenotype at baseline.

Figure 2D shows a representative picture of RFLP analysis to determine the M and R alleles.

TNFa-independent proinflammatory activity of TNFR2-R variant

To investigate whether there is differential function we overexpressed recombinant TNFR2-M and TNFR2-R in cultured ECs using lentiviral approach (Fig 3A). We then determined downstream effects by measuring mRNA levels of a set of proinflammatory genes in the presence or absence of TNFα treatment. As shown in Figure 3B, upon TNFa treatment, both recombinant TNFR2-M and TNFR2-R overexpressing cells showed similar mRNA levels of ICAM-1 and interleukin (IL)-1b. Importantly, we found an increase of basal IL-1b ($P < .05$) and an increasing trend in ICAM-1 (not reached statistical significance) expression in TNFR2-R expressing cells compared to TNFR2-M expressing cells. To rule out that this effect is not cell type-specific, we investigated gene expression on Jurkat T cells expressing either recombinant TNFR2-M or TNFR2-R. Similar to EC, we found a robust increase in basal ICAM-1 gene expression in TNFR2-R expressing Jurkat T cells (not previously activated) in the absence of TNFα (Fig 3C, colourless bars). TNFR2-M expressing cells did not show this effect. To investigate whether this activity was due to secreted TNFα acting on TNFR2-R in an autocrine fashion, we included a TNFα-neutralising antibody. The TNFα-neutralising antibody, but not the control, isotypic antibody (Iso-IgG) inhibited TNFa induction of ICAM-1 in TNFR2-M expressing cells, but in TNFR2-R cells, the ICAM-1 mRNA remained at heightened level (Fig 3C, black bars vs chequered bars), reiterating the TNFa-independent activity of TNFR2-R. Given, soluble ICAM-1 is increased in psoriatic disease conditions [23,24], we determined whether ICAM-1levels in the circulation is associated with TNFR2 variants. We found significant differences in soluble CAM-1 levels among M/M, M/R or R/R genotype (Fig 3D). This suggests that although ICAM expression is increased in TNFR2-R, ICAM-1 shedding is not affected.

Next, we determined whether TNFR2-R at endogenous condition shows the TNFa-independent proinflammatory activity. We utilised cultured ECs isolated from umbilical cord of subjects carrying TNFR2-M, TNFR2-R, or TNFR2-M/R alleles for this study. The genotypes were determined by RFLP analysis. We found higher levels of IL-1β, ICAM-1, Colony stimulating factor 2 (CSF2), Chemokine (C-X-C motif) ligand 2 (CXCL2), and IL-8 expression in cells with TNFR2-R (Fig 3E). Importantly, the TNFa-independent expression levels of these proinflammatory genes, except for CSF2, were increased in terms of TNFR2-R gene dose; expression levels were significantly higher with 2 copies TNFR2-R alleles compared to 1 copy.

TNFa-independent proinflammatory activity of TNFR2-R variant depends on Rho kinase activity

TNFR2 is capable of activating signalling pathways such as Mitogen-activated protein kinase (MAPK) [21,25], Nuclear Factor-kappa B (NF-kB) [21,25], and Rho kinase (ROCK) [22], and these pathways independently or in combination are involved in TNFα induction of proinflammatory genes [22]. Furthermore, we have demonstrated that ROCK activity is upstream to p38 MAP kinase and NFkB activation in TNFR2 signalling pathways [22]. Here, using specific chemical inhibitors, we tested involvement of these pathways in TNFα-independent activity of TNFR2-R in ECs expressing either 1 copy of TNFR2-R (M/R) or 2 copies of TNFR2-R (R/R). The expression levels of IL-1b and ICAM-1 in M/R and R/R were plotted fold change compared to cells expressing 2 copies of TNFR2-M (M/M) on corresponding treatment conditions. In the case of IL-b, we found a significant increase in basal expression with M/R vs R/R ($P < .01$) and the increase was not statistically significant in ICAM-1 expression. We found that inhibition of ROCK activity blocked the heightened basal expression of IL-1b and ICAM-1 in cells expressing TNFR2-R, whereas inhibitions of p38 MAPK and NF-kB pathways showed partial effects (Fig 4A). This suggests that the ROCK activity that triggers multiple downstream pathways is a better drug target. The level of expression of IL-b and ICAM-1 in M/M cells were unaffected by inhibitors of ROCK, p38 or IKK.

There are 2 ROCK isoforms namely ROCK1 and ROCK2 [26]. Our earlier studies showed that TNFα treatment activates ROCK1, but not ROCK2 through TNFR2 signalling [22]. We next compared ROCK1activity induced in TNFR2-M and TNFR2-R expressing cells in the presence or absence of TNF-a. In this experiment, we reconstituted TNFR2-M or TNFR2-R in endogenous TNFR1- and TNFR2-depleted ECs by RNAi approach

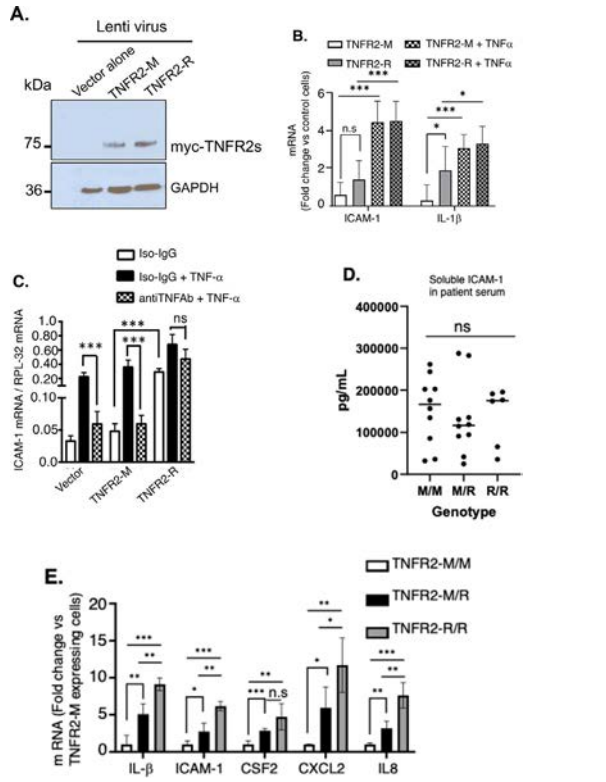

Figure 3. TNFa-independent proinflammatory activity of TNFR2-R. (A) Western blot showing expression of myc-tagged TNFR2-M or myc-tagged TNFR2-R in cultured human umbilical endothelial cells (EC) by lentiviral approach with anti-myc antibody used for detection. GAPDH serves as the loading control. (B) Measurement of ICAM-1 and IL-b mRNA by qPCR in EC expressing either TNFR2-M or TNFR2-R, in the presence or absence of TNFa. Results are presented as fold induction of mRNA compared to mRNAs in empty vector infected cells with RPL-32 mRNA level used for normalisation. (C) Recombinant TNFR2-R expressing Jurkat T cells (by lentiviral approach) show an increased basal ICAM-1 mRNA expression compared to cells expressing TNFR2-M (white bars). ICAM-1 expression in TNFR2-M expressing cells, but not in TNFR2-R expressing cells was inhibited by a TNFα-neutralising antibody. Iso-IgG: isotypic control antibody. (D) Soluble ICAM-1 levels in the serum of patients with PsA with indicated TNFR2 variants or soluble ICAM-1 in the serum of healthy subjects. (E) Proinflammatory gene induction in EC isolated from subjects with TNFR2-M or TNFR2-R alleles, in the absence of TNFa treatment. TNFR2-M/M: 2 copies of TNFR2-M, TNFR2-M/R: 1 copy each of TNFR2-M and TNFR2-R and TNFR2-R/R: 2 copies of TNFR2-R. Results are expressed as fold induction of mRNA compared to mRNA levels in TNFR2-M/M expressing cells. $*P < .05$, $**P < .01$ and $***P < .001$. Values in B-D represented as mean ± Std (n = 3 independent experiments using cells transfected /infected with separate cDNA or using separate primary endothelial cell isolates). CSF2, Colony stimulating factor 2; CXCL2, Chemokine (C-X-C motif) ligand 2; GAPDH, Glyceraldehyde 3-phosphate dehydrogenase; ICAM-1, Intercellular adhesion molecule 1; IL-b, interleukin b; ns, not significant; PsA, psoriatic arthritis; qPCR, quantitative PCR; TNFα, tumour necrosis factor alpha; TNFR2, TNFα receptor 2.

(Fig 4B), to make sure that ROCK1 activity of TNFR2s is independent of TNFR1 activity. Here, we found that the basal ROCK1 activity, measure as phosphorylation of MYPT1 (ROCK substrate) is higher in TNFR2-R variant expressing cells compared to TNFR2-M expressing cells (Fig 4C, D). However, upon TNFa treatment, the ROCK1 activity showed similar magnitude both in TNFR2-M and TNFR2-R expressing cells. The ROCK activity reaches the basal level in TNFR2-M cells within 30 minutes post TNFa treatment, whereas in TNFR2-R cells it persists to a higher level. We then determined the status of ROCK1 activity on cells expressing TNFR2-MM, TNFR2-MR and TNFR2-RR endogenously. Similar to recombinant TNFR2-R expressing cells, we found an increase in basal ROCK1 activity in cultured ECs isolated from subjects with TNFR2-MR and TNFR2-RR genotypes compared to TNFR2-MM cells (Fig 4 E, F).

DISCUSSION

Although anti-TNFα therapy has revolutionised our treatment paradigm for psoriatic diseases, over 40% of patients show inadequate response [5]. Many approaches to predicting response to TNFi have been explored, including signature gene expression patterns, genome-wide association studies, and protein markers in blood [10,27–32]. Despite these efforts, currently no reliable clinical test to predict responsiveness to anti-TNF therapy is available. This is mainly due to a lack of mechanistic understanding for the heterogeneity in response. Our study identifies that the TNFR2-R variant gains a TNFα-independent proinflammatory activity, potentially overriding TNFα neutralisation. Our findings demonstrate a clinically relevant mechanistic basis for the inadequate response to TNFi therapy exhibited by a subset of patients with PsA and potentially other immune-mediated inflammatory diseases carrying TNFR2-R variant, present up to 26% of general population [33].

Previous studies demonstrated evidence for the involvement of TNFa pathways in TNFi therapy response. For example, it has been shown that specific SNPs in TNFa gene and TNFAIP3, a gene encoding A20 protein are associated with TNFi therapy response in rheumatologic diseases [34,35]. While the relationship between TNFi use and TNFR2 rs1061622 polymorphisms has been studied in other immune-mediated diseases including psoriasis, rheumatoid arthritis, and inflammatory bowel disease [9–12,36], this study marks the first detailed characterisation of rs1061622 polymorphisms and TNFi response in patients with PsA. Findings from our study indicate that patients with PsA with at least 1 allele for TNFR2-R were approximately 5 times more likely to discontinue TNFi therapy within 1 year. Our findings are clinically significant and could lead the way to develop pharmacogenetic approaches to stratify responders versus nonresponders before starting TNFi therapy, in a subset of patients with PsA.

Currently, there are no pharmacogenetic tests used in rheumatology to predict treatment effectiveness. The American College of Rheumatology recommends screening certain populations for HLA-B*58:01 before initiation of allopurinol therapy [37], but that is for the prediction of adverse events (severe cutaneous adverse reactions) rather than predicting response to the medication. While not approved by the Food and Drug Administration the PrismRA test has been shown to predict response to TNFi among patients with rheumatoid arthritis (RA) [38], but does not include genetic markers. Nevertheless, the potential role for pharmacogenetics as a clinical aid to predict treatment response before beginning a new medication is not a new concept with classic examples including variants of CYP2C9 and VKORC1 to predict dosing recommendations of warfarin [39] and longstanding evidence in multiple other medications for a variety of rheumatic diseases [7,40].

Mechanistically, here, we demonstrated that TNFR2-R-expressing human cells show a TNFα-independent proinflammatory activity. Importantly, the increased gene expression at basal condition was not inhibited by a TNFα-neutralising antibody, further supporting that TNFR2-R acquired a gain of proinflammatory function, which is TNFa independent, thus providing pathways for inflammation to propagate even in the presence of TNFi. However, our studies did not completely rule out the

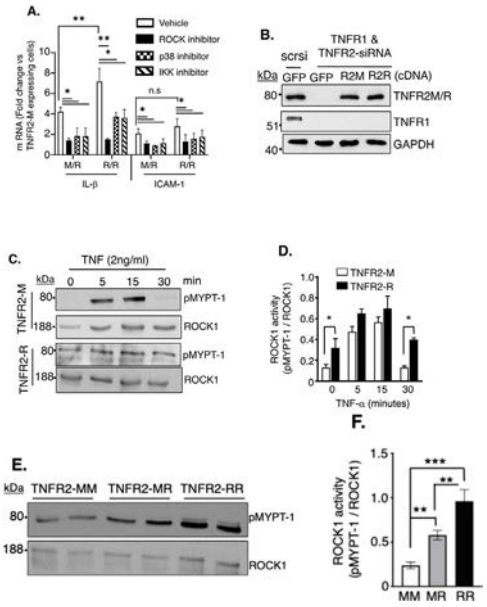

Figure 4. TNFa-independent activity of TNFR2-R is ROCK activity dependent. (A) Basal IL-b and ICAM-1 expression (measured by qPCR) in cultured human umbilical vein endothelial cells (EC) isolated from subjects with 1 copy of TNFR2-R allele (M/R) or 2 copies of TNFR2-R (R/R) in the presence or absence of chemical inhibitors of either ROCK (Y27632), p38 MAP kinase (SB203580) or NFkB pathways (IKK-16). Results are presented as fold induction of mRNA compared to mRNAs of the corresponding genes in cells expressing 2 TNFR2-M alleles. RPL-32 mRNA level was used for normalisation. (B) Reconstitution of recombinant myc-tagged TNFR2-M or TNFR2-R in endogenous TNFR1- and TNFR2-depleted EC (by siRNA) confirmed by Western blotting. TNFR2s (top panel) and TNFR1 (middle panel) are detected by anti-TNFR2 and anti-TNFR1 antibody, respectively. (C) A higher level of ROCK1 activity in cells expressing recombinant TNFR2-R, determined by immunoprecipitation of ROCK1 and subsequent kinase activity assay using ROCK1 substrate MYPT-1 (myosin phosphatase target subunit 1) as described previously [22]. (D) ROCK1 activity detected in (C) is quantified by measuring the image intensity using ImageQuant software. (E) Endogenous ROCK1 activity in endothelial cells isolated from subjects with TNFR2-MM, TNFR2-MR and TNFR2-RR using ROCK1 substrate MYPT-1, which was measured using ImageQuant t software (F). $*P < .05$, $**P < .01$, $***P < .01$. Values in A-F represented as mean ± Std (n = 3 independent experiments, using cells transfected/infected with separate cDNA or using separate primary endothelial cell isolates). IL-b, interleukin b; GFP, Green fluorescent protein; GAPDH, Glyceraldehyde 3-phosphate dehydrogenase; ICAM-1, Intercellular adhesion molecule 1; IKK-16, Inhibitory kappa B kinase - 16; MAP kinase, Mitogen-activated protein kinase; NFkB, Nuclear Factor-kappa B; qPCR, quantitative PCR; ROCK, Rho kinase; TNFα, tumour necrosis factor alpha; TNFR2, TNFα receptor 2.

possibility that this gain-of-function is ligand independent. It is possible that TNFR2-R, but not TNFR2-M, could bind non-TNFa ligands present in the culturing medium to induce proinflammatory signalling. While rs1061622 has not been previously reported to be in strong linkage disequilibrium with other immune-related genes, the potential contribution of unidentified linkage cannot be excluded. We also acknowledge that RNA sequencing would provide a broader and more detailed view of the transcriptional landscape and downstream signalling pathways influenced by the TNFR2 rs 1061622 polymorphism. Nevertheless, the TNFa-independent, constitutive, proinflammatory activity is a plausible explanation for the poor TNFi responsiveness among TNFR2-R carriers.

To better understand of the structural implications that could affect functional differences, we used Alphafold3 server to predict structures of TNFR2-M and TNFR2-R (Supplementary Fig S1). Interestingly, the predicted structures show that the aminoacidic 196 in the CRD4 motif of TNFR2 is sandwiched between glycosylations at N171 and N193. The sugar moiety of N193 is in a close distance (3-4Å) from aa196. It is possible that the substitution of arginine in place of methionine can impact receptor conformation and signalling pathways by the influence of glycosylation in multiple ways. This altered or lack of glycosylation can lead to constitutive TNFR2 activation. Future mutagenesis and mass spectral work should clarify the precise mode of activation due to the M to R substitution in TNFR2.

TNFa induces a variety of signalling cascades through TNFR1 and TNFR2 depending on the cell type and context [41]. We have earlier showed that ROCK activity is critical regulator of TNFR2 signalling and upstream to p38 MAP kinase and NFkB activation [22]. In this study, we identified that ROCK activity is necessary to propagate the TNFa-independent proinflammatory gene induction in the TNFR2-R-expressing cells. The gene-dose dependent (1 allele vs 2 alleles of TNFR2-R) induction of these inflammatory genes aligns with our clinical observations; worse TNFi therapy responses among individuals with 2 TNFR2-R alleles.

This study has certain limitations. Due to the retrospective nature of our study and lack of consistent baseline clinical measures, we were unable to fully adjust for potential confounders such as prior treatment exposures and disease activity. Although efforts were made to recruit participants sequentially, variability in research infrastructure means that this cohort should be considered an observational cohort. Future studies in prospectively enrolled, treatment-naïve populations will be necessary to validate and expand on these findings.

In our study population, we had only 6 patients with homozygotes for TNFR2-R (RR genotype). Although M/M and M/R patients were comparable (91 and 76 patients respectively), and M/R population showed lower responsiveness, it is important to determine validate our findings in an independent cohort. We attempted to address this by analysing an independent cohort of patients with RA-another chronic inflammatory disease in which TNF inhibitors are frequently used. In this RA, we found that individuals with the MR or RR genotype had significantly higher odds of being nonresponders to TNF inhibitor therapy compared to those with the MM genotype (https://acrabstracts.org/abstract/defining-a-personalised-treatment-approach-to-rheumatoid-arthritis-using-genetic-markers-of-tnfi-response/). These findings further support the hypothesis that the presence of at least 1 R allele is associated with reduced TNFi responsiveness.

TNFR2-R gain-of-function variant likely represents only 1 piece of a complex regulatory network influencing TNFi responsiveness. Other elements within the TNF signalling axis—including TNFR1, circulating TNF-α levels, and the shedding of soluble TNFR1 and TNFR2—could independently or synergistically modulate treatment outcomes. For instance, elevated circulating TNFα could potentially overcome the neutralising effect of TNF inhibitors, thereby reducing treatment efficacy. We have ruled out this as we found that circulating TNFa levels were not significantly different among the patients with M/M, M/R and R/R before TNFi initiation (Supplementary Fig S2). Additionally, the development of antidrug antibodies to TNF inhibitors is a well-established mechanism of secondary treatment failure. The potential relationship between the TNFR2-R variant and immunogenicity remains an important area for future investigation. Furthermore, dysregulated shedding of TNFR1 or TNFR2 could alter receptor availability or TNF bioactivity, affecting the therapeutic response.

Due to the retrospective nature of our study, we could not adjust for potential confounders, such as baseline disease activity. Only a limited subset of the analytic cohort (<25%) had baseline disease activity measures before initiation of TNFi. In addition, there was variability in the type of disease activity measures recorded, which precluded the consistent application of a single metric across the study. Since baseline disease activity can impact treatment decisions, follow-up studies that adjust for baseline disease activity in regression models are warranted. Another limitation is the largely homogeneous Caucasian group (95% self-reported white, 99% self-reported non-Hispanic) within this study cohort. Thus, caution is needed in generalising these findings to non-white and non-Hispanic population. This is particularly important as cohorts of previous studies that analysed the involvement of these polymorphisms on drug responsiveness were also predominantly Caucasian population [9,10,13]. Future prospective studies must be conducted in cohorts that include greater racial and ethnic diversity to better understand the effects of TNFR2 rs1061622 polymorphisms on PsA treatment outcomes. Although endogenously expressing TNFR2 variants are in our mechanistic studies additional studies using immune cells isolated from patients and healthy controls will strengthen the conclusions. Nevertheless, to our knowledge, this study is the first to demonstrate plausible a mechanism underlying the frequently reported association between TNFR2 polymorphisms rs1061622 and medication response.

The findings from clinical data analysis underscore the significance of TNFR2 rs1061622 polymorphism status in determining efficacy of TNFi therapy among patients with PsA. Our findings reveal a distinct association between TNFR2-R genotype and diminished responsiveness to TNFi treatment, potentially resulting in premature discontinuation compared to individuals with the TNFR2-M genotype. Moreover, we identified that TNFR2-R acquired a gain-of-function with an increased ROCK activity and inflammatory gene expression, a potential underlying mechanism for the inadequate responsiveness to TNFi therapy. These results together suggest a possible role for pharmacogenetics as a predictive test for determining response to TNFi treatment and ROCK pathway inhibitors as an alternate therapeutic approach for patients with TNFR2-R in PsA. Our findings can pave the way for personalised therapeutic strategies tailored to suit their genetic make-up, an approach that may optimise treatment outcomes by reducing inappropriate disease burden in patients with PsA.

TNF/TNFR2 system plays multifaceted role in normal physiology that includes triggering adaptive immune response through promoting dendritic cell/T cell interaction [42], cellresolving inflammation via T reg cell proliferation and expansion [43,44], EC activation and angiogenesis [22,45,46], inhibition of neuronal inflammation and neuron regeneration [47,48] and metabolic remodelling [49]. Therefore, it will be also interesting to determine whether people in the general population carrying TNFR2-R variant have an advantage or disadvantage over TNFR2-M carriers in combating infection, wound repair and maintaining neuronal and cardiovascular health.

Competing interests

The authors declare the following financial interests/personal relationships which may be considered as potential competing interests: MEH reports a relationship with AbbVie Inc that includes: consulting or advisory. MEH reports a relationship with Bristol Myers Squibb Co that includes: consulting or advisory. MEH reports a relationship with Eli Lilly and Company that includes: consulting or advisory. MEH reports a relationship with Janssen Pharmaceuticals Inc that includes: consulting or advisory. MEH reports a relationship with Novartis as consulting or advisory. MEH reports a relationship with UCB Inc that includes: consulting or advisory. MEH reports a relationship with National Psoriasis Foundation that includes: board membership. MEH reports a relationship with Rheumatology Research Foundation that includes: board membership. If there are other authors, they declare that they have no known competing financial interests or personal relationships that could have appeared to influence the work reported in this paper.

CRediT authorship contribution statement

James K. Sullivan: Writing – original draft, Validation, Methodology, Investigation, Funding acquisition, Formal analysis, Data curation, Conceptualization. **Vandana Rai:** Methodology, Investigation. **Jennifer Harvey:** Methodology, Investigation. **Vincent Del Signore:** Methodology, Investigation. **Shashank Cheemalavagu:** Methodology, Investigation. **Jean Lin:** Methodology, Investigation. **Sujay S. Ithychanda:** Methodology, Investigation. **Jun Qin:** Writing – review & editing, Formal analysis, Conceptualization. **Unnikrishnan M. Chandrasekharan:** Writing – review & editing, Supervision, Funding acquisition, Formal analysis, Conceptualization. **M. Elaine Husni:** Writing – review & editing, Resources, Project administration, Funding acquisition, Formal analysis, Conceptualization.

Acknowledgements

The authors gratefully acknowledge the invaluable assistance of our research coordinator, Saima Goul, in the recruitment of psoriatic arthritis patients and the collection of biosamples for this study.

Funding

This work is supported by NIH Grant R01AR075777 to MEH and UMC, National Psoriasis Foundation (NPF) Bridge-Grant: NPF1808UC to UMC and MEH, and Rheumatology Research Foundation (RRF) Medical & Graduate Student Preceptorship to JKS and MEH.

Patient consent for publication

Not applicable.

Ethics

The study was conducted in accordance with the Helsinki Declaration. The sera of the human subjects were collected under the IRB study # 07-623.

Provenance and peer review

Not commisioned, externally peer reviewed.

Supplementary materials

Supplementary material associated with this article can be found in the online version at doi:10.1016/j.ard.2025.10.014.

Orcid

James K. Sullivan: http://orcid.org/0000-0001-5853-1590
Jean Lin: http://orcid.org/0000-0002-7012-9729
Sujay S. Ithychanda: http://orcid.org/0000-0001-8979-246X
Unnikrishnan M. Chandrasekharan: http://orcid.org/0000-0002-0761-2590
M. Elaine Husni: http://orcid.org/0000-0002-3181-4205

REFERENCES

[1] Silva LCR, Ortigosa LCM, Benard G. Anti-TNF-α agents in the treatment of immune-mediated inflammatory diseases: mechanisms of action and pitfalls. Immunotherapy 2010;2(6):817–33.
[2] Ogdie A, Weiss P. The epidemiology psoriatic arthritis. Rheum Dis Clin North Am 2015;41(4):545–68.
[3] Mease PJ, Gladman DD, Papp KA, Khraishi MM, Thaçi D, Behrens F, et al. Prevalence of rheumatologist-diagnosed psoriatic arthritis in patients with psoriasis in European/North American dermatology clinics. J Am Acad Dermatol 2013;69(5):729–35.
[4] Singh JA, Guyatt G, Ogdie A, Gladman DD, Deal C, Deodhar A, et al. Special article: 2018 American College of Rheumatology/National Psoriasis Foundation guideline for the treatment of psoriatic arthritis. Arthritis Rheumatol 2019;71(1):5–32.
[5] Brahe CH, Ørnbjerg LM, Jacobsson L, Nissen MJ, Kristianslund EK, Mann H, et al. Retention and response rates in 14 261 PsA patients starting TNF inhibitor treatment-results from 12 countries in EuroSpA. Rheumatology (Oxford) 2020;59(7):1640–50.
[6] Aneesh TP, Sonal Sekhar M, Jose A, Chandran L, Zachariah SM. Pharmacogenomics: the right drug to the right person. J Clin Med Res 2009;1(4):191–4.
[7] Aluko A, Ranganathan P. Pharmacogenetics of drug therapies in rheumatoid arthritis. Methods Mol Biol 2022;2547:527–67.
[8] Daniel LL, Dickson AL, Chung CP. Precision medicine for rheumatologists: lessons from the pharmacogenomics of azathioprine. Clin Rheumatol 2021;40(1):65–73.
[9] Canet LM, Filipescu I, Cáliz R, Lupiañez CB, Canhão H, Escudero A, et al. Genetic variants within the TNFRSF1B gene and susceptibility to rheumatoid arthritis and response to anti-TNF drugs: a multicenter study. Pharmacogenet Genomics 2015;25(7):323–33.
[10] Bek S, Nielsen JV, Bojesen AB, Franke A, Bank S, Vogel U, et al. Systematic review: genetic biomarkers associated with anti-TNF treatment response in inflammatory bowel diseases. Aliment Pharmacol Ther 2016;44(6):554–67.
[11] Xing-Rong W, Sheng-Qian X, Wen L, Shan Q, Fa-Ming P, Jian-Hua X. Role of TNFRSF1A and TNFRSF1B polymorphisms in susceptibility, severity, and therapeutic efficacy of etanercept in human leukocyte antigen-B27-positive Chinese Han patients with ankylosing spondylitis. Medicine (Baltimore) 2018;97(31):e11677.
[12] González-Lara L, Batalla A, Coto E, Gómez J, Eiris N, Santos-Juanes J, et al. The TNFRSF1B rs1061622 polymorphism (p.M196R) is associated with biological drug outcome in Psoriasis patients. Arch Dermatol Res 2015;307(5):405–12.
[13] Ovejero-Benito MC, Muñoz-Aceituno E, Reolid A, Fisas LH, Llamas-Velasco M, Prieto-Pérez R, et al. Polymorphisms associated with anti-TNF drugs response in patients with psoriasis and psoriatic arthritis. J Eur Acad Dermatol Venereol 2019;33(4):e175–7.
[14] TNFRSF1B: Chr1 - Genome Data Viewer - NCBI [Internet]. [cited 2022 Mar 11]. Available from: https://www.ncbi.nlm.nih.gov/genome/gdv/browser/gene/?id=7133
[15] Stark GL, Dickinson AM, Jackson GH, Taylor PR, Proctor SJ, Middleton PG. Tumour necrosis factor receptor type II 196M/R genotype correlates with circulating soluble receptor levels in normal subjects and with graft-versus-host disease after sibling allogeneic bone marrow transplantation. Transplantation 2003;76(12):1742–9.
[16] Peral B, San Millán JL, Castello R, Moghetti P, Escobar-Morreale HF. Comment: the methionine 196 arginine polymorphism in exon 6 of the TNF receptor 2 gene (TNFRSF1B) is associated with the polycystic ovary syndrome and hyperandrogenism. J Clin Endocrinol Metab 2002;87(8):3977–83.
[17] Al-Ansari AS, Ollier WE, Villarreal J, Ordi J, Teh LS, Hajeer AH. Tumor necrosis factor receptor II (TNFRII) exon 6 polymorphism in systemic lupus erythematosus. Tissue Antigens 2000;55(1):97–9.
[18] Kumthekar A, Ogdie A. Obesity and psoriatic arthritis: a narrative review. Rheumatol Ther 2020;7(3):447–56.
[19] Queiro R, Tejón P, Alonso S, Coto P. Age at disease onset: a key factor for understanding psoriatic disease. Rheumatology (Oxford) 2014;53(7):1178–85.
[20] Gottenberg JE, Brocq O, Perdriger A, Lassoued S, Berthelot JM, Wendling D, et al. Non−TNF-targeted biologic vs a second anti-TNF drug to treat rheumatoid arthritis in patients with insufficient response to a first anti-TNF drug: a randomized clinical trial. JAMA 2016;316(11):1172–80.
[21] Chandrasekharan UM, Siemionow M, Unsal M, Yang L, Poptic E, Bohn J, et al. Tumor necrosis factor alpha (TNF-alpha) receptor-II is required for TNF-alpha-induced leukocyte-endothelial interaction in vivo. Blood 2007;109(5):1938–44.
[22] Chandrasekharan UM, Dechert L, Davidson UI, Waitkus M, Mavrakis L, Lyons K, et al. Release of nonmuscle myosin II from the cytosolic domain of tumor necrosis factor receptor 2 is required for target gene expression. Sci Signal 2013;6(284):ra60.
[23] Schopf RE, Naumann S, Rehder M, Morsches B. Soluble intercellular adhesion molecule-1 levels in patients with psoriasis. Br J Dermatol 1993;128(1):34–7.
[24] Ruscitti P, Esposito M, Di Cola I, Pellegrini C, De Berardinis A, Mastrangelo M, et al. Cytokine profile characterization of naïve patients with psoriasis and psoriatic arthritis: implications for a pathogenic disease continuum. Front Immunol 2023;14:1229516.
[25] Faustman D, Davis M. TNF receptor 2 pathway: drug target for autoimmune diseases. Nat Rev Drug Discov 2010;9(6):482–93.
[26] Riento K, Ridley AJ. Rocks: multifunctional kinases in cell behaviour. Nat Rev Mol Cell Biol 2003;4(6):446–56.
[27] Arijs I, Li K, Toedter G, Quintens R, Van Lommel L, Van Steen K, et al. Mucosal gene signatures to predict response to infliximab in patients with ulcerative colitis. Gut 2009;58(12):1612–9.
[28] Han BK, Kuzin I, Gaughan JP, Olsen NJ, Bottaro A. Baseline CXCL10 and CXCL13 levels are predictive biomarkers for tumor necrosis factor inhibitor therapy in patients with moderate to severe rheumatoid arthritis: a pilot, prospective study. Arthritis Res Ther 2016;18(1):93.
[29] Kalden JR, Schulze-Koops H. Immunogenicity and loss of response to TNF inhibitors: implications for rheumatoid arthritis treatment. Nat Rev Rheumatol 2017;13(12):707–18.
[30] Plant D, Bowes J, Potter C, Hyrich KL, Morgan AW, Wilson AG, et al. Genome-wide association study of genetic predictors of anti-tumor necrosis factor treatment efficacy in rheumatoid arthritis identifies associations with polymorphisms at seven loci. Arthritis Rheum 2011;63(3):645–53.
[31] Umićević Mirkov M, Cui J, Vermeulen SH, Stahl EA, Toonen EJM, Makkinje RR, et al. Genome-wide association analysis of anti-TNF drug response in patients with rheumatoid arthritis. Ann Rheum Dis 2013;72(8):1375–81.
[32] Julià A, Fernandez-Nebro A, Blanco F, Ortiz A, Cañete JD, Maymó J, et al. A genome-wide association study identifies a new locus associated with the response to anti-TNF therapy in rheumatoid arthritis. Pharmacogenomics J 2016;16(2):147–50.
[33] Phan L, Jin Y, Zhang H, Qiang W, Shekhtman E, Shao D, et al. ALFA: allele frequency aggregator [Internet]. National Center for Biotechnology Information, U.S. National Library of Medicine; 2025. Available from: https://www.ncbi.nlm.nih.gov/snp/docs/gsr/alfa/ALFA_20250407153717/.
[34] Tejasvi T, Stuart PE, Chandran V, Voorhees JJ, Gladman DD, Rahman P, et al. *TNFAIP3* gene polymorphisms are associated with response to TNF blockade in psoriasis. J Invest Dermatol 2012;132(3, Pt 1):593–600.
[35] Seitz M, Wirthmüller U, Möller B, Villiger PM. The -308 tumour necrosis factor-alpha gene polymorphism predicts therapeutic response to TNFalpha-blockers in rheumatoid arthritis and spondyloarthritis patients. Rheumatology (Oxford) 2007;46(1):93–6.
[36] Chen W, Xu H, Wang X, Gu J, Xiong H, Shi Y. The tumor necrosis factor receptor superfamily member 1B polymorphisms predict response to anti-TNF therapy in patients with autoimmune disease: a meta-analysis. Int Immunopharmacol 2015;28(1):146–53.
[37] Dean L, Kane M. Allopurinol therapy and HLA-B*58:01 genotype. In: Pratt VM, Scott SA, Pirmohamed M, Esquivel B, Kattman BL, Malheiro AJ, editors. Medical genetics summaries [Internet]. Bethesda, MD: National Center for Biotechnology Information (US); 2012. [cited 2024 Mar 22]Available from: https://www.ncbi.nlm.nih.gov/books/NBK127547/.
[38] Bergman MJ, Kivitz AJ, Pappas DA, Kremer JM, Zhang L, Jeter A, et al. Clinical utility and cost savings in predicting inadequate response to anti-TNF therapies in rheumatoid arthritis. Rheumatol Ther 2020;7(4):775–92.

[39] Flockhart DA, O'Kane D, Williams MS, Watson MS, Flockhart DA, Gage B, et al. Pharmacogenetic testing of CYP2C9 and VKORC1 alleles for warfarin. Genet Med 2008;10(2):139–50.
[40] Davila L, Ranganathan P. Pharmacogenetics: implications for therapy in rheumatic diseases. Nat Rev Rheumatol 2011;7(9):537–50.
[41] Sedger LM, McDermott MF. TNF and TNF-receptors: from mediators of cell death and inflammation to therapeutic giants - past, present and future. Cytokine Growth Factor Rev 2014;25(4):453–72.
[42] Shiga T, Sato K, Kataoka S, Sano S. TNF inhibitors directly target Th17 cells via attenuation of autonomous TNF/TNFR2 signalling in psoriasis. J Dermatol Sci 2015;77(1):79–81.
[43] Ye LL, Wei XS, Zhang M, Niu YR, Zhou Q. The significance of tumor necrosis factor receptor type II in CD8 + regulatory T cells and CD8 + effector T cells. Front Immunol 2018;9:583.
[44] Fischer R, Sendetski M, del Rivero T, Martinez GF, Bracchi-Ricard V, Swanson KA, et al. TNFR2 promotes Treg-mediated recovery from neuropathic pain across sexes. Proc Natl Acad Sci 2019;116(34):17045–50.
[45] Goukassian DA, Qin G, Dolan C, Murayama T, Silver M, Curry C, et al. Tumor necrosis factor-α receptor p75 is required in ischemia-induced neovascularization. Circulation 2007;115(6):752–62.
[46] Luo Y, Xu Z, Wan T, He Y, Jones D, Zhang H, et al. Endothelial-specific transgenesis of TNFR2 promotes adaptive arteriogenesis and angiogenesis. Arterioscler Thromb Vasc Biol 2010;30(7):1307–14.
[47] Desu HL, Thougaard E, Carney BN, Illiano P, Plastini MJ, Florimon Y, et al. TNFR2 signaling in oligodendrocyte precursor cells suppresses their immune-inflammatory function and detrimental microglia activation in CNS demyelinating disease. Brain Behav Immun 2025;123:81–98.
[48] Pozniak PD, Darbinyan A, Khalili K. TNF-α/TNFR2 regulatory axis stimulates EphB2-mediated neuroregeneration via activation of NF-κB. J Cell Physiol 2016;231(6):1237–48.
[49] de Kivit S, Mensink M, Hoekstra AT, Berlin I, Derks RJE, Both D, et al. Stable human regulatory T cells switch to glycolysis following TNF receptor 2 costimulation. Nat Metab 2020;2(10):1046–61.

Ann Rheum Dis 85 (2026) 640–646

Contents lists available at ScienceDirect

Annals of the Rheumatic Diseases

journal homepage: https://www.sciencedirect.com/journal/annals-of-the-rheumatic-diseases

Systemic lupus erythematosus

25-Hydroxyvitamin D levels are associated with mortality and cardiovascular events in systemic lupus erythematosus

Theerada Assawasaksakul[1,*], Andrea Fava[1], Daniel Goldman[1], Laurence S. Magder[2], Michelle Petri[1]

[1] *Johns Hopkins University, Baltimore, MD, USA*
[2] *University of Maryland, Baltimore, MD, USA*

ARTICLE INFO

Article history:
Received 9 July 2025
Received in revised form 4 October 2025
Accepted 11 October 2025

ABSTRACT

Objectives: We assessed the association between 25-hydroxyvitamin D (25(OH)D) levels and rates of mortality and cardiovascular events (stroke, myocardial infarction, angina/bypass) in patients with systemic lupus erythematosus (SLE).
Methods: The Hopkins Lupus Cohort began measuring 25(OH)D quarterly in 2009. We examined associations between 25(OH)D levels—baseline, mean in the last year, and most recent values—and both mortality and cardiovascular events (stroke, myocardial infarction, angina/bypass). Two analyses were conducted: (i) a prospective analysis of events occurring after the first 25 (OH)D measurement, and (ii) a lifetime analysis including events before cohort entry. All models adjusted for age, sex (female or male), race, and body mass index.
Results: The prospective analysis included 11,302 person-years from 1768 patients. Patients with 25(OH)D <20 ng/mL had the highest mortality and cardiovascular event rates. Compared to those with levels of 30-39 ng/mL, those with levels <20 ng/mL at cohort entry had significantly increased risk of death (hazard ratio [HR] 2.05, 95% CI: 1.19-3.54, $P = .0095$) and cardiovascular events (HR 2.98, 95% CI: 1.30-6.85, $P = .010$). Risk of myocardial infarction alone was not statistically significant (HR 1.90, $P = .30$), but risk of angina/bypass was elevated (HR 3.53, 95% CI: 1.13-11.0, $P = .030$). The lifetime analysis suggested these associations, with a U-shaped pattern for myocardial infarction risk.
Conclusions: An initial 25(OH)D level <20 ng/mL was associated with increased mortality and cardiovascular events (but not stroke) in SLE. The U-shaped curve for myocardial infarction mirrors our previous work in adverse pregnancy outcomes. Lack of association with mean or recent 25(OH)D levels questions the impact of supplementation on risk modification.

INTRODUCTION

Systemic lupus erythematosus (SLE) increases mortality by 2.87-fold compared to the general population, with cardiovascular events being one of the leading causes [1]. Vitamin D plays a crucial role in bone metabolism, immune modulation, and inflammatory regulation [2–4], making it more accurately classified as a sterol hormone rather than a conventional vitamin [5]. Vitamin D insufficiency and deficiency are almost universal in SLE [6–8]. In the general population, most meta-analyses have found an inverse correlation between serum 25-hydroxyvitamin D (25(OH)D) levels and all-cause or cause-specific mortality [9–14], but some did not [15–17]. Mendelian randomisation studies, which assess individuals with genetically

*Correspondence to Dr. Theerada Assawasaksakul.
E-mail address: theerada.azza@gmail.com (T. Assawasaksakul).
Handling editor Josef S. Smolen.

https://doi.org/10.1016/j.ard.2025.10.013

WHAT IS ALREADY KNOWN ON THIS TOPIC

- Systemic lupus erythematosus (SLE) is associated with a markedly increased risk of mortality and cardiovascular disease.
- Vitamin D deficiency is highly prevalent in SLE and has been associated with increased cardiovascular risk and mortality in the general population.
- Previous studies in SLE have not comprehensively investigated the relationship between serum 25-hydroxyvitamin D (25(OH)D) levels and both mortality and cardiovascular outcomes using longitudinal and lifetime analytical approaches.

WHAT THIS STUDY ADDS

- Initial (baseline) 25(OH)D levels <20 ng/mL are significantly associated with higher risks of mortality and cardiovascular events, including stroke, in patients with SLE.
- A U-shaped relationship was observed between 25(OH)D levels and myocardial infarction, suggesting that both low and high levels may increase risk.

HOW THIS STUDY MIGHT AFFECT RESEARCH, PRACTICE OR POLICY

- Highlights the potential utility of early 25(OH)D screening to identify patients with SLE at heightened risk for cardiovascular events.
- Reinforces the need for future research to elucidate mechanistic pathways and define optimal 25(OH)D thresholds for cardiovascular protection in SLE.

determined low 25(OH)D levels to minimise confounding, have also been inconsistent [15,18–24]. Meta-analyses have demonstrated a strong association between very low 25(OH)D levels and increased myocardial infarction (MI) risk compared to higher levels [25,26]. Additionally, a nonlinear inverse relationship exists between 25(OH)D concentrations and recurrent cardiovascular events, with risk reduction plateauing around 20 ng/mL (hazard ratio [HR]: 0.78; 95% CI: 0.65-0.94) [27]. Vitamin D deficiency is associated with an approximately 82% increased risk of ischaemic stroke [28]. Conversely, individuals with 25(OH)D levels above 22 ng/mL have about a 36% lower risk of stroke compared to those with lower levels [29].

In patients with SLE, the risk of death from cardiovascular events, including MI and stroke, is significantly elevated (standardised mortality ratio for cardiovascular diseases: 2.931; 95% CI: 1.802-4.061) [1], but no studies have directly examined the link between 25(OH)D, levels, MI and stroke, nor the impact of supplementation in this population. The design of the Hopkins Lupus Cohort, with longitudinal follow-up and systematic assessment of 25(OH)D, allowed us to address this relationship.

METHODS

Study design

The Hopkins Lupus Cohort, begun in 1987, includes patients with confirmed SLE classification based on the Systemic Lupus International Collaborating Clinics (SLICC) 2012 classification criteria [30]. Patients in the cohort were seen quarterly or biannually. The cohort was approved by the Johns Hopkins University School of Medicine Institutional Review Board (Protocol Review Number NA_00039294). Patients' rights, safety, and well-being were protected based on the principles of the Declaration of Helsinki. All patients gave written informed consent. The participants' health and private data were kept confidential.

The prospective analysis for this study was based on cohort data from 2009 through July 2024. The lifetime analysis included events that occurred before cohort entry.

Ascertainment of mortality

Death was ascertained by the National Death Index.

Ascertainment of cardiovascular events

The diagnosis of MI was established based on patient symptoms, electrocardiographic findings, cardiac echocardiogram results, and/or elevated cardiac biomarkers. Angina (if present for more than 6 months) and coronary procedures were classified according to the SLICC/American College of Rheumatology Damage Index criteria [31]. Thrombotic stroke was defined as the rapid onset of neurological deficit not attributable to brain trauma (such as a closed head injury), tumour, infection (eg, encephalitis or meningitis), or other nonvascular causes. Additionally, there had to be a clinically relevant lesion evident on brain imaging, or the symptoms had to persist for more than 24 hours or result in death within 24 hours. The lifetime analysis included events occurring before cohort entry, based on review of medical records using the same criteria.

Measurements of 25(OH)D

The quantitative determination of total 25(OH)D levels was measured at each cohort visit since the first visit by automated chemiluminescence immunoassay (LIAISON 25 OH Vitamin D TOTAL Assay; DiaSorin Inc.) throughout the study period. All testing was conducted in the Clinical Laboratory Improvement Amendments (CLIA)-certified and College of American Pathologists (CAP)-accredited clinical laboratory at Johns Hopkins Hospital, following standard internal quality control procedures, including the use of manufacturer-provided calibrators and multiple-level controls, to ensure long-term assay precision and comparability.

Definition of 25(OH)D categories

For analysis, 25(OH)D status was classified as: deficiency (<20 ng/mL), insufficiency (20-29 ng/mL), and sufficiency (≥30 ng/mL). To explore potential nonlinear associations, the sufficiency category was further subdivided into 30 to 39 ng/mL, 40 to 49 ng/mL, and ≥50 ng/mL. These cut-points were based on commonly used clinical definitions and previous literature, while the subdivision within the sufficient range allowed assessment of whether risk varied across different concentrations.

Consideration of vitamin D supplementation

Information on vitamin D supplementation was not included as a separate covariate because serum 25(OH)D levels—measured quarterly—reflect the combined effects of supplementation, diet, sun exposure, and metabolism. Therefore, measured 25(OH)D concentrations were used as the primary exposure in all analyses.

Statistical analysis

In the prospective analysis, we divided each patient's cohort follow-up into months and characterised each patient month based on the clinical history and treatments that occurred during or before that month. We also determined whether they had an outcome event (death, or cardiovascular event) during each month. The resulting person-month data set was then analysed with logistic regression. This is sometimes referred to as 'pooled logistic regression' and is a way to perform discrete-time survival analysis with time-varying predictors whose results are interpretable as rate ratios. We classified months with respect to 25(OH)D levels in several different ways: (i) based on the first 25(OH)D measure after cohort entry, (ii) based on the mean 25 (OH)D level in the last year, and (iii) based on the most recent 25(OH)D level. We included only the first cardiovascular event in the analysis and excluded patients who had an event before their first 25(OH)D measure in the prospective (but not the lifetime) analysis.

In the lifetime analysis, we examined the relationship between the first measure of 25(OH)D in the cohort and a patient's lifetime history of cardiovascular events (including events that occurred before cohort entry and before SLE diagnosis). To assess the statistical significance of the relationship between 25(OH)D levels and a lifetime history of cardiovascular events, we used a Cox proportional hazards model with age as the time scale. We also adjusted for race, sex (female or male), and body mass index. SAS 9.4 software (SAS Institute) was used for the analysis.

In an exploratory analysis, we evaluated whether improvements in 25(OH) vitamin D status influenced cardiovascular risk among patients with initially low 25(OH)D levels (<30 ng/mL). We grouped patients based on whether their mean 25(OH)D in the last year remained <30 ng/mL or increased to ≥30 ng/mL, and compared event rates using rate ratios adjusted for age, sex, race, and body mass index.

In sensitivity analyses, models were additionally adjusted for education as a marker of socioeconomic status. Education data were available for 96% of participants; missing values were excluded.

RESULTS

Patients in the cohort were 92% female, 48% White, and 40% African American, with a mean age at cohort entry of 42 years. A total of 50.3% had hypertension, 9.4% had diabetes, 52.6% had hyperlipidaemia, and 14% had hypothyroid. 33.7% had ever smoked and 12.3% were current smokers. 42.6% were obese. In terms of the prevalence of the SLICC classification criteria, 68.2% had acute cutaneous lupus, 21.3% had chronic cutaneous lupus, 55.2% had lupus alopecia, 51.4% had oral or nasal ulcers, 73.2% had arthritis, 45.7% had serositis, 54.7% had lupus nephritis, 51.8% had neurologic involvement, 9.5% had haemolytic anaemia, 61.1% had leukopenia or lymphopenia, 20.2% had thrombocytopenia, 96.6% had antinuclear antibodies (ANA), 62.2% had antidouble stranded DNA, 23.8% had anti-Smith, 62% had low complement, and 58.1% had antiphospholipid antibodies.

The prospective analysis of the broadest definition of clinical events (MI, stroke, angina, or bypass surgery) was based on 11,302 person-years of follow-up from 1768 different patients. Of them, 67 patients experienced an event during cohort participation. Table 1 shows the rate of events overall and as a function of the various ways of classifying follow-up with respect to 25 (OH)D levels.

To determine whether initial, mean (last year), or most recent 25(OH)D levels best predicted the risk of mortality and cardiovascular events, we prospectively analysed their associations with cardiovascular outcomes, adjusting for age, sex, race, and BMI. Table 2 presents the prospective analysis associations using the 3 approaches. Notably, only the initial 25(OH)D levels were significantly associated with mortality and cardiovascular outcomes, but neither the mean nor most recent level showed a consistent relationship with risk. In sensitivity analyses using <15 ng/mL as a separate category, patients with very low vitamin D (<15 ng/mL) demonstrated the highest risks of mortality and cardiovascular events compared to the reference group (30-39 ng/mL) (Supplementary Table S1). When further adjusted for education as a marker of socioeconomic status, results were materially unchanged (Supplementary Table S2). Specifically, individuals with initial 25(OH)D levels below 20 ng/mL had a significantly higher mortality risk than the reference group (30-39 ng/mL) (rate ratio: 2.05, 95% CI: 1.19-3.54, $P = .0095$). Similarly, initial levels <20 ng/mL were associated to an increased risk of composite cardiovascular events (rate ratio: 2.98, 95% CI: 1.30-6.85, $P = .0100$) and stroke (rate ratio: 3.53, 95% CI: 1.13-11.0, $P = .0302$) after adjusting for age, race, sex, and body mass index. These results indicate that later cardiovascular events were overrepresented among patients with low 25(OH)D

Table 1
Rates of cardiovascular events (myocardial infarction, stroke, angina, or bypass), by 25(OH)D levels

Variable	Value	Person-years of follow-up	Number of events	Rate (per 1000 person-years)
All		11,302	67	5.9
First vitamin D in cohort	<20	2785	24	8.6
	20-29	2665	18	6.8
	30-39	3011	8	2.7
	40-49	1778	15	8.4
	50+	1064	2	1.9
Mean vitamin D in last year	<20	588	5	8.5
	20-29	1526	10	6.6
	30-39	2800	19	6.8
	40-49	2579	14	5.4
	50+	2941	16	5.4
Most recent past vitamin D	<20	626	5	8.0
	20-29	1562	8	5.1
	30-39	2577	18	7.0
	40-49	2348	12	5.1
	50+	3243	20	6.2

25(OH)D, 25-hydroxyvitamin D.

Table 2
Prospective analysis 25(OH)D levels measured at the first cohort visit, mean, most recent 25(OH)D levels, and mortality and cardiovascular events (stroke, myocardial infarction [MI] , or angina; stroke; and MI) observed after the first 25(OH)D measure in the cohort

25(OH)D (ng/mL)	Initial 25(OH)D				Mean 25(OH)D in last year				Most recent past 25(OH)D			
		95% CI				95% CI				95% CI		
	Rate ratio[a]	Lower	Upper	*P* value[a]	Rate ratio[a]	Lower	Upper	*P* value[a]	Rate ratio[a]	Lower	Upper	*P* value[a]
Mortality												
<20	2.05	1.19	3.54	.0095	2.01	0.86	4.72	.1089	1.67	0.67	4.18	.2735
20-29	1.01	0.53	1.94	.9760	1.95	1.08	3.54	.0273	2.21	1.23	3.99	.0084
30-39	1 (ref)				1 (ref)				1 (ref)			
40-49	1.01	0.52	1.96	.9761	0.92	0.53	1.61	.7821	0.99	0.55	1.79	.9810
50+	1.20	0.58	2.49	.6232	0.57	0.32	1.02	.0566	0.70	0.40	1.24	.2184
Stroke, myocardial infarction, or angina/bypass												
<20	2.98	1.30	6.85	.0100	1.40	0.51	3.80	.5126	1.24	0.46	3.41	.6696
20-29	2.62	1.13	6.06	.0247	1.01	0.47	2.19	.9747	0.76	0.33	1.77	.5292
30-39	1 (ref)				1 (ref)				1 (ref)			
40-49	3.49	1.47	8.27	.0045	0.77	0.39	1.55	.4713	0.72	0.35	1.51	.3900
50+	0.82	0.17	3.89	.8045	0.76	0.39	1.50	.4313	0.87	0.46	1.66	.6774
Stroke												
<20	3.53	1.13	11.0	.0302	0.73	0.16	3.26	.6787	0.76	0.17	3.43	.7158
20-29	2.39	0.73	7.82	.1478	0.68	0.24	1.89	.4561	0.87	0.32	2.32	.7746
30-39	1 (ref)				1 (ref)				1 (ref)			
40-49	5.24	1.68	16.3	.0042	0.51	0.21	1.28	.1537	0.62	0.24	1.58	.3176
50+	None				0.64	0.28	1.48	.2987	0.70	0.31	1.61	.4011
Myocardial infarction												
<20	1.90	0.57	6.33	.2979	3.59	0.94	13.7	.0625	3.65	0.89	15.0	.0720
20-29	1.82	0.53	6.27	.3436	1.05	0.25	4.44	.9424	0.78	0.14	4.27	.7731
30-39	1 (ref)				1 (ref)				1 (ref)			
40-49	1.44	0.32	6.45	.6370	1.63	0.52	5.18	.4033	1.78	0.50	6.32	.3731
50+	0.91	0.10	8.23	.9316	1.07	0.31	3.76	.9143	1.61	0.47	5.55	.4520

25(OH)D, 25-hydroxyvitamin D.
[a] Adjusted for age, race, sex, and body mass index.

at the initial visit. In contrast, neither mean nor most recent 25 (OH)D levels were significantly associated with mortality or cardiovascular outcomes. Although neither mean nor most recent 25(OH)D levels showed statistically significant associations, the overall trends suggested higher mortality and cardiovascular event rates among those with lower 25(OH)D levels across all exposure definitions. For example, point estimates for mortality in the 20-29 ng/mL category for mean and recent levels were both elevated and statistically significant in some models, indicating that low vitamin D levels at follow-up may also contribute to risk.

Table 3 illustrates that low 25(OH)D levels (<20 ng/mL) were associated with an increased lifetime risk of cardiovascular events, including stroke, MI, and angina/bypass. Specifically,

Table 3
Lifetime analysis of 25(OH)D levels measured at the first cohort visit and lifetime risk of stroke, myocardial infarction, or angina/bypass; stroke alone, and myocardial infarction alone

25(OH)D (ng/mL)	Unadjusted analysis				Adjusted analysis[a]			
		95% CI				95% CI		
	Hazard ratio	Lower	Upper	*P* value	Hazard ratio	Lower	Upper	*P* value
Stroke, myocardial infarction, or angina/bypass								
<20	1.83	1.282	2.63	.0009	1.74	1.20	2.54	.0038
20-29	1.44	0.99	2.08	.055	1.46	0.99	2.13	.052
30-39	1 (ref)				1 (ref)			
40-49	1.31	0.88	1.94	.19	1.35	0.91	2.02	.14
50+	1.24	0.78	1.95	.36	1.32	0.83	2.10	.25
Stroke								
<20	1.63	1.06	2.50	.026	1.41	0.90	2.20	.14
20-29	1.26	0.81	1.97	.31	1.21	0.77	1.91	.40
30-39	1 (ref)				1 (ref)			
40-49	1.23	0.77	1.97	.40	1.28	0.79	2.06	.31
50+	1.13	0.65	1.96	.68	1.17	0.66	2.06	.60
Myocardial infarction								
<20	2.44	1.18	5.07	.017	2.42	1.12	5.24	.025
20-29	1.93	0.91	4.09	.086	2.10	0.96	4.58	.062
30-39	1 (ref)				1 (ref)			
40-49	1.53	0.68	3.48	.31	1.69	0.73	3.92	.22
50+	2.74	1.24	6.04	.012	3.41	1.50	7.74	.0033

25(OH)D, 25-hydroxyvitamin D.
[a] Adjusted for age, race, sex, and body mass index.

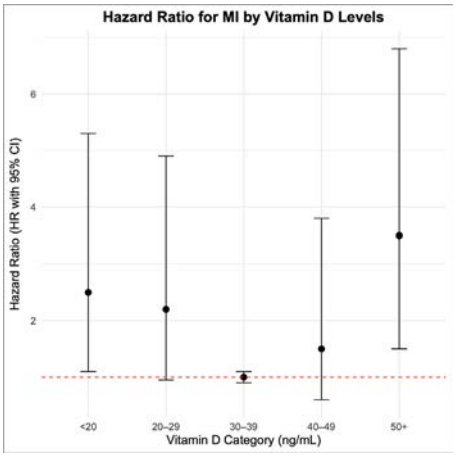

Figure. Initial 25-hydroxyvitamin D (25(OH)D) level and lifetime risk of myocardial infarction. This figure shows U-shaped association between 25(OH)D levels and the risk of myocardial infarction (MI). Both low (<20 ng/mL) and high (≥50 ng/mL) 25(OH)D levels were associated with an increased risk of MI, while the reference group (30-39 ng/mL) had the lowest risk. After adjustment, hazard ratios (HRs) for MI were elevated at both extremes of vitamin D levels, suggesting that both deficiency and excess may contribute to MI.

individuals with 25(OH)D levels below 20 ng/mL had a significantly higher risk of the combined outcome of stroke, MI, or angina/bypass, and this association remained significant after adjusting for race, sex, and body mass index (HR 1.74, $P = .0038$). Low 25(OH)D levels were also associated with a significantly increased risk of MI in both unadjusted and adjusted analyses. However, the association between low 25(OH)D and stroke was not significant after adjustment. Similarly, in lifetime analyses, <15 ng/mL at cohort entry was associated with increased risk of cardiovascular events and mortality (Supplementary Table S1). Adjustment for education did not materially alter these associations (Supplementary Table S3).

Both the unadjusted and adjusted analyses revealed a U-shaped association between 25(OH)D levels and the risk of MI. Compared to the reference group (30-39 ng/mL), individuals with low 25(OH)D levels (<20 ng/mL) had a significantly higher risk of MI (HR: 2.42, 95% CI: 1.12-5.24, $P = .025$). Similarly, those with high 25(OH)D levels (≥50 ng/mL) also had an increased risk of MI (HR: 3.41, 95% CI: 1.50-7.74, $P = .0033$). Although the 20 to 29 ng/mL and 40 to 49 ng/mL groups showed trends towards increased MI risk, these associations did not reach statistical significance. These findings suggest that both vitamin D deficiency and excess may contribute to an elevated risk of MI, supporting a nonlinear, U-shaped relationship between 25(OH)D levels and cardiovascular outcomes, as shown in the Figure.

An exploratory analysis was conducted among patients who had low initial 25(OH)D levels (<30 ng/mL) to assess whether subsequent improvement in 25(OH)D status affected cardiovascular risk (Table 4). Patients whose 25(OH)D levels remained below 30 ng/mL had a cardiovascular event rate of 8.0 per 1000 person-years. Those whose mean 25(OH)D rose to ≥30 ng/mL had a similar event rate of 7.8 per 1000 person-years (adjusted rate ratio 0.88, 95% CI: 0.45-1.72, $P = .71$). These results suggest no appreciable difference in event rates based on 25(OH)D change from low to higher levels during follow-up.

DISCUSSION

Our study is the first study that investigated the relationship between initial 25(OH)D levels, mortality and cardiovascular events, using both prospective and lifetime analyses in patients with SLE.

Initial low 25(OH)D levels (<20 ng/mL) were associated with significantly elevated risks of mortality, cardiovascular events, and stroke. Although the associations for mean and recent levels were not consistently statistically significant, the direction of effect estimates was generally similar, particularly for mortality, where elevated rate ratios were seen for both 20 to 29 and <20 ng/mL categories. These consistent trends suggest a potential role for sustained vitamin D deficiency in adverse outcomes, even beyond what is captured by a single baseline measurement. While the baseline level showed statistically significant associations in several models, for mortality, the point estimates for baseline, mean, and most recent vitamin D were similar—suggesting that no single timepoint clearly outperformed the others as a predictor. However, our data support the observation that later cardiovascular events were overrepresented among patients with low 25(OH)D levels at the initial visit, highlighting the potential importance of early vitamin D status in long-term cardiovascular risk.

In the second (lifetime) analysis, we were able to include events that happened before cohort entry or even before SLE diagnosis. This captures recent advances in the understanding of the natural history of cardiovascular events in SLE, with a peak early in SLE [32].

We observed a potential U-shaped association between initial 25(OH)D levels and the lifetime risk of MI in patients with SLE, with both low (<20 ng/mL) and high (≥50 ng/mL) levels associated with increased risk. This suggests that both extremes of 25(OH)D levels may predispose to adverse outcomes, although the modest number of MI events warrants cautious interpretation. Similar patterns have been reported in the general population [33,34], whereas a Mendelian randomisation study by Sutherland et al [23] described an L-shaped relationship, with HR plateauing at 25(OH)D levels above 50 ng/mL. A U-shaped association was also evident in our prior work on SLE and adverse pregnancy outcomes, where maternal 25(OH)D levels were associated with an increased risk of miscarriage, preterm delivery, and adverse pregnancy outcomes at both low and high

Table 4
Rate of cardiovascular events based on baseline and changing levels of 25(OH)D in the cohort

25(OH)D group	Person-years of follow-up	Number of CV events	Rate per 1000 person-years	Adjusted rate ratio	*P* value
Initial below 30 ng/mL, mean in the last year also below 30 ng/mL	1744	14	8.0	1.0 (ref)	
Initial below 30 ng/mL, mean in the last year above 30 ng/mL	3219	25	7.8	0.88 (0.45, 1.72)	.71
Initial above 30, mean in the last year below 30 ng/mL	370	1	2.7	0.39 (0.05, 3.00)	.37
Initial above 30, mean in the last year above 30 ng/mL	5100	24	4.7	0.57 (0.28, 1.14)	.11

CV, cardiovascular; 25(OH)D, 25-hydroxyvitamin D.

25(OH)D levels [35]. The mechanisms underlying these associations are not fully understood, but several biologically plausible explanations have been proposed. At high 25(OH)D levels, excess intestinal calcium and phosphate absorption increases the calcium–phosphate product, promoting medial and valvular calcification through vascular smooth muscle cell reprogramming and altered regulation of parathyroid hormone (PTH) and fibroblast growth factor 23 (FGF-23) [36]; animal models confirm these effects, and human observational studies have reported associations between high-dose exposure and vascular calcification [37]. At low levels, impaired immune modulation, endothelial dysfunction, Renin–Angiotensin–Aldosterone System (RAAS) activation, oxidative stress, and proinflammatory cytokines may contribute to atherothrombosis and hypertension. Vitamin D acts via the vitamin D receptor in cardiovascular and immune tissues, influencing pathways involved in calcification, inflammation, thrombosis, and vascular tone, providing biologic plausibility for both deficiency- and excess-related risk [36]. The finding that there is a 'therapeutic' window for 25(OH)D (in other words, that higher levels could be harmful) means that a 'one size fits all' approach to supplementation would not be advisable in SLE. In multiple sclerosis, on the other hand, a randomised clinical trial of 100,000 units every other week did reduce disease activity [38], underscoring that optimal dosing thresholds may vary across diseases.

The stronger association of cardiovascular outcomes with initial 25(OH)D levels, rather than later fluctuations, suggests that early deficiency could be linked to vascular and immune changes that persist over time. In SLE, reduced cutaneous synthesis and renal 1α-hydroxylation can impair vitamin D metabolism, promoting endothelial dysfunction, inflammation, and atherogenesis [39,40]. Excess 25(OH)D may conversely favour vascular calcification through calcium–phosphate imbalance [36]. Once these processes are established, later correction may have limited impact, consistent with the lack of benefit seen when low levels improved during follow-up.

Notably, even among patients whose 25(OH)D improved from <30 ng/mL to ≥30 ng/mL during cohort participation, cardiovascular event rates remained similar. This supplemental analysis found no significant reduction in risk associated with 25(OH)D improvement (adjusted rate ratio 0.88, $P = .71$), suggesting that short-term increases in serum levels may not substantially alter long-term cardiovascular risk once deficiency has occurred. This raises the possibility that early or sustained vitamin D sufficiency may be more important in preventing events.

This study has several important strengths. It is the first study in SLE to investigate the relationship between mortality, cardiovascular outcomes, and serum 25(OH)D levels at various time points. Additionally, the extended follow-up period strengthens the reliability of the findings, providing a robust basis for assessing long-term outcomes. The analysis also accounted for racial differences, enabling a more thorough evaluation across diverse populations. However, some limitations should be considered. This is an observational study, and causality cannot be inferred. We did not have an independent validation cohort, which may limit generalisability. Frequent direct measurement of serum 25(OH)D was considered a more accurate integrative marker of vitamin D status than self-reported supplement use, which may be prone to recall bias and incomplete dosage information. Although socioeconomic status and nutritional habits were not comprehensively available, we incorporated education as a proxy for socioeconomic status in sensitivity analyses. Adjustment for education did not materially alter our findings, supporting the robustness of the observed associations. The modest number of MI events also limits precision in assessing nonlinear relationships.

CONCLUSIONS

In this longitudinal study of patients with SLE, low initial 25(OH)D levels (<20 ng/mL) were significantly associated with increased risks of mortality, cardiovascular events, and stroke. While mean and most recent 25(OH)D levels were not consistently statistically significant, similar effect estimates and elevated rate ratios across low categories suggest a persistent trend towards increased risk with lower 25(OH)D levels. A U-shaped association was observed for MI, with both low and high 25(OH)D levels associated to greater risk. Among patients with initially low vitamin D, improving levels during follow-up did not reduce cardiovascular event rates, raising important questions about the timing and long-term impact of vitamin D supplementation in altering cardiovascular outcomes in SLE.

Acknowledgements

We gratefully acknowledge the patients, investigators, and the data management and study teams involved in the Hopkins Lupus Cohort.

Contributors

All authors contributed to the study conception and design. TA, DG, and MP were responsible for data acquisition. TA, AF, LSM, and MP contributed to data analysis and interpretation. All authors contributed to drafting the manuscript or revising it critically for important intellectual content, and all approved the final version for publication. MP had full access to all study data and takes responsibility for the integrity of the data and the accuracy of the analyses.

Funding

This work was supported by NIH grant R01AR069572 (MP) and R01DK134625 (AF).

Competing interests

MP reports financial support was provided by National Institutes of Health. MP reports a relationship with National Institutes of Health that includes: funding grants. The other authors declare they have no competing interests.

Patient consent for publication

Not applicable.

Ethics approval

The Hopkins Lupus cohort was approved by the Johns Hopkins University School of Medicine Institutional Review Board (study number NA_00039294). Patients' rights, safety, and well-being were protected based on the principles of the Declaration of Helsinki. .

Provenance and peer review

Not commissioned; externally peer reviewed.

Supplementary materials

Supplementary material associated with this article can be found in the online version at doi:10.1016/j.ard.2025.10.013.

Orcid

Theerada Assawasaksakul: http://orcid.org/0000-0001-5508-0085
Michelle Petri: http://orcid.org/0000-0003-1441-5373

REFERENCES

[1] Lee YH, Song GG. Mortality in patients with systemic lupus erythematosus: a meta-analysis of overall and cause-specific effects. Lupus 2024;33(9):929–37.
[2] Bikle DD. Vitamin D metabolism, mechanism of action, and clinical applications. Chem Biol 2014;21(3):319–29.
[3] Guillot X, Semerano L, Saidenberg-Kermanac'h N, Falgarone G, Boissier MC. Vitamin D and inflammation. Joint Bone Spine 2010;77(6):552–7.
[4] Cannell JJ, Grant WB, Holick MF. Vitamin D and inflammation. Dermatoendocrinol 2014;6(1):e983401.
[5] Tintut Y, Demer LL. Potential impact of the steroid hormone, vitamin D, on the vasculature. Am Heart J 2021;239:147–53.
[6] Islam MA, Khandker SS, Alam SS, Kotyla P, Hassan R. Vitamin D status in patients with systemic lupus erythematosus (SLE): a systematic review and meta-analysis. Autoimmun Rev 2019;18(11):102392.
[7] Kavadichanda C, Singh P, Maurya S, Tota S, Kiroubagarin A, Kounassegarane D, et al. Clinical and serological association of plasma 25-hydroxyvitamin D (25(OH)D) levels in lupus and the short-term effects of oral vitamin D supplementation. Arthritis Res Ther 2023;25(1):2.
[8] Zhang X, Guo Q, Sun S, Tang X, Shen W, Liang J, et al. Factors associated with 25-hydroxyvitamin D level in Chinese hospitalized patients with systemic lupus erythematosus: a retrospective cohort study. Rheumatol Int 2024;44(10):2067–78.
[9] Zittermann A, Iodice S, Pilz S, Grant WB, Bagnardi V, Gandini S. Vitamin D deficiency and mortality risk in the general population: a meta-analysis of prospective cohort studies. Am J Clin Nutr 2012;95(1):91–100.
[10] Schöttker B, Jorde R, Peasey A, Thorand B, Jansen EH, Groot L, et al. Vitamin D and mortality: meta-analysis of individual participant data from a large consortium of cohort studies from Europe and the United States. BMJ 2014;348:g3656.
[11] Chowdhury R, Kunutsor S, Vitezova A, Oliver-Williams C, Chowdhury S, Kiefte-de-Jong JC, et al. Vitamin D and risk of cause specific death: systematic review and meta-analysis of observational cohort and randomised intervention studies. BMJ 2014;348:g1903.
[12] Garland CF, Kim JJ, Mohr SB, Gorham ED, Grant WB, Giovannucci EL, et al. Meta-analysis of all-cause mortality according to serum 25-hydroxyvitamin D. Am J Public Health 2014;104(8):e43–50.
[13] Gaksch M, Jorde R, Grimnes G, Joakimsen R, Schirmer H, Wilsgaard T, et al. Vitamin D and mortality: individual participant data meta-analysis of standardized 25-hydroxyvitamin D in 26916 individuals from a European consortium. PLoS One 2017;12(2):e0170791.
[14] Zhu A, Kuznia S, Boakye D, Schöttker B, Brenner H. Vitamin D-binding protein, bioavailable, and free 25(OH)D, and mortality: a systematic review and meta-analysis. Nutrients 2022;14(19):3894.
[15] Fang A, Zhao Y, Yang P, Zhang X, Giovannucci EL. Vitamin D and human health: evidence from Mendelian randomization studies. Eur J Epidemiol 2024;39(5):467–90.
[16] Jaiswal V, Ishak A, Peng Ang S, Babu Pokhrel N, Shama N, Lnu K, et al. Hypovitaminosis D and cardiovascular outcomes: a systematic review and meta-analysis. Int J Cardiol Heart Vasc 2022;40:101019.
[17] Liu J, Tian C, Tang Y, Geng B. Associations of the serum vitamin D with mortality in postmenopausal women. Clin Nutr 2024;43(1):211–7.
[18] Trummer O, Pilz S, Hoffmann MM, Winkelmann BR, Boehm BO, März W, et al. Vitamin D and mortality: a Mendelian randomization study. Clin Chem 2013;59(5):793–7.
[19] Ong JS, Gharahkhani P, An J, Law MH, Whiteman DC, Neale RE, et al. Vitamin D and overall cancer risk and cancer mortality: a Mendelian randomization study. Hum Mol Genet 2018;27(24):4315–22.
[20] Aspelund T, Grübler MR, Smith AV, Gudmundsson EF, Keppel M, Cotch MF, et al. Effect of genetically low 25-hydroxyvitamin D on mortality risk: Mendelian randomization analysis in 3 large European cohorts. Nutrients 2019;11(1):74.
[21] Meng X, Li X, Timofeeva MN, He Y, Spiliopoulou A, Wei WQ, et al. Phenome-wide Mendelian-randomization study of genetically determined vitamin D on multiple health outcomes using the UK Biobank study. Int J Epidemiol 2019;48(5):1425–34.
[22] Huang T, Afzal S, Yu C, Guo Y, Bian Z, Yang L, et al. Vitamin D and cause-specific vascular disease and mortality: a Mendelian randomisation study involving 99,012 Chinese and 106,911 European adults. BMC Med 2019;17(1):160.
[23] Sutherland JP, Zhou A, Hyppönen E. Vitamin D deficiency increases mortality risk in the UK Biobank: a nonlinear Mendelian randomization study. Ann Intern Med 2022;175(11):1552–9.
[24] Emerging Risk Factors Collaboration/EPIC-CVD/Vitamin D Studies Collaboration. Estimating dose-response relationships for vitamin D with coronary heart disease, stroke, and all-cause mortality: observational and Mendelian randomisation analyses. Lancet Diabetes Endocrinol 2024;12(1):e2–11.
[25] Brøndum-Jacobsen P, Benn M, Jensen GB, Nordestgaard BG. 25-hydroxyvitamin d levels and risk of ischemic heart disease, myocardial infarction, and early death: population-based study and meta-analyses of 18 and 17 studies. Arterioscler Thromb Vasc Biol 2012;32(11):2794–802.
[26] Huang J, Wang Z, Hu Z, Jiang W, Li B. Association between blood vitamin D and myocardial infarction: a meta-analysis including observational studies. Clin Chim Acta 2017;471:270–5.
[27] Lin X, Chen X, Liu S, Deng Y, Wang Y, Lu Q, et al. Associations of serum 25 (OH)D with risk of recurrent cardiovascular events in individuals with coronary heart disease. J Clin Endocrinol Metab 2023;108(12):e1712–9.
[28] Brøndum-Jacobsen P, Nordestgaard BG, Schnohr P, Benn M. 25-Hydroxyvitamin D and symptomatic ischemic stroke: an original study and meta-analysis. Ann Neurol 2013;73(1):38–47.
[29] Tsai MC, Fan HY, Hsu HY, Tseng PJ, Chuang SM, Yeh TL, et al. Association of serum 25-hydroxyvitamin D with stroke: observational mediation and Mendelian randomization study. J Clin Endocrinol Metab 2025;110(5):e1420–9.
[30] Petri M, Orbai AM, Alarcón GS, Gordon C, Merrill JT, Fortin PR, et al. Derivation and validation of the systemic lupus international collaborating clinics classification criteria for systemic lupus erythematosus. Arthritis Rheum 2012;64(8):2677–86.
[31] Gladman D, Ginzler E, Goldsmith C, Fortin P, Liang M, Urowitz M, et al. The development and initial validation of the systemic lupus international collaborating clinics/American College of Rheumatology damage index for systemic lupus erythematosus. Arthritis Rheum 1996;39(3):363–9.
[32] Garg S, Bartels CM, Bao G, Helmick CG, Drenkard C, Lim SS. Timing and predictors of incident cardiovascular disease in systemic lupus erythematosus: risk occurs early and highlights racial disparities. J Rheumatol 2023;50(1):84–92.
[33] Durup D, Jørgensen HL, Christensen J, Tjønneland A, Olsen A, Halkjær J, et al. A reverse J-shaped association between serum 25-hydroxyvitamin D and cardiovascular disease mortality: the CopD study. J Clin Endocrinol Metab 2015;100(6):2339–46.
[34] Shi JW, Wu JN, Zhu XY, Zhou WH, Yang JY, Li MQ. Association of serum 25-hydroxyvitamin D levels with all-cause and cause-specific mortality among postmenopausal females: results from NHANES. J Transl Med 2023;21(1):629.
[35] Madanchi N, Fava A, Goldman DW, Magder LS, Petri M. Association between 25-hydroxyvitamin D levels and adverse pregnancy outcomes in systemic lupus erythematosus. Arthritis Care Res (Hoboken) 2025;77(4):432–9.
[36] Razzaque MS. The dualistic role of vitamin D in vascular calcifications. Kidney Int 2011;79(7):708–14.
[37] Demer LL, Hsu JJ, Tintut Y. Steroid hormone vitamin D: implications for cardiovascular disease. Circ Res 2018;122(11):1576–85.
[38] Thouvenot E, Laplaud D, Lebrun-Frenay C, Derache N, Le Page E, Maillart E, et al. High-dose vitamin D in clinically isolated syndrome typical of multiple sclerosis: the D-Lay MS randomized clinical trial. JAMA 2025;333(16):1413–22.
[39] Mok CC. Vitamin D and systemic lupus erythematosus: an update. Expert Rev Clin Immunol 2013;9(5):453–63.
[40] Ho LJ, Wu CH, Luo SF, Lai JH. Vitamin D and systemic lupus erythematosus: causality and association with disease activity and therapeutics. Biochem Pharmacol 2024;227:116417.

Ann Rheum Dis 85 (2026) 647–658

Contents lists available at ScienceDirect

Annals of the Rheumatic Diseases

journal homepage: https://www.sciencedirect.com/journal/annals-of-the-rheumatic-diseases

Systemic lupus erythematosus

Treatment nonresponders in lupus nephritis characteristically exhibit persistent type I interferon signalling in monocytes: a longitudinal single-cell transcriptomic analysis

Woo-Joong Kim[1,2,†], Hye-Soon Lee[3,4,5,†], So-Young Bang[3,4,5], Young Bin Joo[3,4,5], Bo-Kyeong Kang[6], Mimi Kim[6], Hyunsung Kim[7], Sung Yul Park[8], Woong-Yang Park[9], Eui-Cheol Shin[1,‡,**], Sang-Cheol Bae[3,4,5,‡,*]

[1] *Graduate School of Medical Science and Engineering, Korea Advanced Institute of Science and Technology, Daejeon, Republic of Korea*
[2] *Department of Rheumatology, Chung-Ang University Hospital, Seoul, Republic of Korea*
[3] *Department of Rheumatology, Hanyang University Hospital for Rheumatic Diseases, Seoul, Republic of Korea*
[4] *Hanyang University Institute for Rheumatology Research, Seoul, Republic of Korea*
[5] *Hanyang Institute of Bioscience and Biotechnology, Hanyang University, Seoul, Republic of Korea*
[6] *Department of Radiology, Hanyang University College of Medicine, Seoul, Republic of Korea*
[7] *Department of Pathology, Hanyang University College of Medicine, Seoul, Republic of Korea*
[8] *Department of Urology, Hanyang University College of Medicine, Seoul, Republic of Korea*
[9] *Samsung Genome Institute, Samsung Medical Center, Sungkyunkwan University School of Medicine, Seoul, Republic of Korea*

ARTICLE INFO

Article history:
Received 6 August 2025
Received in revised form 15 November 2025
Accepted 4 December 2025

ABSTRACT

Objectives: We aimed to characterise the dynamic transcriptional changes associated with treatment responses in lupus nephritis (LN) through longitudinal single-cell RNA sequencing analysis of peripheral blood mononuclear cells (PBMCs) during standard-of-care induction therapy.

Methods: We leveraged the Korean Unlimited multi-Dimensional Omics research in Systemic lupus erythematosus cohort, comprising patients with biopsy-proven active proliferative LN. Single-cell RNA sequencing of PBMCs was conducted at baseline and subsequently at 3, 6, and 12 months following initiation of therapy (n = 10). For validation purposes, bulk RNA sequencing of monocytes was performed in an independent patient group at baseline and at 3 months (n = 13). Renal response was classified as complete response or nonresponse at 12 months according to predefined criteria.

Results: In single-cell RNA sequencing analysis of patients with LN, the myeloid cell population—particularly classical and intermediate monocytes—demonstrated the highest number of differentially expressed genes following induction therapy. Weighted gene coexpression network analysis identified distinct gene modules closely associated with treatment responses. Complete responders exhibited progressive suppression of type I interferon (IFN-I) signalling, whereas nonresponders maintained persistent IFN-I-driven gene expression characterised by sustained inflammatory features. Bulk RNA sequencing of monocytes from an independent group of

*Correspondence to Dr. Sang-Cheol Bae, Hanyang University Hospital for Rheumatic Diseases, Seoul, Republic of Korea.
**Correspondence to Dr. Eui-Cheol Shin, Korea Advanced Institute of Science and Technology, Daejeon, Republic of Korea.
E-mail addresses: ecshin@kaist.ac.kr (E.-C. Shin), scbae@hanyang.ac.kr (S.-C. Bae).
Handling editor Josef S. Smolen.
† Woo-Joong Kim and Hye-Soon Lee are joint first authors.
‡ Eui-Cheol Shin and Sang-Cheol Bae are joint senior authors.

https://doi.org/10.1016/j.ard.2025.12.002

patients with LN confirmed that 6 IFN-I-responsive genes (IRF7, ISG15, LY6E, IFI44, IFI44L, and IFI6) were significantly downregulated by 3 months in complete responders, but not in nonresponders. This gene signature correlated with both proteinuria and disease activity scores.
Conclusions: This study demonstrates that persistent IFN-I-driven gene expression in monocytes characterises treatment resistance in LN. Our findings suggest that early transcriptional profiling may enable timely identification of nonresponders and warrant further investigation in larger, independent cohorts.

WHAT IS ALREADY KNOWN ON THIS TOPIC

- Type I interferons (IFN-Is) are key pathogenic drivers in systemic lupus erythematosus and lupus nephritis (LN). IFN-Is upregulates various interferon-stimulated genes (ISGs) through canonical and noncanonical signalling pathways. However, the dynamics of cellular IFN-I signalling pathways in patients with LN during induction treatment remain unexplored, particularly in relation to treatment responses.

WHAT THIS STUDY ADDS

- We conducted the time-series single-cell RNA sequencing of peripheral blood mononuclear cells from patients with LN, enabling a dynamic view of transcriptional changes according to treatment responses.
- This study reveals that nonresponder monocytes retained elevated ISG expression, in contrast to complete responders who effectively suppressed IFN-I-driven gene expression.
- Bulk RNA sequencing of monocytes from independent patients showed that divergent IFN-I-responsive gene patterns emerge as early as 3 months posttreatment.
- The expression of 6 IFN-I-responsive genes (IRF7, ISG15, LY6E, IFI44, IFI44L, and IFI6) was correlated with both proteinuria and overall disease activity after treatment.

HOW THIS STUDY MIGHT AFFECT RESEARCH, PRACTICE OR POLICY

- This study elucidates the mechanistic anchoring of the complex IFN-I pathways in treatment response to induction therapy. By identifying persistent upregulation of ISGs as a molecular signature of nonresponse, our findings provide insights for developing early prognostic tools in LN. Prospective studies are needed to determine whether IFN-I-targeted interventions could benefit patients with persistent signatures.

INTRODUCTION

Systemic lupus erythematosus (SLE) is a chronic autoimmune disease characterised by widespread inflammation and multiorgan involvement, with lupus nephritis (LN) being one of its most severe manifestations. LN develops in roughly 35% to 60% of patients with SLE and is a leading contributor to both morbidity and mortality [1,2]. Although current standard-of-care immunosuppressive therapies have improved LN outcomes over the past decades, a substantial proportion of patients fail to achieve remission or experience frequent disease flares [3,4]. Clinicians often face the therapeutic dilemma of balancing an intensified immunosuppressive regimen to preserve kidney function against escalating medication burden. To address this challenge, a deeper understanding of the immunological mechanisms underlying therapeutic resistance in LN is essential for developing more targeted and effective treatment strategies.

Type I interferons (IFN-Is; eg, IFN-α and IFN-β) are pivotal amplifiers of SLE pathogenesis. They orchestrate multiple proinflammatory processes—promoting autoreactive B cell survival, activating T cells, and stimulating cytokine production—thereby driving tissue damage [5,6]. Phase 3 trials (Treatment of Uncontrolled Lupus via the Interferon Pathway (TULIP)-1 and -2) of anifrolumab, an IFN-I receptor antagonist, underscored the importance of IFN-I signalling by showing that blocking this pathway markedly reduces interferon-stimulated gene (ISG) expression [7]. Although the 'IFN signature'—increased ISG expression in blood cells used to assess IFN-I pathway activation—correlates with disease activity in most patients with SLE, its value for predicting treatment response has not been established [8–11]. Moreover, different assays measure different ISGs, introducing methodological heterogeneity that hampers the clinical application [12].

IFN-I signalling classically involves the phosphorylation of STAT1 and STAT2 proteins, which then complex with IRF9 to form the canonical transcription factor ISGF3, activating rapid and transient expression of ISGs (Supplementary Fig S1). However, evidence suggests that alternative 'noncanonical' IFN-I signalling pathways may sustain ISG expression [13,14]. Specifically, prolonged IFN-I exposure leads to accumulation of STAT1, STAT2, and IRF9 proteins, which can form U-ISGF3—an unphosphorylated ISGF3 complex that drives expression of a distinct ISG subset. This exaggerated IFN-I response, characterised by sustained expression of U-ISGF3–inducible genes, has been shown to contribute to hyperinflammation in high-risk patients with COVID-19 [15]. Interestingly, corticosteroid treatment significantly suppressed the expression of U-ISGF3–inducible genes by downregulating STAT1 expression in monocytes.

In LN kidney biopsy tissues, ISGs are highly expressed across immune cell populations, but are notably absent in renal epithelial cells [16]. The strong correlation observed between IFN-I signatures in matched blood and kidney samples suggests that IFN-I pathway activation in LN is predominantly driven by extrarenal mechanisms. However, the mechanisms driving persistent intrarenal inflammation despite aggressive immunosuppressive therapies remain poorly understood. We conducted systematic single-cell analyses of temporal gene expression dynamics in circulating immune cells from patients with LN undergoing induction treatment, aiming to identify molecular signatures that complement existing clinical indicators and reveal immunoregulatory networks that distinguish responders from nonresponders.

METHODS

Study design and participants

This study was based on data and biospecimens obtained from the Korean Unlimited multi-Dimensional Omics research in SLE (KUDOS) cohort, a prospective registry of patients with biopsy-proven LN at Hanyang University Hospital for Rheumatic Diseases in South Korea. Patients were recruited between March 2018 and July 2020 [17]. All patients were ≥18 years old and fulfilled either the 2012 Systemic Lupus International

Collaborating Clinics or 2019 European League Against Rheumatism/American College of Rheumatology (ACR) classification criteria for SLE [18,19].

From the KUDOS cohort, we retrospectively selected a homogeneous population of 10 patients for single-cell RNA sequencing, including only those who demonstrated either complete response (CR, n = 5) or nonresponse (NR, n = 5) at 12 months, excluding partial responders (group 1). To validate the study findings, an additional 13 patients (CR, n = 7; NR, n = 6) were selected from the same cohort for bulk RNA sequencing of monocytes (group 2). Eligible participants had active, proliferative LN confirmed by renal biopsy, with persistent proteinuria (urine protein-to-creatinine ratio [UPCR] ≥500 mg/g or 24-hour urine protein ≥500 mg/d) and/or active urinary sediment (>5 red or white blood cells per high-power field or presence of cellular casts).

All patients received standard-of-care induction therapy with high-dose corticosteroids and mycophenolate mofetil (MMF, 2 g/d) according to LN management guidelines [20−23], after renal biopsy and baseline blood sampling. No patient received biologic agents such as anifrolumab, belimumab, or rituximab. This study was conducted in accordance with the Declaration of Helsinki and was approved by the Institutional Review Board (IRB) of the Hanyang University Hospital (IRB No: HYUH2017-08-035). All study participants provided written informed consent.

Sample collection and clinical assessment

Blood samples were prospectively collected from all participants in the KUDOS cohort at predefined timepoints. Peripheral blood mononuclear cells (PBMCs) were isolated by Ficoll-Paque density gradient centrifugation (GE Healthcare), resuspended in freezing medium (RPMI 1640 with 20% foetal bovine serum and 10% DMSO), and stored in liquid nitrogen. For group 1 (single-cell RNA sequencing), PBMC samples were analysed at 4 timepoints: baseline (before high-dose corticosteroids and MMF administration) and at 3, 6, and 12 months following therapy initiation. For group 2 (bulk RNA sequencing), monocytes were isolated from PBMCs collected at baseline and 3 months posttreatment. Baseline sampling in both groups was performed on the same day as the renal biopsy, immediately before the procedure.

Baseline and follow-up clinical data on renal function were collected, including serum creatinine, estimated glomerular filtration rate, blood urea nitrogen, and UPCR obtained from either spot urine samples or 24-hour urine collections. Additionally, SLE-related autoantibodies (such as anti-dsDNA antibodies) and complement levels (C3, C4, and CH50) were assessed. Disease activity was measured using the SLE Disease Activity Index 2000 (SLEDAI-2K) [24]. Histopathological classification of LN, including activity index and chronicity index, was performed according to the revised 2018 International Society of Nephrology/Renal Pathology Society guideline [25]. Treatment responses were classified according to the ACR and Kidney Disease: Improving Global Outcomes criteria [26,27].

Single-cell RNA sequencing and data processing

Single-cell RNA sequencing was performed using the 10 × Genomics Chromium platform and sequenced on an Illumina sequencer. Raw data were processed with Cell Ranger (v6.1.2), aligned to human genome reference GRCh38-2020-A, and imported into Seurat (v4.3). Quality control removed cells expressing fewer than 200 or more than 6000 genes, mitochondrial content >10%, or identified as doublets by scDblFinder (v1.13.10). Data were normalised (Seurat's SCTransform), batch-corrected (Batchelor v1.19.0, Harmony v1.2.0), and visualised with uniform manifold approximation and projection, using top 20 mutual nearest neighbour components for PBMCs and top 16 principal components for myeloid cells.

Differential gene expression and functional enrichment analysis

Differential expression analyses were performed on pseudobulk profiles using DESeq2 (v1.30.1). Transcripts with adjusted P values < .05 and absolute $\log_2$ fold change > 0.25 after adaptive shrinkage were considered significant. Gene set module scores were computed using Seurat's AddModuleScore. Overrepresentation analyses were conducted using a hypergeometric test (fgsea v1.16.0) with gene sets from the Hallmark, Gene Ontology, Reactome, TRRUST (version 2), and published IFN signatures [14,28−36].

Weighted gene coexpression network analysis

Weighted gene coexpression network analysis (WGCNA) was conducted on longitudinal single-cell RNA sequencing data, using genes filtered by variance. Following standard quality filtering to remove low-quality genes and samples, a signed weighted correlation matrix was generated using pairwise Pearson correlations (soft-threshold $\beta = 6$). Modules were identified using hierarchical clustering of topological overlap matrices and the dynamic hybrid tree-cut algorithm (minimum module size = 50, threshold = 0.3).

Monocytes RNA sequencing and analysis

Monocytes were isolated from PBMCs using magnetic-activated cell sorting (Pan Monocyte Isolation Kit, Miltenyi Biotec). RNA was extracted using TRIzol (Thermo Fisher Scientific) and depleted of rRNA and globin mRNA (QIAseq FastSelect−rRNA HMR Kit, Qiagen). Libraries prepared with QIAseq FX Single Cell RNA Kit were sequenced (Illumina Novaseq X, 150-bp paired-end reads). Reads were aligned (GRCh38-2020-A) with BWA (v0.7.17) and counts generated using SAMtools (v1.17).

Statistics and reproducibility

All analyses were performed in R (R Foundation for Statistical Computing, Vienna, Austria), and visualisation of the findings used ggplot2 (v3.4.2) and GraphPad Prism (GraphPad Software, San Diego, CA, USA, v9.0.0). Group differences were assessed with Student's t-test (Welch's correction), Mann-Whitney test, or Fisher's exact test. For metagene analysis, a standardised approach was employed to quantitatively compare the collective expression activity of gene sets across different samples and conditions. Normalised expression values for genes of interest were extracted from relevant cell populations. To account for intergene expression variability and different baseline expression levels, z-scores were computed across all cells for each gene. A 10% trimmed mean of these z-scores across all genes in the signature was then calculated per cell, providing a robust metagene score less sensitive to outliers. These cell-level metagene scores were then aggregated by sample to generate sample-level scores for statistical comparison. Linear mixed-effects models were fitted to metagene z-scores using restricted maximum likelihood, with patient identity as a random effect and sampling timepoints as fixed effects. Linear regression identified predictors of continuous variables. P values < .05 were considered statistically significant, with multiple testing correction

performed using the Benjamini-Hochberg method (false discovery rate (FDR) < 0.05). For validation, we employed leave-one-donor-out cross-validation for single-cell WGCNA analysis (excluding all longitudinal samples from each donor iteratively) and leave-one-out cross-validation for bulk transcriptomic analysis. Gene-level stability was assessed using bootstrap resampling (1000 iterations), and random forest classification was applied to validate feature importance.

RESULTS

Baseline characteristics of study participants

A total of 23 patients from the KUDOS cohort were included in this study: group 1 (n = 10) underwent single-cell transcriptomic analysis of PBMCs, and group 2 (n = 13) underwent bulk transcriptomic analysis of isolated monocytes. Baseline clinical characteristics of both groups are summarised in Table 1 and Supplementary Figure S2.

The 2 groups showed comparable baseline clinical features. Median age was 33 years in group 1 and 38 years in group 2, with female predominance in both groups. Clinical parameters were similar between groups: median SLEDAI-2K score (17 vs 16), serum creatinine (0.6 mg/dL in both), and UPCR (1616 vs 1218 mg/g). All patients had biopsy-proven proliferative LN, with predominantly class IV in group 1 but more heterogeneous in group 2. Histologic activity and chronicity indices were similarly comparable. All patients received MMF and oral glucocorticoids for induction therapy.

Table 1
Baseline characteristics of study participants

	Group 1: scRNA-seq analysis	Group 2: bulk RNA-seq analysis
Number	10	13
Demographics		
Age (y)	33 (21, 52)	38 (23, 58)
Female	10 (100)	11 (84.6)
LN activity parameters		
Urine protein-to-creatinine (mg/g)	1616 (846, 5308)	1218 (534, 2939)
Serum creatinine (mg/dL)	0.6 (0.4, 1.6)	0.6 (0.5, 1.4)
C3 (mg/dL)	48 (24, 61)	50 (39, 106)
C4 (mg/dL)	9 (2, 15)	9 (4, 23)
Anti-dsDNA antibody positive	6 (60)	11 (84.6)
SLEDAI-2K	17 (10, 22)	16 (8, 21)
Renal histology		
ISN/RPS class		
III	0	6 (46.2)
III + V	0	2 (15.4)
IV	9 (90)	4 (30.8)
IV + V	1 (10)	1 (7.7)
LN activity index	8 (5, 14)	6 (2, 11)
LN chronicity index	1 (0, 5)	1 (0, 5)
Treatment		
Prior immunosuppressive therapy (ever exposed)		
Hydroxychloroquine	10 (100)	13 (100)
Mycophenolate mofetil	7 (70)	7 (54)
Cyclophosphamide	2 (20)	7 (54)
Azathioprine	3 (30)	6 (46)
Cyclosporine	2 (20)	1 (8)
Tacrolimus	1 (10)	3 (23)
Methotrexate	4 (40)	4 (31)
Mizoribine	1 (10)	1 (8)
Induction treatment regimen		
Mycophenolate mofetil based	10 (100)	13 (100)
Glucocorticoids	10 (100)	13 (100)
Renal response		
Complete response	5 (50)	7 (53.8)
Nonresponse	5 (50)	6 (46.2)

C3, complement 3; C4, complement 4; ISN/RPS, International Society of Nephrology/Renal Pathology Society; LN, lupus nephritis; scRNA-seq, single-cell RNA sequencing; SLEDAI-2K, systemic lupus erythematosus disease activity index 2000.
Data are presented as n (%) or median (min, max).
No significant differences were observed between groups 1 and 2; individual *P* values are not reported.

Treatment outcomes were evenly distributed in group 1 (50% CR, 50% NR), whereas group 2 showed 53.8% CR and 46.2% NR. Prior MMF exposure was more frequent in the NR subgroup compared with the CR subgroup. A statistically significant baseline difference was not detected for clinical disease activity parameters and renal histological features between CR and NR subgroups (Supplementary Table S1).

Immune cell transcriptomic alterations following induction therapy

To explore the transcriptional dynamics underlying treatment response in LN, we performed single-cell transcriptomic profiling of PBMCs from the 10 female patients in group 1. Blood samples were collected at baseline (before high-dose corticosteroids and MMF administration) and at 3, 6, and 12 months following standard induction therapy (Fig 1A).

Analysis of all 40 samples yielded a total of 238,366 high-quality single cells. Unsupervised hierarchical clustering identified 5 major immune compartments: natural killer (NK) and T cells, monocytes and dendritic cells (DCs), B cells, plasmablasts, and plasmacytoid DCs, comprising 13 distinct annotated cell types (Fig 1B, Supplementary Fig S3A). Following immunosuppressive treatment, no cell populations showed statistically significant temporal changes in relative abundance compared to baseline (Supplementary Fig S3B).

All subjects in group 1 achieved their respective treatment response (CR or NR) by 6 months and maintained this status through 12 months, with highly similar transcriptomic profiles between these timepoints, thus supporting our approach of combining data from both 6-month and 12-month timepoints as ‘posttreatment’ samples when generating the pseudobulk expression matrix.

Analysis of these posttreatment samples revealed that monocytes and DCs exhibited the largest number of differentially expressed genes (DEGs) among all immune cell compartments (Fig 1C). Pathway enrichment analysis using the Hallmark gene sets revealed that treatment-associated transcriptional changes occur across multiple immune compartments (Supplementary Fig S4). Despite this response pattern, monocytes and DCs exhibited substantially greater pathway enrichment scores and dynamic ranges compared with NK/T cells or B cells following induction treatment (Supplementary Fig S5). This indicates that myeloid cells serve as highly sensitive sentinels of systemic immune status, providing an analytical framework for identifying key transcriptional signatures associated with treatment responses in LN.

Classical and intermediate monocytes exhibit convergent transcriptional changes

Focusing on myeloid cell–specific profiles, we analysed 31,536 single-cell transcriptomes and identified 4 principal cell types consistently present across samples: classical monocytes (CMs), intermediate monocytes (IMs), nonclassical monocytes (NMs), and DCs (Fig 2A, Supplementary Fig S6A). Differential

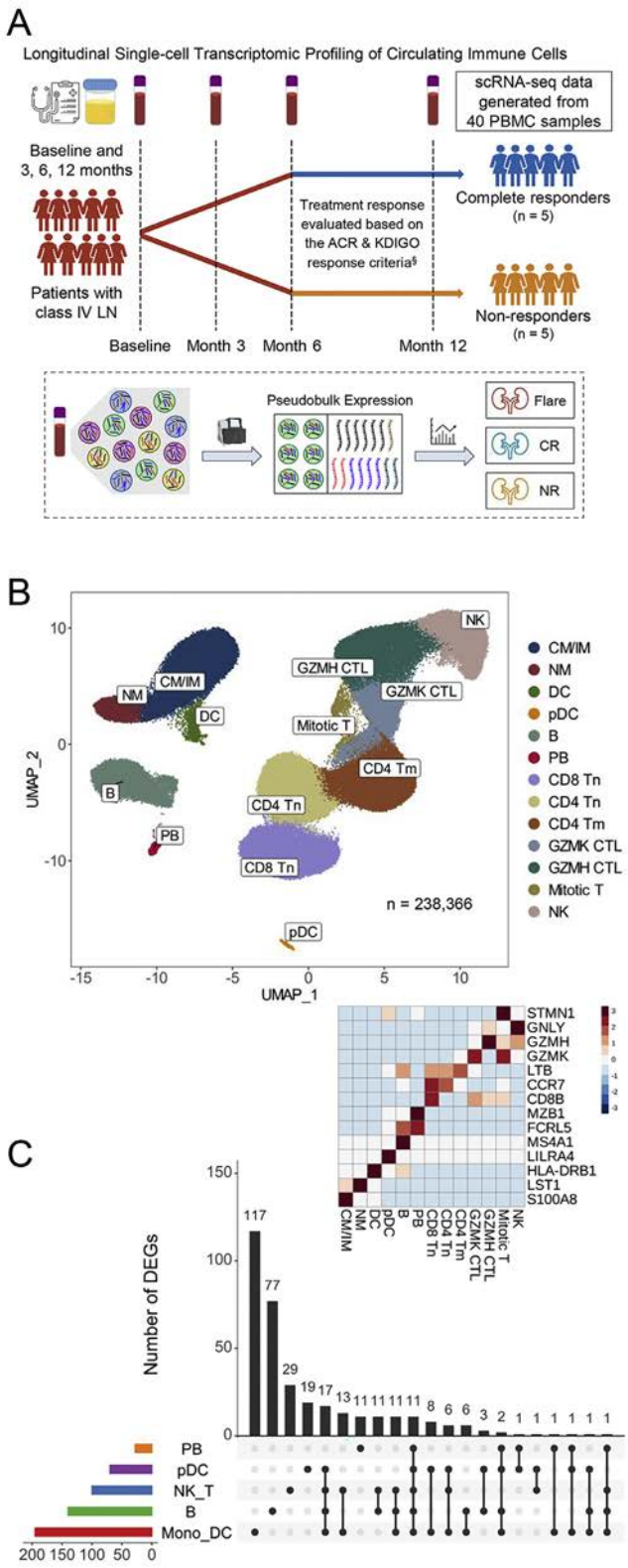

Figure 1. Longitudinal single-cell workflow and the landscape of immune cell gene expression. (A) Schematic representation of the study design and data generation workflow. For single-cell RNA sequencing, peripheral blood samples from 10 patients with LN (5 complete responders, 5 nonresponders) were collected at 4 time points: baseline (before corticosteroid and MMF administration), and at 3, 6, and 12 months following therapy initiation. §Renal responses were defined at 6 and 12 months according to the 2006 American College of Rheumatology response criteria and the 2012 The Kidney Disease: Improving Global Outcomes guideline. (B) Uniform manifold approximation and projection (UMAP) of 238,366 high-quality single cells, coloured by annotated immune cell types. The accompanying heatmap (bottom right) displays the average expression of representative marker genes across each identified cell population. (C) Quantification of differentially expressed genes (DEGs) between complete responders and nonresponders across circulating immune cell compartments at 6 and 12 months posttreatment timepoints. Bar plots indicate the number of DEGs (adjusted *P* value < .05) per cell type, highlighting transcriptional differences associated with treatment response. ACR, American College of Rheumatology; CM, classical monocyte; CR, complete response; CTL, cytotoxic T cell; DC, conventional dendritic cell; IM, intermediate monocyte; KDIGO, Kidney Disease: Improving Global Outcomes; LN, lupus nephritis; MMF, mycophenolate mofetil; NK, natural killer cell; NM, nonclassical monocyte; NR, nonresponse; PB, plasmablast; PBMC, peripheral blood mononuclear cell; pDC, plasmacytoid dendritic cell; scRNA-seq, single-cell RNA sequencing; Tm, memory T cell; Tn, naïve T cell.

expression analysis between complete responders and nonresponders at 6 and 12 months revealed distinct patterns of gene expression across each subset, identifying 146 DEGs in CMs, 110 DEGs in IMs, 71 DEGs in NMs, and 68 DEGs in DCs. Among these populations, CMs and IMs not only exhibited the most DEGs (both upregulated and downregulated) but also shared more than one-third of these DEGs (Fig 2B), consistent with their remarkably high transcriptional similarity (Pearson r = 0.950; Supplementary Fig S6B). These findings suggest common biological mechanisms underlying treatment-related immune modulation. Based on these findings, we hypothesise that integrating gene expression profiles specifically from CMs and IMs could yield a unique signature reflecting treatment responses in patients with LN. Notably, baseline comparison revealed no significant DEGs between complete responders and nonresponders in CMs and IMs (Fig 2C).

Identification of treatment-associated gene coexpression modules

To elucidate gene coexpression patterns associated with immune transcriptional changes during treatment, we performed WGCNA on transcriptomic data from CMs and IMs across longitudinal samples. After selecting 2479 genes exhibiting expression variance above the 75th percentile (by default) based on variance-stabilising transformation, we compared baseline transcriptional states with those of patients achieving CR or NR. Using the dynamic hybrid tree-cut algorithm for module clustering, we identified 8 distinct modules of coexpressed gene networks (Fig 3A). We subsequently calculated Pearson correlation coefficients between each module eigengene—representing the summarised principal component of gene expression—and relevant treatment responses. This modular framework allowed us to systematically identify coexpressed transcriptional networks with strong clinical associations.

Among these gene modules, 4 demonstrated significant correlations with renal outcomes after induction treatment (Fig 3B). The green module, strongly correlated with early treatment response at 3 months in complete responders (r = 0.72, *P* = 9e-07), was defined as the 'Early signature'. The yellow module was positively correlated with CR (r = 0.61, *P* = 8e-05) and named 'CR-up'. The brown module showed negative correlations with both CR (r = −0.55, *P* = 6e-04) and NR (r = −0.76, *P* = 1e-07), designated as 'Common-down'. The blue module, negatively associated with CR (r = −0.58, *P* = 2e-04) but positively associated with NR (r = 0.54, *P* = 7e-04), was labelled 'CR-down/NR-up'. To clearly illustrate temporal shifts in these transcriptional profiles, mean eigengene values of each module were plotted at baseline and at 3, 6, and 12 months posttreatment for both CR and NR groups (Fig 3C).

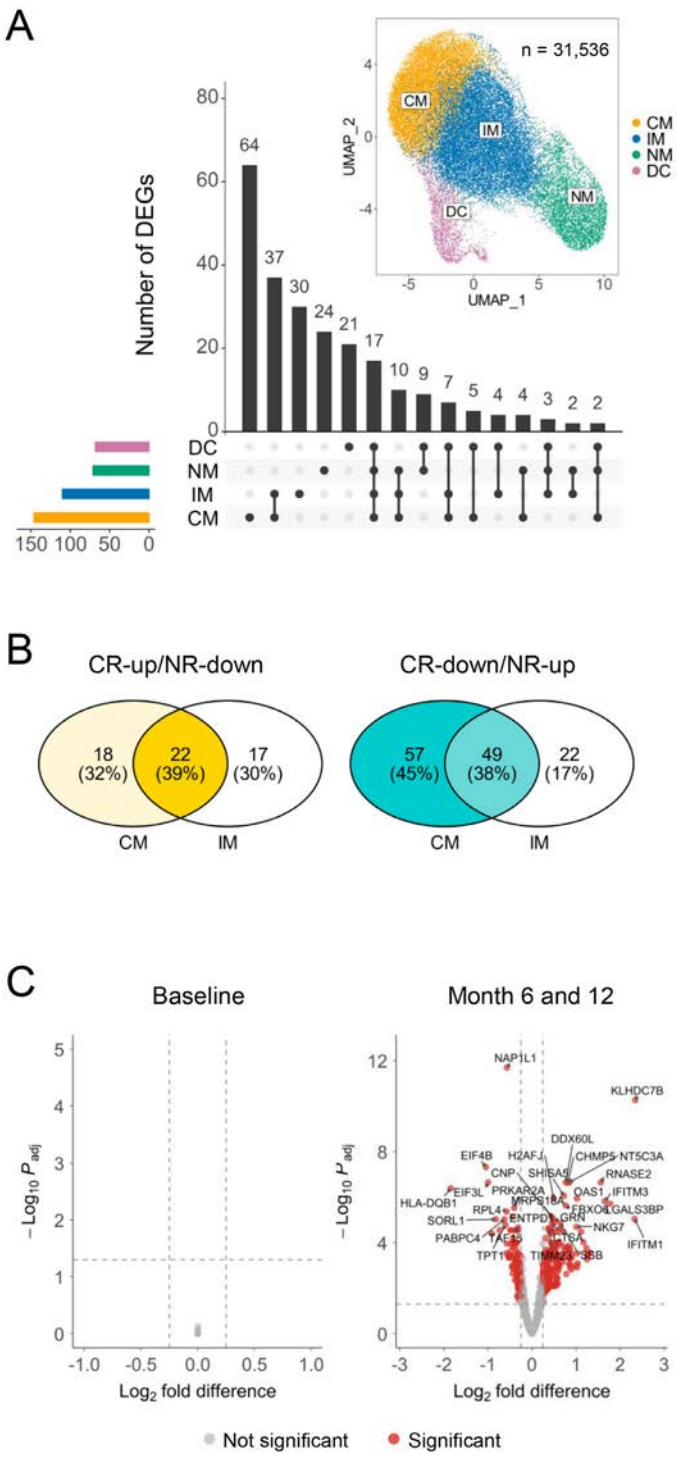

Figure 2. Monocyte transcriptional signatures distinguish treatment responders from nonresponders. (A) Four distinct myeloid cell subclusters identified by single-cell RNA sequencing analysis (top right). The shared and unique patterns of differential gene expression between complete responders and nonresponders across subclusters at 6 and 12 months posttreatment. (B) Venn diagrams showing the number and proportion of overlapping upregulated and downregulated genes shared between classical monocytes and intermediate monocytes at 6 and 12 months posttreatment. (C) Volcano plots of DEGs between complete responders and nonresponders in integrated classical and intermediate monocyte profiles, before and after induction therapy. CM, classical monocyte; CR, complete response; DC, dendritic cell; DEGs, differentially expressed genes; IM, intermediate monocyte; NM, nonclassical monocyte; NR, nonresponse.

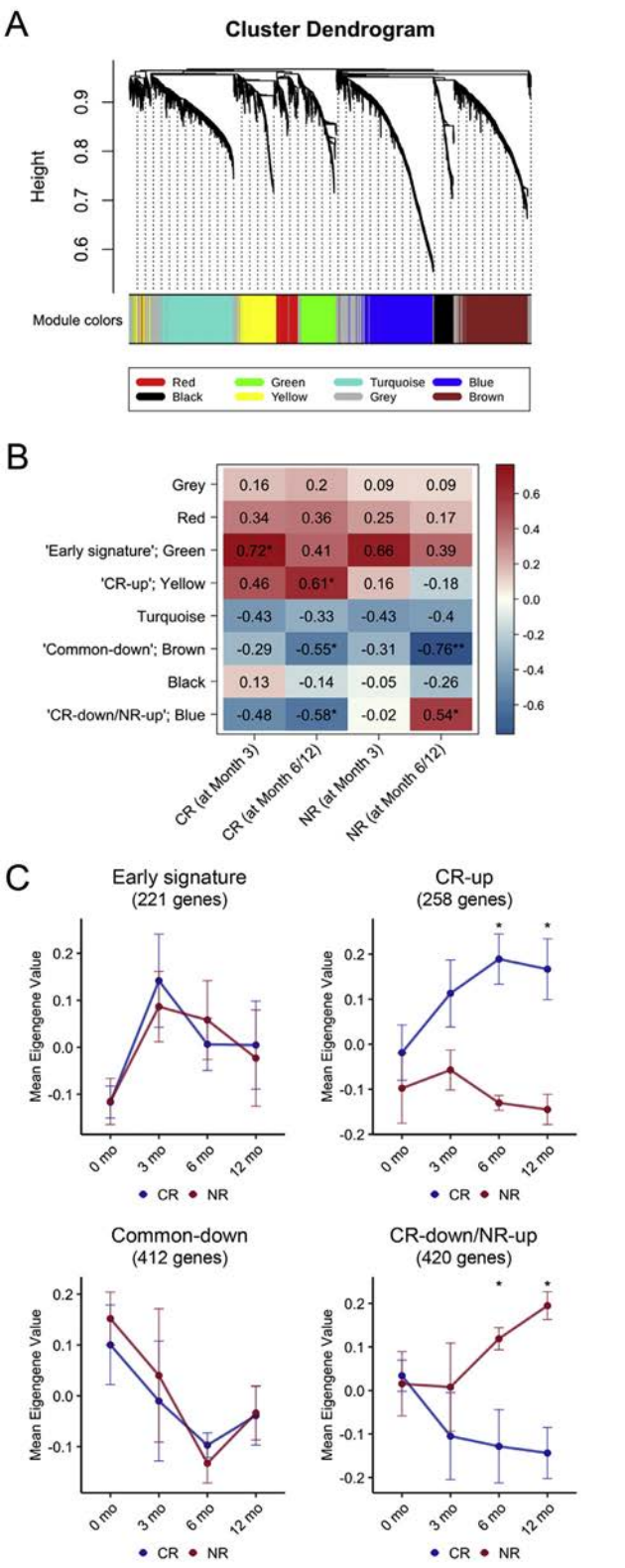

Figure 3. Gene coexpression network analysis reveals induction treatment-associated modules. (A) Hierarchical cluster dendrogram of 2479 genes included in the weighted gene coexpression network analysis (WGCNA). Each module was assigned an arbitrary colour, with genes that did not cluster into any module designated as grey. (B) Heatmap showing correlations between module eigengenes and treatment outcomes. Correlation coefficients and statistical significance are displayed in each cell. (C) Temporal dynamics of eigengene expression for 4 clinically relevant modules from baseline through 3, 6, and 12 months posttreatment in complete responders (CR, blue, n = 5) and nonresponders (NR, red, n = 5). Lines represent mean expression with error bars showing SE. Statistical comparisons between CR and NR at each timepoint were performed using Mann-Whitney *U* tests. $^{*}P < .05$; $^{**}P < .01$.

Persistent IFN-I signalling pathway activation in nonresponders

We next performed overrepresentation analysis to assess the functional significance of each module, aiming to identify key biological pathways mediating monocyte-specific immunoregulation. The 'Early signature' module was significantly enriched in a glucocorticoid-related gene signature previously reported in peripheral blood leukocytes from patients with SLE, featuring key genes such as FKBP5, IL1R2, PHC2, and IRAK3 (Fig 4A) [37]. This module also overlapped with genes predominantly regulated by glucocorticoids rather than IFN-Is, as demonstrated by Northcott et al [38], with both signatures sharing 5 common genes: DUSP1, ZBTB16, ECHDC3, SLA, and FAR2.

The 'CR-up' module showed enrichment in 2 Reactome pathways related to eukaryotic translation (Fig 4B). Specifically, 36 ribosomal protein-coding genes were common to the translation initiation and elongation pathways, including members of both the large and small ribosomal subunit families. Distinct from these modules, the 'Common-down' module consisted of genes consistently downregulated regardless of renal outcomes (Fig 4C). Within this signature, canonical proinflammatory cytokines (eg, tumour necrosis factor [TNF], IL1B, and CXCL chemokines) and transcriptional regulators (eg, CD83, JUNB, KLF6, and NR4A3) showed coordinated expression, with a striking enrichment of the Hallmark TNF signalling pathway.

In the 'CR-down/NR-up' module, genes from the Hallmark IFN-α response pathway were highly represented (Fig 4D). To further dissect the IFN-I signalling components, we curated gene sets from published literature [14,28–36], focusing on genes that have been experimentally validated in human cells (Supplementary Table S2). Since U-ISGF3–inducible genes are a subset of total ISGs that can be transcribed through both phosphorylation-dependent (ISGF3) and phosphorylation-independent (U-ISGF3) pathways (Supplementary Fig S1) [13,14], we curated IFN-I pathway gene sets for analytical purposes: 'ISGF3-inducible gene set' comprising ISGs that require phosphorylated ISGF3 and cannot be induced by U-ISGF3; 'U-ISGF3-inducible gene set' comprising ISGs that can be transcribed through both ISGF3 and U-ISGF3 complexes. Notably, all 29 U-ISGF3-inducible genes, including IFI35, IFIT3, IRF7, and EPSTI1 were present within the 'CR-down/NR-up' module, showing greater enrichment than ISGF3-inducible genes. In contrast, 30 of the 48 ISGF3-inducible genes were absent from this module, including many prototypical ISGs such as CXCL16, MYD88, HLA-F, and UBA7.

To confirm the 'CR-down/NR-up' module, we employed 2 orthogonal approaches: leave-one-donor-out cross-validation demonstrated high module preservation (87.8% mean overlap; Supplementary Fig S7), whereas bootstrap resampling indicated gene stability with 68.9% of module genes exceeding the 80% consistency threshold across 1000 iterations. These analyses represent a robust biological signature associated with persistent IFN-I pathway activity in nonresponders.

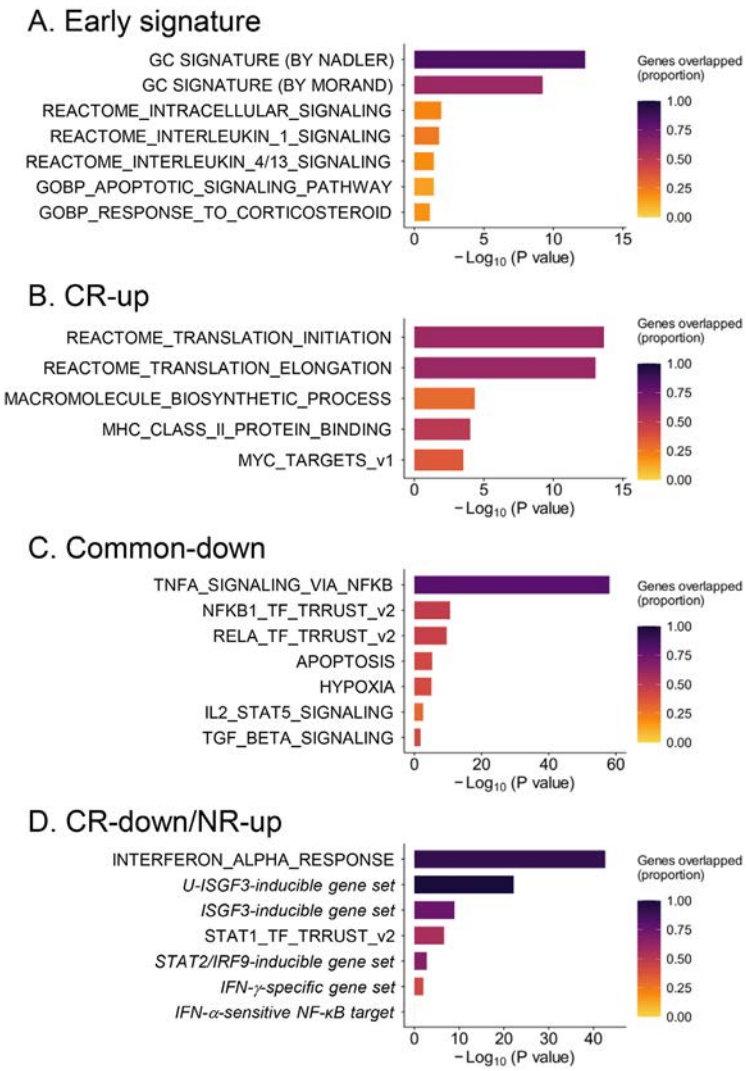

Figure 4. Biological pathway enrichment analysis of gene coexpression modules. Functional enrichment analysis of 4 clinically relevant WGCNA modules using gene sets from the Hallmark, GOBP, Reactome, TRRUST v2, and curated literature sources (shown in italics). Bar plots display enrichment *P* values and the proportion of overlapping genes, revealing dominant biological themes for each module. CR, complete response; GOBP; Gene Ontology Biological Processes; WGCNA, weighted gene coexpression network analysis.

Assessment of monocyte IFN-I-responsive signature in independent patients

The selective enrichment of U-ISGF3-inducible genes in the 'CR-down/NR-up' module suggested a specific role for this noncanonical IFN-I pathway in treatment resistance. Building on these module-based insights, we selected 18 representative genes from the 'CR-down/NR-up' module to create a focused gene signature, capturing over 95% of the module's variance; notably, 11 of these were U-ISGF3-inducible genes (Supplementary Table S3). The 18-gene metagene expression (10% trimmed mean of z-scores) showed significant differences between patients achieving CR and NR at 6 and 12 months posttreatment across monocytes, NK/T cells, and B cells (Supplementary Fig S8).

This signature was then tested in an independent group of 13 patients with active, proliferative LN (group 2), comprising 7 complete responders and 6 nonresponders (Fig 5A, Table 1). To identify early gene signatures associated with LN treatment outcomes, bulk RNA sequencing was conducted on monocytes isolated from PBMCs collected at baseline (before induction therapy) and at 3 months posttreatment, with renal responses determined at 12 months. Among patients ultimately achieving CR at 12 months, 5 (71.4%) had reached CR by 3 months, whereas 2 showed partial response at the 3-month timepoint. Within the 18 genes representing the 'CR-down/NR-up' module, 6 ISGs (IRF7, ISG15, LY6E, IFI44, IFI44L, and IFI6, highlighted in red in Fig 5B) exhibited significant reductions in expression by 3 months in patients achieving CR, whereas no comparable changes were observed in patients achieving NR. Machine learning analysis of the 6-gene signature achieved 69.2% leave-one-out cross-validation accuracy. When compared to 1000 random 6-gene combinations from the 'CR-down/NR-up' module, the signature ranked in the 73rd percentile. Permutation testing showed marginal significance (P = .098). These results suggest potential predictive value but require validation in larger cohorts.

Temporal dynamics of IFN-I signature define treatment outcomes

To evaluate the performance of the IFN-I signature in tracking treatment responses, we employed a linear mixed-effects model to analyse the expression of all 18 representative genes from the 'CR-down/NR-up' module in a longitudinal single-cell RNA sequencing dataset, accounting for both interdonor and intradonor variability. Forest plots for multiple posttreatment timepoints (3, 6, and 12 months) revealed that while several genes demonstrated treatment-related changes in monocytes, 6 ISGs (IRF7, ISG15, LY6E, IFI44, IFI44L, and IFI6) along with IFITM3 consistently exhibited the most pronounced and reproducible response patterns between complete responders and nonresponders (Supplementary Fig S9).

Next, a 10% trimmed mean of the z-scores across the 6 genes (or all 18 genes) was calculated per cell to generate a metagene score. Linear mixed-effects models were fitted to metagene z-scores using restricted maximum likelihood, with patient identity as a random effect and sampling timepoints as fixed effects (Fig 6A, left panel). Among complete responders, the analysis revealed significant and sustained downregulation of 6 IFN-I-responsive metagene expression at all posttreatment timepoints:

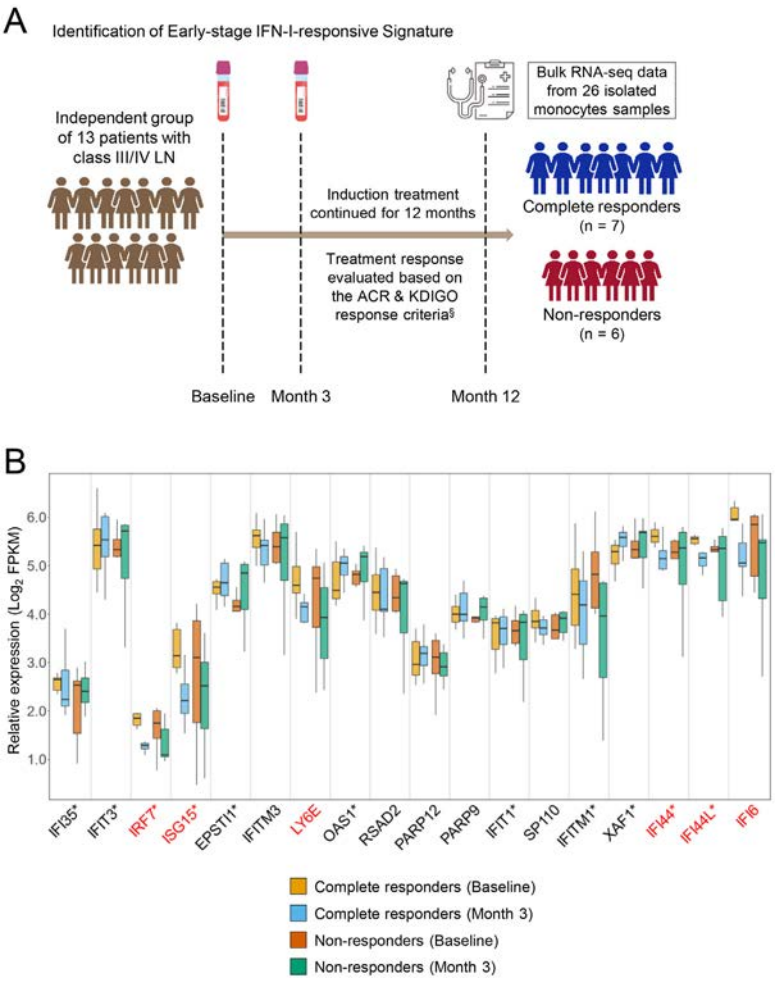

Figure 5. Identification of early responsive signature by bulk RNA sequencing in independent patients. (A) Monocytes were isolated from 13 patients with active proliferative LN at baseline and 3 months postinduction therapy, with clinical outcomes assessed after 1 year of follow-up. For bulk RNA sequencing, peripheral blood samples were collected at baseline (prior to corticosteroid and MMF administration) and at 3 months following therapy initiation. §Renal responses were defined at 6 and 12 months according to the 2006 American College of Rheumatology response criteria and the 2012 The Kidney Disease: Improving Global Outcomes guideline. (B) Expression changes of 18 representative 'CR-down/NR-up' module genes between baseline and 3 months. Red text indicates genes with significant downregulation in complete responders but not in nonresponders. Asterisks denote U-ISGF3-inducible genes (Supplementary Table S2). ACR, American College of Rheumatology; CR, complete response; FPKM, fragments per kilobase of transcript per million mapped reads; IFN-I, type I interferon; KDIGO, Kidney Disease: Improving Global Outcomes; LN, lupus nephritis; MMF, mycophenolate mofetil; NR, nonresponse.

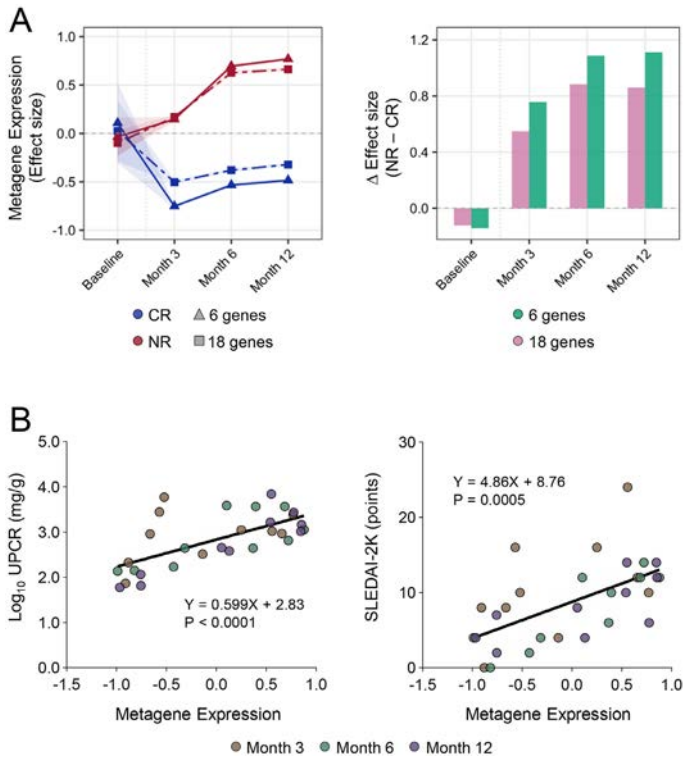

Figure 6. Divergent interferon-responsive signatures distinguish treatment responses. (A) Linear mixed-effects model analysis of interferon-responsive metagene expression in monocytes during induction therapy. Left panel: temporal dynamics showing effect sizes with 95% CIs for the 6-gene (or 18-gene) signature in complete responders (CR, blue) and nonresponders (NR, red). Right panel: statistical comparison of effect size differences between the 6-gene signature and the broader 18-gene panel at each timepoint. (B) Association of the 6-gene interferon-responsive signature in monocytes with proteinuria levels and global disease activity (SLEDAI-2K), assessed by linear regression analysis. SLEDAI-2K, Systemic Lupus Erythematosus Disease Activity Index 2000; UPCR, urine protein-to-creatinine ratio.

3 months ($\beta = -0.753$, $P < .001$), 6 months ($\beta = -0.534$, $P < .001$), and 12 months ($\beta = -0.485$, $P < .001$) compared to baseline. In striking contrast, nonresponders demonstrated progressive upregulation of metagene expression, with effect sizes increasing from 3 months ($\beta = 0.146$) to 6 months ($\beta = 0.695$) and 12 months ($\beta = 0.769$), all significant compared to baseline ($P < .001$).

To quantitatively assess whether the 6-gene signature provides enhanced discriminatory power compared with the broader 18-gene panel, we performed a statistical comparison of effect size differences at each time point (Fig 6A, right panel). At baseline, no significant difference existed between the 6-gene vs 18-gene signatures (difference in effect sizes = 0.019, $P = .944$). However, following treatment initiation, the 6-gene signature demonstrated significantly greater discrimination between response groups at all timepoints: 3 months (difference = −0.207, $P < .001$), 6 months (difference = −0.204, $P < .001$), and 12 months (difference = −0.252, $P < .001$). This convergent evidence from both bulk and single-cell analyses suggests that our 6-gene IFN-I-responsive signature captures the core transcriptional response to induction therapy in LN.

Clinical associations of the IFN-I-responsive signature

Linear regression analysis further demonstrated significant associations between the 6-gene IFN-I-responsive signature in monocytes and clinical parameters after induction treatment. The signature correlated with both proteinuria ($R^2 = 0.435$, $P < .0001$) and total SLEDAI-2K scores ($R^2 = 0.352$, $P = .0005$) (Fig 6B). However, no significant associations were observed with complement levels (C3 and C4) or extrarenal SLEDAI components (Supplementary Fig S10A). Although NK/T and B cell compartments showed similar trends for proteinuria, these associations were less pronounced than in monocytes (Supplementary Fig S10B). Collectively, our findings suggest that persistent expression of selected IFN-I-responsive genes in circulating immune cells represents a valuable signature of treatment NR in LN.

DISCUSSION

In this study, we leveraged time-series single-cell transcriptomics to elucidate how induction treatment reshapes immune cell gene expression in patients with LN. Although treatment-associated transcriptional changes occurred across multiple immune compartments, monocytes served as sensitive sentinels that capture systemic inflammatory states. Using WGCNA, we identified 4 distinct gene modules that correlated with treatment responses. Notably, the ‘Early signature’ module captured a transient surge of immunomodulatory gene expression, featuring known glucocorticoid-responsive genes previously identified in patients with SLE (Figs 3C and 4A). This highlights the rapid and potent immunosuppressive effects of induction therapy, driven primarily by high-dose corticosteroids. In contrast, the ‘CR-down/NR-up’ module showed strong correlation with divergent clinical outcomes. Specifically, this module—downregulated in complete responders but paradoxically sustained or even elevated in nonresponders—was highly enriched for ISGs, particularly for U-ISGF3-inducible genes (Figs 3C and 4D).

Collectively, these networks illustrate distinct transcriptional programmes during the induction treatment of LN.

Recent work by the PRECISESADS consortium identified 3 LN subgroups based on differential IFN signature intensity (low, intermediate, and high) compared with nonrenal patients with SLE [39]. Our longitudinal analysis extends these findings by demonstrating that downstream IFN-I pathway activity distinguishes complete responders from nonresponders within the LN population. Although complete responders showed progressive downregulation of IFN-I-driven gene expression by 3 months postinduction, nonresponders maintained persistently elevated signatures despite treatment. Notably, our 'CR-down/NR-up' module analysis suggested that a subset of ISGs contributed significantly to this differential response pattern.

Our data suggest that nonresponders sustain IFN-I-driven inflammation through prolonged IFN-I signalling activity, which might be caused by U-ISGF3 activation, incomplete suppression of upstream IFN-I signalling, or dysregulated negative feedback in the IFN-I pathway. Whether early detection of persistent IFN-I signatures could enable therapeutic modification requires prospective interventional trials. This is particularly important given that changes in proteinuria and/or kidney function typically lag behind underlying immune processes.

Furthermore, IFN-I-responsive signature reflecting immune perturbations in LN is especially relevant in the rapidly evolving era, where anifrolumab has emerged as a promising therapy for SLE following its approval in 2021. Notably, all patients in our study were enrolled prior to anifrolumab's approval, and this therapy remains unavailable in South Korea, providing a unique opportunity to examine regulatory mechanisms of the IFN-I pathway underlying therapeutic resistance to standard immunosuppressive regimens. The clinical implication of our findings is supported by existing evidence from pooled analyses of the TULIP-1 and TULIP-2 trials, which demonstrated that anifrolumab significantly downregulated numerous ISGs, including all 6 IFN-I-responsive genes (IRF7, ISG15, LY6E, IFI44, IFI44L, and IFI6) we identified [7]. However, the TULIP trials enrolled patients with moderate-to-severe SLE without active severe LN, highlighting the need for LN-specific validation of anifrolumab's efficacy in modulating these molecular signatures.

Our stratified analyses revealed that all nonresponders had prior MMF exposure yet maintained persistent IFN-I-driven gene expression, whereas complete responders achieved suppression of IFN-I activity regardless of MMF history (Supplementary Fig S11). Although limited statistical power precludes causal inference, this pattern reinforces our primary finding that prolonged activation of the IFN-I pathway distinguishes treatment responders from nonresponders. Prospective studies with larger cohorts and controlled treatment protocols will be necessary to determine whether prior MMF exposure influences IFN-I pathway regulation and treatment responses. In addition, individuals with higher expression of the 6-gene IFN-I-responsive signature in circulating immune cells showed associations with more severe proteinuria and higher SLEDAI-2K scores. Although these correlations support the biological plausibility of our findings, we acknowledge that proteinuria and global disease activity scores are imperfect surrogates for underlying renal inflammation and long-term prognosis in LN.

Furthermore, our findings also refine the understanding of TNF- and IL-1β-mediated inflammatory pathways during LN treatment. Previous studies suggest that crosstalk between IFN-I and TNF signalling in lupus monocytes can drive inflammatory reprogramming and trigger unconventional IL-1β secretion, potentially contributing to disease pathogenesis [36,40]. Nevertheless, our results demonstrate that TNF/NF-κB pathways were uniformly suppressed by treatment in both complete responders and nonresponders (Fig 4C, Supplementary Fig S5).

Limitations

This study has several limitations. First, although our study design enabled detailed transcriptional analysis, the sample size was relatively small, and participants were recruited from a single centre, potentially limiting the generalisability of our findings. Validation in larger, multicentre cohorts is needed to confirm the IFN-I-responsive signature as a treatment response marker in diverse patients with LN.

Second, our focus on extreme phenotypes (complete responders vs nonresponders) to maximise molecular contrast excluded partial responders, who constitute approximately 30% to 50% of patients in real-world clinical practice. The molecular profiles of these partial responders remain unexplored, limiting the clinical applicability of our findings across the full spectrum of treatment responses. In addition, the higher prevalence of prior MMF exposure in nonresponders raises questions about potential treatment resistance. This imbalance may reflect selection bias where patients with inherently more refractory disease both receive prior MMF and subsequently fail treatment. However, baseline IFN-I signatures were comparable, and current clinical guidelines do not stratify treatment based on prior MMF exposure. Nevertheless, the imbalance in prior MMF exposure warrants careful interpretation when extrapolating our findings to treatment-naïve populations.

Third, our single-cell RNA sequencing analysis was limited to circulating immune cells, which may not reflect intrarenal immune processes. Although we observed persistent IFN-I-driven gene expression in nonresponders, the lack of paired kidney biopsy transcriptomic data precludes confirmation that these peripheral signatures mirror inflammation associated with renal damage. Future studies incorporating matched kidney and blood transcriptomes will be essential to determine whether systemic IFN-I signatures are mechanistically linked to renal pathology. Nevertheless, peripheral blood-based biomarkers offer important practical advantages. They are readily accessible, minimally invasive, and well suited for longitudinal monitoring, making them clinically attractive tools for early risk stratification and response assessment.

Fourth, the bulk RNA sequencing approach used for validation in the independent patients limited our ability to distinguish between monocyte subsets that may differentially contribute to the IFN-I signalling activity observed in nonresponders. Our single-cell analyses, however, showed highly conserved pathway signals (90%-100%) across classical, intermediate, and nonclassical monocytes, indicating that subset resolution may not be critical.

Lastly, given the observational nature of this study, causality cannot be established and transcriptional inferences should be experimentally validated in future studies. IFN-I-responsive signature correlated with proteinuria and SLEDAI-2K but not with complement levels or extrarenal manifestations—an interpretive challenge unresolved by our data. This dissociation likely reflects glucocorticoids' minimal effect on ISGs vs potent suppression of complement consumption and systemic inflammation in corticosteroid-treated nonresponders [38]. However, the robust correlation between transcriptional patterns and clinical outcomes, combined with the temporal dynamics showing molecular divergence following treatment initiation, provides a

strong rationale for further exploration of IFN-I signalling pathways as both biomarkers and therapeutic targets.

CONCLUSION

To our knowledge, this is the first study to comprehensively delineate the divergent monocyte IFN-I trajectories associated with renal outcomes in LN through longitudinal single-cell analysis. We demonstrate that CR is characterised by timely resolution of IFN-I-driven inflammation, whereas NR is marked by persistent IFN-I signalling activation that evades standard immunosuppressive therapies. This divergent molecular trajectory provides a candidate biomarker for early identification of treatment outcomes. Future interventional studies are needed to validate whether this biological insight can be translated into improved therapeutic strategies.

Acknowledgements

The authors thank patients for their generous and enthusiastic participation in this study.

Contributors

W-JK, H-SL, E-CS, and S-CB were involved in the conceptualization of the study. S-CB recruited and took care of patients, collected blood samples, and extracted clinical data. W-JK, H-SL, and E-CS performed analysis. W-JK and H-SL drafted the manuscript with contributions from all authors. E-CS and S-CB supervised the study and the writing. All authors read and approved the final manuscript for publication.

Funding

This work was supported by the Basic Science Research Program through the National Research Foundation of Korea (NRF-2021R1A6A1A03038899).

Competing interests

All authors confirm that there are no interests to declare

Patient and public involvement

Patients or the public were not involved in the design, or conduct, or reporting, or dissemination plans of this research.

Patient consent for publication

Not applicable.

Ethics approval

The study was conducted in accordance with the principles of the Declaration of Helsinki and approved by the IRB of the Hanyang University Hospital for Rheumatic Diseases (IRB No: HYUH2017-08-035). All study participants provided written informed consent.

Provenance and peer review

Not commissioned; externally peer reviewed.

Data availability statement

The data that support the findings of this study are available from the corresponding authors upon reasonable request.

Supplementary materials

Supplementary material associated with this article can be found in the online version at doi:10.1016/j.ard.2025.12.002.

Orcid

Sang-Cheol Bae: http://orcid.org/0000-0003-4658-1093

REFERENCES

[1] Hanly JG, O'Keeffe AG, Su L, Urowitz MB, Romero-Diaz J, Gordon C, et al. The frequency and outcome of lupus nephritis: results from an international inception cohort study. Rheumatology (Oxford) 2016;55(2):252–62.
[2] Anders HJ, Saxena R, Zhao MH, Parodis I, Salmon JE, Mohan C. Lupus nephritis. Nat Rev Dis Primers 2020;6(1):7.
[3] Mok CC, Teng YKO, Saxena R, Tanaka Y. Treatment of lupus nephritis: consensus, evidence and perspectives. Nat Rev Rheumatol 2023;19(4):227–38.
[4] Kidney Disease: Improving Global Outcomes (KDIGO) Lupus Nephritis Work Group. KDIGO 2024 Clinical Practice Guideline for the management of LUPUS NEPHRITIS. Kidney Int 2024;105(1S):S1–S69.
[5] Caielli S, Wan Z, Pascual V. Systemic lupus erythematosus pathogenesis: interferon and beyond. Annu Rev Immunol 2023;41:533–60.
[6] Crow MK, Olferiev M, Kirou KA. Standing on shoulders: interferon research from viral interference to lupus pathogenesis and treatment. Arthritis Rheumatol 2024;76(7):1002–12.
[7] Baker T, Sharifian H, Newcombe PJ, Gavin PG, Lazarus MN, Ramaswamy M, et al. Type I interferon blockade with anifrolumab in patients with systemic lupus erythematosus modulates key immunopathological pathways in a gene expression and proteomic analysis of two phase 3 trials. Ann Rheum Dis 2024;83(8):1018–27.
[8] Mai L, Asaduzzaman A, Noamani B, Fortin PR, Gladman DD, Touma Z, et al. The baseline interferon signature predicts disease severity over the subsequent 5 years in systemic lupus erythematosus. Arthritis Res Ther 2021;23(1):29.
[9] Miyachi K, Iwamoto T, Kojima S, Ida T, Suzuki J, Yamamoto T, et al. Relationship of systemic type I interferon activity with clinical phenotypes, disease activity, and damage accrual in systemic lupus erythematosus in treatment-naive patients: a retrospective longitudinal analysis. Arthritis Res Ther 2023;25(1):26.
[10] Catalina MD, Bachali P, Geraci NS, Grammer AC, Lipsky PE. Gene expression analysis delineates the potential roles of multiple interferons in systemic lupus erythematosus. Commun Biol 2019;2:140.
[11] Northcott M, Jones S, Koelmeyer R, Bonin J, Vincent F, Kandane-Rathnayake R, et al. Type 1 interferon status in systemic lupus erythematosus: a longitudinal analysis. Lupus Sci Med 2022;9(1):e000625.
[12] Rodriguez-Carrio J, Burska A, Conaghan PG, Dik WA, Biesen R, Eloranta ML, et al. 2022 EULAR points to consider for the measurement, reporting and application of IFN-I pathway activation assays in clinical research and practice. Ann Rheum Dis 2023;82(6):754–62.
[13] Cheon H, Stark GR. Unphosphorylated STAT1 prolongs the expression of interferon-induced immune regulatory genes. Proc Natl Acad Sci U S A 2009;106(23):9373–8.
[14] Cheon H, Holvey-Bates EG, Schoggins JW, Forster S, Hertzog P, Imanaka N, et al. IFNbeta-dependent increases in STAT1, STAT2, and IRF9 mediate resistance to viruses and DNA damage. EMBO J 2013;32(20):2751–63.
[15] Jeong HW, Lee JS, Ko JH, Hong S, Oh ST, Choi S, et al. Corticosteroids reduce pathologic interferon responses by downregulating STAT1 in patients with high-risk COVID-19. Exp Mol Med 2023;55(3):653–64.
[16] Arazi A, Rao DA, Berthier CC, Davidson A, Liu Y, Hoover PJ, et al. The immune cell landscape in kidneys of patients with lupus nephritis. Nat Immunol 2019;20(7):902–14.
[17] Park DJ, Joo YB, Bang SY, Lee J, Lee HS, Bae SC. Predictive factors for renal response in lupus nephritis: a single-center prospective cohort study. J Rheum Dis 2022;29(4):223–31.
[18] Petri M, Orbai AM, Alarcon GS, Gordon C, Merrill JT, Fortin PR, et al. Derivation and validation of the Systemic Lupus International Collaborating Clinics classification criteria for systemic lupus erythematosus. Arthritis Rheum 2012;64(8):2677–86.

[19] Aringer M, Costenbader K, Daikh D, Brinks R, Mosca M, Ramsey-Goldman R, et al. 2019 European League Against Rheumatism/American College of Rheumatology classification criteria for systemic lupus erythematosus. Ann Rheum Dis 2019;78(9):1151–9.
[20] Hahn BH, McMahon MA, Wilkinson A, Wallace WD, Daikh DI, Fitzgerald JD, et al. American College of Rheumatology guidelines for screening, treatment, and management of lupus nephritis. Arthritis Care Res (Hoboken) 2012;64(6):797–808.
[21] Bertsias GK, Tektonidou M, Amoura Z, Aringer M, Bajema I, Berden JHM, et al. Joint European League Against Rheumatism and European Renal Association-European Dialysis and Transplant Association (EULAR/ERA-EDTA) recommendations for the management of adult and paediatric lupus nephritis. Ann Rheum Dis 2012;71(11):1771–82.
[22] Mok CC, Yap DY, Navarra SV, Liu Z-H, Zhao MH, Lu L, et al. Overview of lupus nephritis management guidelines and perspective from Asia. Int J Rheum Dis 2013;16(6):625–36.
[23] Fanouriakis A, Kostopoulou M, Alunno A, Aringer M, Bajema I, Boletis JN, et al. 2019 update of the EULAR recommendations for the management of systemic lupus erythematosus. Ann Rheum Dis 2019;78(6):736–45.
[24] Gladman DD, Ibanez D, Urowitz MB. Systemic lupus erythematosus disease activity index 2000. J Rheumatol 2002;29(2):288–91.
[25] Bajema IM, Wilhelmus S, Alpers CE, Bruijn J, Colvin RB, Cook HT, et al. Revision of the International Society of Nephrology/Renal Pathology Society classification for lupus nephritis: clarification of definitions, and modified National Institutes of Health activity and chronicity indices. Kidney Int 2018;93(4):789–96.
[26] Renal Disease Subcommittee of the American College of Rheumatology Ad Hoc Committee on Systemic Lupus Erythematosus Response Criteria. The American College of Rheumatology response criteria for proliferative and membranous renal disease in systemic lupus erythematosus clinical trials. Arthritis Rheum 2006;54(2):421–32.
[27] Kidney Disease: Improving Global Outcomes (KDIGO) Glomerulonephritis Work Group. KDIGO Clinical Practice Guideline for Glomerulonephritis. Kidney Int Suppl 2012;2(2):139–274.
[28] Sung PS, Cheon H, Cho CH, Hong SH, Park DY, Seo HI, et al. Roles of unphosphorylated ISGF3 in HCV infection and interferon responsiveness. Proc Natl Acad Sci U S A. 2015;112(33):10443–8.
[29] Brierley MM, Marchington KL, Jurisica I, Fish EN. Identification of GAS-dependent interferon-sensitive target genes whose transcription is STAT2-dependent but ISGF3-independent. FEBS J 2006;273(7):1569–81.
[30] Sarkis PT, Ying S, Xu R, Yu XF. STAT1-independent cell type-specific regulation of antiviral APOBEC3G by IFN-alpha. J Immunol 2006;177(7):4530–40.
[31] Lou YJ, Pan XR, Jia PM, Li D, Xiao D, Zhang ZL, et al. IRF-9/STAT2 [corrected] functional interaction drives retinoic acid-induced gene G expression independently of STAT1. Cancer Res 2009;69(8):3673–80.
[32] Blaszczyk K, Olejnik A, Nowicka H, Ozgyin L, Chen YL, Chmielewski S, et al. STAT2/IRF9 directs a prolonged ISGF3-like transcriptional response and antiviral activity in the absence of STAT1. Biochem J 2015;466(3):511–24.
[33] Kirou KA, Lee C, George S, Louca K, Papagiannis LG, Peterson MGE, et al. Coordinate overexpression of interferon-alpha-induced genes in systemic lupus erythematosus. Arthritis Rheum 2004;50(12):3958–67.
[34] Morrow AN, Schmeisser H, Tsuno T, Zoon KC. A novel role for IFN-stimulated gene factor 3II in IFN-gamma signaling and induction of antiviral activity in human cells. J Immunol 2011;186(3):1685–93.
[35] Hall JC, Casciola-Rosen L, Berger AE, Kapsogeorgou EK, Cheadle C, Tzioufas AG, et al. Precise probes of type II interferon activity define the origin of interferon signatures in target tissues in rheumatic diseases. Proc Natl Acad Sci U S A. 2012;109(43):17609–14.
[36] Park SH, Kang K, Giannopoulou E, Qiao Y, Kang K, Kim G, et al. Type I interferons and the cytokine TNF cooperatively reprogram the macrophage epigenome to promote inflammatory activation. Nat Immunol 2017;18(10):1104–16.
[37] Hu Y, Carman JA, Holloway D, Kansal S, Fan L, Goldstine C, et al. Development of a molecular signature to monitor pharmacodynamic responses mediated by in vivo administration of glucocorticoids. Arthritis Rheumatol 2018;70(8):1331–42.
[38] Northcott M, Gearing LJ, Nim HT, Nataraja C, Hertzog P, Jones SA, et al. Glucocorticoid gene signatures in systemic lupus erythematosus and the effects of type I interferon: a cross-sectional and in-vitro study. Lancet Rheumatol 2021;3(5):e357–e70.
[39] Parodis I, Lindblom J, Toro-Dominguez D, Beretta L, Borghi MO, Castillo J, et al. Interferon and B-cell signatures inform precision medicine in lupus nephritis. Kidney Int Rep 2024;9(6):1817–35.
[40] Caielli S, Balasubramanian P, Rodriguez-Alcazar J, Balaji U, Robinson L, Wan Z, et al. Type I IFN drives unconventional IL-1beta secretion in lupus monocytes. Immunity 2024;57(11):2497–513.

Ann Rheum Dis 85 (2026) 659–668

Contents lists available at ScienceDirect

Annals of the Rheumatic Diseases

journal homepage: https://www.sciencedirect.com/journal/annals-of-the-rheumatic-diseases

Systemic lupus erythematosus

Antimitochondrial antibodies in systemic lupus erythematosus are associated with and predict nephritis, arterial vascular events, and mortality

Yann L.C. Becker[1,2], Éric Boilard[1,2], Emmanuelle Rollet-Labelle[1,2], Christian Lood[3], Anne-Sophie Julien[4], Michal Abrahamowicz[5], Isabelle Allaeys[1,2], May Choi[6], Joannie Leclerc[1], Tania Lévesque[1,2], Murray Urowitz[7], John G. Hanly[8], Caroline Gordon[9], Sang-Cheol Bae[10], Juanita Romero-Diaz[11,12], Jorge Sanchez-Guerrero[7,13], Ann E. Clarke[6], Sasha Bernatsky[5,14], Daniel Wallace[15], David Isenberg[16], Anisur Rahman[16], Joan Merrill[17], Dafna D. Gladman[7], Ian N. Bruce[18,19], Michelle Petri[20], Ellen Ginzler[21], Mary Anne Dooley[22], Rosalind Ramsey-Goldman[23], Susan Manzi[24], Andreas Jönsen[25], Graciela S. Alarcón[26], Ronald van Vollenhoven[27], Cynthia Aranow[28], Guillermo Ruiz-Irastorza[29], Sam Lim[30], Murat Inanc[31], Kenneth Kalunian[32], Soren Jacobsen[33], Christine Peschken[12], Diane Kamen[34], Anca Askanase[35], Jill Buyon[36], Paul R. Fortin[1,2,37,*]

[1] *Centre de Recherche ARThrite—Université Laval, Quebec City, QC, Canada*
[2] *Axe Maladies Infectieuses et Immunitaires, Centre de Recherche du CHU de Québec—Université Laval, Quebec City, QC, Canada*
[3] *Division of Rheumatology, University of Washington, Seattle, WA, USA*
[4] *Department of Mathematics and Statistics, Université Laval, Québec City, QC, Canada*
[5] *Department of Epidemiology & Biostatistics, McGill University, Montréal, Québec City, QC, Canada*
[6] *Division of Rheumatology, Cumming School of Medicine, University of Calgary, Calgary, AB, Canada*
[7] *University of Toronto, Toronto Western Hospital, University Health Network, Schroeder Arthritis Institute, Krembil Research Institute, Toronto, ON, Canada*
[8] *Division of Rheumatology, Department of Medicine, Queen Elizabeth II Health Sciences Center (Nova Scotia Rehabilitation Site) and Dalhousie University, Halifax, NS, Canada*
[9] *Rheumatology Research Group, Institute of Inflammation and Ageing, College of Medical and Dental Sciences, University of Birmingham, Birmingham, UK*
[10] *Department of Rheumatology, Hanyang University Hospital for Rheumatic Diseases, Hanyang University Institute for Rheumatology Research and Hanyang Institute of Bioscience and Biotechnology, Seoul, Republic of Korea*
[11] *Instituto Nacional de Ciencias Médicas y Nutrición "Salvador Zubirán", Mexico City, Mexico*
[12] *University of Manitoba, Winnipeg, MB, Canada*
[13] *Mount Sinai Hospital, University of Toronto, Toronto, ON, Canada*
[14] *Research Institute of the McGill University Health Centre, Montréal, QC, Canada*
[15] *Cedars Sinai Medical Center, Los Angeles, CA, USA*
[16] *Centre for Rheumatology, Department of Medicine, University College London, London, UK*
[17] *Oklahoma Medical Research Foundation, Oklahoma City, OK, USA*

*Correspondence to Dr. Paul R. Fortin, CHU de Québec—Université Laval, Quebec City, QC, Canada.
E-mail address: Paul.Fortin@crchudequebec.ulaval.ca (P.R. Fortin).
Handling editor Josef S. Smolen.

https://doi.org/10.1016/j.ard.2025.11.007

[18] *Centre for Musculoskeletal Research, Faculty of Biology, Medicine and Health, The University of Manchester, Manchester, UK*
[19] *Centre for Public Health, Faculty of Medicine, Health and Life Sciences, Queen's University, Belfast, UK*
[20] *Division of Rheumatology, Johns Hopkins University School of Medicine, Baltimore, MD, USA*
[21] *Department of Medicine, SUNY Downstate Health Sciences University, Brooklyn, NY, USA*
[22] *Raleigh Neurology Associates, Raleigh, NC, USA*
[23] *Northwestern University Feinberg School of Medicine, Chicago, IL, USA*
[24] *Allegheny Health Network, Lupus Center of Excellence, Pittsburgh, PA, USA*
[25] *Department of Clinical Sciences, Lund, Section for Rheumatology, Lund University, Lund and Skåne University Hospital, Lund, Sweden*
[26] *Marnix E. Heersink School of Medicine, The University of Alabama at Birmingham, Birmingham, AL, USA*
[27] *Amsterdam University Medical Centers, Amsterdam, The Netherlands*
[28] *Feinstein Institutes for Medical Research, Manhasset, NY, USA*
[29] *Biobizkaia Health Research Institute, UPV/EHU, Barakaldo, País Vasco, Spain*
[30] *Emory University, Atlanta, GA, USA*
[31] *Division of Rheumatology, Department of Internal Medicine, Istanbul Medical Faculty, Istanbul University, Istanbul, Turkey*
[32] *University of California San Diego, San Diego, CA, USA*
[33] *Rigshospitalet, Copenhagen, Denmark*
[34] *Medical University of South Carolina, Charleston, SC, USA*
[35] *Columbia University Medical Center, New York, NY, USA*
[36] *New York University Grossman School of Medicine, New York, NY, USA*
[37] *Division of Rheumatology, Department of Medicine, CHU de Québec — Université Laval, Quebec City, QC, Canada*

ARTICLE INFO

Article history:
Received 6 May 2025
Received in revised form 15 October 2025
Accepted 7 November 2025

ABSTRACT

Objectives: Systemic lupus erythematosus (SLE) remains a deadly disease, yet our ability to predict adverse outcomes is poor. Mitochondria are organelles recognised by the immune system when released from cells, and antimitochondrial antibodies (AMA) can be detected in people with SLE. We assessed AMA as markers of nephritis, arterial vascular events (AVE), and other outcomes including mortality.

Methods: We studied sera and data from 1114 participants of the Systemic Lupus International Collaborating Clinics inception cohort. We measured antiwhole mitochondria (AwMA), antimitochondrial DNA (AmtDNA), and antimitochondrial RNA (AmtRNA) antibodies by direct Enzyme-Linked ImmunoSorbent Assays (ELISAs). Separate multivariable Cox proportional hazards regression models estimated associations of either baseline or most recent measures of AMA with the outcomes, adjusted for biological sex, age, medications, and other clinical factors. Interactions of AMA with biological sex were tested for each outcome.

Results: All AMA titres were elevated in SLE vs healthy individuals. Higher AMA levels were associated with a higher hazard of nephritis, with the strongest associations for most recent AmtDNA (adjusted hazard ratio [aHR] =1.61 for increase of 1 SD, 95% CI 1.43-1.82) and AmtRNA (aHR =1.59, 1.46-1.73). Higher baseline AwMA levels predicted early mortality (aHR =1.19, 1.02-1.40). Most recent AmtDNA (aHR =1.68, 1.28-2.19) was associated with higher mortality throughout the follow-up. For AVE, the impact of higher AmtRNA was stronger in females.

Conclusions: Baseline and most recent assessments of AMA levels may help identify individuals at higher risk of severe outcomes in SLE, including mortality. Integrating AMA into precision medicine strategies will allow deeper exploration of lupus heterogeneity.

WHAT IS ALREADY KNOWN ON THIS TOPIC

- Mitochondria, the intracellular organelles responsible for energy production, are postulated to be bacteria that merged with primitive cells billions of years ago. Under conditions of cellular stress, mitochondrial DNA can escape the organelle and trigger a type 1 interferon response. Additionally, mitochondria can be released into the extracellular environment during cell activation or death and studies performed by us and others have demonstrated that mitochondria are extruded from neutrophils and platelets in lupus.
- The antigenicity of mitochondria has been recognised for several decades. Different sets of antimitochondrial antibodies (AMA), namely AMA-M1 to -M9, have been characterised. These autoantibodies are associated with disease such as primary biliary cirrhosis, hepatitis, cardiomyopathy, and myocarditis.
- We have recently developed assays to measure new AMAs and have documented their occurrence in systemic lupus erythematosus (SLE). They include autoantibodies against the outer membrane of whole mitochondria (AwMA) as well as mitochondrial DNA (AmtDNA) and RNA (AmtRNA). Previous studies reported possible associations between increased AMA levels and SLE clinical manifestation such as arterial vascular events (AVE) and nephritis. Yet, these early studies were limited to cross-sectional analyses with modest sample sizes.
- The Systemic Lupus International Collaborating Clinic lupus inception cohort offers the unique opportunity to study a large number of patients from the time of their diagnosis and for up to 21 years of follow-up. The quality of the clinical data and the availability of repeated sera measurements allowed the exploration of the role of not only the baseline AMA measures but also of their updated, most recent values.

WHAT THIS STUDY ADDS

- Mapping markers of inflammation and autoantibodies, along with their connections to clinical manifestations, remains a significant challenge in lupus. We show here that by leveraging AMA repertoire profiling, we can improve our understanding of mitochondrial biomarkers and their value for patient stratification and outcome prediction in large prospective cohorts. All 3 new AMAs titres were higher in individuals with lupus when compared to healthy controls. Each AMA was found to be associated with different outcomes in lupus. AwMA predicts early mortality while most recent AmtDNA predicts overall mortality and nephritis. Interestingly, we found AmtRNA associated with a higher risk of AVE in females.

HOW THIS STUDY MIGHT AFFECT RESEARCH, PRACTICE OR POLICY

- In addition to classical clinical and immune (eg, complement C3 and C4 levels or antibodies targeting nuclear antigens) markers that help characterise lupus, integrating antibodies directed to the mitochondrial organelle will help understand lupus pathophysiology and how to better classify those at risk of severe lupus outcomes.

INTRODUCTION

The pathogenesis of systemic lupus erythematosus (SLE) leads to the production of an array of autoantibodies [1]. The 2019 European League Against Rheumatism/American College of Rheumatology (ACR) classification criteria for SLE require a positive antinuclear antibody as an entry criterion [2]. However, few lupus autoantibodies meet the standards required for SLE classification criteria or clinical utility. This is a major impediment to personalised care in SLE [3].

There is renewed interest in the role of antimitochondrial antibodies (AMAs) in patients with SLE [4]. AMAs were first described more than 50 years ago in autoimmune liver diseases [5]. Various mitochondrial targets for AMA have been identified in SLE [4,6–10] and displayed associations with arterial vascular events (AVE) [9,11], lupus nephritis [7,8], and disease activity [12].

This study assesses 3 newly defined AMA in patients with lupus enrolled in the Systemic Lupus International Collaborating Clinic (SLICC) inception cohort. We assessed AMA as markers of nephritis, AVE, and other outcomes including mortality.

METHODS

Study population

In 1999, 33 SLICC centres in 11 countries started the SLICC inception lupus cohort. Recruitment was active between 1999 and 2011, and the cohort includes 1827 patients followed for up to 21 years, with a median of 9 years. Participants were diagnosed with lupus, according to the 1997 Updated ACR Classification Criteria for SLE [13,14], within 15 months before cohort entry, and provided consent as required by their Research Ethic Board (REB). Sera paired with demographic and clinical data were collected at baseline and annually. The institutional REB of the leading research team and the SLICC Biological Material and Data Utilization Committee approved this secondary use of the SLICC inception cohort biobank and data. All participants with at least a baseline serum were included, and subsequent sera were taken at or closest to 1, 2, and 5 years of follow-up. Healthy controls, representative of the age and biological sex of the lupus cohort, with no known illnesses or active infection, were recruited for this study from 2 centres to define AMA levels in a healthy population. All sera were aliquoted and stored at −80°C until needed and each aliquot was thawed a maximum of 3 times.

AMA testing

We developed 3 new AMA assays that target the outside membrane of the mitochondria (antiwhole mitochondria antibody [AwMA]), the antimitochondrial DNA (AmtDNA), and antimitochondrial RNA (AmtRNA). The methods for the isolation of the mitochondrial antigens have been published [7,8], and the quantification of AMA by direct ELISA is detailed in Supplemental Methods. We avoided commercial mitochondrial isolation kits, as these do not achieve the purity required and often coprecipitate nuclei, ER, or cytosolic components (mRNA). Instead, we used our own methods, which yield highly purified mitochondria. With these methods, we isolated pure mitochondrial organelles, and we confirmed that both mtRNA and mtDNA preparations originate specifically from mitochondria [6,7,8]. To ensure the reproducibility of the results, we used the same 3 internal controls on each plate. All plates were read in kinetics to quantify the linear part of the reaction.

Outcomes

We explored the following key clinical endpoints: death of any cause, new-onset nephritis, new incident AVE, neuropsychiatric lupus, and the SLICC/ACR Damage Index (SDI), a validated measurement of organ damage [15]. Outcomes were recorded at each annual visit, with exact event date available only for death and AVE. Lupus nephritis was defined as either the new development after entry into the cohort of the criteria for nephritis in the 1997 ACR SLE classification criteria or the report of lupus nephritis, classes I to VI, on a kidney biopsy report. AVE was defined by the first of any of the following: myocardial infarction, stroke, angina, transient ischemic attack, and intermittent claudication, with insertion of a pacemaker or congestive heart failure as surrogate markers for cardiac AVE. For the development of neuropsychiatric lupus, we used the strict SLICC definition of the attribution model A based on the publication by Hanly et al [16].

Other clinical and laboratory variables. Sociodemographic, health habits, lupus disease characteristics, comorbidities, and lupus medication use were collected at baseline and yearly. These included the 1997 Updated ACR classification criteria [14], disease duration, and assessment of disease activity by the SLE Disease Activity Index−2000 (SLEDAI-2K), a validated lupus activity measure [17]. The 1999 protocol only collected information on biological sex, and it did not extensively collect information on ethnicity besides self-identification as being Hispanic. Clinical blood test results from each participating centre (complete blood counts, urine analyses, complement levels, anti-double-stranded DNA antibodies, etc.) were used to calculate the annual SLEDAI-2K measures.

Unfortunately, SLICC did not have a central laboratory to measure with a single assay the traditional lupus biomarkers such as anti-dsDNA, complement C3 and C4, anti-Sm, or the antiphospholipid antibodies. To palliate to this limitation, we abstracted the dichotomous variable presence/absence of items anti-dsDNA and complement from the SLEDAI-2K scores and studied their associations with AMA. In addition, we were able to access the results from Choi's laboratory on a subset of

578 patients of our SLICC cohort at baseline. The following autoantibodies were measured as described in Choi et al [18]: anti-dsDNA, anti-Sm, anti-cardiolipin immunoglobulin G (IgG) and immunoglobulin M (IgM), anti-beta-2 glycoprotein-1 IgG and IgM, antiphosphatidylserine/prothrombin complex (anti-PS/PT) IgG and IgM. Lupus anticoagulant was derived as present or absent from the SLICC original data. This allowed us to estimate which of these were associated with our AMAs.

Statistical analyses

Sample size considerations are presented in Supplemental Methods. The number of participants, samples, and repeat visits was sufficient to allow detection of clinically relevant associations. Baseline AMA levels were compared between groups with Wilcoxon tests. Linear mixed models, with random effects for sites and patients, were used to test for associations of each AMA with follow-up duration, and with SLEDAI-2K scores (with and without the anti-dsDNA item). Transformations (square root for AwMA and SLEDAI-2K, logarithm for others) were used to satisfy the normality assumptions.

Separate time-to-event analyses explored associations between each AMA and each outcome: all-cause mortality, the first diagnosis of lupus nephritis after entry into the cohort, new AVE, new damage, and new neuropsychiatric lupus. Time zero was the date of SLICC cohort entry, and patients who had no event during the follow-up were censored at the earliest of last SLICC visit, death (except for mortality analyses), or loss to follow-up. The patients who had the event of interest at baseline or before, and those without follow-up, were excluded from the corresponding time-to-event analyses.

For each outcome, 4 multivariable Cox proportional hazards regression models were estimated. Models A and B included only the baseline values of AMA and covariates, while models C and D relied on the most recent of the repeated AMA measurements (with 1-4 measurements per patient) and covariates, all represented by time-varying variables. Specifically, model A included the 3 AMAs at baseline in the same model, mutually adjusted for each other and for the baseline covariates values. Model B was estimated separately for each AMA and included only a single AMA at baseline per model, with baseline covariates. Model C included, in the same model, updated values of all 3 AMAs, available at baseline and during the follow-up, adjusted for the time-varying covariates. Finally, model D was similar to model C, except that it was estimated separately for each AMA. To account for clustering by centres, we used a marginal approach with a robust sandwich covariance estimate [19].

The following baseline *a priori* selected covariates were adjusted for in models A and B: sex, Caucasian race/ethnicity, age, and use (baseline or before cohort entry) of prednisone, antimalarials, and immunosuppressors. In addition, body mass index (BMI) and past AVE were included for AVE analyses. Models for all outcomes except death were further adjusted for hypertension and hypercholesterolaemia. In models C and D, which assessed time-varying most recent AMA, other time-varying covariates captured cumulative prednisone dose, current use of antimalarials and immunosuppressors, hypertension, and hypercholesterolaemia. Proportional hazards and linearity assumptions were tested with martingale residuals [20,21]. Interactions between sex and AMA were tested in each model. In time-varying models C and D, we have carried forward the most recent AMAs or covariates measurements as typically done in time-to-event analyses with sparsely measured time-varying covariates [22].

Several sensitivity analyses were performed to assess the potential impact of relevant data limitations (missing values, interval censoring of selected outcomes) and modelling decisions (see *Statistical Analysis Plan* for details). To this end, in separate sensitivity analyses, we relied on, respectively, multiple imputations, dates of events without exact date redefined as the mid-point of the interval between the 2 adjacent clinic visits, inclusion of additional covariates, logarithmic transformation of AMA, and flexible extension of Cox modelling to simultaneous test and account for nonlinear and/or time-dependent effects [23]. Additional sensitivity analyses were done to evaluate the effects of the SLEDAI-2K score, the anti-cardiolipin IgG and anti-PS/PT IgG antibodies, the exclusion of classes I and II lupus nephritis, and finally, by limiting the time-varying models for death to the events occurring in the first year after each AMA measure.

Results were presented as adjusted hazard ratios (aHR) with 95% CIs for an increase of 1 SD of the baseline distribution of a given AMA. Sex-specific estimates were presented if the AMA-by-sex interaction was statistically significant at a 2-tailed 0.05 level. SAS software, version 9.4 (SAS Institute Inc.) was used for analyses. Flexible Cox models were implemented using a customised program in R version 4.2.1.

RESULTS

Descriptive results

Among 1827 patients in the SLICC inception cohort, 1114 (61%) had between 1 and 4 sera available in the first 7 follow-up years, including at least baseline, for a total of 3450 samples (Supplementary Table S1). Table 1 summarises sociodemographic characteristics, BMI, smoking, SLE disease characteristics, comorbidities, baseline medications, and outcomes.

The patients with SLE were 89% female with a mean age (SD) of 35.4 (13.4) years and a mean disease duration of 0.46 (0.35) years, and most had low-to-moderate disease activity (mean [SD] SLEDAI = 5.3 [5.3] at baseline). There were 9788 clinic visits with a median follow-up of 9 years, during which 56 patients died, 120 developed nephritis, 76 had an AVE, 452 developed new damage, and 91 developed neuropsychiatric lupus (Table 2).

Sera were available from 127 healthy controls. Their mean age was 35.2 years (16.1) and 82% were females.

AMAs were elevated in the SLICC inception cohort, and their levels varied over time. At baseline, all 3 AMAs were higher in SLE vs healthy controls (medians of 0.12 vs 0.08, 0.10 vs 0.07, and 0.25 vs 0.09 for, respectively, AwMA, AmtDNA, and AmtRNA, all P values $\leq$ .0001) (Supplementary Table S2). Across all available baseline and follow-up sera, AwMA and AmtRNA generally increased overtime in patients with lupus, whereas AmtDNA levels remained relatively stable (Fig 1). Among the 1114 patients with at least 1 serum available, 366 had a complete set of measurements at prespecified times 0, 1, 2, and 5 years, and were used for sensitivity analysis which revealed the same patterns of change over time (Supplementary Fig S1). When compared to healthy controls, the medians of the 3 subtypes of AMAs remained systematically higher in SLE at baseline and every follow-up (Fig 1).

When comparing AMA with other lupus biomarkers, we found significant associations between higher levels of each AMA and the presence of anti-dsDNA or low complement using

Table 1
Baseline characteristics of SLICC inception cohort lupus patients

Sociodemographic and health habits	SLICC inception cohort lupus patients (N = 1114)[a] Average value (mean ± SD) or Number of patients (N (%))
Age	35.44 ± 13.42
Female	987 (88.60)
Race/ethnicity	
Caucasian	615 (55.21)
Black	201 (18.04)
Asian	196 (17.59)
Hispanic	54 (4.85)
Mixed	26 (2.33)
Other	22 (1.97)
Smoking (n − 1)	169 (15.17)
BMI (kg/m^2)	25.18 ± 5.26
Lupus disease characteristics	
ACR criteria	
Malar rash	399 (35.82)
Discoid rash	137 (12.30)
Photosensitivity	406 (36.45)
Oral ulcers	411 (36.89)
Arthritis	822 (73.79)
Serositis	287 (25.76)
Renal disorders	270 (24.24)
Neurological disorders	50 (4.49)
Haematological disorders	683 (61.31)
Immunological disorders	850 (76.30)
Antinuclear antibodies	1079 (98.86)
Disease duration (y)	0.46 ± 0.35
Lupus disease activity (SLEDAI-2K)	5.34 ± 5.31[b]
Outcome variables at baseline	
Deaths	0
Lupus nephritis	286 (25.67)
Arterial vascular events	
More than 6 mo prediagnosis	53 (4.76)
From 6 mo preceding diagnosis to baseline	41 (3.68)
Lupus disease damage (SDI) >0	91 (8.17)
Neurolupus	70 (6.28)
Comorbidities	
Hypertension (n−2)	374 (33.57)
Diabetes (n−31)	34 (3.14)
Hypercholesterolaemia	379 (34.02)
Obesity (n−51)	192 (17.24)
Menopause	107 (10.84)
Medications	
Antimalarials (n−1)	799 (71.72)
Corticosteroid use	763 (68.49)
Daily dose (mg)	23.47 ± 16.34
Immunosuppressors	425 (38.15)

ACR, American College of Rheumatology; BMI, body mass index; N, number; SDI, SLICC/ACR damage index; SLEDAI-2K, Systemic Lupus Erythematosus Disease Activity Index − 2000; SLICC, Systemic Lupus International Collaborating Clinic.

[a] N = 1114 except when specified in brackets next to a variable. Sera from 127 controls were used for some analyses. Their age (mean ± SD) was 35.16 ± 16.10 and there were 104/127 = 82% females.

[b] SLEDAI-2K median (IQR) = 4 (2-8).

the data derived from the SLEDAI-2K from all patients (results not shown). When restricting our comparisons to the subset of 578 patients from Choi's laboratory (Supplementary Table S4), we replicated our finding of a significant association with anti-dsDNA, and found additional associations with anti-Sm, anticardiolipin IgG (but not IgM) and anti-PS/PT IgG (but not IgM), and no association with the lupus anticoagulant for all 3 AMAs. In addition, we found an association between higher AwMA and the presence of anti-beta-2-glycoprotein-1 IgG, both membrane-bound antigens.

Table 2
Deaths, new nephritis, new AVEs, new damage, and new neurolupus during follow-up in the SLICC inception cohort

Outcome of interest	Number of patients (N = 1114)
Deaths, N (%)	56 (5.03)
Cause of death (lupus as immediate contributing factor[a])	
Lupus	2
Infection	14 (2)
Cardiovascular	10 (3)
Malignancy	7 (1)
Renal	2 (1)
Pulmonary	4 (3)
Other[b]	6 (3)
Unknown	11
New[c] lupus nephritis N (%)	120 (10.77)
Class	
I	3
II	2
II + V	1
III	15
III + V	2
IV	19
IV + V	1
V	7
ACR definition—no biopsy	70
New[c] AVE N (%)	76 (6.82)
Type of AVE	
Myocardial infarction	9
Stroke	21
Angina	13
Transient ischaemic attack	12
Intermittent claudication	7
Pacemaker	3
Congestive heart failure	11
New[c] damage, N (%)	452 (40.57)
1 y	67
5 y	238
10 y	95
15 y	45
20 y	7
New[c] neurolupus N (%)	91 (8.17)
Type of neurolupus	
Acute inflammatory demyelinating syndrome	1
Myelopathy	1
Neuropathy, cranial	11
Polyneuropathy	7
Seizures and seizure disorders	18
Seizures and acute confusional state	1
Acute confusional state	2
Cognitive dysfunction	6
Mood disorders	16
Psychosis	6
Aseptic meningitis	1
Autonomic disorder	1
Cerebrovascular disease	11
Mononeuropathy	8
Myasthenia gravis	1

ACR, American College of Rheumatology; AVE, arterial vascular events; N, number; SLICC, Systemic Lupus International Collaborating Clinic.

[a] Numbers in parentheses account for deaths attributed to a nonlupus cause but the investigators included lupus as a contributing factor to this death.

[b] Other causes of deaths: cerebral haemorrhage post trauma (1); anoxia (1); multiorgan failure post heart transplant (1); seizures (1); Thrombotic Thrombocytopenic Purpura (TTP) in pregnancy (1); neurodegenerative (1).

[c] Patients having a nephritis, AVE, damage, or neurolupus between diagnosis and enrolment (see Table 1) are automatically excluded for new events during this follow-up period.

Higher baseline AwMA was associated with early death in SLE. In multivariable Cox's regression models, higher baseline levels of each AMA, assessed separately, were associated with higher mortality (model B in Table 3), but only baseline AwMA

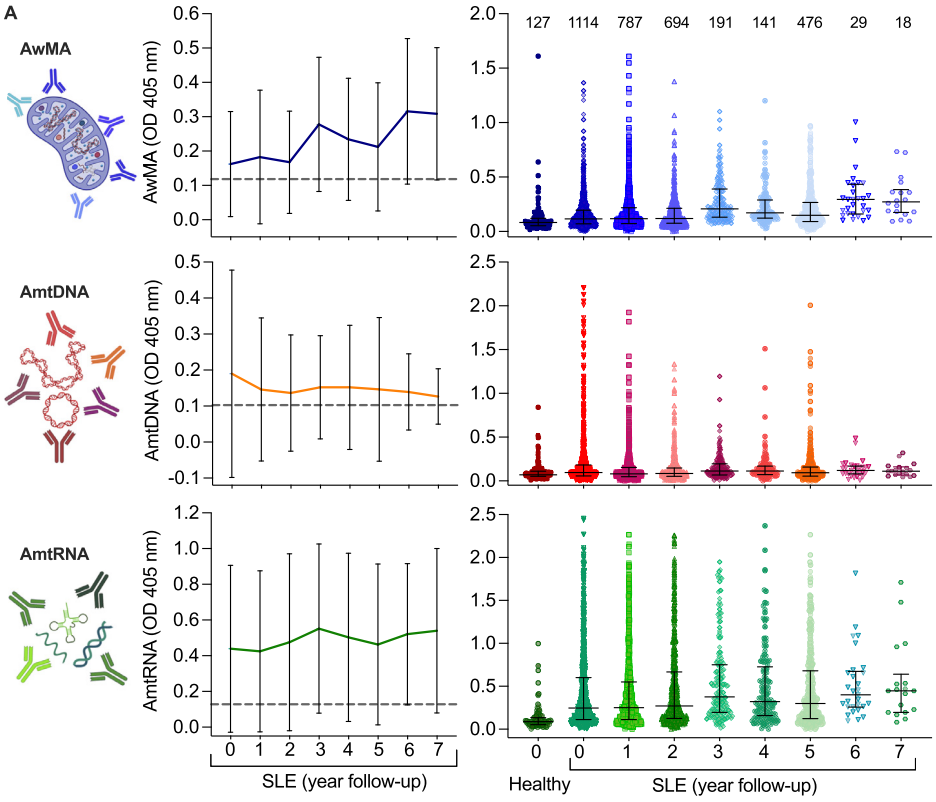

B

Slope estimates for the visit effect over time			
Outcome	Beta (95% confidence interval)	t statistic with degree of freedom	P value
Sqrt_AwMA	0.01699 (0.0143;0.0197)	$t_{3419} = 12.37$	<.0001
Log_AmtDNA	-0.00592 (-0.0179;0.0061)	$t_{3419} = -0.96$	0.3362
Log_AmtRNA	0.03352 (0.0200;0.0470)	$t_{3419} = 4.87$	<.0001

Figure 1. Fluctuations of AMA levels during the disease course and slope estimates for the visit effect over time. (A, left graphs) Mean of OD values of the 3 AMA targeting whole organelles (AwMA, blue colour), mitochondrial DNA (AmtDNA, red colour) or RNA (AmtRNA, green colour) were assessed in sera from healthy individuals (n = 127) and over time for patients with SLE included in the SLICC cohort (n = 1114 patients at baseline) (3577 samples in total). All participants with at least a baseline serum were included and subsequent sera were taken at, or closest to, 1, 2, and 5 years in the first 7 years of follow-up with a maximum of 4 visits per patient. Data are reported as mean ± SD, dotted horizontal lines display mean levels of corresponding AMA measured in healthy donors. (A, right graphs) Box-plot representation of the distributions of AwMA, AmtDNA, and AmtRNA for healthy controls and patients with SLE at each visit. Number of patients with SLE for each subgroup is indicated at the top. The horizontal line within the box represents the median and the lower and upper limits of the box are the 25th and 75th percentiles. (B) Reports on the results of the linear mixed models, with random effects for sites and patients, to test a linear slope between each AMA and years of follow-up. A transformation (square root for AwMA, logarithm for others) was used to satisfy the assumptions. AMA, antimitochondrial antibodies; AmtDNA, antimitochondrial DNA; AmtRNA, antimitochondrial RNA; AVE, arterial vascular events; AwMA, antiwhole mitochondria antibodies; OD, optical density; SLE, systemic lupus erythematosus; SLICC, Systemic Lupus International Collaborating Clinic.

remained statistically significant after adjustment for the 2 other AMAs (model A) with an aHR =1.19, 95% CI 1.02-1.40 for 1 SD increase. However, flexible analyses indicated violations of proportional hazards and linearity assumptions, with the association of baseline AwMA with higher mortality becoming weaker over time and limited to the first 3 years of follow-up (Fig 2). Moreover, among AMA measures updated during the entire follow-up, only higher recent AmtDNA values were significantly associated with higher mortality (aHR 1.68, 1.28-2.19 for model C; aHR 1.54, 1.23-1.93 for model D) (Table 3).

Since AMA values vary within subjects over time, we performed additional sensitivity analyses using the most recent AMA values temporarily censoring each patient at 1 year after their most recent AMA measurement (including the baseline). The censored patients could then be reintegrated in the risk sets later, starting at the time of the next (if any) AMA measurement. This approach evaluated the strength of the associations limited to AMA values observed in the past 12 months. The new estimated HRs in these sensitivity analyses were similar to, and not systematically stronger than those estimated in the main time-varying analyses (Supplementary Table S5). These results do not suggest that more recent AwMA values are better predictors of death.

AmtDNA and AmtRNA were associated with SLE nephritis. When considered separately, higher baseline values of all AMAs were significantly associated with nephritis (Table 3, model B), with both AmtDNA (aHR 1.42, 1.24-1.63) and AmtRNA (aHR

Table 3
Prediction of deaths, nephritis, or AVE by AMA at baseline only or using repeated measures over time

Deaths Model	AwMA	AmtDNA	AmtRNA
A	1.19 (1.02-1.40)	1.27 (0.97-1.66)	1.07 (0.78-1.48)
B	1.22 (1.05-1.42)	1.35 (1.16-1.56)	1.23 (1.02-1.49)
C	0.91 (0.70-1.20)	1.68 (1.28-2.19)	0.90 (0.63-1.28)
D	0.98 (0.79-1.22)	1.54 (1.23-1.93)	1.13 (0.83-1.54)
Nephritis **Model**	**AwMA**	**AmtDNA**	**AmtRNA**
A	1.01 (0.82-1.23)	1.31 (1.13-1.52)	1.28 (1.16-1.41)
B	1.19 (1.06-1.34)	1.42 (1.24-1.63)	1.45 (1.31-1.61)
C	1.02 (0.92-1.14)	1.37 (1.19-1.58)	1.37 (1.26-1.48)
D	1.17 (1.07-1.27)	1.61 (1.43-1.82)	1.59 (1.46-1.73)
AVE **Model**	**AwMA**	**AmtDNA**	**AmtRNA**
A	0.99 (0.83-1.18)	0.99 (0.79-1.23)	F 1.17 (0.96-1.41) M 0.57 (0.35-0.92) Interaction *P* value = .0203
B	1.02 (0.87-1.19)	0.98 (0.79-1.21)	F 1.15 (0.94-1.42) M 0.56 (0.34-0.93) Interaction *P* value = .0174
C	1.08 (0.89-1.30)	1.15 (0.92-1.45)	F 1.24 (0.98-1.58) M 0.62 (0.36-1.06) Interaction *P* value = .0384
D	1.12 (0.94-1.33)	1.22 (1.009-1.47)	F 1.34 (1.07-1.67) M 0.67 (0.39-1.14) Interaction *P* value = .0361

Summary of models		AMA included in the models	
		Three AMA in the same model	Three separate models for each AMA
Visits included in the models	Baseline only	A	B
	All available visits (time-varying variables)	C	D

AMA, antimitochondrial antibodies; AmtDNA, antimitochondrial DNA; AmtRNA, antimitochondrial RNA; AVE, arterial vascular events; AwMA, antiwhole mitochondria antibodies; HR, hazard ratio.
Values are HR (95% CI) for 1 SD increase. SD are 0.153 for AwMA, 0.288 for AmtDNA and 0.468 for AmtRNA.
Model A includes the 3 AMAs at baseline in the same model with covariates at baseline. Model B includes 1 AMA at baseline per model with covariates at baseline. Model C includes the 3 AMAs available at baseline and with 0 to 3 additional measures over time per patient in the same model with the time-varying covariates. Model D includes 1 AMA available at baseline and with 0 to 3 additional measures over time per patient in the same model with the time-varying covariates.

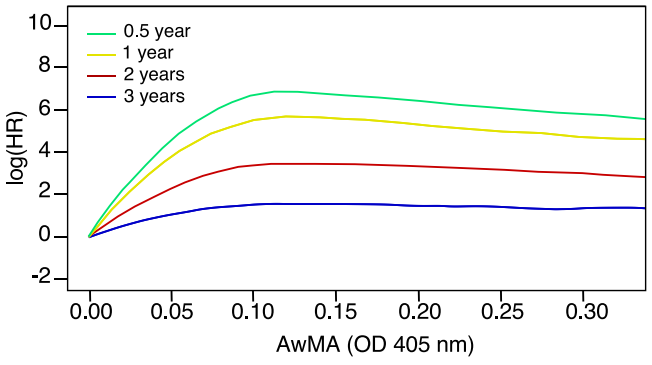

Figure 2. The effect of time on the association between AwMA and mortality. Flexible analyses indicated violations of proportional hazards and linearity assumptions, with the association of baseline AwMA with higher mortality becoming weaker over time and limited to the first 3 years of follow-up. As can be seen on this figure, the risk of death, measured as log(HR) on the y-axis, associated with AwMA, measured as OD on the x-axis, is highest early on, eg, at 6 months (green curve) and 1 year (yellow curve), less at 2 years (red curve) and almost back to nil at 3 years (blue curve). AwMA, antiwhole mitochondria antibodies; HR, hazard ratio; OD, optical density.

1.45, 1.31-1.61) displaying strong relationships. A similar pattern, with slightly stronger associations, was observed for most recent AmtDNA and AmtRNA values in time-varying models C and D (Table 3).

Risk of AVE increased with higher recent AmtDNA levels in the time-varying model D (aHR 1.22, 1.009-1.47, Table 3) when adjusted for other AMAs. However, the associations of AVE with AmtRNA differed by sex with *P* values for sex interactions ranging between 0.02 and 0.04 in all AVE models (Table 3). In males with SLE, AVE risks decreased with higher baseline AmtRNA either when considered alone (aHR 0.56, 0.34-0.93) or adjusted for the other AMAs (aHR 0.57, 0.35-0.92), with similar associations for most recent AmtRNA values (Table 3). In contrast, for female patients, higher values of either baseline or most recent AmtRNA were systematically associated with *higher* AVE hazards (Table 3), and the association reached statistical significance for most recent AmtRNA, when not adjusted for the other AMAs (aHR 1.34, 1.07-1.67, model D). Males with SLE had more cardiac AVE (angina, myocardial infarction, and pacemaker) whereas females had more cerebral AVE (stroke and transient ischemic attacks) ($P = .06$ for chi-square test of sex differences in AVE type).

Since lupus disease activity could be a confounder, because it may be associated with AMA and have an effect on our outcomes, we further studied the relation between each of the 3 AMAs and the disease activity measure SLEDAI-2K. We found significant associations between each of the 3 AMAs and SLEDAI-2K both with and without the SLEDAI-2K item anti-dsDNA or low complement (Supplementary Table S3). Given these associations, we repeated all our multivariable models and found that adding the variable SLEDAI-2K as an adjustment covariate did *not* affect materially any of the results reported in Table 3 (Supplementary Table S5). We are therefore confident that the clinical associations we found do *not* reflect a potential confounding by SLEDAI-2K. Similarly, the following sensitivity analyses did not affect our overall results: adding anticardiolipin IgG or anti-PS/PT IgG antibodies to the models, excluding classes I and II lupus nephritis, and finally, limiting the models for death to the events occurring in the first year after the AMA measure.

We were unable to establish clear associations of either baseline or most recent AMA values in any of the models for either damage or neuropsychiatric lupus (data not shown).

DISCUSSION

We have demonstrated in this large and unique longitudinal inception cohort of patients with SLE that AMAs are associated with critically important clinical outcomes such as death, nephritis, and AVE. Previous studies reported possible associations between increased AMA levels and SLE clinical manifestations [4,6–9,12] such as AVE and nephritis. Yet, these early studies were limited to cross-sectional analyses with modest sample sizes [24]. Here, we have sought to capture key outcomes which could be verified easily across all 33 centres, notably renal involvement, AVE, and deaths, using a large cohort with long follow-up. Importantly, we demonstrate that AMA increases can antedate the development of those outcomes and remain independent predictors after adjustment for several covariates. Furthermore, our analyses helped establish new associations between AMA and early mortality, new development of nephritis, and AVE.

The SLICC lupus inception cohort offers the unique opportunity to study a large number of patients from diagnosis and for up to 21 years of follow-up. This is a racially and ethnically diverse population from centres all around the world. The quality of the clinical data and the availability of repeated sera measurements allowed the exploration of the role of not only the baseline AMA measures but also of their updated, most recent values. An important clinical question remains whether these new autoantibodies add to the information carried by traditional autoantibodies such as anti-dsDNA, anti-Sm, or the different antiphospholipid antibodies. Our substudy of patients with available baseline measures of these traditional autoantibodies performed in Choi's laboratory showed, as expected, that AMA positivity was associated with higher mean levels of some of these autoantibodies.

We have previously demonstrated that AwMA, AmtDNA, and AmtRNA performed differently than anti-M2 AMA associated with primary biliary cholangitis (PBC) [7,8]. We found the most likely antigenic target of AwMA to be C1q-binding protein and mitofusin-1 [6]. Preliminary results show that anti-mitofusin-1 appears to discriminate lupus sera from those derived from healthy controls, as well as from patients with PBC and several other connective tissue diseases (data not shown). Interestingly, anti-mitofusin-1 has recently been reported as a marker of erosive, more severe rheumatoid arthritis [25] and polymyalgia rheumatica [26].

We conducted a complex analysis with multiple models that could potentially lead to an inflated overall risk of type I error. However, across all models considered, among the 60 tests of associations of individual AMA (either baseline or repeated time-varying) values with different outcomes, 24 (40%) yielded $P < .05$, compared to 3 expected by chance ($P < .0001$). Thus, a vast majority of the significant associations we report are very unlikely to reflect just chance.

We acknowledge that we did not determine the relative usefulness of AMA in combination with other known biomarkers of organ involvement, damage, or death, including anti-dsDNA antibodies. Furthermore, the low number of male patients, typical of SLE cohorts, limited our ability to establish more definitively the possible protective effect on AVE of AmtRNA in males with SLE.

Overall, our results support the use of AMA in the clinic both as new possible diagnostic biomarkers and definitively as predictors of clinically important outcomes. They may have a greater role in monitoring rather than diagnosing disease, particularly when used in combination with other autoantibodies or cytokine signatures. The addition of AMA may enhance previously published clinically relevant lupus profiles [18]. This may lead to the identification of clinically relevant subgroups of patients that may require different treatments or monitoring models.

Higher baseline AwMA was a marker for early mortality in SLE. In lupus, cells and platelets can release mitochondria and mitochondrial components [4,27]. Mitochondria are recognised as damage-associated molecular patterns (DAMPs) that can elicit immune responses [4,28]. In genetically predisposed individuals, immune responses to circulating mitochondria or mitochondrial antigens may be amplified, potentially marking more severe disease. Conversely, accumulating evidence suggests a beneficial role for mitochondrial transfer between cells [29] a process that could be disrupted by the presence of AMA. Furthermore, B-cell subsets, including specific B-cell clones or polyreactive B cells activated by circulating DAMPs [30], may generate AMAs that interfere with intercellular mitochondrial exchange. More research is required to determine whether AMAs play a direct pathogenic role or instead represent an epiphenomenon.

We found that higher AwMA levels in newly SLE-diagnosed patients are associated with early mortality, while high recent AmtDNA levels were associated with mortality across the follow-up. The immune response to mitochondrial antigens in predisposed individuals may evolve over time from the recognition of a surface antigen on the outer wall of the mitochondria, such as anti-mitofusin-1 [6], to that of the internal antigens such as mitochondrial DNA or RNA. Clinically, detection of elevated AwMA at the time of diagnosis, or persistently elevated AmtDNA or AmtRNA, should prompt careful assessment and follow-up.

Higher levels of all AMAs were consistently associated with a higher risk of developing lupus nephritis, across the various models, with the strongest relationships for AmtDNA, followed closely by AmtRNA. The presence of antibodies to genomic DNA (AgDNA) is a known risk factor for lupus nephritis. We have previously reported that, although moderately correlated, AmtDNA captures antibodies with different specificities than AgDNA, maybe due to different methylation patterns and structures [4,7]. This suggests that patients with both AmtDNA and AgDNA or autoantibodies with higher

affinity may generate more pathogenic immune complexes that lead to worse disease.

AmtDNA was associated with AVE overall. We also found an intriguing potential sex difference in the association between AmtRNA and AVE with higher levels of AmtRNA clearly associated with AVE in females while having a possible *protective* effect in males. AmtRNA might promote Fc-mediated internalisation of mtRNA in intracellular compartments, where endosomal toll-like receptors (TLRs) such as TLR-7 and 8 may recognise mtRNA to promote activation. How exactly AmtRNA may play contrasting roles in males and females is unclear, but this may be linked to the presence of TLR-7 and -8 genes on the X chromosome and their potential to escape X chromosome inactivation, thus leaving females with more gene copies of these TLRs [31,32]. Moreover, the long noncoding RNA Xist, which is uniquely transcribed from the inactivated X chromosome in females, forms complexes with ribonucleoproteins that drive sex-driven autoimmunity [33]. Whether AmtRNA cross react with these Xist-containing antigens is unknown.

In conclusion, detection of elevated AwMA at the time of diagnosis, or persistently elevated AmtDNA or AmtRNA during disease course, should prompt careful initial assessment and cautious follow-up. Integrating antibodies directed to the mitochondrial organelle into precision medicine strategies will allow deeper exploration of lupus heterogeneity.

Competing interests

YLCB, PRF, and EB have filed a provisional patent regarding kits to detect antimitochondrial antibodies in systemic lupus erythematosus.

Acknowledgements

We acknowledge the contribution of Dr. Joyce Rauch (McGill University, Montréal, Canada) and Dr Mélanie Dieudé in the conception of the experiments presented herein. The study participants, individual center support staff as well as investigators of the Systemic Lupus International Collaborating Clinics (SLICC) Inception Cohort project who for a period of 21 years have made this study possible. Paul R. Fortin holds the tier 1 Canada Research Chair in Systemic Autoimmune Rheumatic Diseases. This work was previously presented in the following references:

1 Becker YL, Boilard É, Rollet-Labelle E, et al. 103 Exploratory segregation of patients upon their levels of anti- mitochondrial antibodies (AMAs) reveals associations between AMAs and disease manifestations. Lupus Science & Medicine 2022;9:doi: 10.1136/lupus-2022-lupus21century.3

2 Becker Y, Boilard E, Fortin PR, Bernatsky S, Clarke AE et Al. Mapping Anti-Mitochondrial Antibodies over Time in a Lupus Inception Cohort. ACR Convergence 2022 in Philadelphia, Pennsylvania, Session: SLE – Diagnosis, Manifestations, and Outcomes Poster I: Diagnosis. Saturday, November 12. Abstract ID: 1287449.

Contributors

EB, A-SJ, MA, PRF, and YLCB researched data for the article and wrote the article. YB, ER-L, IA, JL, and TL contributed to the handling of the samples and reagents, and to the acquisition of the OD values. MC contributed data for the subanalyses of 578 patients to test associations between AMAs and lupus biomarkers. A-SJ, MA, and PRF contributed to the biostatistical analyses performed. Tables and figures were designed by A-SJ, IA, and YLCB. Biological samples and clinical information were harvested by the investigators of the SLICC Inception Cohort. All authors contributed substantially to the discussion of the content and reviewed and/or edited the manuscript before submission.

Funding

This study was supported by CIHR CIB grant PJT-162353. YLCB is supported by fellowships from the Fonds de Recherche du Québec en Santé (FRQS) and from the ARThrite Research Center. CL is supported by awards from the NIH (1 R21 AR077565, 1 R21 AR079542, and 1 R01 HL158606). S-CB is supported by Basic Science Research Program through the National Research Foundation of Korea (NRF) funded by the Ministry of Education (NRF-2021R1A6A1A03038899). EB is supported by a senior award from the FRQS. The SLICC neuropsychiatric study led by JGH was supported by CIHR grants MOP-57752, MOP-86526, and MOP-88526.

Patient consent for publication

Patient consent for publication was not required.

Ethics approval

1- The original REB was done at the SLICC Inception Cohort coordinating center at University Health Network in Toronto (University Health Network Research Ethics Board - REB#: 00-0279); 2- Each participating center then had their own institutional REB review and approve the study; 3- The present substudy was submitted and approved by the SLICC Biological Materials and Data Utilization Committee; 4- The REB of the CHU de Québec - Université Laval approved the substudy (Comité d'Éthique à la recherche du CHU de Québec - Université Laval, CER#: 2019-4592); and 5- all research on humans performed in the SLICC Inception Study and in the present substudy was done in compliance with the Declaration of Helsinki.

Provenance and peer review

Not commissioned; externally peer reviewed.

Supplementary materials

Supplementary material associated with this article can be found in the online version at doi:10.1016/j.ard.2025.11.007.

Orcid

Paul R. Fortin: http://orcid.org/0000-0002-7278-2596

REFERENCES

[1] Yaniv G, Twig G, Shor DB, Furer A, Sherer Y, Mozes O, et al. A volcanic explosion of autoantibodies in systemic lupus erythematosus: a diversity of 180 different antibodies found in SLE patients. Autoimmun Rev 2015;14(1):75–9.

[2] Aringer M, Costenbader K, Daikh D, Brinks R, Mosca M, Ramsey-Goldman R, et al. 2019 European League Against Rheumatism/American College of Rheumatology classification criteria for systemic lupus erythematosus. Ann Rheum Dis 2019;78(9):1151–9.

[3] Aringer M, Johnson SR. Classifying and diagnosing systemic lupus erythematosus in the 21st century. Rheumatology (Oxford) 2020;59(Suppl5):v4–11.

[4] Becker YLC, Duvvuri B, Fortin PR, Lood C, Boilard E. The role of mitochondria in rheumatic diseases. Nat Rev Rheumatol 2022;18(11):621–40.
[5] Kaplowitz N, Finlayson NDC, Walmsley P, Thurnherr N, Javitt NB. Hepatobiliary diseases associated with serum antimitochondrial antibody (AMA). Am J Med 1973;54(6):725–30 PMID: 4710306. doi: 10.1016/0002-9343(73)90058-2.
[6] Becker YLC, Gagné JP, Julien AS, Lévesque T, Allaeys I, Gougeard N, et al. Identification of mitofusin 1 and complement component 1q subcomponent binding protein as mitochondrial targets in systemic lupus erythematosus. Arthritis Rheumatol 2022;74(7):1193–203.
[7] Becker Y, Loignon RC, Julien AS, Marcoux G, Allaeys I, Lévesque T, et al. Anti-mitochondrial autoantibodies in systemic lupus erythematosus and their association with disease manifestations. Sci Rep 2019;9(1):4530.
[8] Becker Y, Marcoux G, Allaeys I, Julien AS, Loignon RC, Benk-Fortin H, et al. Autoantibodies in systemic lupus erythematosus target mitochondrial RNA. Front Immunol 2019;10:1026.
[9] Becker YL, Julien AS, Godbout A, Boilard É, Fortin PR. Pilot study of anti-mitochondrial antibodies in antiphospholipid syndrome. Lupus 2020;29(12):1623–9.
[10] Caielli S, Athale S, Domic B, Murat E, Chandra M, Banchereau R, et al. Oxidized mitochondrial nucleoids released by neutrophils drive type I interferon production in human lupus. J Exp Med 2016;213(5):697–713.
[11] Dieudé M, Correa JA, Neville C, Pineau C, Levine JS, Subang R, et al. Association of autoantibodies to heat-shock protein 60 with arterial vascular events in patients with antiphospholipid antibodies. Arthritis Rheum 2011;63(8):2416–24.
[12] Pisetsky DS, Spencer DM, Mobarrez F, Fuzzi E, Gunnarsson I, Svenungsson E. The binding of SLE autoantibodies to mitochondria. Clin Immunol 2020;212:108349.
[13] Tan EM, Cohen AS, Fries JF, Masi AT, McShane DJ, Rothfield NF, et al. The 1982 revised criteria for the classification of systemic lupus erythematosus. Arthritis Rheum 1982;25(11):1271–7.
[14] Hochberg MC. Updating the American College of Rheumatology revised criteria for the classification of systemic lupus erythematosus. Arthritis Rheum 1997;40(9):1725.
[15] Gladman D, Ginzler E, Goldsmith C, Fortin P, Liang M, Urowitz M, et al. Systemic lupus international collaborative clinics: development of a damage index in systemic lupus erythematosus. J Rheumatol 1992;19(11):1820–1.
[16] Hanly JG, Gordon C, Bae SC, Romero-Diaz J, Sanchez-Guerrero J, Bernatsky S, et al. Neuropsychiatric events in systemic lupus erythematosus: predictors of occurrence and resolution in a longitudinal analysis of an international inception cohort. Arthritis Rheumatol 2021;73(12):2293–302.
[17] Gladman DD, Ibañez D, Urowitz MB. Systemic lupus erythematosus disease activity index 2000. J Rheumatol 2002;29(2):288–91.
[18] Choi MY, Chen I, Clarke AE, Fritzler MJ, Buhler KA, Urowitz M, et al. Machine learning identifies clusters of longitudinal autoantibody profiles predictive of systemic lupus erythematosus disease outcomes. Ann Rheum Dis 2023;82(7):927–36.
[19] Lee EW, Wei LJ, Amato DA, Leurgans S. Survival analysis: state of the art. In: Klein JP, Goel PK, editors. Survival analysis: state of the art. Dordrecht, Netherlands: Kluwer Academic; 1992. p. 237–47.
[20] Grambsch P, Therneau TM. Proportional hazards tests and diagnostics based on weighted residuals. Biometrika 1994;81(3):515–26.
[21] Lin DY, Wei LJ, Ying Z. Checking the Cox model with cumulative sums of martingale-based residuals. Biometrika 1993;80:557–72.
[22] Andersen PK, Liestøl K. Attenuation caused by infrequently updated covariates in survival analysis. Biostatistics 2003;4(4):633–49.
[23] Abrahamowicz M, MacKenzie TA. Joint estimation of time-dependent and nonlinear effects of continuous covariates on survival. Stat Med 2007;26(2):392–408.
[24] Piga M, Arnaud L. The main challenges in systemic lupus erythematosus: where do we stand? J Clin Med 2021;10(2):243.
[25] Moore RE, Wang T, Duvvuri B, Feser ML, Deane KD, Solomon JJ, et al. Prediction of erosive disease development by antimitochondrial antibodies in rheumatoid arthritis. Arthritis Rheumatol 2023;75(6):890–9.
[26] Michailidou D, Johansson L, Chapa JAG, Wang T, Chen J, López JA, et al. Mitochondrial-mediated platelet activation in polymyalgia rheumatica. ACR Open Rheumatol 2025;7(3):e70021.
[27] Melki I, Allaeys I, Tessandier N, Lévesque T, Cloutier N, Laroche A, et al. Platelets release mitochondrial antigens in systemic lupus erythematosus. Sci Transl Med 2021;13(581):eaav5928.
[28] Marchi S, Guilbaud E, Tait SWG, Yamazaki T, Galluzzi L. Mitochondrial control of inflammation. Nat Rev Immunol 2023;23(3):159–73.
[29] Brestoff JR, Singh KK, Aquilano K, Becker LB, Berridge MV, Boilard E, et al. Recommendations for mitochondria transfer and transplantation nomenclature and characterization. Nat Metab 2025;7(1):53–67.
[30] Mashiko S, Shihab RR, See SB, Schahadat LGZ, Aguiar TFM, Roy P, et al. Broad responses to chemical adducts shape the natural antibody repertoire in early infancy. Sci Adv 2023;9(19):eade8872.
[31] Brown GJ, Cañete PF, Wang H, Medhavy A, Bones J, Roco JA, et al. TLR7 gain-of-function genetic variation causes human lupus. Nature 2022;605(7909):349–56.
[32] Youness A, Cenac C, Faz-López B, Grunenwald S, Barrat FJ, Chaumeil J, et al. TLR8 escapes X chromosome inactivation in human monocytes and CD4. Biol Sex Differ 2023;14(1):60.
[33] Dou DR, Zhao Y, Belk JA, Casey KM, Chen DC, Li R, et al. Xist ribonucleoproteins promote female sex-biased autoimmunity. Cell 2024;187(3):733–749.e16.

Ann Rheum Dis 85 (2026) 669–679

Contents lists available at ScienceDirect

Annals of the Rheumatic Diseases

journal homepage: https://www.sciencedirect.com/journal/annals-of-the-rheumatic-diseases

Systemic sclerosis

The incidence of interstitial lung disease in patients with systemic sclerosis: rate, risk factors and prognostic implications in a EUSTAR cohort analysis (CP 133)

Liubov Petelytska[1,2], Lorenzo Tofani[3], Arthiha Velauthapillai[4], Rucsandra Dobrota[1], Mike Oliver Becker[1], Carina Mihai[1], Sinziana Muraru[1], Muriel Elhai[1], Suzana Jordan[1], Eric Hachulla[5], Ulf Müller-Ladner[6], Elise Siegert[7], Yannick Allanore[8], Gabriela Riemekasten[9], Christina Bergmann[10,11], Radim Becvar[12], Kamal Solanki[13], Branimir Anic[14], Iulia Szabo[15,16], Bojana Stamenkovic[17], Jörg Distler[18,19], Patricia E. Carreira[20], Giovanna Cuomo[21], Ivan Castellví[22], Alexandra Balbir-Gurman[23], Paolo Airò[24], Ira Litinsky[25], Lesley Ann Saketkoo[26,27], Bruno Bertaccini[3], Madelon C Vonk[4], Jeska de Vries-Bouwstra[28], Anna-Maria Hoffmann-Vold[1,29], Marco Matucci-Cerinic[30,31,32], Oliver Distler[1], Cosimo Bruni[1,33,*], on behalf of the EUSTAR collaborators

[1] *Department of Rheumatology, University Hospital Zurich, University of Zurich, Zurich, Switzerland*
[2] *Department of Internal Medicine n 3, Bogomolets National Medical University, Kyiv, Ukraine*
[3] *Department of Statistics Informatics & Applications, University of Florence, Florence, Italy*
[4] *Department of Rheumatology, Radboud University Medical Center, Nijmegen, The Netherlands*
[5] *Department of Internal Medicine and Clinical Immunology, National Referral Centre for Rare Systemic Auto-immune and Auto-inflammatory Diseases, Inserm, CHU Lille, U1286 – INFINITE, University of Lille, Lille, France*
[6] *Department of Internal Medicine and Clinical Immunology, Justus-Liebig-University Giessen, Bad Nauheim, Germany*
[7] *Department of Rheumatology and Clinical Immunology, Charité – Universitätsmedizin Berlin, Berlin, Germany*
[8] *Department of Rheumatology, Cochin Hospital, Université Paris Cité, Paris, France*
[9] *Department of Rheumatology and Clinical Immunology, University Clinic Schleswig-Holstein, University of Lübeck Ratzeburger Allee, Lübeck, Germany*
[10] *Department of Internal Medicine 3, Rheumatology and Immunology, Friedrich-Alexander-University Erlangen-Nürnberg (FAU), Erlangen, Germany*
[11] *University Hospital Erlangen, Erlangen, Germany*
[12] *Institute of Rheumatology and Department of Rheumatology, 1st Medical School Charles University, Prague, Czech Republic*
[13] *Department of Rheumatology, Te Whatu Ora Health New Zealand Waikato, Hamilton City, New Zealand*
[14] *Department of Internal Medicine, Division of Clinical Immunology and Rheumatology, University of Zagreb School of Medicine, University Hospital Center Zagreb, Zagreb, Croatia*
[15] *Department of Rheumatology, "Iuliu Haţieganu" University of Medicine and Pharmacy, Cluj-Napoca, Romania*
[16] *Department of Rheumatology, County Emergency Hospital, Cluj-Napoca, Romania*

*Correspondence to Dr. Cosimo Bruni, Department of Rheumatology, University Hospital Zurich, University of Zurich, Rämistrasse 100, 8006, Zurich, Switzerland.
E-mail address: cosimo.bruni@usz.ch (C. Bruni).
Handling editor Josef S. Smolen.

https://doi.org/10.1016/j.ard.2025.12.008

[17] Institute for Prevention Treatment and Rehabilitation Rheumatic and Cardiovascular Disease, Niška Banja, Serbia
[18] Clinic for Rheumatology, University Hospital Düsseldorf Heinrich-Heine University, Düsseldorf, Germany
[19] Hiller Research Center, University Hospital Düsseldorf Heinrich-Heine University, Düsseldorf, Germany
[20] Servicio de Reumatología, Hospital 12 de Octubre, Madrid, Spain
[21] Department of Precision Medicine "Luigi Vanvitelli", University of Campania, Naples, Italy
[22] Department of Rheumatology, Hospital Universitari de la Santa Creu i Sant Pau, Barcelona, Spain
[23] B. Shine Rheumatology Institute, Rambam Health Care Campus, Rappaport Faculty of Medicine Technion, Haifa, Israel
[24] Scleroderma UNIT, UOC Reumatologia ed Immunologia Clinica, ASST Spedali Civili, Brescia, Italy
[25] Centre Tel Aviv Sourasky. Rheumatology Institute, Tel Aviv, Israel
[26] Tulane University, New Orleans, LA, USA
[27] Scleroderma and Sarcoidosis Patient Care and Research Center, Louisiana State University Schools of Medicine/University Medical Center, New Orleans, Los Angeles, USA
[28] Department of Rheumatology, Leiden University Medical Center, Leiden, The Netherlands
[29] Department of Rheumatology, Oslo University Hospital, Rikshospitalet, Oslo, Norway
[30] Unit of Immunology Rheumatology Allergy and Rare Diseases (UniRAR), IRCCS Ospedale San Raffaele, Milan, Italy
[31] Inflammation, Fibrosis and Aging Initiative (INFLAGE), IRCCS Ospedale San Raffaele, Milan, Italy
[32] Vita Salute University San Raffaele, Milan, Italy
[33] Department of Experimental and Clinical Medicine, University of Florence, Florence, Italy

ARTICLE INFO

Article history:
Received 3 February 2025
Received in revised form 25 August 2025
Accepted 16 December 2025

ABSTRACT

Objectives: Interstitial lung disease (ILD) carries significant morbidity and mortality risk in systemic sclerosis (SSc). We aimed to estimate the incidence of new-onset SSc-ILD and the associated risk factors, as well as its impact on the prognosis.

Methods: Patients classified as having SSc, with the absence of ILD signs on high-resolution computed tomography (HRCT) at baseline and having at least 1 follow-up visit with available HRCT data, were selected. SSc-ILD incidence was calculated as a rate per 100 person-years. Predictors of new-onset ILD and risk factors for ILD progression and mortality were chosen according to the literature and expert opinion. Risk factors for new-onset ILD, as well as its prognostic impact on ILD progression and mortality, were tested by generalised logistic estimating equation and Cox regression models, respectively.

Results: Among 5331 patients with SSc with negative baseline HRCT, the incidence of new-onset ILD was 3.83 cases per 100 person-years. Notably, there was a continuous detection of new ILD onset up to 10 years from baseline. Risk factors for new-onset ILD included New York Heart Association stage ≥2, muscle weakness, high inflammatory markers, and SSc-specific autoantibodies, but not disease duration. Despite a lower risk of ILD progression compared with prevalent ILD diagnosed at baseline, incident ILD still carried an increased risk for mortality, which was almost double when compared with ILD-negative cases.

Conclusions: Patients with SSc should be considered for regular screening following a negative baseline HRCT, in particular when carrying high-risk features for new ILD onset, given its incidence and prognostic implications.

INTRODUCTION

Interstitial lung disease (ILD) is among the most important factors influencing the clinical course of systemic sclerosis (SSc), in terms of quality of life, morbidity, and mortality [1].

The epidemiology of ILD in SSc varies depending on the different methodologies used to detect it. Although ILD overall affects from 2.3 to 19 per 100,000 persons in the general population [2,3], its frequency is higher in patients with SSc, ranging from 13.9 to 88.1 per 100 cases [4–9]. When considering representative population-based studies, the lifetime prevalence of SSc-ILD turns out to be approximately 50% [10].

With the availability of effective treatments [11,12], consensus statements [13] and guidelines for the management of SSc-ILD have been published [14–16]. Accordingly, patients with SSc-ILD have been well characterised, and risk factors associated with the presence of SSc-ILD have been identified. These include anti-topoisomerase I (ATA) positivity, diffuse cutaneous SSc (dcSSc), oesophagal involvement, male sex, African-American ethnicity, lower % predicted forced vital capacity (FVC), and lower % predicted diffusing capacity of the lungs for carbon monoxide (DLCO) [17–21].

As most SSc-ILD studies are cross-sectional or consider baseline SSc-ILD cases in a longitudinal observation, less is known about the incidence of SSc-ILD following a negative baseline high-resolution computed tomography (HRCT) [22,23]. Single-centre and national cohort analysis revealed incidence rates of new-onset SSc-ILD between 2.0 and 4.4 per 100 patients-years [7,24,25]. However, different definitions of baseline negative patients have been applied (ie, negative HRCT but also negative chest X-ray, no symptoms, or low suspicion of ILD). In these studies, certain risk factors for new onset of SSc-ILD were proposed, including baseline pulmonary function tests (PFTs), autoantibody status, haemoglobin concentrations, age at onset of Raynaud's phenomenon (RP) [22], and rapid progression of skin fibrosis [23].

Later onset of ILD, not detectable at first presentation, might suggest a milder phenotype and better outcome. However, data

WHAT IS ALREADY KNOWN ON THIS TOPIC

- Limited studies estimated the incidence of interstitial lung disease (ILD) in systemic sclerosis.
- The optimal combination of risk factors for accurately predicting ILD in patients with systemic sclerosis (SSc) has not yet been identified.
- The impact of new-onset, incident ILD, in comparison with prevalent ILD diagnosed at baseline, is unknown in terms of risk of progression and mortality.

WHAT THIS STUDY ADDS

- There is a continuous incidence of new-onset ILD cases in SSc, stable up to 10 years from baseline.
- We have identified factors associated with new ILD onset following a negative baseline high-resolution computed tomography, including age, dyspnoea, autoantibody profile, diffusion capacity of the lung for carbon oxide and increased inflammatory markers.
- New-onset incident ILD has a lower risk of functional progression than prevalent ILD, but determines a higher mortality burden in comparison with patients without ILD.

HOW THIS STUDY MIGHT AFFECT RESEARCH, PRACTICE, OR POLICY

- The prognostic implication of new-onset incident ILD should support continuous screening for ILD in patients with SSc following a negative baseline.
- Risk factors have been identified to further support the screening and the rescreening of patients at higher risk.

to prove this hypothesis are lacking. This uncertainty might have also led to a lack of consensus about rescreening initially negative cases [13–16,26]. In addition, it is unclear whether the incidence of new-onset ILD is decreasing over the disease course. This is of high practical importance, as rescreening for new-onset ILD might be adapted in patients with longer disease duration, if the incidence of new-onset ILD is decreasing over time. Identifying patients at risk of new-onset ILD might further help to stratify patients for more or fewer screenings. Notably, the findings of reduced survival, even in patients with mild lung fibrosis and normal FVC [10], might argue for a relevant disease burden in patients with new-onset ILD, after a negative baseline screening.

We therefore aimed to (1) estimate the annual incidence of new-onset SSc-ILD in baseline HRCT-negative patients in the large European Scleroderma Trials And Research (EUSTAR) cohort, (2) identify risk factors for new SSc-ILD onset, and (3) evaluate the impact of new-onset SSc-ILD on ILD progression and mortality.

METHODS

Patient population and characteristics

Patients with SSc classified according to the 2013 ACR/EULAR criteria [27] from the EUSTAR group database were eligible for this study if they showed available data for ILD on HRCT at baseline, as defined by the local expert radiologist evaluation and as reported in the database, and at least 1 follow-up visit with available HRCT data. The dataset extraction took place in June 2022 (data from September 2003 to February 2022 were available). The framework of the EUSTAR database, the structure of the presented data, and definitions of clinical variables, including ILD and disease duration (from the first non-RP sign or symptom), have been previously provided [17]. Patients with pulmonary hypertension, defined as mean pulmonary artery pressure >20 mmHg on right heart catheterisation, were excluded, as well as those with unknown ILD status on HRCT and inconsistent cases. Presence of overlapping rheumatic conditions, such as rheumatoid arthritis or idiopathic inflammatory myopathies, did not represent an exclusion criterion.

The first visit with available HRCT data recorded was considered as the baseline visit. Based on the baseline ILD status, patients were divided into 2 groups: those with ILD on baseline HRCT (prevalent ILD group) and those without ILD on baseline HRCT. Based on follow-up HRCTs, patients without ILD on baseline HRCT were further classified into patients with new onset of ILD on HRCT at follow-up (incident ILD group) and patients who remained ILD negative (ILD-negative group).

Primary outcome

The primary outcome of this post hoc analysis of prospectively collected data was the estimation of the crude incidence of SSc-ILD. The incidence was calculated by dividing the number of patients with SSc who developed ILD according to HRCT during follow-up by the number of patients with SSc without ILD at baseline. The incidence rate was presented as a rate per 100 person-years (dividing the number of incidental ILD cases by the total number of person-years accumulated by the cohorts of ILD-negative patients), starting from the baseline visit and from disease onset (corresponding to the date of the first non-RP sign or symptom).

Secondary outcomes

In addition, we tested the risk factor for new onset of SSc-ILD, both for 1-year and long-term (ever) incidence. Secondly, we tested the impact of incident SSc-ILD compared with prevalent SSc-ILD on progression at 12±3 months intervals. The following 3 different definitions of progression were applied: (1) absolute FVC decline ≥5% predicted [28], (2) absolute FVC decline ≥5% predicted or absolute DLCO decline ≥10% predicted [29], and (3) relative FVC decline ≥10% predicted or 5% to 9% with relative DLCO decline ≥15% predicted [30]. Finally, we tested the association of new-onset SSc-ILD with mortality, compared with prevalent or negative ILD.

Statistical methods

Categorical variables were reported as number (%) and continuous variables as mean with SD or median with IQR, depending on distribution. Poisson rate CI were calculated for measuring the 95% CI for each incidence rate.

Multivariable, logistic, generalised estimating equation models, using backward selection, with odds ratio (OR) and 95% CI, were applied to identify risk factors for 1-year SSc-ILD incidence, as well as for ILD progression. Generalised estimating equation modelling accounts and balances for multiple observations of the same patient, and the adjusting factors refer to the start of each observation (ie, each yearly interval).

Cox regression models, using backward selection, were used to estimate adjusted hazard ratio (HR) and 95% CI of incident ILD ever and for mortality. In these longitudinal analyses, risk factors and adjusting covariates from the baseline visit were included.

All prediction models included adjusting confounders, based on previous preliminary data and expert opinion [22,23,31,32]. Common adjusting factors to all models belonged to demographics (age, sex, disease duration, and smoking), clinical (cutaneous subtype, arthritis ever, muscle weakness, oesophageal symptoms, digital ulcers, digital pitting scars, dyspnoea—defined as New York Heart Association [NYHA] stage ≥2), functional (DLCO%, FVC%), and laboratory features. The latter included SSc-specific autoantibodies (including ATA, anticentromere [ACA], anti-RNA polymerase III [ARA], and anti-PM/Scl antibodies), increased inflammatory markers (defined as C-reactive protein or erythrocyte sedimentation rate above the upper level of normality according to local laboratory).

For both ILD onset analyses, body mass index, ethnicity, modified Rodnan's skin score, tendon friction rubs, and haemoglobin level represented additional covariates. All ILD progression models included as predictor of interest the categorisation of patients with ILD into incident vs prevalent. The mortality analysis also included ILD status (in terms of incident, prevalent, or negative), the abovementioned adjusting factors, as well as further mortality risk factors such as left ventricle ejection fraction, pericardial effusion, diastolic dysfunction and estimated systolic pulmonary artery pressure, measured through echocardiography.

Additionally, the number of HRCTs during follow-up, the average time between HRCTs and the exposure to immunosuppressants (including corticosteroids above 10 mg/d, methotrexate, azathioprine, cyclophosphamide, mycophenolate mofetil, rituximab, and tocilizumab) during the observation were also included in the long-term incidence model.

To account for the variation in time of onset of ILD during follow-up, the number of visits and the follow-up duration, sensitivity analyses for ILD incidence as outcome were performed and restricted to 1) patients with at least 3 visits within 5 years from baseline, and 2) patients with disease duration ≤5 years.

Finally, hypothesising a major role for ATA for ILD incidence, we implemented the final steps of both ILD onset prediction models by adding interaction terms between ATA and the other predictors to confirm their predictive role among the ATA status strata. To quantify this, marginal estimates effects were computed.

The survival analysis included patients with at least 6 months of follow-up after the first visit with an HRCT reporting the presence of ILD (for prevalent and incident cases). For ILD-negative patients, a minimum of 6 months follow-up from the first HRCT available was required. In addition to the Cox regression model, a Kaplan-Meier analysis was performed to compare survival among groups.

All statistical analyses were performed with SAS 9.4 M7. Missing data on the predictors and confounders were handled with an imputation algorithm (Random Forest) [33], when at least 51% information was present. The variables considered for imputation, with the prevalence of missing data, are presented in the supplementary annex S1. Given the high percentage of missingness, exposure to immunosuppressants was not imputed and tested only as an exploratory evaluation.

RESULTS

Baseline demographics

Within the EUSTAR database, 11,601 patients fulfilled inclusion criteria (Fig 1). Among them, we identified 6270 (54.5%) patients with prevalent ILD at baseline. Among 5331 ILD-negative patients at baseline, new ILD onset occurred in 1075 (20.2%) cases over a median 3.8 (1.6-7.3) years follow-up, with a median time to ILD detection of 3.23 (95% CI: 1.39-6.74) years from the baseline visit.

Similar results were obtained in the sensitivity analysis, including 3358 patients with at least 3 visits with available

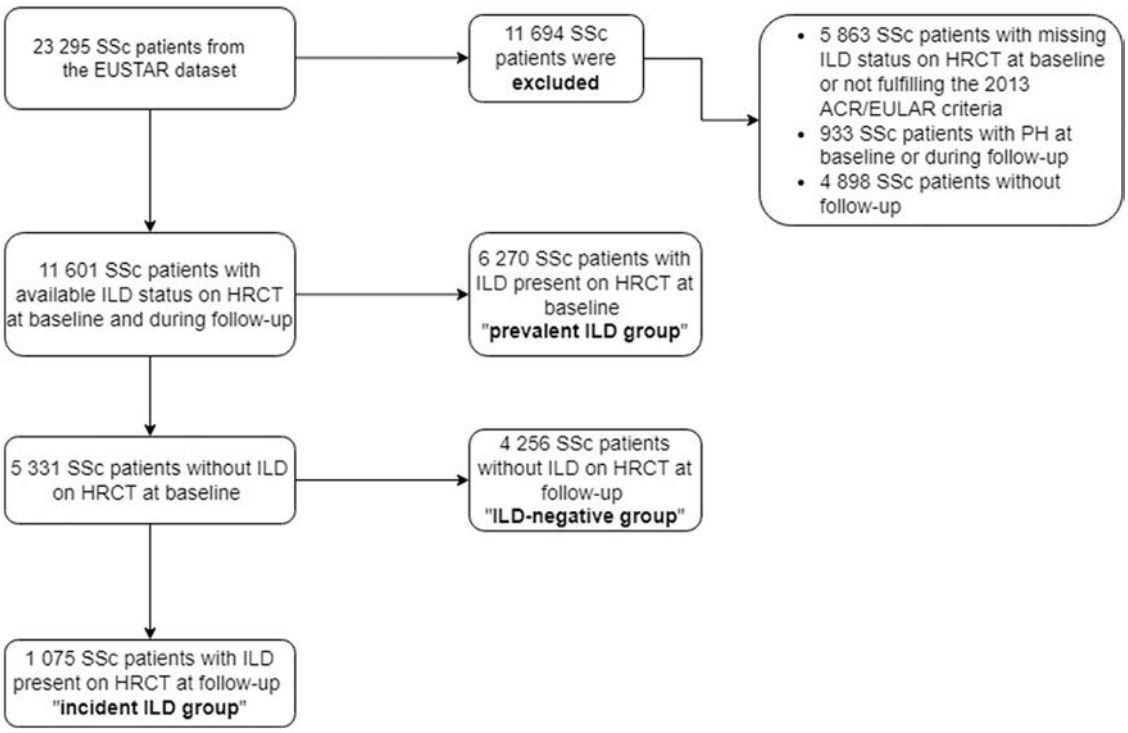

Figure 1. Flow chart of the study population. ACR/EULAR, American College of Rheumatology/European Alliance of Associations for Rheumatology; EUSTAR, European Scleroderma Trials And Research; PH, pulmonary hypertension; HRCT, high-resolution computed tomography; ILD, interstitial lung disease; PAH, pulmonary arterial hypertension; SSc, systemic sclerosis.

HRCTs within 5 years from baseline. Among them, 2727 (81.2%) were ILD negative at baseline, and 631 (18.8%) developed ILD during follow-up. Interestingly, we noted a numerically shorter time to new ILD detection, at a median of 2.25 (1.23-3.75) years after baseline.

In the second sensitivity analysis focusing on patients with disease duration ≤5 years, 576/2674 (21.5%) patients developed ILD after a median 3.1 (1.3-6.4) years of follow-up (Supplementary Table S1). Time to ILD onset was comparable with the whole population, with a median time to ILD onset of 3.05 (1.60-7.36) years.

In comparison with the prevalent ILD group, the incident ILD group was characterised by shorter disease duration, lower prevalence of peripheral vascular manifestations, arthritis, and smoking exposure at baseline (Table). Similarly, compared with patients who remained ILD-negative during follow-up, patients with incident ILD were younger at baseline, more frequently men, with dcSSc subset, ATA positivity, and increased inflammatory markers, but less frequently smokers. Moreover, patients with incident ILD already had a higher dyspnoea NYHA class at baseline, as well as lower FVC% and DLCO% (Table).

Except for age and NYHA functional class, the sensitivity analyses confirmed the baseline differences between incident ILD and ILD-negative cases (Supplementary Table S1).

Incidence rate of new-onset ILD

The overall ILD incidence rate was 3.83 (95% CI, 3.12-4.63) per 100 person-years. There was a continuous detection of new onset of ILD for up to 10 years from baseline (range of incidence rates 2.40-5.14 per 100 person-years; Fig 2, left panel). Interestingly, when the incidence rate was quantified from disease onset, we confirmed the persistent incidence of new cases up to 15 years, with an overall ILD incidence rate of 1.66 (95% CI, 1.19-2.25) per 100 person-years (Fig 2, right panel). Similar rates and ranges over time were confirmed in the 2 sensitivity analyses (Supplementary Figs S1-S2).

Predictors of 1-year incidence of SSc-ILD

Given the annual follow-up of patients with SSc and the potential design of a 1-year preventive clinical trial, we focused our ILD incidence analysis on patients having at least a 1-year observation period. This resulted in the analysis of 13,339 yearly follow-ups from 4067 baseline negative patients, with 482 new ILD onset detected. In multivariable analysis, male sex (OR, 1.42; 95% CI, 1.10-1.84), older age (OR, 1.01; 95% CI, 1.00-1.02), dyspnoea NYHA stage ≥2 (OR, 1.38; 95% CI, 1.13-1.67), ATA (OR, 2.10; 95% CI, 1.60-2.76) and increased inflammatory markers (OR, 1.31; 95% CI, 1.03-1.67) were associated

Table
Baseline characteristics of patients with SSc according to the ILD status

	ILD prevalent group (n = 6270)	ILD incident group (n = 1075)	ILD-negative group (n = 4256)
Age (y), mean±SD	57±13	52±14	53±14
Sex female, n (%)	4054 (80)	873 (81)	3692 (87)
Disease duration (y), mean±SD	9±8	6±7	7±7
Caucasian, n (%)	5823 (92)	1007 (94)	4057 (95)
Smoking ever, n (%)	916 (15)	75 (7)	409 (10)
BMI, mean±SD	25±4	25±4	25±4
Diffuse cutaneous SSc, n (%)	3062 (49)	490 (46)	1023 (24)
Raynaud's phenomenon present, n (%)	5876 (94)	880 (82)	3595 (85)
Modified Rodnan skin score, median (IQR)	9 (0-51)	7 (3-13)	4 (2-10)
Digital ulcers ever, n (%)	2007 (32)	186 (17)	577 (14)
Pitting scars on fingertips, n (%)	2485 (40)	358 (33)	1184 (28)
Puffy fingers, n (%)	3249 (55)	568 (53)	2141 (50)
Telangiectasia, n (%)	717 (66)	4123 (66)	2644 (64)
Arthritis ever, n (%)	780 (12)	21 (2)	133 (3)
Tendon friction rubs, n (%)	473 (8)	75 (7)	192 (5)
Muscle weakness, n (%)	1044 (17)	168 (16)	503 (12)
Oesophagal symptoms, n (%)	4159 (66)	653 (61)	2521 (59)
Scleroderma renal crisis, n (%)	118 (2)	7 (0.7)	20 (0.5)
Dyspnoea NYHA stage ≥2, n (%)	3403 (54)	372 (35)	1258 (30)
Pericardial effusion, n (%)	365 (6)	29 (3)	113 (3)
Diastolic function abnormal, n (%)	1280 (20)	166 (15)	481 (11)
DLCO% predicted, mean±SD	61±18	70±17	75±17
FVC % predicted, mean±SD	86±21	93±18	99±18
TLC% predicted, mean±SD	84±20	93±19	101±17
Systolic PAP on ECHO (mmHg), mean±SD	31±9	30±6	29±7
ACA, n (%)	1187 (19)	312 (29)	2495 (59)
ATA, n (%)	3297 (53)	521 (48)	770 (18)
ARA, n (%)	206 (3)	29 (3)	170 (3)
PM/Scl, n (%)	125 (2)	13 (1)	40 (1)
None of above or other, n (%)	1455 (23)	200 (19)	807 (19)
Increased inflammatory markers, n (%)	1470 (23)	195 (18)	495 (12)
Hb (g/dL), mean±SD	12±3	12±2	12±3
Immunosuppressants ever, n (%)	1588/2058 (77)	432/ 577 (75)	593/955 (62)
Immunosuppressants ongoing, n (%)	1586/2056 (77)	375/562 (67)	593/955 (62)

ACA, anticentromere antibodies; ARA, anti-RNA polymerase III antibodies; ATA, anti-topoisomerase antibodies; BMI, body mass index; CRP, C-reactive protein; DLCO/SB, carbon monoxide diffusing capacity; ESR, erythrocyte sedimentation rate; FVC, forced vital capacity; ILD, interstitial lung disease; NYHA, New York Heart Association; PAP on ECHO, pulmonary artery pressure on echocardiogram; PM/Scl, anti-PM/Scl antibodies; SSc, systemic sclerosis; TLC, total lung capacity.

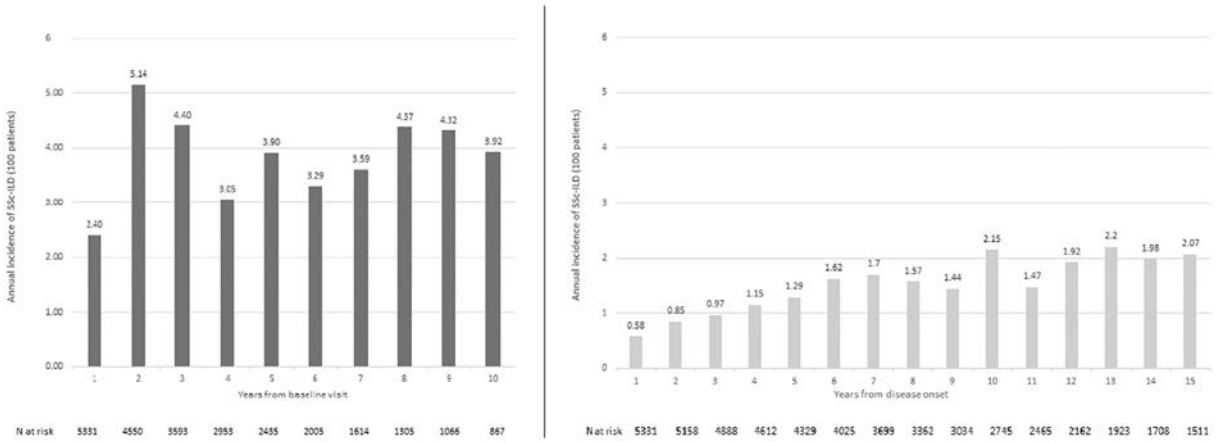

Figure 2. Annual incidence rate of new onset of ILD per 100 patients from the baseline visit (left panel) and from disease onset, defined as the date of first non-Raynaud's phenomenon sign or symptom (right panel). ILD, interstitial lung disease; SSc, systemic sclerosis.

with an increased risk of 1-year SSc-ILD incidence. Conversely, higher DLCO% (OR, 0.98; 95% CI, 0.98-0.99) and haemoglobin level (OR, 0.98; 95% CI, 0.98-0.99), arthritis ever (OR, 0.66; 95% CI, 0.50-0.87), ACA (OR, 0.40; 95% CI, 0.29-0.54), and ARA (OR, 0.52; 95% CI, 0.28-0.97) were independent protective factors of 1-year SSc-ILD incidence (Fig 3A). When exposure to immunosuppressants was forced into the 2 models, as an exploratory evaluation, this was not retained as a protective factor. When testing the interaction of ATA with the other predictors, no statistically significant result was detected, supporting a comparable role of the risk factors regardless of autoantibody specificity (data not shown).

Predictors of incidence of SSc-ILD ever

In the Cox regression analysis of the cumulative incidence over the whole observation period, new-onset SSc-ILD was independently predicted by dyspnoea NYHA stage ≥2 (HR, 1.15;

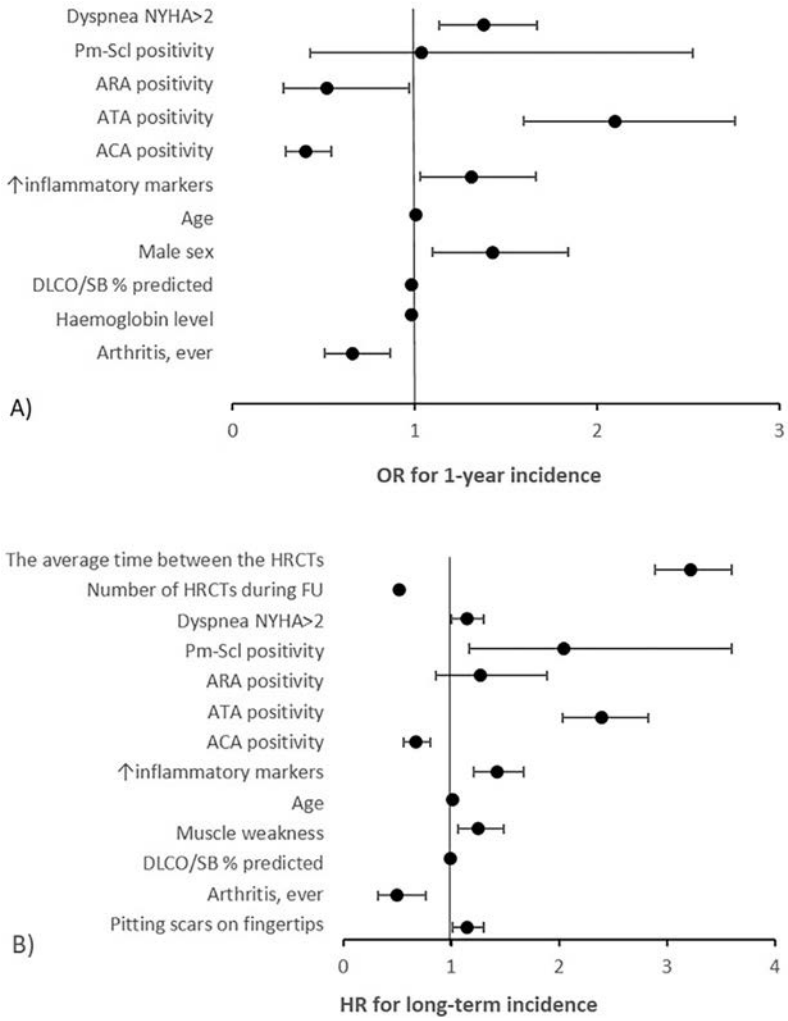

Figure 3. Multivariable prediction models of new onset of ILD for 1- (A) and long-term observation (B), respectively, applying logistic and Cox regression. ACA, anticentromere antibodies; ARA, anti-RNA polymerase III antibodies; ATA, anti-topoisomerase antibodies; DLCO/SB, carbon monoxide diffusing capacity; FU, follow-up; HR, hazard ratio; HRCT, high-resolution computed tomography; ILD, interstitial lung disease; NYHA, New York Heart Association; OR, odds ratio.

95% CI, 1.01-1.30), digital pitting scars (HR, 1.15; 95% CI, 1.01-1.31), muscle weakness (HR, 1.26; 95% CI, 1.06-1.49), age (HR, 1.01; 95% CI, 1.01-1.02), increased inflammatory markers (HR, 1.42; 95% CI, 1.21-1.67), ATA (HR, 2.40; 95% CI, 2.03-2.82) and anti-Pm/Scl antibodies (HR, 2.05; 95% CI, 1.16-3.60). A higher DLCO% (HR, 1.77; 95% CI, 1.49-2.08) was mildly associated with a reduced risk of incidence, as well as ACA (HR, 0.68; 95% CI, 0.56-0.81) and arthritis ever (HR, 0.50; 95% CI, 0.32-0.77) (Fig 3B). These results were independent of the average time between HRCTs and the number of HRCTs performed during the follow-up. Notably, the incidence of new onset of ILD was independent of disease duration. When testing the interaction of ATA with the other predictors, we observed a significant interaction between ATA and age (P = .02) and ATA and dyspnoea, NYHA stage ≥2 (P = .04). Combining the results into marginal estimates, we observed that dyspnoea NYHA stage ≥2 (HR, 1.32; 95% CI, 1.11-1.58) and age (HR, 1.02; 95% CI, 1.01-1.02) were confirmed as independent predictors of new ILD onset ever in the ATA negative population, hypothesising a more prominent role for these risk factors in this subpopulation. Conversely, in patients with ATA positive, these 2 predictors were not independently associated with the ILD onset (dyspnoea NYHA stage ≥2, HR, 0.99; 95% CI, 0.82-1.21: age, HR, 1.00; 95% CI, 0.99-1.01).

Impact of ILD on overall survival in patients with SSc

During a median of 4.1 (IQR, 2.0-7.7 years) years of follow-up, 708/9003 (7.8%) deaths were recorded. The survival rate was lower in the prevalent ILD group (88.1%), compared with both the incident ILD (92.2%) and ILD-negative (96.4%) groups (P = .0008 by Log-rank test). In the adjusted Cox regression model (Fig 4), both incident ILD (HR, 0.68; 95% CI: 0.51-0.89) and ILD-negative (HR, 0.35; 95% CI, 0.29-0.42) status showed a lower mortality risk than the prevalent ILD. Additionally, the incident ILD group had a higher risk of mortality than the ILD-negative group (HR, 1.94; 95% CI, 1.41-2.67), even after adjustment for confounders.

SSc-ILD progression in incident and prevalent groups

ILD progression was analysed in 7337 follow-ups of 2803 patients with SSc-ILD, including both incident and prevalent SSc-ILD cases for a median observation of 3.15 (1.52-6.42) years. Incident and prevalent cases were similarly observed, respectively for 3.03 (1.50-5.99) years and 3.18 (1.53-6.50) years. Overall, progression occurred in 25%, 35%, and 19% yearly follow-ups, respectively, according to the 3 abovementioned definitions. In comparison to the ILD prevalent group, the ILD incident group was associated with a decreased risk of ILD progression by definition B (*absolute FVC decline ≥5% or absolute DLCO decline ≥10% predicted*; OR, 0.85; 95% CI, 0.79-0.97; P = .02) and C (*relative FVC decline ≥10% predicted or 5-9% predicted with relative DLCO decline ≥15% predicted* − OR, 0.83; 95% CI, 0.69-0.98; P = .03), after adjustment for covariates. This association was not confirmed for definition A (*absolute FVC decline ≥5% predicted*—Fig 5).

DISCUSSION

Our EUSTAR study shows an incidence rate for new-onset SSc-ILD of 3.8 cases per 100 person-years and, to our knowledge, for the first time, a continuous detection of new onset of ILD up to 10 years from baseline visit. Additionally, we confirmed a negative impact on survival also for incident SSc-ILD compared with ILD-negative cases, in addition to the already known increased risk for prevalent ILD.

ILD incidence is not a rare event

Our incidence rate data are in line with recent results from national registries (2.0-4.4 per 100 person-years) [3,4,7,24,25,34]. Compared with these cohorts, our multicentre study included larger numbers and considered HRCT as the gold standard sole method to confirm both the presence and absence of ILD. In contrast, the previous studies identified new ILD [24,25], also based on other criteria, such as chest X-ray or 'velcro-like crackles' on physical examination. The high number of patients with SSc included in the EUSTAR cohort and the long follow-up allowed us to perform sensitivity analyses, show new SSc-ILD cases up to 10 years after baseline and to determine the independence of this phenomenon with respect to disease duration.

Risk factors of incident ILD

Our study identified risk factors of incident ILD both at 1-year follow-up and overall, long-term observation, confirming predictors such as DLCO% [21,22,35], older age [21,22], ATA or ACA positivity [21,22,25], haemoglobin [10], and increased inflammatory markers [36]. Some risk factors were identified only in one of the two prediction analyses, such as ARA reducing the risk of 1-year ILD incidence and of anti-PM/Scl antibody increasing the risk of SSc-ILD onset ever. In fact, ARA has been

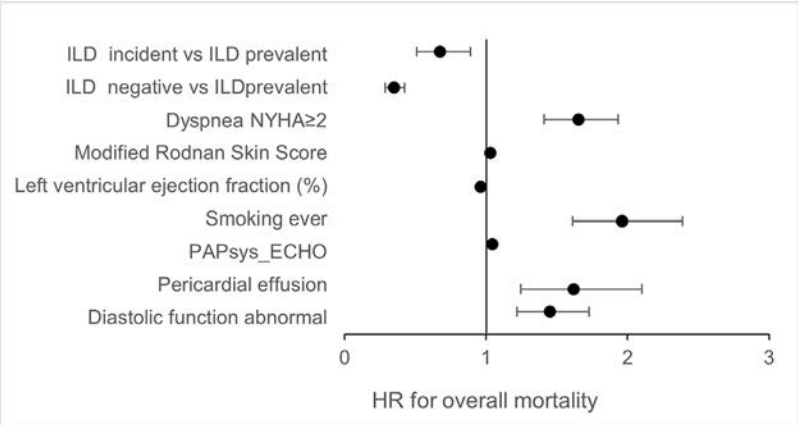

Figure 4. Prediction model of mortality in patients with SSc according to ILD status. ILD, interstitial lung disease; NYHA, New York Heart Association functional class; OR, odds ratio; PAPsys_ECHO, systolic pulmonary artery pressure estimated on echocardiogram; SSc, systemic sclerosis.

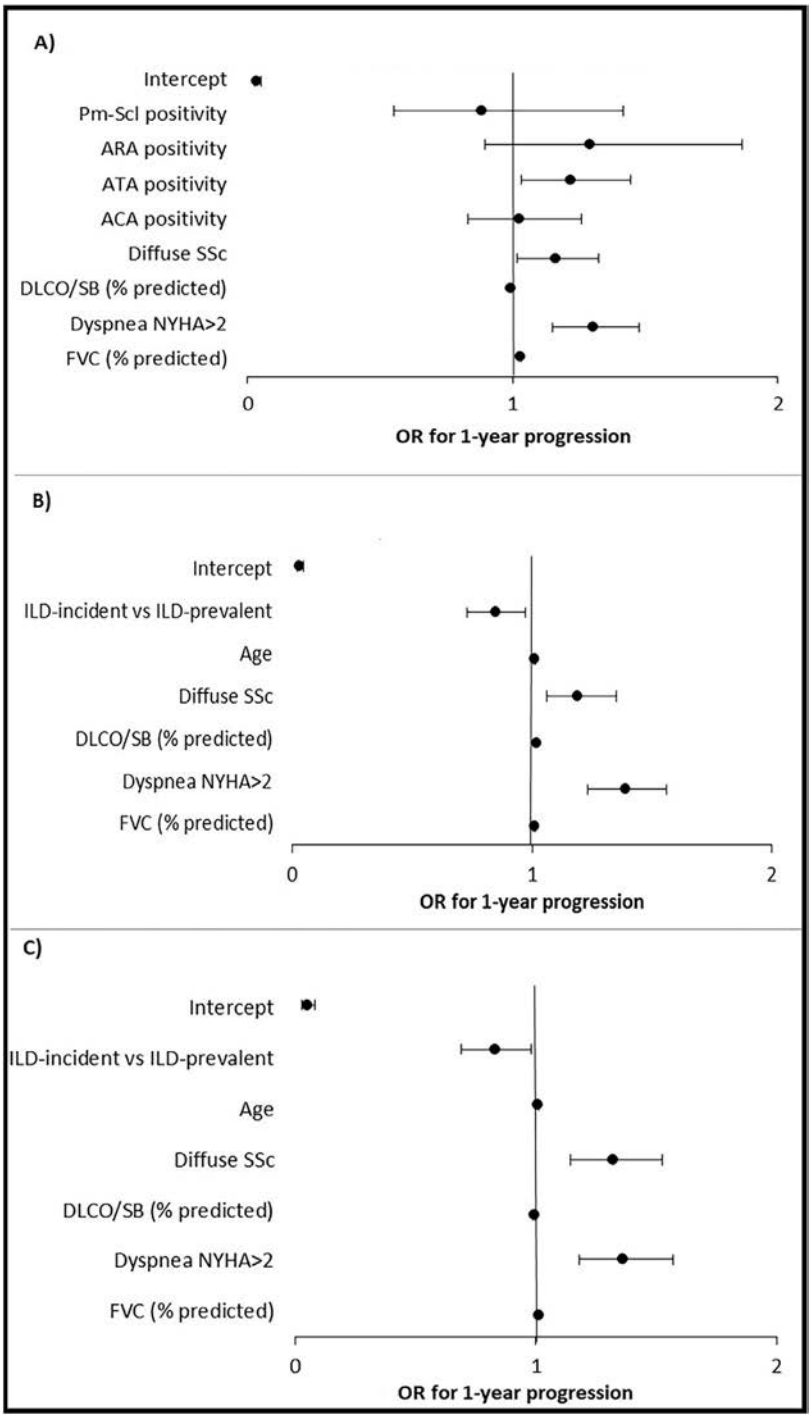

Figure 5. Prediction models of SSc-ILD progression according to definition A (*absolute FVC decline ≥5% predicted*), definition B (*absolute FVC decline ≥5% or absolute DLCO decline ≥10% predicted*), and (C) (*relative FVC decline ≥10% predicted or 5-9% predicted with relative DLCO decline ≥15% predicted*), over 12±3 mo intervals. ACA, anticentromere antibodies; ARA, anti-RNA polymerase III antibodies; ATA, anti-topoisomerase antibodies; DLCO/SB, carbon monoxide diffusing capacity; FVC, forced vital capacity; ILD, interstitial lung disease; NYHA, New York Heart Association; PM/Scl, anti-PM/Scl antibodies; SSc, systemic sclerosis; TLC, total lung capacity.

previously associated with the hazard of clinically significant pulmonary fibrosis that peaked in the first 3 years, whereas this hazard was increased after the first decade in patients with anti-PM/Scl-positive SSc [37]. Interestingly, arthritis ever was associated with lower ILD incidence: this might be related to the coexistence in the model of increased inflammatory biomarkers (potentially representing an active musculoskeletal disease status), as well as to the disease-modifying drugs these patients might have received for the very same complication, for which we cannot exclude a potential protective effect.

Once validated, the prediction models derived from our data would define the patient phenotype at higher risk of incident ILD. Practically, this would represent the phenotype of patients who could benefit from a more intensive observation and rescreening, In fact, our analysis also indirectly supports the rescreening for ILD in patients with an initially negative HRCT, as we observed patients undergoing more frequent HRCTs were detected with new-onset ILD almost 1 year earlier. This is an advance in the *window of opportunity* for the treatment of SSc-ILD, to possibly start treating earlier, as well as the basis for an enrichment cohort for preventive trials, in which pharmacologic and nonpharmacologic interventions might be tested.

Progression and prognosis of incident vs prevalent ILD

Early progression of ILD based on PFTs is associated with an increased risk of mortality in both clinical trials [38] and observational studies [10,30], which highlights the importance of

early detection and treatment of SSc-ILD. In our cohort, we could detect a variable incidence of ILD functional progression in line with previous EUSTAR data [28]. Importantly, we observed a significantly lower risk of progression in patients with incident ILD, compared with prevalent ILD, within a comparable follow-up observation. This might be partially explained by the lower ILD extent on HRCT [39] and previous immunosuppressive treatment for organ involvement [25]. Regarding prognosis, our results indicate an increased mortality risk even for incident SSc-ILD, despite mild functional impairment at baseline compared with prevalent ILD cases. Although this difference might also be explained by a milder ILD extent [40], we could not confirm this due to the high amount of missing data in the visual quantification of ILD extent in the EUSTAR database. Additionally, we hypothesise that the new detection of incident ILD could be associated with a prompt initiation of immunosuppressive therapy, which would be theoretically less delayed compared with prevalent ILD cases, in which the baseline detection of ILD determines the impossibility to date its onset.

Limitations of our analysis

Limitations of our study are derived from its observational nature, including decentralised reading of HRCT images. Additionally, our population presented with long disease duration [21]. However, this possible bias was neutralised by the sensitivity analysis, showing comparable incidence rates in cases with disease duration <5 years. In addition, not all patients with ILD-negative baseline underwent a follow-up HRCT, which might determine a selection bias and overestimate the incidence rate of SSc-ILD, as only more severe cases could have been referred to additional HRCTs. To control for this selection bias, we performed a subanalysis focusing on patients followed up more tightly, which did not show a meaningfully higher incidence. However, HRCT represents the current gold standard for the detection of SSc-ILD and, therefore, has face validity supporting our decision. Despite a possible slight overestimation, the data still show that ILD has an impact on survival, making its application very relevant. Another potential limitation was using the exposure to immunosuppressant as a composite group, without specification of the compound, intermittent exposure, or total duration of treatment. This decision was based on the different availability of medications across centres, as well as on the large time span of the patients recorded in the EUSTAR registry, going over almost 20 years, which determines profound changes in availability and prescriptions. Additionally, data about exposure to immunosuppressants were present in less than half of the study population and not balanced within the groups, also determining a certain risk of bias. Although Hoa et al [25] showed the protective role of mycophenolate mofetil on SSc-ILD development, larger size, prospective studies, using dedicated matching methods to balance risk factors, are needed to evaluate the potential role of immunosuppressive drugs and other categories of medications on the primary prevention of SSc-ILD. It is also important to point out that our progression analysis was limited to definitions based on PFTs deterioration [28–30], and did not include the recent complex definition of progressive pulmonary fibrosis [29,41,42], due to the lack of detailed information on the worsening of clinical symptoms and radiological progression in the EUSTAR dataset. However, not all these multidomains definitions have been specifically validated for SSc-ILD [29].

In conclusion, our study showed that new-onset ILD can appear at any time after SSc diagnosis, with stable numerical incidence during the disease course, after a negative baseline HRCT. We have identified a clinical phenotype of patients with SSc at risk of developing new ILD, which would be a candidate for an intensified screening approach following a negative baseline HRCT, which could be feasible using noninvasive and validated screening tools [43], as well as a hypothetical target population for preventive medicine approaches. In fact, even though incident ILD might represent a milder phenotype of pulmonary involvement, at lower risk of functional progression in comparison to SSc-ILD detected at the first presentation, it still has a relevant impact on patient survival.

Competing interests

LP has received research grant from the Swiss National Research Foundation/Scholars at risk. ME has received for the last 3 years grant/research support from Pfizer, Novartis Foundation for Bio-Medical Research, Iten Kohaut foundation, Kurt und Senta Herrmann foundation, Foundation for research in Rheumatology (FOREUM), University Zurich, Walter and Gertrud Siegenthaler Foundation and Theodor und Ida Herzog-Egli – Stiftung. Congress Support from Astrazeneca and Janssen. RD has received for the last 3 years grant/research support from Iten Kohaut, Walter und Gertrud Siegenthaler Fellowship; congress/workshop participation support: Amgen, Otsuka. CM is consultant for Janssen Cilag AG and Boehringer Ingelheim, speakers bureau for Boehringer Ingelheim, Medbase, Mepha, MED Talks Switzerland, Novartis and PlayToKnow AG, and has received travel support for congress from Boehringer Ingelheim. SM has received congress participation support from AstraZeneca. EH is on speakers bureau of Johnson & Johnson, GlaxoSmithKline, Astra Zeneca; research funding from CSL Behring, GlaxoSmithKline, Johnson & Johnson, Pfizer; consultant of Bayer, Boehringer Ingelheim, GlaxoSmithKline, Astra Zeneca; Johnson & Johnson, Sanofi Genzyme, Novartis, Grant/research support from GlaxoSmithKline, Roche-Chugai, Sanofi Genzyme, Sobi, Novartis. PEC is on speakers bureau: (last 5 years) of Janssen Lilly VivaCell Emerald Health Pharmaceuticals Gesynta Pharma Boehringer Ingelheim Abbie Sanofi Genzyme Mitsubishi Tanabe Consultant of: (last 5 years): Janssen, Lilly, VivaCell, Emerald Health Pharmaceuticals, Gesynta Pharma, Boehringer Ingelheim, AbbVie, Sanofi, Genzyme, and Mitsubishi Tanabe. IC is on speakers bureau (last 5 years) of Janssen, Kern Pharma, BMS, Roche, Boehringer Ingelheim, Sanofi Genzyme, and Gebro; is a consultant of (last 5 years) Janssen, Boehringer Ingelheim, Kern, Novartis, Innovaderm, GSK. ABG received support from AbbVie, Novartis, Boehringer Ingilheim, Pfizer, Sanofi, Astra Zeneca, Genetec, and Elli Lily, in the last 5 years. PA is on speakers bureau of Bristol Myers Squibb, Bohringer Ingelheim; received grant/research support from Bristol Myers Squibb, Bohringer Ingelheim; Roche; Novartis; CSL Behring; Janssen- Cilag: CSL Vifor, Gruppo Italiano Lotta alla Sclerodermia (GILS), European Scleroderma Trials and Research Group (EUSTAR). YA: is a consultant of AbbVie, AstraZeneca, Bayer, Boehringer Ingelheim, Mylan, Janssen, Medsenic, and Prometheus; grant/research support from Alpine Immunosciences Medsenic and Corvus. GR is a consultant of Boehringer Ingelheim. Janssen; grants from Sanofi; speaker fees from AbbVie, Janssen, Boehringer Ingelheim, Galapagos, Roche, MSD, and Novartis; all outside the submitted study. KS is an Honorary Adjunct International Professor of Apollo Hospitals Educational and Research Foundation (AHERF). MCV received research grants from Boehringer Ingelheim, Ferrer, Galapagos and Janssen Pharmaceutical

Companies of Johnson & Johnson; received consulting fees from Boehringer Ingelheim and Janssen Pharmaceutical Companies of Johnson & Johnson; received speaker fees from Boehringer Ingelheim, Bristol Myers Squibb, GSK, Janssen Pharmaceutical Companies of Johnson & Johnson, MSD, Novartis, and Roche; served as a data safety monitoring board member at Corbus; and is treasurer of EUSTAR and steering committee member of the ERN ReCONNET. JdV-B is on speakers bureau of AbbVie, Janssen, Boehringer-Ingerlheim, consultant of: ABBvie, Janssen, Boehringer- Ingerlheim, grant/research support from: Janssen Cilag, Galapagos, and Roche. A-MH-V has received fees as speaker for Boehringer Ingelheim, Janssen, Medscape, Merck Sharp & Dohme, Novartis and Roche; consultant for AbbVie, ARXX, Boehringer Ingelheim, Bristol Myers Squibb, Genentech, Janssen, Medscape, Merck Sharp & Dohme, Pliant Therapeutics, Roche and Werfen; research grant from Boehringer Ingelheim, Janssen. EULAR study group leader on the lung in rheumatic and musculoskeletal diseases, CTD-ILD ERS/EULAR convenor. MM-C is on speakers bureau of Actelion, Janssen, Inventiva, Bayer, Biogen, Boehringer CSL, Behring, Corbus, Galapagos, Mitsubishi, Samsung, Regeneron, Acceleron, MSD, Chemomab, Lilly, Pfizer, and Roche; consultant of Actelion, Astra Zeneca, Janssen, Inventiva, Bayer, Biogen, Boehringer CSL, Behring, Corbus, Argenx, Galapagos, Mitsubishi, Samsung, Regeneron, Acceleron, MSD, Chemomab, Lilly, Pfizer, and Roche. OD has/had consultancy relationships with and/or has served as a speaker for the following companies in the area of potential treatments for systemic sclerosis and its complications in the last 3 calendar years: 4P-Pharma, AbbVie, Acceleron, Acepodia Biotech, Aera, Alcimed, Altavant, Amgen, AnaMar, Anaveon AG, Argenx, AstraZeneca, Blade, Bayer, Boehringer Ingelheim, Calluna (Arxx), Cantargia AB, Catalyze Capital, Corbus, CSL Behring, Galderma, Galapagos, Glenmark, Gossamer, Horizon, Janssen, Kymera, Lupin, Medscape, MSD Merck, Miltenyi Biotec, Mitsubishi Tanabe, Nkarta Inc., Novartis, Orion, Pilan, Prometheus, Quell, Redxpharma, Roivant, EMD Serono, Topadur and UCB. Patent issued "mir-29 for the treatment of systemic sclerosis" (US8247389, EP2331143). Cofounder of CITUS AG. Research grants: BI, Kymera, Mitsubishi Tanabe, UCB. CBruni received consulting fees for Boehringer Ingelheim. Research grants from Gruppo Italiano Lotta alla Sclerodermia (GILS), Scleroderma Clinical Trials Consortium (SCTC), EMDO Foundation, Novartis Foundation for medical-biological research. Congress participation support from Boehringer Ingelheim. All other authors have no conflicts of interest to disclose.

Acknowledgements

We acknowledge the contribution of all EUSTAR collaborators, see attached supplementary file.

Contributors

CBruni, LT, and OD made substantial contributions to conception and design of the study. LP, AV, RD, MOB, CM, SM, ME, SJ, EH, UM-L, ES, YA, GR, CBergmann, RB, KS, BA, IS, BS, JD, PEC, GC, EH, IC, AB-G, PA, IL, LAS, MCV, JdV-B, A-MH-V, MM-C, OD, and CBruni contributed substantially to data acquisition. All authors contributed substantially to data analysis and interpretation, drafted the article or revised it critically for important intellectual content, and approved the final manuscript for publication.

Patient consent for publication

Patients were not actively involved in this study; we thank all of them for their research contribution to the whole EUSTAR database.

Ethics approval

The EUSTAR registry protocol was reviewed and approved by the local committee of each centre. Written informed consent was obtained from all participants. The study was approved by the EUSTAR board (number CP 133) and conducted according to the Declaration of Helsinki.

Provenance and peer review

Not commissioned; externally peer reviewed.

Data availability statement

Anonymised data might be available from OD at the Department of Rheumatology, University Hospital Zurich, University of Zurich, Switzerland on reasonable request.

Supplementary materials

Supplementary material associated with this article can be found in the online version at doi:10.1016/j.ard.2025.12.008.

Orcid

Liubov Petelytska: http://orcid.org/0000-0001-8330-8681
Lorenzo Tofani: http://orcid.org/0000-0001-9965-7667
Rucsandra Dobrota: http://orcid.org/0000-0001-9819-7574
Carina Mihai: http://orcid.org/0000-0002-8627-8817
Sinziana Muraru: http://orcid.org/0009-0004-2896-153X
Christina Bergmann: http://orcid.org/0000-0001-5257-9171
Kamal Solanki: http://orcid.org/0000-0002-2953-9064
Iulia Szabo: http://orcid.org/0000-0001-8598-2848
Patricia E. Carreira: http://orcid.org/0000-0001-8279-3806
Lesley Ann Saketkoo: http://orcid.org/0000-0002-1878-8591
Madelon C Vonk: http://orcid.org/0000-0002-2266-9907
Jeska de Vries-Bouwstra: http://orcid.org/0000-0002-5624-1415
Cosimo Bruni: http://orcid.org/0000-0003-2813-2083

REFERENCES

[1] Tyndall AJ, Bannert B, Vonk M, Airò P, Cozzi F, Carreira PE, et al. Causes and risk factors for death in systemic sclerosis: a study from the EULAR Scleroderma Trials and Research (EUSTAR) database. Ann Rheum Dis 2010;69(10):1809–15.
[2] Pope JE, Quansah K, Hassan S, Seung SJ, Flavin J, Kolb M. Systemic sclerosis and associated interstitial lung disease in Ontario, Canada: an examination of prevalence and survival over 10 years. J Rheumatol 2021;48(9):1427–34.
[3] Li Q, Wallace L, Patnaik P, Alves M, Gahlemann M, Kohlbrenner V, et al. Disease frequency, patient characteristics, comorbidity outcomes and immunosuppressive therapy in systemic sclerosis and Systemic Sclerosis-Associated Interstitial Lung Disease: a US cohort study. Rheumatology (Oxford) 2021;60(4):1915–25.
[4] Kuwana M, Saito A, Sakamoto W, Raabe C, Saito K. Incidence rate and prevalence of systemic sclerosis and Systemic Sclerosis-Associated Interstitial Lung Disease in Japan: analysis using Japanese claims databases. Adv Ther 2022;39(5):2222–35.

[5] Morrisroe K, Stevens W, Sahhar J, Ngian GS, Ferdowsi N, Hansen D, et al. The clinical and economic burden of systemic sclerosis related interstitial lung disease. Rheumatology (Oxford) 2020;59(8):1878–88.
[6] Fairley JL, Hansen D, Proudman S, Sahhar J, Ngian GS, Walker J, et al. Clinical features of systemic sclerosis-mixed connective tissue disease and systemic sclerosis overlap syndromes. Arthritis Care Res (Hoboken) 2021;73(5):732–41.
[7] Vandecasteele E, Melsens K, Vanhaecke A, Blockmans D, Bonroy C, Carton C, et al. Incidence, prevalence and long-term progression of Goh algorithm rated interstitial lung disease in systemic sclerosis in two independent cohorts in flanders: a retrospective cohort study. Semin Arthritis Rheum 2021;51(5):969–76.
[8] Wangkaew S, Euathrongchit J, Wattanawittawas P, Kasitanon N, Louthrenoo W. Incidence and predictors of interstitial lung disease (ILD) in Thai patients with early systemic sclerosis: Inception cohort study. Mod Rheumatol 2016;26(4):588–93.
[9] Bergamasco A, Hartmann N, Wallace L, Verpillat P. Epidemiology of systemic sclerosis and Systemic Sclerosis-Associated Interstitial Lung Disease. Clin Epidemiol 2019;11:257–73.
[10] Hoffmann-Vold AM, Fretheim H, Halse AK, Seip M, Bitter H, Wallenius M, et al. Tracking impact of interstitial lung disease in systemic sclerosis in a complete nationwide cohort. Am J Respir Crit Care Med 2019;200(10):1258–66.
[11] Distler O, Highland KB, Gahlemann M, Azuma A, Fischer A, Mayes MD, et al. Nintedanib for systemic sclerosis-associated interstitial lung disease. N Engl J Med 2019;380(26):2518–28.
[12] Khanna D, Lin CJF, Furst DE, Goldin J, Kim G, Kuwana M, et al. Tocilizumab in systemic sclerosis: a randomised, double-blind, placebo-controlled, phase 3 trial. Lancet Respir Med 2020;8(10):963–74.
[13] Hoffmann-Vold AM, Maher TM, Philpot EE, Ashrafzadeh A, Barake R, Barsotti S, et al. The identification and management of interstitial lung disease in systemic sclerosis: evidence-based European consensus statements. Lancet Rheumatol 2020;2(2):e71–83.
[14] Antoniou K, Distler O, Gheorghiu A, Moor CC, Vikse H, Bizymi N, et al. ERS/EULAR clinical practice guidelines for connective tissue diseases associated interstitial lung disease. Ann Rheum Dis 2026;85(1):22–60.
[15] Johnson SR, Bernstein EJ, Bolster MB, Chung JH, Danoff SK, George MD, et al. 2023 American College of Rheumatology (ACR)/American College of Chest Physicians (CHEST) guideline for the screening and monitoring of interstitial lung disease in people with systemic autoimmune rheumatic diseases. Arthritis Rheumatol 2024;76(8):1201–13.
[16] Raghu G, Montesi SB, Silver RM, Hossain T, Macrea M, Herman D, et al. Treatment of systemic sclerosis-associated interstitial lung disease: evidence-based recommendations. An official American Thoracic Society clinical practice guideline. Am J Respir Crit Care Med 2024;209(2):137–52.
[17] Walker UA, Tyndall A, Czirják L, Denton C, Farge-Bancel D, Kowal-Bielecka O, et al. Clinical risk assessment of organ manifestations in systemic sclerosis: a report from the EULAR Scleroderma Trials And Research group database. Ann Rheum Dis 2007;66(6):754–63.
[18] Peoples C, Medsger Jr. TA, Lucas M, Rosario BL, Feghali-Bostwick CA. Gender differences in systemic sclerosis: relationship to clinical features, serologic status and outcomes. J Scleroderma Relat Disord 2016;1(2):177–240.
[19] Hussein H, Lee P, Chau C, Johnson SR. The effect of male sex on survival in systemic sclerosis. J Rheumatol 2014;41(11):2193–200.
[20] Al-Sheikh H, Ahmad Z, Johnson SR. Ethnic variations in systemic sclerosis disease manifestations, internal organ involvement, and mortality. J Rheumatol 2019;46(9):1103–8.
[21] Nihtyanova SI, Schreiber BE, Ong VH, Rosenberg D, Moinzadeh P, Coghlan JG, et al. Prediction of pulmonary complications and long-term survival in systemic sclerosis. Arthritis Rheumatol 2014;66(6):1625–35.
[22] Kapralik J MR, Farooqi M, Beattie K, Hambly N, Larche M. Predictors of ILD development and timing of onset in systemic sclerosis: a Canadian cohort. Arthritis Rheumatol 2021;73(Suppl 9).
[23] Wangkaew S, Thongwitokomarn H, Prasertwittayakij N, Euathrongchit J. Rapid skin thickness progression rate is associated with high incidence rate of cardiopulmonary complications in patients with early diffuse cutaneous systemic sclerosis: inception cohort study. Clin Exp Rheumatol 2020;38(Suppl 125(3)):98–105.
[24] Hurtubise R, Hudson M, Gyger G, Wang M, Steele RJ, Baron M, et al. Association between gastroprotective agents and risk of incident interstitial lung disease in systemic sclerosis. Respir Med 2021;185:106482.
[25] Hoa S, Bernatsky S, Baron M, Proudman S, Stevens W, Sahhar J, et al. Association between immunosuppressive therapy and incident risk of interstitial lung disease in systemic sclerosis. Chest 2021;160(6):2158–62.
[26] Bruni C, Chung L, Hoffmann-Vold AM, Assassi S, Gabrielli A, Khanna D, et al. High-resolution computed tomography of the chest for the screening, re-screening and follow-up of systemic sclerosis-associated interstitial lung disease: a EUSTAR-SCTC survey. Clin Exp Rheumatol 2022;40(10):1951–5.
[27] van den Hoogen F, Khanna D, Fransen J, Johnson SR, Baron M, Tyndall A, et al. 2013 classification criteria for systemic sclerosis: an American College of Rheumatology/European League against Rheumatism collaborative initiative. Arthritis Rheum 2013;65(11):2737–47.
[28] Hoffmann-Vold AM, Allanore Y, Alves M, Brunborg C, Airó P, Ananieva LP, et al. Progressive interstitial lung disease in patients with systemic sclerosis-associated interstitial lung disease in the EUSTAR database. Ann Rheum Dis 2021;80(2):219–27.
[29] Raghu G, Remy-Jardin M, Richeldi L, Thomson CC, Inoue Y, Johkoh T, et al. Idiopathic pulmonary fibrosis (an update) and progressive pulmonary fibrosis in adults: an official ATS/ERS/JRS/ALAT clinical practice guideline. Am J Respir Crit Care Med 2022;205(9):e18–47.
[30] Goh NS, Hoyles RK, Denton CP, Hansell DM, Renzoni EA, Maher TM, et al. Short-term pulmonary function trends are predictive of mortality in interstitial lung disease associated with systemic sclerosis. Arthritis Rheumatol 2017;69(8):1670–8.
[31] Distler O, Assassi S, Cottin V, Cutolo M, Danoff SK, Denton CP, et al. Predictors of progression in systemic sclerosis patients with interstitial lung disease. Eur Respir J 2020;55(5):1902026.
[32] Elhai M, Meune C, Boubaya M, Avouac J, Hachulla E, Balbir-Gurman A, et al. Mapping and predicting mortality from systemic sclerosis. Ann Rheum Dis 2017;76(11):1897–905.
[33] Tang F, Ishwaran H. Random forest missing data algorithms. Stat Anal Data Min 2017;10(6):363–77.
[34] Fan Y, Bender S, Shi W, Zoz D. Incidence and prevalence of systemic sclerosis and systemic sclerosis with interstitial lung disease in the United States. J Manag Care Spec Pharm 2020;26(12):1539–47.
[35] Lepri G, Bruni C, Tofani L, Moggi-Pignone A, Orlandi M, Tomassetti S, et al. The performance of pulmonary function tests in predicting systemic sclerosis-interstitial lung disease in the European Scleroderma Trial and Research Database. Diagnostics (Basel) 2024;14(3):295.
[36] Stock CJW, Bray WG, Kouranos V, Jacob J, Kokosi M, George PM, et al. Serum C-reactive protein is associated with earlier mortality across different interstitial lung diseases. Respirology 2024;29(3):228–34.
[37] Nihtyanova SI, Sari A, Harvey JC, Leslie A, Derrett-Smith EC, Fonseca C, et al. Using autoantibodies and cutaneous subset to develop outcome-based disease classification in systemic sclerosis. Arthritis Rheumatol 2020;72(3):465–76.
[38] Volkmann ER, Tashkin DP, Sim M, Li N, Goldmuntz E, Keyes-Elstein L, et al. Short-term progression of interstitial lung disease in systemic sclerosis predicts long-term survival in two independent clinical trial cohorts. Ann Rheum Dis 2019;78(1):122–30.
[39] Moore OA, Goh N, Corte T, Rouse H, Hennessy O, Thakkar V, et al. Extent of disease on high-resolution computed tomography lung is a predictor of decline and mortality in systemic sclerosis-related interstitial lung disease. Rheumatology (Oxford) 2013;52(1):155–60.
[40] Landini N, Orlandi M, Bruni C, Carlesi E, Nardi C, Calistri L, et al. Computed tomography predictors of mortality or disease progression in systemic sclerosis-interstitial lung disease: a systematic review. Front Med (Lausanne) 2022;8:807982.
[41] Flaherty KR, Wells AU, Cottin V, Devaraj A, Walsh SLF, Inoue Y, et al. Nintedanib in progressive fibrosing interstitial lung diseases. N Engl J Med 2019;381(18):1718–27.
[42] Petelytska L, Bonomi F, Cannistra C, Fiorentini E, Peretti S, Torracchi S, et al. Heterogeneity of determining disease severity, clinical course and outcomes in systemic sclerosis-associated interstitial lung disease: a systematic literature review. RMD Open 2023;9(4):e003426.
[43] Bruni C, Tofani L, Fretheim H, Liem SIE, Velauthapillai A, Bjørkekjær H, et al. A screening tool to detect interstitial lung disease in systemic sclerosis: the ILD-RISC score. Rheumatology (Oxford) 2025;64(12):6285–93.

Ann Rheum Dis 85 (2026) 680–692

Contents lists available at ScienceDirect

Annals of the Rheumatic Diseases

journal homepage: https://www.sciencedirect.com/journal/annals-of-the-rheumatic-diseases

Systemic sclerosis

Identification of novel fibroblast subsets in diffuse cutaneous systemic sclerosis

Ann-Helen S Rosendahl[1,*], Anna Bornikoel[1], Isabel Zeinert[1], Lena Keufgens[2], Frederik Tellkamp[2], Niklas Kleinenkuhnen[3], Till Baar[3], Katrin Schönborn[1], Marcus Krüger[2,4], Achim Tresch[2,3], Bent Brachvogel[5], Beate Eckes[1], Pia Moinzadeh[6], Thomas Krieg[1,2,4,6]

[1] *Translational Matrix Biology, Faculty of Medicine, University of Cologne, Cologne, Germany*
[2] *Cologne Excellence Cluster on Cellular Stress Responses in Ageing-Associated Diseases (CECAD), University of Cologne, Cologne, Germany*
[3] *Institute of Medical Statistics and Computational Biology, Faculty of Medicine, University of Cologne, Cologne, Germany*
[4] *Center for Molecular Medicine (CMMC), University of Cologne, Cologne, Germany*
[5] *University Hospital for Pediatrics and Adolescent Medicine, Experimental Neonatology, Faculty of Medicine, University of Cologne, Cologne, Germany*
[6] *Department of Dermatology, University of Cologne, Cologne, Germany*

ARTICLE INFO

Article history:
Received 31 July 2025
Received in revised form 17 November 2025
Accepted 28 November 2025

ABSTRACT

Objectives: Systemic sclerosis (SSc) is an autoimmune-driven fibrotic disease, characterised by excessive extracellular matrix (ECM) deposition and fibroblast activation. Our study aimed to identify novel fibroblast subpopulations in SSc and determine their functional role.

Methods: We performed single-cell RNA sequencing on cultured dermal fibroblasts from healthy donors and patients with diffuse cutaneous SSc, verified selected, specific genes at the protein level and used siRNA knockdown experiments to provide evidence for a functional role of these proteins.

Results: SSc fibroblasts revealed high heterogeneity and in specific activated subsets strong upregulation of CD9 and four and a half LIM domain 1 (FHL1), previously described as a muscle-related protein. Overexpression of FHL1 and CD9 was also detected in fibroblast subsets in patient skin. CD9 was associated with the regulation of *FHL1* expression. Downmodulation of *FHL1* in primary skin fibroblasts correlated with downregulation of the vestigial-like family member 3 (*VGLL3*) gene, which is known to be expressed in myofibroblasts in a stiff and fibrotic environment and to upregulate collagen synthesis. Further, VGLL3 was confirmed to be upregulated in SSc donor skin.

Conclusions: Our study identified novel fibroblast subsets in SSc, characterised by CD9 and/or FHL1 upregulation. The data indicate a functional role of FHL1 in fibroblasts and its involvement in the regulation of ECM production and provide a new mechanistic link to VGLL3 regulation. Our findings suggest new avenues for therapeutic exploration targeting the perpetuating fibroblast activation by the fibrotic environment.

*Correspondence to Dr. Ann-Helen S Rosendahl, PhD.
E-mail address: ann-helen.rosendahl@hus.fi (A.-H.S. Rosendahl).
Handling editor Josef S. Smolen.

https://doi.org/10.1016/j.ard.2025.11.027

WHAT IS ALREADY KNOWN ON THIS TOPIC

- Systemic sclerosis (scleroderma) is a chronic fibrosing disease that has a major impact on the quality of life of the patients.
- Vascular damage and an inflammatory reaction lead to the activation of fibroblasts and the excessive deposition of connective tissue.
- Fibroblasts are now known to have many different functions; they produce extracellular matrix material, but also play a key role in the regulation of inflammation.
- Several populations of fibroblasts have already been described in normal and fibrotic skin. These are thought to differ in their function.

WHAT THIS STUDY ADDS

- In this study, we describe novel populations of fibroblast subsets in scleroderma skin, and we characterise their gene and protein expression profiles and demonstrate that these populations are also detected in the involved skin of the patients and in fibrotic murine skin.
- The data support a functional role of these proteins in the ongoing fibrosing reaction.

HOW THIS STUDY MIGHT AFFECT RESEARCH, PRACTICE OR POLICY

- We provide data for the characterisation of unique, activated fibroblast populations.
- These populations can be identified in the skin of the patients providing new biomarkers for activated fibroblasts.
- In addition, these described genes/proteins represent potential targets for new therapeutic approaches to limit fibrosing processes. Systemic sclerosis might represent a model for fibrotic diseases in general.

INTRODUCTION

Scleroderma or systemic sclerosis (SSc) is a chronic autoimmune-driven fibrotic disease affecting the skin and many internal organs; it can occur in a diffuse cutaneous SSc (dcSSc) and a limited cutaneous SSc (lcSSc) subset [1,2]. Although the early pathophysiology involves initial vascular damage and a subsequent inflammatory reaction, the final activation of fibroblasts leads to the characteristic excessive deposition of extracellular matrix (ECM) and tissue damage.

Fibroblasts are a heterogeneous cell type, and several subsets in normal and fibrotic skin can be differentiated [3–5]. They play a fundamental role in the structural support of tissues by producing ECM proteins, but also secrete cytokines and growth factors that act in autocrine and paracrine fashions. They are crucial for ensuring tissue homeostasis, modulate inflammatory responses and are key players in all tissue repair processes [6,7].

Single-cell transcriptomic analyses (single-cell RNA sequencing [scRNA-seq]) revealed details about heterogeneity of fibroblasts in sclerodermatous skin [8–10]. However, many of these studies are descriptive and it remains unclear whether these cells have a causal relationship to the ongoing pathogenetic events. It should also be emphasised that the heterogeneity of cells characterised by transcriptome analysis at a given time point does not necessarily define stable subsets of fibroblasts but may just reflect a particular dynamic cellular state. In addition, many of these recently published investigations were derived from cells released by enzymatic dissociation of rigid fibrotic tissue, a procedure that could lead to damage and loss of certain sensitive or fragile cell populations and therefore result in subsequent bias.

To overcome some of these restrictions, we concentrated on an alternative approach and used bulk fibroblast cultures obtained from skin biopsies of patients with SSc as described previously [11–13]. Using scRNA-seq analysis, this strategy allowed us to identify fibroblast subsets with a stable phenotype after several cell divisions. We then validated the gene expression by determining protein levels in fibroblast cultures and directly in patient tissue. We here describe new unique subsets, characterised by induced expression of CD9 and the four and a half LIM domain protein (FHL) 1, respectively [14,15]. We also identify these subsets in patient skin and in a bleomycin-induced fibrosis model in mice and propose a functional role of these proteins. Finally, we show that induced expression of CD9 and FHL1 is associated with the induction of vestigial-like family member 3 (VGLL3), a transcriptional cofactor known to induce ECM production [16].

METHODS

Study design

Scleroderma is a rare, still incurable disease. Our study was conducted to find possible new biomarkers that could aid in early diagnosis and open new treatment avenues. Examining the transcriptome of patient-derived cultured fibroblasts compared to healthy controls by scRNA-seq, we identified markers overexpressed in specific fibroblast subsets, including *CD9* and *FHL1*. We confirmed our results by western blot (WB) or Fluorescence-Activated Cell Sorting as well as immunofluorescent (IF) staining using fibroblasts from the same patients/controls and skin sections from patients with SSc and controls. For functional analysis, we performed knockdown experiments using siRNAs for *CD9* and *FHL1* in human fibroblasts, examining both the transcriptome and secretome. In addition, we employed an experimentally induced fibrosis model in mice to correlate CD9 and FHL1 expression with fibrotic conditions. The number of independent experiments (biological replicates, n) is indicated in each figure legend; no outliers were removed for statistical analysis.

Study population

Patient and control samples used in this study were age- and sex-matched (female or male) (Supplementary Table S1). All patients included in the scRNA-seq analysis were diagnosed with dcSSc.

Detailed descriptions of all materials and methods are provided in the Supplementary Materials [17–23].

Initiation of primary dermal fibroblast cultures

4 mm skin biopsies were obtained from study patients after informed consent. Primary dermal fibroblasts were obtained by outgrowth from the skin explants and cultured in Dulbecco's Modified Eagle Medium (Gibco Invitrogen, 41965-039) with 100 U/mL penicillin, 100 μg/mL streptomycin (Sigma, P0781), 2 mM L-glutamine (Biozym, 882027) 50 μg/mL Na-ascorbate (Sigma-Aldrich, A4034), and 10% fetal calf serum (Gibco, 10270-106) in 5% CO_2 at 37°C, harvested and analysed in passage 2-5.

Study approval

Skin biopsies were obtained from female and male healthy individuals or patients with scleroderma (SSc) after written consent and with approval of the local ethics committee (Ethics committee of the medical faculty of University of Cologne, 21-1072). The study was conducted in accordance with the criteria set by the Declaration of Helsinki.

Data and materials availability

All data generated during this study are included in this published article (and its supplementary information files). The RNA sequencing data were deposited in National Center for Biotechnology Information/Gene Expression Omnibus under the following accession numbers: scRNAseq—GSE294431, siRNA HPF Bulk—GSE294430 and CD9 MEF Bulk—GSE294429. The proteomics data have been deposited in PRoteomics IDEntifications Database (PRIDE) with the following accession numbers: Secretome—PXD062591 and proteome—PXD062597. Additional detailed information is available from the corresponding authors on request.

RESULTS

Fibroblasts were grown from dermal tissue explants, obtained from 4 patients with early diffuse cutaneous SSc [24] and 4 age-matched healthy controls (Supplementary Table S1). After 4 passages, we investigated these confluent fibroblast cultures by scRNA-seq analysis.

SSc dermal fibroblasts show altered transcriptional signatures and increased heterogeneity

We performed scRNA-seq on 37,343 cultured dermal fibroblasts from biopsies of 4 healthy donors (19,083 cells) and 4 patients with SSc (18,260 cells) (Supplementary Table S2). Unsupervised uniform manifold approximation and projection clustering (Louvain algorithm, resolution 0.28, see also Supplementary Table S3) identified 10 distinct fibroblast clusters (Fig 1A), with a clear separation between SSc and control fibroblasts (Fig 1B). Control fibroblasts primarily grouped into 2 major clusters (Fig 1B,C, Supplementary Fig S1), whereas the transcriptional signature of SSc fibroblasts displayed greater diversity (Fig 1B,C) including clusters 3 (IGFBP4^{hi}), 5 (POSTN^{hi}), 6 (MMP3^{hi}), 7 (SFRP1^{hi}), and 10 (FHL1^{hi}). Cluster 3, the largest of the SSc-specific clusters (28%), expressed genes involved in inflammation, fibroblast functions, and fibrosis (Fig 1B,C, Supplementary Table S4). Over 17% of the SSc-associated fibroblasts were found in cluster 5, with upregulated genes associated with fibrotic activity (Fig 1B,C, Supplementary Table S4). Cluster 6 (~14% of SSc fibroblasts) showed enrichment for genes involved in Bone Morphogenetic Protein signalling (BMP) signalling (Fig 1B,C, Supplementary Fig S2A, Supplementary Table S4). Genes in cluster 7 (12% of SSc fibroblasts) showed enrichment for response to oestrogen, and negative regulation of kinase and transferase activity (Fig 1B,C, Supplementary Fig S2B, Supplementary Table S4). Cluster 10 (FHL1^{hi}) was a small SSc-specific cluster (0.87%) with genes involved in muscle organ development, muscle cell differentiation, ECM, and extracellular structure organisation (Fig 1B,C, Fig 2B,C, Supplementary Fig S2C, Supplementary Table S4) indicating a special role of these fibroblasts for ECM deposition and remodelling.

Next, we asked if we could identify published marker genes of fibroblast clusters in our dataset. Papillary fibroblasts have been shown to be DPP4^{+}/ATXN1^{-}, while reticular fibroblasts mostly express PDPN and ATXN1 [3,4]. Our scRNA-seq data did

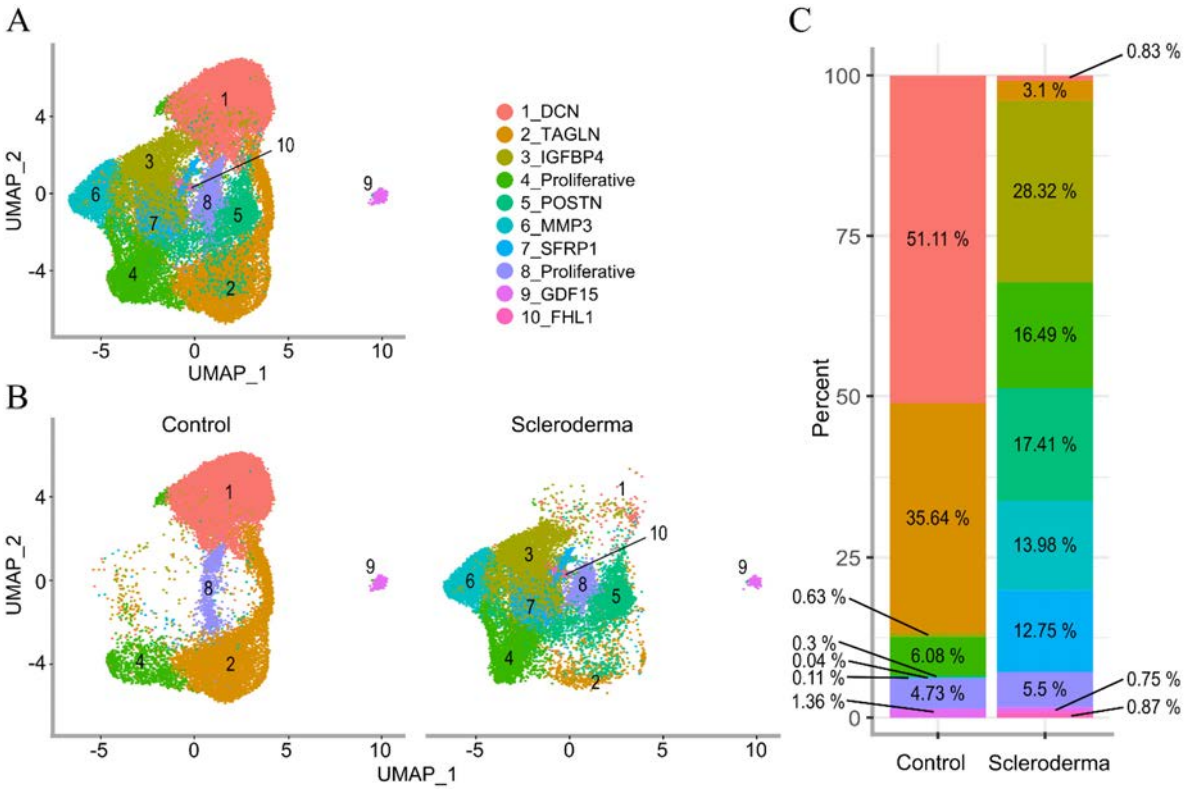

Figure 1. ScRNA-seq analysis of human dermal fibroblasts from 4 healthy control donors and 4 individuals with dcSSc. (A) UMAP representation of dermal fibroblasts processed from all 4 healthy controls and 4 samples obtained from patients with dcSSc, identified by marker genes. (B) Separated UMAP representation of all dermal fibroblasts processed from 4 healthy controls (left) and from 4 dcSSc fibroblast samples (right). dcSSc-specific clusters were clusters 3, 5, 6, 7, and 10. (C) Percentage of each cluster of control fibroblasts (left) and SSc fibroblasts (right). Colours of clusters in the UMAP (A, B) and the bar plot (C) correlate to the colours of the clusters 1–10, identified by marker genes. dcSSc, diffuse cutaneous systemic sclerosis; UMAP, Uniform Manifold Approximation and Projection; *DCN*, Decorin; *TAGLN*, Transgelin; *IGFBP4*, Insulin Like Growth Factor Binding Protein 4; *POSTN*, Periostin; *MMP3*, Matrix Metallopeptidase 3; *SFRP1*, Secreted Frizzled Related Protein 1; *GDF15*, Growth Differentiation Factor 15; *FHL1*, four and a half LIM domain 1; scRNA-seq, single-cell RNA sequencing; SSc, systemic sclerosis.

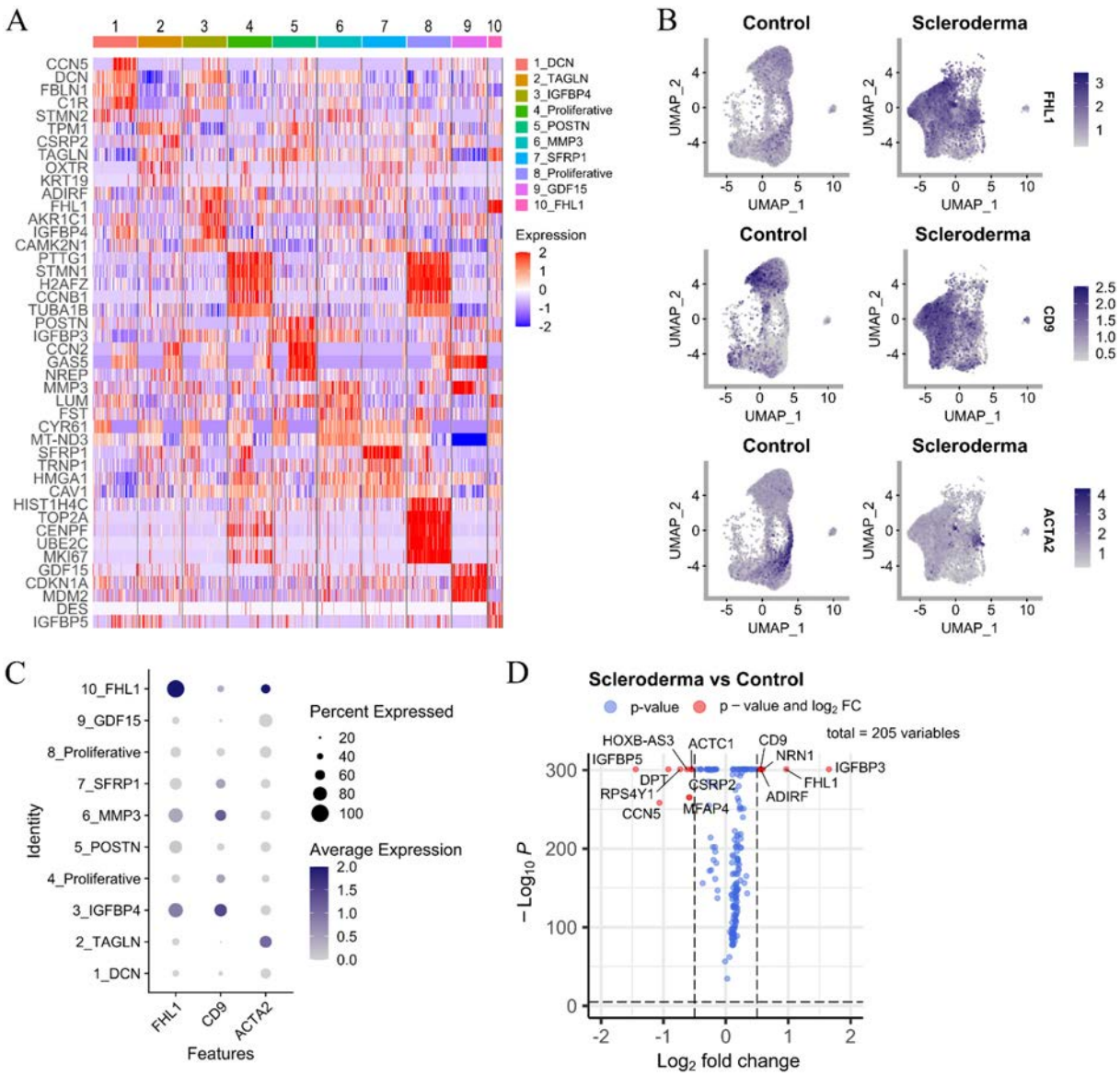

Figure 2. ScRNA-seq analysis of DEGs in fibroblasts obtained from patients with dcSSc compared to controls. (A) Heat map of scaled gene expression data for the top 5 DEGs for each cluster. (B) Feature plots of selected genes: *FHL1*, *CD9*, and *ACTA2*. Each dot represents a cell; the colour intensity of the dots correlates with increased expression. (C) Dot plot of selected genes: *FHL1*, *CD9*, and *ACTA2*. The size of the dot indicates the percentage of cells per cluster expressing the gene. The intensity of the colour shade of each dot correlates with the scaled average expression intensity in these cells. (D) Volcano plot of the most upregulated and downregulated genes in the SSc dermal fibroblasts when compared to control fibroblasts. Red dots indicate the significant genes that have an adjusted *P* value <.05 and that have a log2FC greater than .5. Significant genes are all labelled in the figure. DEGs, differentially expressed gene(s); dcSSc, diffuse cutaneous systemic sclerosis; *FHL1*, four and a half LIM domain 1; *ACTA2*, Actin Alpha 2; scRNA-seq, single-cell RNA sequencing; UMAP, Uniform Manifold Approximation and Projection.

not identify a clear pattern of these typical papillary or reticular markers (Supplementary Fig S3A,B). *DPP4* and *ATXN1* were expressed to some extent in all clusters, while *PDPN* was mostly expressed in control cluster 1 (DCN^{hi}) and SSc cluster 3 (IGFBP4^{hi}) (Supplementary Fig S3A,B). The same was found for other papillary fibroblast marker genes, such as *APCDD1*, *HSPB3*, and *WIF1*, as well as reticular fibroblast marker gene *CD36* [5]. We saw higher expression levels of *APCDD1* and *HSPB3* in cluster 3 (IGFBP4^{hi}), but again, no clear separation between reticular and papillary fibroblasts was detected (Supplementary Fig S3B).

However, in cluster 1, we identified expression of *SFRP2* (Supplementary Fig S3B), which together with *DPP4* marks a major fibroblast population in human skin [8] (Supplementary Fig S3A,B). In several of our clusters, we identified genes that were reported to correlate with the severity of SSc, such as *COMP* and *THBS1*, *CTGF*, *TNC*, *THY1*, *CDH11*, and *CCL2* [9] (Supplementary Fig S3C). These genes were found to some extent in all our fibroblast cultures but no clear differences were seen between SSc and controls.

Specific SSc fibroblast clusters reveal increased expression of FHL1 *and* CD9

The most striking observation was significantly increased *FHL1* expression in SSc fibroblasts, particularly in cluster 3 (IGFBP4^{hi}) and 10 (FHL1^{hi}), and to a lesser extent in cluster 6 (MMP3^{hi}) (Fig 2A-D). *FHL1* expression is highly abundant in muscle tissue [25], but has been found at low levels in multiple other tissues, such as heart, lung, and testis, but also in fibroblasts [14,26]. Its function in fibroblasts, however, has remained unknown. In cluster 10 (FHL1^{hi}), 100% and in clusters 3 (IGFBP4^{hi}) and 6 (MMP3^{hi}),

about 80% of the fibroblasts expressed *FHL1* at a high level (Fig 2C). These clusters were highly specific to SSc.

A second key observation was that we found an overall significant upregulation of *CD9* in our SSc-derived fibroblasts (Fig 2B-D). In our data, ~70% of the cells in cluster 3 (IGFBP4^{hi}) and ~60% of the fibroblasts in cluster 6 (MMP3^{hi}) expressed *CD9* at a high level (Fig 2C).

In cluster 10 (FHL1^{hi}), we further saw increased expression of profibrotic and ECM-related genes, such as *TAGLN*, *LUM*, *IGFBP5*, and *MFAP5*, but also muscle-related genes, such as *SYNPO2* and *MYL9* (Fig 2A, Supplementary Table S4). In addition, ~60% of the fibroblasts in the small profibrotic cluster 10 expressed smooth muscle α-2 actin (*ACTA2*; α-SMA). Even though *ACTA2* expression intensity was high in these cells, the fibroblasts did not cluster together with the other *ACTA2*$^{+}$ (myo)fibroblasts in clusters 2 and 5 (Fig 2B,C).

Cluster 3 (IGFBP4^{hi}) and 6 (MMP3^{hi}) expressed *FHL1* and *CD9* but lacked *ACTA2* expression (Fig 2B,C). *CD9* expression was also seen at a moderately high level in ~50% of the fibroblasts in clusters 7 (SFRP1^{hi}) and 4 (proliferative) with a discernible *FHL1* or *ACTA2* expression (Fig 2B,C).

High expression of *CD9* and *FHL1* genes in SSc was characteristic of SSc and prompted us to (i) validate these data at the protein level, (ii) search for expression of CD9 and FHL1 *in vivo* in patient skin, and (iii) demonstrate the functional relevance of these proteins.

Validation of increased FHL1 and CD9 protein in fibroblast cultures and patients with SSc

Next, we analysed several fibroblast cultures from controls and patients with SSc (6 independent biological replicates) by WB. These data clearly demonstrate that FHL1 protein amount was significantly increased in SSc fibroblasts *in vitro* (Fig 3A,B). The relative FHL1 protein amount in SSc fibroblasts was more than 4 times higher than in controls (Fig 3B). We also investigated fibroblasts from lcSSc samples, in which the clinical fibrosis was considerably less prominent. These samples only showed a slight increase in FHL1 (Fig 3B). IF staining confirmed FHL1 expression in many more SSc-derived fibroblasts in monolayer culture compared to controls (Fig 3C,D). Some cells in the SSc cultures showed markedly higher expression

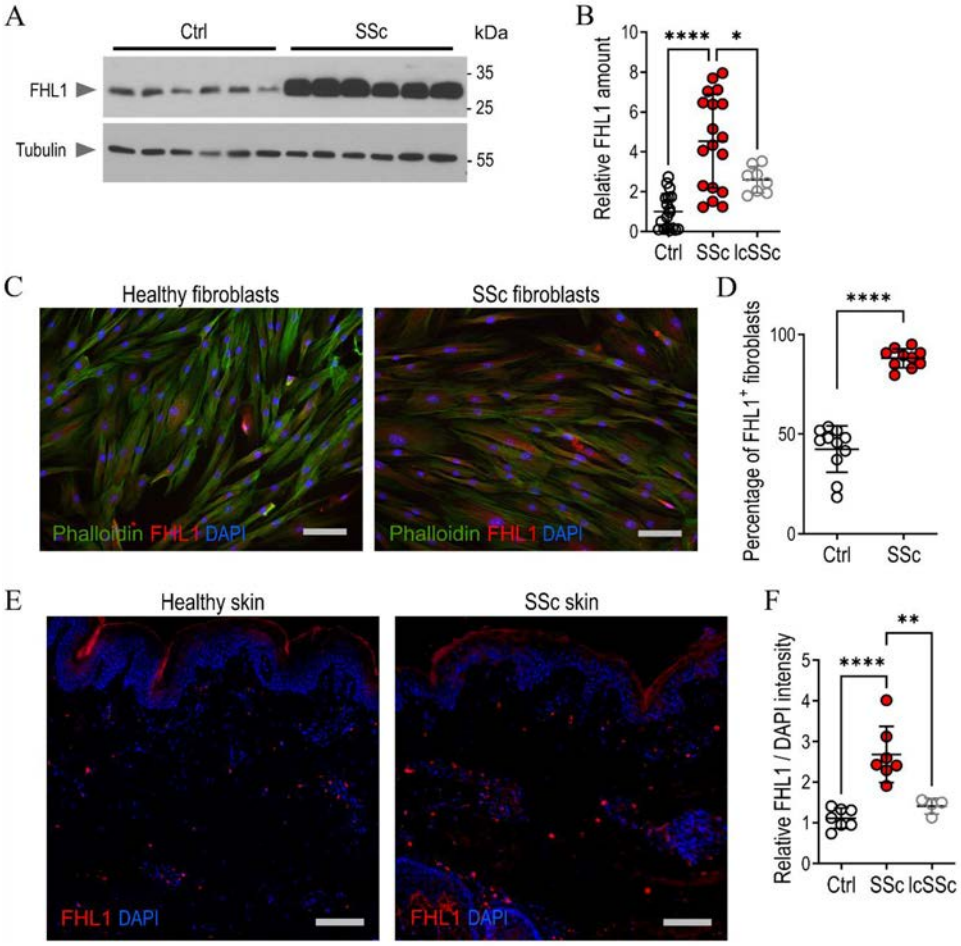

Figure 3. FHL1 protein amount is increased in specific subsets of SSc fibroblasts. (A) Representative western blot staining of FHL1 and β-tubulin in fibroblasts obtained from controls and patients with dcSSc. (B) Corresponding quantification from primary human dermal fibroblasts derived from healthy control skin, dcSSc skin and lcSSc skin (N = 18/18/8 independent samples or 6 Ctrl/6 SSc/4 patients with lcSSc, *P* values calculated with one-way ANOVA). (C) Representative IF staining of DAPI (blue), phalloidin (green) and FHL1 (red) in human healthy (left) and dcSSc fibroblasts (right) and (D) quantification of FHL1 positive fibroblasts (N = 11/12 measured images or 2 Ctrl/2 SSc patients; *P* values calculated with Welch's t-test, two-tailed). (E) IF staining of DAPI (blue) and FHL1 (red) in human healthy skin (left) and dcSSc skin (right). (F) Quantification of IF staining intensity of FHL1 normalised to cell number (DAPI) in human healthy, dcSSc, and lcSSc dermis. Data shown as relative values compared to control (N = 7 Ctrl/7 dcSSc /4 lcSSc donors, *P* values calculated with one-way ANOVA). **** $P \leq .0001$, ** $P = .0013$, * $P = .0166$; data shown as mean ± SD. Scale bar = 100 µm. ANOVA, analysis of variance; Ctrl, control; FHL1, four and a half LIM domain 1; IF, immunofluorescent; DAPI, 4',6-diamidino-2-phenylindole; dcSSc, diffuse cutaneous systemic sclerosis; lcSSc, limited cutaneous systemic sclerosis; SSc, systemic sclerosis.

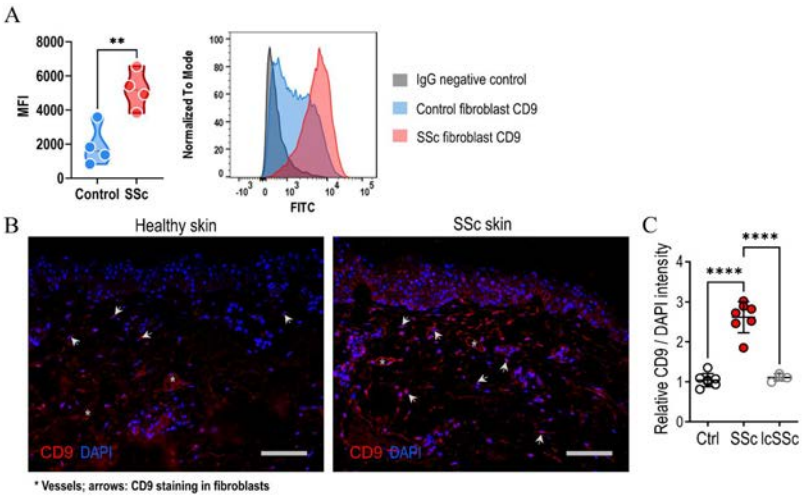

Figure 4. CD9 protein amount is increased in fibroblasts obtained from patients with dcSSc. (A) FACS analysis of CD9 staining in fibroblasts obtained from patients with dcSSc compared to control shown as violin plots. MFI = mean fluorescence intensity, N = 4 Ctrl/4 SSc donors; ** P = .0074, quantified with unpaired t-test, two-tailed. (B) IF staining of DAPI (blue) and CD9 (red) in human healthy (left) and dcSSc skin (right). (C) Quantification of CD9 staining intensity normalised to DAPI in human healthy, dcSSc, and lcSSc dermis. Data shown as relative values compared to control. N = 7 Ctrl/ 7 SSc/4 lcSSc donors; **** $P \leq .0001$, P values calculated with one-way ANOVA; data shown as mean ± SD. Scale bar = 100 μm. ANOVA, analysis of variance; Ctrl, control; FACS, Fluorescence-Activated Cell Sorting; dcSSc, diffuse cutaneous systemic sclerosis; IF, immunofluorescent; lcSSc, limited cutaneous systemic sclerosis; DAPI, 4',6-diamidino-2-phenylindole; FITC , Fluorescein Isothiocyanate; IgG, Immunoglobulin G.

than others. Notably, IF staining of skin biopsies obtained from patients with dcSSc also revealed significantly increased FHL1 expression, observed in many—but not all—fibroblasts (Fig 3E, F). The relative levels of FHL1 protein in the dermis of SSc skin, normalised to cell number, were up to 2.5 times higher than in healthy donor skin (Fig 3F). In contrast, in our lcSSc samples, we could only detect a slight increase in the intensity of FHL1 staining (Fig 3F).

In addition, we determined CD9 protein levels in dermal SSc fibroblasts. Flow cytometry of primary fibroblasts revealed a significant increase in CD9^{hi} fibroblasts in SSc vs control cultures (Fig 4A). Strikingly, significantly increased CD9 protein was also found *in vivo* in the dermis of skin biopsies obtained from patients with dcSSc (Fig 4B,C). The relative CD9 protein levels in SSc skin, quantified in the dermis only, were about 2.5 times higher than in healthy donor skin (Fig 4C). In contrast, we could not detect clear differences in the CD9 staining between control and lcSSc samples (Fig 4C). Of note, there was also increased CD9 staining of keratinocytes in the SSc biopsies (Fig 4B). To demonstrate the association of CD9 and FHL1 expressing fibroblast subsets with the development of fibrosis, we employed an independent system, the bleomycin-induced fibrosis in mice, which demonstrated that CD9- and FHL1-expressing fibroblasts are induced with the development of a fibrotic reaction upon injection of bleomycin into the dermis (Fig 5).

Loss of FHL1 *and* CD9 *from fibroblasts negatively impacts ECM deposition*

The striking upregulation of FHL1 and CD9 at both the transcript and protein levels in SSc fibroblast cultures obtained from patients with dcSSc and skin biopsies prompted us to investigate potential functional consequences. We therefore treated primary dermal fibroblasts from healthy donors with siRNAs targeting *FHL1* using siRNA against *Renilla reniformis* luciferase (*RLuc*) as a control. *FHL1* siRNA treatment resulted in a significant downregulation of *FHL1* expression (log2FC of −4.86; Supplementary Fig S4A,B) and fibroblasts also revealed a significant downregulation of genes associated with ECM or in fibrosis such as transforming growth factor beta-induced protein (*TGFBI*) (an ECM component involved in ECM organisation and pulmonary fibrosis [27]), Reticulocalbin 3 (*RCN3*) (involved in pulmonary fibrosis and activating fibroblasts [28]), collagen V α1 chain (*COL5A1*) (an ECM component required for correct assembly of fibril-forming collagens [29]), *VGLL3*, nidogen 2 (*NID2*) and prolyl 4-

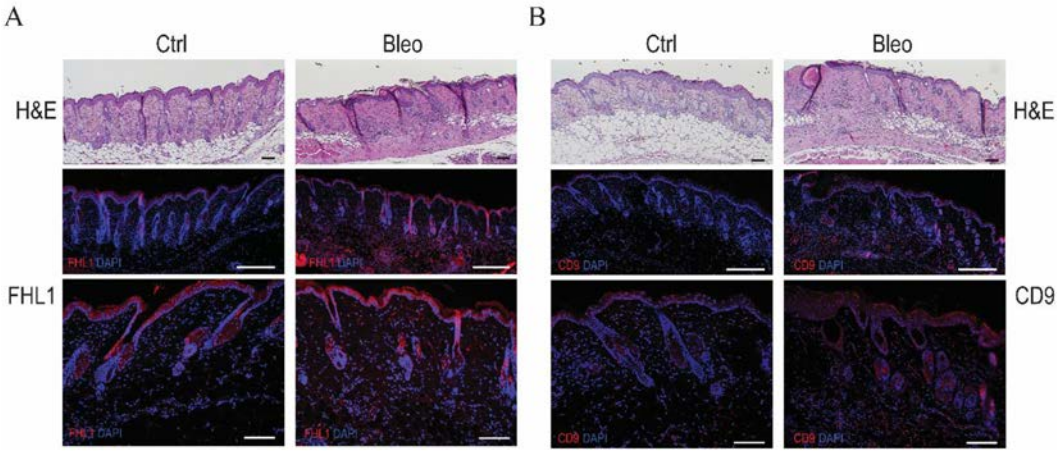

Figure 5. Increased amounts of FHL1 and CD9 protein in fibrotic skin of mice. Skin fibrosis was induced by intradermal bleomycin injections in mice. Sections were evaluated by histology (haematoxylin and eosin [H&E]) and IF staining of control (Ctrl) and fibrotic (Bleo) skin lesions. (A) H&E and IF staining of FHL1 (red); (B) H&E and IF staining of CD9 (red) of control (left) and fibrotic (right) skin. Nuclei are marked by DAPI (blue). Upper IF panels show overviews and bottom panels show higher magnification. Scale bars: 100 μm in H&E, 300 μm in IF overviews (top panels), and 100 μm in higher magnification images (bottom panels). FHL1, four and a half LIM domain 1; IF, immunofluorescent; DAPI, 4',6-diamidino-2-phenylindole.

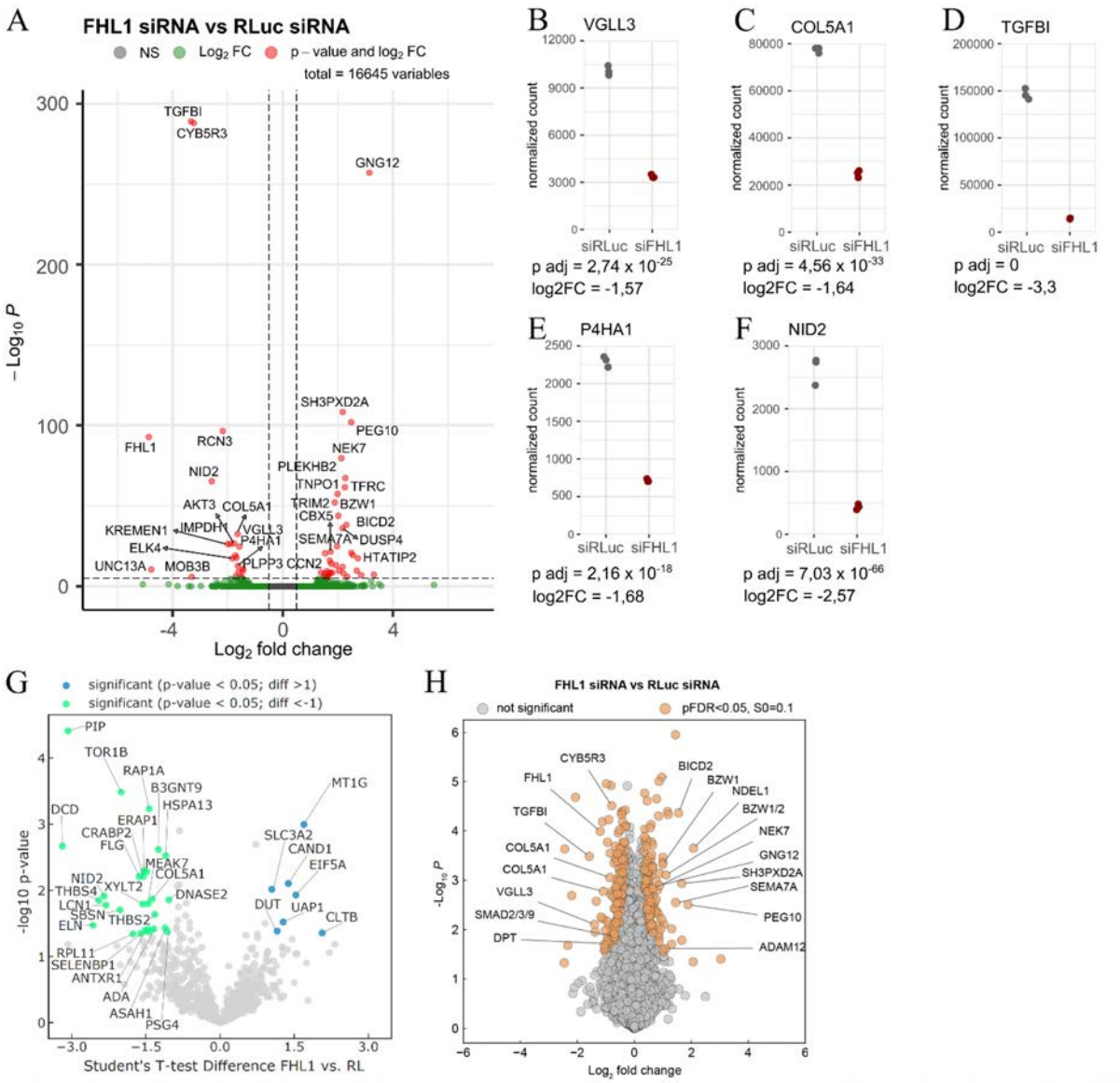

Figure 6. Omics data of *FHL1* siRNA (siFHL1) and *RLuc* siRNA (siRLuc) treated primary fibroblasts and their supernatants. (A) Volcano plot of bulk RNA-seq data, depicting the most upregulated and downregulated genes in siFHL1-treated samples compared to siRLuc-treated. Grey dots: nonsignificant (NS) genes; green dots: genes with a significant Log2FC; red dots: genes with a significant *P* adjusted and Log2FC value. Log2FC smaller than −0.5 or larger than 0.5 and *P* adjusted value <.05 were considered significant, cutoffs are displayed by a dotted line. (B) *VGLL3*, (C) *COL5A1*, (D) *TGFBI*, (E) *P4HA1*, and (F) *NID2* expression in siRLuc- and siFHL1-treated fibroblasts from the bulk RNA-seq data. Transcriptomics: N = 3/3 independent samples. (G) Volcano plot showing the log2 fold change and -log10 *P* value of secreted proteins after treatment with siFHL1 compared to siRLuc (RL). Significantly enriched proteins were determined by an unpaired 2-sided Student's *t*-test. (H) Volcano plot depicting the log2 fold change and −log10 *P* value of proteins in the cell lysate following downregulation of *FHL1* compared to siRLuc-treated samples. Orange: significantly regulated proteins. Significance determined by paired Welch's t-test with permutation-based FDR <0.05 and S0 = 0.1. Secretomics and proteomics: N = 5/5 independent samples. COL5A1, collagen V α1 chain; FHL1, four and a half LIM domain 1; NID2, nidogen 2; P4HA1, prolyl 4-hydroxylase subunit alpha 1; SSc, systemic sclerosis; TGFBI, transforming growth factor beta-induced protein; VGLL3, vestigial-like family member 3; FDR, False Discovery Rate.

hydroxylase subunit alpha 1 (*P4HA1*) (Fig 6A-F). Gene ontology (GO) term analysis for downregulated genes included chaperone-mediated protein folding and metabolic processes, yet a more significant correlation was seen for the terms extracellular structure organisation, ECM organisation, and external encapsulating structure organisation, while the upregulated GO terms were closely linked to proliferation and mitosis (Supplementary Fig S4C).

Focusing on genes involved in ECM homeostasis or its regulation, *VGLL3* stood out. It acts as a transcription cofactor for TEA (Transcriptional Enhancer Factor-1 DNA-binding domain) domain-containing transcription factors and is known to promote collagen expression and production in myofibroblasts and to be induced by matrix stiffness, creating a positive feedback loop for collagen production by myofibroblasts [16]. Our data revealed that knockdown of *FHL1* significantly reduced *VGLL3* expression (Fig 6B).

Secretomics analysis of supernatants from *FHL1* siRNA-treated cells supported the gene expression pattern examined in the transcriptome analysis following *FHL1* downregulation (Fig 6G). Notably, extracellular proteins COL5A1, NID2, and elastin (ELN) were significantly less abundant in the culture supernatants (Fig 6G).

Also, proteomics analysis of the cell layer from *FHL1* siRNA-treated fibroblasts not only demonstrated a ~50% downregulation of FHL1 protein, but further corroborated the significant downregulation of TGFBI and COL5A1 as well as the significant

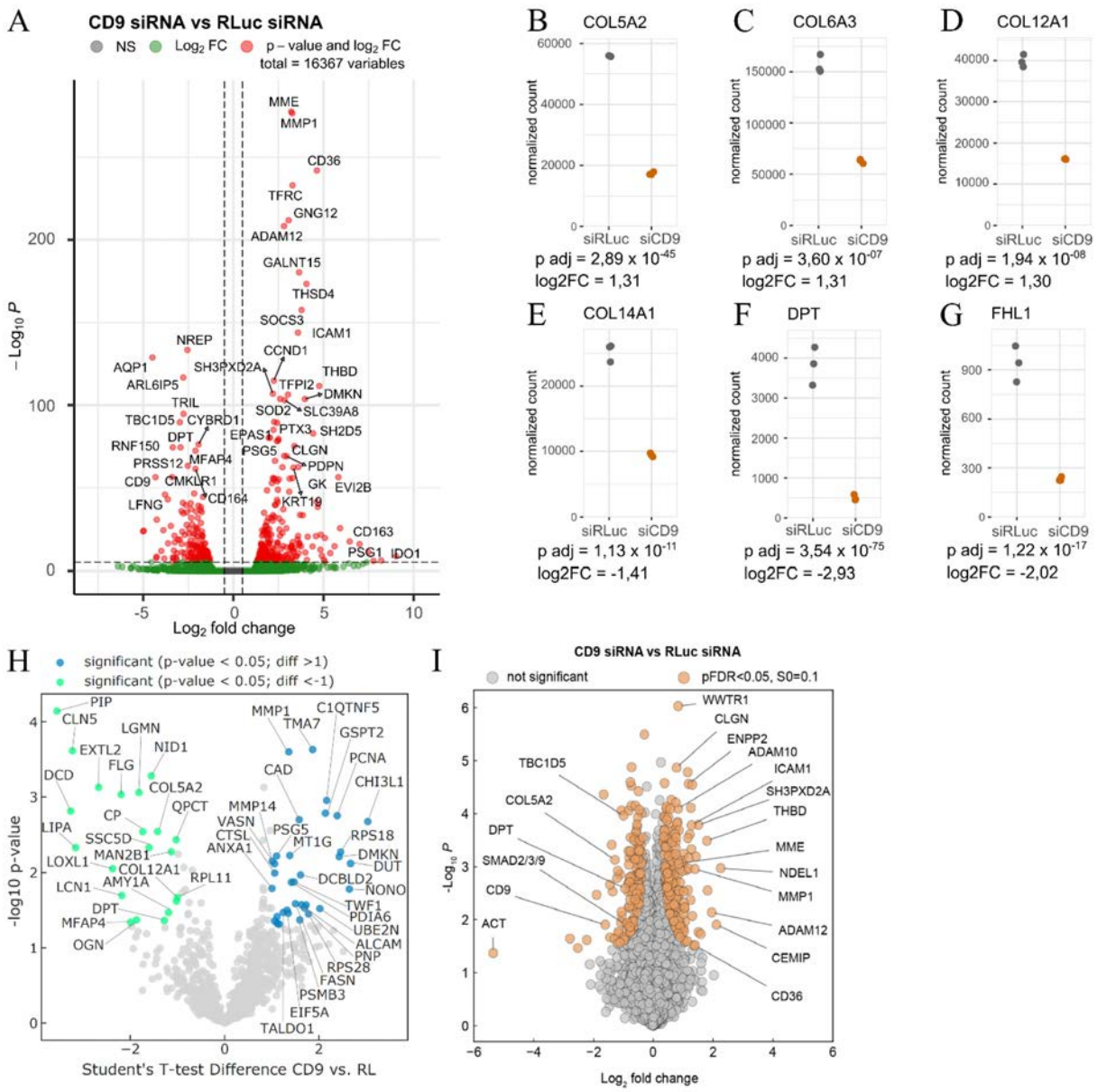

Figure 7. Omics data from *CD9* siRNA (siCD9) and siRLuc-treated primary dermal fibroblasts. (A) Volcano plot from bulk transcriptomics data showing the most upregulated and downregulated genes in siCD9-treated samples compared to siRLuc-treated. Grey dots: nonsignificant (NS) genes; green dots: genes with a significant Log2FC; red dots: genes with a significant *P* adjusted and Log2FC value. Log2FC less than −0.5 or larger than 0.5 and *P* adjusted value <.05 were considered significant, cutoffs depicted with a dotted line. Transcriptomics data of (B) *COL5A2*, (C) *COL6A3*, (D) *COL12A1*, (E) *COL14A1*, (F) *DPT*, and (G) *FHL1* expression in siRLuc- and siCD9-treated fibroblasts. Transcriptomics: N = 3/3 independent samples. (H) Volcano plot showing the log2 fold change and −log10 *P* value of secreted proteins after treatment with siCD9 compared to siRLuc. Significantly enriched proteins were determined by a 2-sided Student's *t*-test. (I) Volcano plot depicting proteomic changes upon downregulation of *CD9* compared to siRLuc-treated samples. Orange: significantly regulated proteins. Significance determined by Welch's t-test with permutation-based FDR <0.05 and S0 = 0.1. Secretomics and proteomics: N = 5/5 independent samples. COL5A2, collagen V α2 chain; COL6A3, Collagen 6 α3 chain; COL12A1, Collagen 12 α1 chain; COL14A1, Collagen 14 α1 chain; DPT, dermatopontin; FHL1, four and a half LIM domain 1; SSc, systemic sclerosis; FDR, False Discovery Rate.

upregulation of SH3 And PX Domains 2A (SH3PXD2A) and NIMA-Related Kinase 7 (NEK7). Notably, *FHL1* siRNA treatment significantly downregulated VGLL3, SMAD2, and SMAD3, which are both key to TGF-beta signalling [30], as well as SMAD9 (Fig 6H), linked to BMP signalling [31].

Similarly, we saw significant differences in the gene expression profiles when comparing *CD9* siRNA and *RLuc* siRNA-treated samples (Supplementary Fig S5A), showing significant CD9 downregulation (−4.32 log2FC; Supplementary Fig S5B). Fibroblasts treated with *CD9* siRNA revealed a significant downregulation of genes such as neuronal regeneration related protein (*NREP*), aquaporin 1 (*AQP1*), *ARL6IP5* (Adenosine diphosphate (ADP)−ribosylation factor−like GTPase 6 −interacting protein 5), dermatopontin (*DPT*), and microfibril associated protein 4 (*MFAP4*); and a significant upregulation of genes such as membrane metalloendopeptidase (*MME*), matrix metallopeptidase 1 (*MMP1*), ADAM metallopeptidase domain 12 (*ADAM12*), and thrombospondin type 1 domain containing 4 (*THSD4*) (Fig 7A). In addition, GO-term enrichment analysis identified that upregulated genes were mainly involved in DNA replication and mitosis checkpoint signalling (Supplementary Fig S5C). In contrast, the downregulated genes were associated with cytoplasmic translation, negative regulation of endothelial cell migration and phospholipase C-activating G protein-coupled receptor signalling (Supplementary Fig S5C). Notably, we also identified a number of genes involved in ECM production or its

regulation, including a significant downregulation of collagens *COL5A2*, *COL6A3*, *COL12A1*, *COL14A1*, and *COL21A1* (Fig 7B-E, Supplementary Fig S5D). In addition, *IGFBP5* (Supplementary Fig S5E), *DPT*, and most interestingly *FHL1* were downregulated (Fig 7F,G).

To functionally link CD9 expression with regulation of ECM deposition, fibroblasts from *CD9*$^{-/-}$ mouse embryonic fibroblasts (*CD9* KO MEFs) and control MEFs were analysed by bulk RNA sequencing (Supplementary Fig S6A-C). Several major collagens and *Acta2* (α-SMA) were significantly downregulated in the *CD9* KO MEFs, also at the protein level (Supplementary Fig S6C-I, Supplementary Fig S7A-E).

Findings based on *CD9* knockout MEFs were further corroborated by *CD9* gene silencing in human skin fibroblasts. Secretomic analysis of supernatants from *CD9* siRNA and *RLuc* siRNA-treated human primary fibroblasts revealed similar changes at the protein level. Secreted extracellular proteins COL5A2, COL12A1, and DPT were significantly reduced in the *CD9* siRNA-treated samples (Fig 7H). In addition, MFAP4, an ECM protein regulating elastic fibre assembly [32], Lysyl oxidase like 1 (LOXL1), which crosslinks elastin and collagens and has been associated with fibrosis [33], and osteoglycin (OGN), which is involved in the organisation and maintenance of ECM and was described as a key regulator of fibrosis, were all significantly decreased following *CD9* knockdown (Fig 7H).

In addition, proteomics analysis of cell lysates from *CD9* siRNA-treated fibroblasts supports the transcriptomics analysis and the biological relevance of CD9. This was further underscored by a decrease of TGF-beta signalling associated SMAD2 and SMAD3 as well as SMAD9 in response to *CD9* knockdown (Fig 7I).

VGLL3 is significantly upregulated in subsets of SSc dermal fibroblasts and SSc skin

Downregulation of *FHL1* by siRNA demonstrated that VGLL3 expression was markedly reduced. Because VGLL3 is known to play an important role in promoting ECM expression, we also analysed its expression in the different clusters representing fibroblast subpopulations. Although our scRNA-seq data indicated no significant difference in the overall *VGLL3* expression between SSc and healthy control fibroblasts, we observed the highest expression levels of *VGLL3* overall in cluster 3 (IGFBP4^{hi}), which also had high expression levels of both *FHL1* and *CD9* (Fig 8A,B; Fig 2B,C). In addition, clusters 1 (DCN^{hi}) and 10 (FHL1^{hi}) also displayed increased expression levels of *VGLL3*, yet to a lesser extent than cluster 3 (IGFBP4^{hi}) (Fig 8A,B).

Of note, the number of *FHL1*$^{+}$/*VGLL3*$^{+}$ double-positive fibroblasts in our scRNA-seq data was significantly increased in SSc when compared to healthy control fibroblasts: 243 control compared to 2197 SSc fibroblasts with high expression of both, *FHL1* and *VGLL3* (expression level >1.2), equivalent to 1.27% of control and 12.01% of SSc fibroblasts (Supplementary Fig S8A, B). Cells coexpressing *VGLL3* and *FHL1* mainly localised to cluster 1 (DCN^{hi}) in control fibroblasts and to an even higher extent to cluster 3 (IGFBP4^{hi}) in SSc fibroblasts (Fig 8C).

Likewise, the abundance of *CD9*$^{+}$/*VGLL3*$^{+}$ double-positive fibroblasts was also significantly augmented in SSc compared to healthy control fibroblasts: 225 control vs 787 SSc fibroblasts with high expression of both, *CD9* and *VGLL3* (expression level >1.2), equating to 1.17% of control and 4.30% of SSc fibroblasts (Supplementary Fig S8C,D). *CD9*$^{+}$/*VGLL3*$^{+}$ fibroblasts mainly localised to cluster 3 (IGFBP4^{hi}) in SSc fibroblasts, as did the *FHL1*$^{+}$/*VGLL3*$^{+}$ fibroblasts (Supplementary Fig S8E).

Strikingly, we also identified fibroblasts that coexpressed all 3 genes (*CD9*, *FHL1*, and *VGLL3*) with high intensity (expression level >1.2). Their abundance was significantly increased in SSc compared to controls: we identified 393 *CD9*$^{+}$/*FHL1*$^{+}$/*VGLL3*$^{+}$ fibroblasts in SSc, but only 4 such fibroblasts in controls, which was equivalent to 2.14% of the SSc vs 0.02% of the control fibroblast population (Supplementary Fig S8F,G). Given that *CD9*$^{+}$/*FHL1*$^{+}$/*VGLL3*$^{+}$ fibroblasts were predominantly found in SSc samples, they may represent a specific subtype of fibroblasts present in SSc. Importantly, IF staining confirmed increased VGLL3 expression in SSc fibroblast cultures and in addition in patient biopsies (Fig 8D-F) indicating potential diagnostic and therapeutic implications.

DISCUSSION

SSc (scleroderma; SSc) is an autoimmune-driven disease, where an initial inflammatory reaction leads to activation of fibroblasts and excessive deposition of ECM [1,2,34]. Fibroblasts cultured from skin biopsies obtained from patients with SSc show induced collagen synthesis even after several passages [11–13]. We here provide evidence by scRNA-seq that fibroblast cultures obtained by outgrowth from skin biopsies from fibrotic skin of patients with dcSSc are composed of a heterogenous group of fibroblasts and represent an important source to identify altered fibroblast subsets with a stable phenotype independent of the environment. In these, we demonstrate upregulation of novel genes characteristic of SSc fibroblast clusters and propose that they have a functional role in ECM deposition.

Extensive scRNA-seq data from fibroblasts isolated directly from the skin of patient with SSc also characterised distinct fibroblast subsets [9,35–38]. This experimental approach has the advantage of better reflecting the state of activity of cells in their biological environment. On the other hand, the sensitivity of certain fibroblasts to enzymatic digestion may result in the selection of more resistant populations. Comparison of this kind of scRNA-seq data with our fibroblast populations revealed only limited similarities and did not detect several clusters reported previously [8,9]. This can be due to the culture conditions modifying the gene expression profile to a certain extent. Another contributing difference may be that the heterogeneity of fibroblasts detected directly after isolation from the tissue might only reflect a transient dynamic state of the cells at a distinct point in time and not the presence of stable fibroblast populations. In contrast, our cultured fibroblasts were analysed after 4 passages and revealed a relatively stable phenotype.

Our data indicate that the fibroblasts obtained from the patients with SSc did not reveal a clear papillary or reticular gene signature. We identified the papillary marker gene, *DPP4*, in all fibroblasts, but simultaneously also the expression of the reticular marker gene, *ATXN1*. However, in cluster 1 (DCN^{hi}) and interestingly in cluster 3 (IGFBP5^{hi}), we saw *PDPN* expression, characteristic for reticular fibroblasts that are derived from deep dermal tissue, where most of the fibrotic activity in SSc takes place. Furthermore, several of the subsets in our scleroderma cultures did exhibit markers of activation that were previously identified by several other groups [3,39].

FHL1 and CD9 overexpressing fibroblasts in SSc and in fibrotic murine skin

Of note, we report the detection of unique populations characterised by high overexpression of CD9 and FHL1. This raised the question whether these populations represent activated

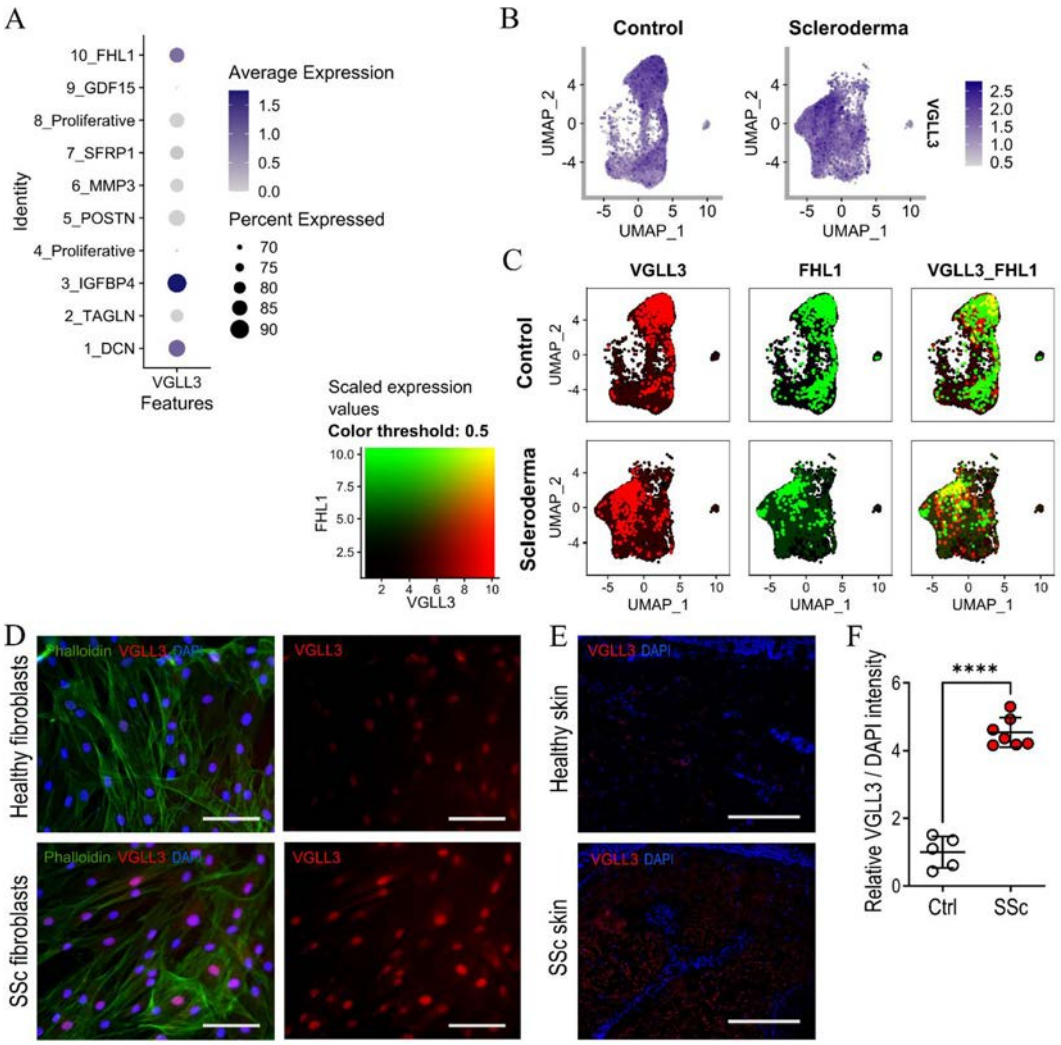

Figure 8. VGLL3 expression is increased in specific subsets of fibroblasts obtained from patients with dcSSc. (A) scRNA-seq dot plot of *VGLL3*. The size of the dot is proportional to the percentage of cells per cluster expressing the gene. The colour intensity correlates with the scaled average expression intensity in these cells. (B) scRNA-seq feature plots of *VGLL3* for control (left) and dcSSc (right) fibroblasts. Each dot represents a cell; the darker the colour intensity of the dots, the more increased the gene expression. (C) Coexpression feature plot of *VGLL3* and *FHL1* comparing healthy control (top row) and dcSSc (bottom row) fibroblasts. Red dots represent the expression of *VGLL3*, green dots the expression of *FHL1*; high coexpression of *VGLL3* and *FHL1* can be seen as yellow. Each dot represents a cell, and the increased intensity of the colour of the dots represents increased expression. The colour scale (on the left) depicts increased coexpression in a cell with a yellow to orange colour scale. (D) Representative IF staining of DAPI (blue), phalloidin (green), and VGLL3 (red) in human healthy (top row) and dcSSc fibroblasts (bottom row). Scale bar = 100 μm. (E) IF staining of DAPI (blue) and VGLL3 (red) in human healthy skin (top) and skin from patients with dcSSc (bottom). Scale bar = 300 μm. (F) Quantification of IF staining intensity of VGLL3 normalised to DAPI in human healthy and SSc dermis. Data are shown as relative values compared to control (N = 4 Ctrl/7 SSc donors; **** $P \leq .0001$). *P* values calculated with Welch's t-test, two-tailed; data shown as mean ± SD. Ctrl, control; dcSSc, diffuse cutaneous systemic sclerosis; FHL1, four and a half LIM domain 1; IF, immunofluorescent; scRNA-seq, single-cell RNA sequencing; SSc, systemic sclerosis; VGLL3, vestigial-like family member 3; UMAP, Uniform Manifold Approximation and Projection; DAPI, 4',6-diamidino-2-phenylindole.

fibroblasts. Given the expression of several markers for activated fibroblasts in these subpopulations, such as the profibrotic markers *THY1* (CD90), *CTGF*, *TNC*, *IGFBP5*, *ACTA2*, among others, we think they do. Expression of *ACTA2*, in particular, has been described as a characteristic marker of myofibroblasts [40,41], which play a key role in tissue repair and fibrotic diseases [42].

However, we also identified clusters characterised by *FHL1* and *CD9* overexpression, where *ACTA2* was not overexpressed. Also, *CD9* overexpression was found to be associated only partially with *FHL1* co-overexpression. This indicates further heterogeneity within the still insufficiently characterised myofibroblasts [9] and suggests the presence of at least 3 related but distinct subpopulations of $CD9^+$, $CD9^+/FHL1^+$, and $FHL1^+$ cells, with presumably specific functions.

FHL1 has been shown to play an essential role in muscle development and related diseases. It is also reported to be downregulated in cancer. There are studies indicating that the isoform FHL1A is expressed in skeletal muscle, myocardium and in fibroblasts [14,26]. To date, its role in the biology of fibroblasts is unknown and it has not previously been described in the context of fibrotic diseases.

CD9 is a tetraspanin transmembrane protein and is thought to mark exosomes. It is associated with many cellular functions in various cell types and interacts with integrins and other cell surface molecules that are involved in cell–matrix interactions. It has been linked to multiple diseases associated with dysregulated inflammatory responses and various types of cancer [15]. Mice lacking *CD9* have severe fertility issues [43], and exhibit delayed wound healing [44]. In addition, CD9 levels were reported to be

increased in SSc dermal fibroblasts [39]. However, due to the broad cellular distribution of CD9, a causal relationship with the fibrotic process and its role in fibroblasts is still speculative.

Our western blots and proteomics analysis comparing patients with SSc-derived cultured fibroblasts with healthy controls further corroborated the increased levels for CD9 and FHL1 that we detected by scRNA-seq and confirmed previous findings by Nakamura et al [39] for CD9. Moreover, we also detected the FHL1 and CD9 overexpressing subpopulations *in vivo* in biopsies from patients with SSc by immunofluorescence. Together, these findings argue strongly against a culture condition-dependent artefact and indicate that these subpopulations represent a stable subset of activated fibroblasts in SSc.

Immunostaining of biopsies obtained from severe fibrotic skin from patients with dcSSc revealed that FHL1 staining was most prominent in spindle-shaped cells with the histological appearance of fibroblasts in the reticular layer of the dermis. Interestingly, CD9 was also overexpressed in keratinocytes in these biopsies compared to controls. Keratinocyte involvement in the pathophysiology of scleroderma has recently been discussed, but it remains to be clarified, whether this is directly related to the disease or represents a secondary phenomenon [45–47].

We also found that fibroblasts obtained from patients with lcSSc did not overexpress FHL1 to the same extent as fibroblasts from patients with dcSSc. Also, FHL1 and CD9 staining in biopsies from patients with lcSSc were similar to controls or showed only a slight increase. Since the development of fibrosis was much more intense in the patients with dcSSc, this indicates that induced FHL1 and CD9 expression are characteristic of heavily involved fibrotic skin and reflects the intensity of fibrosis. This might indicate that the expression of these markers in distinct fibroblast subsets can be used as biomarkers for following the severity of fibrosis.

The association of CD9 and FHL1 overexpressing fibroblasts with the initiation of a fibrotic reaction is further supported by the demonstration of increased numbers of CD9 and FHL1 strongly positive fibroblasts in the bleomycin-induced fibrotic skin in mice.

FHL1 and CD9 have a functional role in activated fibroblast subpopulations

Evidently, the elevated expression levels and also the induced protein levels in culture and *in vivo* represent a descriptive analysis and do not allow a causal connection between CD9/FHL1 and the activation of fibroblast subsets. Knockdown experiments were therefore conducted to reveal if FHL1 and CD9 have functional roles in the activation of these fibroblast subsets. The functional analysis of *CD9* downregulation in human fibroblasts revealed reduced expression of genes involved in cytoplasmic protein translation, but also of *MFAP4*, dermatopontin, several collagens, and other ECM-related genes. In addition, we obtained independent evidence for a functional role of CD9 from another system. Analysis of murine *CD9* KO MEFs by RNA-seq revealed a very significant downregulation of both *Col1a1* and *Col1a2* along with other collagens. Interestingly, *Acta2* was also significantly downregulated in these murine fibroblasts. Notably, collagen I, fibrillin 1, and fibronectin were also downregulated in the *CD9* KO MEFs at the protein level. We were able to confirm that a lack of CD9 has a negative impact on ECM-related genes and proteins in several different cross-species assays.

Similarly, downregulation of *FHL1* resulted in reduced expression of TGFBI, known to be involved in the organisation of the ECM [48], as well as of several genes encoding ECM or ECM-modifying enzymes. Moreover, both *FHL1* and *CD9* downregulation by siRNA treatment resulted in downregulation of SMAD2 and SMAD3 proteins, as targets in the TGF-β signalling pathways, indicating a direct impact on ECM gene transcription.

Interestingly, also the transcription cofactor VGLL3 was downregulated after FHL1 knockdown. VGLL3 was previously reported to be involved in regulating the induction of collagen synthesis in myofibroblasts in response to mechanical stress [16], and it is also involved in myogenesis, cell proliferation [49], and autoimmune diseases [50]. Altered interaction of fibroblasts with the surrounding ECM in a very stiff tissue is thought to play a key role in the persistent activation of fibroblasts during fibrosis. VGLL3 was recently reported to be translocated to the nucleus in response to substrate stiffness and to induce collagen production by suppressing miR-29b, which is known to target collagen mRNA [16]. Our data demonstrated an upregulation of VGLL3 in SSc-derived dermal fibroblasts in culture and also in SSc skin sections of the fibrotic tissue. This strongly supports a role of VGLL3 in fibrosis and provides a molecular explanation for the perpetuation of an activated phenotype of the myofibroblast subsets in SSc due to the increased mechanical stiffness of the tissue, which is mediated through the integrin-cytoskeleton axis [51–53].

Downregulation of *FHL1* resulted in the regulation of several other ECM genes, eg, collagen V (COL5A1), NID2, *P4HA1*, and ELN. The decrease in COL5A1 and NID2 was confirmed by proteomic analysis of secreted proteins. This altered expression of distinct molecules that are involved in the collagen suprastructure and macromolecular association is in accordance with the disturbed structure of collagen bundles seen in biopsies from patients with SSc by electron microscopy [54]. The subsequently altered macromolecular ECM organisation is thought to contribute to the increased stiffness of the tissue, which again leads to activation of certain fibroblast subsets and contributes to the perpetuation of the activation.

Strikingly, *CD9* downmodulation by siRNA resulted in reduced *FHL1* transcript levels, as well as other ECM-related genes, such as collagen V (*COL5A2*), *DPT*, and *MFAP4*. Other ECM-related proteins were also impacted, including LOXL1 and collagen XII (COL12A1). The downregulation of *FHL1* after *CD9* knockdown indicates a close link between these proteins in the differently activated subsets of (myo)fibroblasts. It still remains unclear if a hierarchical process exists placing CD9 upstream of FHL1 that results in VGLL3 induction, whether shared upstream pathways exist or whether these players act independently. Nevertheless, the induction of VGLL3 is in line with the activation of collagen synthesis in the fibroblast populations reported here and demonstrated in a recent report on its role in cardiac fibrosis [16].

Conclusion

We identify a novel subset of fibroblasts characterised by high expression of CD9 and FHL1 in fibrotic lesions of patients with dcSSc and present evidence in different experimental systems supporting a functional role of these proteins for ECM production and fibrosis development. The data provide the basis for new biomarker development and the identification of novel therapeutic targets.

Competing interests

The authors have declared that no conflict of interest exists.

CRediT authorship contribution statement

Ann-Helen S Rosendahl: Writing – review & editing, Writing – original draft, Visualization, Methodology, Investigation, Conceptualization. **Anna Bornikoel:** Writing – review & editing, Writing – original draft, Visualization, Methodology, Investigation. **Isabel Zeinert:** Writing – review & editing, Methodology. **Lena Keufgens:** Writing – review & editing, Visualization, Methodology. **Frederik Tellkamp:** Writing – review & editing, Visualization, Methodology. **Niklas Kleinenkuhnen:** Writing – review & editing, Methodology. **Till Baar:** Writing – review & editing, Methodology, Investigation. **Katrin Schönborn:** Writing – review & editing, Visualization, Funding acquisition. **Marcus Krüger:** Writing – review & editing, Supervision. **Achim Tresch:** Writing – review & editing, Supervision. **Bent Brachvogel:** Writing – review & editing, Methodology, Funding acquisition, Conceptualization. **Beate Eckes:** Writing – review & editing, Project administration, Funding acquisition, Conceptualization. **Pia Moinzadeh:** Writing – review & editing, Investigation. **Thomas Krieg:** Writing – review & editing, Writing – original draft, Supervision, Project administration, Funding acquisition, Conceptualization.

Acknowledgements

We thank Dr Claude Boucheix, Dr Eric Rubinstein, and Dr Stephanie Charrin (INSERM, Paris, France) for the kind gift of *CD9* KO and control MEFs, Dr Miloš Gojković (CECAD Cologne) for help and expert advice with the fluorescence-activated cell sorting data, and Susanne Neumann for excellent technical assistance. Some of the data reported here were presented at ISID2023 conference in Tokyo (DOI:10.1016/j.jid.2023.03.1472), and at the ESDR 2022 conference in Amsterdam (DOI:10.1016/j.jid.2022.09.018).

Funding

A-HSR was generously supported by the Young researcher grant, year 2021 from Emil Aaltonen Foundation, Finland. Parts of this work were funded by CMMC (SRG 2), CECAD (both to TK), Edith Busch Foundation (to BE and KS) and the German Research Foundation through KR 558/17-1, project ID 468236352 (to TK) and RU 2722, project ID 384170921 (to BB). CECAD/ZMMK Proteomics Facility appreciates the funding of DFG Grossgeräteantrag 'INST 216/1020-1 FUGG'.

Patient consent for publication

Written informed consent was obtained from the patients.

Ethics approval

This study has the approval of the local ethics committee (Ethics committee of the medical faculty of University of Cologne, 21-1072). The study was conducted in accordance with the criteria set by the Declaration of Helsinki. Mouse handling and experimentation were performed according to the German Law for Welfare of Laboratory Animals and were approved by the North Rhine Westphalia State Office for Nature, Environment and Consumer Protection Germany (LANUV NRW) under the license 84-02.04.2020.A155.

Provenance and peer review

Not commissioned; externally peer reviewed.

Supplementary materials

Supplementary material associated with this article can be found, in the online version, at doi:10.1016/j.ard.2025.11.027.

Orcid

Ann-Helen S Rosendahl: http://orcid.org/0000-0001-7968-0990
Anna Bornikoel: http://orcid.org/0000-0002-1921-7205
Thomas Krieg: http://orcid.org/0000-0001-5616-8476

REFERENCES

[1] Gabrielli A, Avvedimento EV, Scleroderma Krieg T. N Engl J Med 2009;360(19):1989–2003.
[2] Varga J, Abraham D. Systemic sclerosis: a prototypic multisystem fibrotic disorder. J Clin Invest 2007;117(3):557–67.
[3] Driskell RR, Lichtenberger BM, Hoste E, Kretzschmar K, Simons BD, Charalambous M, et al. Distinct fibroblast lineages determine dermal architecture in skin development and repair. Nature 2013;504(7479):277–81.
[4] Driskell RR, Watt FM. Understanding fibroblast heterogeneity in the skin. Trends Cell Biol 2015;25(2):92–9.
[5] Philippeos C, Telerman SB, Oulès B, Pisco AO, Shaw TJ, Elgueta R, et al. Spatial and single-cell transcriptional profiling identifies functionally distinct human dermal fibroblast subpopulations. J Invest Dermatol 2018;138(4):811–25.
[6] Sawant M, Hinz B, Schönborn K, Zeinert I, Eckes B, Krieg T, et al. A story of fibers and stress: matrix-embedded signals for fibroblast activation in the skin. Wound Repair Regen 2021;29(4):515–30.
[7] Koliaraki V, Prados A, Armaka M, Kollias G. The mesenchymal context in inflammation, immunity and cancer. Nat Immunol 2020;21(9):974–82.
[8] Tabib T, Morse C, Wang T, Chen W, Lafyatis R. SFRP2/DPP4 and FMO1/LSP1 define major fibroblast populations in human skin. J Invest Dermatol 2018;138(4):802–10.
[9] Tabib T, Huang M, Morse N, Papazoglou A, Behera R, Jia M, et al. Myofibroblast transcriptome indicates SFRP2^{hi} fibroblast progenitors in systemic sclerosis skin. Nat Commun 2021;12(1):4384.
[10] Valenzi E, Bulik M, Tabib T, Morse C, Sembrat J, Trejo Bittar H, et al. Single-cell analysis reveals fibroblast heterogeneity and myofibroblasts in systemic sclerosis-associated interstitial lung disease. Ann Rheum Dis 2019;78(10):1379–87.
[11] LeRoy EC. Increased collagen synthesis by scleroderma skin fibroblasts in vitro: a possible defect in the regulation or activation of the scleroderma fibroblast. J Clin Invest 1974;54(4):880–9.
[12] LeRoy EC, Mercurio S, Sherer GK. Replication and phenotypic expression of control and scleroderma human fibroblasts: responses to growth factors. Proc Natl Acad Sci U S A. 1982;79(4):1286–90.
[13] Fleischmajer R, Perlish JS, Krieg T, Timpl R. Variability in collagen and fibronectin synthesis by scleroderma fibroblasts in primary culture. J Invest Dermatol 1981;76(5):400–3.
[14] Shathasivam T, Kislinger T, Gramolini AO. Genes, proteins and complexes: the multifaceted nature of FHL family proteins in diverse tissues. J Cell Mol Med 2010;14(12):2702–20.
[15] Brosseau C, Colas L, Magnan A, Brouard S. CD9 Tetraspanin: a new pathway for the regulation of inflammation? Front Immunol 2018;9:2316.
[16] Horii Y, Matsuda S, Toyota C, Morinaga T, Nakaya T, Tsuchiya S, et al. VGLL3 is a mechanosensitive protein that promotes cardiac fibrosis through liquid-liquid phase separation. Nat Commun 2023;14(1):550.
[17] Satija R, Farrell JA, Gennert D, Schier AF, Regev A. Spatial reconstruction of single-cell gene expression data. Nat Biotechnol 2015;33(5):495–502.
[18] McGinnis CS, Murrow LM, Gartner ZJ. DoubletFinder: doublet detection in single-cell RNA sequencing data using artificial nearest neighbors. Cell Syst 2019;8(4):329–37 .e4.
[19] Stuart T, Butler A, Hoffman P, Hafemeister C, Papalexi E, Mauck 3rd WM, et al. Comprehensive integration of single-cell data. Cell 2019;177(7):1888–902 .e21.
[20] Sawant M, Wang F, Koester J, Niehoff A, Nava MM, Lundgren-Akerlund E, et al. Ablation of integrin-mediated cell-collagen communication alleviates fibrosis. Ann Rheum Dis 2023;82(11):1474–86.

[21] Nolte H, MacVicar TD, Tellkamp F, Krüger M. Instant clue: a software suite for interactive data visualization and analysis. Sci Rep 2018;8(1):12648.
[22] Demichev V, Messner CB, Vernardis SI, Lilley KS, Ralser M. DIA-NN: neural networks and interference correction enable deep proteome coverage in high throughput. Nat Methods 2020;17(1):41–4.
[23] Tusher VG, Tibshirani R, Chu G. Significance analysis of microarrays applied to the ionizing radiation response. Proc Natl Acad Sci U S A 2001;98(9):5116–21.
[24] LeRoy EC, Medsger TA. Jr. Criteria for the classification of early systemic sclerosis. J Rheumatol 2001;28(7):1573–6.
[25] Selva-O'Callaghan A, Trallero-Araguás E, MT Sanz-Martínez. Anti-FHL1 antibody: welcome to a novel autoantibody in myositis. Rheumatology (Oxford) 2022;61(10):3887–8.
[26] Tao Y, Wu Y, Shen R, He S, Miao X. Role of four and a half LIM domain protein 1 in tumors (Review). Oncol Lett 2025;29(1):37.
[27] Yang K, Huang N, Sun J, Dai W, Chen M, Zeng J. Transforming growth factor-beta induced protein regulates pulmonary fibrosis via the G-protein signaling modulator 2 /Snail axis. Peptides 2022;155:170842.
[28] Wu M, Wang Z, Shi X, Zan D, Chen H, Yang S, et al. TGFβ1-RCN3-TGFBR1 loop facilitates pulmonary fibrosis by orchestrating fibroblast activation. Respir Res 2023;24(1):222.
[29] Sun M, Chen S, Adams SM, Florer JB, Liu H, Kao WW, et al. Collagen V is a dominant regulator of collagen fibrillogenesis: dysfunctional regulation of structure and function in a corneal-stroma-specific Col5a1-null mouse model. J Cell Sci 2011;124(Pt 23):4096–105.
[30] Peng D, Fu M, Wang M, Wei Y, Wei X. Targeting TGF-beta signal transduction for fibrosis and cancer therapy. Mol Cancer 2022;21(1):104.
[31] Tsukamoto S, Mizuta T, Fujimoto M, Ohte S, Osawa K, Miyamoto A, et al. Smad9 is a new type of transcriptional regulator in bone morphogenetic protein signaling. Sci Rep 2014;4:7596.
[32] Mohammadi A, Sorensen GL, Pilecki B. MFAP4-Mediated effects in elastic fiber homeostasis, integrin signaling and cancer, and its role in teleost fish. Cells 2022;11(13):2115.
[33] Greene AG, Eivers SB, Dervan EWJ, O'Brien CJ, Wallace DM. Lysyl oxidase like 1: biological roles and regulation. Exp Eye Res 2020;193:107975.
[34] Distler JHW, Györfi AH, Ramanujam M, Whitfield ML, Königshoff M, Lafyatis R. Shared and distinct mechanisms of fibrosis. Nat Rev Rheumatol 2019;15 (12):705–30.
[35] Werner G, Sanyal A, Mirizio E, Hutchins T, Tabib T, Lafyatis R, et al. Single-cell transcriptome analysis identifies subclusters with inflammatory fibroblast responses in localized scleroderma. Int J Mol Sci 2023;24(12):9796.
[36] Li Z, Cao T, Li Q, Zhang J, Du J, Chen J, et al. Cross-disease characterization of fibroblast heterogeneities and their pathogenic roles in skin inflammation. Clin Immunol 2023;255:109742.
[37] Clark KEN, Xu S, Attah M, Ong VH, Buckley CD, Denton CP. Single-cell analysis reveals key differences between early-stage and late-stage systemic sclerosis skin across autoantibody subgroups. Ann Rheum Dis 2023;82(12):1568–79.
[38] Zhu H, Luo H, Skaug B, Tabib T, Li YN, Tao Y, et al. Fibroblast subpopulations in systemic sclerosis: functional implications of individual subpopulations and correlations with clinical features. J Invest Dermatol 2024;144(6):1251–61 .e13.
[39] Nakamura K, Jinnin M, Harada M, Kudo H, Nakayama W, Inoue K, et al. Altered expression of CD63 and exosomes in scleroderma dermal fibroblasts. J Dermatol Sci 2016;84(1):30–9.
[40] Majno G, Gabbiani G, Hirschel BJ, Ryan GB, Statkov PR. Contraction of granulation tissue in vitro: similarity to smooth muscle. Science 1971;173 (3996):548–50.
[41] Hirschel BJ, Gabbiani G, Ryan GB, Majno G. Fibroblasts of granulation tissue: immunofluorescent staining with antismooth muscle serum. Proc Soc Exp Biol Med 1971;138(2):466–9.
[42] Hinz B, Lagares D. Evasion of apoptosis by myofibroblasts: a hallmark of fibrotic diseases. Nat Rev Rheumatol 2020;16(1):11–31.
[43] Le Naour F, Rubinstein E, Jasmin C, Prenant M, Boucheix C. Severely reduced female fertility in CD9-deficient mice. Science 2000;287(5451):319–21.
[44] Zhang J, Dong J, Gu H, Yu S, Zhang X, Gou Y, et al. CD9 is critical for cutaneous wound healing through JNK signaling. J Invest Dermatol 2012;132 (1):226–36.
[45] Aden N, Shiwen X, Aden D, Black C, Nuttall A, Denton CP, et al. Proteomic analysis of scleroderma lesional skin reveals activated wound healing phenotype of epidermal cell layer. Rheumatology (Oxford) 2008;47 (12):1754–60.
[46] Aden N, Nuttall A, Shiwen X, de Winter P, Leask A, Black CM, et al. Epithelial cells promote fibroblast activation via IL-1alpha in systemic sclerosis. J Invest Dermatol 2010;130(9):2191–200.
[47] Nikitorowicz-Buniak J, Shiwen X, Denton CP, Abraham D, Stratton R. Abnormally differentiating keratinocytes in the epidermis of systemic sclerosis patients show enhanced secretion of CCN2 and S100A9. J Invest Dermatol 2014;134(11):2693–702.
[48] Yin J, Liu JS, Feng M, Li JM, Lu S, Yang M, et al. Comprehensively investigating the expression levels and the prognostic role of transforming growth factor beta-induced (TGFBI) in glioblastoma multiforme. Transl Cancer Res 2020;9(10):6487–504.
[49] Figeac N, Mohamed AD, Sun C, Schönfelder M, Matallanas D, Garcia-Munoz A, et al. VGLL3 operates via TEAD1, TEAD3 and TEAD4 to influence myogenesis in skeletal muscle. J Cell Sci 2019;132(13):jcs225946.
[50] Billi AC, Gharaee-Kermani M, Fullmer J, Tsoi LC, Hill BD, Gruszka D, et al. The female-biased factor VGLL3 drives cutaneous and systemic autoimmunity. JCI Insight 2019;4(8):e127291.
[51] Schulz JN, Plomann M, Sengle G, Gullberg D, Krieg T. Eckes B. New developments on skin fibrosis - essential signals emanating from the extracellular matrix for the control of myofibroblasts. Matrix Biol 2018;68-69:522–32.
[52] Wickström SA, Lange A, Montanez E, Fässler R. The ILK/PINCH/parvin complex: the kinase is dead, long live the pseudokinase!. EMBO J 2010;29(2):281–91.
[53] Nüchel J, Ghatak S, Zuk AV, Illerhaus A, Mörgelin M, Schönborn K, et al. TGFB1 is secreted through an unconventional pathway dependent on the autophagic machinery and cytoskeletal regulators. Autophagy 2018;14 (3):465–86.
[54] Perlish JS, Lemlich G, Fleischmajer R. Identification of collagen fibrils in scleroderma skin. J Invest Dermatol 1988;90(1):48–54.

Ann Rheum Dis 85 (2026) 693–703

Contents lists available at ScienceDirect

Annals of the Rheumatic Diseases

journal homepage: https://www.sciencedirect.com/journal/annals-of-the-rheumatic-diseases

IgG4 related disease

Genome-wide association studies reveal new insights into the genetic basis of IgG4-related disease in the Chinese Han population

Songxin Yan[1,2], Yu Peng[3,4], Jingkai Xu[5], Yanying Liu[6,7], Zhan Li[1], Yue Yang[5], Linyi Peng[3], Jiaxin Zhou[3], Liubing Li[8], Chenxi Liu[9], Haizhen Chen[10], Mu Wang[11], Ziyan Wu[1], Shulan Zhang[3], Honglin Xu[1], Haolong Li[1], Futai Feng[1], Yunyun Fei[3], Yu Chen[12], Lingli Dong[12], Mengtao Li[3], Zhanguo Li[6], Fengchun Zhang[3], Xianbo Zuo[5,**], Wen Zhang[3,***], Yongzhe Li[1,*]

[1] *Department of Clinical Laboratory, State Key Laboratory of Complex Severe and Rare Diseases, Peking Union Medical College Hospital, Chinese Academy of Medical Science and Peking Union Medical College, Beijing, China*
[2] *Department of Laboratory Medicine, Gene Diagnosis Research Center, Fujian Key Laboratory of Laboratory Medicine, The First Affiliated Hospital, Fujian Medical University, Fuzhou, China*
[3] *Department of Rheumatology, National Clinical Research Center for Dermatologic and Immunologic Diseases, Key Laboratory of Rheumatology and Clinical Immunology, Ministry of Education, State Key Laboratory of Complex Severe and Rare Diseases, Peking Union Medical College Hospital, Chinese Academy of Medical Science and Peking Union Medical College, Beijing, China*
[4] *Department of Rheumatology, the Second Affiliated Hospital of Zhejiang University, School of Medicine, Zhejiang, China*
[5] *Department of Big Data Center, Department of Dermatology, NHC Key Laboratory of Clinical Big Data Standardization & Integration, China-Japan Friendship Hospital, Beijing, China*
[6] *Department of Rheumatology and Immunology, Beijing Key Laboratory for Rheumatism Mechanism and Immune Diagnosis, Peking University People's Hospital, Beijing, China*
[7] *Department of Rheumatology and Immunology, Beijing Friendship Hospital, Capital Medical University, Beijing, China*
[8] *Department of Laboratory Medicine, The First Affiliated Hospital, Sun Yat-sen University, Guangzhou, Guangdong Province, China*
[9] *Department of Laboratory Medicine, West China Second University Hospital, Sichuan University, Chengdu, Sichuan, China*
[10] *Clinical Laboratory, The First Hospital of Jilin University, Changchun, China*
[11] *Department of Stomatology, Peking Union Medical College Hospital, Chinese Academy of Medical Sciences & Peking Union Medical College, Wangfujing, Dongcheng District, Beijing, China*
[12] *Department of Rheumatology and Immunology, Tongji Hospital, Tongji Medical College, Huazhong University of Science and Technology, Wuhan, Hubei, China*

*Correspondence to Prof Yongzhe Li, Department of Clinical Laboratory, State Key Laboratory of Complex Severe and Rare Diseases, Peking Union Medical College Hospital, Chinese Academy of Medical Science and Peking Union Medical College, Beijing, China.

**Correspondence to Prof Xianbo Zuo, Department of Big Data Center, Department of Dermatology, NHC Key Laboratory of Clinical Big Data Standardization & Integration, China-Japan Friendship Hospital, Beijing, China.

***Correspondence to Prof Wen Zhang, Department of Rheumatology, National Clinical Research Center for Dermatologic and Immunologic Diseases, Key Laboratory of Rheumatology and Clinical Immunology, Ministry of Education, State Key Laboratory of Complex Severe and Rare Diseases, Peking Union Medical College Hospital, Chinese Academy of Medical Science and Peking Union Medical College, Beijing, China.

E-mail addresses: zuoxianbo@qq.com (X. Zuo), zhangwen91@sina.com (W. Zhang), liyz@pumch.cn (Y. Li).

Handling editor Josef S Smolen

Songxin Yan, Yu Peng, Jingkai Xu, and Yanying Liu contributed equally.

https://doi.org/10.1016/j.ard.2025.10.028

ARTICLE INFO

Article history:
Received 12 May 2025
Received in revised form 30 August 2025
Accepted 27 October 2025

ABSTRACT

Objectives: IgG4-related disease (IgG4-RD) is an immune-mediated fibroinflammatory disorder of unknown aetiology, potentially linked to genetic factors. This study conducted the first genome-wide association study on IgG4-RD in the Chinese Han population to identify genetic susceptibility loci.

Methods: The study analysed data from 1161 patients with IgG4-RD and 10,539 controls across 2 independent cohorts, with 1115 patients and 10,154 controls passing quality control criteria. Using the Han-MHC reference dataset of the Chinese Han population, IgG4-RD genotyping data were imputed for the human leukocyte antigen (HLA) locus. Additionally, the study assessed the association between genetic variants and clinical characteristics, including disease activity, subtype classification, and relapse.

Results: We identified 22 single nucleotide polymorphisms (SNPs) that surpassed genome-wide significance thresholds ($P < 5E-08$) and replicated consistently across both cohorts, defining 16 distinct genetic susceptibility loci. The strongest signal mapped to chromosome 6 in the extended major histocompatibility complex region. Notably, chromosome 1 harboured significant loci involving immune-related genes such as the FC-γ receptor gene family. Fine mapping identified 6 independent HLA alleles, 2 amino acid mutations, and SNP rs3888777 as independent significant signals. Genetic variants were significantly associated with clinical manifestations such as serum immunoglobulin G4 levels, extent and pattern of organ involvement, clinical subtypes, and relapse risk. Furthermore, meta-analysis integrating Japanese cohort data confirmed known loci and revealed novel susceptibility variants.

Conclusions: This study identified multiple susceptibility loci for IgG4-RD, uncovering novel genetic variants closely linked to clinical features and disease prognosis. These findings provide valuable genomic insights, advancing the understanding of IgG4-RD pathogenesis.

WHAT IS ALREADY KNOWN ON THIS TOPIC

- Before this study, we thoroughly examined existing literature on IgG4-related disease (IgG4-RD), focusing on genetic studies. We conducted searches in databases like PubMed and Web of Science, not limited to English-language publications, up to December 2023. Search terms included 'IgG4-RD', 'genetics', 'GWAS', and 'HLA genotyping'. A key earlier study of 850 Japanese patients identified human leukocyte antigen DR beta 1 (HLA-DRB1) and *FC-γ receptor IIb* (*FCGR2B*) as potential susceptibility loci for IgG4-RD but faced limitations due to ethnic specificity.

WHAT THIS STUDY ADDS

- Our study represents a significant advancement over previous research by analysing a larger and ethnically distinct cohort consisting of 1161 Chinese Han patients with IgG4-RD and 15,299 healthy controls. This comprehensive analysis enabled the identification of multiple novel susceptibility loci, including crucial genetic markers such as the extended major histocompatibility complex region, *FCGR2B/FCRLA/FCGR3A/FCGR3B* gene cluster, and *transmembrane phosphatase with tensin homology 2* locus, significantly associated with disease prognosis and clinical features.

HOW THIS STUDY MIGHT AFFECT RESEARCH, PRACTICE OR POLICY

- When integrated with previous studies, our results reinforce the significance of conducting population-specific genetic investigations in IgG4-RD. The discovery of distinct genetic variants linked to clinical outcomes and prognosis in the Chinese Han population underscores opportunities for developing precision medicine approaches, highlighting the critical role that genome-wide association study plays in unravelling the genetic complexity underlying autoimmune diseases such as IgG4-RD.

INTRODUCTION

IgG4-related disease (IgG4-RD) is a chronic immune-mediated fibrotic disorder with a progressive course, affecting various organs throughout the body [1,2]. It often presents as tumour-like masses in affected organs with elevated serum immunoglobulin G4 (IgG4) levels. Pathological features include dense lymphoplasmacytic infiltration, predominantly IgG4+ plasma cells, and storiform fibrosis—an irregular, whorled pattern of fibrosis [3,4]. IgG4-RD primarily affects males, typically between 40 and 70 years of age [5]. Epidemiological studies report its prevalence at 1.39 to 3.1 per 100,000 individuals, with potential ethnic and geographic differences [6,7].

The aetiology and pathogenesis of IgG4-RD remain poorly understood. Evidence suggests an autoimmune basis, including the accumulation of hyperreactive T and B cells in affected tissues [8], antigen-driven interactions, secretion of profibrotic molecules, and the identification of potential autoantibodies such as anti-Laminin 511, anti-Galectin-3, and anti-Annexin A11 [9–11]. Genetic factors also play a significant role in autoimmune diseases [12]. A family study of IgG4-RD identified a heterozygous single-base deletion in fibroblast growth factor binding protein type 2, leading to a frameshift mutation [13]. Additionally, studies on human leukocyte antigen (HLA) polymorphisms revealed a significant association between the substitution of aspartic acid at position 57 in DQB1 with a nonaspartic acid residue and the relapse of autoimmune pancreatitis (AIP) [14].

Genome-wide association studies (GWASs) are a key method for identifying genetic factors underlying complex diseases [15]. A previous GWAS involving 850 Japanese patients with IgG4-RD highlighted the *Human leukocyte antigen DR beta 1* (*HLA-DRB1)* and *FC-γ receptor IIb* (*FCGR2B*) regions as potential susceptibility loci, emphasising the genetic basis of the disease [16]. However, this study was limited by potential ethnic variations and might not fully capture the genetic landscape of IgG4-

RD. To address this, we conducted the first GWAS on IgG4-RD in the Chinese Han population, aiming to uncover susceptibility genes and provide deeper insights into the genetic mechanisms of IgG4-RD in this demographic.

METHODS

Study population

This study included genome-wide genotyped data from 1161 patients with IgG4-RD and 10,539 healthy individuals from 2 GWAS cohorts in a Chinese population. IgG4-RD diagnosis was based on the 2019 American College of Rheumatology/European League Against Rheumatism classification criteria [17] and/or the 2020 Revised Comprehensive Diagnostic Criteria for IgG4-RD [18]. The study adhered to the Declaration of Helsinki guidelines and was approved by the Institutional Review Committee of Peking Union Medical College Hospital (ZS-3193). Written informed consent was obtained from all participants.

Genotyping, quality control, and imputation

We genotyped 743,722 single nucleotide polymorphisms (SNPs) in 1161 patients with IgG4-RD and 10,539 healthy individuals using the Illumina Asian Screening Array. To improve GWAS resolution, genome-wide genotype imputation was performed using the 1000 Genomes Project (phase 3, version 5) as the reference panel. Imputation for the extended major histocompatibility complex (MHC) region (chromosome 6, 29-34 Mb), covering SNPs, classical HLA alleles, and amino acid variants, was conducted using SNP2HLA, as previously described [19], with reference panels derived from a Han-MHC database [20]. Detailed quality control (QC) and imputation methods are provided in the Supplementary Appendix (p. 2).

Clinical subtypes of IgG4-RD

Basic clinical data of patients were collected at enrolment, with detailed data available in the Supplementary Appendix (p. 2). Enrolled patients with IgG4-RD were classified into clinical subtypes based on organ involvement [21]: (1) proliferative subtype: involvement of proliferative organs, including lacrimal gland, submandibular gland, parotid gland, pancreas, bile duct, kidney, lung, pituitary gland, paranasal sinus, and lymph nodes; (2) fibrotic subtype: involvement of fibrotic organs, including retroperitoneum, aortitis/periarteritis, mesentery, mediastinum, endocranium, and thyroid gland; (3) mixed subtype: involvement of both proliferative and fibrotic organs.

Disease activity and relapse

IgG4-RD activity was assessed at each visit using the IgG4-RD Responder Index (RI) score [22]. Disease relapse was defined as the recurrence, exacerbation, or new onset in the affected organs, including the changes in symptoms or image findings [23]. Prognostic analysis was conducted for patients with a follow-up period of 12 months or longer.

Statistical analysis

The genome-wide significance was established at a P value ≤5.E-08. Quantile-quantile (QQ) plots and Manhattan plots for GWAS results were generated using R 4.2.1 with the CMplot and ggplot2 packages. Logistic regression was used for case-control association analysis, and the genomic inflation factor (λ) was calculated to evaluate population stratification. Principal component analysis (PCA) was performed to characterise population structure, selecting 20 principal components (PCs) to mitigate confounding effects from population stratification. Sex and the top 10 PCs were included as covariates in the association analysis. To reduce redundancy and enhance efficiency, linkage disequilibrium pruning was conducted before GWAS using PLINK (v1.9). Highly correlated SNPs were removed through independent pairwise analysis with a 50 kb window, a step size of 5 variants, and $r^2 > 0.2$. This approach reduced dataset dimensionality while preserving genetic diversity, enabling more efficient and reliable analyses. As the 2 cohorts were genotyped separately, a meta-analysis was performed using the inverse-variance fixed-effects method in PLINK v1.09 to combine results. Heterogeneity was assessed using Cochran's Q test and the I^2 statistic, excluding SNPs with $I^2 > 30$ from further analysis. To ensure consistency and minimise imputation biases, a combined GWAS using unimputed chip data was conducted to validate significant SNPs. This method enhanced reliability, increased statistical power by pooling data from both cohorts, and validated imputed results against directly observed data, reducing spurious associations and strengthening signal robustness. Logistic regression models in PLINK software were employed for stepwise regression analysis, assuming an additive model for each locus. Summary-level statistics from a Japanese dataset were integrated using fixed-effects meta-analysis. Associations between variants and clinical characteristics were analysed using linear regression or Chi-square tests in SPSS 25.0. Kaplan-Meier curves and log-rank tests were employed to compare relapse rates among patients with different genotypes.

Patient and public involvement

There was no patient or public involvement in this study.

RESULTS

Subjects' enrolment and GWAS design

As depicted in Figure 1, after genotyping and QC, the analysis ultimately included 1115 patients with IgG4-RD, 10,154 healthy controls (HCs), and 8,067,112 genetic variants, composed of 2 independent cohorts: cohort 1 with 372 patients with IgG4-RD and 3385 HCs, and cohort 2 with 743 patients with IgG4-RD and 6769 HCs. The baseline clinical characteristics of both patients with IgG4-RD and HCs are detailed in Supplementary Table S1. PCA of the GWAS showed no significant population stratification between patients with IgG4-RD and HCs, as illustrated in Supplementary Figure S1. The λ was calculated separately for each cohort, yielding values of 1.018 for cohort 1 and 1.019 for cohort 2, as presented in Supplementary Figure S2A. The QQ plots for cohort 1 and cohort 2 demonstrated an enrichment of SNP P values deviating from the expected distribution under the null hypothesis, reflecting a consistent pattern across both cohorts.

GWAS identified the significant loci for IgG4-RD

As shown in Supplementary Figure S2, 44 SNPs reached genome-wide significance ($P < 5E-08$) in cohort 1, while 122 SNPs met this threshold in cohort 2. A total of 22 SNPs achieved significance in both cohorts and were considered potential susceptibility loci. These 22 SNPs were then subjected to meta-

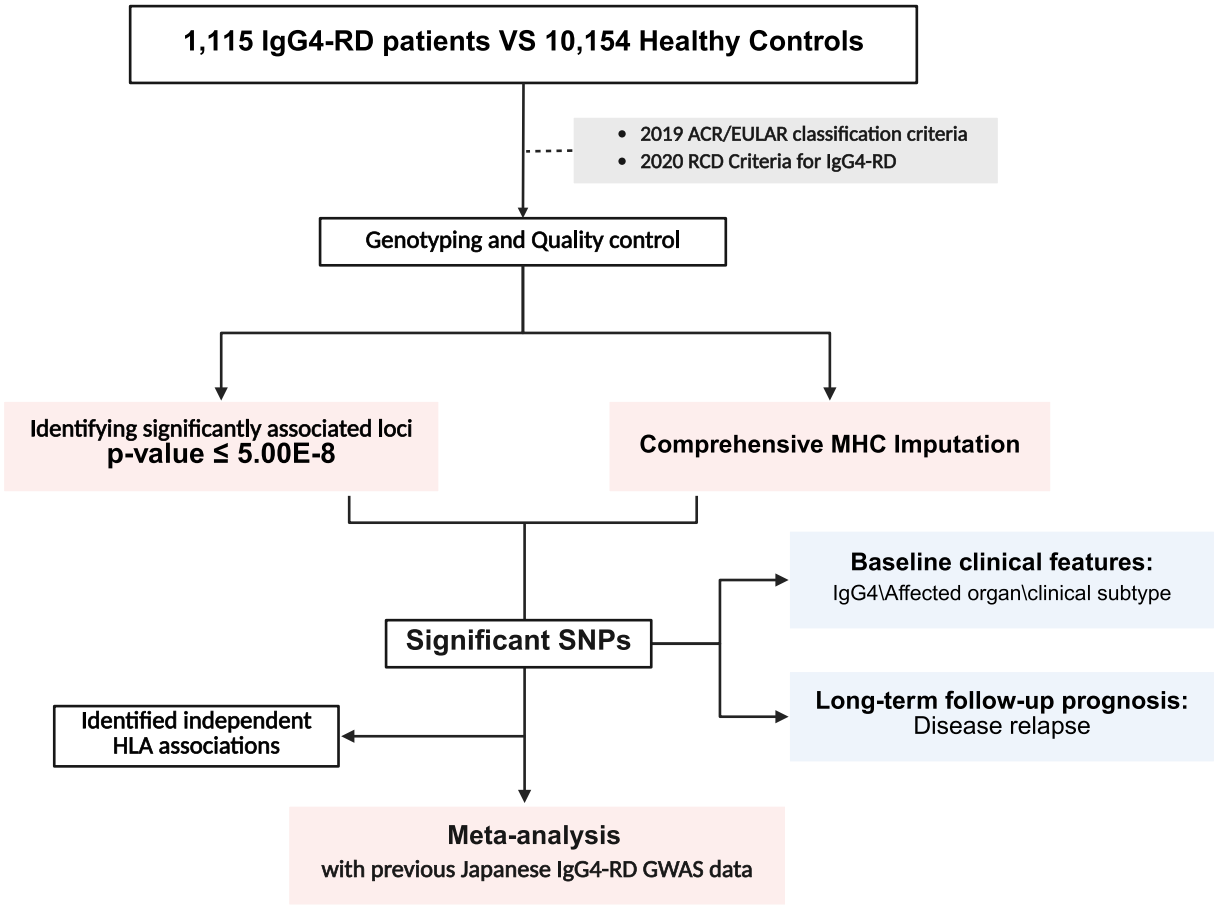

Figure 1. The workflow diagram of this study. ACR/EULAR, American College of Rheumatology/European League Against Rheumatism; GWAS, genome-wide association study; HLA, human leukocyte antigen; IgG4, immunoglobulin G4; IgG4-RD, IgG4-related disease; MHC, major histocompatibility complex; RCD, revised comprehensive diagnostic; SNP, single nucleotide polymorphism.

analysis, with the results presented in Supplementary Table S2. As shown in Table 1, these signals consolidated into 16 distinct genomic loci, implicating candidate susceptibility genes for IgG4-RD.

Notably, 4 loci were mapped to chromosome 1, highlighting regions encompassing immune-relevant genes such as *NBPF1*, *NBPF12*, and the immunoglobulin receptor family *FCGR3A/FCGR3B*. The strongest genome-wide association signal localised

Table 1
Summary of significant loci identified in the GWAS using imputed genotype data

CHR	BP	SNP	Nearest gene	A1/A2	Meta-analysis		
					P value	OR	95% CI
1	16,869,900	rs390042	NBPF1	G/A	1.03E-29	1.69	1.54-1.85
1	146,542,208	rs636329	NBPF12	T/G	3.27E-25	0.59	0.53-0.65
1	161,590,743	rs35181127	FCGR3A/FCGR3B	G/A	4.30E-19	1.49	1.37-1.63
1	207,371,824	rs117561933	LOC107985251	T/G	2.55E-39	3.22	2.7-3.84
2	114,123,517	rs113257032	LINC02966	T/C	1.32E-36	1.93	1.74-2.14
6	30,529,816	rs3888777	PRR3	A/G	2.67E-96	3.44	3.06-3.86
6	32,568,967	rs9270772	HLA	T/C	2.16E-32	1.70	1.56-1.86
7	6,947,285	rs7802039	CCZ1B/C1GALT1	T/A	1.58E-85	3.42	3.03-3.87
7	63,349,473	rs4717156	LOC124901654	G/T	2.40E-21	1.71	1.55-1.86
7	76,726,994	rs2537431	FAM185BP	G/C	2.58E-65	2.89	2.56-3.26
9	104,419,918	rs57235233	GRIN3A	A/G	1.96E-34	3.78	3.06-4.68
11	59,249,312	rs1453536	OR4D10/OR4D11	T/C	1.24E-44	2.10	1.89-2.33
13	20,091,685	rs150048756	TPTE2	A/G	5.51E-80	8.67	6.93-10.84
13	111,619,632	rs9559915	LINC00431	T/C	1.73E-10	1.33	1.22-1.45
14	47,402,789	rs73237216	MDGA2	A/T	3.82E-38	5.41	4.18-6.98
20	46,612,538	rs6066576	LINC01522	T/A	7.69E-29	2.03	1.82-2.24

A1, minor allele; A2, major allele; BP, base pair position; CHR, chromosome; F_A, minor allele frequency in cases; F_U, minor allele frequency in controls; GWAS, genome-wide association study; HLA, human leukocyte antigen; OR, odds ratio; SNP, single nucleotide polymorphism.
BP position based on build hg19.

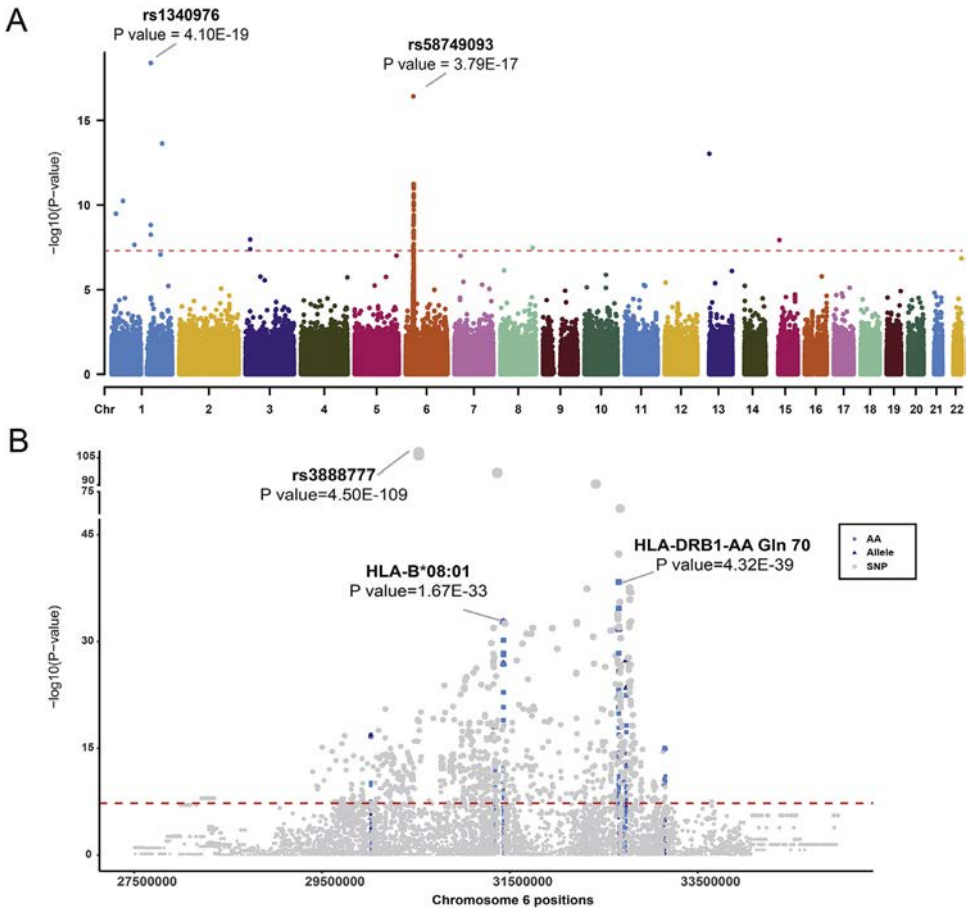

Figure 2. Association analysis of patients with IgG4-related disease. (A) Manhattan plot of the genome-wide association study. (B) Association signals in the MHC region. The plots display variants with their genomic position on the x-axis and the strength of association on the y-axis. The red horizontal line represents genome-wide significance (P = 5E-08). GWAS, genome-wide association study; HLA, human leukocyte antigen; HLA-DRB1, human leukocyte antigen DR beta 1; IgG4, immunoglobulin G4; MHC, major histocompatibility complex; SNP, single nucleotide polymorphism.

to chromosome 6 in the extended MHC region (rs3888777, *PRR3*; odds ratio [OR] = 3.44, P = 2.67E-96), accompanied by an independent secondary signal near the HLA region (rs9270772). Three loci on chromosome 7 were identified, involving *CCZ1B/C1GALT1* (rs7802039), *FAM185BP* (rs2537431), and *LOC124901654* (rs4717156). Additional genome-wide significant associations were detected on chromosomes 2 (*LINC02966*), 9 (*GRIN3A*), 11 (*OR4D10/OR4D11*), 13 (*TPTE2* and *LINC00431*), 14 (*MDGA2*), and 20 (*LINC01522*).

To further validate the findings and minimise potential biases introduced by imputation, we conducted a combined analysis using unimputed chip genotype data from both cohorts. This direct analysis provided robust confirmation of the associations identified in the imputed dataset. As shown in Figure 2A, the combined GWAS with unimputed genotype data identified 66 SNPs reaching genome-wide significance (P < 5E-08), including 54 SNPs within the MHC region on chromosome 6 (Supplementary Table S3) and 12 SNPs on nonchromosome 6 loci (Table 2), distributed across 9

Table 2
Summary of nonchromosome 6 significant loci identified in the combined GWAS with unimputed genotype data

CHR	BP	SNP	Nearest gene	A1/A2	F_A	F_U	*P* value	OR	95% CI
1	161,661,489	rs1340976	FCGR2B/FCRLA	C/A	0.601	0.486	4.10E-19	1.65	1.48-1.85
1	207,929,340	rs11118516	CD46	A/G	0.3712	0.2613	2.37E-14	1.55	1.39-1.74
1	47,611,598	rs2405599	CYP4A22	T/C	0.3294	0.4035	5.75E-11	0.68	0.61-0.76
1	18,464,526	rs74428983	IGSF21	A/C	0.1094	0.06945	3.29E-10	1.77	1.48-2.12
1	161,656,631	rs56402041	FCGR2B/FCRLA	A/G	0.1384	0.1959	1.52E-09	0.63	0.54-0.73
1	161,669,427	rs12078337	FCGR2B/FCRLA	C/A	0.1343	0.1923	5.73E-09	0.64	0.55-0.74
1	94,449,342	rs28555322	ABCA4/GCLM	C/T	0.2327	0.1656	2.24E-08	1.44	1.26-1.63
3	18,784,423	rs6809854	STAB1/KCNH8	G/A	0.1655	0.1102	1.11E-08	1.55	1.33-1.80
3	18,812,072	rs7644430	STAB1/KCNH8	G/A	0.1668	0.1115	4.06E-08	1.52	1.31-1.77
8	131,954,652	rs12334868	ADCY8	C/T	0.3593	0.2786	3.37E-08	1.37	1.22-1.53
13	20,119,312	rs9508453	TPTE2	A/C	0.1802	0.09227	9.41E-14	1.85	1.58-2.18
15	27,180,915	rs11263708	GABRA5	C/T	0.4144	0.4707	1.19E-08	0.73	0.66-0.82

A1, minor allele; A2, major allele; BP, base pair position; CHR, chromosome; F_A, minor allele frequency in cases; F_U, minor allele frequency in controls; FCGR2B, FC-γ receptor IIb; GWAS, genome-wide association study; OR, odds ratio; SNP, single nucleotide polymorphism.
BP position based on build hg19.

Table 3
Independent HLA association results after the sequential conditional analysis

CHR	SNP	BP	A1/A2	F_A	F_U	OR	95% CI	*P* value	Conditioned *P* value
6	HLA-B*08:01	31,431,272	P/A	0.03549	0.007887	4.63	3.52-6.08	1.67E-33	
6	HLA-DRB1*09:01	32,660,042	P/A	0.06559	0.1606	0.37	0.31-0.44	1.62E-32	2.10E-27
6	HLA-DQB1*06:02	32,739,039	P/A	0.1473	0.08277	1.92	1.69-2.18	3.30E-24	3.42E-17
6	HLA-B*46:01	31,431,272	P/A	0.04672	0.1251	0.34	0.28-0.42	1.11E-27	5.40E-12
6	HLA-B*40:01	31,431,272	P/A	0.06424	0.1091	0.56	0.47-0.67	5.10E-11	1.08E-10
6	HLA-DRB1*04	32,660,042	P/A	0.1631	0.1156	1.49	1.32-1.68	6.64E-11	7.17E-10
6	HLA-DRB1-AA Gln 70	32,659,938	P/A	0.4645	0.3262	1.79	1.64-1.96	4.32E-39	–
6	HLA-B-AA Ser 24	31,432,644	P/A	0.2471	0.1521	1.83	1.65-2.03	6.30E-31	8.33E-23
6	rs3888777	30,529,816	A/G	0.2077	0.06988	3.49	3.11-3.92	4.50E-109	–

A, absent; A1, minor allele; A2, major allele; BP, base pair position; CHR, chromosome; F_A, minor allele frequency in cases; F_U, minor allele frequency in controls; HLA, human leukocyte antigen; HLA-DRB1, human leukocyte antigen DR beta 1; HLA-DQB1, human leukocyte antigen DQ beta 1; OR, odds ratio; P, present; SNP, single nucleotide polymorphism.
BP position based on build hg19. Sequential conditional association analyses were performed separately for each variant type.

genomic loci. Among the nonchromosome 6 SNPs, rs1340976, located between the *FCGR2B* and *FCRLA* genes, showed the strongest association (P = 4.10E-19, OR = 1.65).

Importantly, 2 genomic loci—*FCGR2B/FCRLA/FCGR3A/FCGR3B* on chromosome 1 and *TPTE2* on chromosome 13—were consistently replicated in both the imputed and unimputed genotype analyses, underscoring their robust association with IgG4-RD susceptibility and further highlighting their biological relevance.

Fine mapping identified independent HLA associations

Given the critical role of the MHC region in the immune system and autoimmunity, a specialised fine mapping imputation was conducted for the MHC region. After imputation and QC of the MHC region in the GWAS data, a total of 182 HLA alleles, 897 AA, and 9921 SNP loci were included for further analysis (Fig 2B). Among them, 1285 MHC region loci reached genome-wide significance (P < 5E-08), including 28 alleles, 178 AA mutations, and 1079 SNPs.

Twenty-eight HLA alleles were found to be significantly associated with IgG4-RD (P < 5E-08). After stepwise conditional analysis, 6 independent allele signals were observed (Table 3). Among them, the strongest association was observed with *HLA-B*08:01* (P = 1.67E-33, OR = 4.63). Further stepwise conditional analysis revealed 5 additional independent significant allele associations.

One hundred seventy-eight amino acid mutations significantly associated with IgG4-RD have been found (P < 5E-08). The most significant amino acid residue signal was HLA-DRB1-AA Gln 70 (P = 4.32E-39, OR = 1.79). Stepwise conditional analysis identified 1 additional significant independent amino acid position (HLA-B-AA Ser 24, P = 6.30E-31, OR = 1.83). rs3888777 (*PRR3*) was found to be the sole independent SNP locus within the MHC region after imputation (OR = 3.49), and it exhibited the highest statistical significance (P = 4.50E-109).

Genetic loci linked to IgG4-RD clinical features and prognosis

We subsequently explored the potential clinical implications of the significant genetic variants. Linear regression analysis revealed that 4 SNPs, rs35139848, rs2125685, rs56402041, and rs12078337, were significantly associated with serum IgG4 levels, showing a negative correlation (Supplementary Fig S3A-D). In contrast, rs1340976 demonstrated a strong positive association with IgG4 levels, with each additional C-allele corresponding to a stepwise increase in serum concentration (P < .0001, Fig 3A). Furthermore, 20 genetic signals were linked to the number of affected organs (Fig 3B-I, Supplementary Fig S3E-P). Among these, independent signals such as rs3888777, rs113257032, rs7802039, rs1453536, and rs150048756 showed robust positive correlations (P < .0001), while rs13227207 was significantly associated with a lower number of affected organs.

Patients were classified into proliferative, fibrotic, and mixed subtypes based on organ involvement. Comparative analysis revealed associations between multiple SNPs and clinical subtypes. Allelic distributions varied across proliferative, fibrotic, and mixed phenotypes. Notably, several variants showed higher frequencies in the mixed subtype, including rs113257032 (70.4%, P = .0035, Supplementary Fig S4A), rs7802039 (56.8%, P = .011, Supplementary Fig S4B), rs4717156 (77.8%, P = .018, Supplementary Fig S4C), rs3888777 (63%, P = .011, Supplementary Fig S4D), and rs2537431 (53.1%, P = .037, Supplementary Fig S4F), highlighting their role in more diverse clinical presentations. Conversely, variants such as rs636329 (39.1%, P = .00035, Supplementary Fig S4G), rs3011806 (39.1%, P = .0008, Supplementary Fig S4E), and HLA-DQB1*06:02 (42.2%, P = .014, Supplementary Fig S4H) were enriched in the fibrotic subtype than in the proliferative and mixed subtypes. Kaplan-Meier survival analysis identified 4 variants significantly associated with relapse risk during follow-up (Fig 4). In a subset of follow-up patients, rs10231721 (P = .033, hazard ratios [HRs] = 0.5917, Fig 4B), rs35181127 (P = .047, HR = 0.724, Fig 4C), and rs113257032 (P = .02, HR = 0.6947, Fig 4D) were significantly associated with a reduced risk of disease relapse. Patients carrying these alleles exhibited a lower likelihood of disease relapse during long-term follow-up. Conversely, the *HLA-DRB1*09:01* allele was significantly associated with an increased relapse risk (P = .031, HR = 1.597, Fig 4A), highlighting its potential utility as a genetic marker for identifying patients at higher risk of disease recurrence.

GWAS meta-analysis identified the significant loci for IgG4-RD

Given the previous GWAS study on IgG4-RD published by a Japanese research team [16], we further conducted a meta-analysis of the summary-level statistics they provided. The meta-analysis results identified a total of 25 significant SNPs, some of which had not been reported in the previous Japanese study (Supplementary Table S4), yielding novel associations that did

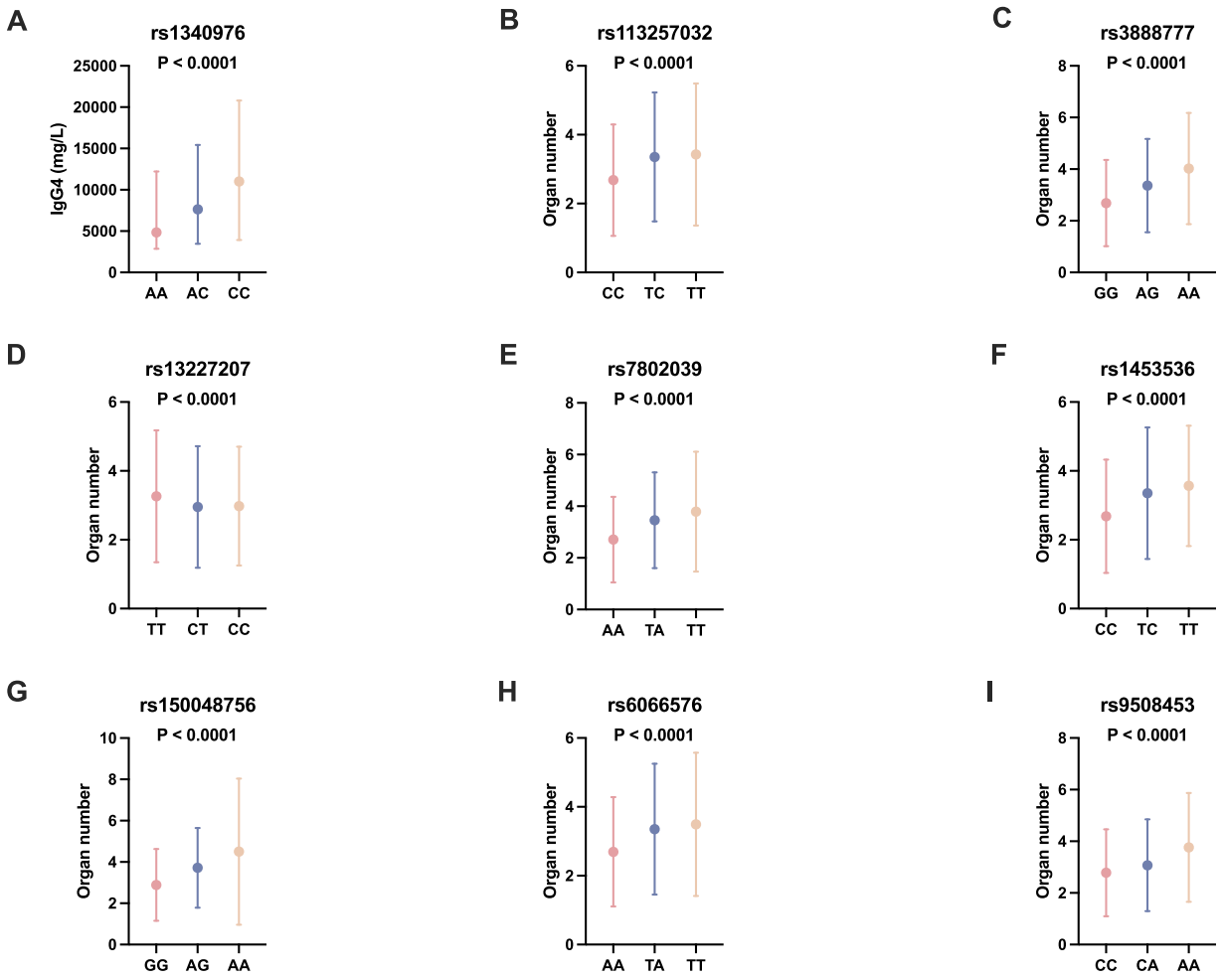

Figure 3. Correlation analysis between clinical characteristics and sentinel genotypes. (A) Serum IgG4 concentration stratified by rs1340976 genotype (AA, AC, CC). (B-I) Number of affected organs plotted against genotype for 8 risk variants-mrs13227207, rs150048756, rs113257032, rs7802039, rs6066576, rs3888777, rs1453536, and rs9508453 ($P < .0001$). IgG4, immunoglobulin G4.

not reach genome-wide significance in either cohort alone. Notably, our meta-analysis also confirmed rs28371251 as the most significant MHC imputed SNP and rs1340976 as the most significant nonchromosomal SNP, highlighting its potential importance.

DISCUSSION

To explore the potential genetic variants for IgG4-RD, we conducted the first GWAS study on patients with IgG4-RD in the Chinese Han population, including 1161 patients with IgG4-RD and 10,539 HCs. We identified 22 genome-wide significant SNPs mapping to 16 independent loci.

The most prominent signal resided in the MHC region on chromosome 6p, with the lead SNP rs3888777 (within the MHC) showing the strongest association. Notably, rs3888777 is located within the coding region of *PRR3* but represents a synonymous variant, meaning it does not alter the amino acid residue. Although synonymous mutations do not change the protein sequence directly, accumulating evidence indicates they may influence gene expression or function via mechanisms such as altered mRNA stability, translational efficiency, or alternative splicing. Such alterations could substantially affect *PRR3* mRNA splicing patterns, potentially influencing isoform expression or nearby gene regulatory networks. This finding reinforces the pivotal role of HLA genes in IgG4-RD susceptibility, consistent with earlier studies in Japan that first implicated the *HLA-DRB1* locus as a primary genetic risk factor [16]. In fact, our fine mapping of the MHC region revealed multiple independent risk factors: 6 specific HLA alleles, 2 amino acid polymorphisms, and the SNP rs3888777, all contributing independently to disease risk. The involvement of *HLA-DRB1* (class II) and *HLA-B* (class I) alleles indicates that both CD4 T-cell (HLA class II-restricted) and CD8 T-cell or natural killer (NK) cell (HLA class I-restricted) immune responses may be driving IgG4-RD pathogenesis. Notably, previous HLA candidate studies have similarly pointed to class II alleles (eg, the *HLA-DRB1*0405-DQB1*0401* haplotype in AIP) as risk factors, supporting the notion that antigen presentation is a critical element in this disease [24]. Our data extend those observations by also implicating class I HLA variation (HLA-B-AA Ser 24), suggesting that antigen presentation to CD8 cytotoxic T cells or interactions with innate lymphocytes (via HLA-B) could also contribute to IgG4-RD—a new insight that earlier GWAS in the Japanese population, which primarily highlighted *HLA-DRB1*, had not reported.

In our IgG4-RD cohort, *HLA-B*08:01* emerged as the most significant association, consistent with its involvement in a broad autoimmune spectrum including the idiopathic inflammatory myopathies (notably antisynthetase syndrome) [25] and systemic lupus erythematosus [26]. We also detected independent protective effects for *HLA-B*46:01* and *HLA-B*40:01*, paralleling prior observations that *HLA-B*46:01* confers resistance to type 1 diabetes and latent autoimmune diabetes in Asian populations [27], while *HLA-B*40:01* is protective in autoimmune

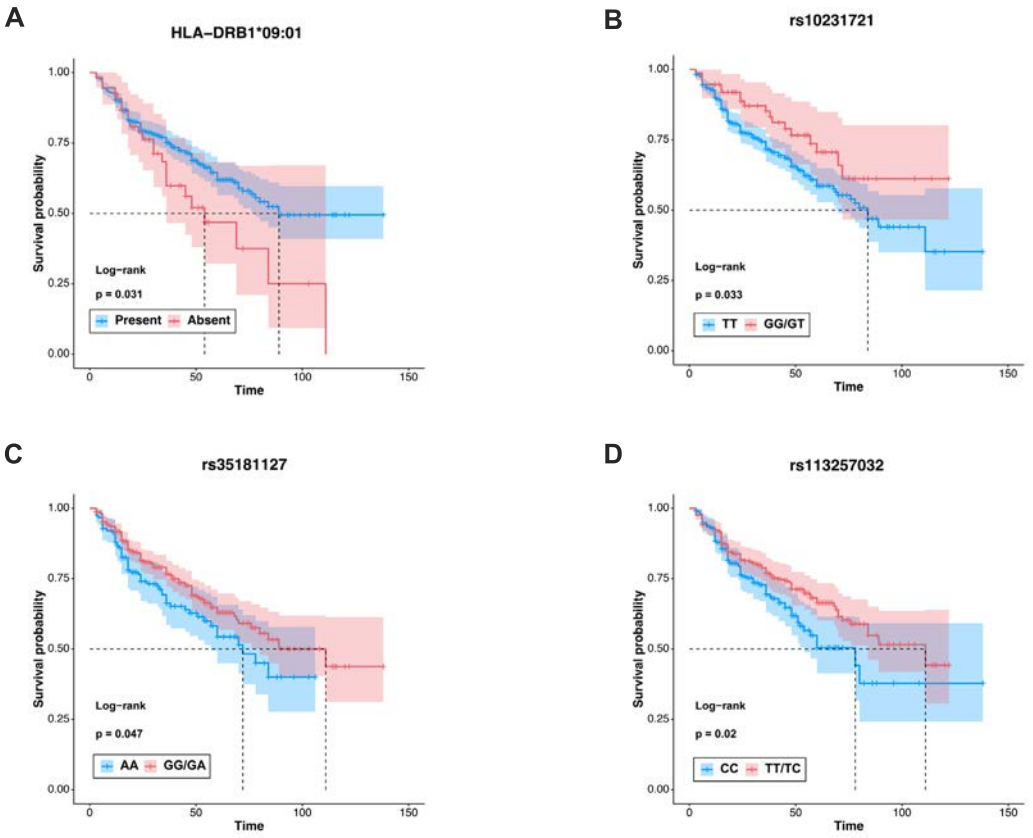

Figure 4. Genotype-specific risk of disease relapse. (A) HLA-DRB1*09:01; (B) rs10231721; (C) rs35181127; (D) rs113257032. Hazard ratios (HRs) and *P* values were derived from Cox proportional-hazards models, $P < .05$ denotes statistical significance. HLA-DRB1, major histocompatibility complex, class II, DR beta 1.

hepatitis [28]. After conditioning on these signals, an additional association was uncovered at *HLA-DRB1*09:01*; this allele has been implicated in IgG4-RD by a Japanese GWAS and is a known risk factor across multiple autoimmune diseases—eg, mixed connective tissue disease [29], type 1 diabetes [30], and rheumatoid arthritis [31]. Finally, *HLA-DRB1*04* was identified as an independent risk allele for IgG4-RD, in line with the role of certain 04 subtypes as disease-predisposing variants [32]. Taken together, these findings underscore the complex genetic architecture of IgG4-RD and highlight how key HLA susceptibility and protective alleles intersect with the broader landscape of autoimmunity, offering insight into shared and population-dependent genetic drivers of autoimmune disease.

In addition to the MHC locus, we confirmed and broadened the association at the fragment crystallizable region of IgG (Fc) gamma receptor gene cluster on chromosome 1q23. This locus, encompassing *FCGR2B*, *FCRLA*, *FCGR3A*, and *FCGR3B*, was strongly associated with IgG4-RD risk in our study. The involvement of *FCGR2B* is especially noteworthy, as it was 1 of only 2 loci identified in the first GWAS of IgG4-RD (in Japanese patients) [16]. We replicated the *FCGR2B* signal and further showed that it likely represents a broader haplotype of risk in the Fc receptor region, possibly including neighbouring immunoregulatory genes (*FCRLA* encodes an intracellular Fc receptor-like protein in B cells, and *FCGR3A/3B* encode activating Fcγ receptors on NK cells and neutrophils). Intriguingly, the specific *FCGR2B*-linked SNP first noted in Japanese IgG4-RD, rs1340976 has been shown to increase the expression of the inhibitory Fcγ receptor IIb. This is somewhat counterintuitive, as higher *FCGR2B* expression typically dampens B-cell and immune cell activation [33,34]. However, such observation aligns well with the unique T helper type 2 (Th2)-dominant and immunoregulatory milieu characteristic of IgG4-RD. It is known that IL-4, a cytokine essential for IgG4 class switching, also strongly upregulates Fc gamma receptor IIb (FcγRIIB) expression on B cells, suggesting a potential feedback loop wherein elevated Th2 cytokines (eg, IL-4, IL-13) further amplify FcγRIIB-mediated modulation of B-cell responses [33,35]. Although Fc receptors, including FcγRIIB, do not directly drive Ig class switching to IgG4, they can indirectly shape antibody subclass distributions by modulating B-cell activation thresholds and clone selection during germinal centre reactions [36,37]. Elevated FcγRIIB expression could raise the activation threshold of B cells, thereby restricting responses to those clones receiving robust regulatory cytokine signals, including IL-4 and IL-10. Such a scenario would preferentially promote IgG4 class switching, which occurs in environments characterised by repeated antigen exposure and strong regulatory (tolerogenic) signalling [38]. Furthermore, IgG4 immune complexes have been reported to interact with FcγRIIB on macrophages to induce IL-10 production, subsequently fostering further IgG4 production in a positive regulatory loop [39]. The observed association between the rs1340976 risk allele and elevated serum IgG4 levels further supports its indirect but meaningful contribution to sustained Th2 cytokine-dependent class switching towards IgG4. Importantly, this pattern contrasts with autoimmune conditions such as systemic lupus erythematosus, in which a coding variant in *FCGR2B* that reduces its inhibitory function (Ile232Thr, rs1050501) confers increased disease risk characterised by pathogenic IgG1 and IgG3 autoantibodies [34]. Thus, the association of IgG4-RD susceptibility with a gain-of-expression *FCGR2B* variant suggests a distinct immune-regulatory imbalance in IgG4-

RD pathogenesis compared to classical autoimmune diseases. Nonetheless, our findings firmly establish the *FCGR2B/FCGR* region as a key susceptibility locus, reinforcing earlier reports that *FCGR2B* plays an important role in IgG4-RD development.

Beyond HLA and Fc receptor genes, our GWAS identified several novel risk loci for IgG4-RD. One highlighted locus is on chromosome 13 at *Transmembrane Phosphoinositide 3-Phosphatase And Tensin Homolog 2* (*TPTE2*), which, to our knowledge, has not been previously implicated in IgG4-RD or autoimmunity. *TPTE2* encodes a membrane-associated phosphatidylinositol-3 phosphatase related to the Phosphatase and tensin homolog (PTEN) family, potentially involved in cell signalling [40]. Although its immunological function is unclear, its genome-wide significant association in both our imputed analysis and validation with unimputed genotypes suggests *TPTE2* could represent a novel pathway contributing to IgG4-RD risk. This discovery expands the spectrum of genetic contributors beyond the classical immune genes, and future studies will be needed to unravel how variants in *TPTE2* might influence immune or fibrotic processes in this disease.

Importantly, all the key loci we identified—including the MHC region, the *FCGR2B/FCRLA/FCGR3A/3B* cluster, and *TPTE2*—were corroborated in analyses of both imputed data and unimputed (directly genotyped) data. This consistency underlines the robustness of our associations and reduces concerns that imputation artefacts might have driven our top signals. We further bolstered confidence in these findings by conducting a meta-analysis that incorporated data from the prior Japanese GWAS. The meta-analysis confirmed the known loci (*HLA-DRB1* and *FCGR2B*) and improved our power to detect additional signals, yielding novel associations that did not reach genome-wide significance in either cohort alone. This trans-ethnic approach demonstrates that many IgG4-RD risk variants are shared across East Asian populations, while also enabling the discovery of subtler effects. For example, some suggestive loci in our Chinese Han cohort became significant upon combining with the Japanese data, emphasising common genetic architecture. At the same time, any differences observed between Chinese and Japanese results may point to ethnic-specific effects or differences in allele frequencies—an aspect that will require further investigation in diverse populations.

Our results align well with, and significantly extend, previous research on IgG4-RD genetics. Before this study, genetic insights into IgG4-RD were limited to 1 moderate-sized GWAS and a handful of candidate-gene studies. The Japanese GWAS (857 cases, 2082 controls) had pinpointed HLA-DRB1 and *FCGR2B* as risk loci, which we now validate in a larger cohort with genome-wide significance. Smaller studies had suggested other risk candidates, such as *FCRL3* [41] and *CTLA4* [42], *KCNA3* [43], and *IL1R1* [44]. Some of these candidates overlap with or lie near the loci detected in our GWAS. While our study did not find genome-wide significance for every previously reported candidate, the overall convergence on immune pathways (T-cell regulation via CTLA4, B-cell regulation via FCRL/FCGR, innate cytokine signalling via IL1R1, etc) underscores a common theme. Notably, our fine mapping of the MHC region revealed that *HLA-DRB1*09:01* and HLA-DRB1-Gln70 independently contribute to IgG4-RD susceptibility. These HLA class II variants were reported to be significantly associated with total immunoglobulin E (IgE) levels [45] and likely contribute Th2/T follicular helper (Tfh) polarisation by shaping antigen presentation to CD4+ T cells, thereby promoting IL-4/IL-13 production—a cytokine milieu directly driving B-cell class switching to IgG4. This mechanism bridges genetic risk with IgG4-RD's hallmark immunopathology. In summary, our comprehensive genetic mapping firmly establishes IgG4-RD as a polygenic immune-mediated disease, with risk alleles clustering in genes related to antigen presentation, B-cell/antibody function, and immune regulation. These discoveries provide important context and confirmation to the groundwork laid by earlier research, while charting new directions by revealing additional novel loci for further study.

An important aspect of our study was the exploration of how genetic variation correlates with clinical heterogeneity in IgG4-RD. We found that several risk alleles not only predispose to disease susceptibility but also influence quantitative traits and subphenotypes of IgG4-RD. For example, genetic variants in the FCGR region showed a significant association with serum IgG4 levels at diagnosis and the number of organs involved by the disease. This was observed previously in Japanese patients. We also observed that certain loci were linked to clinical subtypes of IgG4-RD. In our cohort, patients have been clinically categorised into 'proliferative' vs 'fibrotic' vs 'mixed' disease types based on their presentations. While sample sizes for each subtype analysis were smaller, a few SNPs showed differential association with these subgroups. Though these subtype associations need to be interpreted cautiously, they raise the possibility that the balance of immune cell-mediated inflammation vs fibrosis in IgG4-RD could be partly genetically determined. Supporting this, prior studies have found that IgG4-related periaortitis (a notably fibrotic manifestation) has a unique genetic association with *IL1R1* variants, emphasising that organ-specific fibrosis in IgG4-RD may have a distinct genetic signature [44]. Another clinically relevant genetic correlation we identified was with disease relapse. Our analysis revealed that certain HLA alleles and SNPs were enriched in patients who had recurrent disease flares. Notably, 1 of the HLA class II variants associated with overall susceptibility was also a significant predictor of relapse risk, independent of its effect on susceptibility. This finding resonates with reports in IgG4-related AIP, where specific HLA alleles (eg, HLA-DQB1 and certain class I alleles) were linked to higher relapse rates [46]. For patients with IgG4-RD and clinicians, this could mean that genotyping might one day help identify those who need more aggressive or maintenance therapy to prevent relapse. Similarly, we observed that the FCGR2B risk haplotype (associated with high IgG4 and multiorgan disease) might also predispose to relapse, potentially because such patients have an underlying tendency for persistent B-cell activity even after treatment. This is consistent with clinical observations that patients with higher baseline IgG4 or multiorgan involvement often require more prolonged immunosuppression. The genotype-phenotype analyses in our study reinforce that IgG4-RD's genetic risk factors are not just binary switches for disease vs health, but modulators of disease expression. They influence how severe the disease gets, what pattern it takes, and how it evolves over time. These insights hold promise for personalised medicine: as we validate these associations in larger cohorts, we could integrate genetic profiling into risk stratification. For example, a patient carrying multiple 'severe disease' alleles (certain *HLA* types plus the *FCGR2B* haplotype) might be monitored more closely for relapse or considered for early biologic therapy, whereas a patient lacking those might be managed with a higher expectation of maintaining remission once achieved. That said, these applications are still exploratory—current findings would need to be replicated and built into predictive models before clinical use.

This study has several limitations that highlight future directions of research. Firstly, the sample size of this study was still relatively small, given that IgG4-RD is a rare disease with a low prevalence rate; this was the maximum sample size that could be achieved at the end of this study. Future studies should continue to expand the sample size to validate the conclusions. Secondly, polymorphisms on the sex chromosomes were not analysed in this study. Given that IgG4-RD has a well-documented male predominance, genetic variants on the sex chromosomes may play important roles in disease susceptibility or progression. Future studies should incorporate sex chromosome analyses, employing sex-aware analytical approaches to fully clarify their potential contribution to IgG4-RD pathogenesis. Finally, further functional studies and gene-engineered animal models are required to elucidate the physiological and pathological implications of susceptibility genes in IgG4-RD.

In conclusion, our GWAS of IgG4-RD has substantially deepened the genetic understanding of this complex disorder. We have provided strong evidence linking IgG4-RD to specific immune pathways, notably HLA class I/II antigen presentation and Fc receptor-mediated B-cell regulation, and discovered new candidate genes that broaden the scope of pathogenesis hypotheses. By contextualising our results with previous research, we see a coherent story emerging: genetic predisposition sets the stage for an abnormal immune tolerance response that manifests as IgG4-RD. Our findings highlight the polygenic and immune-mediated nature of IgG4-RD and underscore the potential for these genetic markers to enhance clinical stratification, prognosis, and targeted therapeutic strategies. Future functional validation and broader multiethnic studies will further clarify the pathophysiological mechanisms underlying these genetic associations, providing essential insights towards personalised and precision medicine for patients with IgG4-RD.

Competing interests

The authors declare that they have no known competing financial interests or personal relationships that could have appeared to influence the work reported in this paper.

Acknowledgements

We gratefully acknowledge Peking Union Medical College Hospital, Peking University People's Hospital, Tongji Hospital, Tongji Medical College, Huazhong University of Science and Technology, China-Japan Friendship Hospital, and Tianjin First Central Hospital for their indispensable contributions to this work. These institutions provided critical support in recruiting participants, collecting and processing biospecimens, and curating clinical data. We sincerely thank the clinicians, research nurses, laboratory personnel, and all patients and healthy volunteers whose commitment made this study possible.

Contributors

YL, XZ, and WZ designed and supervised the study. FZ, ML, YF, YL, MW, LP, JZ, CL, LL, HC, SZ, ZL, FF, HL, contributed to samples and data collection. SY, YP, and JX, YY contributed to data analysis and the figures. SY and YP contributed to the writing of the article. All authors revised, reviewed, and edited the manuscript. All authors read and approved the final manuscript. YL, XZ, and WZ are the guarantors for the article, accept full responsibility for the work and the conduct of the study, and had final responsibility for the decision to submit for publication. SY, XZ, and YP directly accessed and verified the underlying data reported in the manuscript.

Funding

This research was supported by grants from the National Key Research and Development Program of China (2024YFA1307604, 2024YFA1307601, 2018YFE0207300, 2022YFC2703104), the National High Level Hospital Clinical Research Funding (2022-PUMCH-B-124, 2022-PUMCH-C-006, 2022-NHLHCRF-LX-02-03, 2023-NHLHCRF-YXHZ-ZRZD-06), National Natural Science Foundation of China (82472348, 82273523, 82271848, 82471829), Beijing Natural Science Foundation (M23008, 7232113), the Nonprofit Central Research Institute Fund of Chinese Academy of Medical Sciences (2019XK320038, 2022-I2M-C&T-B-005), Capital's Funds for Health Improvement and Research (CFH 2020-1-2031, 2022-2-2026), and Tongzhou District Science and Technology Committee (No. KJ2023CX004).

Patient consent for publication

Not applicable.

Ethics approval

The study was approved by the Institutional Review Committee of Peking Union Medical College Hospital (ZS-3193).

Provenance and peer review

Not commissioned; externally peer reviewed.

Data availability statement

The full GWAS summary statistics are provided without restriction in the Supplementary data: cohort 1 (Supplementary data 1), cohort 2 (Supplementary data 2), the meta-analysis of the 2 Chinese cohorts (Supplementary data 3), and the trans-ethnic meta-analysis incorporating the Japanese GWAS (Supplementary data 4).

Declaration of generative AI and AI-assisted technologies in the writing process

During the preparation of this work, the authors used ChatGPT in order to enhance the readability and language quality. After using this tool, the authors reviewed and edited the content as needed and take full responsibility for the content of the published article.

Supplementary materials

Supplementary material associated with this article can be found in the online version at doi:10.1016/j.ard.2025.10.028.

REFERENCES

[1] Umehara H, Okazaki K, Masaki Y, Kawano M, Yamamoto M, Saeki T, et al. A novel clinical entity, IgG4-related disease (IgG4RD): general concept and details. Mod Rheumatol 2012;22(1):1–14 Feb.

[2] Kamisawa T, Zen Y, Pillai S, Stone JH. IgG4-related disease. Lancet 2015;385 (9976):1460–71 Apr 11.

[3] Kamisawa T, Funata N, Hayashi Y, Eishi Y, Koike M, Tsuruta K, et al. A new clinicopathological entity of IgG4-related autoimmune disease. J Gastroenterol 2003;38(10):982–4.
[4] Deshpande V, Zen Y, Chan JK, Yi EE, Sato Y, Yoshino T, et al. Consensus statement on the pathology of IgG4-related disease. Mod Pathol 2012;25 (9):1181–92 Sep.
[5] Beyer G, Schwaiger T, Lerch MM, Mayerle J. IgG4-related disease: a new kid on the block or an old aquaintance? United European Gastroenterol J 2014;2 (3):165–72 Jun.
[6] Masamune A, Kikuta K, Hamada S, Tsuji I, Takeyama Y, Shimosegawa T, et al. Nationwide epidemiological survey of autoimmune pancreatitis in Japan in 2016. J Gastroenterol 2020;55(4):462–70 Apr.
[7] Wallace ZS, Miles G, Smolkina E, Petruski-Ivleva N, Madziva D, Cook C, et al. Incidence, prevalence and mortality of IgG4-related disease in the USA: a claims-based analysis of commercially insured adults. Ann Rheum Dis 2023;82(7):957–62 Jul.
[8] Lanzillotta M, Mancuso G, Della-Torre E. Advances in the diagnosis and management of IgG4 related disease. BMJ 2020;369:m1067. Jun 16.
[9] Shiokawa M, Kodama Y, Sekiguchi K, Kuwada T, Tomono T, Kuriyama K, et al. Laminin 511 is a target antigen in autoimmune pancreatitis. Sci Transl Med 2018;10(453):eaaq0997. Aug 8.
[10] Perugino CA, AlSalem SB, Mattoo H, Della-Torre E, Mahajan V, Ganesh G, et al. Identification of galectin-3 as an autoantigen in patients with IgG_4-related disease. J Allergy Clin Immunol 2019;143(2) Feb736-45.e736.
[11] Hubers LM, Vos H, Schuurman AR, Erken R, Oude Elferink RP, Burgering B, et al. Annexin A11 is targeted by IgG4 and IgG1 autoantibodies in IgG4-related disease. Gut 2018;67(4):728–35 Apr.
[12] Farh KK, Marson A, Zhu J, Kleinewietfeld M, Housley WJ, Beik S, et al. Genetic and epigenetic fine mapping of causal autoimmune disease variants. Nature 2015;518(7539):337–43 Feb 19.
[13] Newman JH, Shaver A, Sheehan JH, Mallal S, Stone JH, Pillai S, et al. IgG4-related disease: association with a rare gene variant expressed in cytotoxic T cells. Mol Genet Genomic Med 2019;7(6):e686. Jun.
[14] Park DH, Kim MH, Oh HB, Kwon OJ, Choi YJ, Lee SS, et al. Substitution of aspartic acid at position 57 of the DQbeta1 affects relapse of autoimmune pancreatitis. Gastroenterology 2008;134(2):440–6 Feb.
[15] Welter D, MacArthur J, Morales J, Burdett T, Hall P, Junkins H, et al. The NHGRI GWAS Catalog, a curated resource of SNP-trait associations. Nucleic Acids Res 2014;42:D1001–6 Jan.
[16] Terao C, Ota M, Iwasaki T, Shiokawa M, Kawaguchi S, Kuriyama K, et al. IgG4-related disease in the Japanese population: a genome-wide association study. Lancet Rheumatol 2019;1(1):e14–22 Sep.
[17] Wallace ZS, Naden RP, Chari S, Choi HK, Della-Torre E, Dicaire JF, et al. The 2019 American College of Rheumatology/European League Against Rheumatism classification criteria for IgG4-related disease. Ann Rheum Dis 2020;79 (1):77–87 Jan.
[18] Umehara H, Okazaki K, Kawa S, Takahashi H, Goto H, Matsui S, et al. The 2020 revised comprehensive diagnostic (RCD) criteria for IgG4-RD. Mod Rheumatol 2021;31(3):529–33 May.
[19] Su G, Zhong Z, Zhou Q, Du L, Ye Z, Li F, et al. Identification of novel risk loci for Behçet's disease-related uveitis in a Chinese population in a genome-wide association study. Arthritis Rheumatol 2022;74(4):671–81 Apr.
[20] Zhou F, Cao H, Zuo X, Zhang T, Zhang X, Liu X, et al. Deep sequencing of the MHC region in the Chinese population contributes to studies of complex disease. Nat Genet 2016;48(7):740–6 Jul.
[21] Peng L, Zhang X, Zhou J, Li J, Liu Z, Lu H, et al. Comparison of clinical features and outcomes of proliferative, fibrotic, and mixed subtypes of IgG4-related disease: a retrospective cohort study. Chin Med J (Engl) 2024;137:303–11 Feb 5.
[22] Wallace ZS, Khosroshahi A, Carruthers MD, Perugino CA, Choi H, Campochiaro C, et al. An international multispecialty validation study of the IgG4-related disease responder Index. Arthritis Care Res (Hoboken) 2018;70 (11):1671–8 Nov.
[23] Peng Y, Li JQ, Zhang PP, Zhang X, Peng LY, Chen H, et al. Clinical outcomes and predictive relapse factors of IgG4-related disease following treatment: a long-term cohort study. J Intern Med 2019;286(5):542–52 Nov.
[24] Kawa S, Ota M, Yoshizawa K, Horiuchi A, Hamano H, Ochi Y, et al. HLA DRB10405-DQB10401 haplotype is associated with autoimmune pancreatitis in the Japanese population. Gastroenterology 2002;122(5):1264–9 May.
[25] Remuzgo-Martínez S, Atienza-Mateo B, Ocejo-Vinyals JG, Pulito-Cueto V, Prieto-Peña D, Genre F, et al. HLA association with the susceptibility to antisynthetase syndrome. Joint Bone Spine 2021;88(3):105115 May.
[26] Hanscombe KB, Morris DL, Noble JA, Dilthey AT, Tombleson P, Kaufman KM, et al. Genetic fine mapping of systemic lupus erythematosus MHC associations in Europeans and African Americans. Hum Mol Genet 2018;27(21):3813–24 Nov 1.
[27] Xia Y, Chen Y, Li X, Luo S, Lin J, Huang G, et al. HLA class I association with autoimmune diabetes in Chinese people: distinct implications in classic type 1 diabetes and LADA. J Clin Endocrinol Metab 2023;108(7):e404–14 Jun 16.
[28] Lammert C, McKinnon EJ, Chalasani N, Phillips EJ. Novel HLA class I alleles outside the extended DR3 haplotype are protective against autoimmune hepatitis. Clin Transl Gastroenterol 2019;10(6):e00032 Jun.
[29] Wu YL, Chang TY, Chu CC, Huang CY, Lo FS, Ting WH, et al. The HLA-DRB1 gene and Graves disease in Taiwanese children: a case-control and family-based study. Tissue Antigens 2012;80(3):224–30 Sep.
[30] Kawabata Y, Ikegami H, Kawaguchi Y, Fujisawa T, Shintani M, Ono M, et al. Asian-specific HLA haplotypes reveal heterogeneity of the contribution of HLA-DR and -DQ haplotypes to susceptibility to type 1 diabetes. Diabetes 2002;51(2):545–51 Feb.
[31] Furuya T, Hakoda M, Ichikawa N, Higami K, Nanke Y, Yago T, et al. Differential association of HLA-DRB1 alleles in Japanese patients with early rheumatoid arthritis in relationship to autoantibodies to cyclic citrullinated peptide. Clin Exp Rheumatol 2007;25(2):219–24 Mar-Apr.
[32] Selvaraja M, Chin VK, Abdullah M, Arip M, Amin-Nordin S. HLA-DRB1*04 as a risk allele to systemic lupus erythematosus and lupus nephritis in the Malay population of Malaysia. Front Med (Lausanne) 2020;7:598665.
[33] Panda SK, Wigerblad G, Jiang L, Jiménez-Andrade Y, Iyer VS, Shen Y, et al. IL-4 controls activated neutrophil FcγR2b expression and migration into inflamed joints. Proc Natl Acad Sci U S A. 2020;117(6):3103–13 Feb 11.
[34] Floto RA, Clatworthy MR, Heilbronn KR, Rosner DR, MacAry PA, Rankin A, et al. Loss of function of a lupus-associated FcgammaRIIb polymorphism through exclusion from lipid rafts. Nat Med 2005;11(10):1056–8 Oct.
[35] Smith KG, Clatworthy MR. FcgammaRIIB in autoimmunity and infection: evolutionary and therapeutic implications. Nat Rev Immunol 2010;10 (5):328–43 May.
[36] Nimmerjahn F, Ravetch JV. Fcgamma receptors as regulators of immune responses. Nat Rev Immunol 2008;8(1):34–47 Jan.
[37] Espéli M, Smith KG, Clatworthy MR. FcγRIIB and autoimmunity. Immunol Rev 2016;269(1):194–211 Jan.
[38] Aalberse RC, Platts-Mills TA, Rispens T. The developmental history of IgE and IgG4 antibodies in relation to atopy, eosinophilic esophagitis, and the modified TH2 response. Curr Allergy Asthma Rep 2016;16(6):45. Jun.
[39] Bianchini R, Roth-Walter F, Ohradanova-Repic A, Flicker S, Hufnagl K, Fischer MB, et al. IgG4 drives M2a macrophages to a regulatory M2b-like phenotype: potential implication in immune tolerance. Allergy 2019;74 (3):483–94 Mar.
[40] Liu Y, Bankaitis VA. Phosphoinositide phosphatases in cell biology and disease. Prog Lipid Res 2010;49(3):201–17 Jul.
[41] Umemura T, Ota M, Hamano H, Katsuyama Y, Kiyosawa K, Kawa S. Genetic association of Fc receptor-like 3 polymorphisms with autoimmune pancreatitis in Japanese patients. Gut 2006;55(9):1367–8 Sep.
[42] Umemura T, Ota M, Hamano H, Katsuyama Y, Muraki T, Arakura N, et al. Association of autoimmune pancreatitis with cytotoxic T-lymphocyte antigen 4 gene polymorphisms in Japanese patients. Am J Gastroenterol 2008;103 (3):588–94 Mar.
[43] Ota M, Ito T, Umemura T, Katsuyama Y, Yoshizawa K, Hamano H, et al. Polymorphism in the KCNA3 gene is associated with susceptibility to autoimmune pancreatitis in the Japanese population. Dis Markers 2011;31 (4):223–9.
[44] Umemura T, Fujinaga Y, Ashihara N, Ozawa M, Kuraishi Y, Watanabe T, et al. IL1R1 gene variants associate with disease susceptibility to IgG4-related periaortitis/periarteritis in IgG4-related disease. Gene 2022;820:146212 Apr 30.
[45] Vince N, Limou S, Daya M, Morii W, Rafaels N, Geffard E, et al. Association of HLA-DRB1∗09:01 with tIgE levels among African-ancestry individuals with asthma. J Allergy Clin Immunol 2020;146(1):147–55 Jul.
[46] Ota M, Katsuyama Y, Hamano H, Umemura T, Kimura A, Yoshizawa K, et al. Two critical genes (HLA-DRB1 and ABCF1)in the HLA region are associated with the susceptibility to autoimmune pancreatitis. Immunogenetics 2007;59 (1):45–52 Jan.

Ann Rheum Dis 85 (2026) 704–714

Contents lists available at ScienceDirect

Annals of the Rheumatic Diseases

journal homepage: https://www.sciencedirect.com/journal/annals-of-the-rheumatic-diseases

Autoinflammatory disorders

TBXAS1 deficiency causes autoinflammation responsive to IL-6 inhibitor

Lin Liu[1,2], Jun Wang[2], Yan Ding[3], Li Guo[4], Mikhail Kostik[5], Meiping Lu[4], Yudie Fei[2], Xiangwei Sun[2], Yi Zeng[2], Yusha Wang[2], Qian Ma[4], Yang Liu[6], Xinghui Yang[7], Yali Wu[3], Bin Zhu[1], Xiangmin Tong[8], Xiaomin Yu[2,**], Qing Zhou[2,*]

[1] *Urology & Nephrology Center, Department of Nephrology, Zhejiang Provincial People's Hospital (Affiliated People's Hospital, Hangzhou Medical College), Hangzhou, China*
[2] *Department of Rheumatology, Sir Run Run Shaw Hospital, Zhejiang University School of Medicine, and Liangzhu Laboratory of Zhejiang University, Hangzhou, China*
[3] *Department of Rheumatology and Immunology, Wuhan Children's Hospital (Wuhan Maternal and Child Healthcare Hospital), Tongji Medical College, Huazhong University of Science and Technology, Wuhan, China*
[4] *Department of Rheumatology Immunology and Allergy, Children's Hospital, Zhejiang University School of Medicine, Hangzhou, China*
[5] *Saint-Petersburg State Pediatric Medical University, Saint-Petersburg, Russia*
[6] *Department of Pathology, Children's Hospital, Zhejiang University School of Medicine, Hangzhou, China*
[7] *Department of Radiology, Children's Hospital, Zhejiang University School of Medicine, Hangzhou, China*
[8] *Department of Laboratory Medicine, Affiliated Hangzhou First People's Hospital, School of Medicine, Westlake University, Hangzhou, China*

ARTICLE INFO

Article history:
Received 19 March 2025
Received in revised form 16 August 2025
Accepted 28 September 2025

ABSTRACT

Objectives: Thromboxane A synthase 1 (*TBXAS1*) deficiency results in Ghosal haematodiaphyseal dysplasia (GHDD). We identified 2 patients with *TBXAS1* deficiency characterised by autoinflammation. Our objective was to explore molecular mechanisms underlying the disease and investigate the targeted therapy.

Methods: Whole-exome sequencing and Sanger sequencing were used to identify and confirm the mutations. Quantitative reverse transcription polymerase chain reaction and Western blotting were conducted to analyse the pathway. Cytometric bead arrays, enzyme-linked immunosorbent assay, and mass spectrometry were used to detect the concentrations of cytokines, cyclic adenosine monophosphate (cAMP), and arachidonic acid metabolites. Cytometry time-of-flight and single-cell RNA sequencing were utilised to evaluate inflammatory responses and *IL6* signaling activation.

Results: We identified 2 patients with *TBXAS1* deficiency presented with systemic inflammation, in addition to increased bone density and anaemia. *TBXAS1* deficiency led to abnormal eicosanoid accumulation. The elevated prostaglandin E2 induced the expression of interleukin 6 (IL-6) via E-type prostanoid receptor 2/cAMP/cAMP response element-binding protein pathway.

*Correspondence to Qing Zhou, Department of Rheumatology, Sir Run Run Shaw Hospital, Zhejiang University School of Medicine, and Liangzhu Laboratory of Zhejiang University, Hangzhou, China.

**Correspondence to Xiaomin Yu, Department of Rheumatology, Sir Run Run Shaw Hospital, Zhejiang University School of Medicine, and Liangzhu Laboratory of Zhejiang University, Hangzhou, China.

E-mail addresses: yuxiaomin@zju.edu.cn (X. Yu), zhouqingnwu@gmail.com (Q. Zhou).

Lin Liu, Jun Wang, Yan Ding, Li Guo, and Mikhail Kostik contributed equally to this work.

Handling editor Josef S. Smolen.

https://doi.org/10.1016/j.ard.2025.09.014

Patients' peripheral blood mononuclear cells showed strong inflammatory signatures, particularly in monocytes and activation of *IL6* signaling in various immune cell populations. Based on these critical findings, we treated both patients with the IL-6 inhibitor tocilizumab, resulting in complete resolution of symptoms and laboratory abnormalities, as indicated by normalised erythrocyte sedimentation rate, C-reactive protein, and eicosanoid metabolite levels, as well as improvements in bone density.

Conclusions: We provided new insights into the pathophysiology of GHDD, which highlighted a novel link between the arachidonic acid pathway and systemic autoinflammation, and proposed an effective targeted therapy for patients with GHDD or potentially other diseases associated with the dysregulation of the arachidonic acid pathway.

WHAT IS ALREADY KNOWN ON THIS TOPIC

- Thromboxane A synthase 1 (*TBXAS1)* deficiency leads to an autosomal recessive inherited disease Ghosal haematodiaphyseal dysplasia (GHDD), characterised by increased bone density and corticosteroid-sensitive normocytic anaemia.
- Corticosteroid and nonsteroidal anti-inflammatory drugs have been reported to be effective in treating GHDD.

WHAT THIS STUDY ADDS

- This is the first report revealing that *TBXAS1* deficiency drives early-onset systemic autoinflammation, which broadens the clinical spectrum of GHDD.
- Mechanistic studies demonstrate that elevated prostaglandin E2 upregulates interleukin-6 (IL-6) expression through the EP2/cyclic adenosine monophosphate (cAMP)/cAMP response element-binding protein pathway.
- Tocilizumab, targeting IL-6, alleviates systemic inflammation, improves bone density, and corrects anaemia in patients, providing an effective treatment for *TBXAS1* deficiency.

HOW THIS STUDY MIGHT AFFECT RESEARCH, PRACTICE OR POLICY

- This is the first study linking dysregulation of the arachidonic acid pathway with autoinflammatory diseases.
- This study provides a novel and effective therapeutic regimen targeting IL-6 for GHDD.

INTRODUCTION

The arachidonic acid (AA) pathway plays a crucial role in cardiovascular biology, carcinogenesis, and inflammatory diseases [1]. AA is metabolised by cyclooxygenases, lipoxygenases and cytochrome P450 enzymes to a range of bioactive mediators, which include prostanoids, leukotrienes, epoxyeicosatrienoic acids, dihydroxyeicosatetraenoic acid, eicosatetraenoic acids, and lipoxins [1]. Prostanoids, comprising prostaglandins (PGs) and thromboxanes (TXs), are synthesised via cyclooxygenase-mediated oxidation of 20-carbon unsaturated fatty acids [2].

Prostaglandin E2 (PGE2), the most abundantly detected PG in various tissues, mediates diverse biological processes through its 4 G protein-coupled receptors (GPCRs, E-type prostanoid receptor, EP1 to EP4), each activating distinct downstream signaling pathways [2,3]. PGE2 is markedly upregulated at sites of inflammation across multiple pathologies, including synovial fluid and cartilage from patients with osteoarthritis and rheumatoid arthritis [4], which implicates it as a key mediator in acute inflammatory responses. In addition, PGE2 elevation triggering interleukin-6 (IL-6) production is mechanistically linked to cyclooxygenase 2 (COX2) upregulation, suggesting a sequential inflammatory signaling pathway [5].

TX A synthase 1 (*TBXAS1*) encodes TX A synthase (TXAS), an enzyme that converts prostaglandins H2 (PGH2) into TX A2 (TXA2). Biallelic loss-of-function variants in the *TBXAS1* can lead to an autosomal recessive inherited disease, Ghosal haematodiaphyseal dysplasia (GHDD) [6,7]. Most patients with GHDD presented increased bone density and corticosteroid-sensitive normocytic anaemia [7–10]. Corticosteroid and nonsteroidal anti-inflammatory drugs (NSAIDs) have been reported to be effective in treating GHDD [9,11]. However, the underlying mechanisms of the disease require further investigation, which could inform the development and utilisation of more effective targeted therapy.

METHODS

Patients

This study was performed according to the protocol approved by the institutional review boards of the Wuhan Children's Hospital (2024R076-E01) and Children's Hospital, Zhejiang University School of Medicine (2021-IRB-0172). Both patients provided written informed consent, including consent to publish.

Whole-exome sequencing and Sanger sequencing

Whole genomic DNA was extracted from whole blood using the Maxwell RSC Whole Blood DNA Kit (Promega, AS1520), and 1 μg of DNA was used for whole-exome sequencing (WES). Data were analysed as previously described [12]. Sanger sequencing was performed to confirm mutations identified by WES.

RNA isolation and quantitative reverse transcription polymerase chain reaction

Total RNA was isolated using the RNeasy Mini Kit (Qiagen, 74104). 1 μg of RNA was reverse transcribed using the HiScript III All-in-one RT SuperMix Perfect for quantitative polymerase chain reaction (qPCR) Kit (Vazyme #R333). Quantitative reverse transcription polymerase chain reaction (PCR) was performed on Roche LightCycler 480 II using 2 × Universal SYBR Green Fast qPCR Mix (Abclonal, RK21203). Relative mRNA expression levels were normalised to the reference gene glyceraldehyde-3-phosphate dehydrogenase (*GAPDH*) using the 2-DDCt method.

Cell lines, culture, and treatments

Human peripheral blood mononuclear cells (PBMCs) were separated from peripheral blood samples using density gradient centrifugation with lymphocyte separation medium (MP

Biomedicals, 50494). *TBXAS1*-knockout (*TBXAS1*-KO) U937 cells were generated using the clustered regularly interspaced short palindromic repeats (CRISPR)/CRISPR-associated protein 9 (Cas9) system with sgRNA targeting *TBXAS1* (sgRNA-F: CACCGTAAAACGCTATGCGGAATCT; sgRNA-R: AAACAGATTCCGCATAGCGTTTTAC). Wild-type (WT) U937 cells were generated using empty lentiCRISPR v2. U937 cells were infected by lentivirus followed by selection with 3 μg/mL puromycin. The efficiency of knockout was assessed by immunoblotting.

PBMCs, U937 cells, and HEK293T cells were cultured in Roswell Park Memorial Institute (RPMI) 1640 (Gibco) or Dulbecco's Modified Eagle Medium (Gibco, C11995500BT) supplemented with 10% fetal bovine serum (Noverse, NFBS-2500A) and 1% penicillin/streptomycin (Gibco, 15140-122). PGE2 (MedChemExpress (MCE), HY-101952), AA (MCE, HY-109590), and cyclic adenosine monophosphate (cAMP) agonist Forskolin (MCE, HY-15371) were used to stimulate cells as indicated conditions. EP2 antagonist TG6-10-1 (MCE, HY-16978), EP4 antagonist L-161982 (MCE, HY-108559), protein kinase A (PKA) inhibitor H-89 (MCE, HY-15979), and tocilizumab (Selleck, A2012) were used to pretreat cells as indicated conditions.

Western blotting

Cells were harvested and lysed in 0.5% NP-40 lysis buffer containing protease and phosphatase inhibitors (Thermo Fisher, 78442). Concentrations of protein were measured using bicinchoninic acid (BCA) protein assay kit (Thermo Fisher, 23225). Immunoblotting was conducted as described previously with the following specific antibodies.

Antibodies and plasmids

The antibodies used were listed as follows: TXAS (A1988) was purchased from ABclonal. GAPDH (5174), p-cyclic AMP response element (CRE)-binding protein (CREB) (Ser133) (9198), CREB (9197), phosphorylated signal transducer and activator of transcription 3 (p-STAT3) (Tyr705) (9145), and signal transducer and activator of transcription 3 (STAT3) (9139) were purchased from Cell Signaling Technology. Myc (60003-2-Ig) was purchased from Proteintech.

Myc-tagged wild-type TBXAS1 (TBXAS1-WT) expression plasmids were generated by PCR amplification from the cDNA of the PBMCs, and then cloned into the pLenti vector. The mutant plasmids were constructed by site-directed mutagenesis.

Cytokine detection

Human serum cytokines were detected by cytometric bead arrays (CBAs, BD Biosciences) and enzyme-linked immunosorbent assay (ELISA) (Multi Sciences: EK-106) according to the manufacturer's guidelines. CBA data were analysed by FCAP Array V3 software (BD Biosciences). PGE2, prostaglandin D2 (PGD2), TX B2 (TXB2) and cAMP were detected by ELISA (Multi Sciences, EK8103; Sangon Biotech, D751029; Elabsience, E-EL-H2191 and Elabsience, E-EL-0056).

Cytometry by time-of-flight

For the mass cytometry experiment, purified antibodies were purchased from Biolegend, Thermo Fisher, Bio-Rad, and R&D Systems using the clones detailed in Supplementary Table S1. Sample preparation, flow cytometer setup, and operation procedures were performed largely according to the previous pipeline [12]. To be specific, the MaxPAR antibody labelling kit (Fluidigm) was used for antibody labelling with the indicated metal tag. Optimal concentration for conjugated antibodies was titrated before use.

1 × phosphate-buffered saline (PBS) was used for washing cells, and cells were subsequently stained with 100 μL of 250 nM cisplatin (Fluidigm) for 5 minutes on ice to exclude dead cells, and then incubated in Fc receptor blocking solution before being stained with surface antibodies cocktail for 30 minutes on ice. Cells were washed twice with fluorescence-activated cell sorting (FACS) buffer (0.5% bovine serum albumin (BSA) in PBS) and fixed in 200 μL of intercalation solution (Maxpar Fix and Perm Buffer containing 250 nM 191/193Ir, Fluidigm) overnight. After fixation, cells were washed once with FACS buffer and then perm buffer (eBioscience), stained with intracellular antibodies cocktail for 30 minutes on ice. Cells were washed and resuspended with deionised water, adding 20% EQ beads (Fluidigm), acquired on a mass cytometer (Helios, Fluidigm).

The cytometry by time-of-flight (CyTOF) data were exported as FCS files, and FCS files were standardised and debarcoded using the Nolan Lab Beads Normalizer package (V0.3). All FCS files were manually gated in FlowJo (v10.0.7) to remove doublets, and CD45+ single cells were identified by DNA (191Ir and 193Ir), 194Pt and event length. A total of 30,000 CD45+CD66- cells were randomly selected from each sample for downstream analysis. FCS files were transformed using the arcsinh function with a cofactor of 5. Phenograph clustering in cytofkit (0.99.0) R package was performed on all subsampled sample events, and the k value (k = 30) used in Phenograph clustering was calculated with the elbow algorithm. The transformed values of all events were subjected to t-Distributed Stochastic Neighbor Embedding (t-SNE) dimension reduction using R-tsne (0.15) package.

Ultraperformance liquid chromatography-mass spectrometry

Serum samples were analysed using an ultraperformance liquid chromatography system (Waters UPLC I-Class). The mass spectrometry analysis was conducted using a 5500 QTRAP mass spectrometer (AB SCIEX) in negative ion mode. The results were analysed under the technical assistance of Shanghai Applied Protein Technology Co., Ltd.

Single-cell RNA sequencing

PBMCs of 2 patients and 3 healthy controls were isolated, and 8000 to 10,000 single cells were captured by 10 × Genomics Chromium for cDNA library construction. Single-cell sequencing data were analysed as previously described [12]. In short, Seurat v3.2.3 R package (https://satijalab.org/seurat/) was used for downstream analysis. 'WP_IL6_SIGNALING_PATHWAY' score was calculated using Seurat AddModuleScore function. The gene list of 'WP_IL6_SIGNALING_PATHWAY' was selected according to the Wiki Pathways (https://www.wikipathways.org/pathways/WP364.html).

Statistical analysis

All values were represented as mean ± SEM. Data were analysed by a 2-tailed unpaired Students' t-test unless otherwise stated. Statistical analysis was performed by GraphPad Prism 8 software.

RESULTS

Autoinflammation in patients with biallelic loss-of-function variants in TBXAS1

Patient 1 (P1) is a 16-year-old Chinese boy who had presented with progressive muscle weakness, joint pain, mild anaemia, and low body weight since the age of 4. Magnetic resonance imaging and x-ray showed joint oedema and long bones cortical thickening (Fig 1A—a and b). Muscle biopsy showed focal inflammatory cell infiltration (Fig 1A—d-f). Laboratory testing revealed elevated C-reactive protein (CRP) and erythrocyte sedimentation rate (ESR) (Supplementary Table S2). He initially received treatment with corticosteroids and NSAIDs, and achieved complete remission. However, he experienced a recurrence of symptoms upon steroid tapering. Patient 2 (P2) is a 6-year-old Caucasian boy from Russia. He presented with anaemia, abdominal bloating, weight deficiency at 3 months of age, followed by splenomegaly at 5 months, and fevers, muscle hypotonia at 6 months of age. X-ray showed increased bone density (Fig 1A—c). Laboratory testing revealed increased CRP and ESR and decreased haemoglobin from 1 year old until the last admission (Supplementary Table S3).

WES revealed compound heterozygous *TBXAS1* variants c.176dup (p.R60Pfs*33) and c.210del (p.R71Efs*25) in P1, which were derived from the mother and father (Supplementary Fig S1), respectively, and a homozygous *TBXAS1* variant c.228del (p.L77Cfs*19) in P2 (Fig 1B). These variants were subsequently confirmed by Sanger sequencing (Fig 1C). The mRNA levels of *TBXAS1* in patients' PBMCs were decreased remarkably, suggesting the involvement of nonsense-mediated RNA decay (Fig 1D). Consequently, no full-length or truncated TXAS protein was detected in patients' PBMCs or in HEK293T cell lysates transfected with the indicated mutated plasmids (Fig 1E). Therefore, both patients carry loss-of-function variants in *TBXAS1*, which resulted in a deficiency of TXAS.

Since both patients presented with inflammatory manifestations, we measured the proinflammatory cytokines in P2's serum using CBA. Consistently, the results showed significantly increased levels of proinflammatory cytokines, including IL-6, IL-8 and IL-1β in the patient, compared to healthy controls (HCs) (Fig 1F). Elevated level of IL-6 was also detected in the supernatant of cultured PBMCs from the patient (Fig 1G), further demonstrated that IL-6 was a critical proinflammatory cytokine in *TBXAS1* deficiency. To investigate the inflammatory responses at single-cell levels, we conducted CyTOF on PBMCs from the P2 and HCs. CyTOF confirmed elevated production of proinflammatory cytokines IL-6, IL-8, and IL-1β in P2's monocytes compared to HCs (Supplementary Fig S2A-D), suggesting an important role of monocytes in driving inflammation in GHDD.

We then test the eicosanoid levels of the AA pathway, as it has been reported that abnormal eicosanoids accumulate in patients with GHDD [9]. Elevated proinflammatory PG metabolites—PGE2 and PGD2, hydroxyicosatetraenoic acid (HETE) metabolites, as well as leukotrienes leukotriene B4 in serum of P2 were detected using an ELISA kit or metabolic mass spectrometry (Fig 1H). TXB2 was undetectable in the patient, which supported a total loss-of-function of *TBXAS1* (Fig 1H). In addition, we generated *TBXAS1*-KO U937 cell line using CRISPR/Cas9 technology. We confirmed that PGE2 increased significantly in the supernatant of cultured *TBXAS1*-KO U937 cells under stimulation of AA, compared with WT U937 cells (Fig 1I), consistent with the elevated level of PGE2 observed in *TBXAS1* deficiency patients. Overexpression of the TBXAS1-WT plasmid dose dependently increased the concentration of TXB2 and attenuated AA-induced PGE2 elevation in HEK293T cells, which lack endogenous TXAS expression (Fig 1J and Supplementary Fig S3A). Mutant constructs, including our frameshift mutations and the missense founder mutation p.R412Q, failed to catalyse TXB2 production and demonstrated no inhibitory effect on PGE2 generation (Fig 1J). These functional assays demonstrate that the pathogenic mutations lead to PGE2 production.

To investigate whether the dysregulation of the AA metabolism pathway exhibits specificity in autoinflammatory diseases (AIDs), we measured serum levels of PGE2, PGD2, and TXB2 in 15 patients with AIDs (Supplementary Table S4). Both PGE2 and PGD2 were found elevated in some patients with AIDs and *TBXAS1* deficiency (Fig 1K), while TXB2 was undetectable in *TBXAS1* deficiency patients. Furthermore, the markedly elevated PGE2 levels observed in *TBXAS1* deficiency patients compared to other patients (Fig 1K), when considered in the context of its biosynthetic pathway, indicate a mutation-specific pattern of PG dysregulation. Overall, our results suggest a potential association between PGE2 levels and systemic inflammation, although formal correlation analysis was not performed.

Elevated PGE2 induces IL6 expression through EP2/cAMP/CREB pathway

To investigate the differential responses to accumulated PGE2 between the WT and *TBXAS1*-KO U937 cells, we stimulated the cells with PGE2 or AA. At the basal level, *TBXAS1*-KO U937 cells exhibited higher mRNA expression of proinflammatory cytokines and *COX2* compared to WT cells (Fig 2A,B). Moreover, both PGE2 and AA significantly induced the upregulation of transcriptional levels of *COX2* and proinflammatory cytokines, including *IL6* and *CXCL8* (Fig 2A,B). Previous studies have reported that PGE2 could upregulate the expression of *CXCL8* and *COX2* [13,14]. We demonstrated that *IL6* was directly modulated by PGE2 at the transcriptional level. In addition, IL-6 expression was constantly and significantly increased in a time-dependent manner following PGE2 or AA stimulation in *TBXAS1*-KO U937 cells compared to WT U937 cells (Fig 2C,D).

PGE2 exerts its effects via 4 subtypes of GPCRs, namely EP1 to EP4 [3]. The CREB was reported as a transcription factor of *COX2* and *IL6* [15]. To investigate the regulation of *IL6* by PGE2, EP2, and EP4 inhibitors were used to block the GPCRs, since EP1 and EP3 were rarely expressed in the immune cells [16]. Only EP2 inhibitor, but not EP4 inhibitor, partially inhibited the increased phosphorylation of CREB and consistently suppressed the upregulation of gene expression of *IL6, CXCL8,* and *COX2* induced by PGE2, in both WT and *TBXAS1*-KO U937 cells (Fig 2E,F). To further elucidate the mechanism, we measured cAMP production and found that PGE2 induced a more rapidly increase and a higher level of cAMP in *TBXAS1*-KO U937 cells, compared to WT U937 cells (Fig 2G). Additionally, cAMP agonist Forskolin significantly increased *IL6* expression in both WT and *TBXAS1*-KO U937 cells (Fig 2H). Moreover, the PKA inhibitor effectively reversed the phosphorylation of CREB and the upregulation of *IL6* induced by PGE2 in a dose-dependent manner (Fig 2I,J). Taken together, these findings suggested that PGE2 regulates IL6 expression through the EP2-cAMP-PKA axis.

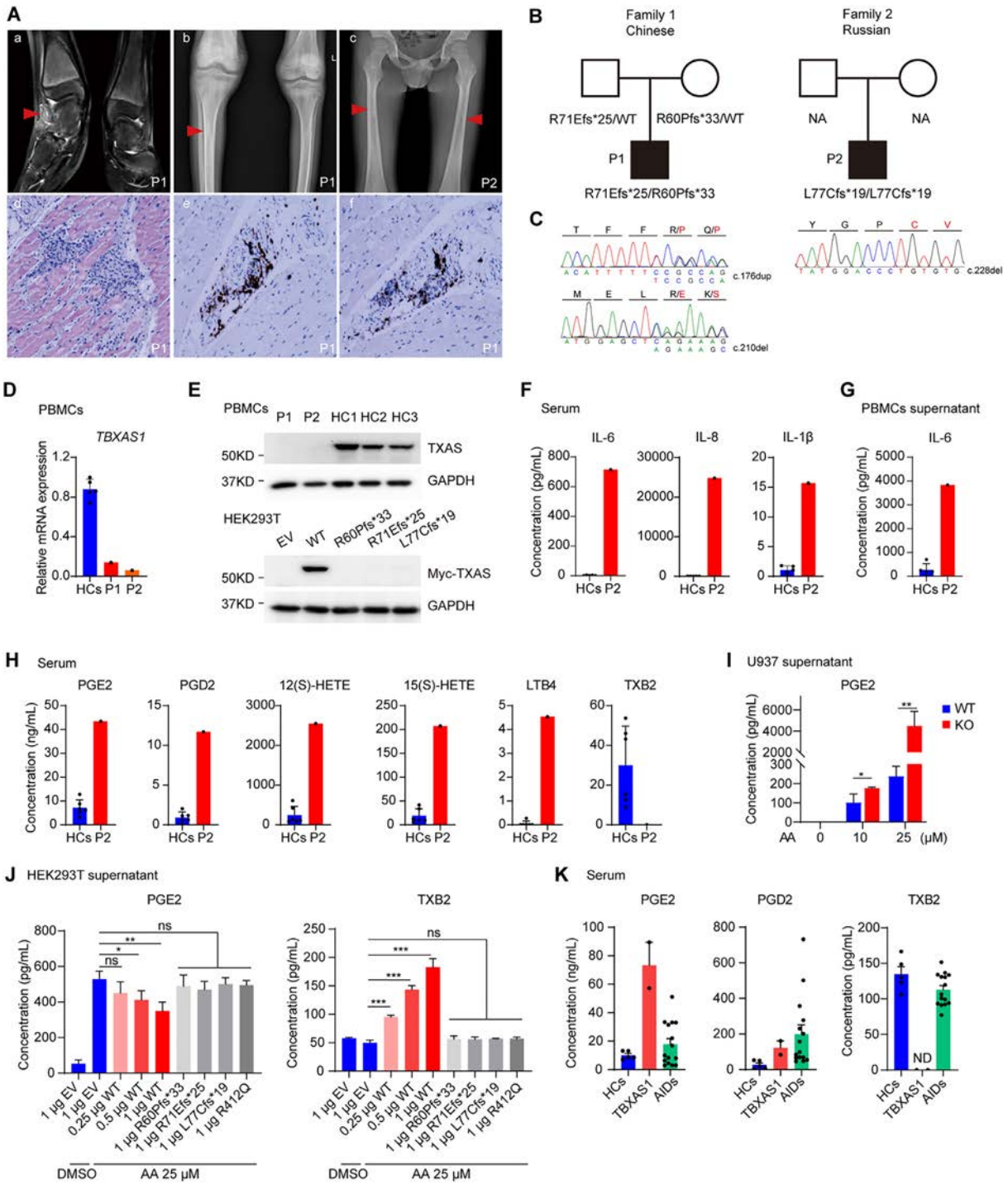

Figure 1. Clinical manifestations, arachidonic acid metabolism profiles, and inflammatory signatures of 2 patients with *TBXAS1* pathogenic variants. (A) Radiological and pathological manifestations of the patients. (a) Joint effusion on MRI (red arrows). (b and c) X-ray images showed increased density of femoral shafts of 2 patients (red arrows). (d) Oedema in gastrocnemius muscle with lymphocyte infiltration (HE, 200 ×). (e and f) CD3 and CD20 immunohistochemical staining in gastrocnemius muscle biopsy (200 ×). (B) Pedigrees of the 2 families with *TBXAS1* pathogenic variants (compound heterozygous frameshift mutation in family 1 and homozygous frameshift mutation in family 2). (C) Sanger sequencing verification of the variants of *TBXAS1*. (D) qPCR analysis of *TBXAS1* mRNA expression in 5 healthy controls (HCs) and patients. (E) Protein levels of TXAS in PBMCs from 2 patients and 3 HCs (upper panel) and in HEK293T cells transfected with indicated constructed plasmids (lower panel). (F) Levels of cytokines IL-6, IL-1β, and chemokine IL-8 in serum of 4 HCs and patient 2 (P2) detected by cytometric bead array (CBA). (G) Concentration of cytokine IL-6 in supernatants of PBMCs from 4 HCs and P2 cultured in RPMI 1640 for 24 hours measured by CBA. (H) Mass spectrometry analysis of serum arachidonic acid metabolites in 6 HCs and P2 before treatment with tocilizumab. (I) ELISA analysis of PGE2 concentrations in the supernatants of wild-type (WT) and *TBXAS1*-knockout (KO) U937 cell lines treated with indicated doses of arachidonic acid (AA). (J) ELISA analysis of PGE2 and TXB2 concentrations in the supernatants of HEK293T cells transfected with indicated constructed TBXAS1 plasmids, after treatment with 25 μM AA. (K) ELISA analysis of serum levels of PGE2, PGD2, and TXB2 in HCs, patients with *TBXAS1* variants and patients with autoinflammatory diseases (AIDs, n = 15). The experiments were repeated 3 times. *, $P < .05$; **, $P < .01$; ***, $P < .001$. DMSO, dimethyl sulfoxide; ELISA, enzyme-linked immunosorbent assay; EV, empty vector; 15(S)-HETE, 15(S)-hydroxyeicosatetraenoic acid; HE, haematoxylin and eosin; IL, interleukin; MRI, magnetic resonance imaging; ND, not detected; ns, no significance; PBMC, peripheral blood mononuclear cell; PGE2, prostaglandin E2; PGD2, prostaglandin D2; qPCR, quantitative polymerase chain reaction; TBXAS1, thromboxane A synthase 1; 12(S)-HETE, 12(S)-hydroxyeicosatetraenoic acid; TXB2, thromboxane B2.

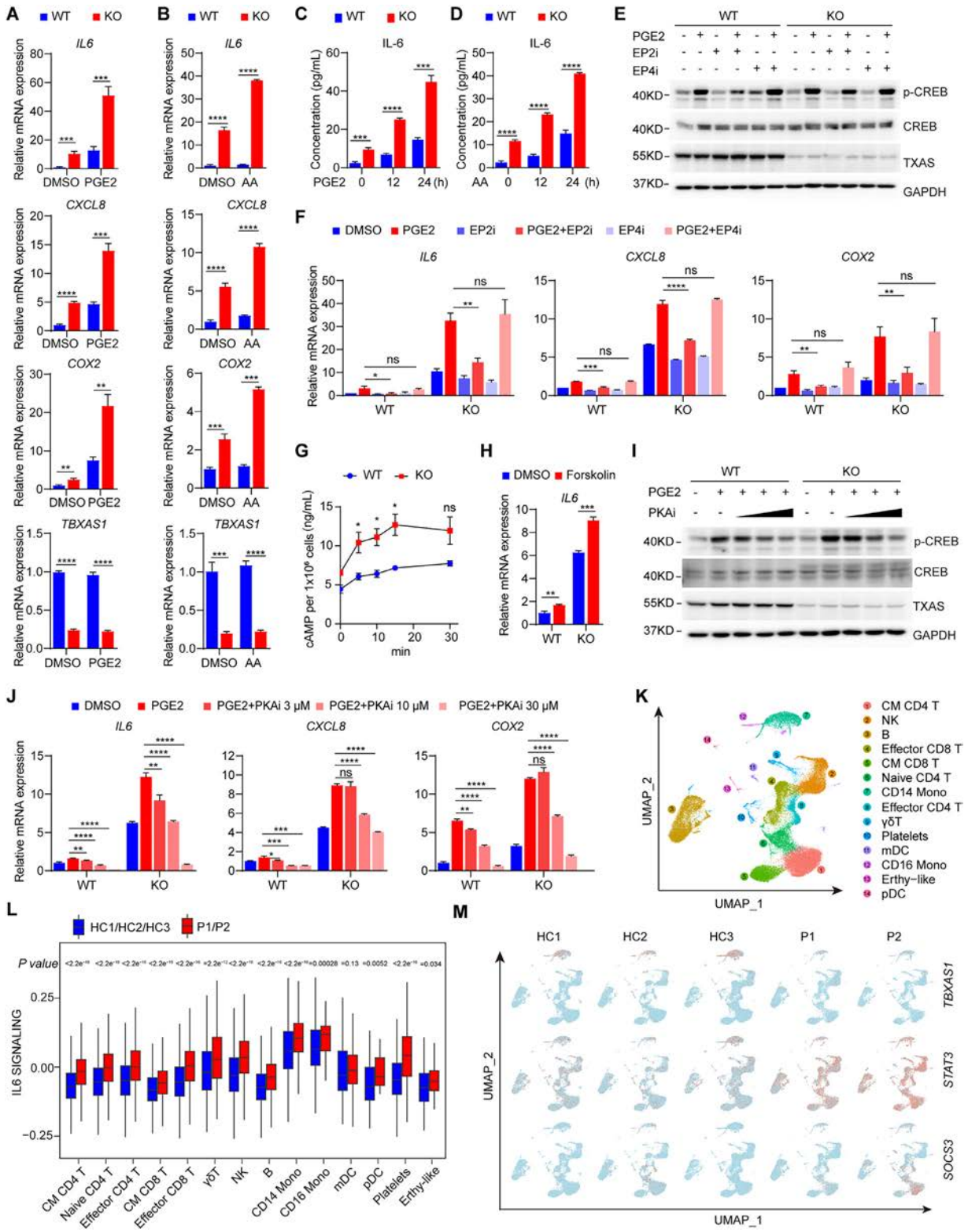

Figure 2. Elevated PGE2 induces IL6 expression through EP2/cAMP/CREB pathway. (A) qPCR analysis of *IL6, CXCL8, COX2,* and *TBXAS1* mRNA expression in wild-type (WT) and *TBXAS1*-knockout (KO) U937 cells treated with 10 μM PGE2 for 2 hours. (B) qPCR analysis of *IL6, CXCL8, COX2,* and *TBXAS1* mRNA expression in WT and KO U937 cells treated with 25 μM AA for 3 hours. (C) WT and KO U937 cells were treated with 10 μM PGE2 for indicated time, and supernatants were collected to measure IL-6 concentrations by ELISA. (D) WT and KO U937 cells were treated with 25 μM AA for indicated time, and supernatants were collected to measure IL-6 concentrations by ELISA. (E) Western blots of WT and KO U937 cells pretreated with 10 μM EP2 inhibitor (EP2i) or EP4 inhibitor (EP4i) before 10 μM PGE2 stimulation or not. (F) qPCR analysis of *IL6, CXCL8, COX2* mRNA expression in WT and KO U937 cells pretreated with 10 μM EP2i or EP4i before PGE2 stimulation or not. (G) cAMP concentrations in the cell lysate of WT and KO U937 cells treated with 10 μM PGE2 for indicated time were detected by ELISA. (H) qPCR analysis of *IL6* mRNA expression in WT and KO U937 cells treated with or without 10 μM Forskolin. (I) Western blots of WT and KO U937 cells pretreated with 3 μM, 10 μM, or 30 μM PKA inhibitor (PKAi) before 10 μM PGE2 stimulation. (J) qPCR analysis of *IL6, CXCL8, COX2* mRNA expression in WT and KO U937 cells pretreated with 3 μM, 10 μM, or 30 μM PKAi before 10 μM PGE2 stimulation. (K) Uniform manifold approximation and projection (UMAP) visualisation and marker-based annotation of 14 cell subtypes from 3 HCs and 2 patients. (L) Single-cell RNA sequencing analysis of IL-6 signaling score in 2 patients compared to 3 HCs across different cell types. Statistical significance was determined using the Wilcoxon test. (M) Visualisation of expression of *TBXAS1, STAT3,* and

To further investigate the specific cell populations linked to the patient's clinical manifestations, we performed single-cell RNA sequencing on PBMCs from 2 patients and 3 HCs. Unsupervised graph-based clustering of approximately 33,000 cells integrated from patients and controls resolved 14 clusters annotated in a semisupervised fashion based on marker gene expression profiles (Fig 2K). We noticed elevated gene expression in IL-6 signaling across most of the immune cell types (Fig 2L), with notable upregulation of *STAT3* and *SOCS3*, indicating hyperactivation of the *IL6* signaling in patients' PBMCs (Fig 2M). Among immune cell populations, *TBXAS1* was selectively expressed in monocytes in HCs (Fig 2M), which further highlighting the pathogenic role of *TBXAS1* deficiency in monocyte-driven inflammatory responses. This is consistent with the inflammatory responses detected in monocytes from patients' PBMCs by CyTOF analysis.

Clinical improvement with tocilizumab treatment

Considering the distinct inflammatory phenotypes of both patients and the dramatic upregulation of IL-6 signaling caused by TXAS deficiency, the IL-6 receptor monoclonal antibody tocilizumab was considered as a more specific and potent treatment for patients. To evaluate its efficacy, we tested the effect of tocilizumab in cell lines and on patients' PBMCs *ex vivo*. The basal level of phosphorylation of STAT3 was increased in *TBXAS1*-KO U937 cells compared to WT U937 cells, which indicated an activation of IL-6 signaling in *TBXAS1*-KO U937 cells (Fig 3A). PGE2 and AA treatment further increased phosphorylation of STAT3, which was effectively inhibited by tocilizumab (Fig 3A, B). This suggests that tocilizumab may be a potential treatment. Next, we treated the patients' PBMCs with tocilizumab *ex vivo*. Tocilizumab alleviated the increase of *IL6, CXCL8* and *COX2* induced by AA stimulation (Fig 3C).

Subsequently, the P1 was prescribed tocilizumab (8 mg/kg, per 4 weeks) on his second relapse during the course of methylprednisolone tapering (Fig 3D). The patient experienced significant relief from joint and muscle pain. Haemoglobin, CRP, and ESR levels normalised rapidly and remained stable until the last follow-up on 11 November 2024 (Fig 3E and Supplementary Table S2). Glucocorticoid was successfully withdrawn on 25 January 2024. Until now, the patient P1 has been doing well and attending school as normal. The x-ray taken before the preparation of this manuscript showed marked improvement in cortical thickening of long bones (Fig 3F). In addition, the serum level of IL-8 was decreased after treatment (Fig 3G). The elevated level of IL-6 was attributed to the inhibition of IL-6R-mediated consumption (Fig 3G) [17]. We tested the concentrations of eicosanoid and found that PGE2, PGD2, and HETE metabolites returned to normal, although TXB2 remained undetectable (Fig 3H). The most recent follow-up on 10 May 2025 demonstrated normalised inflammatory markers (CRP 0.83 mg/L; ESR 4 mm/h) and PGE2 concentration (13.46 ng/mL), confirming sustained clinical remission. Given the P1's excellent response to tocilizumab, we recommended P2 to receive the same treatment. The P2 received the first infusion of tocilizumab on 20 November 2024. Elevated CRP returned to normal quickly by the third day after treatment. Haemoglobin, CRP, and ESR levels returned to normal within a week (Supplementary Table S2). The P2 is also doing well currently.

DISCUSSION

Here, we reported 2 patients with *TBXAS1* deficiency manifesting with early-onset AID and identified an inflammatory signaling pathway that drives IL-6 overproduction (Fig 4). Treatment targeting IL-6 alleviated all symptoms, including resolution of systemic inflammation, improved bone density, correction of anaemia, and normalisation of eicosanoid metabolite levels.

To our knowledge, only 7 missense and 3 truncating mutations in *TBXAS1* have been reported to date [6−10,18−22] (Supplementary Fig S3B, C). Here, we identified 3 novel frameshift variants in *TBXAS1*, resulting in reduced *TBXAS1* mRNA expression and complete loss of TXAS protein. Previous studies have shown that PGE2 level was higher in platelet-rich plasma of patients with *TBXAS1* mutations, and increased more intensely upon AA induction [7]. Loss of TXAS results in an abnormal accumulation of PGH2 for other PG synthases [9]. TXAS-deleted mice also exhibit a compensatory increase in PGE2 and a lesser extent in PGD2 and PGF2α [23]. An increase in eicosanoid metabolites, especially PGE2, was similarly detected in our patients, which is consistent with previous reports. Additionally, both of our patients exhibited a systemic inflammatory phenotype, which was previously indicated in only 6 of 23 cases (Supplementary Table S5). The observed systemic inflammation and PGE2 elevation in our patients suggest PG-mediated pathophysiology, consistent with PGE2's known regulatory functions in inflammation [24]. A recent work reveals a strong correlation between PGE2 and systemic inflammation during the courses of treatment with high-dose aspirin/ibuprofen, off therapy and low-dose aspirin/ibuprofen [9], which is concordant with our observations. The pronounced inflammatory phenotype observed in our patients may be attributable to their total loss-of-function frameshift mutation in *TBXAS1*, suggesting a genotype-driven inflammatory mechanism. Although our patients also had osteosclerosis, the degree was milder and the haematopoietic function was less affected, with mild anaemia and normal white blood cells and platelets. Because the anaemia resolved rapidly after treatment with tocilizumab within 2 days, we speculated that the anaemia was due to inflammation rather than myelofibrosis.

Osteosclerosis is a common manifestation in patients with GHDD with *TBXAS1* variants, while the underlying mechanisms remain to be further explored. Although no experimental data on bone pathophysiology are provided, the low TXA2 levels resulting from *TBXAS1* mutations likely feed into complex pathways of bone dysregulation in patients with *TBXAS1* deficiency (GHDD). Decreased generation of TXA2 and excessive production of PGE2 might both contribute to the development of osteosclerosis in patients with GHDD. Pharmacological inhibition of TXAS in primary cultured osteoblasts suppresses the expression

SOCS3 (coloured single cells) on UMAP plot projecting PBMCs from 3 HCs and 2 patients. All the *in vitro* experiments were repeated at least 3 times. *, $P < .05$; **, $P < .01$; ***, $P < .001$; ****, $P < .0001$. AA, arachidonic acid; cAMP, cyclic adenosine monophosphate; CM, central memory; CREB, cyclic AMP response element (CRE)-binding protein; DMSO, dimethyl sulfoxide; ELISA, enzyme-linked immunosorbent assay; EP2, E-type prostanoid receptor 2; Erthy-like, erythroid-like and erythroid precursor cell; GAPDH, glyceraldehyde-3-phosphate dehydrogenase; HC, healthy control; IL, interleukin; mDC, myeloid dendritic cell; Mono, monocyte; NK, natural killer cell; PBMC, peripheral blood mononuclear cell; pDC, plasmacytoid dendritic cell; PGE2, prostaglandin E2; qPCR, quantitative polymerase chain reaction; STAT3, signal transducer and activator of transcription 3; TBXAS1, thromboxane A synthase 1; TXAS, thromboxane A synthase.

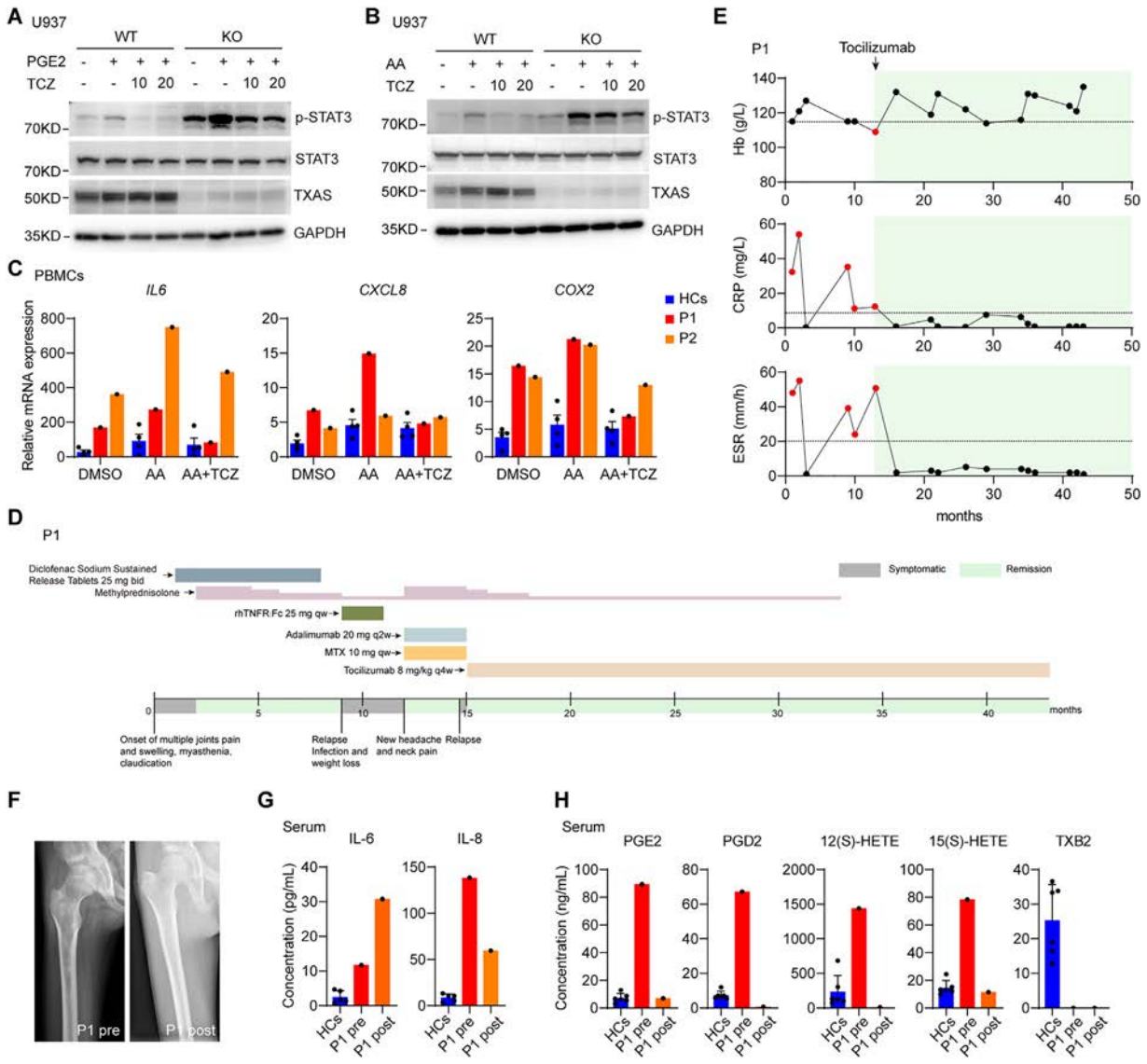

Figure 3. Effective treatment with tocilizumab (TCZ) *in vitro, ex vivo,* and *in vivo*. (A) Western blots of wild-type (WT) and *TBXAS1*-knockout (KO) U937 cells treated with 10 μM PGE2, combined with 10 ng/mL or 20 ng/mL TCZ for 36 hours. (B) Western blots of WT and KO U937 cells treated with 25 μM AA, combined with 10 ng/mL or 20 ng/mL TCZ for 36 hours. (C) qPCR analysis of *IL6, CXCL8*, and *COX2* mRNA expression in 4 HCs' and patients' PBMCs pretreated with 10 ng/mL TCZ before challenged with 25 μM AA stimulation. (D) Schematic representation of the P1's symptoms and treatment from the onset of illness. P1 suffered from joint pain and swelling, myasthenia, and claudication at the onset of the disease. After treatment with NSAIDs and methylprednisolone, he received complete remission. However, the disease recurred when attempting to reduce the dosage of methylprednisolone to 4 mg and 6 mg every other day. The use of rhTNFR:Fc failed to improve the status. The patient received complete remission again after using a combination of methylprednisolone (24 mg once daily), adalimumab and methotrexate, but suffered relapse again during the glucocorticoid tapering to 12 mg once daily. Then, based on our findings, the patient was prescribed with TCZ and attained remission until now. During the course of TCZ treatment, the glucocorticoid was gradually reduced and subsequently tapered off completely on January 25, 2024. The dose and frequency of the medicine are shown in the figure. (E) Haemoglobin (Hb), C-reactive protein (CRP), and erythrocyte sedimentation rate (ESR) from the first assessment of the P1 at the time of onset to the present were shown. Horizontal dotted lines indicate age-specific low levels of Hb or high levels of CRP or ESR. Red dots represent the abnormal values. The green rectangle covers the course of treatment with TCZ. (F) X-ray images showed improved density of femoral shafts of P1 after treatment with TCZ for 3 doses of 240 mg and 12 doses of 320 mg (weight-based, 8 mg/kg). (G) Levels of cytokine IL-6 and chemokine IL-8 in serum of 5 HCs and P1 before and after treatment of TCZ were detected by CBA. (H) Mass spectrometry analysis of serum arachidonic acid (AA) metabolites in 6 HCs and P1 before and after treatment with TCZ. All the *in vitro* experiments were repeated at least 3 times. *, $P < .05$; **, $P < .01$; ***, $P < .001$; ****, $P < .0001$. CBA, cytometric bead array; DMSO, dimethyl sulfoxide; 15(S)-HETE, 15(S)-hydroxyeicosatetraenoic acid; GAPDH, glyceraldehyde-3-phosphate dehydrogenase; HC, healthy control; IL, interleukin; MTX, methotrexate; NSAID, nonsteroidal anti-inflammatory drug; PBMC, peripheral blood mononuclear cell; PGE2, prostaglandin E2; PGD2, prostaglandin D2; qPCR, quantitative polymerase chain reaction; 12(S)-HETE, 12(S)-hydroxyeicosatetraenoic acid; STAT3, signal transducer and activator of transcription 3; TXB2, thromboxane B2.

of *TNFSF11*, encoding the receptor activator of nuclear factor kappa-B ligand (RANKL), but increases the expression of *TNFRSF11B*, encoding osteoprotegerin (OPG) [7]. This shift in the OPG/RANKL ratio reduces osteoclast differentiation but favours osteoblast-mediated bone formation, ultimately promoting osteosclerosis. The addition of the analogue of TXA2 has an opposite effect [7]. Thus, TXA2 may have a proresorptive function on osteoclasts.

While intermittent PGE2 elevation can stimulate osteoclasts, chronic PGE2 exposure promotes osteoblast differentiation and increases bone formation via EP4, insulin-like growth factor 1 (IGF-1), Wnt pathway activation [25]. Long-term PGE2 infusion

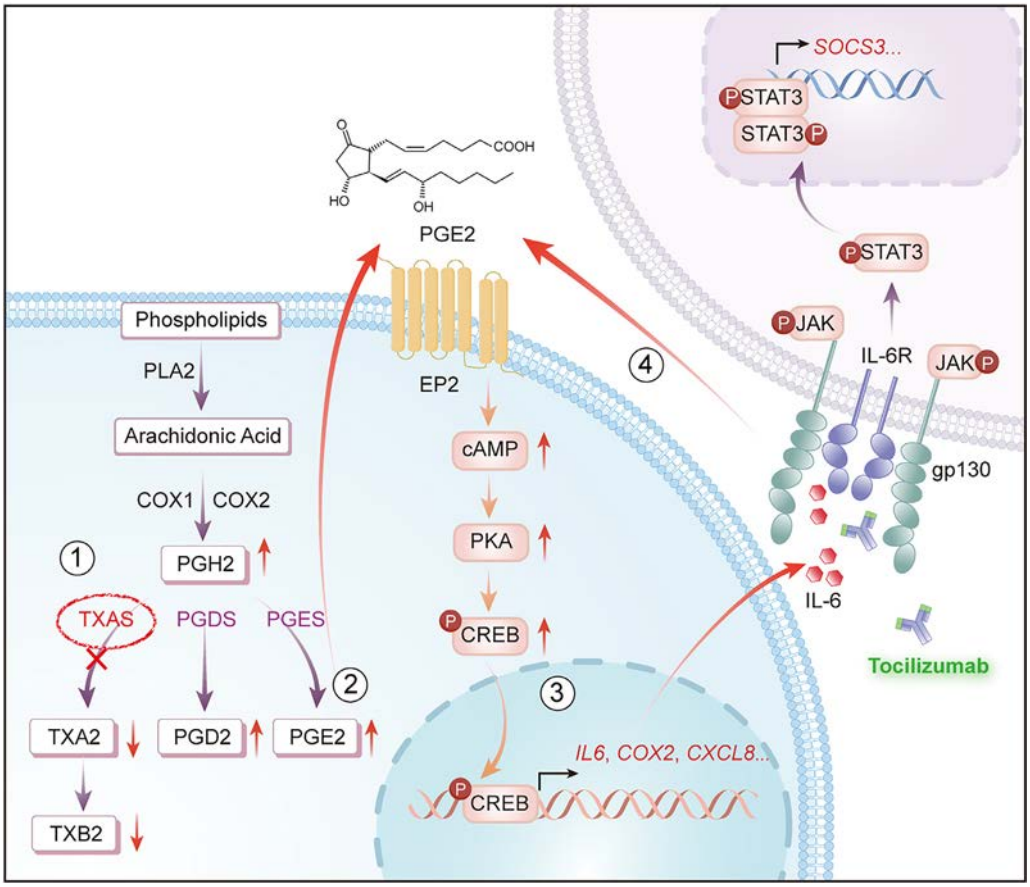

Figure 4. Graphic overview of TBXAS1 deficiency leading to upregulation of IL-6, which could be effectively blocked by tocilizumab. 1 *TBXAS1* loss-of-function mutations lead to a deficiency of TXAS, resulting in decreased TXA2 and TXB2 levels and accumulation of PGH2. 2 Increased PGH2 is funnelled through prostaglandin E synthase (PGES) and PGDS (encoded by *PTGES* and *PTGDS*, respectively), leading to increased PGE2 and PGD2. 3 PGE2 activates the cAMP-PKA-CREB pathway to produce IL-6, COX2, and IL-8. 4 IL-6 and other inflammatory cytokines promote a feed-forward mechanism that leads to excessive PGE2 production, which can be interrupted by IL-6R inhibitor tocilizumab. cAMP, cyclic adenosine monophosphate; COX2, cyclooxygenase 2; CREB, cyclic AMP response element (CRE)-binding protein; EP2, E-type prostanoid receptor 2; IL, interleukin; JAK; Janus kinase; PGD2, prostaglandin D2; PGDS, prostaglandin D2 synthase; PGE2, prostaglandin E2; PGES, prostaglandin E2 synthase; PGH2, prostaglandins H2; PKA, protein kinase A; PLA2, phospholipase A2; SOCS3, suppressor of cytokine signaling 3; STAT3, signal transducer and activator of transcription 3; TBXAS1, thromboxane A synthase 1; TXAS, thromboxane A synthase; TXA2, thromboxane A2; TXB2, thromboxane B2.

results in cortical hyperostosis of the long bones in humans [26], suggesting a direct effect of PGE2 in promoting bone sclerosis. Loss-of-function variants in *SLCO2A1* gene [27] (encoding solute carrier organic anion transporter family member 2A1 that mediates the transport of PG) and *HPGD* gene [28] (encoding 15-hydroxyprostaglandin dehydrogenase that is responsible for PG degradation) can lead to chronically elevated PGE2 levels and result in bone and joint pain and diaphyseal periosteal thickening. We observed the improvement of bone density in patients with decreasing levels of PGE2, which provided an effective therapeutic target and highlighted the importance of monitoring PGE2 levels in evaluating the effectiveness of treatment. Thus, the bidirectional regulation between TX and PG pathways progressively exacerbates bone sclerosis.

PGE2 is thought to be a key mediator of inflammation and pain in both rheumatoid arthritis and osteoarthritis, with high levels of PG E synthase in the synovial membrane [4]. In addition, pathogen-derived endotoxins activate macrophage production of pyrogenic cytokines, which subsequently circulate to circumventricular organs and induce local PGE2 synthesis and release, leading to fever [29], one of the most prominent symptoms in AIDs. We observed elevated PGE2 levels in a subset of patients with AIDs, which may be associated with disease activity. Beyond the hallmark PGE2 elevation and inflammatory manifestations, patients with GHDD consistently present with distinctive clinical features as osteosclerosis. However, high serum CRP and IL-6 levels are typically associated with osteoporosis [30], so we speculate that the increase in CRP and IL-6 is secondary to the elevated PGE2. Abnormal generation of TXA2 and excessive production of PGE2 are mainly responsible for osteosclerosis in patients with GHDD.

Mechanistically, we demonstrated that PGE2 induces IL-6 expression through the EP2/cAMP/CREB pathway. Single-cell RNA sequencing and CyTOF revealed that monocytes were primarily responsible for the production of inflammatory factors, consistent with the specific expression of TBXAS1 in monocytes. Elevated PGE2 has been consistently reported to stimulate IL-6 secretion in diverse pathological conditions, including IL-1β-stimulated synovial fibroblasts [31], endoplasmic reticulum stress in glial cells [32], chronic rhinosinusitis [33], and chronic peritonitis [5], suggesting a conserved inflammatory mechanism. Several studies have demonstrated that cerebral COX2 and PGE2 are not induced by lipopolysaccharide (LPS)-driven inflammation in IL-6-deficient mice or in the presence of IL-6-specific neutralising antibodies [34,35]. IL-6 trans-signaling upregulates the expression of COX2 and increases the production of PGE2 in human granulosa-lutein cells [36]. These researches indicate that IL-6 may play a positive feedback role

in *TBXAS1* deficiency-induced inflammation. Inhibition of IL-6 signaling can block the production of COX2 and PGE2, which reveals the underlying mechanism of tocilizumab treatment.

While glucocorticoids have been reported to be effective in treating GHDD [10,21], their long-term use is limited by adverse side effects such as opportunistic infections [37], diabetes mellitus [38] and glucocorticoid withdrawal syndrome [39]. One of our patients relapsed when methylprednisolone dose was reduced to 12 mg/d, prompting him to seek alternative treatment. Full or intermediate-dose NSAIDs targeting COX2 are effective to normalise haematologic and inflammatory parameters [9]. However, the long-term therapy with NSAIDs is associated with high incidences of adverse events in the gastrointestinal tract and acute kidney injury [40]. Drugs with fewer side effects and suitable for long-term use still need to be sought. We successfully treated 2 patients with tocilizumab based on the molecular mechanism of PGE2-induced IL-6 elevation, which provides an option for the treatment of GHDD, especially in patients with prominent inflammatory phenotypes.

Many AIDs have been clearly defined based on shared signaling pathways or pathogenic mechanisms, such as the type I interferonopathy and inflammasomopathy [41]. However, AIDs resulting from defects in the AA pathway, which is an important source of inflammatory mediators, have not yet been systematically classified. Further studies are needed to determine whether additional monogenic defects in the AA pathway give rise to a distinct group of inflammatory diseases.

Competing interests

The authors have no conflicts of interest to disclose.

Acknowledgements

We thank the patients, their families, and the unaffected controls for their support during this research study.

Contributors

QZ and XY designed the study and supervised the research. LL, JW, YD, LG, and MK contributed equally. LL and JW performed the experiments and analysed the data. YD, YW, LG, QM and ML enrolled the P1, collected, interpreted clinical information and administered the treatment. YL and XY collected and analysed the image data of the P1. MK enrolled the P2, collected, interpreted clinical information and administered the treatment. YF and YZ performed some of the experiments and analysed data. XS and YW contributed to data analysis. BZ recruited some patients as disease controls. BZ and XT interpreted clinical information and edited the manuscript. LL, JW and QZ wrote the manuscript. All authors edited and approved the final version of the manuscript.

Funding

The works of QZ were supported by grants 82225022, 32141004 and 32321002 from the National Natural Science Foundation of China, and 2024YFC2511002 from the National Key Research and Development Program of China. LL received the grant 82000667 from the National Natural Science Foundation of China. XY received the grants 82394420, 82394424 and 82471844 from the National Natural Science Foundation of China, the Hundred-Talent Program of Zhejiang University, the grant 2024Z221 from Key Technology Breakthrough Program of Ningbo Sci-Tech Innovation YONGJIANG 2035 and grant 2021R01012 from Leading Innovative and Entrepreneur Team Introduction Program of Zhejiang. JW received the grants 82394423, 82394420, and 82402121 from the National Natural Science Foundation of China, 2023M733104 from the China Postdoctoral Science Foundation. LG received the grant LHDMY23H100005 from the Joint Funds of the Zhejiang Provincial Natural Science Foundation of China.

Patient consent for publication

Written informed consent for publication was obtained from both participating patients.

Ethics approval

This study was performed according to the protocol approved by the institutional review boards of the Wuhan Children's Hospital (2024R076-E01) and Children's Hospital, Zhejiang University School of Medicine (2021-IRB-0172).

Provenance and peer review

Not commissioned; externally peer reviewed.

Data availability statement

The research data, including patient data, are available on reasonable request to the corresponding authors.

Supplementary materials

Supplementary material associated with this article can be found in the online version at doi:10.1016/j.ard.2025.09.014.

REFERENCES

[1] Wang B, Wu L, Chen J, Dong L, Chen C, Wen Z, et al. Metabolism pathways of arachidonic acids: mechanisms and potential therapeutic targets. Signal Transduct Target Ther 2021;6(1):94.
[2] Narumiya S, Sugimoto Y, Ushikubi F. Prostanoid receptors: structures, properties, and functions. Physiol Rev 1999;79(4):1193–226.
[3] Tsuge K, Inazumi T, Shimamoto A, Sugimoto Y. Molecular mechanisms underlying prostaglandin E2-exacerbated inflammation and immune diseases. Int Immunol 2019;31(9):597–606.
[4] Park JY, Pillinger MH, Abramson SB. Prostaglandin E2 synthesis and secretion: the role of PGE2 synthases. Clin Immunol 2006;119(3):229–40.
[5] Hinson RM, Williams JA, Shacter E. Elevated interleukin 6 is induced by prostaglandin E2 in a murine model of inflammation: possible role of cyclooxygenase-2. Proc Natl Acad Sci U S A. 1996;93(10):4885–90.
[6] Isidor B, Dagoneau N, Huber C, Genevieve D, Bader-Meunier B, Blanche S, et al. A gene responsible for Ghosal hemato-diaphyseal dysplasia maps to chromosome 7q33-34. Hum Genet 2007;121(2):269–73.
[7] Geneviève D, Proulle V, Isidor B, Bellais S, Serre V, Djouadi F, et al. Thromboxane synthase mutations in an increased bone density disorder (Ghosal syndrome). Nat Genet 2008;40(3):284–6.
[8] Selina A, Kandagaddala M, Madhuri V. A recurrent biallelic pathogenic variant in TBXAS1 gene causing Ghosal hematodiaphyseal dysplasia. Indian J Pediatr 2021;88(4):381–2.
[9] Brown TJ, Barrett N, Meng H, Ricciotti E, McDonnell C, Dancis A, et al. Nonsteroidal anti-inflammatory drugs as a targeted therapy for bone marrow failure in Ghosal hematodiaphyseal dysplasia. Blood 2023;141(13):1553–9.
[10] Kim SY, Ing A, Gong SY, Yap KL, Bhat R. Novel compound heterozygous variants of TBXAS1 presenting with Ghosal hematodiaphyseal dysplasia treated with steroids. Mol Genet Genomic Med 2021;9(3):e1494.
[11] Mazaheri P, Nadkarni G, Lowe E, Hines P, Vuica M, Griffin M, et al. Ghosal hematodiaphyseal dysplasia: a rare cause of a myelophthisic anemia. Pediatr Blood Cancer 2010;55(6):1187–90.

[12] Wang Y, Wang J, Zheng W, Zhang J, Wang J, Jin T, et al. Identification of an IL-1 receptor mutation driving autoinflammation directs IL-1-targeted drug design. Immunity 2023;56(7):e1487.
[13] Yu Y, Chadee K. Prostaglandin E2 stimulates IL-8 gene expression in human colonic epithelial cells by a posttranscriptional mechanism. J Immunol 1998;161(7):3746–52.
[14] Cho WJ, Choe J. Prostaglandin E2 stimulates COX-2 expression via mitogen-activated protein kinase p38 but not ERK in human follicular dendritic cell-like cells. BMC Immunol 2020;21(1):20.
[15] Mayr B, Montminy M. Transcriptional regulation by the phosphorylation-dependent factor CREB. Nat Rev Mol Cell Biol 2001;2(8):599–609.
[16] Punyawatthananukool S, Matsuura R, Wongchang T, Katsurada N, Tsuruyama T, Tajima M, et al. Prostaglandin E_2-EP2/EP4 signaling induces immunosuppression in human cancer by impairing bioenergetics and ribosome biogenesis in immune cells. Nat Commun 2024;15(1):9464.
[17] Nishimoto N, Terao K, Mima T, Nakahara H, Takagi N, Kakehi T. Mechanisms and pathologic significances in increase in serum interleukin-6 (IL-6) and soluble IL-6 receptor after administration of an anti-IL-6 receptor antibody, tocilizumab, in patients with rheumatoid arthritis and Castleman disease. Blood 2008;112(10):3959–64.
[18] Khandelwal S, Khurana R, Kanvinde P, Khan S, Shah D, Dhabale T, et al. Steroid-responsive anemia with bony dysplasias: what lurks behind!. J Trop Pediatr 2024;70(5) fmae028.
[19] Jeevan A, Doyard M, Kabra M, Daire VC, Gupta N. Ghosal type hematodiaphyseal dysplasia. Indian Pediatr 2016;53(4):347–8.
[20] Joy P, Yoganathan S, Korula S, Abraham SSC, Barney AM, Walter VM, et al. Ghosal hematodiaphyseal dysplasia and response to corticosteroid therapy. Am J Med Genet A 2021;185(2):596–9.
[21] Sharma R, Sierra Potchanant E, Schwartz JE, Nalepa G. Chronic steroid-response pancytopenia and increased bone density due to thromboxane synthase deficiency. Pediatr Blood Cancer 2018;65(1):e26777.
[22] Sudhakar M, Sharma M, Kandasamy S, Gummadi A, Rawat A, Vignesh P. Novel TBXAS1 variants in two Indian children with Ghosal hematodiaphyseal dysplasia: a concise report. Eur J Med Genet 2022;65(5):104498.
[23] Yu IS, Lin SR, Huang CC, Tseng H-Y, Huang P-H, Shi G-Y, et al. TXAS-deleted mice exhibit normal thrombopoiesis, defective hemostasis, and resistance to arachidonate-induced death. Blood 2004;104:135–42.
[24] Davies P, Bailey PJ, Goldenberg MM, Ford-Hutchinson AW. The role of arachidonic acid oxygenation products in pain and inflammation. Annu Rev Immunol 1984;2:335–57.
[25] Smith WL, DeWitt DL, Garavito RM. Cyclooxygenases: structural, cellular, and molecular biology. Annu Rev Biochem 2000;69:145–82.
[26] Jørgensen HRI, Svanholm H, Høst A. Bone formation induced in an infant by systemic prostaglandin-E2 administration. Acta Orthop Scand 1988;59(4):464–6.
[27] Kimball TN, Rivero-García P, Barrera-Godínez A, Domínguez-Cherit J. Genotype and phenotype characterization of primary hypertrophic osteoarthropathy type 2 and chronic enteropathy associated with SLCO2A1: report of two cases and literature review. Am J Med Genet A 2024;194(3):e63446.
[28] Uppal S, Diggle CP, Carr IM, Fishwick CWG, Ahmed M, Ibrahim GH, et al. Mutations in 15-hydroxyprostaglandin dehydrogenase cause primary hypertrophic osteoarthropathy. Nat Genet 2008;40(6):789–93.
[29] Blatteis CM, Sehic E. Cytokines and fever. Ann N Y Acad Sci 1998;840:608–18.
[30] Qiu J, Lu C, Zhang L, Zhou X, Zou H. Osteoporosis in patients with rheumatoid arthritis is associated with serum immune regulatory cellular factors. Clin Rheumatol 2022;41(9):2685–93.
[31] Inoue H, Takamori M, Shimoyama Y, Ishibashi H, Yamamoto S, Koshihara Y. Regulation by PGE2 of the production of interleukin-6, macrophage colony stimulating factor, and vascular endothelial growth factor in human synovial fibroblasts. Br J Pharmacol 2002;136(2):287–95.
[32] Hosoi T, Honda M, Oba T, Ozawa K. ER stress upregulated PGE_2/IFNgamma-induced IL-6 expression and down-regulated iNOS expression in glial cells. Sci Rep 2013;3:3388.
[33] Shieh JM, Tsai YJ, Ma MC, Chen CL, Wu WB. The cyclooxygenase-2 upregulation mediates production of PGE2 autacoid to positively regulate interleukin-6 secretion in chronic rhinosinusitis with nasal polyps and polyp-derived fibroblasts. Sci Rep 2024;14(1):7559.
[34] Turnbull AV, Prehar S, Kennedy AR, Little RA, Hopkins SJ. Interleukin-6 is an afferent signal to the hypothalamo-pituitary-adrenal axis during local inflammation in mice. Endocrinology 2003;144(5):1894–906.
[35] Rummel C, Sachot C, Poole S, Luheshi GN. Circulating interleukin-6 induces fever through a STAT3-linked activation of COX-2 in the brain. Am J Physiol Regul Integr Comp Physiol 2006;291(5):R1316–26.
[36] Li SJ, Chang HM, Xie J, Wang JH, Yang J, Leung PCK. The interleukin 6 trans-signaling increases prostaglandin E2 production in human granulosa cells†. Biol Reprod 2021;105(5):1189–204.
[37] Chastain DB, Spradlin M, Ahmad H, Henao-Martínez AF. Unintended consequences: risk of opportunistic infections associated with long-term glucocorticoid therapies in adults. Clin Infect Dis 2024;78(4):e37–56.
[38] Li JX, Cummins CL. Fresh insights into glucocorticoid-induced diabetes mellitus and new therapeutic directions. Nat Rev Endocrinol 2022;18(9):540–57.
[39] Oray M, Abu Samra K, Ebrahimiadib N, Meese H, Foster CS. Long-term side effects of glucocorticoids. Expert Opin Drug Saf 2016;15(4):457–65.
[40] Bindu S, Mazumder S, Bandyopadhyay U. Non-steroidal anti-inflammatory drugs (NSAIDs) and organ damage: a current perspective. Biochem Pharmacol 2020;180:114147.
[41] Rood JE, Behrens EM. Inherited autoinflammatory syndromes. Annu Rev Pathol 2022;17:227–49.

Ann Rheum Dis 85 (2026) 715–729

Contents lists available at ScienceDirect

Annals of the Rheumatic Diseases

journal homepage: https://www.sciencedirect.com/journal/annals-of-the-rheumatic-diseases

Autoinflammatory disorders

A de novo dominant-negative *PSMB8* mutation causes severe CANDLE/PRAAS due to arrested proteasome biogenesis

Sophie Wolfgramm[1], Sara Alehashemi[2], Martin Wendlandt[1], Franziska G. Thiel[1], Adriana A. de Jesus[2], Jonas J. Papendorf[1], Hannes Wolfgramm[3], Flavia Llorente Alvarez[1], Emely Borngräber[1], Kat Uss[2], Farzana Bhuyan[2], Anvitha Metpally[2], Leif Steil[3], Christian Hentschker[3], Simone Venz[1], Ruba Al Abdulla[1], Léa Poirier[4], Christopher Friend[2], Fabiola Castello Casta[5], Iren Horkayne-Szakaly[6], Shoghik Akoghlanian[7], Peter J. Mustillo[8], Roshini S. Abraham[9], Paul Bastard[10,11,12,13], Thais C.L. Moura[14], Mayra B. Dorna[14], Katia T. Kozu[14], Jesper Kers[15,16,17], Y. K. Onno Teng[18], Robbert G.M. Bredius[19], Karin Palmblad[20], AnnaCarin Horne[20], Petter Brodin[20], Pilar Blanco-Lobo[21], José Bernabeu-Wittel[21], Laura Fernandez-Silveira[21], Olaf Neth[21], Anne Pagnier[22], Guilaine Boursier[23], Maud Tusseau[24], Thomas W.J. Huizinga[25], Benjamin Fournier[11,13], Bénédicte Neven[11,13], Uwe Völker[3], Gijs W.E. Santen[26], Jason M. Brenchley[5], Katherine R. Calvo[27], David Kleiner[28], Frédéric Ebstein[1,4], Elke Krüger[1,*], Raphaela Goldbach-Mansky[2,**]

[1] *Institute of Medical Biochemistry and Molecular Biology, University Medicine Greifswald, Greifswald, Germany*
[2] *Translational Autoinflammatory Diseases Section (TADS), Laboratory of Clinical Immunology and Microbiology, National Institute of Allergy and Infectious Diseases, National Institutes of Health, Bethesda, MD, USA*
[3] *Department of Functional Genomics, University Medicine Greifswald, Greifswald, Germany*
[4] *Nantes Université, CNRS, INSERM, L'Institut du Thorax, 44000 Nantes, France*
[5] *Barrier Immunity Section, Laboratory of Viral Diseases, National Institute of Allergy and Infectious Diseases, National Institutes of Health Bethesda, MD, USA*
[6] *Joint Pathology Center, Silver Spring, MD, USA*
[7] *Division of Rheumatology, Department of Pediatrics, Nationwide Children's Hospital, Columbus, OH, USA*
[8] *Division of Allergy and Immunology, Department of Pediatrics, Nationwide Children's Hospital, Columbus, OH, USA*
[9] *Department of Pathology and Laboratory Medicine, Nationwide Children's Hospital, Columbus, OH, USA*
[10] *Laboratory of Human Genetics of Infectious Diseases, Necker Branch, INSERM U1163, Necker Hospital for Sick Children, Paris, France*
[11] *University Paris Cité, Institut des Maladies Génétiques (Imagine) Institute, Paris, France*

*Correspondence to Dr. Elke Krüger, Institute of Medical Biochemistry and Molecular Biology, University Medicine Greifswald, Greifswald, Germany.
**Correspondence to Dr. Raphaela Goldbach-Mansky, Translational Autoinflammatory Diseases Section (TADS), National Institute of Allergy and Infectious Diseases, NIH, Bethesda, MD, USA.
E-mail addresses: elke.krueger@uni-greifswald.de (E. Krüger), raphaela.goldbach-mansky@nih.gov (R. Goldbach-Mansky).
Sophie Wolfgramm and Sara Alehashemi contributed equally.
Handling editor Josef S. Smolen.

https://doi.org/10.1016/j.ard.2025.10.021

[12] St. Giles Laboratory of Human Genetics of Infectious Diseases, Rockefeller Branch, The Rockefeller University, New York, NY, USA
[13] Pediatric Hematology-Immunology and Rheumatology Unit, Necker Hospital for Sick Children, Assistance Publique-Hôpitaux de Paris (AP-HP), Paris, France
[14] Children's Hospital of the University of Sao Paulo, Sao Paulo, Brazil
[15] Department of Pathology, Leiden University Medical Center, Leiden, Netherlands
[16] Department of Pathology, Erasmus Medical Center, Rotterdam, Netherlands
[17] Department of Pathology, Amsterdam University Medical Center, Amsterdam, Netherlands
[18] Center of expertise for Lupus-, Vasculitis- and Complement-Associated Systemic Autoimmune Diseases, Department of Internal Medicine, Section of Nephrology, Leiden University Medical Center, Leiden, Netherlands
[19] Department of Pediatrics, Leiden University Medical Center, Leiden, Netherlands
[20] Karolinska University Hospital, Stockholm, Sweden
[21] Hospital Universitario Virgen del Rocío, Instituto de Biomedicina de Sevilla (IBiS), CSIC/Universidad de Sevilla, Seville, Spain
[22] French National Reference Center of Autoinflammatory Diseases and Amyloidosis (CeRéMAIA), Immuno-Hémato-Oncologie (IHO), Grenoble Alpes University-Hospital, Grenoble, France
[23] French National Reference Center of Autoinflammatory Diseases and Amyloidosis (CeRéMAIA), CHU Montpellier, Department of Molecular Genetics and Cytogenomics, IRMB, INSERM U1183, Univ Montpellier, Montpellier, France
[24] University Hospital of Lyon, Department of Medical Genetics, CIRI, Inserm U1111, University Claude Bernard Lyon 1, UMR5308, ENS de Lyon, Lyon, France
[25] Department of Rheumatology, Leiden University Medical Center, Leiden, Netherlands
[26] Department of Clinical Genetics, Leiden University Medical Center, Leiden, Netherlands
[27] Hematology Section, Department of Laboratory Medicine, Clinical Center, NIH, Bethesda, MD, USA
[28] Laboratory of Pathology Center for Cancer Research, National Cancer Institute, National Institutes of Health, Bethesda, MD, USA

ARTICLE INFO

Article history:
Received 24 July 2025
Received in revised form 17 October 2025
Accepted 19 October 2025

ABSTRACT

Objectives: Proteasome-associated autoinflammatory syndromes (PRAAS) include a group of autoinflammatory interferonopathies caused by 20S proteasome dysfunction. We characterised pathomechanisms and treatment responses of patients with a de novo, dominant-negative (DN)-proteasome subunit beta type-8 (*PSMB8*) variant.
Methods: Patients with the DN-*PSMB8* p.G209R variant encoding a mutant β5i subunit of the 20S immunoproteasome were evaluated. Interferon biomarkers, proteasome activity, structural modelling, and proteotoxic stress responses were assessed. Patients' T cells underwent integrated transcriptomic and proteomic profiling to characterise immune dysregulation, proteotoxic stress responses, mitochondrial function, and type I interferon (IFN-I) associated stress signalling.
Results: Patients with DN-PRAAS presented with early-onset systemic inflammation, panniculitis, cytopenias, infections, and porto-sinusoidal vascular liver disease (PSVD), indicating broader immune dysfunction that partially responds to Janus kinase inhibition and/or interferon-α/β receptor blockade (anifrolumab). Mechanistically, the *PSMB8* p.G209R variant caused steric hindrance that impaired β5i propeptide processing and final 20S proteasome formation, resulting in intracellular protein aggregation, impaired mitochondrial metabolism, and altered neutral lipid processing. The IFN-I signature of patients' T cells was reduced by blockade of 2 integrated stress response (ISR)-regulating kinases, protein kinase R (PKR) and general control nonderepressible 2 (GCN2), and by Janus kinase signalling.
Conclusions: The DN-*PSMB8* p.G209R variant broadens the clinical and mechanistic PRAAS spectrum by causing 20S proteasome maturation arrest and uncovering a convergence between mitochondrial dysfunction and the ISR. Our findings implicate cytopenia in a pattern of vascular pathology, including PSVD of the liver. We further identify PKR and GCN2 as key mediators of maladaptive IFN-I responses and potential therapeutic targets.

INTRODUCTION

The discovery of loss-of-function (LOF) mutations in proteasome genes as a cause of the autoinflammatory disease spectrum of proteasome-associated autoinflammatory syndromes (PRAAS) has linked the 20S proteasome dysfunction to type I interferon (IFN-I)-driven autoinflammation and spurred investigations into mechanisms connecting impaired proteasome function with chronic inflammation and immune dysregulation, including aberrant IFN-I production [1]. The ubiquitin-proteasome system (UPS) is the principal pathway for degrading misfolded, damaged, or regulatory proteins, thereby maintaining protein homeostasis. In addition to proteolysis, the UPS intersects with a broad spectrum of cellular and metabolic pathways, including autophagy and lysosomal degradation [2–4], nutrient sensing [5,6], lipid metabolism [7], mitochondrial function [8], and immune signalling [9]. Mechanistically, the standard 26S proteasome consists of a 20S core particle with catalytic β1, β2, and β5 subunits, and 1 or 2 19S regulatory particle (s) (RP) for substrate recognition and unfolding, with the latter

WHAT IS ALREADY KNOWN ON THIS TOPIC

- Proteasome-associated autoinflammatory syndromes (PRAAS) are predominantly autosomal recessive diseases caused by variants in immuno- or standard-proteasome subunit genes with type I interferon (IFN-I)-driven autoinflammation that is responsive to Janus kinase inhibition.
- PRAAS is associated with proteotoxic cell stress due to reduced peptide hydrolysis of the 20S proteasome with increased IFN-I signalling dependent on the upregulation of the integrated stress response kinase PKR.

WHAT THIS STUDY ADDS

- Compared to homozygous or compound heterozygous (biallelic) PRAAS, 8 unrelated patients with the first dominant-negative (DN)-proteasome subunit beta type-8 (*PSMB8*) variant presented with broader immune dysregulation, including cytopenias, infections, and porto-sinusoidal vascular liver disease (PSVD), and may require baricitinib and anifrolumab to improve inflammatory control.
- Different cell models and structural modelling uncover the pathomechanism of the DN effect of the *PSMB8* p.G209R variant that results in steric hindrance and stalled propeptide processing at the preholo-proteasome stage that affects ~75% of all 20S immunoproteasomes.
- Molecular profiling of patients' expanded T cells reveals elevated mitochondrial stress and impaired lipid metabolism in DN-PRAAS, likely contributing to T cell dysfunction and cytopenias, which are associated with increased viral susceptibility and the development of PSVD, and contrasts with the milder phenotype observed in biallelic *PSMB8* CANDLE/PRAAS.
- Functional inhibition studies identify GCN2, another serine/threonine kinase that, in concert with PKR, modifies the integrated stress response and IFN-I signalling. Accumulation of intracellular protein aggregates, expansion of exhausted $CD8^+$ T cells, a mitochondrial stress signature, and lipid droplet formation may serve as additional biomarkers, beyond the IFN-I signature, to identify patients at risk for immunodeficiency and PSVD, and to guide treatment stratification.

HOW THIS STUDY MIGHT AFFECT RESEARCH, PRACTICE OR POLICY

- The study identifies a novel pathogenic variant causing DN-PRAAS with immune dysregulation and immunodeficiency, highlights the role of proteasome dysfunction in driving both PSVD and immune impairment, expands the spectrum of therapeutic targets, and proposes a tailored treatment approach within the broader CANDLE/PRAAS continuum.

targeting polyubiquitylated proteins [10,11]. The immunoproteasome, a specialised proteasome complex, is defined by the high-efficiency inducible catalytic subunits, β1i, β2i, and β5i, encoded by (*PSMB10*), *PSMB9,* and (*PSMB8*), that emerged following the genome-wide duplication ~500 million years ago, at the beginning of vertebrate diversification and adaptive immunity evolution [12]. It enhances antigen presentation and provides protection during IFN-induced oxidative stress and cytokine exposure [9,13–15]. The immunoproteasome subunits are upregulated in immune and nonimmune cells in response to IFNs and depend on the proper assembly involving proteasome maturation protein (POMP) and other chaperones [16–19].

LOF variants in 20S proteasome subunits underlie the spectrum of PRAAS, originally described in Hispanic [20,21] and Japanese [22,23] founder populations with *PSMB8* variants causing the same disease that is referred to as NNS: Nakajo-Nishimura syndrome; JASL: Japanese autoinflammatory syndrome with lipodystrophy, or CANDLE: chronic atypical neutrophilic dermatosis with lipodystrophy and elevated temperature [24]. Later discoveries of variants in genes encoding other 20S subunits (eg, proteasome subunit alpha type-3 (*PSMA3*), *PSMA5, PSMB4, PSMB9, PSMB10*) [25–32] and assembly chaperones (eg, *POMP* and proteasome assembly chaperone 2 (*PSMG2*)) [26,33–35] have expanded the clinical spectrum to include immunodeficiencies and infections. These range from recessive homozygous or (compound) heterozygous *PSMB8* variants [20,22–26,36–45] and DN variants including *POMP, PSMB9,* and *PSMB10,* the latter presenting with more prominent features of immunodeficiency [26,29–33,35]. CANDLE/PRAAS patients typically exhibit a prominent IFN-I signature [46], and the robust clinical response to Janus kinase inhibitors (JAKi), which block IFN signalling, provides clinical validation of a central role of IFN in driving inflammatory disease manifestations [47]. However, prolonged or high-dose JAKi treatment can lead to infections, including viral reactivation, which is particularly concerning in patients with more severe immune dysregulation. Recent studies have identified a role of the integrated stress response (ISR) serine/threonine kinase, protein kinase R (PKR), as sensor of proteotoxic stress through binding to misfolded indicator protein, interleukin 24 (IL-24), and activation of IFNβ signalling [48]; however, integration with other proteasome-mediated cell stress responses including mitochondrial dysfunction and metabolic dysregulation and their impact on organ dysfunction and damage are not well understood.

We report the first de novo *PSMB8* variant, p.G209R, that causes a dominant-negative (DN)-PRAAS phenotype with clinical features of immune dysregulation, which is not seen in CANDLE patients with disease-causing biallelic *PSMB8* variants. Through structural modelling and cellular profiling, we characterise mitochondrial and metabolic lipid stress, in addition to intracellular protein aggregates in patients' T cells, and thus expand the characterisation of maladaptive cell stress responses that contribute to immune dysregulation and provide novel treatment targets.

MATERIALS AND METHODS

Ethic statement

Patients 1 to 7 and healthy donors (HDs) were enrolled in the Natural History, Pathogenesis, and Outcomes of Autoinflammatory Diseases protocol (NCT02974595) at the National Institutes of Health (NIH), in Bethesda, MD, USA, with written informed consent obtained from participants or their legal guardians. Buffy coats from HDs and previously published HDs [49] were obtained for some experiments under protocol (BB 209/18 and BB 014/14). Patient 8 was enrolled at Imagine Institute, France (IRB number: 22.00729.000060).

Patient studies

DN patients were clinically assessed, and genetic analysis, clinical biomarkers assessment, including IFN signature and response to JAKi, and IFNAR blockade. Expanded T cells were generated from DN-PRAAS patients (Pt 1, Pt 2, Pt 4 and Pt 8), biallelic *PSMB8* (β5i) CANDLE/PRAAS patients, and from HDs (see Supplementary Methods).

Additional methods and materials can be found in the Supplementary Methods.

RESULTS

Clinical description

Through international collaboration, the cohort included 8 patients (5 female), aged 2 to 30 years, who all harbour a heterozygous *PSMB8* p.Gly209Arg (G209R) variant (6/8 de novo, 2/8 assumed de novo). Disease onset occurred in the neonatal period, and in 7/8 presented with fever, rash, and systemic inflammation (Fig 1A-F; S1 A-C). Patient 1 died at age 25 years from complications of portal hypertension, in the context of nodular regenerative hyperplasia (NRH). Patient 3 passed away at the age of 5 years due to cytomegalovirus (CMV) pneumonia. The clinical description of the cohort is summarised in Table S1.

Compared to patients with biallelic or digenic PRAAS, infections were frequent in all patients from an early age, including pneumonia and sepsis. Hepatosplenomegaly, abdominal distention, and ascites were common (7/8). Two patients were also diagnosed with congenital thyroid gland agenesis in infancy (Fig 1F, Table S1). The clinical characteristics of the DN cohort, including cytopenias, infections, and organ involvement, are depicted in comparison to biallelic PRAAS in Figure 1F. Haematologic and immunologic abnormalities were prominent in the cohort. Anaemia was observed in all patients (8/8), while persistent lymphopenia and hypogammaglobulinemia were observed in 7 out of 8 patients, who were all placed on immunoglobulin replacement therapy. Thrombocytopenia in 6 patients with splenomegaly was suggestive of splenic sequestration. Serial bone marrow biopsies (patient 2) showed variable hypocellularity, ranging from approximately 20% during systemic viral infection, to 60% −70% on treatment with anifrolumab and JAKi. The biopsies demonstrated preserved trilineage hematopoiesis, a marked reduction in B-cell lymphoid precursors, and preserved or increased myeloid cells. Flow analysis showed normal neutrophil maturation. (Fig S2). $CD4^+$, $CD8^+$ T-cell, and $CD19^+$ B-cell counts in the peripheral blood were plotted as a function of age. In comparison to age-matched controls, $CD19^+$ B cell lymphopenia with borderline $CD4^+$ T cell lymphopenia was documented and was lower in DN patients compared with digenic and biallelic *PSMB8* CANDLE patients. (Fig S3). Early in life, transient increases in CD19 counts and $CD4^+$ and $CD8^+$ T cells following documented viral infections suggested appropriate bone marrow responses (Fig 1G). Seven out of 8 patients had elevated acute phase reactants, and all had elevated IFN-I scores supporting an interferon-driven inflammatory process (Fig 1H and Supplementary Methods). All patients (8/8) experienced recurrent infections. Viral infections (8/8) included Epstein-Barr virus, CMV, norovirus, adenovirus, rotavirus, rhinovirus, coronavirus, parainfluenza, human herpesvirus 6, and human herpesvirus 8. Bacterial infections (5/8) included *Pneumocystis jirovecii* pneumonia (n = 2), *Pseudomonas aeruginosa* (n = 2), pneumococcal pneumonia (n = 1), and *Mycoplasma pneumoniae* (n = 1). Fungal infections (3/8) comprised pulmonary aspergillosis and cutaneous candidiasis and parasitic infection with *cryptosporidium* (n = 1).

NRH was identified in all patients who underwent liver biopsy (4/4) during the evaluation of transaminitis and hepatosplenomegaly. Serum levels of intestinal fatty acid−binding protein (I-FABP), a marker of gut epithelial damage and increased intestinal permeability, were markedly elevated in 2 patients (3 samples) with the DN-*PSMB8* variant. Patients with digenic PRAAS (2 patients, 4 samples) also showed elevated I-FABP levels, albeit to a lesser extent, whereas levels in biallelic PRAAS patients (3 patients, 4 samples) remained within the normal range (Fig 1I). These findings suggest that increased gut permeability in DN-PRAAS may contribute to bacterial translocation and liver pathology [50].

Seven of 8 patients received systemic corticosteroids (0.2−1 mg/kg/day), and 5 received additional disease-modifying therapies, including hydroxychloroquine (1/5), mycophenolate (3/5), methotrexate (2/5), infliximab (2/5), rituximab (1/5), antithymocyte globulin (1/5), and colchicine (1/5). Responses were partial and transient.

JAK inhibitors were initiated in 5 of 8 patients (3 received tofacitinib and 2 received baricitinib). All JAKi-treated patients demonstrated clinical improvement and discontinued disease-modifying drugs as outlined in Table S1. However, in contrast to biallelic *PSMB8* patients, who show normalisation of type I and type II IFN signatures on baricitinib, DN-PRAAS patients exhibited resolution of cutaneous manifestations and improvement in myositis but only partial normalisation of systemic inflammatory markers and IFN signatures (Fig 1K,L).

Two patients (patient 2 and patient 4) with incomplete responses to JAKis were subsequently treated with anifrolumab, a monoclonal antibody targeting the type I interferon receptor (IFNAR1). Both achieved normalisation of IFN scores (Fig 1J,K) and were able to discontinue systemic corticosteroids and taper high-dose JAKis. However, lymphopenia and susceptibility to recurrent viral infections persisted, and both patients showed progression of liver disease, including worsening splenomegaly and transaminitis.

Discontinuation of JAKi on anifrolumab treatment in 1 patient led to a clinical flare with elevation of C-X-C motif chemokine 9 (CXCL9) and re-emergence of skin lesions that subsided with reinstation of baricitinib (Fig 1J), suggesting that clinically relevant immune dysregulation in DN-CANDLE/PRAAS may extend beyond type I IFN signalling.

Compared with ‘classic PRAAS’ (biallelic *PSMB8* CANDLE/PRAAS), the DN cohort exhibits both overlapping features—such as panniculitis, lipodystrophy, and elevated IFN scores—and unique manifestations, including more pronounced cytopenias, susceptibility to infections, nodular regenerative hyperplasia, and nephropathy (Fig 1L). Patient 2 is currently undergoing evaluation for haematopoietic stem cell transplantation (HSCT) due to chronic *Pseudomonas aeruginosa* infections, early bronchiectasis, and progression of NRH with worsening splenomegaly.

The de novo heterozygous PSMB8 *p.G209R variant is predicted to be pathogenic and causes decreased immunoproteasome formation*

In silico predictions using MetaRNN (scores of 0.9511 and 0.9514) and AlphaMissense prediction (score of 0.842) support the pathogenicity of the *PSMB8/β*5i variant (c.625G>A and c.625G>C), which substitutes glycine with arginine at protein position 209, without predicted splicing impact (SpliceAI <0.2) (Table S2). Unlike the common founder mutation, p.T75M (minor allele frequency (MAF) 0.000025), p.G209R is absent from population databases, further supporting pathogenicity per ACMG/AMP criteria and suggesting a likely DN effect. Patient 4 also harboured 2 inherited *ADRM1* variants, affecting a 19S RP subunit of the 26S proteasome. ACMG predictions were benign and likely benign (Fig 1E, Table S1), and transfected variants had no significant impact on proteasome function. Additional variants observed in individual patients (Table S1) were not

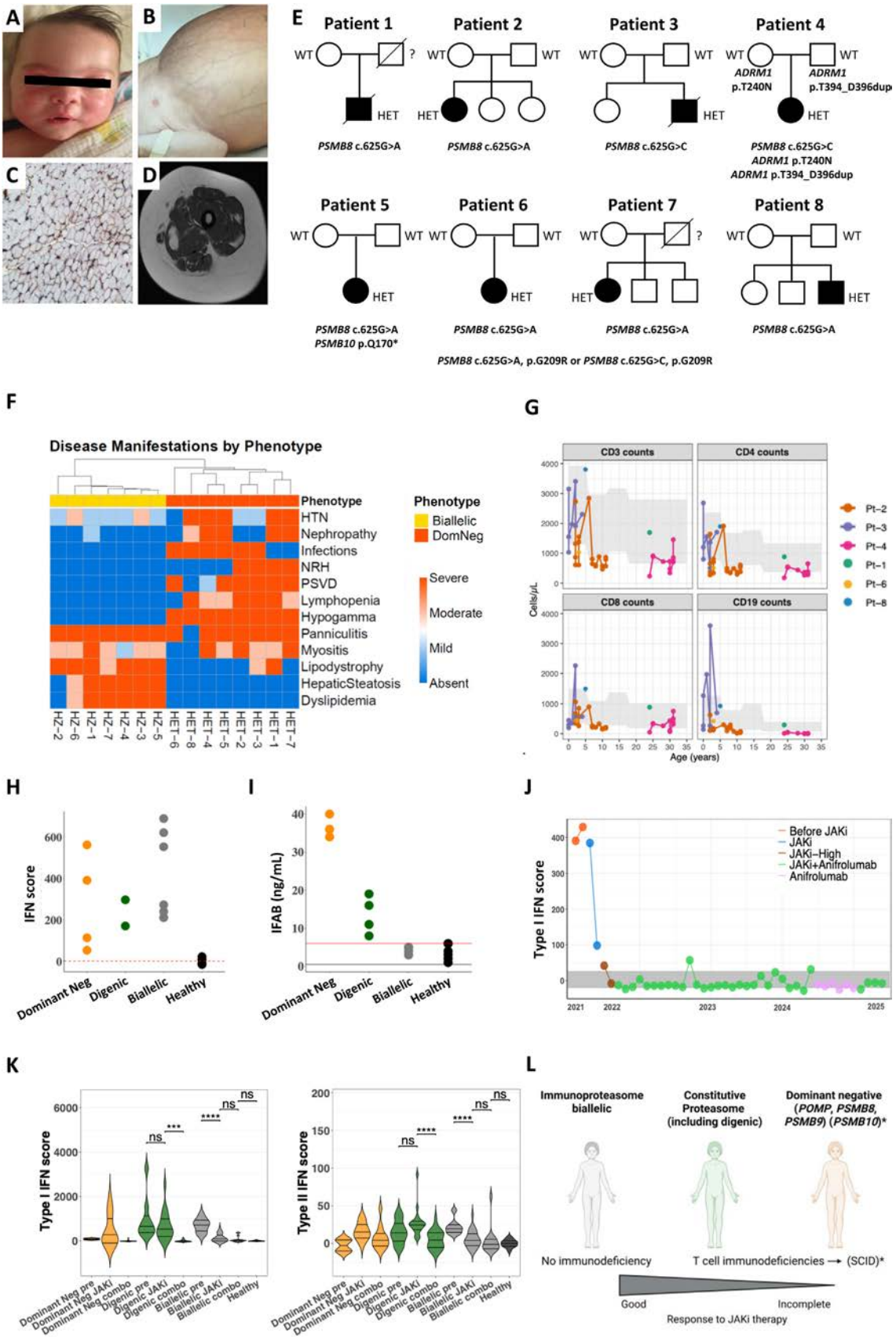

Figure 1. Clinical, histologic, genetic, and biomarker characterisation of patients with dominant-negative *PSMB8* mutations. A–B, Clinical photos showing a violaceous facial rash with periorbital oedema (A) and abdominal distention with prominent abdominal veins, indicative of portal hypertension, ascites, and hepatosplenomegaly (B). C, Muscle biopsy (20 ×) showing diffuse MHC class I upregulation and perifascicular myofibre atrophy, consistent with chronic inflammatory myopathy. D, Axial T1-weighted MRI of the lower extremities showing symmetrical patchy fat replacement and muscle atrophy (left thigh image shown). E, Pedigrees of affected individuals with heterozygous *PSMB8* p.G209R mutations, de novo in most cases. Additional heterozygous proteasome-related variants (*ADRM1* and *PSMB10*) are indicated, whereas proteasome-unrelated variants are mentioned in Table S1. Filled symbols represent affected individuals. Patients 1 and 3 are deceased. F, Heatmap summarizing clinical phenotypes in heterozygous (HET, n = 8) and homozygous (HZ, n = 7) *PSMB8* mutation carriers. Colour intensity reflects severity scores (0–3, absent, mild, moderate, severe)

considered relevant, as the de novo *PSMB8* p.G209R variant was shared across all patients and was selected for in-depth analysis.

To characterise proteasome activity of the *PSMB8* p.G209R variant, we assessed proteasomal chymotrypsin-like activity in expanded T cells from patients and controls in native PAGE assays, which was decreased in proteasome complexes (Fig 2A-D; S4A-D). Total proteasomal activity staining was decreased in proteasome-specific activity-based assessment (Fig S4E), similarly to caspase and trypsin-like activity that were assessed in patient 4 compared to the controls (Fig S4F). Staining of proteasome complexes, α6 and β5i, indicated a partial assembly defect with accumulation of 20S precursor complexes at lower molecular weight (Fig 2D). The decreased β5i signal suggested less incorporation of the mutant subunit into active proteasomes, a finding consistent with haploinsufficiency (Fig 2D; S4A). The staining for 19S cap component, Rpn5, was similar to HDs (Fig S4B), suggesting normal recruitment of the 19S regulatory cap.

Immunoblotting showed higher standard β5 subunit expression than control with unchanged total β5i protein levels (proform and matured form), while incorporation of the other standard catalytic subunits, β1 and β2, and the induced subunits, β1i and β2i, were similar to controls (Fig 2E) suggesting decreased incorporation of the β5i G209R variant into the active proteasome with a partial compensatory replacement by the constitutive β5 subunit accounting for the decreased β5i activity observed. Accumulation of proteasome precursor complexes (Fig 2D, left panel) and increased residual levels of the assembly helper chaperone POMP (Fig 2E, right panel; S4G) indicate that the β5i G209R variant perturbed proteasome assembly, resulting in POMP retention in an incompletely matured proteasome complex.

Transfection studies confirm a proteasome maturation defect caused by the PSMB8 *p.G209R variant*

To study the impact of the *PSMB8* p.G209R variant on proteasome maturation and assembly *in vitro*, we transfected V5-epitope-tagged mutant and wild-type *PSMB8* constructs into C20 microglia cells, EA.hy926 human endothelial cells, and HeLa cells, a human epithelial cell line (Fig 3; S5-7). Two cell lines (C20 and EA.hy926) were CRISPR/Cas9 engineered to lack endogenous *PSMB8*/β5i (*PSMB8* knock out (KO)). V5-epitope-tagged versions of β5i were quantified in immunoblots (Fig 3A-B; S5A-B; S6A-B). Strikingly, in all parental and KO cells transduced with the mutant β5i G209R-V5 construct, the mutant propeptide was not cleaved off completely, suggesting failed propeptide processing for maturation of the subunit (Fig 3B; S5B; S6A). In contrast, the WT construct and the known CANDLE-causing β5i T75M-variant allowed for pro-β5i cleavage and final proteasome maturation, albeit decreased efficiency was seen with β5i T75M-V5 [26].

These data suggest that the p.G209R variant may exert the DN effect by affecting proteasome formation even if WT β5i is endogenously expressed in parental cells. We studied proteasome precursor complexes and identified accumulation of a 20S proteasome intermediate complex in all β5i G209R-V5-expressing cells (Fig 3C; S5C; S6B) that migrates slower and retains the assembly chaperone POMP, which identifies a premature 20S proteasome complex [51] (Fig 3C; S5C). These experiments further indicate that POMP cannot be degraded in the maturation-arrested β5i G209R-mutant proteasome complex. Despite these defects, the cell models do not show striking alterations in the chymotrypsin-like activity (Fig S5E; S6C; S7C).

POMP is required for the incorporation of β5 and β5i; however, β5i has a significantly higher affinity to POMP and is thus preferentially incorporated [18]. Co-immunoprecipitation of FLAG-tagged POMP with wild-type β5i WT-V5 or mutant β5i G209R-V5 showed less association of mutant β5i G209R with POMP compared to the β5i WT-V5 in HeLa cells (Fig 3D; S6D). These results led to the conclusion that a better compensation of proteasome activity by β5 was blocked by β5i G209R mutant interaction with POMP and the incorporation of the mutant variant into nascent proteasome complexes that cannot mature.

The β5i G209R variant blocks conformational changes required for proteasome maturation

To interrogate the structural basis for the proteasome maturation arrest at the preholo-proteasome stage, we used updated structural models of standard 20S-proteasome precursors [51] and immunoproteasomes from various mammalian species, combining available structures with AlphaFold3 predictions for the subunit variant. Proteasome assembly involves multiple steps and chaperones, including POMP and proteasome assembly chaperones (Fig 4A) [19,51]. The glycine at β5i position G209 resides within a compact helix (p.N204 to p.G214) that closely interacts with 2 helices of the opposing β4-subunit, suggesting a critical interface during proteasome biogenesis (Fig 4B,C). Substituting glycine (G) with a bulky, positively charged arginine (R) at p.G209 introduces a steric hindrance, as the arginine side chain clashes with β4 residues T139 and E166,

across 10 clinical domains. HTN, hypertension; NRH, nodular regenerative hyperplasia; PSVD, porto-sinusoidal vascular disease of the liver. G, Age-dependent distribution of $CD3^+$, $CD4^+$, $CD8^+$ T-cell, and $CD19^+$ B cell counts in representative dominant negative CANDLE patients compared with age-appropriate reference ranges (grey shading). Each dot represents a single measurement for an individual subject. Subjects Pt-2, Pt-3, and Pt-4 had longitudinal assessments, and connecting lines trace serial values over time. Subjects with a single available time point, including Pt-1, Pt-6, and Pt-8 are displayed as individual dots. The shaded grey area corresponds to published normative ranges for each lymphocyte subset. H, Type I interferon (IFN) scores measured using a 28-gene panel in HET (n = 5), HZ (n = 2), and biallelic (n = 7) *PSMB8* mutation carriers compared to healthy controls (HC, n = 6). Red lines indicate assay thresholds. I, Circulating intestinal fatty acid binding protein (IFABP) levels in HET (2 patients, 3 samples), digenic (2 patients, 4 samples), biallelic (3 patients, 4 samples), and HC (n = 6). Red lines indicate assay thresholds. J, Longitudinal IFN scores over three years in a patient treated with JAK inhibitor (JAKi) and IFNAR1 blockade with anifrolumab. Initial JAKi monotherapy with baricitinib (0.2 mg/kg) incompletely suppressed the IFN signature, requiring high-dose systemic steroids. Escalation to 0.3 mg/kg daily is limited by recurrent infections. Combination JAKi and anifrolumab therapy achieved durable IFN suppression, enabling baricitinib tapering (0.1 mg/kg daily) and steroid discontinuation. IFNAR1 blockade monotherapy with anifrolumab maintained low IFN scores but was associated with disease flare (rash, myositis, and CXCL9 elevation). Resumption of combination therapy restored remission. K, Type-I and type-II IFN scores by DN (yellow, n = 4 patients), digenic (green, n = 2 patients) and biallelic (grey, n = 9 patients) CANDLE/PRAAS patients before and during JAKi and on JAKi + anifrolumab (combo) therapy compared to controls (black, n = 21 patients). For DN, combo therapy data reflect a single patient. Significant differences were detected for digenic JAKi vs combo (***$P < 0.001$) and biallelic pretreatment vs JAKi (***$P < 0.001$); all other comparisons were not significant (ns). L, Overview of inherited or dominant-negative CANDLE/PRAAS variants and their response to JAKi therapy. Created in BioRender. Venz, S. (2025) https://BioRender.com/ow4aslt.

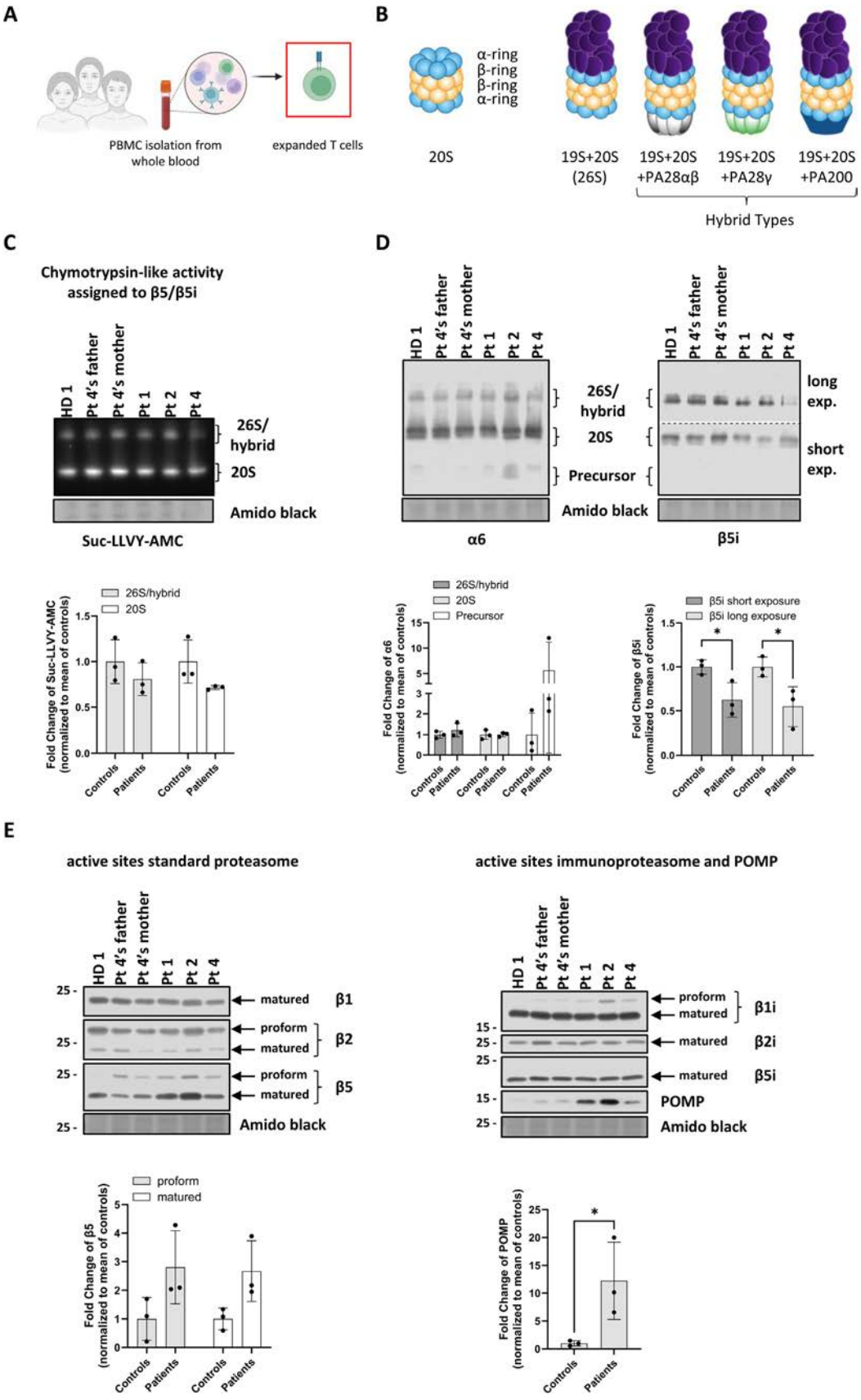

Figure 2. Analyses of proteasome activity and proteasome complexes in patients' expanded T cells. A, Expanded T cells derived from peripheral blood mononuclear cells (PBMCs) from patients and healthy donors were used for analysis. B, Representative illustration of 20S proteasome, 26S proteasome, and hybrid proteasomes. C, In-gel activity assay of chymotrypsin-like activity (Suc-Leu-Leu-Val-Tyr-7-amino-4-methylcoumarin, Suc-LLVY-AMC) and its densitometric analysis from patients 1, 2, and 4 (Pt 1, 2, and 4), including healthy donors: HD 1 and the unaffected parents from patient 4. D, Immunoblots of native PAGE gels and their densitometric analysis from patients 1, 2, and 4 (Pt 1, 2, and 4), including healthy donors: HD 1 and the unaffected parents from patient 4 that were stained with an α6 and β5i antibody to visualise proteasome complexes. The horizontal black dotted line indicates a border to visualise 2 different exposure (exp.) times (long and short) of the same membrane. E, Immunoblots and densitometric analyses showing alterations within the protein expression regarding the catalytically active sites of the standard and immunoproteasomes and the assembly

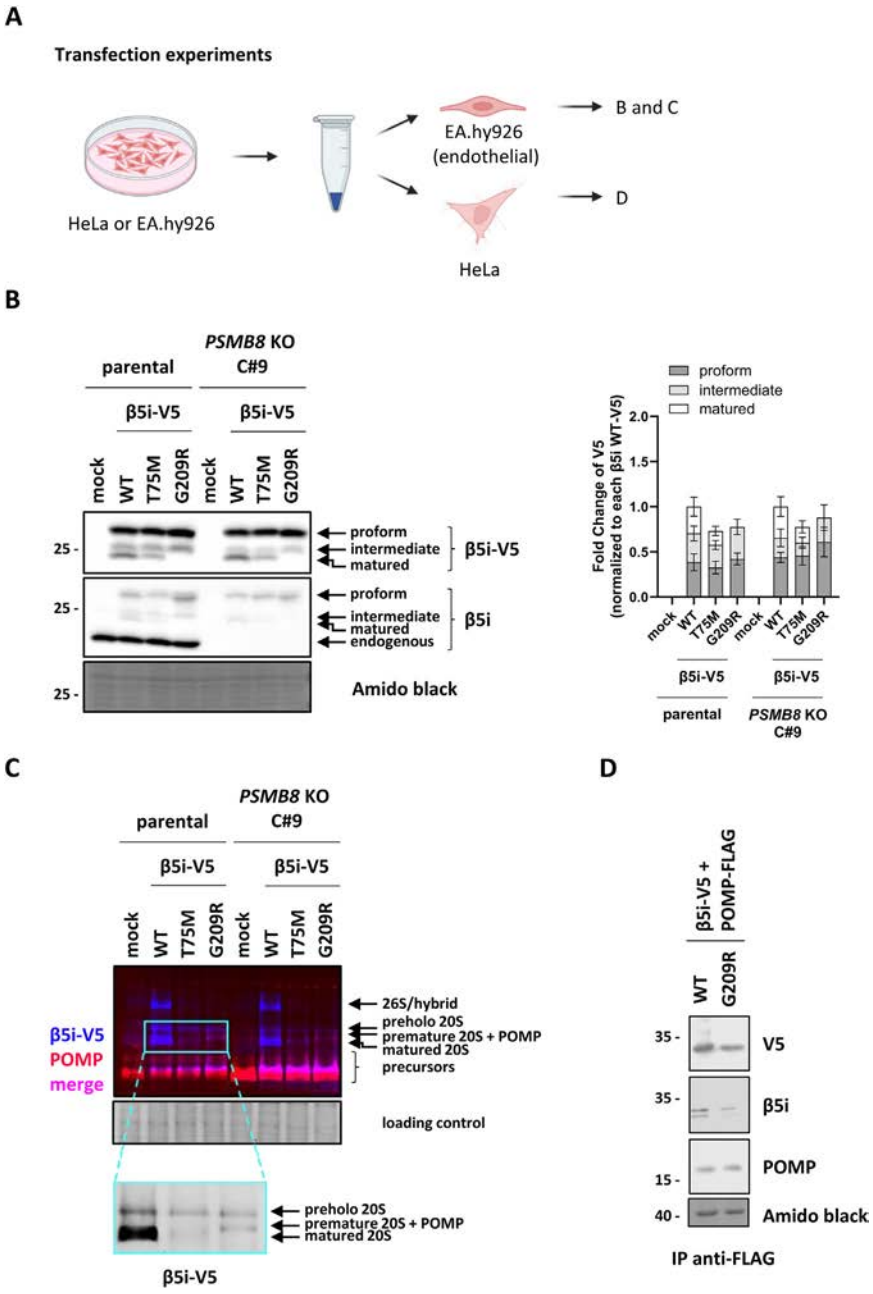

Figure 3. Molecular and functional analyses of EA.hy926 and HeLa *PSMB8*/β5i variants in transfected cells. A, Scheme of cell models used for analysis in B-D. B, SDS-PAGE immunoblot of β5i and V5-tagged β5i in EA.hy926 β5i WT-V5/HIS, β5i T75M-V5/HIS, and β5i G209R-V5/HIS transfected cells depicting the propeptide processing of β5i. Densitometric analysis was performed with n = 5. C, Cofluorescence staining (V5-tagged β5i and POMP) of EA.hy926 β5i WT-V5/HIS, β5i T75M-V5/HIS, and β5i G209R-V5/HIS transfected cells in native PAGE showing different proteasome complexes (n = 3). D, Immunoprecipitation of FLAG-tagged POMP in HeLa transfected β5i WT-V5/HIS and β5i G209R-V5/HIS cells depicting the interaction with β5i (n = 2). Densitometric analysis was normalised to the respective loading control using ImageJ and GraphPad Prism (v.10.2.2). Statistic was applied using the Friedman test with Dunn's correction in GraphPad Prism (v.10.2.2) (Table S3). Created in BioRender. Venz, S. (2025) https://BioRender.com/tsiovsf.

destabilising β4/β5i interactions and preventing proper proteasome maturation (Fig 4C). This likely disrupts the required conformational 'twist' necessary for propeptide processing and final proteasome maturation (Fig 4D), providing a mechanism for the observed maturation defect. Furthermore, the variant perturbs the close approximation of residues within the C-terminal arm of β7/*PSMB4* and the opposing β1/β2 subunits that upon fusion reposition a catalytic lysine triad to activate a catalytic threonine through autocatalysis. The disruption results in β1 propeptide retention [52,53]. This steric clash/hindrance occurs when one or both half-proteasomes incorporate the DN-*PSMB8* variant and thus may affected up to ~75% of immunoproteasomes, consistent with a DN effect (Fig 4E).

Molecular profiling of patient T cells revealed a mitochondrial and metabolic stress signature and an ISR-dependent IFN-signature

The more pronounced cytopenias and T cell-related pathology in the DN-PRAAS patients compared to biallelic PRAAS suggested broader immune dysregulation caused by the β5i G209R-variant, prompting a comparative omics approach to identify cell stress signatures beyond the ISR (Fig 5A). Proteasome

helper POMP of patients 1, 2, and 4 (Pt 1, 2, and 4) to healthy donors, including HD 1 and the unaffected parents from patient 4. Representative Amidoblack stainings show loading and transfer efficiency. All densitometric analyses were normalised to the respective loading controls using ImageJ and GraphPad Prism (v.10.2.2). For statistical testing, an unpaired *t* test was performed, considering a *P* value ≤ 0.05 (*) as significant. Created in BioRender. Venz, S. (2025) https://BioRender.com/jgt88oy; https://BioRender.com/tsiovsf.

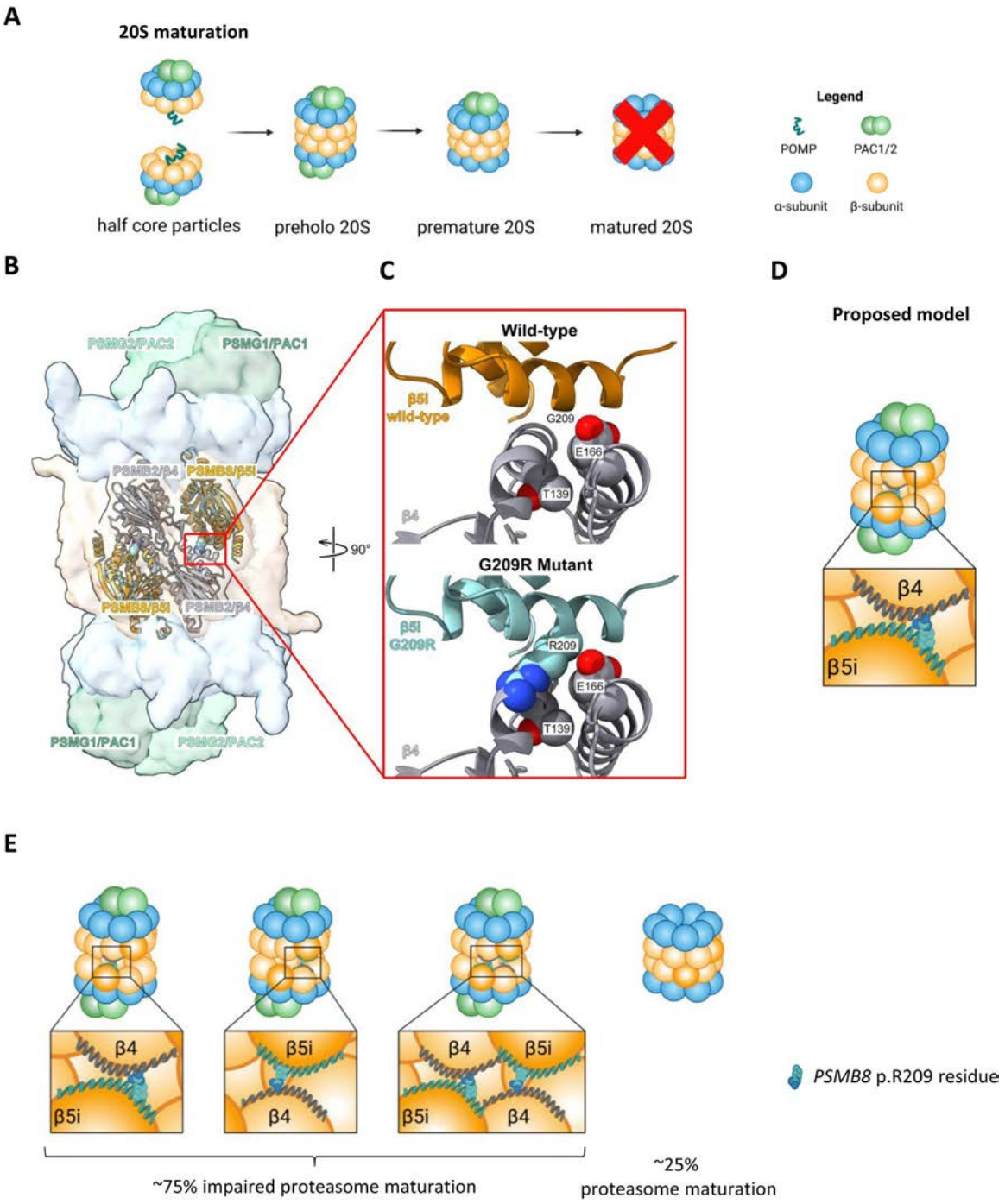

Figure 4. *In silico* steric modelling of de novo PSMB8 Gly209Arg mutation using the preholo-proteasome crystal structure. A, Illustration of the standard 20S maturation. The frame highlights the used structural model for B. B, Cartoon of the standard 20S preholo-proteasome (PDB:8QYS) and the superpositioned β5i (*PSMB8*) with its close interaction side to β4 (*PSMB2*). The red frame indicates the region of interest (C). C, Zoom-in of β5i structure (orange) within the preholo-proteasome, highlighting the variant's position at 209 in the wild-type structure and the closely related amino acids of β4 (grey). The steric clash between the mutated β5i (turquoise) and β4 (grey) is shown by using AlphaFold3 to introduce the amino acid exchange of β5i at position 209 from a glycine (G) to an arginine (R). D, Proposed model of β5i-G209R incorporated proteasomes based on the preholo-proteasome structure, indicating a maturation stop (A). E, Probability of *PSMB8* p.G209R incorporation within the proteasome biogenesis process. Created in BioRender. Venz, S. (2025) https://BioRender.com/s7 × 9ft6; https://BioRender.com/lp7rt0z.

defects can initiate a vicious cycle with mitochondrial impairment, compounding cellular stress [54]. To assess this interplay, we profiled phytohaemagglutinin-lectin (PHA-L) + IL-2 activated T cells (Supplementary Methods), which represent a maximally activated and metabolically stressed state that models immune activation-induced cellular stress. Proteomic and transcriptomic analyses revealed that hallmark cellular and metabolic pathways are more disrupted in DN than biallelic PRAAS T cells, with a prominent cell death signature in DN-PRAAS in transcriptomic (Fig S8A) and proteomic profiling (Fig S9A). Proteomic profiling suggested mitochondrial dysfunction and related metabolic pathways in CANDLE/PRAAS compared to controls (Fig S9A). Activated T cells from both DN and biallelic *PSMB8* PRAAS patients showed protein signatures of impaired mitochondrial respiration (reduced COX5B, SYNE2, AK4), but only DN-PRAAS T cells downregulated proteins critical for

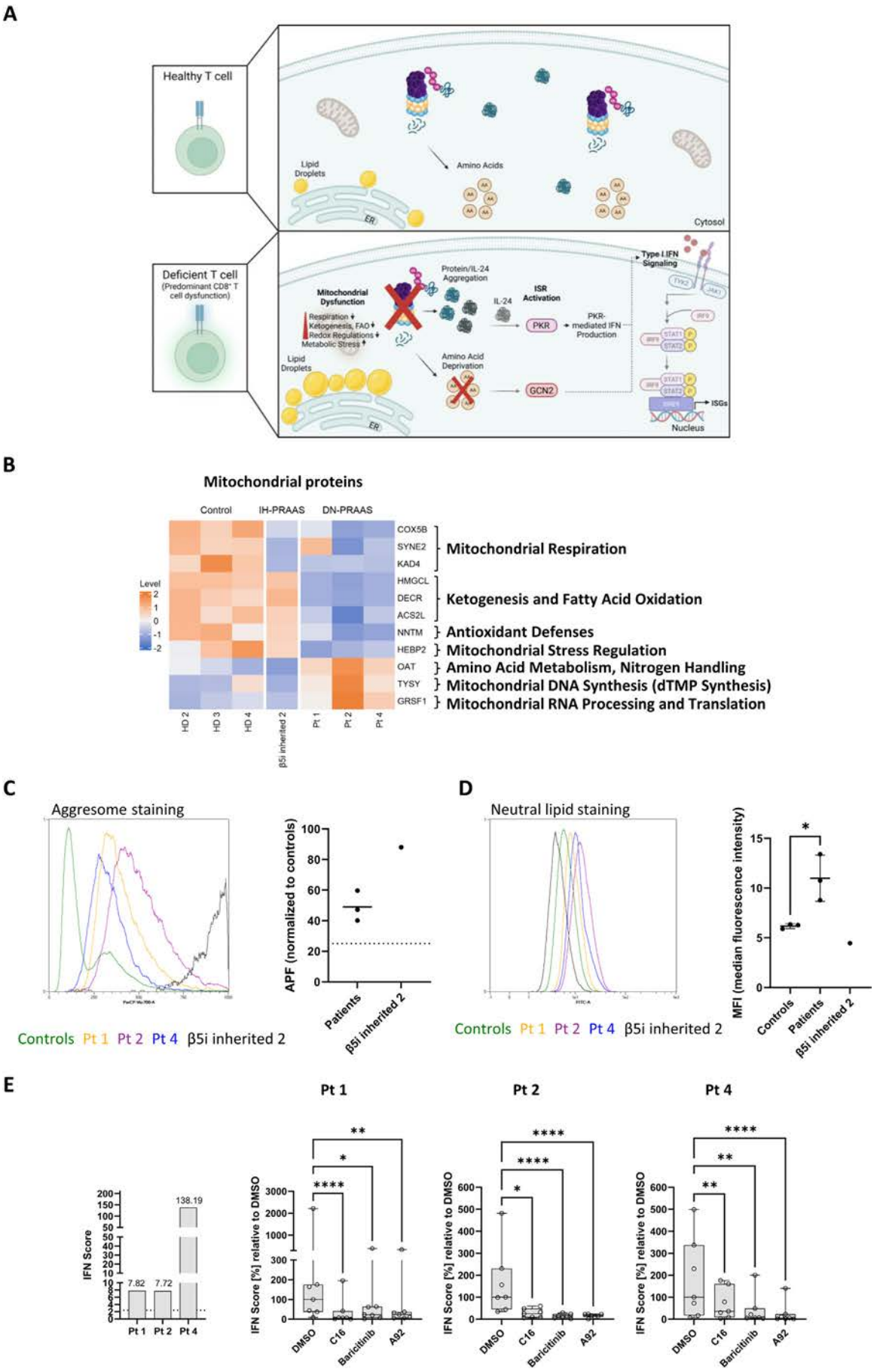

Figure 5. Molecular analysis of the patient's expanded T cells. A, Summary of affected cellular processes in deficient T cells. B, Heatmap of regulated mitochondrial proteins from proteomic profiling of patients 1, 2, and 4 (Pt 1, 2, and 4) and healthy donors (HD 2, 3, and 4), including the pathogenic variant β5i C135* homozygous (β5i inherited 2). C, Fluorescent-based protein aggregate staining assay was performed in patients' T cells (Pt 1, 2, and 4) and healthy donors (HD 1, father and mother of patient 4), including a known inherited PRAAS variant, β5i C135* (β5i inherited 2). The aggresome

ketogenesis and fatty acid oxidation (eg, HMGCL, DECR1, ACSL2), lost protective mitochondrial redox regulation (eg, NNTM and HEBP2), and upregulated proteins indicating increased amino acid metabolism and mitochondrial DNA and RNA processing (Fig 5B). These changes drive mitochondrial dysfunction that has been linked to cellular exhaustion (eg, *CTLA4* and *PDCD1*) and increased cell death (Fig S8A-B) [55]. Of note, an altered CD4/CD8 ratio of the expanded T cells for 2 patients could be observed (Fig S8C).

Protein aggregate staining confirmed disrupted proteostatic processes in both DN and biallelic PRAAS T cells compared to healthy controls (Fig 5C) with increased lysine 48 (K48)-linked ubiquitin-conjugates (Fig S9B). In addition, lipid droplet formation, a sign of impaired fatty acid utilisation and maladaptive proteotoxic stress buffering [56,57], was notably increased in DN-PRAAS T cells, but not in biallelic cases (Fig 5D). These droplets were recently found to sequester ubiquitylated proteins under stress [58], reflecting a dysfunctional response to severe cell stress.

Several cell stress pathways converge on eIF2α phosphorylation to activate the ISR [59,60]. Proteasome impairment also depletes the intracellular free amino acid pool, activating general control nonderepressible 2 (GCN2) via uncharged tRNA sensing [61]. Inhibitor studies in patient T cells confirmed that PKR inhibition (C16) and GCN2 inhibition (A92) significantly reduced IFN-I scores, comparable to the JAKi baricitinib (Fig 5E). In contrast, inhibition of an endoplasmic reticulum stress sensor, IRE1α (by 4μ8c), or of the dinucleotide sensor stimulator of interferon gene (by H-151) had no significant effect (Fig S9C). These findings highlight the increased mitochondrial, proteotoxic, and lipotoxic stress responses as central features of T cell activation in DN-PRAAS over biallelic PRAAS and suggest PKR and possibly GCN2 as potential therapeutic targets.

DISCUSSION

PRAAS comprises a spectrum of IFN-I-driven autoinflammatory disorders caused by LOF variants in 20S proteasome subunits or their assembly factors. We report a heterozygous, de novo, DN-*PSMB8* mutation, p.G209R, that expands the genophenotype associations of *PSMB8*-related CANDLE/PRAAS beyond recessive inheritance, introducing immune dysregulation and cytopenias as dominant clinical features. This variant deepens our understanding of proteasome dysfunction by integrating structural and functional modelling of progressive 20S proteasome impairment and supporting a severity-dependent disease model with novel biomarkers and implications for a personalised therapeutic approach.

Unlike the 'classic PRAAS' phenotype associated with homozygous founder mutations p.T75M and p.G201V in Hispanic [20,21] and Japanese populations [22,23], respectively, DN-*PSMB8* PRAAS manifests with immunodeficiency, T and B cell lymphopenia, perinatal infections, and vascular liver and renal involvement, resembling features of POMP-related autoinflammation and immune dysregulation [33].

The de novo *PSMB8* p.G209R variant leads to severe impairment of β5i-propeptide processing, affecting ~75% of the immunoproteasomes. Structural modelling revealed that the 'bulky', positively charged mutant arginine residue at position 209 that replaces the highly conserved wild-type glycine protrudes into the β4/β5i interface, creating steric clashes with β4-subunit residues (p.T139 and p.E166), and prevents proper propeptide maturation (Fig 4). Functional assays confirmed a block in final proteasome maturation at a POMP-retaining preholoproteasome state (Fig 3), explaining the profound dysfunction caused by the DN, disease-causing variant. These findings align with functional assays in previously reported DN variants, including truncating POMP variants that escape nonsense-mediated decay and incorporate into proteasome precursors [26,33], the DN-*PSMB9* variant, p.G156D (Fig S10) [29,30], and DN-*PSMB10* variants p.D56H and p.G201R [31,32]. AlphaFold3-based structural modelling of these variants suggested a similar mechanism of a steric hindrance due to altered charges or sizes of mutated amino acid residues, preventing late-stage proteasome maturation in published DN variants; moving forward, AlphaFold3-based structural modelling will likely improve pathogenesis predictions of novel proteasome variants and of variants of uncertain significance.

Our observations link T cell-intrinsic stress to pathomechanisms likely contributing to cytopenias and related complications, including recurrent infections and porto-sinusoidal vascular liver disease (PSVD) of the liver. While transient cytopenias (including lymphopenia and hypogammaglobulinemia) can occur in response to high levels of IFN-I and often improve with IFN-blocking therapies [62], the persistent and severe cytopenias observed in DN-PRAAS patients point to a multifactorial aetiology. Molecular profiling identifies mitochondrial and metabolic stress markers as being associated with disease severity. While intracellular protein aggregates reflect proteotoxic stress, they do not correlate with clinical phenotype. In contrast, lipid droplet accumulation and progressive upregulation of mitochondrial stress response genes offer a more reliable readout of proteotoxic, lipotoxic, and mitochondrial dysfunction, likely driving T cell exhaustion and cell death in activated cells, contributing to cytopenias and the immunodeficiency-related disease manifestations in DN-PRAAS patients, which are most pronounced during infections. Importantly, these markers also associate with clinical manifestations of immune deficiency such as viral susceptibility and liver pathology, supporting their potential for risk stratification. Proteasome dysfunction is known to disrupt the development and maintenance of medullary thymic epithelial cells (mTEC), leading to thymic hypoplasia or involution and T cell repertoire reduction and impaired central T cell tolerance [63–65]. Notably, the DN-*PSMB10* variant, p.G201R, has been associated with profound cytopenias mimicking SCID- or Omenn-like phenotypes in infants, particularly in the context of perinatal infections [31,32]. Proteasome dysfunction appears to disproportionately affect $CD8^+$ T cell repertoire development and antiviral competence [66,67], which is caused by $CD8^+$ T cells undergoing positive selection in the thymus based on cytosolic peptides processed by proteasomes and presented in a major histocompatibility complex (MHC) class I-

propensity factor (APF) was calculated for each sample using the mean of controls. D, Neutral lipid staining assay for triglycerides was used to stain patients' T cells (Pt 1, 2, and 4) and healthy donors (HD 1, father and mother of patient 4), including a known inherited PRAAS variant β5i C135* (β5i inherited 2). E, RT-qPCR analysis of 7 interferon-stimulated genes (ISGs) was performed to calculate the interferon (IFN) score of patients' expanded T cells (Pt 1, 2, and 4), including 16-hour inhibitor treatments for: PKR (5 μM C16), JAK1 (1 μM baricitinib), and GCN2 (10 μM A92). Statistical testing was applied by performing a Friedman test with Dunn's correction in GraphPad Prism (v.10.2.2). *P* value ≤0.05 (*), ≤0.01 (**), ≤0.001 (***), ≤0.0001(****). Created in BioRender. Venz, S. (2025) https://BioRender.com/9bknfxj.

restricted manner by cortical thymic epithelial cells. Disruption of this pathway reduces thymic selection efficiency and narrows the $CD8^+$ T cell repertoire [32,68]. In contrast, $CD4^+$ T cells, which are selected on antigens processed independent of the proteasome in endosomal/lysosomal compartments and presented via MHC class II, are comparatively spared [69,70]. The impact of the disease-causing variants on CD8+ and CD4+ T cell repertoire development is currently unknown, and future studies are needed to provide further insights into T cell dysfunction and repertoire restricting in contributing to the immunodeficiency phenotype of DN patients.

The divergent hepatic manifestations between PRAAS genotypes, hepatic steatosis in biallelic PRAAS and PSVD/NRH in DN-PRAAS, align with differences in mitochondrial and lipid stress. We found that the DN variant *PSMB8* p.G209R causes a more profound defect in proteasome biogenesis, leading to heightened proteotoxic and metabolic stress. This disrupts key mitochondrial pathways critical for lipid metabolism, including ketogenesis and fatty acid β-oxidation, which remain relatively preserved in the biallelic CANDLE/PRAAS patients. Consequently, DN-PRAAS patients may lack hepatic steatosis due to impaired lipid handling and oxidative stress–mediated inhibition of β-oxidation, whereas patients with homozygous PRAAS retain partial mitochondrial function and accumulate hepatic lipid stores [71,72]. Nonalcoholic fatty liver disease/nonalcoholic steatohepatitis models support this dichotomy with mild mitochondrial dysfunction promoting steatosis and severe dysfunction resulting in hepatocyte injury [73,74].

Additional factors that may exacerbate liver pathology include increased gut permeability resulting in microbial translocation [50]. This could amplify immune-mediated endothelial damage, driving PSVD, including NRH and thrombotic microangiopathy, which have been reported in inborn errors of immunity associated with cytopenias, T cell–targeted immunosuppression post-HSCT [75,76], and IFN-I–mediated immune dysregulation [77]. Notably, 4 DN-PRAAS patients developed transient but prolonged expansions of activated, cytotoxic $CD8^+$ T cells postinfection (Table S1), suggesting oligoclonal T cell activation that may contribute to sinusoidal endothelial damage and NRH, similar to what has been proposed in common variable immunodeficiency [78] and chronic granulomatous disease [79]. These findings indicate that severe proteasome assembly defects, compounded by mitochondrial and lipotoxic stress and impaired redox regulation, likely drive the collapse of hepatocyte lipid homeostasis and cytopenia-mediated endothelial and sinusoidal injury. This highlights the need for disease severity biomarkers beyond proteasome activity. Whether cell stress signatures in activated T cells can identify patients at risk for PSVD warrants further investigation.

Previous studies underscore a central role for the ISR in propagating disease [48]. PKR, a key eIF2α kinase, amplifies IFN-I signalling in response to misfolded IL-24 under proteotoxic stress, a process exacerbated by amino acid starvation [48,80–82]. Although GCN2 was not directly implicated in that study, its known activation under amino acid deprivation suggests it also contributes to the ISR signalling in PRAAS [48,83,84]. Our findings demonstrate that pharmacologic inhibition of GCN2 reduces IFN-I signalling, supporting convergence with PKR in modulating IFN output and orchestrating eIF2α-driven cell-fate transitions.

These insights may inform treatment stratification. While JAK inhibitors remain the cornerstone of treatment in PRAAS, IFNAR blockade (eg, anifrolumab) may provide added benefit in patients with incomplete responses or T cell-mediated immunodeficiencies [85]. Given the variability in HSCT outcomes across PRAAS genotypes [46], personalised treatment approaches that include rigorous management of the inflammatory disease manifestations are essential. Stress-response biomarkers may prove valuable in guiding therapy and predicting disease progression.

In summary, the *PSMB8* p.G209R variant causes a DN form of PRAAS characterised by severe immune and metabolic stress, cytopenias, and organ involvement. Structural modelling elucidates the molecular basis of its disruptive effect, while integration of genotype, functional biomarkers, and clinical features supports a continuum of mitochondrial, proteotoxic, and lipotoxic stress responses that contribute to maladaptive responses that drive disease severity. Future research should focus on dissecting tissue-specific stress pathways and exploring their therapeutic modulation. Ultimately, PRAAS provides a compelling model for investigating the intersection of proteostasis failure, maladaptive tissue stress responses, and immune dysfunction, with broader implications for immunologic, metabolic, and degenerative diseases.

Acknowledgements

We thank Prof. Dr Oliver Otto and his group, especially Doreen Biedenweg, for supporting this work with technical equipment and knowledge for single-cell sorting. We also want to thank the group of Prof. Dr. Jens Fielitz and Caterina Redwanz for providing and supervising on the device to perform the NanoString measurements, and we would like to additionally thank Prof. Dr. Lars Kaderali and his group, especially Dr. Yonatan Mekonnen, for initial support. We are grateful for the excellent technical assistance from Anne Brandenburg, Robert Beyer, and Katrin Schoknecht. We would like to thank Katherine Myint-Hpu for her assistance in bone marrow biopsies and lumbar punctures. We would like to thank Renata R. Dias for her contribution to the collection of patient data and clinical assessment of patient 3, as well as Adriana Maluf Elias and Lucia Campos for the clinical evaluation of patient 3. We thank Dr. Julien Thevenon and the 2025 French Genomic Medicine Initiative for data on patient 7 and Dr Jérémie Rosain for the genetic analysis of patient 8. We thank the patients and their families for their commitment.

Schematic illustrations were designed in BioRender.com.

Contributors

SW: Performed experiments, data interpretation, data analysis, figure design, manuscript writing, and manuscript revision. SA: Performed experiments, clinical data collection, data interpretation, data analysis, figure design, manuscript writing, and manuscript revision. MW: Bioinformatic predictions of mutations, molecular modelling, data interpretation, figure design, manuscript writing, and manuscript revision. FGT: Performed experiments, data analysis, and manuscript revision. AJ: Genetic analysis, clinical data collection, and manuscript revision. JJP: Performed experiments, data analysis, and manuscript revision. HW: Data analysis and manuscript revision. FLA: Performed experiments. EB: Performed experiments and manuscript revision. KU: Patient care, clinical data collection, and manuscript revision. FB: Clinical biomarker analysis and manuscript revision. AM: Patient data collection and manuscript revision. LS: Data analysis and manuscript revision. CH: Performed experiments and manuscript revision. SV: Methodology and manuscript revision. RAA: Data analysis and manuscript revision. LP:

Performed cell culture cultivation. C and F: Biomarker assessment and manuscript revision. FCC: Patient care, clinical data collection, and manuscript revision. IHS: Clinical data collection and interpretation and manuscript revision. SAk: Patient care, data collection and interpretation, and manuscript revision. PJM: Patient care and manuscript revision. RSA: Patient care, clinical and laboratory data collection and interpretation, and manuscript revision. PB: Patient care and manuscript revision. TCLM: Patient care, clinical data collection, and manuscript revision. MB.D and KTK: Patient care and manuscript revision. JK and YKOT: Patient care, clinical data collection, and manuscript revision. RGMB: Patient care, genetic diagnosis, and manuscript revision. KP: Patient care and manuscript revision. ACH: Patient care, clinical data collection, and manuscript revision. PBr: Biomarker analysis and interpretation and manuscript revision. PBL, JBW, and LFS: Patient care and manuscript revision. ON: Patient care, clinical data collection and interpretation, and manuscript revision. AP: Patient care, clinical data collection, and manuscript revision. GB: Patient care and manuscript revision. MT: Patient care, clinical data collection, and manuscript revision. TWJH, BF, and BN: Patient care and manuscript revision. UV: Data analysis, funding acquisition, and manuscript revision. GWES: Manuscript revision. JMB: Biomarker assessment and interpretation and manuscript revision. KRC and DK: Clinical data collection and interpretation and manuscript revision. FE: Study design, performed experiments, and manuscript revision. EK: Study design, figure design, data interpretation, manuscript writing and revision, and funding acquisition. RGM: Study design, figure design, data interpretation, manuscript writing, revision, and funding.. All authors improved and accepted the final version of the manuscript.

Funding

This work was funded by the Deutsche Forschungsgemeinschaft (DFG, German Research Foundation, 443535983; RTG 2719) and the DFG-Priority Program ‘Integration of mitochondria into the cellular proteostasis network’ (DFG SPP 2453 KR1915/11-1). This research was supported in part by the Intramural Research Program of the National Institutes of Health (NIH). RGM’s program receives intramural support ZIA AI001220. The contributions of the NIH authors were made as part of their official duties as NIH federal employees, are in compliance with agency policy requirements, and are considered Works of the United States Government. However, the findings and conclusions presented in this paper are those of the author (s) and do not necessarily reflect the views of the NIH or the U. S. Department of Health and Human Services. Additional support was provided by the I-SITE Nantes Excellence Trajectory (NExT) program (project NDD-UBIPRO). P.B. was supported by the French Foundation for Medical Research (FRM, EA20170638020), the MD-PhD program of the Imagine Institute (with the support of the Fondation Bettencourt-Schueller), and a ‘Poste CCA-INSERM-Bettencourt’ (with the support of the Fondation Bettencourt-Schueller).

Competing interests

All authors declare they have no competing interests.

Patient consent for publication

Not applicable.

Ethics approval

Please see ethics statement in materials and methods section.

Provenance and peer review

Not applicable.

Data availability statement

The proteome dataset (PXD062316) is available at the PRIDE website (http://www.ebi.ac.uk/pride). The transcriptome dataset (GSE308642) is available at the GEO website (https://www.ncbi.nlm.nih.gov/geo/).

Supplementary materials

Supplementary material associated with this article can be found in the online version at doi:10.1016/j.ard.2025.10.021.

Orcid

Sophie Wolfgramm: http://orcid.org/0009-0004-0353-6457
Sara Alehashemi: http://orcid.org/0000-0002-6531-6108
Martin Wendlandt: http://orcid.org/0009-0007-7151-3961
Franziska G. Thiel: http://orcid.org/0000-0001-6322-9222
Adriana A. de Jesus: http://orcid.org/0000-0001-8966-8362
Hannes Wolfgramm: http://orcid.org/0000-0002-6028-0046
Flavia Llorente Alvarez: http://orcid.org/0009-0007-4453-1507
Farzana Bhuyan: http://orcid.org/0000-0003-2316-1221
Leif Steil: http://orcid.org/0000-0002-0733-8421
Simone Venz: http://orcid.org/0009-0004-6544-8524
Ruba Al Abdulla: http://orcid.org/0000-0002-5194-9801
Léa Poirier: http://orcid.org/0009-0003-7400-8363
Christopher Friend: http://orcid.org/0009-0000-3277-026X
Shoghik Akoghlanian: http://orcid.org/0000-0002-8264-316X
Peter J. Mustillo: http://orcid.org/0000-0002-8420-8655
Roshini S. Abraham: http://orcid.org/0000-0001-8109-8502
Paul Bastard: http://orcid.org/0000-0002-5926-8437
Jesper Kers: http://orcid.org/0000-0002-2418-5279
Y. K. Onno Teng: http://orcid.org/0000-0001-9920-2195
Robbert G.M. Bredius: http://orcid.org/0000-0001-8151-1539
Karin Palmblad: http://orcid.org/0000-0003-1197-5201
AnnaCarin Horne: http://orcid.org/0000-0002-2878-4463
Petter Brodin: http://orcid.org/0000-0002-8103-0046
Pilar Blanco-Lobo: http://orcid.org/0000-0003-1893-8198
José Bernabeu-Wittel: http://orcid.org/0000-0002-3639-8482
Olaf Neth: http://orcid.org/0000-0001-5018-0466
Guilaine Boursier: http://orcid.org/0000-0002-2903-3135
Maud Tusseau: http://orcid.org/0009-0001-2699-3827
Thomas W.J. Huizinga: http://orcid.org/0000-0001-7033-7520
Benjamin Fournier: http://orcid.org/0000-0003-4383-7524
Bénédicte Neven: http://orcid.org/0000-0001-8941-0935
Uwe Völker: http://orcid.org/0000-0002-5689-3448
Gijs W.E. Santen: http://orcid.org/0000-0003-1959-3267
Jason M. Brenchley: http://orcid.org/0000-0001-8357-2984
Frédéric Ebstein: http://orcid.org/0000-0002-3729-7878
Elke Krüger: http://orcid.org/0000-0002-2551-242X
Raphaela Goldbach-Mansky: http://orcid.org/0000-0001-7865-5769

REFERENCES

[1] Goldbach-Mansky R, Alehashemi S, De Jesus AA. Emerging concepts and treatments in autoinflammatory interferonopathies and monogenic systemic lupus erythematosus. Nat Rev Rheumatol 2025;21:22–45. doi: 10.1038/s41584-024-01184-8.

[2] Vargas JNS, Hamasaki M, Kawabata T, Youle RJ, Yoshimori T, et al. The mechanisms and roles of selective autophagy in mammals. Nat Rev Mol Cell Biol 2023;24:167–85. doi: 10.1038/s41580-022-00542-2.

[3] Dikic I. Proteasomal and autophagic degradation systems. Annu Rev Biochem 2017;86:193–224. doi: 10.1146/annurev-biochem-061516-044908.

[4] Kwon YT, Ciechanover A. The ubiquitin code in the ubiquitin-proteasome system and autophagy. Trends Biochem Sci 2017;42:873–86. doi: 10.1016/j.tibs.2017.09.002.

[5] Enenkel C, Ernst OP. Proteasome dynamics in response to metabolic changes. Front Cell Dev Biol 2025;13. doi: 10.3389/fcell.2025.1523382.

[6] Bard JAM, Goodall EA, Greene ER, Jonsson E, Dong KC, Martin A. Structure and function of the 26S proteasome. Annu Rev Biochem 2018;87:697–724. doi: 10.1146/annurev-biochem-062917-011931.

[7] Sam PN, Avery E, Claypool SM. Proteolytic control of lipid metabolism. ACS Chem Biol 2019;14:2406–23. doi: 10.1021/acschembio.9b00695.

[8] Kodroń A, Mussulini BH, Pilecka I, Wiśniewska M, Dobrowolska A, Pałka M, et al. The ubiquitin-proteasome system and its crosstalk with mitochondria as therapeutic targets in medicine. Pharmacol Res 2021;163:105248. doi: 10.1016/j.phrs.2020.105248.

[9] Çetin G, Klafack S, Studencka-Turski M, Krüger E, Ebstein F, Dubiel W, et al. The ubiquitin–proteasome system in immune cells. Biomolecules 2021;11:60. doi: 10.3390/biom11010060.

[10] Coux O, Tanaka K, Goldberg AL. Structure and functions of the 20s and 26s proteasomes. Annu Rev Biochem 1996;65:801–47. doi: 10.1146/annurev.bi.65.070196.004101.

[11] Dahlmann B. Proteasomes. Essays Biochem 2005;41:31–48. doi: 10.1042/bse0410031.

[12] Kasahara M, Flajnik MF. Origin and evolution of the specialized forms of proteasomes involved in antigen presentation. Immunogenetics 2019;71:251–61. doi: 10.1007/s00251-019-01105-0.

[13] Groettrup M, Kirk CJ, Basler M. Proteasomes in immune cells: more than peptide producers? Nat Rev Immunol 2010;10:73–8. doi: 10.1038/nri2687.

[14] Ebstein F, Kloetzel P-M, Krüger E, Seifert U, Budeus B, Schlosser A, et al. Emerging roles of immunoproteasomes beyond MHC class I antigen processing. Cell Mol Life Sci 2012;69:2543–58. doi: 10.1007/s00018-012-0938-0.

[15] Seifert U, Bialy LP, Ebstein F, Bech-Otschir D, Voigt A, Schröter F, et al. Immunoproteasomes preserve protein homeostasis upon interferon-induced oxidative stress. Cell 2010;142:613–24. doi: 10.1016/j.cell.2010.07.036.

[16] Basler M, Groettrup M. On the role of the immunoproteasome in protein homeostasis. Cells 2021;10:3216. doi: 10.3390/cells10113216.

[17] Ebstein F, Poli Harlowe MC, Studencka-Turski M, Krüger E, Kloetzel P-M, Seifert U, et al. Contribution of the unfolded protein response (UPR) to the pathogenesis of proteasome-associated autoinflammatory syndromes (PRAAS). Front Immunol 2019;10:2756. doi: 10.3389/fimmu.2019.02756.

[18] Heink S, Ludwig D, Kloetzel P-M, Krüger E, Freitag L, Schmidt F, et al. IFN-γ-induced immune adaptation of the proteasome system is an accelerated and transient response. Proc Natl Acad Sci 2005;102:9241–6. doi: 10.1073/pnas.0501711102.

[19] Bai M, Zhao X, Sahara K, Kawano H, Tanaka K, Ichihara A, et al. Assembly mechanisms of specialized core particles of the proteasome. Biomolecules 2014;4:662–77. doi: 10.3390/biom4030662.

[20] Liu Y, Ramot Y, Torrelo A, Paller AS, Si N, Babay S, et al. Mutations in proteasome subunit β type 8 cause chronic atypical neutrophilic dermatosis with lipodystrophy and elevated temperature with evidence of genetic and phenotypic heterogeneity. Arthritis Rheum 2012;64:895–907. doi: 10.1002/art.33368.

[21] Garg A, Hernandez MD, Sousa AB, Subramanyam L, Martínez de Villarreal L, dos Santos HG, et al. An autosomal recessive syndrome of joint contractures, muscular atrophy, microcytic anemia, and panniculitis-associated lipodystrophy. J Clin Endocrinol Metab 2010;95:E58–63. doi: 10.1210/jc.2010-0488.

[22] Kitamura A, Maekawa Y, Uehara H, Izumi K, Kawachi I, Nishizawa M, et al. A mutation in the immunoproteasome subunit PSMB8 causes autoinflammation and lipodystrophy in humans. J Clin Invest 2011;121:4150–60. doi: 10.1172/JCI58414.

[23] Arima K, Kinoshita A, Mishima H, Kanazawa N, Kaneko T, Mizushima T, et al. Proteasome assembly defect due to a proteasome subunit beta type 8 (PSMB8) mutation causes the autoinflammatory disorder, Nakajo-Nishimura syndrome. Proc Natl Acad Sci 2011;108:14914–9. doi: 10.1073/pnas.1106015108.

[24] Arimochi H, Sasaki Y, Kitamura A, Yasutomo K, Nishikomori R, Nakagawa K. Dysfunctional immunoproteasomes in autoinflammatory diseases. Inflamm Regen 2016;36. doi: 10.1186/s41232-016-0011-8.

[25] Papendorf JJ, Ebstein F, Alehashemi S, Staufner C, Wolf NI, Schmickel K, et al. Identification of eight novel proteasome variants in five unrelated cases of proteasome-associated autoinflammatory syndromes (PRAAS). Front Immunol 2023;14:1190104. doi: 10.3389/fimmu.2023.1190104.

[26] Brehm A, Liu Y, Sheikh A, Marrero B, Omoyinmi E, Zhou Q, et al. Additive loss-of-function proteasome subunit mutations in CANDLE/PRAAS patients promote type I IFN production. J Clin Invest 2015;125:4196–211. doi: 10.1172/JCI81260.

[27] Sarrabay G, Méchin D, Salhi A, Bastard P, Touitou I, Jeru I, et al. PSMB10, the last immunoproteasome gene missing for PRAAS. J Allergy Clin Immunol 2020;145:1015–7 e6. doi: 10.1016/j.jaci.2019.11.024.

[28] Verhoeven D, Schonenberg-Meinema D, Ebstein F, Krüger E, van Royen-Kerkhof A, van Gijn M E, et al. Hematopoietic stem cell transplantation in a patient with proteasome-associated autoinflammatory syndrome (PRAAS). J Allergy Clin Immunol 2022;149:1120–7 e8. doi: 10.1016/j.jaci.2021.07.039.

[29] Kataoka S, Kawashima N, Okuno Y, Fujio K, Yamamoto K, Kanazawa N, et al. Successful treatment of a novel type I interferonopathy due to a de novo PSMB9 gene mutation with a Janus kinase inhibitor. J Allergy Clin Immunol 2021;148:639–44. doi: 10.1016/j.jaci.2021.03.010.

[30] Kanazawa N, Hemmi H, Kinjo N, Fujimoto N, Amano H, Ohmura K, et al. Heterozygous missense variant of the proteasome subunit β-type 9 causes neonatal-onset autoinflammation and immunodeficiency. Nat Commun 2021;12:6819. doi: 10.1038/s41467-021-27085-y.

[31] Van Der Made CI, Kersten S, Chorin O, van den Berge K, van Diemen CC, Verhoeven D, et al. Expanding the PRAAS spectrum: de novo mutations of immunoproteasome subunit β-type 10 in six infants with SCID-Omenn syndrome. Am J Hum Genet 2024;111:791–804. doi: 10.1016/j.ajhg.2024.02.013.

[32] Kuehn HS, Bosticardo M, Arrieta AC, van der Made CI, Oliveira JB, Notarangelo LD, et al. Thymic and T-cell intrinsic critical roles associated with severe combined immunodeficiency and Omenn syndrome due to a heterozygous variant (G201R) in PSMB10. J Allergy Clin Immunol 2025;155:1378–85 e2. doi: 10.1016/j.jaci.2024.12.1082.

[33] Poli MC, Ebstein F, Nicholas SK, de Guzman MM, Forbes LR, Chinn IK, et al. Heterozygous truncating variants in POMP escape nonsense-mediated decay and cause a unique immune dysregulatory syndrome. Am J Hum Genet 2018;102:1126–42. doi: 10.1016/j.ajhg.2018.04.010.

[34] De Jesus AA, Brehm A, VanTries R, Pillet P, Parentelli AS, Sanchez GAM, et al. Novel proteasome assembly chaperone mutations in *PSMG2*/PAC2 cause the autoinflammatory interferonopathy CANDLE/PRAAS4. J Allergy Clin Immunol 2019;143:1939–43 e8. doi: 10.1016/j.jaci.2018.12.1012.

[35] Meinhardt A, Ramos PC, Dohmen RJ, Jansen NS, Lankester AC, Ebstein F, et al. Curative treatment of POMP-related autoinflammation and immune dysregulation (PRAID) by hematopoietic stem cell transplantation. J Clin Immunol 2021;41:1664–7. doi: 10.1007/s10875-021-01067-7.

[36] Cavalcante MPV, Brunelli JB, Miranda CC, Fonseca EOL, da Rocha Sobrinho HM, Magalhães T, et al. CANDLE syndrome: chronic atypical neutrophilic dermatosis with lipodystrophy and elevated temperature—a rare case with a novel mutation. Eur J Pediatr 2016;175:735–40. doi: 10.1007/s00431-015-2668-4.

[37] McDermott A, Jesus AA, Liu Y, Kim P, Jacks J, Sanchez GAM, et al. A case of proteasome-associated auto-inflammatory syndrome with compound heterozygous mutations in PSMB8. J Am Acad Dermatol 2013;69:e29–32. doi: 10.1016/j.jaad.2013.01.015.

[38] Jia T, Zheng Y, Feng C, Yang J, Zhang J, Li C, et al. A Chinese case of Nakajo–Nishimura syndrome with novel compound heterozygous mutations of the PSMB8 gene. BMC Med Genet 2020;21:126. doi: 10.1186/s12881-020-01060-8.

[39] Contreras-Cubas C, Cárdenas-Conejo A, Rodríguez-Velasco A, Gómez-Díaz B, Gómez-Ruiz C, Córdova EJ, et al. A homozygous mutation in the *PSMB8* gene in a case with proteasome-associated autoinflammatory syndrome. Scand J Rheumatol 2018;47:251–4. doi: 10.1080/03009742.2017.1342273.

[40] Boyadzhiev M, Marinov L, Boyadzhiev V, Iliev E, Stefanova P, Ivanov I, et al. Disease course and treatment effects of a JAK inhibitor in a patient with CANDLE syndrome. Pediatr Rheumatol 2019;17:19. doi: 10.1186/s12969-019-0322-9.

[41] Agarwal AK, Xing C, DeMartino GN, Mizrachi D, Hernandez MD, Sousa AB, et al. *PSMB8* encoding the β5i proteasome subunit is mutated in joint contractures, muscle atrophy, microcytic anemia, and panniculitis-induced lipodystrophy syndrome. Am J Hum Genet 2010;87:866–72. doi: 10.1016/j.ajhg.2010.10.031.

[42] Yamazaki-Nakashimada MA, Santos-Chávez EE, de Jesus AA, Ramírez-Vargas N, Alarcón-Segovia D, Orozco L, et al. Systemic autoimmunity in a patient with CANDLE syndrome. J Investig Allergol Clin Immunol 2019;29:75–6. doi: 10.18176/jiaci.0338.

[43] Patel PN, Hunt R, Pettigrew ZJ, Al Hammadi R, McEwen FS, Wilson N, et al. Successful treatment of chronic atypical neutrophilic dermatosis with

lipodystrophy and elevated temperature (CANDLE) syndrome with tofacitinib. Pediatr Dermatol 2021;38:528–9. doi: 10.1111/pde.14517.
[44] Kluk J, Rustin M, Brogan PA, Lachmann HJ, Elefftheriou D, Omoyinmi E, et al. Chronic atypical neutrophilic dermatosis with lipodystrophy and elevated temperature syndrome: a report of a novel mutation and review of the literature. Br J Dermatol 2014;170:215–7. doi: 10.1111/bjd.12600.
[45] Miyamoto T, Honda Y, Izawa K, Yoshida M, Kawai T, Nishikomori R, et al. Assessment of type I interferon signatures in undifferentiated inflammatory diseases: a Japanese multicenter experience. Front Immunol 2022; 13:905960. doi: 10.3389/fimmu.2022.905960.
[46] Zhang J, Tao P, Deuitch NT, Liu Y, Goldbach-Mansky R, Brogan PA, et al. Proteasome-associated syndromes: updates on genetics, clinical manifestations, pathogenesis, and treatment. J Clin Immunol 2024;44:88. doi: 10.1007/s10875-024-01692-y.
[47] Sanchez GAM, Reinhardt A, Ramsey S, Wittkowski H, Hashkes PJ, Berkun Y, et al. JAK1/2 inhibition with baricitinib in the treatment of autoinflammatory interferonopathies. J Clin Invest 2018;128:3041–52. doi: 10.1172/JCI98814.
[48] Davidson S, Yu C-H, Steiner A, Ebstein F, Sedghi M, Nicchitta C, et al. Protein kinase R is an innate immune sensor of proteotoxic stress via accumulation of cytoplasmic IL-24. Sci Immunol 2022;7:eabi6763. doi: 10.1126/sciimmunol.abi6763.
[49] Isidor B, Ebstein F, Hurst A, Pasquier L, Bézieau S, Thevenon J, et al. Stankiewicz-Isidor syndrome: expanding the clinical and molecular phenotype. Genet Med 2022;24:179–91. doi: 10.1016/j.gim.2021.09.005.
[50] Llorente C, Schnabl B. The gut microbiota and liver disease. Cell Mol Gastroenterol *Hepatol* 2015;1:275–84. doi: 10.1016/j.jcmgh.2015.04.003.
[51] Adolf F, Du J, Goodall EA, van der Lee R, Ben-Nissan G, Guo X, et al. Visualizing chaperone-mediated multistep assembly of the human 20S proteasome. Nat Struct Mol Biol 2024;31:1176–88. doi: 10.1038/s41594-024-01268-9.
[52] Ramos PC, Marques AJ, London MK, Dohmen RJ. Role of C-terminal extensions of subunits β2 and β7 in assembly and activity of eukaryotic proteasomes. J Biol Chem 2004;279:14323–30. doi: 10.1074/jbc.M308757200.
[53] Huber EM, Heinemeyer W, Li X, Arendt CS, Hochstrasser M, Groll M. A unified mechanism for proteolysis and autocatalytic activation in the 20S proteasome. Nat Commun 2016;7:10900. doi: 10.1038/ncomms10900.
[54] Ross J, Olson L, Coppotelli G. Mitochondrial and ubiquitin proteasome system dysfunction in ageing and disease: two sides of the same coin? Int J Mol Sci 2015;16:19458–76. doi: 10.3390/ijms160819458.
[55] Wu H, Zhao X, Hochrein SM, Dülmen M, Gao X, Yin J, et al. Mitochondrial dysfunction promotes the transition of precursor to terminally exhausted T cells through HIF-1α-mediated glycolytic reprogramming. Nat Commun 2023;14. doi: 10.1038/s41467-023-42634-3.
[56] Meçe O, Houbaert D, Sassano M-L, De Decker M, de Waele J, Eelen G, et al. Lipid droplet degradation by autophagy connects mitochondria metabolism to Prox1-driven expression of lymphatic genes and lymphangiogenesis. Nat Commun 2022;13. doi: 10.1038/s41467-022-30490-6.
[57] Geltinger F, Schartel L, Wiederstein M, Tevini J, Stelzer L, Jungwirth H, et al. Friend or foe: lipid droplets as organelles for protein and lipid storage in cellular stress response, aging and disease. Molecules 2020;25:5053. doi: 10.3390/molecules25215053.
[58] Kumar AV, Mills J, Parker WM, Lu Y, Harnett B, Babcock DT, et al. Lipid droplets modulate proteostasis, SQST-1/SQSTM1 dynamics, and lifespan in C. elegans. iScience. 2023;26:107960. doi: 10.1016/j.isci.2023.107960
[59] Acosta-Alvear D. Common signaling principles and interconnectivity in the ISR-UPR networks. FASEB J 2022;36. doi: 10.1096/fasebj.2022.36.s1.0i138.
[60] Pakos-Zebrucka K, Koryga I, Mnich K, Ljujic M, Samali A, Gorman AM. The integrated stress response. EMBO Rep 2016;17:1374–95. doi: 10.15252/embr.201642195.
[61] Wek SA, Zhu S, Wek RC. The histidyl-tRNA synthetase-related sequence in the eIF-2α protein kinase GCN2 interacts with tRNA and is required for activation in response to starvation for different amino acids. Mol Cell Biol 1995;15:4497–506. doi: 10.1128/mcb.15.8.4497.
[62] Fischer S, Proschmann U, Akgün K, Ziemssen T. Lymphocyte counts and multiple sclerosis therapeutics: between mechanisms of action and treatment-limiting side effects. Cells 2021;10:3177. doi: 10.3390/cells10113177.
[63] Murata S, Takahama Y, Kasahara M, Tanaka K. The immunoproteasome and thymoproteasome: functions, evolution and human disease. Nat Immunol 2018;19:923–31. doi: 10.1038/s41590-018-0186-z.
[64] Matsuda-Lennikov M, Ohigashi I, Takahama Y. Tissue-specific proteasomes in generation of MHC class I peptides and CD8+ T cells. Curr Opin Immunol 2022;77:102217. doi: 10.1016/j.coi.2022.102217.
[65] Yamaguchi N, Takakura Y, Akiyama T. Autophagy and proteasomes in thymic epithelial cells: essential bulk protein degradation systems for immune homeostasis maintenance. Front Immunol 2024;15. doi: 10.3389/fimmu.2024.1488020.
[66] Schmidt ME, Varga SM. The CD8 T cell response to respiratory virus infections. Front Immunol 2018;9. doi: 10.3389/fimmu.2018.00678.
[67] Cai Q, Chen K, Young KH. Epstein–Barr virus-positive T/NK-cell lymphoproliferative disorders. Exp Mol Med 2015;47 e133-e133. doi: 10.1038/emm.2014.105.
[68] Frantzeskakis M, Takahama Y, Ohigashi I. The role of proteasomes in the thymus. Front Immunol 2021;12. doi: 10.3389/fimmu.2021.646209.
[69] Klein L, Kyewski B, Allen PM, Hogquist KA. Positive and negative selection of the T cell repertoire: what thymocytes see (and don't see). Nat Rev Immunol 2014;14:377–91. doi: 10.1038/nri3667.
[70] Wu C, Aichinger M, Nedjic J, Klein L. Thymic epithelial cells use macroautophagy to turn their inside out for CD4 T cell tolerance. Autophagy 2013;9:931–2. doi: 10.4161/auto.24374.
[71] Wei Y, Rector RS, Thyfault JP, Ibdah JA. Nonalcoholic fatty liver disease and mitochondrial dysfunction. World J Gastroenterol 2008;14:193. doi: 10.3748/wjg.14.193.
[72] Das D, Paul A, Lahiri A, Chakraborty S, Bhattacharjee P, Ghosh S. Proteasome dysfunction under compromised redox metabolism dictates liver injury in NASH through ASK1/PPARγ binodal complementary modules. Redox Biol 2021;45:102043. doi: 10.1016/j.redox.2021.102043.
[73] Pecoraro A, Crescenzi L, Varricchi G, Marano L, Spadaro G, Triggiani M. Heterogeneity of liver disease in common variable immunodeficiency disorders. Front Immunol 2020;11. doi: 10.3389/fimmu.2020.00338.
[74] Fuss IJ, Friend J, Yang Z, et al. Nodular regenerative hyperplasia in common variable immunodeficiency. J Clin Immunol 2013;33:748–58. doi: 10.1007/s10875-013-9873-6.
[75] Elfeky R, Lucchini G, Lum S-H, Dvorak CC, Veys P, Amrolia PJ. New insights into risk factors for transplant-associated thrombotic microangiopathy in pediatric HSCT. Blood Adv 2020;4:2418–29. doi: 10.1182/bloodadvances.2019001315.
[76] Riller Q, Fourgeaud J, Bruneau J, Melotti A, Thomas C, Neven B. Late-onset enteric virus infection associated with hepatitis (EVAH) in transplanted SCID patients. J Allergy Clin Immunol 2023;151:1634–45. doi: 10.1016/j.jaci.2022.12.822.
[77] Tydén H, Lood C, Gullstrand B, Jönsen A, Leanderson T, Bengtsson AA. Endothelial dysfunction is associated with activation of the type I interferon system and platelets in patients with systemic lupus erythematosus. RMD Open 2017;3:e000508. doi: 10.1136/rmdopen-2017-000508.
[78] Daza-Cajigal V, Segura-Guerrero M, López-Cueto M, García-García E, Martínez-Banaclocha H, Campos-Caro A. Clinical manifestations and approach to the management of patients with common variable immunodeficiency and liver disease. Front Immunol 2023;14:1197361. doi: 10.3389/fimmu.2023.1197361.
[79] Feld JJ, Hussain N, Wright EC, Mistry N, Lee DY, Markowitz J. Hepatic involvement and portal hypertension predict mortality in chronic granulomatous disease. Gastroenterology 2008;134:1917–26. doi: 10.1053/j.gastro.2008.02.081.
[80] Ebstein F, Küry S, Most V, Syrbe S, Wiemann M, Fehling HJ. PSMC3 proteasome subunit variants are associated with neurodevelopmental delay and type I interferon production. Sci Transl Med 2023;15:eabo3189. doi: 10.1126/scitranslmed.abo3189.
[81] Deb W, Rosenfelt C, Vignard V, Girard S, Laflamme N, Roux-Dalvai F, et al. PSMD11 loss-of-function variants correlate with a neurobehavioral phenotype, obesity, and increased interferon response. Am J Hum Genet 2024;111:1352–69. doi: 10.1016/j.ajhg.2024.05.016.
[82] Küry S, Stanton JE, Van Woerden G, Kichler S, Morel A, Houge G, et al. Unveiling the crucial neuronal role of the proteasomal ATPase subunit gene PSMC5 in neurodevelopmental proteasomopathies. 2024.
[83] Suraweera A, Münch C, Hanssum A, Bertolotti A. Failure of amino acid homeostasis causes cell death following proteasome inhibition. Mol Cell 2012;48:242–53. doi: 10.1016/j.molcel.2012.08.003.
[84] Zhao C, Guo H, Hou Y, Zhang H, Wang Y, Zhang J, et al. Multiple roles of the stress sensor GCN2 in immune cells. Int J Mol Sci 2023;24:4285. doi: 10.3390/ijms24054285.
[85] Cetin Gedik K, Ortega-Villa AM, Materne G, Ombrello MJ, Zavialov AV, Biancotto A, et al. Disease flares with baricitinib dose reductions and development of flare criteria in patients with CANDLE/PRAAS. Ann Rheum Dis 2024;83:1181–8. doi: 10.1136/ard-2023-225463.

Ann Rheum Dis 85 (2026) 730–742

Contents lists available at ScienceDirect

Annals of the Rheumatic Diseases

journal homepage: https://www.sciencedirect.com/journal/annals-of-the-rheumatic-diseases

Autoimmunity

Cigarette smoke-primed citrullinated HLA-DR4 T cell reactivity is modulated by γδ-T cells

Matthias Jarlborg[1,2], Tine Decruy[1,2], Teddy Manuello[1,2], Julie Coudenys[1,2], Renée Van der Cruyssen[1,2], Thomas L.A. Malfait[3], Leander Meuris[4], Tania Maes[5], Ken R. Bracke[5], Diane van der Woude[6], Aegli Athanasiadou[6], Ruth Wittoek[2], Peggy Jacques[2], Dirk Elewaut[1,2], Koen Venken[1,2,*]

[1] *Molecular Immunology and Inflammation Unit, Vlaams Instituut voor Biotechnologie (VIB) Center for Inflammation Research, Ghent University, Ghent, Belgium*
[2] *Faculty of Medicine and Health Sciences, Department of Internal Medicine and Pediatrics (Rheumatology Unit), Ghent University, Ghent, Belgium*
[3] *Department of Respiratory Medicine, Ghent University Hospital, Ghent, Belgium*
[4] *Vlaams Instituut voor Biotechnologie (VIB)-UGent Center for Medical Biotechnology, Ghent, Belgium*
[5] *Laboratory for Translational Research in Obstructive Pulmonary Diseases, Department of Respiratory Medicine, Ghent University Hospital, Ghent, Belgium*
[6] *Leiden University Medical Center, Leiden, The Netherlands*

ARTICLE INFO

Article history:
Received 30 July 2025
Received in revised form 9 October 2025
Accepted 29 October 2025

ABSTRACT

Objectives: Cigarette smoke (CS) increases the risk of seropositive rheumatoid arthritis (RA), particularly in individuals carrying HLA-DR4 (Human Leukocyte Antigen-DR4) shared epitope (SE) alleles, though the underlying mechanisms remain unclear. This study aimed to investigate the interaction between these 2 key risk factors—CS and HLA-DR4—and their effect on T cell responses to citrullinated antigens in early RA and in HLA-DR4 transgenic mice.

Methods: Major histocompatibility complex (MHC)-II tetramer technology was used to detect CD4+ T cells specific for citrullinated antigens in patients with early SE+ RA and in HLA-DR4 transgenic mice. Mice were exposed to CS or immunised with citrullinated α-enolase (Cit-ENOL) to assess T cell responses. Systemic interleukin (IL)-23 overexpression was induced by hydrodynamic injection of IL-23-enhanced episomal vector.

Results: CS exposure enhanced T cell reactivity to citrullinated peptides, including Cit-ENOL, in the lungs of both patients and mice. While Cit-ENOL T cells, either induced by CS or immunisation, did not directly trigger arthritis development, IL-23 overexpression unleashed their arthritogenic potential in immunised HLA-DR4 mice. Interestingly, CS exposure and Cit-ENOL immunisation led to γδ-T cell activation strongly correlating with Cit-ENOL T cell responses. Furthermore, γδ-T cell-deficient HLA-DR4 mice exhibited an aggravated arthritis phenotype, mirrored by altered functional Cit-ENOL T cell responses.

Conclusions: These findings reveal a selective impact of CS on pulmonary T cell subsets and suggest that γδ T cells act as gatekeepers of HLA-DR4-mediated autoimmune responses in RA pathogenesis. They also highlight a potential 2-hit model involving IL-23 in driving T cell-mediated arthritis.

*Correspondence to Prof. Dr. Koen Venken.
E-mail address: koen.venken@ugent.be (K. Venken).
Handling editor Josef S. Smolen.
Dirk Elewaut and Koen Venken are joint senior authors.

https://doi.org/10.1016/j.ard.2025.10.031

WHAT IS ALREADY KNOWN ON THIS TOPIC

- Cigarette smoking is a well-established risk factor for rheumatoid arthritis (RA) and has been linked to the induction of autoantibodies. However, its impact on T cell autoreactivity to citrullinated antigens remains poorly understood.

WHAT THIS STUDY ADDS

- This study provides direct evidence supporting a lung-joint axis in RA by linking cigarette smoking to T cell responses against citrullinated antigens—particularly citrullinated α-enolase (Cit-ENOL)—in anti-citrullinated protein antibody-positive patients with RA and HLA-DR4 transgenic mice.
- Using a human transgenic mouse model, we demonstrate that T cell responses to Cit-ENOL are regulated by $\gamma\delta$ T cells and require a secondary interleukin (IL)-23–driven inflammatory signal to induce arthritis.

HOW THIS STUDY MIGHT AFFECT RESEARCH, PRACTICE OR POLICY

- Our findings highlight the selective impact of smoking on lung-resident T cell subsets and reveal a novel immunomodulatory role for $\gamma\delta$ T cells in RA pathogenesis.
- We provide further evidence implicating IL-23 as a potentially proarthritogenic cytokine in the early stages of RA, underscoring its potential as a target for preventive therapeutic strategies.

INTRODUCTION

Rheumatoid arthritis (RA) is a chronic autoimmune disease affecting ~1% of the population, characterised by symmetric polyarthritis and progressive joint destruction [1]. Disease onset is thought to result from a complex interplay between genetic and environmental factors. Among these, cigarette smoke (CS) is a major environmental risk factor, particularly in individuals carrying specific human leukocyte antigen (HLA)-DRB1 alleles of the major histocompatibility complex (MHC) class II locus—collectively referred to as the 'shared epitope' (SE) [2]. These alleles encode a common 5-amino acid motif at positions 70 to 74 of the HLA-DRβ chain and are associated with increased risk of seropositive RA and the development of anticitrullinated protein antibodies (ACPAs), a key disease hallmark. Citrullinated peptides bind SE alleles with high affinity, particularly at the P4 pocket, facilitating the emergence of autoreactive T cells early in disease development [3,4]. Consistently, T cells specific for citrullinated peptides are enriched in patients with RA compared to healthy controls [5–9].

The mechanisms by which CS contributes to RA pathogenesis, particularly in genetically susceptible individuals, remain poorly defined. Smoke-induced lung inflammation and microdamage may upregulate immune mediators and danger-associated molecular patterns, priming adaptive responses to modified self-antigens. CS affects both innate and adaptive immunity but appears to have a more persistent impact on the latter [10]. Notably, CS enhances protein citrullination in the lung by upregulating peptidyl arginine deiminase 2 [11,12], potentially driving local ACPA production, as evidenced in bronchoalveolar lavage (BAL) samples from patients with RA [13,14]. CS has also been linked to ACPA immunoglobulin (Ig)-A isotype responses, supporting the involvement of mucosal immunity [15]. These findings are supportive for a link between lung and joint inflammation in RA aetiology. However, the mechanisms underlying the loss of tolerance and the emergence of HLA-DR4-restricted autoreactive T cells remain unclear. We recently showed that shared T cell clonotypes exist between the lung and synovial tissue in early patients with ACPA$^+$ RA, with a strong association to smoking, supporting the mucosal origin hypothesis [16]. Nevertheless, the specific antigenic drivers and local events that breach mucosal tolerance and lead to systemic joint inflammation are yet to be elucidated. Here, we hypothesise that CS promotes citrullinated T cell subsets at mucosal barriers in early stages of the disease. By means of tetramer technology, we assessed citrulline-specific T cells in the lungs of early patients with RA. In parallel, we modelled key RA risk factors—CS and SE—*in vivo* in HLA-DR4 transgenic mice to evaluate their impact on T cell responses and arthritis pathology.

METHODS

Patients samples

BAL fluid and peripheral blood mononuclear cells (PBMCs) were collected from 21 patients with early ACPA-positive RA, fulfilling the 2010 American College of Rheumatology (ACR) and the European League Against Rheumatism (EULAR) classification criteria, as previously described [16]. Patients were recruited at the Rheumatology Department, Ghent University Hospital, based on the following criteria: newly diagnosed, symptom duration <6 months, ≥1 clinically active joint, elevated inflammatory markers (C-reactive protein and/or erythrocyte sedimentation), and no prior treatment with Disease-Modifying Antirheumatic Drugs (DMARDs), biologics, or intra-articular corticosteroids (Table 1). Following informed consent, heparinised and EDTA blood samples, along with BAL fluid, were obtained on the same day. HLA-DRB1 genotyping was conducted via PCR with sequence-specific oligonucleotide probes (Luminex, Belgian Red Cross), classifying patients as SE-positive (HLA-DRB1*0101, *0401, or *0404) or SE-negative. PBMCs and BAL cells were isolated as described [16], and 10-25 million cells per sample were used in flow cytometry assays (see Supplementary Methods). MHC-II tetramer technology was used to detect CD4+ T cells reactive to 5 citrullinated peptides and a noncitrullinated control peptide (haemagglutinin [HA]) in human and HLA-DR4 transgenic mice. A combinatorial MHC class II (DRB1*04:01) tetramer approach was optimised for parallel detection of reactivity to citrullinated autoantigens including aggrecan, vimentin, fibrinogen, cartilage intermediate layer protein (CILP)2, and α-enolase (Table 2). Cells were incubated with tetramers and surface-stained with various monoclonal antibodies to identify specific T cell subsets. Flow cytometry analysis was performed using a FACSCanto II instrument and FlowJo software (v10.8.1). Data analyses were done in a blinded fashion (meaning investigators were not aware of smoking or HLA status) at the moment of analyses.

Mice

HLA-DR4 transgenic mice (C57BL/6 background -Abb knockout; Taconic), expressing a chimeric MHC class II molecule composed of human HLA-DRA and HLA-DRB1*0401 peptide-binding domains and a murine I-E proximal domain, were bred under specific pathogen-free conditions in individually ventilated cages following standard animal care guidelines. Both male and female mice were used, with no sex-specific differences observed. HLA-DR4$^+$Rag2$^{-/-}$ and HLA-DR4$^+$Rag2$^{+/+}$ mice were generated by backcrossing HLA-DR4 transgenics with

Table 1
Patients' characteristics

Parameters	SE− (n = 10)	SE+ (n = 11)	*P* value
Sex (female), n, %	40	45.5	
Age (y), median, IQR	59.5 (54.8-64.3)	58 (48-59)	.36
Symptoms duration (months), median, IQR	2 (1.75-6)	4.5 (2-6)	.22
CS (current or past), %	80	72.3	
Swollen joint count, median, IQR	2 (1-6.3)	3 (2-6)	.77
Tender joint count, median, IQR	4.5 (2-7)	4 (2-7)	.64
ACPA (U/mL, max 340), mean ± SEM	340 (152-340)	340 (149-340)	.9
RF (IU/mL), mean ± SEM	184.2 ± 76.2	114 ± 41.7	
RF positivity, n, %	70	63.6	
ESR (mm/s), mean ± SEM	47.7 ± 11.6	30.1 ± 9.2	.24
CRP (mg/mL), mean ± SEM	30 ± 9.1	28 ± 17.9	.93
TCD4/mL of BAL, mean ± SEM	4120 ± 2675	11,886 ± 7596	.6
TCD4/mL blood, mean ± SEM	277,772 ± 87,839	227,001 ± 75,667	.71
T$\gamma\delta$/mL of BAL, mean ± SEM	122.1 ± 42.4	295 ± 181.9	.25
T$\gamma\delta$/mL blood, mean ± SEM	7128 ± 3845	7242 ± 2085	.18
Cit-tetra+ cells per million TCD4+ in BAL, mean ± SEM	0	2047 ± 611	.005
Cit-tetra+ cells per million TCD4+ in blood, mean ± SEM	0	60.6 ± 10	.007

ACPA, anticitrullinated protein antibody; BAL, bronchoalveolar lavage; CRP, C-reactive protein; CS, cigarette smoke; ESR, erythrocyte sedimentation rate; RF, rheumatoid factor; SE, shared epitope; TCD4, conventional CD4+ T cells; Tgd, gamma delta T cells, .

Rag2$^{-/-}$ mice and interbreeding heterozygotes. HLA-DR4 × Tcrd$^{-/-}$ mice were obtained by crossing HLA-DR4 with Tcrd$^{-/-}$ mice (Jackson Laboratory). Mice were exposed to cigarette smoke (CS) or immunised with citrullinated α-enolase (Cit-ENOL) peptide sequence 11-25 (IFDSXGNPTVEVD; with X = Citrulline), with or without interleukin (IL)-23 overexpression (see Supplementary Methods for details).

Statistics

Statistical analysis was performed using GraphPad Prism (version 10.4.1) or Genstat. A conjugate Hierarchical Generalised Linear Model (HGLM) as implemented in Genstat v24 was applied to tetramer count data. Depending on normality testing, a 2-tailed unpaired t-test/Mann-Whitney *U* test was used when comparing 2 groups, one-way analysis of variance (ANOVA)/Kruskal-Wallis with correction for multiple testing (Bonferroni/Dunn's test) was used for multigroup analysis, and Pearson/Spearman coefficients were calculated for correlation analysis. Clinical scores and weight loss were analysed with repeated measurements.

Table 2
Tetramers with their respective peptide and fluorochrome used for T cells staining

Tetramer	Loaded peptide	Fluorochrome
ProT2 MHC class II tetramers DR4 (DRB1*04:01)	Citrullinated vimentin	PE
	Cit-Vimentin 59-78	APC
	GVYAT(CIT)SSAV(CIT)L(CIT)SSVPGVR	
	Citrullinated cartilage intermediate layer protein	PE
	Cit-CILP-2 297-311	BB515
	ATIKAEFV(CIT)AETPYM	
	Citrullinated alpha-enolase	PE
	Cit-α-enolase 11-25	BV421
	IFDS(CIT)GNPTVEVDLF	
	Citrullinated aggrecan	APC
	Cit-Aggrecan 89-103	BB515
	ATEG(CIT)V(CIT)VNSAYQDK	
	Citrullinated fibrinogen	APC
	Cit-Fibrinogen-α 79-91	BV421
	QDFTN(CIT)INKLKNS	
	Hemagglutinin	BB515
	HA306-318 (control peptide)	BV421
	PKYVKQNTLKLAT	

APC, Allophycocyanin; BB515, Brilliant Blue 515; BV421, Brilliant Violet 421; MHC, Major Histocompatibility Complex; PE, Phycoerythrin. Cit-CILP, citrullinated cartilage intermediate layer protein.

Ethics

This study was approved by the Ethics Committee of Ghent University Hospital (EC approval IDs: B670201734033 and B670201629920). All participants provided written informed consent for blood and BAL sampling to support research on RA immunopathogenesis. Animal experiments were approved by the Ethics Committee for Laboratory Animal Welfare of Ghent University (ECD 21-22 and ECD 21-36) and conducted in compliance with institutional, national, and ethical guidelines.

Patient and public involvement

The patients were informed about the study and gave written informed consent for the collection of blood and BAL samples for this project, to improve the understanding of the immunopathogenesis of RA. Patients were not involved in the design of the study, choice of outcome measures, recruitment nor in the dissemination of the study.

RESULTS

CS is associated with increased T cell reactivity towards citrullinated antigens in the lungs of early patients with RA

CS has been linked to citrullination processes and antibody responses to citrullinated self-antigens in RA [12], but a direct impact on autoreactive T cell responses remains unknown. To address this question, we first sought to evaluate the presence of citrullinated antigen reactive T cells in lung (bronchoalveolar lavage fluid) and paired blood (PBMC) samples of 21 ACPA+ early patients with RA in function of smoking. To this end, we applied a combinatorial MHC class II (DRB1*04:01) tetramer approach for the parallel detection of T cell reactivity towards 5 known RA-associated citrullinated peptides (Cit-peptides), including aggrecan, vimentin, fibrinogen B (Cit-FIB), Cit-CILP, and α-enolase (Cit-ENOL), next to HA peptide as a control

antigen (Fig 1A and Supplementary Fig S1). Interestingly, significant DRB1*04:01 tetramer binding could be observed for samples from SE+ (n = 11) but not patients with SE− (n = 10), regardless of smoking status, underscoring the specificity of the tetramer screening assay (Fig 1B and Table 1). Our data clearly indicated that T cells with a specificity for joint-derived citrullinated antigens were present in BAL samples from patients with ACPA+ SE+ RA and were significantly increased in smokers (Fig 1C). Focusing on the individual citrullinated antigen responses (Table 2), we found a significant increased frequency of the citrullinated Cit-CILP, Cit-VIM, Cit-AGC, Cit-FIB and Cit-ENOL tetramer-positive cells detected in lung samples of smokers vs nonsmokers ($P < .05$), which was not seen for the control HA peptide antigen (Fig 1D). In contrast, such selective enrichment in smokers vs nonsmokers was not detected for blood-resident Cit-peptide reactive T cells (Fig 1C), suggesting a predominant local effect of smoke exposure in the lungs. Nevertheless, paired analyses showed that antigen-specific responses occur predominantly in the lung environment, which again was not seen for the control antigen (Supplementary Fig S1B). Altogether, these data clearly show increased citrullinated peptide reactive T cells in the lungs of SE+ RA smokers.

Smoking induces citrullinated antigen T cell responses in HLA-DR4 transgenic mice without arthritis development

Based on the findings in patients with RA samples, we aimed to further explore the role of CS exposure on Cit-peptide T cell reactivity in a humanised HLA-DR4 transgenic mouse model. Hence, we exposed HLA-DR4 transgenic mice to 4 weeks (subacute) or 4 months (chronic) of whole-body CS with 3R4F reference cigarettes or room air (as a control) and collected lung and splenocytes for detection of citrullinated peptide reactive T cells with the HLA-DR4 tetramer panel (Fig 1E,F). Chronic CS led to a significant increase in the absolute numbers of Cit-peptide reactive CD4+ T cells in the lung tissue ($P = .01$; Fig 1G). A similar trend was observed following subacute CS exposure, for which statistical analyses revealed significant increases for both Cit-ENOL and Cit-FIB (data not shown). This increase upon CS was not observed in the spleen (both for subacute and chronic exposure) nor for the control HA peptide between smoking and nonsmoking mice. Regarding peptide specificity, we found a significant increase in the number of Cit-ENOL and Cit-FIB reactive CD4+ T cells in the lungs of mice exposed to chronic CS (Fig 1H).

In correspondence with the known metabolic effects of smoking, we observed a significant weight loss in chronically CS exposed mice compared to air controls (Supplementary Fig S2A). In the lung tissues, chronic CS exposure was associated with the presence of ectopic lymphoid tissue (aggregates and follicles) assessed by CD3/B220 immunostaining (Supplementary Fig S2B), suggestive of immune priming. Given our observations in human RA lung samples and consistent induction of Cit-peptide reactivity in HLA-DR4 mice upon smoking, it was intriguing to explore any signs of (sub) clinical arthritis development in these mice. However, on clinical or histological evaluation, we observed no clear indications for joint pathology development in HLA-DR4 mice up to 4 months of CS exposure (data not shown). In summary, chronic CS exposure in the context of RA risk gene expression seems permissive for (local citrullinated) autoimmune reactivity, but does not directly lead to the development of arthritis.

Immunisation with Cit-ENOL peptide induces proinflammatory T cell responses

Our findings may reflect the extended preclinical phase during which autoimmunity—potentially influenced by smoking—develops before the onset of clinical RA in at-risk individuals [17]. Given that Cit-ENOL reactive T cells emerged in both patients with RA and HLA-DR4 mice following smoking, we further characterised T cell responses using an immunisation model to assess whether Cit-ENOL immunisation would lead to the development of arthritis. We first explored whether Cit-peptide-specific T cell responses could be primed upon short-term foot hock immunisation. Eight days after a single injection of Cit-ENOL in complete Freud's adjuvant (CFA) on each hind paws, T cell reactivity to Cit-ENOL was assessed *ex-vivo* (Fig 2A). Tetramer assay showed an increased number of Cit-ENOL reactive T cells in the draining lymph nodes (popliteal and inguinal) in immunised mice compared to mice receiving CFA only (Fig 2B). Next, we were interested in testing whether active immunisation with Cit-ENOL would result in the development of arthritis in HLA-DR4 mice. Hence, we performed subcutaneous Cit-ENOL immunisation at the base of the tail with a booster immunisation at day 21 (Fig 2C). At day 60 (postprimary immunisation), we were able to observe clear T cell responses towards Cit-ENOL as demonstrated by rechallenge experiments of cultured lymphocytes from immunised HLA-DR4 mice: T cell proliferation (carboxyfluorescein succinimidyl ester (CFSE) dilution assay; Fig 2D) and secretion of proinflammatory cytokines (Fig 2E) were consistent with a specific response towards Cit-ENOL. This T cell response was dose-dependent with an increased and profound interleukin (IL)-17 (and to a lesser extent also interferon (IFN)-γ, Tumor necrosis factor (TNF)-α, and IL-6) production when rechallenged with higher concentrations of Cit-ENOL, which was blocked in the presence of neutralising HLA-DR Abs. Of note, no response was observed upon re-exposure to the native (noncitrullinated) form of the ENOL peptide, but we did observe significant T cell proliferation and cytokine production upon rechallenge with citrullinated cartilage layer intermediate protein (Cit-CILP, ATIKAEFV (CIT)AETPYM), suggesting T cell cross-reactivity towards other citrullinated antigens upon Cit-ENOL immunisation. However, despite clear induction of functional proinflammatory Cit-ENOL T cells in joint-draining lymph nodes, this T cell priming did not trigger arthritis induction in HLA-DR4 mice (data not shown).

Arthritogenic potential of Cit-ENOL immunisation is unleashed by IL-23

Loss of tolerance to Cit-ENOL whether induced by prolonged smoke exposure or immunisation, did not lead to arthritis in HLA-DR4 transgenic mice, suggesting that an additional trigger is required for disease induction. Given its role in early adaptive immunity and antibody maturation in (preclinical) RA, IL-23 was hypothesised as a potential second hit [18]. To test this, systemic IL-23 overexpression was induced in HLA-DR4 mice via hydrodynamic injection of an enhanced episomal vector (IL-23 EEV) [19] (Fig 3A) either alone or in combination with Cit-ENOL immunisation (in addition to CFA controls). IL-23 EEV injection led to sustained serum IL-23 levels in both immunised and CFA-injected HLA-DR4 mice (Fig 3B). While control vector-injected mice remained healthy, IL-23 overexpression alone induced only very mild arthritis, typically involving a single

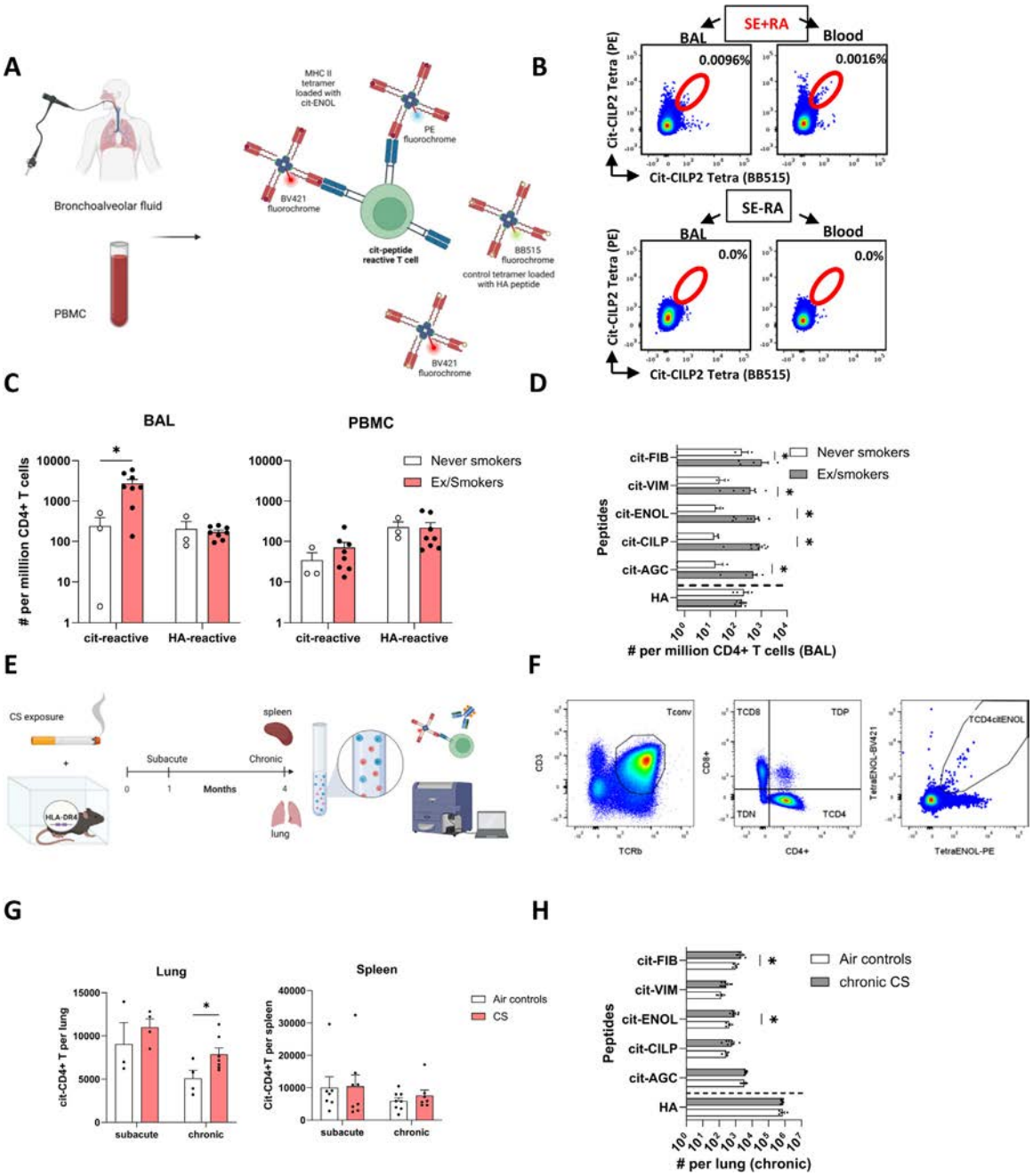

Figure 1. Cigarette smoke is associated with an increased detection of citrullinated peptide-specific T cells by tetramer assay. (A) BAL fluid isolated cells and PBMC from patients with early ACPA+ RA were screened for the presence of Cit-peptide reactive T cells by means of MHC Class II tetramers flow cytometric staining. HLA-DRB1*0401 tetramers using specific combinations of 2 fluorochromes per Ag-Tetra specificity were loaded with citrullinated peptides of aggrecan (Cit-AGC), vimentin (Cit-VIM), fibrinogen B (Cit-FIB), cartilage intermediate layer protein (Cit-CILP), α-enolase (Cit-ENOL), or control influenza peptide (HA). Figure created using Biorender. (B) One representative example shown for Cit-CILP staining of BAL cells from a patient with SE+ (n = 11) and SE− (n = 10) RA. Patients with SE+ RA showed clear tetramer responses, while patients with SE− showed no DRB1 reactivity, underscoring the specificity of the tetramer screening assay. Gating strategy as indicated in Supplementary Figure 1. (C) Quantification of total (sum of) Cit-peptide or HA control tetramer-positive cells in PBMC and BAL samples of patients with SE+ RA, stratified for smoking status: never smokers (n = 3) and ex- and active smokers (n = 8) (statistics: Multiple Mann-Whitney *U* test; **P* value ≤ .05). (D) Quantification of individual tetramer-positive T cells in BAL samples of patients with SE+ RA, stratified for smoking status (statistics: HGLM, **P* value ≤ .05). (E) HLA-DR4 mice (n = 15) were exposed to regular air (n = 8) or mainstream tobacco smoke (n = 7) from 3R4F reference cigarettes for 1 or 4 months. Lungs and spleen samples were collected and processed for HLA-DRB1*0401 tetramer staining (control mice lungs pooled per pair). (F) Dotplots showing the gating strategy used to identify cit-ENOL CD4+ T cells in the lung tissue of an HLA-DR4 mouse exposed to cigarette smoke. (G) The total number of citrullinated peptide reactive CD4+ T cells present in the lung tissue was significantly increased upon chronic CS but not in the spleen (statistics: multiple Mann-Whitney *U* test, **P* value ≤ .05). (H) Quantification of individual tetramer positive T cells in lung tissue of HLA-DR4 mice, stratified for smoking status (statistics: HGLM, **P* value ≤ .05). (A)-(E) were created using Biorender. ACPA, anticitrullinated protein antibody; BAL, bronchoalveolar lavage; CD4, Cluster of Differentiation 4; CD8, Cluster of Differentiation 8; Cit-AGC, Citrullinated aggrecan; Cit-CLIP, citrullinated cartilage intermediate layer protein; Cit-ENOL, citrullinated α-enolase; Cit-FIB, Citrullinated fibrinogen; Cit-VIM, Citrullinated vimentin; CS, cigarette smoke; HA, influenza haemagglutinin; HLA-DRB1, Human Leukocyte Antigen - DR β1; MHC, Major Histocompatibility Complex; PBMC, peripheral blood mononuclear cells; PE, Phycoerythrin; RA, rheumatoid arthritis; SE, shared epitope; TDP, double positive T cells; TDN, double negative T cells.

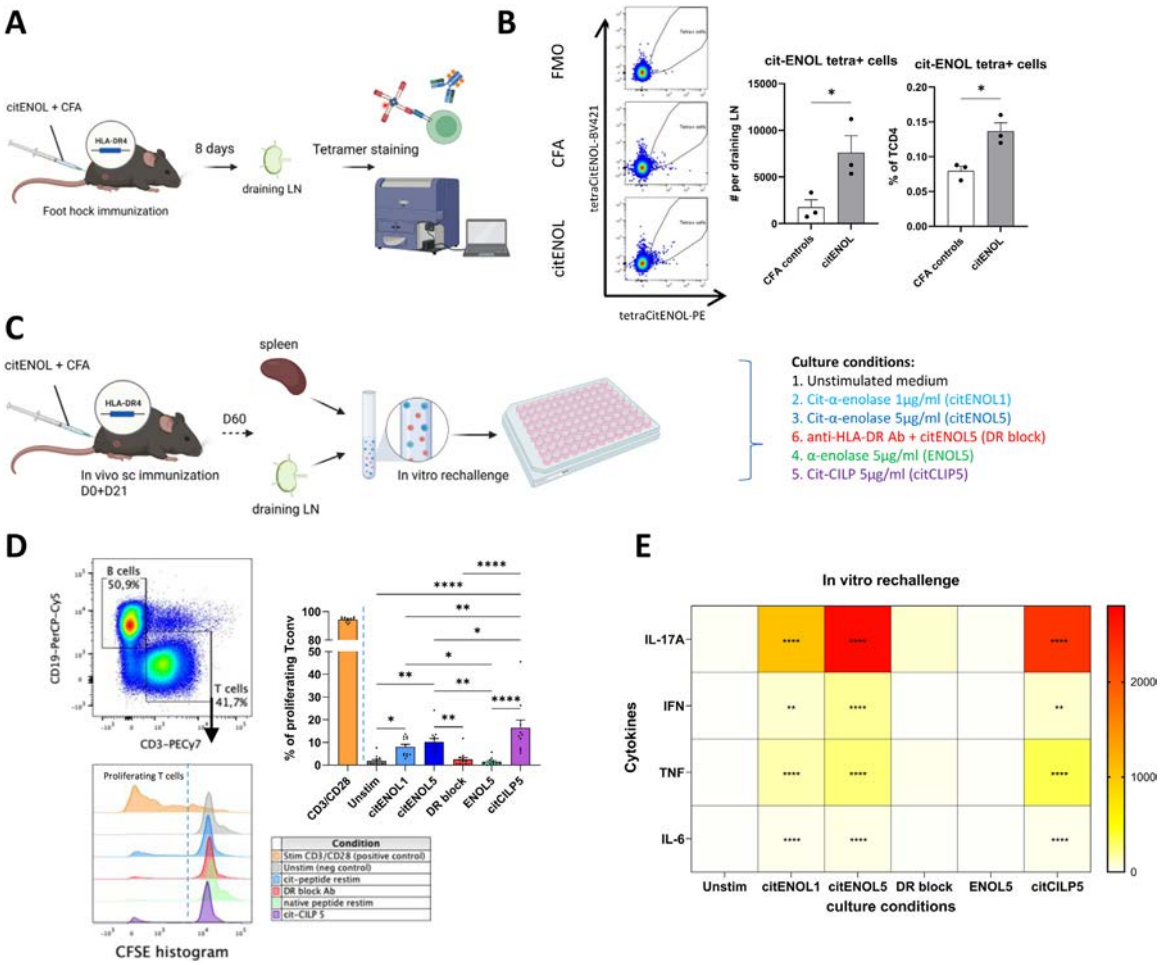

Figure 2. Citrullinated-α-enolase immunisation induces the development of specific citrullinated Ag T cell responses in HLA-DR4 mice. (A) HLA-DR4 mice were injected with 100 μg of Cit-enolase (in CFA) in each foot hock (n = 3) or CFA only (control mice, n = 3). After 8 d, the inguinal lymph nodes were isolated for Cit-ENOL tetramer staining by flow cytometry. (B) Representative flow plots (left figure) and quantification (right figure; frequency and total number) with regard to Cit-ENOL+ tetramer CD4 T cells in draining lymph nodes from immunised vs controlled mice (statistic: unpaired 2-tailed t-test; *P value ≤ .05). (C) HLA-DR4 mice were s.c. injected at day 0 and day 21 with 100 μg of Cit-enolase (in CFA). At day 50 post-immunisation, splenocytes and popliteal together with inguinal lymph nodes were isolated and cells were set up *in vitro* for restimulation with Cit-enolase (1 or 5 µg/mL); unrelated Cit-peptide (Cit-CILP) or, respectively, native peptides (containing arginine instead of citrulline); or Cit-ENOL (5 μg/mL) in the presence of anti-HLADR Ab (DR block) (6 technical replicates per condition). (D) CFSE dilution assay (flow cytometry) showing the percentage of proliferating CD3+. T cells according to the different cultured conditions described in (C) (statistic: one-way ANOVA with Dunnett's multiple comparisons test, specific conditions compared to the unstimulated control condition; *P value ≤ .05, **P ≤ .01, ****P ≤ .0001). (E) Heatmap representing quantification of proinflammatory cytokines (respectively, IL-17A, IFNγ, TNFα, and IL-6) measured by ELISA in the supernatants of the different cultures conditions as described in C (statistic: one-way ANOVA with Dunnett's multiple comparisons test to compare each condition to the unstimulated control condition with *P value ≤ .05, **P ≤ .01, ***P ≤ .001, ****P ≤ .0001). (A) and (C) were created using Biorender. ANOVA, Analysis of Variance; CD3, Cluster of Differentiation 3; CD4, Cluster of Differentiation 4; CFA, Complete Freund's Adjuvant; CFSE, Carboxyfluorescein Succinimidyl Ester; Cit-CILP, citrullinated cartilage intermediate layer protein; Cit-CLIP, citrullinated cartilage intermediate layer protein; Cit-ENOL, citrullinated α-enolase; DR block, anti-HLADR antibodies; ELISA, Enzyme-Linked Immunosorbent Assay; FMO, Fluorescence Minus One; HA, Influenza Hemagglutinin; HLA-DR4, Human Leukocyte Antigen − DR4; IFNγ, Interferon Gamma; IL-17A, Interleukin 17A; IL-6, Interleukin 6; LN, Lymph Node; s.c., subcutaneous; TNFα, Tumor Necrosis Factor Alpha.

hind paw toe (Fig 3C). Strikingly, coadministration of IL-23 EEV and Cit-ENOL immunisation resulted in a robust polyarthritis phenotype, affecting both front and hind paws, beginning after the booster immunisation and progressively worsening until endpoint at day 60 (Fig 3C). Consistently, haematoxylin and eosin (H&E) staining of foot and knee sections from Cit-ENOL IL-23EEV mice at endpoints revealed (mild) inflammatory cell infiltrations in arthritic animals (Fig 3D,E, and Supplementary Fig S2C,D). Interestingly, (mild) erosion development was seen for femur condyles of Cit-ENOL+IL-23 EEV HLA-DR4 mice (which was not seen in the IL-23 EEV alone condition; Fig 3E). No sex-dependent differences were observed regarding clinical phenotype (Supplementary Fig S2E). The combined treatment was associated with increased serum TNF levels, while IL-17 levels did not further increase as compared to either IL-23 alone or Cit-ENOL immunisation alone (Fig 3F). Rag2$^{-/-}$ HLA-DR4 mice, lacking B and T cells, were completely protected from arthritis under the same conditions, confirming the essential role of adaptive immunity in this model (Fig 3G).

To understand how IL-23 overexpression favoured arthritis development, we first explored whether IL-23 would increase the number of specific Cit-ENOL T cells as evaluated by tetramer staining on joint-draining lymph node cells of immunised mice. The number of total T cells (and B cells) did not differ significantly between animal groups (data not shown). Similarly, we could also not observe any differences in the number of antigen-specific CD4$^+$ T cells (Fig 3H). Next, we anticipated IL-23 overexpression may lead to phenotypical changes in the Cit-ENOL

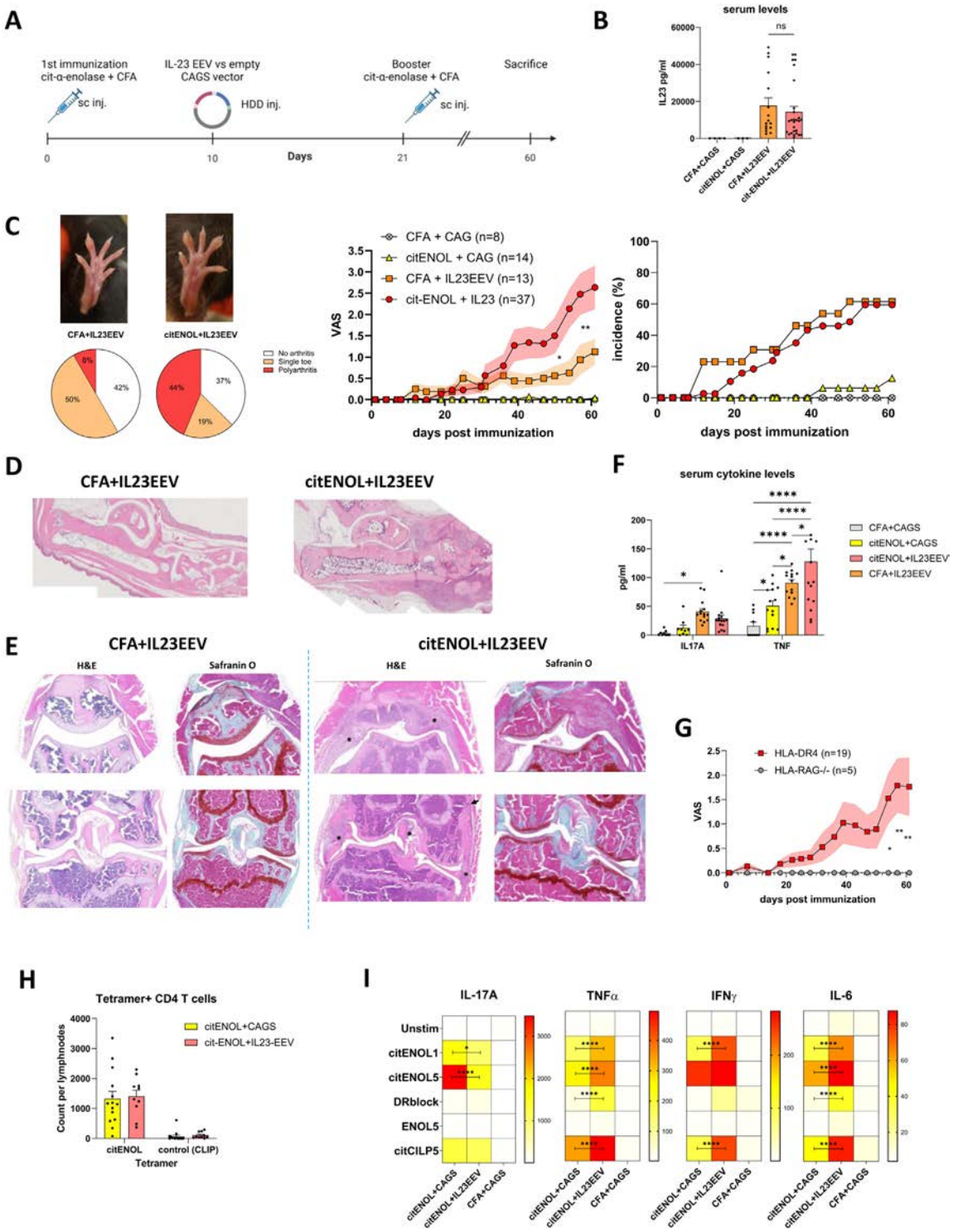

Figure 3. Arthritogenic potential of Cit-ENOL immunisation is unleashed by IL-23. (A) Cit-ENOL immunisation was combined with HDD injection of 40 ng IL-23 EEV (n = 37) or empty vector (CAGS EEV, n = 14) in HLA-DR4 mice. Additional controls included mice receiving IL-23 EEV with CFA (n = 13) and CFA + CAGS (n = 8) (B) Serum levels of IL-23 measured in Cit-ENOL (or CFA control) immunised mice receiving IL-23 EEV or empty vector, and CAGS controls. (C) Photographs illustrating arthritis development in DR4 mice challenged with Cit-ENOL + IL-23 EEV vs CFA + IL-23 EEV, including arthritis phenotype distribution (pie diagrams). Data graphs show visual analogue scale (VAS) clinical arthritis scores and arthritis incidence (%) plotted for each condition and assessed every 3 days after first immunisation (mean ± SEM, statistic: two-way ANOVA with repeated measurement, and Fischer LSD's multiple comparisons test with *P value ≤ .05, **P ≤ .01). (D) Histology of hind feet with representative illustrations from HLA-DR4 mice treated with CFA + IL23EEV (upper panel) and Cit-ENOL + IL23 (lower panel). (E) Histological knee sections from HLA-DR4 mice treated with CFA + IL23EEV (left panel) and Cit-ENOL + IL23 (right panel). The upper panel shows the femoropatellar joint, while the lower panel shows the femorotibial joint. Sections were stained with H&E and Safranin O. In the Cit-ENOL + IL23-treated mice (right), synovial hyperplasia, inflammatory infiltrates (marked with an asterisk), and a marked loss of proteoglycans in the cartilage (indicated by the red decolouration) are observed, suggesting cartilage degradation. In contrast, the CFA + IL23EEV group (left) shows less severe pathological changes. (F) Serum levels of IL-17A and TNF for each group of mice (mean ± SEM, statistic: two-way ANOVA with Fischer LSD's multiple comparisons test with *P value ≤ .05, ****P ≤ .0001). (G) Clinical arthritis scores of HLA-DR4 × RAG$^{-/-}$ compared to HLA-DR4, showing no arthritis in RAG-deficient mice (statistic: two-way ANOVA with repeated measurement, and Fischer LSD's multiple comparisons test with *P value ≤ .05, **P ≤ .01). (H) Absolute number of Cit-ENOL CD4 T cells in the popliteal and inguinal draining lymph nodes of Cit-ENOL immunised mice receiving IL-23 EEV vs CAGS controls. The absolute number of CLIP (Class II-associated invariant chain peptide) specific T cells is shown as negative control. (I) Quantification (heatmap representation)

reactive T cells. To explore this, we specifically measured and compared cytokine secretion by *in vitro* restimulated T cells from Cit-ENOL alone vs Cit-ENOL and IL-23EEV-treated mice (Fig 3I). These experiments demonstrated that *in vivo* IL-23 overexpression enhanced the proinflammatory cytokine profile of lymph node Cit-ENOL-primed T cells, with elevated IFN-γ, TNF, and IL-6 production. Notably, TNF and IL-6 secretion were only partially dependent on HLA-DR4, suggesting additional involved pathways. IL-17 production, unexpectedly, was reduced in IL-23 EEV-treated mice (Fig 3I).

Finally, we assessed the humoral immune response to citrullinated proteins by conducting enzyme-linked immunosorbent assays (ELISAs) with 3 distinct citrullinated antigens. For most mice, including immunised groups, we could not demonstrate the presence of detectable citrulline-specific antibody responses. Interestingly, specific difference in optical density (ΔOD) signals for citrullinated fibrinogen and ovalbumen-specific Ig antibodies were still detectable at high dilutions in the serum of a subset of immunised HLA-DR4 mice (Supplementary Fig S3A). However, these rare antibody responses did not correlate with arthritis severity, joint inflammatory infiltration, or T cell proliferative activity. Since IL-23 may influence antibody pathogenicity via Fc glycosylation [18], we analysed total IgG-Fc sialylation and galactosylation, but found no significant changes following IL-23 overexpression (Supplementary Fig S3B).

Altogether, these findings highlight that the arthritogenic potential of citrullinated antigen-specific T cells in HLA-DR4 mice is unleashed upon IL-23 overexpression, with IL-23 modulating T cell function rather than expanding autoreactive clones, and without clear evidence of autoantibody (ACPA) involvement.

$\gamma\delta$ T cells gatekeep citrullinated autoreactivity development in HLA-DR4 mice

At mucosal surfaces, including the lung barrier, $\gamma\delta$ T cells are enriched and act as immunoregulatory cells bridging the stromal compartment and the conventional immune system. Their strategic positioning exposes them directly to environmental factors such as CS, potentially enabling them to modulate local (adaptive) immune responses [20]. Notably, $\gamma\delta$ T cells are also responsive to IL-23, which is increased in smoke-induced inflammation [21], further supporting our interest in exploring their role in this context. Interestingly, we found that smoking led to a significant increase in $\gamma\delta$-T cells in the lung environment of HLA-DR4 mice (Fig. 4A, BAL, $P < .001$; lung tissue $P = .002$; and mediastinal lymph node, $P = .03$). This was consistent with our observation of elevated $\gamma\delta$-T cell numbers in BAL samples from RA smokers vs nonsmokers or ex-smokers, which was not seen for other innate-like T cell subsets such as invariant natural killer T (iNKT) and mucosal associated invariant T (MAIT) cells (Fig 4B, and Supplementary Fig S4A-C). Moreover, we found a strong positive correlation between the numbers of lung-resident Cit-peptide reactive CD4+ T cells and $\gamma\delta$-T cells after CS exposure in HLA-DR4 transgenic mice, whereas no such correlation was apparent for HA (control antigen) reactive T cells (Fig 4C).

As these data suggest a potential link between Cit-peptide autoreactivity and altered $\gamma\delta$-T responses, we further sought to explore the responses of $\gamma\delta$-T cells after Cit-ENOL immunisation in our experimental arthritis set-up in the presence of IL-23 overexpression. First, we observed that Cit-ENOL immunisation was associated with an increase in the percentage of $\gamma\delta$-T cells in the spleen, compared with mice receiving CFA control (Fig 4D). A significant positive correlation between the number of Cit-ENOL tetramer+ CD4 T cells and $\gamma\delta$-T in the draining lymph node after Cit-ENOL injection was present independently of IL-23 overexpression (Fig 4E). We also checked the levels of cell activation markers, such as PD-1 (CD279), CD137, CD25 (IL-2Ra), and HLA-DR, on lymphocytes (including $\gamma\delta$-T cells) by flow cytometry. Interestingly, the expression of HLA-DR on $\gamma\delta$-T was increased after Cit-ENOL immunisation ($P < .05$, Supplementary Fig 4E). Second, *in vitro* Cit-peptide rechallenge induced the proliferation of $\gamma\delta$-T cells—to an even greater extend as compared to conventional T cells—with up to 20% proliferative cells (when restimulated with Cit-ENOL but not control antigen, Fig 4F,G, Supplementary Fig S4D). Preincubation with blocking anti-HLA-DR Ab prevented $\gamma\delta$-T cells proliferation in response to Cit-peptide rechallenge (Fig. 4G), suggestive for a potential cross-talk upon activation of Cit-peptide reactive conventional T cells. Interestingly, this MHC-II dependency was lost upon IL-23 overexpression, in line with the potential of IL-23 to stimulate $\gamma\delta$-T cells directly [22].

To further study the potential effect of $\gamma\delta$-T cells towards adaptive Cit-peptide T cell responses and arthritis, HLA-DR4 crossed with TCRD$^{-/-}$ mice (lacking $\gamma\delta$-T cells) were similarly immunised with Cit-α-enolase peptide together with IL-23 overexpression. The absence of $\gamma\delta$-T cells led to a worsened arthritis phenotype in Cit-ENOL immunised mice, reflected by a mean visual arthritis score of 2.1 $\pm$ 0.6 vs 0.6 $\pm$ 0.2 at day 50 ($P = .02$) and most strikingly a clear increase in arthritis incidence (Fig 4H). Serum IL-23 levels after IL-23 EEV hydrodynamic delivery (HDD) injections were similar in mice lacking $\gamma\delta$-T cells compared to wild-type HLA-DR4 mice (Fig 4I). Of note, no differences in ACPA responses were detected (see Supplementary Fig S3C). Histological analyses did not show any significant differences in immune cell infiltration as seen on H&E-stained ankle and feet sections of arthritic mice at the endpoint of disease for TCRD$^{-/-}$ $\times$ HLA-DR4 vs HLA-DR4 mice (Fig 4J). This probably indicates the absence of $\gamma\delta$-T cells had a predominant impact on the arthritis incidence and number of affected joints (as reflected in the arthritis disease score in Fig. 4H). Following *in vitro* restimulation with Cit-ENOL, T cells culture from HLA-DR4 $\times$ TCRD$^{-/-}$ mice exhibited enhanced IL17 and IFNγ proinflammatory responses, compared to those from HLA-DR4 $\times$ TCRD$^{+/+}$ control mice (Fig. 4K). Finally, given the effect of CS on $\gamma\delta$-T cells *in vivo*, we thought to assess the additive impact of CS on T cell responses to citrullinated antigens *in vitro* in the context of the absence of $\gamma\delta$-T cells. Cigarette smoke extract (CSE) is commonly used *in vitro* to mimic the biological

of proinflammatory cytokine levels (IL-17A, IFNγ, TNFα, and IL-6) in the supernatant (measured via ELISA) after *in vitro* restimulation with different cultures conditions as described in Figure 2A (statistic: one-way ANOVA with Dunnett's multiple comparisons test; each condition compared to the unstimulated control condition with *P value $\leq .05$, **$P \leq .01$, ***$P \leq .001$, $P \leq .0001$). (A) was created using Biorender. ANOVA, Analysis of Variance; CAGS, Control empty vector; CFA, Complete Freund's Adjuvant; Cit-ENOL, citrullinated α-enolase; EEV, enhanced episomal vector; H&E, haematoxylin and eosin; ELISA, Enzyme-Linked Immunosorbent Assay; HDD, Hydrodynamic delivery; HLA-DR4, Human Leukocyte Antigen – DR4; IFNγ, Interferon Gamma; IL-17A, Interleukin 17A; LSD, Least Significant Difference; RAG, Recombinase Activating Gene; TNF, Tumor Necrosis Factor; TNFα, Tumor Necrosis Factor Alpha.

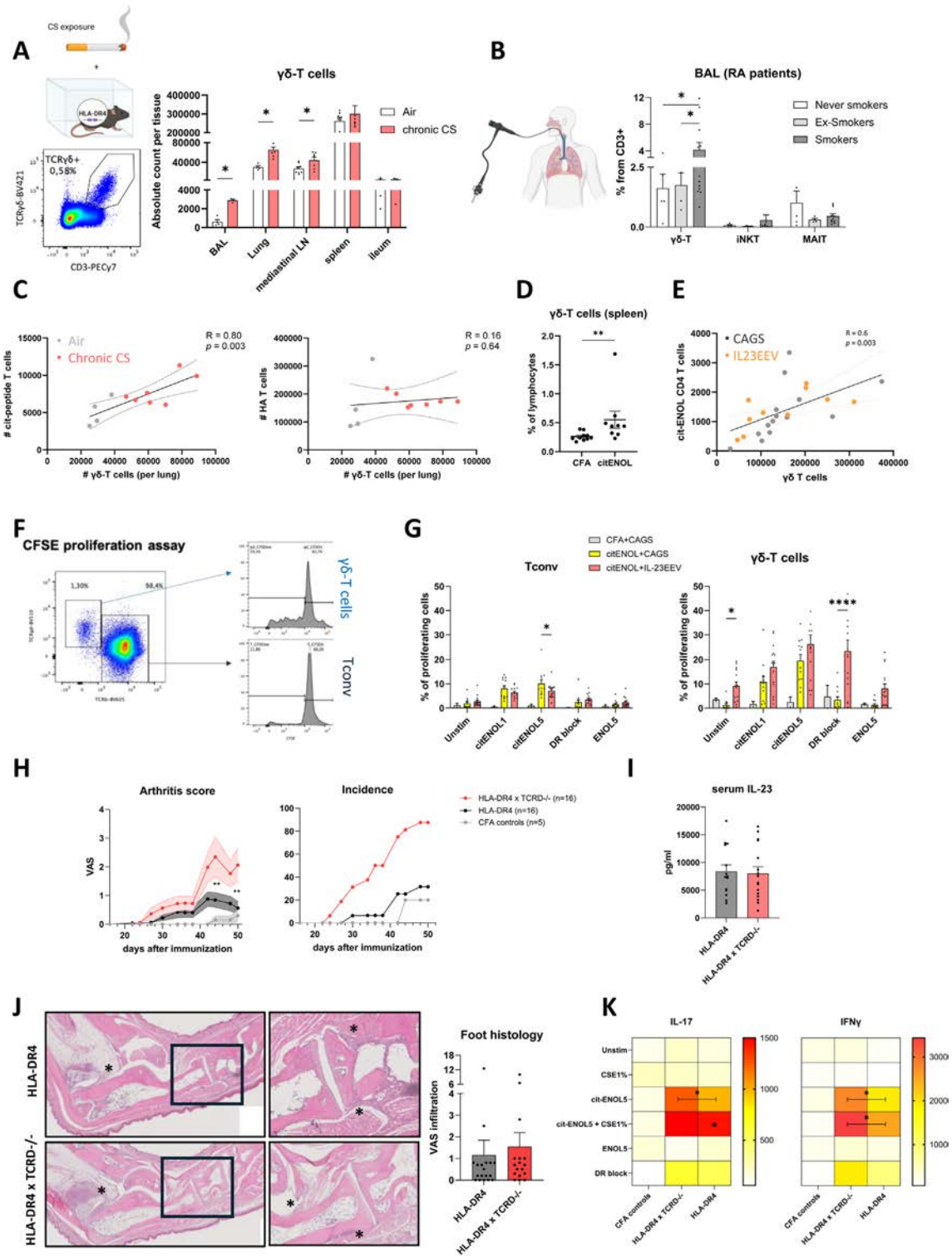

Figure 4. *γδ* T cells gatekeep citrullinated autoreactivity development in HLA-DR4 mice. (A) *γδ*-T cells were quantified by means of flow cytometry of cells from the indicated organs (representative staining of lung shown). Effect of CS on *γδ*-T cell numbers in different tissues of HLA-DR4 mice (chronic CS vs air controls; statistic: multiple unpaired t tests with **P* value ≤ .05). (B) Quantification of innate-like T cell subsets (*γδ*-T, MAIT, and iNKT cells) in BAL fluid of patients with early RA stratified for smoking status (statistic: two-way ANOVA with Fischer LSD's multiple comparisons test with **P* value ≤ .05). (C) Correlation plots between the numbers of lung-residing *γδ*-T cells and Cit-peptide reactive CD4 + T cells (left panel) and HA reactive T cells (right panel); mice exposed to chronic CS are highlighted in red (statistic: Pearson test, with R[rho]- and *P*-values indicated). (D) Cit-ENOL immunisation was associated with a significantly increased number of *γδ*-T cells in the spleen as compared to mice receiving CFA (statistic: unpaired 2-tailed t-test with ** indicating a *P* value ≤ .01). (E) Correlation between the numbers of popliteal/inguinal LN *γδ*-T cells and Cit-peptide reactive CD4 + T cells in mice immunised with Cit-ENOL; mice receiving IL-23 EEV are highlighted in orange (statistic: Pearson test, with R[rho]- and *P* value indicated). (F) CFSE dilution assay (flow cytometry) gated on conventional T and *γδ*-T cells from an immunised mice, showing (G) proliferation percentages of conventional T and *γδ*-T cells as shown for each condition (statistic: two-way ANOVA with Šídák's multiple comparisons test with **P* value ≤ .05, ****P* ≤ .001, *****P* ≤ .0001). (H) Cit-ENOL immunisation combined with IL-23 overexpression in HLA-DR4 × TCRD$^{-/-}$ mice. Arthritis VAS of HLA-DR4 × TCRD$^{-/-}$ compared to HLA-DR4, showing an aggravated arthritis score in mice lacking *γδ*-T cells; graphs show arthritis scores (left) and incidence rates (right) as function of time. (I) Serum levels of IL-23 in HLA-DR4 vs HLA-DR4 × TCRD$^{-/-}$ receiving IL-23 EEV (statistic: unpaired 2-tailed *t*-test). (J) Histology of hind feet, with representative illustrations (left) and inflammation scores (right) of ankle joints (cellular infiltrations, see

effect of CS exposure on cells. CSE alone did not affect the release of IFNγ and IL-17, with supernatant levels similar to controls. However, in combination with Cit-ENOL re-exposure, CSE was associated with an increased production of IL-17 in culture conditions from HLA-DR4 mice immunised mice ($P < .001$). This synergistic effect was not seen in culture from HLA-DR4 mice lacking $\gamma\delta$-T cells (Fig 4K). These results suggested a modulatory effect on $\gamma\delta$-T cells towards HLA-DR4-mediated Cit-peptide T cell responses under the influence of CS.

DISCUSSION

Cigarette smoke is a well-established risk factor for RA, yet the underlying pathogenic mechanisms remain poorly defined. Our study now provides translational evidence linking chronic smoke exposure to increased citrullinated CD4+ T cell responses as observed in lung samples from patients with early SE+ RA and HLA-DR4 transgenic mice. We further demonstrate that these HLA-DR4-restricted autoimmune responses require an additional inflammatory signal (ie, IL23) to trigger joint pathology, with $\gamma\delta$ T cells emerging as key modulators of this process. This study offers substantial new insights on the role of autoimmunity and disease development in the context of the lung-joint axis in RA.

A consistent observation in both human and murine settings was the increased T cell reactivity to Cit-ENOL, a ubiquitously expressed, highly conserved glycolytic enzyme previously implicated in RA [23]. This cross-species homology aligns with the concept of molecular mimicry, where environmental antigens may trigger T cell responses that cross-react with self-antigens, contributing to the initiation and amplification of autoimmunity in RA. Specifically, anti-Cit-ENOL antibodies are found in up to 60% of patients with ACPA+ RA [24,25] and have been detected in synovial fluid [26]. Structural studies revealed a biased T cell receptor (TCR) usage towards HLA-DR4-restricted Cit-ENOL peptides [27]. Hence, our results further support that Cit-ENOL might serve as both an antigenic and arthritogenic target in RA, potentially triggered by CS. Interestingly, T cells from mice immunised with Cit-ENOL also responded strongly to Cit-CILP *in vitro*, despite the low sequence homology between these peptides. This observation suggests that citrullination itself may act as a dominant determinant for MHC class II binding in the context of the SE, with the adjacent amino acids playing a relatively minor role. These findings also support the concept of epitope spreading in the development of autoreactive T cell responses.

Regarding humoral responses, we only observed rare and weak antibody responses to citrullinated antigens in immunised mice. One limitation of this study is the use of a peptide antigen for immunisation, which may restrict B cell activation and the development of antigen-specific antibody responses. While such linear peptides can serve as T cell epitopes, they may not be efficiently recognised by B cell receptors, preventing antibody production. Since autoantibody production and immune complex deposition are key pathogenic drivers in several classical arthritis models, including collagen-induced arthritis, their absence could potentially influence joint pathology, particularly the extent of erosive changes—an effect also modulated by the genetic background of the mouse strain. Despite this limitation, we observed overt arthritis accompanied by clear cartilage erosions in immunised mice, along with IL-23 overexpression. Furthermore, we observed a strong and specific T cell response, suggesting successful T cell priming and a break in tolerance, even in the apparent absence of a detectable anticitrullinated peptide response, adding to the ongoing debate about detectability and pathogenic relevance of ACPA in preclinical models [28,29].

Importantly, neither smoke exposure nor Cit-ENOL immunisation was sufficient to provoke arthritis in HLA-DR4 mice, despite the formation of ectopic lymphoid structures in the lung and robust T cell responses. These are key steps in local immune activation that may contribute to the breakdown of tolerance, especially considering the known role of IL-23 in promoting such immune processes. Notably, Kinloch et al [30] reported that citrullinated human alpha enolase immunisation of DR4-IE-transgenic mice (expressing human SE and no murine MHC-II genes) was associated with arthritis development. In contrast, this finding could not be reproduced by Haag et al [31] despite the constitution of preserved immune responses to Cit-ENOL antigen, suggesting that environmental conditions and exposure to inflammatory triggers or stress are critical factors allowing the development of arthritis. These findings are consistent with a 'second-hit' model of RA pathogenesis, in which loss of tolerance to citrullinated antigens precedes overt disease and requires additional inflammatory cues to precipitate arthritis. IL-23 emerged as a strong candidate based on its elevated expression in early RA [32,33] and its role in mucosal immunity. Recently, expanded Th17/Th22 cells (characterised by a downstream signature of IL-23) were identified in RA at-risk individuals [34]. Here, we show that the combination of Cit-ENOL immunisation with IL-23 overexpression was associated with a robust, MHC class II-dependent polyarthritis phenotype in HLA-DR4 mice. Prior study showed that arthritic phenotype upon IL-23EEV overexpression is MHC class II-dependent, with C57BL/6 mice (in contrast to B10RIII mice, which are more susceptible for arthritis development) being resistant to disease development [35], suggesting—in line with our findings—an important interplay between IL-23 and adaptive MHC-driven immune responses in arthritic disease outcome. Intriguingly, T cell restimulation assays revealed a dominant IFN-γ, TNF-α, and IL-6-driven inflammatory

materials and methods). (K) Splenocytes and inguinal lymph nodes from arthritic mice were isolated, and cells were set up *in vitro* for restimulation with Cit-enolase (5 μg/mL) in the presence or absence of cigarette smoke extract (CSE, 1% of culture medium); native peptides (containing arginine instead of citrulline); and Cit-enolase (5 μg/mL) in the presence of anti-HLADR Ab (aDR Ab, DR block). Quantification by ELISA of proinflammatory cytokines, respectively, IFNγ and IL-17A, in the culture supernatant after *in vitro* rechallenge with Cit-enolase 5 μg/ml vs no stimulation (statistic: one-way ANOVA with Šídák's multiple comparisons test with * indicating a P value $\leq .05$, **$P \leq .01$, ***$P \leq .001$). (A) and (B) were partly created using Biorender. ANOVA, Analysis of Variance; anti-HLADR Ab, Anti-Human Leukocyte Antigen − DR Antibody; BAL, bronchoalveolar lavage; CAGS, control empty vectors; CD4, Cluster of Differentiation 4; CFA, Complete Freund's Adjuvant; CFSE, Carboxyfluorescein Succinimidyl Ester; Cit-ENOL, citrullinated α-enolase; CS, cigarette smoke; EEV, enhanced episomal vector; ELISA, Enzyme-Linked Immunosorbent Assay; IFNγ, Interferon Gamma; HA, Influenza haemagglutinin HLA-DR4, Human Leukocyte Antigen − DR4; iNKT, Invariant Natural Killer T cells; IL-17A, Interleukin 17A; LN, Lymph Node; LSD, Least Significant Difference; MAIT, Mucosal-Associated Invariant T cells; TCRD, T Cell Receptor Delta; RA, rheumatoid arthritis; VAS, visual analogue scale.

profile, with reduced IL-17 production, which seemed counter-intuitive. However, although generally associated with Th17 responses, IL-23 has been shown to promote Th1-like effector function [36]. Hence, our results support alternative IL-23-driven pathways in tissue inflammation, potentially relevant in RA disease development.

This study further highlights the immunomodulatory role of γδ-T cells (a distinct population of innate-like T cells enriched at mucosal barriers [37]) in regulating HLA-DR4-restricted responses during arthritis development. First, we observed a strong correlation between lung-resident Cit-peptide $CD4^+$ T cells and γδ-T cells following smoke exposure. Second, IL-23 overexpression in Cit-ENOL-immunised mice showed a comparable correlation, along with altered Cit-ENOL-specific T cell responses in γδ T cell-deficient mice. Furthermore, γδ-T cells displayed robust proliferative responses upon *in vitro* Cit-ENOL rechallenge, suggesting cross-activation alongside DR4-mediated T cell responses. Finally, HLA-DR4 $TCRD^{-/-}$ mice showed an increased arthritis development following IL-23 EEV and Cit-ENOL cochallenge, indicating a potentially protective role for γδ T cells in this model. The regulatory function of γδ T cells in mucosal immunity has been previously demonstrated using $TCRD^{-/-}$ mice, which exhibit impaired IgA production and germinal centre formation in response to immunisation (tetanus toxoid, cholera toxin, or OVA in CFA) [38,39]. The mechanisms by which γδ-T cells modulate conventional T cell responses and arthritis remain to be elucidated and require further investigations. γδ-T cells constitutively express IL-23R, allowing rapid IL-17, IL-22, and IL-21 secretion in response to IL-23, as shown in IL-23-driven spondyloarthritis models [40]. Conversely, γδ-T cells contribute to protective immunity at lung barriers during respiratory infections and inflammation [41,42]. Their recruitment to the lung upon CS exposure has also been linked to IFN-mediated protection against influenza A virus [20]. Reduced γδ-T cell numbers in chronic obstructive pulmonary disease (COPD) and asthma further suggest a protective role in chronic lung inflammation [43,44]. Collectively, these findings highlight the functional plasticity of γδ-T cells, with context-dependent regulatory roles across tissues and diseases.

This study has several limitations, including a relatively small patient cohort. Furthermore, we did not directly demonstrate the effect of CS on arthritis development, as we employed an immunisation model—as a proxy for smoke-induced changes, specifically the induction of anticitrullinated peptide responses—to circumvent long-term smoke exposure in combination with high IL-23 load in mice. Finally, in both our human and mouse experiments, we focused on the total population of γδ T cells, which excluded γδ T cell subset characterisation and functional involvement to be explored in our model. This warrants further investigation, eg, by a specific focused approach using advanced multicolour flow cytometry and single cell OMIC assays (incl. γδ-TCR sequencing).

In conclusion, our study provides strong evidence supporting the existence of a lung-joint axis in RA pathogenesis, with a direct link between smoking and the development of citrullinated T cells responses in both ACPA+ RA and in HLA-DR4 mice. Our data further suggest that γδ-T cells function as important gatekeepers in light of smoke-induced adaptive immune responses at mucosal barriers with a profound impact on arthritis development. Altogether, these data highlight the selective impact of CS on autoreactive and innate-like T cell subsets in the lung environment, reflecting smoke-induced early immune changes before RA tolerance breakdown.

Competing interests

All authors declare they have no competing interests.

Acknowledgements

The authors would like to thank all the volunteers who participated in the studies, as well as all the lab technicians and team members who assisted with the experiments, including Eric Gracey, Andrea Cere, Emilie Dumas, Srinath Govindarajan, Guillaume Planckaert, Elisabeth Gillis, Karel Van Damme, Eveline Verheugen, Margaux Maelegheer, Nadia Schrijvers, Ann Neesen, Indra De Borle, Katleen De Saedeleer, Greet Barbier, and Anouck Goethals. We would like to thank Marnik Vuylsteke (Gnomixx) for advanced statistical analyses.

Contributors

The project was designed, conceived, and planned by KV, MJ, and DE. Clinical examinations and samples were collected by TM, PJ, RW, and TM. Experiments were performed by MJ, KV, TD, TM, JC, RvdC, DvdW, and AA. The data were analysed by MJ, KV, and DE. The paper was written and edited by MJ, KV, and DE. All authors revised the paper critically for important intellectual content and gave their final approval for submission. DE is the guarantor of this study. KV and DE contributed equally to this paper as shared last authors.

Funding

MJ is supported by the SSR (Swiss Rheumatology Society) training grant for rheumatologists 2020, a travelling grant from the private foundation of Geneva University hospital (Hôpitaux Universitaires de Genève), and the Eugenio Litta grant from The Fondation genevoise de bienfaisance Valeria Rossi di Montelera, Geneva, Switzerland. KV is supported by FWO-Vl (Fonds voor Wetenschappelijk Onderzoek Vlaanderen, Grant G091025N), VLAIO (Flanders Innovation & Entrepreneurship, HBC.2016.0622), Special Research Funds from Ghent University (BOF/BAF/3y/2024/01/006 and 01G03122), and The King Baudouin Foundation (2024-J1820590-0021916). DE is supported by FWO-Vl (G0A9824N and G082023N).

Provenance and peer review

Not commissioned; externally peer reviewed.

Declaration of generative AI and AI-assisted technologies in the writing process

During the preparation of this work the authors used AI-assisted technologies in order to improve the readability and language of the manuscript. After using this tool/service, the authors reviewed and edited the content as needed and take full responsibility for the content of the publication.

Supplementary materials

Supplementary material associated with this article can be found in the online version at doi:10.1016/j.ard.2025.10.031.

Orcid

Koen Venken: http://orcid.org/0000-0002-4950-386X

REFERENCES

[1] Gravallese EM, Firestein GS. Rheumatoid arthritis. Reply. N Engl J Med 2023;388:1919–20. doi: 10.1056/NEJMc2302868.

[2] Linn-Rasker SP, van der Helm-van Mil AH, van Gaalen FA, Kloppenburg M, de Vries RR, le Cessie S, et al. Smoking is a risk factor for anti-CCP antibodies only in rheumatoid arthritis patients who carry HLA-DRB1 shared epitope alleles. Ann Rheum Dis 2006;65:366–71.

[3] Lim JJ, Jones CM, Loh TJ, Ting YT, Zareie P, Loh KL, et al. The shared susceptibility epitope of HLA-DR4 binds citrullinated self-antigens and the TCR. Sci Immunol 2021;6:eabe0896. doi: 10.1126/sciimmunol.abe0896.

[4] Scally SW, Petersen J, Law SC, Dudek NL, Nel HJ, Loh KL, et al. A molecular basis for the association of the HLA-DRB1 locus, citrullination, and rheumatoid arthritis. J Exp Med 2013;210:2569–82. doi: 10.1084/jem.20131241.

[5] Rims C, Uchtenhagen H, Kaplan MJ, Carmona-Rivera C, Carlucci P, Mikecz K, et al. Citrullinated aggrecan epitopes as targets of autoreactive CD4+ T cells in patients with rheumatoid arthritis. Arthritis Rheumatol 2019;71:518–28. doi: 10.1002/art.40768.

[6] Chemin K, Pollastro S, James E, Ge C, Albrecht I, Herrath J, et al. A novel HLA-DRB1*10:01-restricted T cell epitope from citrullinated type II collagen relevant to rheumatoid arthritis. Arthritis Rheumatol 2016;68:1124–35. doi: 10.1002/art.39553.

[7] Song J, Schwenzer A, Wong A, Turcinov S, Rims C, Martinez LR, et al. Shared recognition of citrullinated tenascin-C peptides by T and B cells in rheumatoid arthritis. JCI Insight 2021;6:e145217. doi: 10.1172/jci.insight.145217.

[8] Snir O, Rieck M, Gebe JA, Yue BB, Rawlings CA, Nepom G, et al. Identification and functional characterization of T cells reactive to citrullinated vimentin in HLA-DRB1*0401-positive humanized mice and rheumatoid arthritis patients. Arthritis Rheum 2011;63:2873–83. doi: 10.1002/art.30445.

[9] Pieper J, Dubnovitsky A, Gerstner C, James EA, Rieck M, Kozhukh G, et al. Memory T cells specific to citrullinated α-enolase are enriched in the rheumatic joint. J Autoimmun 2018;92:47–56. doi: 10.1016/j.jaut.2018.04.004.

[10] Saint-André V, Charbit B, Biton A, Rouilly V, Possémé C, Bertrand A, et al. Smoking changes adaptive immunity with persistent effects. Nature 2024;626:827–35. doi: 10.1038/s41586-023-06968-8.

[11] van Wesemael TJ, Ajeganova S, Humphreys J, Terao C, Muhammad A, Symmons DP, et al. Smoking is associated with the concurrent presence of multiple autoantibodies in rheumatoid arthritis rather than with anti-citrullinated protein antibodies per se: a multicenter cohort study. Arthritis Res Ther 2016;18:285. doi: 10.1186/s13075-016-1177-9.

[12] Makrygiannakis D, Hermansson M, Ulfgren A-K, Nicholas AP, Zendman AJ, Eklund A, et al. Smoking increases peptidylarginine deiminase 2 enzyme expression in human lungs and increases citrullination in BAL cells. Ann Rheum Dis 2008;67:1488–92. doi: 10.1136/ard.2007.075192.

[13] Reynisdottir G, Karimi R, Joshua V, Olsen H, Hensvold AH, Harju A, et al. Structural changes and antibody enrichment in the lungs are early features of anti-citrullinated protein antibody-positive rheumatoid arthritis. Arthritis Rheumatol 2014;66:31–9. doi: 10.1002/art.38201.

[14] Joshua V, Loberg Haarhaus M, Hensvold A, Wähämaa H, Gerstner C, Hansson M, et al. Rheumatoid arthritis-specific autoimmunity in the lung before and at the onset of disease. Arthritis Rheumatol 2023;75:1910–22. doi: 10.1002/art.42549.

[15] van Wesemael TJ, Morton FR, Heutz JW, Maurits MP, Dorjée AL, Porter D, et al. Smoking as a risk factor for rheumatoid arthritis: predominant association with IgA autoantibodies - comprehensive analysis of anti-modified protein antibodies with smoking and genetic risk factors in rheumatoid arthritis. Arthritis Res Ther 2025;27:101. doi: 10.1186/s13075-025-03543-6.

[16] Venken K, Jarlborg M, Stevenaert F, Malfait TLA, Vlieghe C, Abraham Y, et al. Shared lung and joint T cell repertoire in early rheumatoid arthritis driven by cigarette smoking. Ann Rheum Dis 2024 ard-2024-226284. doi: 10.1136/ard-2024-226284.

[17] Kokkonen H, Brink M, Hansson M, Lassen E, Mathsson-Alm L, Holmdahl R, et al. Associations of antibodies against citrullinated peptides with human leukocyte antigen-shared epitope and smoking prior to the development of rheumatoid arthritis. Arthritis Res Ther 2015;17:125. doi: 10.1186/s13075-015-0638-x.

[18] Pfeifle R, Rothe T, Ipseiz N, Scherer HU, Culemann S, Harre U, et al. Regulation of autoantibody activity by the IL-23-TH17 axis determines the onset of autoimmune disease. Nat Immunol 2017;18:104–13. doi: 10.1038/ni.3579.

[19] Mortier C, Gracey E, Coudenys J, Manuello T, Decruy T, Maelegheer M, et al. RORγt inhibition ameliorates IL-23 driven experimental psoriatic arthritis by predominantly modulating γδ-T cells. Rheumatology (Oxford) 2023;62:3169–78. doi: 10.1093/rheumatology/kead022.

[20] Hong MJ, Gu BH, Madison MC, Landers C, Tung HY, Kim M, et al. Protective role of γδ T cells in cigarette smoke and influenza infection. Mucosal Immunol 2018;11:894–908. doi: 10.1038/mi.2017.93.

[21] Tian X, Wang S, Zhang C, Prakash YS, Vassallo R. Blocking IL-23 signaling mitigates cigarette smoke-induced murine emphysema. Environ Toxicol 2024;39:5334–46. doi: 10.1002/tox.24405.

[22] Papotto PH, Gonçalves-Sousa N, Schmolka N, Iseppon A, Mensurado S, Stockinger B, et al. IL-23 drives differentiation of peripheral γδ17 T cells from adult bone marrow-derived precursors. EMBO Rep 2017;18:1957–67. doi: 10.15252/embr.201744200.

[23] Pancholi V. Multifunctional alpha-enolase: its role in diseases. Cell Mol Life Sci 2001;58:902–20. doi: 10.1007/pl00000910.

[24] Lundberg K, Kinloch A, Fisher BA, Wegner N, Wait R, Charles P, et al. Antibodies to citrullinated alpha-enolase peptide 1 are specific for rheumatoid arthritis and cross-react with bacterial enolase. Arthritis Rheum 2008;58:3009–19. doi: 10.1002/art.23936.

[25] Kinloch A, Lundberg K, Wait R, Wegner N, Lim NH, Zendman AJ, et al. Synovial fluid is a site of citrullination of autoantigens in inflammatory arthritis. Arthritis Rheum 2008;58:2287–95. doi: 10.1002/art.23618.

[26] Snir O, Widhe M, Hermansson M, von Spee C, Lindberg J, Hensen S, et al. Antibodies to several citrullinated antigens are enriched in the joints of rheumatoid arthritis patients. Arthritis Rheum 2010;62:44–52. doi: 10.1002/art.25036.

[27] Loh TJ, Lim JJ, Jones CM, Dao HT, Tran MT, Baker DG, et al. The molecular basis underlying T cell specificity towards citrullinated epitopes presented by HLA-DR4. Nat Commun 2024;15:6201. doi: 10.1038/s41467-024-50511-w.

[28] Marco-Bonilla M, Fresnadillo M, de la Riva-Bueno M, Herrero-Beaumont G, Largo R, Mediero A. Animal models in rheumatoid arthritis: is there a correlation between autoantibodies in human pathology and animal models? Biology (Basel) 2025;14:460. doi: 10.3390/biology14050460.

[29] Stoop JN, Fischer A, Hayer S, Hegen M, Huizinga TW, Steiner G, et al. Anti-carbamylated protein antibodies can be detected in animal models of arthritis that require active involvement of the adaptive immune system. Ann Rheum Dis 2015;74:949–50. doi: 10.1136/annrheumdis-2014-206797.

[30] Kinloch AJ, Alzabin S, Brintnell W, Wilson E, Barra L, Wegner N, et al. Immunization with porphyromonas gingivalis enolase induces autoimmunity to mammalian α-enolase and arthritis in DR4-IE-transgenic mice. Arthritis Rheum 2011;63:3818–23. doi: 10.1002/art.30639.

[31] Haag S, Uysal H, Bäcklund J, Tuncel J, Holmdahl R, et al. Human α-enolase is immunogenic, but not arthritogenic, in HLA-DR4-transgenic mice: comment on the article by Kinloch et al. Arthritis Rheum 2012;64:1689–91. doi: 10.1002/art.34379.

[32] Cañete JD, Celis R, Yeremenko N, Sanmartí R, van Duivenvoorde L, Ramírez J, et al. Ectopic lymphoid neogenesis is strongly associated with activation of the IL-23 pathway in rheumatoid synovitis. Arthritis Res Ther 2015;17:173. doi: 10.1186/s13075-015-0688-0.

[33] Rasmussen TK, Andersen T, Hvid M, Hetland ML, Hørslev-Petersen K, Stengaard-Pedersen K, et al. Increased interleukin 21 (IL-21) and IL-23 are associated with increased disease activity and with radiographic status in patients with early rheumatoid arthritis. J Rheumatol 2010;37:2014–20. doi: 10.3899/jrheum.100259.

[34] Inamo J, Keegan J, Griffith A, Ghosh T, Horisberger A, Howard K, et al. Deep immunophenotyping reveals circulating activated lymphocytes in individuals at risk for rheumatoid arthritis. J Clin Invest 2025;135:e185217. doi: 10.1172/JCI185217.

[35] Haley EK, Matmusaev M, Hossain IN, Davin S, Martin TM, Ermann J. The impact of genetic background and sex on the phenotype of IL-23 induced murine spondyloarthritis. PLoS One 2021;16:e0247149. doi: 10.1371/journal.pone.0247149.

[36] Pawlak M, DeTomaso D, Schnell A, Meyer Zu Horste G, Lee Y, Nyman J, et al. Induction of a colitogenic phenotype in Th1-like cells depends on interleukin-23 receptor signaling. Immunity 2022;55 1663-79.e6. doi: 10.1016/j.immuni.2022.08.007.

[37] Ribot JC, Lopes N, Silva-Santos B. γδ T cells in tissue physiology and surveillance. Nat Rev Immunol 2021;21:221–32. doi: 10.1038/s41577-020-00452-4.

[38] Fujihashi K, McGhee JR, Kweon MN, Cooper MD, Tonegawa S, Takahashi I, et al. Gamma/delta T cell-deficient mice have impaired mucosal immunoglobulin A responses. J Exp Med 1996;183:1929–35. doi: 10.1084/jem.183.4.1929.

[39] Rezende RM, Lanser AJ, Rubino S, Kuhn C, Skillin N, Moreira TG, et al. γδ T cells control humoral immune response by inducing T follicular helper cell differentiation. Nat Commun 2018;9:3151. doi: 10.1038/s41467-018-05487-9.

[40] Petermann F, Rothhammer V, Claussen MC, Haas JD, Blanco LR, Heink S, et al. γδ T cells enhance autoimmunity by restraining regulatory T cell responses via an interleukin-23-dependent mechanism. Immunity 2010;33:351–63. doi: 10.1016/j.immuni.2010.08.013.

[41] Guo XJ, Dash P, Crawford JC, Allen EK, Zamora AE, Boyd DF, et al. Lung $\gamma\delta$ T cells mediate protective responses during neonatal influenza infection that are associated with type 2 immunity. Immunity 2018;49 531-44.e6. doi: 10.1016/j.immuni.2018.07.011.

[42] Wehrmann F, Lavelle JC, Collins CB, Tinega AN, Thurman JM, Burnham EL, et al. $\gamma\delta$ T cells protect against LPS-induced lung injury. J Leukoc Biol 2016;99:373–86. doi: 10.1189/jlb.4A0115-017RR.

[43] Urboniene D, Babusyte A, Lötvall J, Sakalauskas R, Sitkauskiene B. Distribution of $\gamma\delta$ and other T-lymphocyte subsets in patients with chronic obstructive pulmonary disease and asthma. Respir Med 2013;107:413–23. doi: 10.1016/j.rmed.2012.11.012.

[44] Sjåheim T, Kongerud J, Bjørtuft O, Drabløs PA, Malterud D, Halstensen TS. Reduced bronchial CD4+ T-cell density in smokers with occupational asthma. Eur Respir J 2006;28:1138–44. doi: 10.1183/09031936.06.00032906.

Ann Rheum Dis 85 (2026) 743–760

Contents lists available at ScienceDirect

Annals of the Rheumatic Diseases

journal homepage: https://www.sciencedirect.com/journal/annals-of-the-rheumatic-diseases

Osteoarthritis

A brain-driven neural circuit contributes to tissue regeneration in joint cartilage

Konglin Huo[1], Xuebin Ma[1], Yan Xue[1], Lei Zhao[1], Fanhua Wang[1], Guohao Wang[1], Yu You[1], Wenhao Jiang[1], Ruibin Wang[2,3], Yuan Li[2,3], Qing Shen[2,3], Xiaoqing Cheng[1], Chao Wu[1], Keran Chen[1], Yiyun Wang[1], Meiling Su[1], Yeqing Sun[1], Xizhi Guo[4], Zijing Guan[5], Huatai Xu[6], Liangcai Gao[5], Xinran Ma[5], Tifei Yuan[7], Karan Mehul Shah[8], Ning Wang[8,9], Yue Wang[1,*], Xiaochun Peng[10,**], Jian Luo[1,*]

[1] *Yangzhi Rehabilitation Hospital (Shanghai Sunshine Rehabilitation Centre), Tongji University School of Medicine, Shanghai, PR China*
[2] *Laboratory of Mental Health Research, Tongji University School of Medicine, Shanghai, PR China*
[3] *School of Public Health and General Practice, Tongji University School of Medicine, Shanghai, PR China*
[4] *Bio-X Institutes, Key Laboratory for the Genetics of Developmental and Neuropsychiatric Disorders, Ministry of Education, Shanghai Jiao Tong University, Shanghai, PR China*
[5] *Shanghai Key Laboratory of Regulatory Biology, Institute of Biomedical Sciences and School of Life Sciences, East China Normal University, Shanghai, PR China*
[6] *Lingang Laboratory, Shanghai Center for Brain Science and Brain-Inspired Intelligence Technology, Shanghai, PR China*
[7] *Shanghai Key Laboratory of Psychotic Disorders, Brain Health Institute, National Center for Mental Disorders, Shanghai Mental Health Center, Shanghai Jiaotong University School of Medicine, Shanghai, PR China*
[8] *Division of Clinical Medicine, School of Medicine and Population Health, The University of Sheffield, Sheffield, UK*
[9] *Leicester Cancer Research Centre, Division of Cancer Sciences, School of Medical Sciences, University of Leicester, Leicester, UK*
[10] *Department of Orthopaedics, Shanghai Sixth People's Hospital Affiliated to Shanghai Jiao Tong University School of Medicine, Shanghai, PR China*

ARTICLE INFO

Article history:
Received 9 July 2025
Received in revised form 21 November 2025
Accepted 4 December 2025

ABSTRACT

Objectives: Most mammalian tissues have limited regenerative capacity. It has been speculated that the brain might regulate tissue regeneration, while this concept has yet to be experimentally addressed. Using cartilage, a tissue with limited regenerative capacity as an example, we investigated this hypothesis.

Methods: We employed magnetic resonance imaging, polysynaptic retrograde tracing, chemogenetic/optogenetic manipulations, and single-cell RNA sequencing to characterise a functional brain-cartilage neural circuit regulating cartilage regeneration in human and mouse models.

Results: We found that fractional anisotropy and amplitude of low-frequency fluctuations values of the paraventricular nucleus (PVN) are elevated, and correlate with Western Ontario and McMaster Universities Arthritis Index scores and synovial fluid norepinephrine (NE)

*Correspondence to Dr. Yue Wang and Dr. Jian Luo, Yangzhi Rehabilitation Hospital (Shanghai Sunshine Rehabilitation Center), Tongji University School of Medicine, Shanghai, PR China.

**Correspondence to Dr. Xiaochun Peng, Shanghai Sixth People's Hospital, Shanghai JiaoTong University School of Medicine, Shanghai, PR China.

E-mail addresses: wangyuesh@126.com (Y. Wang), dr.xcpeng@shsmu.edu.cn (X. Peng), jluo@tongji.edu.cn (J. Luo).

Handling editor Josef S. Smolen.

Jian Luo, Xiaochun Peng and Yue Wang contributed equally to this study and are considered joint last authors.

Konglin Huo, Xuebin Ma, and Yan Xue contributed equally to this work.

https://doi.org/10.1016/j.ard.2025.12.004

concentrations in patients with osteoarthritis. We further demonstrate the existence of a functional trans-neuronal circuit to regulate cartilage regeneration, which originates from PVN^{CRH} neurons to sympathetic nerves in the synovium of joint. Inhibition of the circuit is sufficient to strongly promote the production of stable mature articular cartilage instead of fibrocartilage. This process fosters the regeneration of articular cartilage by inhibiting the pathways mediated by NE/articular cartilage via the β2-adrenergic receptor (ADRB2) in Proteoglycan 4^+ cells. Furthermore, treatment with an ADRB2 inverse agonist prevented cartilage degradation in human articular cartilage explants.

Conclusions: Our findings unveil a brain-cartilage circuit that regulates cartilage regeneration, providing valuable insights into the inherent limitations of tissue regeneration and suggesting a promising treatment strategy for enhancing cartilage regeneration.

WHAT IS ALREADY KNOWN ON THIS TOPIC

- The limited regenerative capacity of humans and mammals has significantly impeded our ability to cure various diseases, such as osteoarthritis, kidney failure, and chronic obstructive pulmonary disease. Therefore, what controls organ regeneration is one of the most challenging scientific questions.
- Current clinical cartilage repair strategies primarily produce fibrocartilage tissue with unsatisfactory mechanical properties, and a cartilage morphology that is not maintained for an extended period.
- Psychological disorders (e.g., anxiety and depression) are epidemiologically associated with the progression of knee osteoarthritis, but the direct neural regulatory mechanism linking brain activity to cartilage regeneration remains unclear.

WHAT THIS STUDY ADDS

- Our findings offer a novel explanation for the limited regenerative capacity observed in many human tissues and organs, using joint cartilage as an example. When the brain detects damage in peripheral tissue or organs, it exhibits changes in activity, resulting in a reduced or even complete loss of tissue regeneration ability.
- Our research has revealed a groundbreaking neural circuit that establishes a novel physiological connection between the brain and peripheral tissue regeneration. Specifically, we have discovered that PVNCRH neurons project trans-synaptically to the synovial sympathetic nerve and trigger the release of NE into the synovial fluid, which then binds ADRB2 in PRG4 + cells to suppress cartilage regeneration.
- Our study has successfully demonstrated that the inhibition of PVNCRH neurons, along with the downstream sympathetic nervous system and ADRB2, effectively promotes the regeneration of stable mature articular cartilage instead of fibrocartilage.

HOW THIS STUDY MIGHT AFFECT RESEARCH, PRACTICE OR POLICY

- Our study provides a starting point to explore the neural circuit by which brain regulates tissue and organ regeneration.
- Our findings have the potential to inspire the development of alternative interventions aimed at promoting tissue regeneration. These interventions could make use of established brain-stimulation technologies, including transcranial magnetic stimulation, focused ultrasound, or deep brain stimulation.

INTRODUCTION

Tissue regeneration is the process of repairing or replacing damaged tissues caused by injury or other degenerative diseases. However, it is widely recognised that mammals have, to a significant extent, relinquished the capacity for tissue and organ regeneration [1,2]. Consequently, diseases associated with disorders in tissue regeneration, such as osteoarthritis (OA), kidney failure, and chronic obstructive pulmonary disease, currently face a dearth of effective treatment options and impose a substantial health burden worldwide [3]. Deciphering the intricate mechanisms underlying tissue regeneration and harnessing them to facilitate the regenerative processes remains an evolving field of study. Here, we use articular cartilage as our paradigm to understand tissue regeneration, as OA, a degenerative disease of the cartilage, has one of the highest incidence rates with a lifetime risk of 40% [4]. Moreover, multiple strategies have been employed to regenerate articular cartilage, but with limited success [5]. Attempts to regenerate cartilage in OA via arthroscopic microfracture surgery, cartilage transplantation, and others, result in the regeneration of primarily fibrocartilage tissue which has unsatisfactory mechanical properties, and a cartilage morphology that is not maintained for an extended period [6–8]. Similarly, the implementation of stem cell implantation also does not yield desirable therapeutic results and regeneration of stable mature articular cartilage remains a challenge [9].

Increasing evidence suggests that various psychological disorders, particularly anxiety and depression, are risk factors for OA progression [10,11], and pain severity [12]. However, whether the brain's influence extends beyond pain modulation to directly regulate the regenerative capacity of articular cartilage remains unknown.

In this study, we screened the brains of patients with OA using magnetic resonance imaging (MRI) and found that elevated fractional anisotropy (FA) and amplitude of low-frequency fluctuations (ALFF) values in the paraventricular nucleus (PVN) may serve as a potential biomarker for OA. This observation was validated in animal models, in which we demonstrated the PVN to be a surprisingly robust regulator of cartilage regeneration. We also present novel data that suggest the role of corticotropin-releasing hormone (CRH) neurons within the PVN (PVN^{CRH} neurons) in mediating articular cartilage regeneration and identify the therapeutically targetable β2-adrenergic receptor (ADRB2) pathway in Proteoglycan 4 $(PRG4)^+$ cell as a key player in facilitating these effects. Thus, our findings highlight a powerful strategy for identifying and characterising clinically relevant neural circuits involved in tissue regeneration.

RESULTS

FA and ALFF values of PVN are elevated in patients with knee OA (KOA) and associate positively with cartilage damage.

To investigate whether there is a link between brain and cartilage regeneration, we utilised diffusion tensor imaging (DTI) of the brain in patients with KOA (see Materials and methods for details, Supplementary Fig S1A,B) to assess changes in FA values

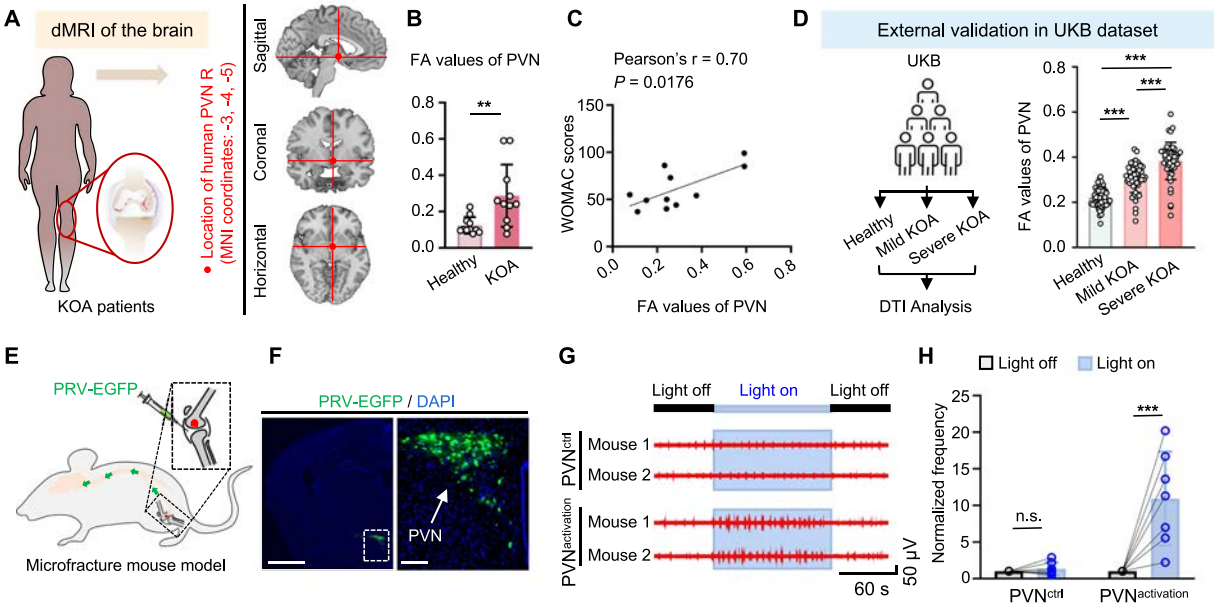

Figure 1. PVN neurons have functional connection to the joint. (A-C) Diagram of clinical recruitment of participants and trial scheme with the location of PVN R highlighted (Montreal Neurological Institute [MNI] coordinates: −3, −4, −5) (A). FA values of PVN between patients with KOA and healthy controls (n = 11 humans in each group) (B). Pearson's correlation between the FA values of PVN and WOMAC scores (n = 11 patients with KOA) (C). (D) FA values of the PVN were compared in patients with mild KOA, severe KOA, and healthy controls using UKB data (n = 50 humans each group). (E and F) Schematic of PRV-EGFP injection into the knee articular cavity (E). Representative images of PRV-infected neurons in the PVN, counterstained with nuclear marker DAPI. Scale bar: 1 mm. The panel on the right shows a magnified view. Scale bar: 100 μm (n = 6 mice) (F). (G, H) Representative traces showing the electrophysiological activities of synovial nerve in PVN^{ctrl} (upper) or $PVN^{activation}$ (lower) mice before and during ChR2-mediated activation of PVN neurons (G). The quantification of optogenetically induced alterations in synovial nerve electrophysiological activity frequency was performed in PVN^{ctrl} or $PVN^{activation}$ mice. Frequency was normalised to the baseline level measured before activation in each trial (n = 7 mice each group) (H). Data information: comparisons between groups were analysed using Student's unpaired *t* test (B, H), or a 1-way ANOVA with Tukey's multiple-comparisons test (D). Pearson's correlation coefficient assay (C). All data are represented as mean ± SD. $^{**}P < .01$, $^{***}P < .001$. ANOVA, analysis of variance; ChR2, channel rhodopsin 2; DAPI, 4',6-diamidino-2-phenylindole; dMRI, diffusion magnetic resonance imaging; DTI, diffusion tensor imaging; FA, fractional anisotropy; KOA, knee osteoarthritis; PRV-EGFP, pseudorabies virus-enhanced green fluorescent protein; PVN, paraventricular nucleus; UKB, UK Biobank; WOMAC, Western Ontario and McMaster Universities Arthritis Index.

of different brain regions (Fig 1A). These regions included key areas associated with anxiety and depression, including the PVN, Amygdala, anterior cingulate cortex (ACC), hippocampus and dorsolateral prefrontal cortex (DLPFC) [13–15]. Our data revealed that the PVN was the only region that displayed significantly higher FA values in individuals with KOA compared to healthy controls (Fig 1B; Supplementary Fig S1C-F), suggesting an enhancement in compensatory neural circuit reorganisation [16–18]. Moreover, the FA values of PVN positively correlated with the Western Ontario and McMaster Universities Arthritis Index (WOMAC) scores (Pearson's $r = 0.70$; $P = .0176$) in these patients with KOA (Fig 1C). Furthermore, we independently validated these findings in populations of diverse ancestries from the UK Biobank (UKB). The results also showed that the PVN was the only region where FA values were elevated in patients with KOA and were positively associated with radiographic OA grading (Fig 1D; Supplementary Fig S1G).

To further investigate the association between articular cartilage defect and PVN activity, we examined the differences in PVN region activity between patients with KOA and healthy controls through the analysis of the ALFF in resting-state functional MRI (rs-fMRI). The results showed that patients with KOA exhibited significantly higher ALFF values in the PVN, which were similarly positively correlated with WOMAC scores (Pearson's $r = 0.76$; $P = .0067$) (Supplementary Fig S1H,I). Taken together, these findings suggest that elevated FA and ALFF values of the PVN may serve as a potential biomarker of OA.

A transneural network exists between the PVN and the joint

We used polysynaptic retrograde tracing system [19–21] to identify the potential anatomical pathways that enable such communication between the PVN and the joint in the mouse model. The modified high-efficiency neurotropic pseudorabies virus (PRV) expressing enhanced green fluorescent protein (EGFP) [22] was injected into the knee articular cavity of the microfracture surgery-induced focal articular cartilage defect mouse model to label neurons upstream of the joint retrogradely and trans-synaptically (Fig 1E). After 96 hours, PRV-EGFP ascended from the joint up into the spinal cord, brainstem and to the forebrain (Supplementary Fig S2A-D; Supplementary Table S1), where the PVN of the hypothalamus exhibited prominent labelling (Fig 1F). These observations were also consistent in a separate microfracture surgery-induced focal articular cartilage defect rat model (Supplementary Fig S2E,F). Moreover, the labelling from joint to PVN neurons was independent of sex as well as surgical intervention (Supplementary Fig S3A,B). Taken together, our results suggest the presence of a trans-neuronal circuit connecting PVN with synovial nerves in the joint of mice and rats.

Electrophysiological activity recording assays are widely used to establish connections between the central nervous system and peripheral organs [23–25]. To further investigate the neural circuit connecting PVN neurons with the synovial nerves, we stereotactically injected an adeno-associated virus (AAV)

that encoded channel rhodopsin 2 (ChR2) fused with EGFP driven by the hSyn promoter (AAV-hSyn-ChR2-EGFP) into the PVN region in C57BL/6J wild-type (WT) mice to optogenetically stimulate PVN neurons, while simultaneously recording electrophysiological activities of the synovial nerves (Supplementary Fig S3C,D). Following activation of PVN neurons ($PVN^{activation}$), we observed that electrophysiological activity at the synovial nerves increased immediately, but not in the PVN^{ctrl} mice, which only expressed EGFP in the PVN (Fig 1G,H), suggesting that the PVN neurons are indeed connected to and can stimulate the synovial nerves.

Inhibition of PVN neuronal activity strongly promotes articular cartilage regeneration

To investigate the potential function of PVN neurons in articular cartilage regeneration, we employed 2 mouse models: a microfracture surgery-induced cartilage defect mouse model and a destabilisation of the medial meniscus (DMM) surgery-induced KOA mouse model. We modulated the activity of PVN neurons in these 2 models using chemogenetic approaches. Specifically, we injected an activator (AAV-hSyn-hM3Dq-EGFP) or inhibitor (AAV-hSyn-hM4Di-EGFP) Designer Receptors Exclusively Activated by a Designer Drug (DREADD)-carrying AAVs into the PVN in the 2 mouse models ($PVN^{activation}$ or $PVN^{inhibition}$, respectively) (Supplementary Fig S4A). Subsequently, the mice were administered with clozapine-N-oxide (CNO), an inert drug that binds to DREADD via the drinking water, which would either stimulate or inhibit the DREADD-carrying neurons.

Our data showed that the cartilage regeneration in $PVN^{inhibition}$ mice was strikingly improved compared to the PVN^{ctrl} mice in the microfracture mouse model (Supplementary Fig S4B), as evidenced by the International Cartilage Repair Society (ICRS) and Oswestry macroscopic grading [26] (Supplementary Fig S4C) and ICRS Visual Histological scores [27] (Supplementary Fig S4D). It is noteworthy that following microfracture surgery, both humans and mice primarily exhibit regeneration of fibrocartilage, which is characterised by increased expression of the fibrocartilage marker (collagen type I alpha 1 chain (COL1A1)) and catabolic factor marker (matrix metalloproteinase 13 (MMP13)), reduced expression of stable mature articular cartilage markers (aggrecan (ACAN) and collagen type II alpha 1 chain (COL2A1)), and a reduction in the elastic modulus of the cartilage [28], which is contrary to the natural stable mature articular cartilage. Interestingly, we observe increased expression, and to a much deeper level, of articular chondroprogenitor cell marker (PRG4) [29], ACAN, and COL2A1 (Supplementary Fig S4E-G), and decreased expression of COL1A1 and MMP13 in $PVN^{inhibition}$ mice cartilages (Supplementary Fig S4H,I). As a result, the elastic modulus of the regenerated cartilage as assessed by atomic force microscopy (AFM) was strikingly increased and almost close to the normal WT articular cartilage when PVN neurons were inhibited (Supplementary Fig S4J). Conversely, the cartilage regeneration was reduced in the $PVN^{activation}$ mice compared to the PVN^{ctrl} mice, including a decrease in ICRS Macroscopic and ICRS Visual Histological scores (Supplementary Fig S4C,D), ACAN expression (Supplementary Fig S4F), while an increase in COL1A1 and MMP13 expression was observed (Supplementary Fig S4H,I). Additionally, microfracture surgery typically induces pain, which is alleviated by the inhibition of PVN neurons (Supplementary Fig S4K,L).

Next, we examined whether inhibition of PVN neurons promoted cartilage regeneration in the DMM mouse model. Consistent with the previous model, the $PVN^{inhibition}$ mice strikingly improved KOA and promoted articular cartilage regeneration (Supplementary Fig S5A), including decrease in Osteoarthritis Research Society International (OARSI) scores [30] (Supplementary Fig S5B), increased expression of PRG4, ACAN, COL2A1 (Supplementary Fig S5,C-E), and decreased expression of MMP13 and COL1A1 (Supplementary Fig S5F,G). In comparison, the $PVN^{activation}$ mice showed deteriorated KOA, including increase in OARSI scores (Supplementary Fig S5B), reduced expression of PRG4 and ACAN (Supplementary Fig S5C,D), and increased of expression of MMP13 and COL1A1 (Supplementary Fig S5F,G). The inhibition of PVN neurons was also suppressed DMM surgery-induced pain (Supplementary Fig S5H,I).

To further confirm whether the PVN could regulate articular cartilage under normal physiological conditions, we activated or inhibited PVN neurons for 6 weeks in a noninjured joint mouse model (Supplementary Fig S5J). Our data revealed that selective activation of PVN neurons led to degeneration of the normal articular cartilage, including increased OARSI scores (Supplementary Fig S5K), downregulation of PRG4, ACAN, and COL2A1 (Supplementary Fig S5L-N), and an upregulation of COL1A1 and MMP13 (Supplementary Fig S5O,P). However, inhibition of PVN neurons had little impact on the cartilage parameters compared to controls (Supplementary Fig S5J-P). Furthermore, we observed increased pain following activation of the PVN neurons (Supplementary Fig S5Q,R).

To investigate whether PVN manipulation directly alters pain thresholds in the absence of structural disease, we conducted short-term chemogenetic activation or inhibition of PVN neurons (via the first CNO administration following stable virus expression) in noninjured joint mice. Our data showed that short-term activation or inhibition of PVN neurons had little impact on pain sensitivity compared to controls (Supplementary Fig S5S,T), suggesting that the pain modulation observed in our OA models is secondary to the level of cartilage damage, rather than a direct effect of PVN activity on pain perception.

Collectively, our results demonstrate that activation of PVN neurons negatively impacts cartilage regeneration, while inhibition of PVN neurons promotes regeneration, enhances anabolism, and suppresses catabolism in cartilage (Supplementary Fig S5U).

PVN^{CRH} neurons regulate the regeneration of articular cartilage

As the PVN represented a primary brain region connecting to synovium, we next sought to identify specific PVN neurons making anatomical connections with synovium. PVN neurons, especially PVN^{CRH} neurons, play a crucial role in regulating anxiety and depression [31–33]. We hypothesised that the activity of PVN^{CRH} neurons might be transmitted as efferent outputs through the synovial nerves to regulate cartilage regeneration. This connection between the PVN^{CRH} neurons and joints was also supported by our immunofluorescence staining in the polysynaptic retrograde tracing mice (Fig 2A).

To further investigate the neural circuit connecting PVN^{CRH} neurons with the synovial nerves, we stereotactically injected an AAV that conditionally expresses double-floxed inverted open reading frame (DIO), for Cre-dependent expression), ChR2 and EGFP (AAV-hSyn-DIO-ChR2-EGFP) into the PVN region of CRH-Cre transgenic mice (Supplementary Fig S6A). In this model, optical stimulation of ChR2 activates neurons in a Cre-dependent manner. After verification of accurate stereotactic targeting (Supplementary Fig S6B), we performed direct electrophysiological recordings from the synovial nerves during optogenetic activation of PVN^{CRH} neurons. Consistent with

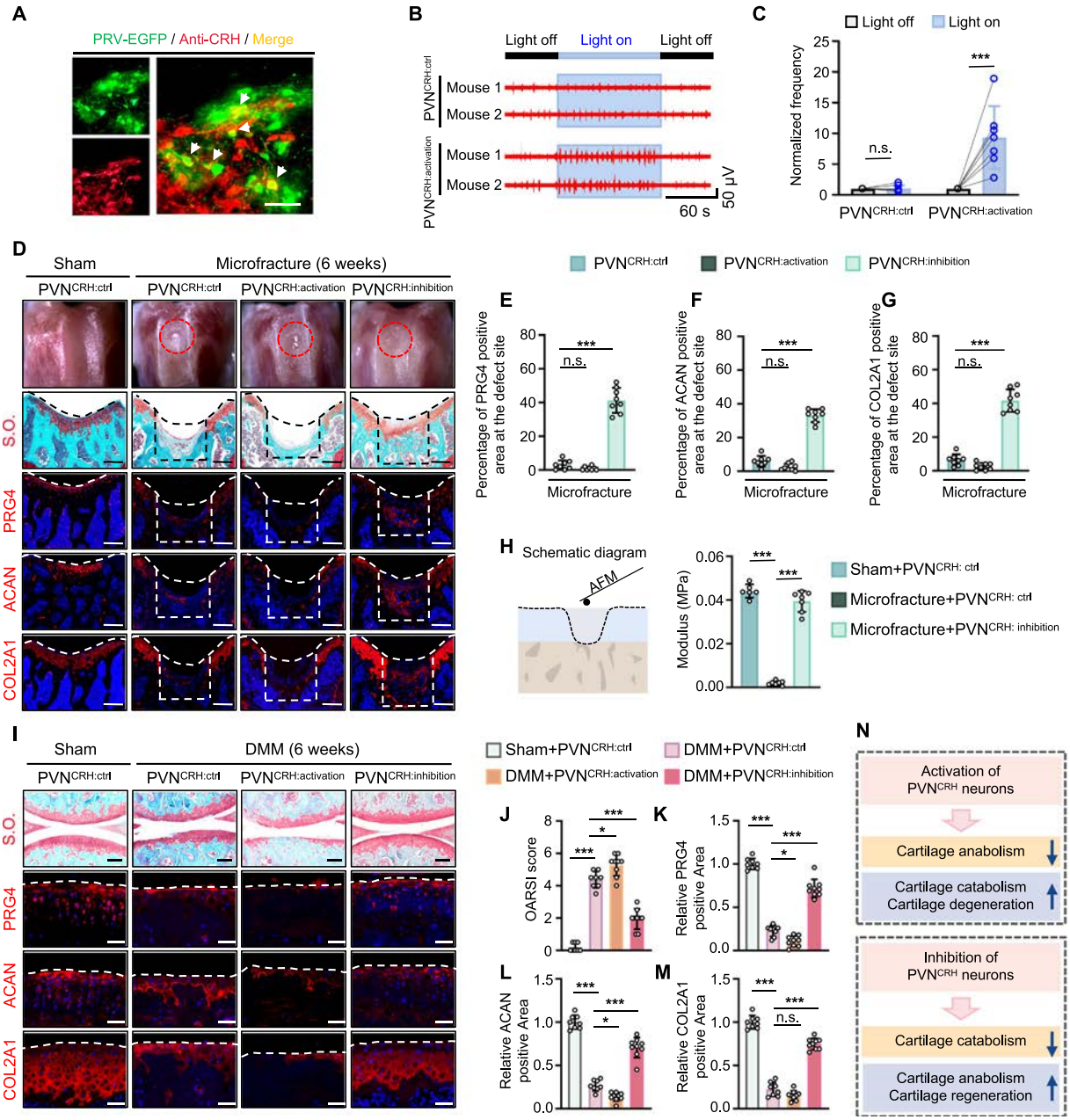

Figure 2. Articular cartilage regeneration is regulated by the CRH-expressing neurons in the PVN. (A) Representative images that illustrate the colocalisation of PRV-EGFP (green) with CRH neurons (immunostaining is in red) in the PVN region. Scale bar: 100 μm (n = 4 mice). (B, C) Representative traces showing the electrophysiological activities of synovial nerve in $PVN^{CRH:\ ctrl}$ (upper) or $PVN^{CRH:\ activation}$ (lower) mice before and during ChR2-mediated activation of PVN^{CRH} neurons (B). The quantification of optogenetically induced alterations in synovial nerve electrophysiological activity frequency was performed in $PVN^{CRH:\ ctrl}$ or $PVN^{CRH:\ activation}$ mice. Frequency was normalised to the baseline level measured before activation in each trial (n = 7 mice each group) (C). (D-G) Representative images of general view, S.O. and immunofluorescence (PRG4, ACAN and COL2A1) staining following activation or inhibition of PVN^{CRH} neurons in microfracture surgery-induced focal articular cartilage defect mouse model. The surgical site is indicated by the red circle, while the rectangular dashed line demarcates the specific location of the defect in the microfracture surgery. Scale bar: 200 μm (D). The graphs represent quantification of PRG4 (E), ACAN (F) and COL2A1 (G) expression in the cartilage tissue at the microfracture surgical defect site (n = 8 mice each group). (H) Quantification for the elastic modulus of the regenerate using AFM at 6 weeks post sham, and microfracture surgery with or without inhibition of PVN^{CRH} neurons (Sham + $PVN^{CRH:\ ctrl}$, n = 6; Microfracture + $PVN^{CRH:\ ctrl}$, n = 7; Microfracture + $PVN^{CRH:\ inhibition}$, n = 7). (I-M) Representative images of S.O. and immunofluorescence (PRG4, ACAN and COL2A1) staining following activation or inhibition of PVN^{CRH} neurons in the DMM surgery-induced KOA mouse model. The dotted lines demarcate the boundary of the articular cartilage surface. Scale bar: 200 μm for S.O. and 100 μm for immunofluorescence (I). OARSI scoring of S.O. stained sections (J). Quantification of PRG4 (K), ACAN (L) and COL2A1 (M) expression in the cartilage tissue (Sham + $PVN^{CRH:\ ctrl}$, n = 8; DMM + $PVN^{CRH:\ ctrl}$, n = 8; DMM + $PVN^{CRH:\ activation}$, n = 9; DMM + $PVN^{CRH:\ inhibition}$, n = 9). (N) Working model illustrating the regulatory role of PVN^{CRH} neurons in cartilage regeneration. Data information: comparisons between groups were analysed using Student's unpaired *t* test (C), or a 1-way ANOVA with Tukey's multiple-comparisons test [(E-H) and (J-M)]. All data are represented as mean ± SD. $^{*}P < .05$, $^{***}P < .001$. ACAN, aggrecan; AFM, atomic force microscopy; ANOVA, analysis of variance; ChR2, channel rhodopsin 2; COL2A1, collagen type II alpha 1 chain; CRH, corticotropin-releasing hormone; DMM, destabilisation of the medial meniscus; KOA, knee osteoarthritis; n.s., not significant; OARSI, Osteoarthritis Research Society International; PRG4, proteoglycan 4; PRV-EGFP, pseudorabies virus-enhanced green fluorescent protein; PVN, paraventricular nucleus; S.O., safranin o/fast green.

activation of PVN neurons, activation of PVN^{CRH} neurons ($PVN^{CRH:\ activation}$ mice) also induces electrophysiological activity in the synovial nerves immediately (Fig 2B,C), suggesting a functional connection between the PVN^{CRH} neurons and the synovial nerves.

To further investigate whether PVN^{CRH} neurons regulate cartilage regeneration, we stereotactically injected the following recombinant AAV vectors within the PVN region of CRH-Cre mice: AAV-hSyn-DIO-EGFP, AAV-hSyn-DIO-hM3Dq-EGFP, or AAV-hSyn-DIO-hM4Di-EGFP to conditionally express EGFP (control), hM3Dq receptor (activation) or hM4Di receptor (inhibition), respectively (Supplementary Fig S7A); and the mice were then subjected to microfracture or DMM surgeries to generate cartilage defects. Consistent with our observations of activated PVN neurons, inhibition of PVN^{CRH} neurons ($PVN^{CRH:\ inhibition}$ mice) strongly improved articular cartilage regeneration and OA scores (Fig 2D,I,J; Supplementary Fig S7B,C), increased expression of PRG4, ACAN, and COL2A1 (Fig 2E-G,K-M), and decreased expression of COL1A1 and MMP13 compared to the $PVN^{CRH:\ ctrl}$ mice (Supplementary Fig S7D-I). The inhibition of PVN^{CRH} neurons also led to the restoration of the elastic modulus of the cartilage, approaching a level similar to the normal physiological state (Fig 2H). Furthermore, inhibition of PVN^{CRH} neurons was also able to relieve both microfracture and DMM-induced pain (Supplementary Fig S7J-M). Conversely, we show that in the DMM model, and to a lesser extent in the microfracture model, activation of the PVN^{CRH} neurons induced cartilage degeneration (Fig 2I,J, Supplementary Fig S7B,C), accompanied by lower expression of PRG4 and ACAN (Fig 2K,L), and increased expression of COL1A1 and MMP13 (Supplementary Fig S7F,H,I). Taken together, we demonstrate that a specific cluster of PVN^{CRH} neurons regulates articular cartilage regeneration (Fig 2N).

Activation of PVN^{CRH} neuronal activity elevates norepinephrine concentration from the synovial sympathetic nerves and facilitates norepinephrine binding to articular chondrocytes

The PVN and PVN^{CRH} neurons have been reported to regulate the sympathetic outflow from the brain to peripheral body tissues [23]. Moreover, previous studies have reported the presence of TH^+ sympathetic nerve fibres in both animal and human synovium and subchondral bone [34], where the sympathetic signal functions primarily through norepinephrine (NE). These findings collectively suggest a potential link between PVN^{CRH} neurons and the sympathetic system within the joint. Therefore, we next examined whether it is the sympathetic neural circuitry linking the brain with the joint occurs via the PVN and the PVN^{CRH} neurons.

Initial data from mice revealed an increase in NE concentration throughout the mouse joint upon PVN^{CRH} neurons activation (Supplementary Fig S8A). Furthermore, we observed that TH^+ sympathetic nerve fibres were more densely localised in the synovium, with some presence in subchondral bone and negligible presence in tendon (Supplementary Fig S8B,C). These findings strongly suggest that NE in the synovial fluid is a consequence of synovial sympathetic nerve terminals, as synovial fluid is predominantly derived from the synovium [35,36].

To further validate whether synovial fluid NE originates from the synovium, and to overcome technical challenges associated with the small size of mouse joints and precise isolation of joint tissues, we employed a rat model to anatomically dissect the source for NE. Our data revealed that chemogenetic activation of PVN neurons elicited an elevation in NE concentration specifically within the synovial fluid and synovium, with no discernible changes in the subchondral bone and tendon of rat (Supplementary Fig S8D-F). Similarly, we induced cartilage defects in rats to explore whether cartilage defect leads to an increase in NE and to identify which tissues' sympathetic nerves were the origin for this NE release. Our results exhibited consistent upregulation of NE concentrations specifically in the synovium and synovial fluid, whereas no significant changes were observed in the subchondral bone and tendon in the microfracture and DMM rat models, while intra-articular administration of 6-hydroxydopamine (6-OHDA) [37], a highly selective neurotoxin targeting sympathetic nerves, effectively abolished the upregulation of NE in the synovium and synovial fluid (Supplementary Fig S8G,H). Together, these results suggest a pivotal role of PVN-sympathetic nervous circuit in stimulating the release of NE from the synovium specifically into the synovial fluid, without influencing NE concentration in subchondral bone or tendons.

Next, we used a G Protein-Coupled Receptor (GPCR) activation-based NE (GRAB_NE) sensor combined with fibre photometry approach [38,39], which allows for the real-time detection of NE travel in living animals [20,40] to investigate whether the released NE of joint by stimulation of PVN^{CRH} neurons binds to articular cartilage. To do this, we stereotactically injected AAVs encoding hChR2 fused with EGFP driven by the mouse CRH (mCRH) promoter (AAV-mCRH-hChR2-EGFP) to the PVN region, to optogenetically stimulate PVN^{CRH} neurons; and a second vector carrying Cre-dependent GRAB_NE (AAV-CMV-DIO-NE2m) into the chondrocytes by injection into the knee articular cavity of *Acan*-CreERT2 transgenic mice, to evaluate the dynamics of cartilage NE in a spatiotemporal manner (Supplementary Fig S9A-D). Our data showed that optical stimulation of PVN^{CRH} neurons elicited an augmentation in GRAB_NE fluorescence intensity in the articular $Acan^+$ chondrocytes about 1 minute post-stimulation (Supplementary Fig S9E,F). This strongly suggests that PVN^{CRH} neuron activation prompts the release of NE, which subsequently binds to NE receptors on articular chondrocytes.

It has been reported that adrenal gland can secrete NE under the activation of PVN^{CRH} neurons [33,41]. To determine whether adrenal glands mediate activation of PVN^{CRH} neurons induced the increase in NE concentration throughout the joint, we surgically removed both adrenal glands (Supplementary Fig S9G). The results showed that while adrenalectomy abolished the increase of NE concentration in the bloodstream of $PVN^{CRH:activation}$ mice compared to sham controls, the NE concentration in the joints was still elevated for $PVN^{CRH:activation}$ mice (Supplementary Fig S9H), suggesting that the PVN^{CRH} neuron-stimulated increase in NE concentration in the joint is independent of adrenal glands.

Collectively, the results obtained from multiple animal models unanimously demonstrate the existence of a functional neuronal circuit between PVN^{CRH} neurons and articular cartilage, which operates through the release of NE from the synovial sympathetic nerve terminals.

Synovial fluid NE concentration correlates with FA, ALFF values of PVN and WOMAC scores in patients with KOA

The data so far suggest that activation of PVN or PVN^{CRH} neurons triggers an increase in NE release from sympathetic nerves in the joint. To explore the potential link between the PVN and synovial sympathetic activity in humans, we measured the concentration of NE in synovial fluid from patients with KOA.

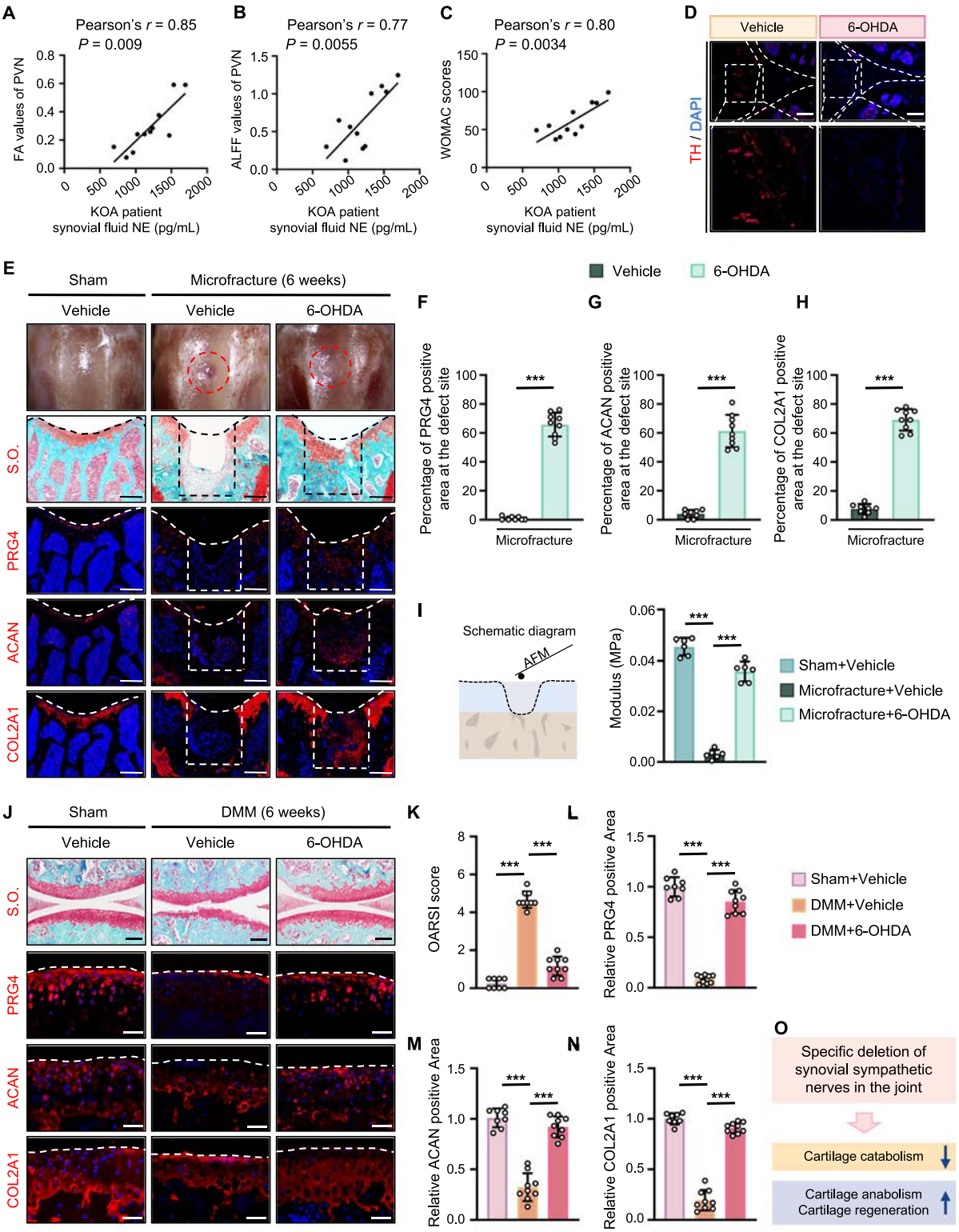

Figure 3. Specific deletion of sympathetic nerves in the joint promotes articular cartilage regeneration. (A) Pearson's correlation between synovial fluid NE concentrations and FA values of PVN in patients with KOA (n = 11 patients with KOA). (B) Pearson's correlation between synovial fluid NE concentrations and ALFF values of PVN in patients with KOA (n = 11 patients with KOA). (C) Pearson's correlation between synovial fluid NE concentrations and WOMAC scores in patients with KOA (n = 11 patients with KOA). (D) Representative images of vehicle-treated (left) or 6-OHDA-treated (right) joint after intra-articular injection. (red: TH-sympathetic nerve fibres, and blue: nuclear staining). Scale bar: 200 μm. (E-H) Representative images of general view, S.O. and immunofluorescence (PRG4, ACAN and COL2A1) staining following the deletion of sympathetic nerves in microfracture surgery-induced focal articular cartilage defect mouse model. The surgical site is indicated by the red circle, while the rectangular dashed line demarcates the specific location of the defect following microfracture surgery. Scale bar: 200 μm (E). The graphs represent quantification of PRG4 (F), ACAN (G) and COL2A1 (H) expression in the cartilage tissue at the microfracture surgical defect site (Microfracture + vehicle, n = 8; Microfracture + 6-OHDA, n = 9). (I) Quantification of the elastic modulus of the regenerated tissue using AFM was conducted at 6 weeks post sham surgery and after microfracture surgery, both with and without the deletion of synovial sympathetic nerves (n = 6 mice each group). (J-N) Representative images of S.O. and immunofluorescence (PRG4, ACAN and COL2A1) staining following the deletion of synovial sympathetic nerves in DMM surgery-induced KOA mouse model. The dotted lines demarcate the boundary of the articular cartilage surface. Scale bar: 200 μm for S.O. staining and 100 μm for immunofluorescence images (J). OARSI scoring of S.O. stained sections (K). Quantification of PRG4 (L), ACAN (M) and COL2A1 (N) expression in

Notably, the synovial fluid NE concentration correlated positively with the FA values (Pearson's $r = 0.85$; $P = .009$), ALFF values (Pearson's $r = 0.77$; $P = .0055$) of PVN and WOMAC scores (Pearson's $r = 0.80$; $P = .0034$) of these patients with KOA (Fig 3A-C). These findings suggest that elevated synovial fluid NE concentration is associated with increased FA, ALFF values in the PVN, and clinical severity in patients with KOA.

Articular sympathetic denervation drives functional cartilage regeneration

To establish an articular sympathetic denervation model, we specifically ablated the local sympathetic innervation in mice through intra-articular injection of 6-OHDA. Our data showed that the ablation effectively eliminated tyrosine hydroxylase (TH)-positive sympathetic fibres in the joint, as confirmed by whole-articulation anti-TH immunolabeling (Fig 3D; Supplementary Fig S10A), and significantly reduced NE concentrations in joint homogenates (Supplementary Fig S10B). We then investigated the role of sympathetic nerves in cartilage regeneration using 2 mouse models: a microfracture model and a DMM model.

Our results revealed that deletion of synovial sympathetic nerves in the microfracture model promotes the formation of stable and mature articular cartilage (Fig 3E,F; Supplementary Fig S10C,D), enhancing cartilage anabolism (Fig 3G,H), and elastic modulus (Fig 3I), inhibiting fibrocartilage formation and cartilage catabolism (Supplementary Fig S10E-G). Similarly, in the DMM mouse model, the deletion of synovial sympathetic nerves effectively reduced structural damage (Fig 3J,K), increasing the expression of PRG4, ACAN, and COL2A1 (Fig 3L-O), decreasing the expression of COL1A1 and MMP13 (Supplementary Fig S10H-J), along with reductions in pain associated with OA (Supplementary Fig S10K-N).

NE intrinsically inhibits the regeneration of articular cartilage via the ADRB2 signalling in PRG4$^+$ cells

To investigate how sympathetic nerve inhibits the regeneration of articular cartilage, we performed single-cell RNA sequencing (scRNA-seq) on cartilage tissue from mice following microfracture surgery, with or without 6-OHDA treatment for local sympathetic ablation (Supplementary Fig S11A). Our results showed an increased expression of *Prg4, Acan*, and *Col2a1*, while decreased expression of *Col1a1* in 6-OHDA-treated cartilage tissue compared to controls (Fig 4A,B; Supplementary Figures S11B-D). Notably, the 6-OHDA-treated cartilage tissue showed intense labelling for chondroprogenitor markers *Prg4* (Fig 4A,B), consistent with their established role in cartilage repair [42]. These findings led us to hypothesise that sympathetic signalling suppresses cartilage regeneration by modulating the activity of PRG4$^+$ cells.

We profiled the mRNA expression of all 9 NE receptor subtypes to systematically identify which predominantly mediates its regulatory effects on cartilage regeneration, and observed *ADRB2* to be the most highly expressed in both mouse (Fig 4C) and human articular chondrocytes (Supplementary Fig S11E). Furthermore, our analysis of immunostaining in relatively intact nonweight-bearing explants of human KOA articular cartilage revealed that 42.4% of PRG4$^+$ cells express ADRB2 (Supplementary Fig S11F,G). This finding was corroborated by scRNA-seq data, which revealed a high percentage of coexpression between *hPRG4* and *hADRB2* in human knee articular cartilage (Fig 4D), but little coexpression between *hPRG4* and *hADRB1* (Supplementary Fig S11H), and no coexpression in other receptors (data not shown). These results suggest that ADRB2 may play a pivotal role in articular cartilage regeneration via regulation of PRG4$^+$ cells.

To investigate whether ADRB2 in PRG4$^+$ cells directly regulates articular cartilage regeneration, we subsequently employed both genetic and pharmacological approaches. First, we used the conditional knockout of *Adrb2* in *Prg4*$^+$ cells (*Adrb2*^{Prg4}) in the microfracture and DMM mouse models. We observed a significantly increase in cartilage proteoglycan content (Fig 4E,J,K; Supplementary Fig S12B), elevated expression of PRG4, ACAN, and COL2A1 (Fig 4F-H,L-N), increase in elastic modulus of the cartilage (Fig 4I), and decrease in COL1A1 and MMP13 expression (Supplementary Fig S12C,D,F-H) in *Adrb2*^{Prg4} mice compared to *Adrb2*$^{f/f}$ controls, for both models of cartilage defect. These results indicate that knocking out *Adrb2* in *Prg4*$^+$ cells enhances stable formation of mature articular cartilage instead of fibrocartilage formation (Fig 4O). Moreover, the conditional knockout of *Adrb2* in PRG4$^+$ cells was also able to suppress both microfracture and DMM-induced pain (Supplementary Fig S12I-L).

Next, we explored whether ICI-118551, a highly selective inverse agonist for ADRB2, could induce articular cartilage regeneration in our microfracture and DMM mouse models. Consistent with the aforementioned findings, intra-articular injection of ICI-118551 promoted the formation of stable and mature articular cartilage by increasing the PRG4$^+$ cell population, enhancing cartilage anabolism and elastic modulus, and suppressing cartilage catabolism (Supplementary Fig S13A-I; Supplementary Fig S14A-G), while also alleviating joint pain (Supplementary Fig S13J,K; Supplementary Fig S14H,I).

Furthermore, we assessed the proliferation of primary chondroprogenitor cells (with high PRG4 expression) with NE or ICI-118551 treatment (Supplementary Fig S15A). Our data showed that NE suppressed primary chondroprogenitor cell proliferation in a concentration-dependent manner, whereas ICI-118551 promoted their proliferation in a concentration-dependent manner (Supplementary Fig S15B).

Inhibition of ADRB2 protects against PVN^{CRH} neuron-induced articular cartilage degeneration

We next aimed to determine if intra-articular administration of ICI-118551 concurrently with PVN$^{CRH:\ activation}$ (PVN$^{CRH:\ activation}$ + ICI-118551) is able to rescue the PVN^{CRH} neuron-induced articular cartilage degeneration in our noninjured joint mouse model. Our data showed that ICI-118551 started to have beneficial effects at 6 weeks, and a striking protective effect at

the cartilage tissue (sham + vehicle, n = 8; DMM + vehicle, n = 9; DMM + 6-OHDA, n = 9). (O) Working model showing the deletion of synovial sympathetic nerves promotes cartilage regeneration. Data information: Pearson's correlation coefficient assay (A-C). Comparisons between groups were analysed using Student's unpaired *t* test (F-H), or a 1-way ANOVA with Tukey's multiple-comparisons test [(I) and (K-N)]. All data are represented as mean ± SD. ***$P < .001$. ACAN, aggrecan; AFM, atomic force microscopy; ALFF, amplitude of low-frequency fluctuation; ANOVA, analysis of variance; COL2A1, collagen type II alpha 1 chain; DAPI, 4',6-diamidino-2-phenylindole; DMM, destabilisation of the medial meniscus; FA, fractional anisotropy; KOA, knee osteoarthritis; NE, norepinephrine; OARSI, Osteoarthritis Research Society International; PRG4, proteoglycan 4; PVN, paraventricular nucleus; 6-OHDA, 6-hydroxydopamine; S.O., safranin o/fast green; WOMAC, Western Ontario and McMaster Universities Arthritis Index.

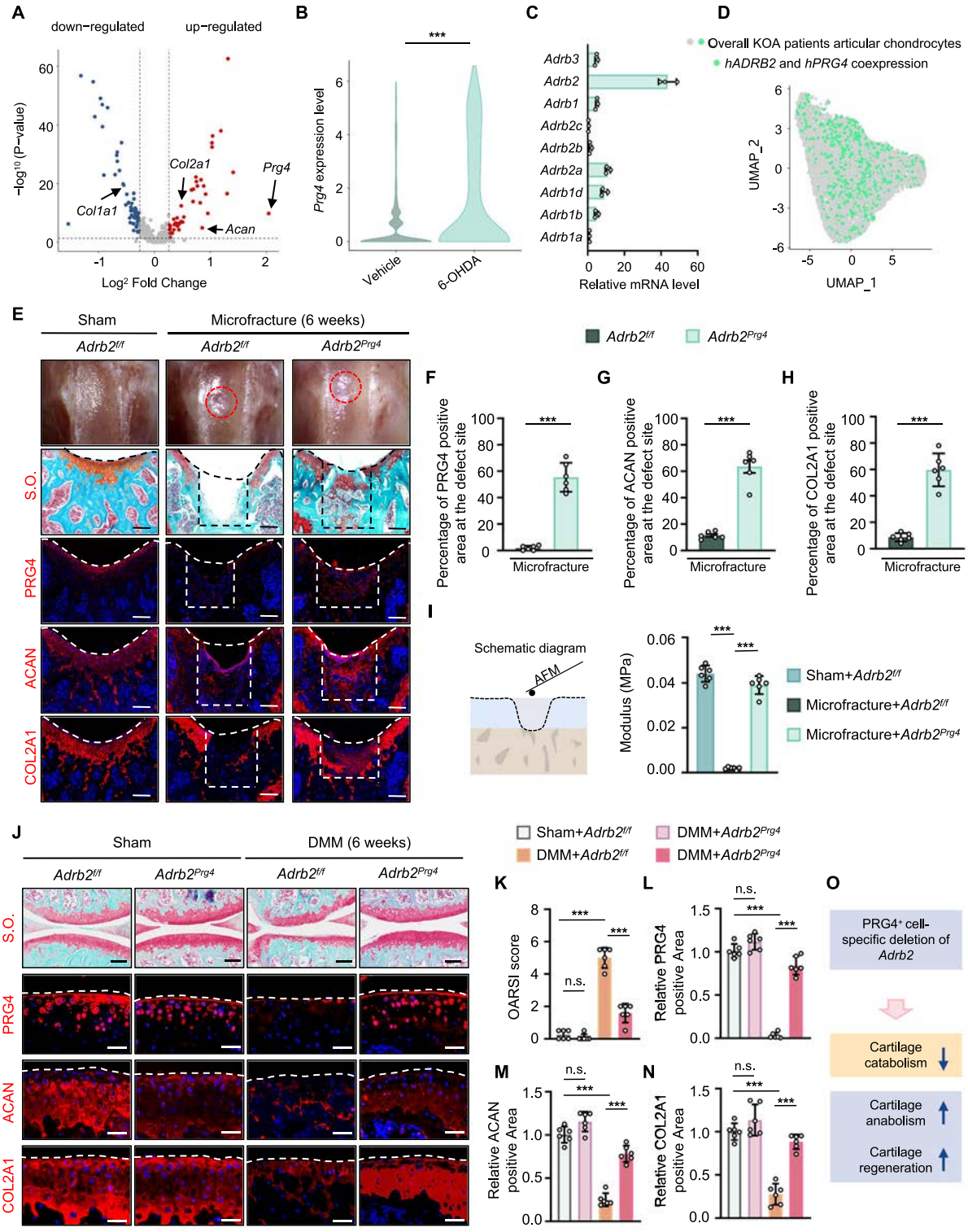

Figure 4. Conditional knockout of *Adrb2* in *Prg4*$^+$ cells regulates the cartilage regeneration. (A, B) Volcano plot showing differentially expressed genes between groups with and without synovial sympathetic nerve deletion induced by 6-OHDA administration in the microfracture model. Red: upregulated (eg, *Prg4, Acan* and *col2a1*); blue: downregulated (eg, *Col1a1*) (A). Quantification of *Prg4* expression at the defect site in mice with or without 6-OHDA-mediated sympathetic ablation (B). (C) qRT-PCR analyses of all 9 NE receptor expression in mouse articular chondrocytes (n = 3 mice). (D) The coexpression of *hPRG4* and *hADRB2* in human chondrocytes was analysed using scRNA-seq data GSE152805. (E-H) Representative images of general view, S.O. and immunofluorescence (PRG4, ACAN and COL2A1) staining following conditional knockout of *Adrb2* in *Prg4*$^+$ cells in the microfracture mouse model. The surgical site is indicated by the red circle, while the rectangular dashed line demarcates the specific location of the defect in the microfracture surgery. Scale bar: 200 μm (E). Quantification of PRG4 (F), ACAN (G) and COL2A1 (H) expression in the cartilage tissue at the microfracture surgical defect site (n = 6 mice each group). (I) Quantification for the elastic modulus of the regenerate using AFM at 6 weeks post sham, and microfracture surgery with or without conditional knockout of *Adrb2* in *Prg4*$^+$ cells (n = 6 mice each group). (J-N) Representative images of S.O. and immunofluorescence (PRG4, ACAN and COL2A1) staining following conditional knockout of *Adrb2* in *Prg4*$^+$ cells in the DMM mouse model. The dotted lines demarcate the boundary of the articular cartilage surface. Scale bar: 200 μm for S.O. and 100 μm for immunofluorescence staining (J). OARSI scoring of S.O. stained sections (K). Quantification of PRG4 (L), ACAN (M) and COL2A1 (N) expression in the cartilage tissue (n = 6 mice each group). (O) Working model illustrating the regulatory role of *Prg4*$^+$ cell-conditional deletion of Adrb2 in cartilage regeneration. Data information: Comparisons between groups were analysed using a Student's unpaired *t* test (B and [F-H]), or a 1-way ANOVA with Tukey's multiple-

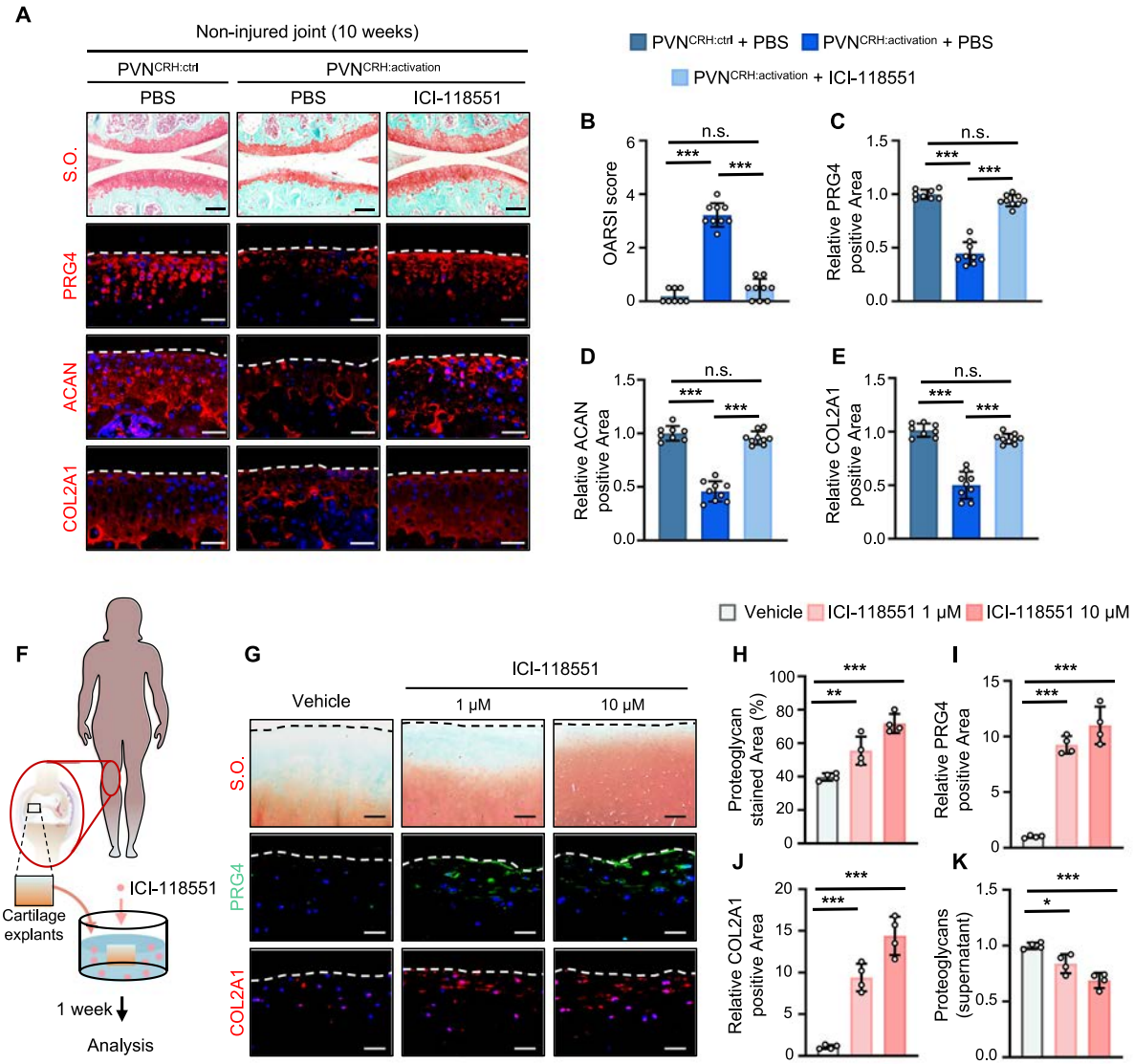

Figure 5. ADRB2 inverse agonist effectively suppresses cartilage degeneration. (A-E) Representative images of S.O. and immunofluorescence (PRG4, ACAN and COL2A1) staining were obtained following the activation of PVN^{CRH} neurons, concurrent with intra-articular injection of ICI-118551 for 10 weeks in mice with noninjured joint. The dotted lines demarcate the boundary of the articular cartilage surface. Scale bars: 200 μm for S.O. staining and 100 μm for immunofluorescence staining (A). OARSI scoring of S.O. stained sections (B). Quantification of PRG4 (C), ACAN (D) and COL2A1 (E) expression in the cartilage tissue ($PVN^{CRH:\ ctrl}$ + PBS, n = 8; $PVN^{CRH:\ activation}$ + PBS, n = 9; $PVN^{CRH:\ activation}$ + ICI-118551, n = 9). (F-K) Relatively intact nonweight-bearing explants of human cartilage were isolated from patients with KOA undergoing total knee replacement (F). S.O. and immunofluorescence staining for PRG4 (green) and COL2A1 (red) of cartilage explants of patient with KOA after 1 week of treatment with ICI-118551 at indicated dosage or vehicle. Scale bars: 200 μm for S.O. and 50 μm for immunofluorescence staining (G). Proteoglycan area (%) from the explants was measured from the S.O. staining (H). Quantification of PRG4 (I) and COL2A1 (J) expression in cartilage tissue. Release of total glycosaminoglycan (GAG) into the media of human articular cartilage explants was measured using the 1,9-dimethylmethylene blue (DMMB) assay. The secreted GAG concentration was normalised to the wet weight of the cartilage explants, and then to the vehicle (K) (n = 4 humans in each group). Data information: comparisons between groups were analysed using a 1-way ANOVA with Tukey's multiple-comparisons test ([B-E] and [H-K]). All data are represented as mean ± SD. *P < .05, **P < .01, ***P < .001. ACAN, aggrecan; ADRB2, articular cartilage via the β2-adrenergic receptor; ANOVA, analysis of variance; COL2A1, collagen type II alpha 1 chain; CRH, corticotropin-releasing hormone; KOA, knee osteoarthritis; n.s., not significant; OARSI, Osteoarthritis Research Society International; PBS, phosphate buffer saline; PRG4, proteoglycan 4; PVN, paraventricular nucleus; S.O., safranin o/fast green.

10 weeks (Fig 5A-E; Supplementary Fig S16A-N), with cartilage parameters almost approaching levels similar to normal physiological state. These data suggest that inhibition of ADRB2 is sufficient to prevent cartilage degeneration caused by PVN^{CRH} neurons activation.

Systematic analysis of signalling pathway in articular cartilage regeneration

To uncover the underlying molecular mechanisms that play a role in the regeneration of articular cartilage following

comparisons test (I and [K-N]). All data are represented as mean ± SD. ***P < .001. ACAN, aggrecan; AFM, atomic force microscopy; ANOVA, analysis of variance; COL2A1, collagen type II alpha 1 chain; DMM, destabilisation of the medial meniscus; KOA, knee osteoarthritis; NE, norepinephrine; OARSI, Osteoarthritis Research Society International; n.s., not significant; PRG4, proteoglycan 4; S.O., safranin o/fast green; UMAP, uniform manifold approximation and projection; 6-OHDA, 6-hydroxydopamine.

inhibition of the NE/ADRB2 signalling pathways in PRG4$^+$ cells, we used integrated *in vivo* and *in vitro* approaches. Pathway analyses of our previously mentioned scRNA-seq data from microfracture surgery mice with or without 6-OHDA treatment (Supplementary Fig S11A) revealed significant enrichment of extracellular matrix (ECM)-receptor interaction, phosphatidylinositol 3-kinase-protein kinase B (PI3K-Akt) signalling, and transforming growth factor-β (TGF-β) signalling kyoto encyclopedia of genes and genomes (KEGG) pathways in *Prg4*$^+$ cells from the 6-OHDA-treated group compared to the vehicle controls (Supplementary Fig S17A). These signalling pathways are known critical early events of cartilage degeneration, regeneration, and homeostasis maintenance [43,44].

Subsequently, we performed RNA-seq analysis on the primary chondroprogenitor cells (with high PRG4 expression) following NE exposure. Our data revealed significant enrichment of the including TNF, PI3K-Akt, Hippo, and ECM-receptor interaction signalling pathways (Supplementary Fig S17B). Cross-comparison of *in vivo* and *in vitro* KEGG results converged on PI3K-Akt, ECM-receptor interaction, and TGF-β signalling pathways. Critically, gene set enrichment analysis (GSEA) confirmed that 6-OHDA treatment suppressed PI3K-Akt signalling pathways (Supplementary Fig S17C) while NE treatment activated it (Supplementary Fig S17D). To further validate these findings, we analysed PI3K-Akt signalling in primary chondroprogenitor cells stimulated with NE or ICI-118551 (Supplementary Fig S17E). Our results showed that NE induced phosphorylation of PI3K and AKT, while this phosphorylation was abolished by treatment with ICI-118551 (Supplementary Fig S17F-H), providing a mechanistic basis for its role in cartilage regeneration.

Inhibition of ADRB2 prevented cartilage degradation in human articular cartilage explants

Finally, we explored the potential of targeting ADRB2 in the regeneration of human articular cartilage. We cultured relatively intact nonweight-bearing explants of human KOA articular cartilage in the presence of ICI-118551 for 1 week and assessed cartilage regeneration-related parameters (Fig 5F). We observed a dose-dependent increase in the percentage area of proteoglycans, as determined by safranin O/Fast Green (S.O.) staining (Fig 5G,H), an increase in PRG4 and COL2A1 expression (Fig 5I,J), and a dose-dependent decrease in glycosaminoglycan release (Fig 5K). Together, these results indicate that inhibition of ADRB2 prevented cartilage degradation in human articular cartilage explants, and they highlight the therapeutic potential of targeting ADRB2 in OA.

DISCUSSION

The limited regenerative capacity of humans and mammals has significantly impeded our ability to cure various diseases [2,3]. Our data, utilising articular cartilage as a paradigm to comprehend tissue regeneration, presented above support the conclusion that when the brain detects damage in peripheral tissue or organs, specific brain regions exhibit changes in activity, resulting in a reduced or even complete loss of tissue regeneration ability.

The role of anxiety and depression as potential risk factors for the development of OA has been well-established [45–47]. PVN neurons, especially PVN^{CRH} neurons, play a crucial role in regulating anxiety and depression [31–33]. In our study, we demonstrated that the activation of PVN^{CRH} neurons could cause the degeneration of normal articular cartilage. In terms of clinical significance, we implemented a therapeutic approach involving intra-articular injections of ADRB2 inverse agonist, which represents a local and minimally invasive approach, which effectively inhibits cartilage degeneration caused by the activation of PVN^{CRH} neurons. Furthermore, treatment with an ADRB2 inverse agonist prevented cartilage degradation in human articular cartilage explants. Therefore, our findings might suggest potential neural mechanisms that underlie the aggravation of OA development associated with anxiety and depression, and identify a promising therapeutic target for interventions in patients with both OA and anxiety/depression comorbidity.

Our findings demonstrate that the deletion of synovial sympathetic nerves enhances the regeneration of articular cartilage by inhibiting the NE/ADRB2-mediated pathway in PRG4$^+$ cells. This observation is consistent with previous studies that sympathetic nervous terminals cause a decline in melanocyte stem cells through NE/ADRB2 signalling [37]. Additionally, the administration of the ADRB2 agonist significantly accelerates cartilage degradation [48] and hinders chondrocyte differentiation by modulating ERK1/2 and PKA signalling [49]. The activation of NE/ADRB2 signalling has been linked to detrimental effects on the maintenance of stem cell homeostasis [50] and ADRA2 antagonist promotes chondrogenesis in human pluripotent stem cells [51]. Nonetheless, the neural circuit responsible for upstream NE release remains unclear. Our study sheds light on the crucial role of the PVN^{CRH} neurons-synovial sympathetic nerves as an upstream regulator of NE release, thereby suppressing the regeneration of cartilage tissue, indicating a novel paradigm in which the central nervous system can modulate tissue stem cells to regulate peripheral tissue regeneration. Interactions between the sympathetic nerves and the immune system have recently emerged as critical regulators of inflammation [21,52]. It is plausible that sympathetic nerves may also impair tissue regeneration via immunomodulatory mechanisms, which warrants further study.

Pain is a dominant clinical symptom of OA and typically presents alongside significant articular cartilage loss [53]. In our study, we demonstrated that the inhibition of PVN neurons could alleviate joint pain of injured joint mouse model. However, short-term activation or inhibition of these neurons did not alter pain sensitivity in noninjured mice. This finding is consistent with previous reports indicating that modulating PVN^{CRH} neuronal activity (eg, with propofol) does not affect mechanical hypersensitivity [54]. These data suggest that the pain modulation observed in our OA models is secondary to the level of cartilage damage, rather than a direct effect of PVN activity on pain perception.

The development of strategies to enable organ regeneration has been a topic of great interest recently. To the best of our knowledge, our study is the first to provide proof-of-concept findings that the brain-cartilage neural circuitry axis can regulate cartilage regeneration. This finding may lead to the development of alternative interventions for promoting tissue regeneration in the future. Specifically, existing brain stimulation technologies including transcranial magnetic stimulation [55], focused ultrasound [56] or deep brain stimulation [57] could be utilised. It is important to note that the implications of our study extend beyond cartilage regeneration, as the role of the brain in regenerating other tissues warrants further investigation, particularly in relation to other diseases.

METHODS

Human participants

This study employed a case-control design and included patients who underwent unicompartmental knee arthroplasty at Shanghai Sixth People's Hospital, Shanghai JiaoTong University School of Medicine, as the case group. The inclusion criteria for the case group were as follows: patients aged between 50 and 70 years with KOA, meeting the diagnostic criteria for KOA set by the American College of Rheumatology in 1995, having Kellgren-Lawrence classification system grade 3 with focal articular cartilage defect, well-functioning ligaments, no significant deformities, no severe chronic pain unrelated to the joints, and no severe knee osteophyte formation. The control group consisted of age- and sex-matched healthy individuals selected from the Physical Examination Center at Yangzhi Rehabilitation Hospital (Shanghai Sunshine Rehabilitation Center), Tongji University School of Medicine. The inclusion criteria for the control group were age between 50 and 70 years, and no diagnosis of KOA. All participants were required to demonstrate willingness and ability to provide informed consent, met the safety criteria for MRI, had no history of psychiatric disorders or psychiatric drug treatment, were not pregnant or breastfeeding, had no severe systemic diseases, and maintained a body mass index not exceeding 30 kg/m^2. This study received approval from the Ethics Committee of Yangzhi Rehabilitation Hospital (Shanghai Sunshine Rehabilitation Center), Tongji University School of Medicine (No. 2022-022) and was registered with the Chinese Clinical Trial Registry (ChiCTR2200065730). Ultimately, the study included 11 patients with KOA (mean age, 59.5 years) and 11 healthy controls (mean age, 59.7 years) (Supplementary Table S2 for details).

WOMAC questionnaire

The WOMAC score is a widely used questionnaire to assess symptoms and functional limitations related to knee and hip OA. It aims to evaluate pain, stiffness, and physical functioning in patients with OA. The WOMAC questionnaire consists of a series of questions related to daily activities and mobility, such as walking, climbing stairs, getting up, and sitting down, where higher scores indicate greater levels of pain, stiffness, and functional impairment.

MRI data acquisition and analysis

MRI data were acquired using 3 Tesla MRI scanner (Ingenia Elition, Philips Healthcare) equipped with a 32-channel head coil at the Department of Radiology in Shanghai Sixth People's Hospital Shanghai JiaoTong University School of Medicine. The MRI protocol included a 3D structural T1-weighted scan, DTI, and rs-fMRI. 3D T1-weighted structure images scan parameters: repetition time (TR) 2500 milliseconds, echo time (TE) 2.2 milliseconds, field of view (FOV) of 200 × 210 mm, matrix size 252 × 262, slice thickness 1.6 mm, slice gap 0.8 mm and 162 transversal slices. This session lasted for about 4 minutes. DTI scan parameters: 62 axial slices, TR 3397 milliseconds, TE 72 milliseconds, B = 0, 1000 s/mm^2, FOV 200 × 229 × 143 mm, diffusion directions 128, slice thickness 2.3 mm. This session lasted for about 7 minutes 28 seconds. rs-fMRI were acquired with an single-shot FE_EPI_RS sequence, TR 2000 milliseconds, TE 35 milliseconds, flip angle 90°, FOV 230 × 230 mm, slice thickness 3 mm, acquisition matrix 76 × 76; voxel size 3 × 3 × 3 mm, multiband acceleration factor 2, slice orientation transverse, number of slices 48, total acquisition time: 6 minutes 52 seconds.

DTI data processing

A reliable tractography software DSI-Studio (http://dsi-studio.labsolver.org) was used for data processing. Diffusion data processing procedures included: (i) image quality control, elimination of images with incomplete scan area or unclear imaging. (ii) Correction for susceptibility-induced distortions, reduction of eddy currents and head motion. (iii) Confirmation of mask coverage on white matter. (iv) Use of Q-space diffeomorphic reconstruction to reconstruct the quantitative anisotropy map with diffusion fibre length ratio at 1.25, and (v) calculation of the FA tensor eigenvalue map. The different anatomical regions of interest (ROIs) were manually delineated. The ROI for the PVN was defined manually based on coordinates in the Montreal Neurological Institute space [58]. The other 4 ROIs (Amygdala, ACC, hippocampus and DLPFC) were derived from their corresponding regions in the Automated Anatomical Labeling 2 atlas [59] (Supplementary Table S3 for details). Subsequently, the DTI-FA values for these regions were calculated utilising the region statistics module within DSI-Studio.

rs-fMRI processing

The rs-fMRI data were preprocessed using RESTplus v1.27 (http://www.restfmri.net/forum/restplus). This included: (i) Removal of the first 10 time points: to allow the longitudinal magnetisation to reach a steady state and to allow the participant to adapt to the scanning environment. (ii) Slice timing correction: to correct for differences in image acquisition time between slices. (iii) Head motion correction: the functional time series were realigned to the initial image for motion correction. Participants with maximum translation greater than 3 mm or rotation greater than 3° were excluded. (iv) The data were then coregistered to the T1 structural images, segmented, and normalised to the deformation field imaging template. (v) Spatial smoothing: spatial smoothing with an isotropic Gaussian kernel with a full width at half maximum of 6 mm. (vi) Removal of the linear trend of the time course to reduce the influence of the MRI equipment. (vii) Nuisance signal regressors include Friston-24 motion parameters, cerebrospinal fluid, white matter.

The ALFF was calculated using the fast Fourier transform, with the time series of each voxel transformed to the frequency band without band-pass filtering. The square root was initially calculated at each frequency of the power spectrum, and subsequently, the mean square root was obtained within the range of 0.01 to 0.08 Hz. All individual ALFF maps were computed and standardised into ALFF *Z*-values.

UKB data acquisition and analysis

Our study utilised data from the UKB (https://www.ukbiobank.ac.uk/), a large-scale prospective cohort study. The UKB protocol received ethical approval from the North West Multicentre Research Ethics Committee (reference number: 16/NW/0274), and all participants provided written informed consent. Our analysis was conducted under UKB application number (102056).

Dual-energy X-ray absorptiometry and radiographic OA grading were used to assess the severity of KOA during participants' visits to the UKB assessment center [60] (Field ID 20321). To obtain neuroimaging data, we utilised the UKB's large-scale imaging enhancement study, which began in 2014 to reinvite

participants for multimodal MRI, including brain scans [61]. From the total UKB cohort, we identified 32,185 participants who had both KOA grades and multiband diffusion MRI data (Field ID 20218).

Based on their KOA grades, these participants were categorised into 3 groups: a healthy group (score 0), a mild KOA group (score 1-2), and a severe KOA group (score 3-4). A random sample of 50 participants was then selected from each group for subsequent analysis. The mean age (and range) was 59.5 years (47-74) for the Healthy group, 60.7 years (48-74) for the mild KOA group, and 62.8 years (49-74) for the severe KOA group, resulting in an overall mean age of 61 years (range 47-74) for the final cohort of 150 participants (Supplementary Table S4 for details). Finally, multiband diffusion MRI data from these 150 participants were processed using the pipeline described in the 'DTI data processing' section to derive FA values for the ROIs.

Animals

The mice and rats were housed under a standardised 12-hour light-dark cycle and had unrestricted access to food and water, unless specified otherwise. Experimental procedures commenced when the mice reached 12 weeks and the rats reached 8 weeks of age, unless specifically stated otherwise. All animal experiments were randomised into different experimental groups and all data were double blinded for recording and analysis, and conducted in accordance with the guidelines of the Ethics Committees at Tongji University and East China Normal University.

C57BL/6J WT mice and Sprague Dawley WT rats were sourced from GemPharmatech Co., Ltd. CRH-IRES-Cre (simplified as CRH-Cre in figures, Jax 012704) C57BL/6J mice were kindly provided by Dr. Huatai Xu (Lin Gang Laboratory), while *Aggrecan*-CreERT2 (simplified as Acan-CreERT2 in figures, Jax 019148) C57BL/6J mice were generously donated by Dr. Jianquan Chen (Soochow University). *Prg4*-GFPCreERT2 (simplified as Prg4-CreERT2 in figures, Jax 022757) C57BL/6J mice from the Jackson Laboratory. *Adrb2*$^{fl/fl}$ C57BL/6J mice were generated by GemPharmatech Co., Ltd (No. TO52308). To produce Prg4-creERT2; *Adrb2*$^{fl/fl}$ (*Adrb2*^{Prg4}) mice, *Adrb2*$^{fl/fl}$ mice were crossed with the Prg4-creERT2 mice.

PRV retrograde tracing from the joint

For retrograde trans-synaptic tracing from the joint, mice were consistently anesthetised with 1.5% to 2.0% isoflurane in oxygen (RWD) and were subsequently positioned on a heated pad to maintain normothermia. A surgical incision was made on the external skin overlying the joint, and a single injection site was established within the articular cavity at a depth of 1 to 2 mm using a glass micropipette. At each injection site, PRV (PRV-CAG-EGFP, 7.0×10^9 vg/mL, 2 μL, Brain Case) was injected using a 10-μL syringe. Following each injection, the glass micropipette was maintained in position for 3 minutes to prevent backflow, then slowly withdrawn over 30 seconds. The brain, spinal cord, and joint were collected at 48 or 96 hours post-PRV-EGFP injection. Prior to collection, the mice were perfused with phosphate buffer saline (PBS), followed by 4% paraformaldehyde (PFA) for subsequent processing. Coronal brain and spinal cord slices (40 μm thickness) and joint slices (15 μm) were prepared using a cryostat microtome. Sections containing the PVN were subsequently counterstained with antibodies specific to CRH for immunolabeling analysis.

Analogously, rats were anesthetised with 2.0% isoflurane in oxygen and underwent intra-articular injection of PRV-CAG-mRFP (7.0×10^9 vg/mL, 3 μL, Brain Case), with brain tissue harvested 96 hours postinjection for sectioning and validation of viral trans-synaptic tracing.

Stereotaxic injection

We followed a previously described procedure [23]. Mice were anesthetised under isoflurane and securely positioned on a stereotaxic apparatus (RWD) to position the skull in parallel to the reference panel. A small incision was made with a scalpel along the midline of the head to expose the skull. A craniotomy was drilled into the skull surface of the target area by a dental drill. Virus was injected bilaterally into the target area using a glass micropipette with a 15 μm tip diameter, connected to a 10 μL syringe (Hamilton). A microinfusion pump (LEGATO 130, kdScientific) was used to control the speed and volume of the injection. The following coordinates for PVN were: anteroposterior (AP), −0.70 mm from bregma; mediolateral (ML), ±0.20 mm; dorsoventral (DV), −4.72 mm. After a 10-minute delay following the completion of the injection, the glass micropipette was slowly withdrawn, and the scalp was sutured closed. The procedure for stereotaxic injection in rats was analogous to that of mice; the following coordinates for PVN were: AP, −1.50 mm from bregma; ML, ±0.40 mm; DV, −7.7 mm. Following surgery, both mice and rats were allowed to recover in their home cages under close monitoring.

Recording of synovial nerves activity during optogenetic stimulation of PVN^{CRH} neurons

For specifically optogenetic stimulation of PVN^{CRH} neurons, groups of CRH-Cre male mice were stereotactically injected with AAV2/9-hSyn-DIO-hChR2 (H134R)-P2A-EGFP-WPRE-hGH polyA (AAV-hSyn-DIO-ChR2-EGFP, 4.7×10^{12} vg/mL, 100 nL, Brain Case) or AAV2/9-hSyn-DIO-EGFP-WPRE-hGH polyA (AAV-hSyn-DIO-EGFP, 6.55×10^{12} vg/mL, 100 nL, Brain Case) into the PVN regions. Fibre implantation was offset relative to the viral injection sites (AP, −0.70 mm from bregma; ML, +0.20 mm; DV, −4.5 mm).

After achieving stable virus expression for 2 weeks, the mice were anesthetised, and the synovium was exposed. We then implanted one custom-made tungsten electrode (Kedou), with an impedance of 1.0 MΩ, into the synovium along the medial parapatellar incision and the electrode probe was in contact with the synovial nerve. The electrode probe was connected to a multichannel physiological recording and signal processing system (Chengdu Instrument Factory, RM6240). To activate PVN^{CRH} neurons expressing ChR2 during each experimental trial, a 465-nm laser light (RWD) was delivered as 2-millisecond pulses at 50 Hz for 200 milliseconds every second. The intensity of the laser light was calibrated with an optical power metre (Sanwa) to reach 10 mW at the end of the implanted fibre stub. To ensure data accuracy, our recording signals were sampled at 1000 Hz. For data analysis, all signals were digitally bandpass-filtered between 10 and 40 Hz to reduce noise [23–25]. Average firing rates during 60 s before and 60 s after optogenetic stimulation of PVN^{CRH} neurons were calculated and statistically analysed by paired t test.

Chemogenetic neuronal manipulation

For chemogenetic activation or inhibition of PVN neurons, groups of WT male mice were stereotactically injected with AAV2/9-hSyn-hM3Dq-EGFP-3flag-WPRE-hGH polyA (AAV-hSyn-hM3Dq-EGFP, 4.5×10^{12} vg/mL, 100 nL, Brain Case),

AAV2/9-hSyn-hM4Di-EGFP-3flag-WPRE-hGH polyA (AAV-hSyn-hM4Di-EGFP, 4.5×10^{12} vg/mL, 100 nL, Brain Case), or AAV2/9-hSyn-EGFP-WPRE-hGH polyA (AAV-hSyn-EGFP, 2.67×10^{12} vg/mL, 100 nL, Brain Case) into the PVN regions.

To specifically target PVN^{CRH} neurons for chemogenetic manipulation, groups of CRH-Cre male mice, respectively, were stereotactically injected with AAV2/9-hSyn-DIO-hM3Dq-EGFP-WPRE-hGH polyA (AAV-hSyn-DIO-hM3Dq-EGFP, 2.1×10^{12} vg/mL, 100 nL, Brain Case), AAV2/9-hSyn-DIO- hM4Di-EGFP-WPRE-hGH polyA (AAV-hSyn-DIO-hM4Di-EGFP, 2.3×10^{12} vg/mL, 100 nL, Brain Case), or AAV2/9-hSyn-DIO-EGFP-WPRE-hGH polyA (AAV-hSyn-DIO-EGFP, 6.25×10^{12} vg/mL, 100 nL, Brain Case) into the PVN regions.

To activate or inhibit the AAV-infected neurons, the mice were provided with drinking water supplemented with CNO to achieve an estimated daily intake of approximately 5 mg/kg of CNO, ensuring an average water consumption of 5 mL/d per mouse.

Surgical-related mouse model of cartilage pathology model

As described previously [62], cartilage wear was surgically induced in mice by DMM in the right joint. Mice aged 12 weeks were anesthetised with 1% pentobarbital (i.p. 100 mg/kg) for general anaesthesia. The skin and muscles of the joint were incised to expose the knee articular cavity. The medial meniscus was carefully dissociated medially using a surgical blade, and then it was returned to the articular cavity. In the sham-operated mice, only the skin and muscles were cut without damaging the medial meniscus. The muscle and skin were sutured, and the animals were placed in a 37°C environment until they fully recovered from surgery. At 6 weeks postoperatively, joint tissue was collected, fixed in 4% PFA overnight at 4°C, decalcified in 0.5 M EDTA for 14 days, embedded in paraffin, and then sectioned into 6 μm slices. The paraffin sections were stained with S.O. The OARSI grading system was used to evaluate cartilage damage by blinded observers [30].

For the microfracture surgery-induced focal articular cartilage defect mouse model, mice aged 12 weeks were used. After the mice were put under general anaesthesia, the skin and muscles of the joint surface were incised, and the patella and surrounding muscles were displaced laterally to expose the surface cartilage of the femur. The cartilage defect with a depth of 1 mm and a diameter of 0.45 mm was created in the centre of the femoral trochlea with a 26 G needle (polished to a flat head). The patella and surrounding muscles were then returned to its original position, and the wound was sutured. The control group underwent a sham operation with no cartilage defect. After the operation, the mice were kept in a 37 °C environment until they fully recovered from surgery from the surgery. At 6 weeks postoperatively, joint tissue was collected, fixed in 4% PFA overnight at 4°C, decalcified in 0.5 M EDTA for 14 days, embedded in paraffin, sectioned into 6 μm slices, and mounted on slides for histological and related analyses.

AFM

The mice were euthanised, and distal femurs were dissected 6 weeks after the microfracture surgery. The defect regions were bisected by a microtome blade. Half of the fresh tissue was cleaned with PBS for measuring further. We then fixed the tissue in place on a plate containing protease-free PBS using tissue glue and imaged using a Bruker Fast Scan Bio-AFM (Bruker Germany). The measurements were made with a precalibrated set of Nanotools 0.10 N/m 12 μm MLCT-O10 biosphere spherical probes (Bruker Germany). All variables were kept constant across each group. Data analysis was performed using the NanoScope Analysis 1.8 Software.

Sympathetic manipulation

Chemical sympathetic ablation was conducted through intra-articular injections of 10 mg/kg 6-OHDA (MedChemExpress), administered 3 days before cartilage defects surgery. Control mice or rats received intra-articular injections of PBS containing 0.4% ascorbic acid (MedChemExpress) as the vehicle for 6-OHDA. In addition, following both cartilage defects surgery, intra-articular injections of 10 mg/kg 6-OHDA or vehicle were administered every 2 weeks.

Adrenalectomy

In this study, adrenalectomy in mice or rats was performed according to standardised protocols described in previous literature [63]. $PVN^{CRH:\ ctrl}$, $PVN^{CRH:\ activation}$ mice or WT rats were anesthetised with 1% pentobarbital (i.p. 100 mg/kg) for general anaesthesia. The mice or rats were then positioned prone on the surgical table, and a dorsal incision was made extending from the first to the third lumbar vertebrae. The latissimus dorsi muscle was dissected and retracted to reveal the kidneys, thereby facilitating access to the adrenal glands. Subsequently, both adrenal glands were carefully excised. As a control, sham-operated rats underwent the same surgical procedure, including gripping of the adrenal glands, but without actual excision. All mice or rats were allowed a 7-day recovery period with close monitoring of their health status.

To assess whether activation of PVN^{CRH} neurons upregulates NE concentrations in joint via the adrenal glands, $PVN^{CRH:activation}$ mice were intraperitoneally injected with 1 mg/kg CNO. Joint tissues and blood were collected 1 hour postinjection, and NE concentration was measured using an enzyme-linked immunosorbent assay (ELISA) kit.

Measurement of NE concentrations by ELISA

To accurately assess the NE concentrations in synovial fluid, prior to collection from rat knee joints, the joints underwent injection with 40 μL of saline, followed by aspiration of the synovial fluid using an insulin syringe for collection. For the quantification of NE concentrations in rat subchondral bone, synovium, tendon, and whole mouse joints, tissues were immediately frozen in liquid nitrogen, pulverised into a fine powder, and weighed. Subsequently, the frozen joint powder was resuspended in a tissue extraction buffer (consisting of 0.01 N HCl, 0.15 mM EDTA, and 0.1% reduced L-glutathione) and neutralised with 1.0 M Tris at pH 8.0 (1/10 volume) before proceeding with the ELISA. We used commercial ELISA kits (Cloud-Clone) and followed the manufacturer's instructions to determine NE concentrations using a competitive enzyme immunoassay method.

Joint viral injection and fibre implantation

To dynamically track the *in vivo* fluctuations of NE concentrations within the extracellular milieu of cartilage cell membranes, adult male *Aggrecan*-creERT2 mice were used. To facilitate Cre-mediated expression of the GRAB_NE sensor (AAV2/9-CMV-DIO-NE2m-WPRE-hGH polyA, 2.20×10^{12} vg/mL, Brain Case)

in active chondrocytes, a daily intraperitoneal injection of 150 mg/kg Tamoxifen (Sigma) was administered for 5 consecutive days prior to viral delivery. The surface of joint was shaved and wiped with 75% ethanol 3 times and a small incision was made with a scalpel to expose the subcutaneous knee articular cavity. Subsequently, a precision microsyringe (Hamilton) was gently inserted into the knee articular cavity, and 2 μL of the viral vector carrying the GRAB_NE sensor was administered.

For targeted optogenetic stimulation of PVN^{CRH} neurons, the aforementioned mice also received stereotactic injections of either AAV2/9-mCrh-hChR2 (H134R)-EGFP (AAV-mCrh-hChR2-EGFP, 2×10^{12} vg/mL, 100 nL, Brain Case) or AAV2/9-mCrh-EGFP (AAV-mCrh-EGFP, 1×10^{13} vg/mL, 100 nL, Brain Case) into the PVN target region. Fibre implantation was offset relative to the viral injection sites (AP: −0.70 mm from bregma; ML: +0.20 mm; DV: −4.5 mm). Following a 2-week period to allow for stable virus expression, mice were consistently anesthetised with 1.5% isoflurane in oxygen (RWD) and were subsequently positioned on a heated pad to maintain normothermia. The knee joint was prepared as previously detailed, with a medial parapatellar incision made to access the articular cartilage within the knee articular cavity. Care was taken to avoid damaging underlying nerve and vascular supplies to the joint. Subsequently, a sleeve-connected conventional optic ferrule (RWD) was inserted into the articular cartilage surface along the medial parapatellar incision. To reduce variance across mice with fibres inserted into the synovium and ensure not free-floating, we wrapped the incision site and fibres with medical bandages. A light shielding tape was applied over the wrap to block ambient light. Fluorescence signals were acquired with a fibre photometric system equipped with a 470 nm excitation laser (RWD). The normalised change in fluorescence signal (ΔF/F) was calculated as (F-F0)/F0, where F0 is the average baseline fluorescent signal before EPS. ΔF/F values were plotted as an average trace bracketed by a shaded area indicating SEM.

Cartilage anatomy and single-cell sequencing

Deletion of synovial sympathetic nerves was achieved by intra-articular administration of 6-OHDA, followed by microfracture 3 days postinjection, with additional 6-OHDA injections every week to ensure complete sympathetic nerve depletion. Two weeks after microfracture, the surgical defect site was harvested using a surgical knife. For each experimental group, cartilage tissue was pooled from 25 mice. Samples were digested with 0.25% collagenase type II from *Clostridium histolyticum* in dulbecco's modified eagle medium (DMEM) at 37 °C overnight. Following enzymatic digestion, cells were pelleted by centrifugation, washed, filtered through a 50 μm cell strainer, and resuspended in 1 ml PBS. Single-cell suspensions were loaded onto a microfluidic chip (Singleron GEXSCOPE platform) to capture single cells and generate barcoded single-cell gel beads in emulsion (GEMs). Reverse transcription, cDNA amplification, and library construction were performed using the GEXSCOPE Single-Cell RNA Library Kit (Singleron Biotechnologies) following the manufacturer's protocol. Libraries were sequenced on an Illumina NovaSeq 6000 platform with 150-bp paired-end reads. Raw sequencing data were processed using the CeleScope pipeline (Singleron Biotechnologies) for demultiplexing, alignment to the mouse genome (GRCm39). Through annotation, we identified a total of 32,818 cells, including 6349 chondrocytes, 2056 monocytes/macrophages, 14,431 neutrophils, 452 endothelial cells, 5452 B cells, 642 NK/T cells, 3225 erythrocytes, and 211 stem cell-like cells.

Bioinformatics analysis

Published bulk RNA-seq and single-cell RNA-seq of knee articular cartilage were obtained from GEO (https://www.ncbi.nlm.nih.gov/gds/) with accession numbers GSE114007 and GSE152805. For bulk RNA-seq data GSE114007, samples from articular cartilage tissues of 20 patients with KOA were used for downstream analysis. Bulk RNA-seq data of GSE280035 induced primary chondrocytes were performed using Illumina system with 2 × 150 paired-end sequencing. Differentially expressed genes were identified using 'DESeq2' and 'limma' packages with criterion of $|\text{Log2(Fold change)}| \geq 1$ and adjusted P values <.05. clusterProfiler was used to perform GSEA.

As for the single-cell RNA-seq data, the 'Seurat4.0' package was applied to integrate different samples with canonical correlation analysis (CCA) (cross-dataset normalisation) method. Then, cells were filtered as criteria of nFeature_RNA > 200 and percent mt <5%. The data are further normalised using the 'SCTransform' method. 'uniform manifold approximation and projection (UMAP)' was used to display the cell distribution.

Cell isolation and cell culture

Primary chondrocytes isolated from newborn mice joint cartilage [62]. In a sterile environment, the knee cartilage tissue of newborn mice was extracted and cut into pieces. The chopped cartilage tissue was digested overnight with 0.1% collagen type II at 37 °C. The chondrocytes released from the matrix were then centrifuged at 800 g for 5 min and cultured in DMEM: F12 (Gibco) medium containing 10% foetal bovine serum (Gibco) in a 37 °C incubator containing 5% CO_2. The medium was replaced every 2 days.

Sulforhodamine B assay

The proliferation of chondrocytes was measured by sulforhodamine B (SRB) assay [64]. Primary chondrocytes of mice were obtained from newborn WT mice. NE or ICI-118551 was added in DMEM: F12 medium (Gibco). After 24 hours of culture, the cells were fixed with precooled trichloroacetic acid (TCA) solution (30%, W/V) at a final concentration of 10% and stained with SRB (0.4%, W/V) at room temperature. Subsequently, the cell-bound dye was dissolved in a tris-base alkaline solution (10 mM, pH = 10.5) and the absorbance read at a wavelength of 510 nm to assess the cell proliferation.

Immunofluorescence staining and immunohistochemistry staining

Immunofluorescence staining was carried out following standard protocol [62]. Briefly, antigen retrieval was performed using citrate buffer and the sections were blocked in 2% horse serum. The sections were stained using anti-COL2A1 (1:200, rabbit, Abcam, ab34712), anti-PRG4 (1:200, rabbit, Abcam, ab28484), anti-ACAN (1:200, rabbit, Proteintech, 13880-1-AP) and anti-TH (1:200, rabbit, Abcam, Ab137869) primary antibodies overnight at 4°C. Subsequently, the sections were washed and incubated in the corresponding secondary antibody for one hour at room temperature.

Immunohistochemistry staining was also performed according to the standard protocol [65]. Antigen retrieval was achieved using citrate buffer, and 3% hydrogen peroxide was used to reduce endogenous peroxidase activity. The sections were then permeabilised with 0.1% Triton X-100 and blocked in 2% horse serum. The sections were stained using anti-MMP13

(1:200, rabbit, Abcam, ab219620), anti-COL1A1 (1:200, rabbit, Abclonal, a1352) overnight primary antibodies at 4°C. Subsequently, the sections were washed and incubated in the corresponding secondary antibody for 1 hour at room temperature. Histological images were collected using the Olympus BX53 microscope and quantitated performed using ImageJ software.

For immunofluorescence staining of the brain tissue, mice were euthanised and perfused transcardially with saline, followed by 4% PFA. The dissected brains were fixed in 4% PFA and then stored in a 30% sucrose solution until sectioning. Coronal slices of 40 μm were obtained by cryostat microtome at −20°C. Similar to the previous staining procedures, sections were blocked with 2% horse serum and sections stained using anti-CRH (1:200, rabbit, Peninsula Laboratories Inc, T-4037), overnight at 4°C. Subsequently, the sections were washed and incubated in the corresponding secondary antibody for 1 hour at room temperature. Histological images were collected using the Olympus BX53 microscope and quantitation was performed using ImageJ software.

qRT-PCR

Total mRNA was extracted with Trizol (Takara). Reverse transcription reaction was performed using the reverse transcription kit (Yeasen, 11202ES). The relative expression level of genes was calculated relative to glyceraldehyde-3-phosphate dehydrogenase (GAPDH). All qRT-PCR primers are described in Supplementary Table S5.

Western blotting analysis

After treatment with NE or ICI-118551, cells were lysed using radio-immunoprecipitation assay (RIPA) buffer for protein extraction. Protein concentration was quantified using the bicinchoninic acid assay (Thermo Fisher Scientific). Following electrophoresis and transfer to nitrocellulose membranes (Beyotime), the membranes were blocked with 5% bovine serum albumin (Beyotime) for 3 hours and incubated overnight at 4 °C with specific antibodies: GAPDH antibody (Abmart), p-PI3K (Tyr467/199) antibody (Abmart), PI3K antibody (Abmart), p-AKT (Ser473) antibody (Abmart), and AKT antibody (Abmart). After washing, membranes were incubated with horseradish peroxidase-conjugated secondary antibodies. Images were acquired using the Western Blot Imager (qTouch, RWD), and band intensity was quantified with Image-Pro Plus 6.0 software. All readings were normalised to GAPDH, and fold changes were calculated by normalising p-AKT to total AKT and p-PI3K to total PI3K.

Collection and preparation of human articular cartilage explants

Human articular cartilage explants were collected from patients with OA who were undergoing total knee replacement surgery, with approval from the Human Ethics Committee of Shanghai Sixth People's Hospital (Approval no. 2021-048). The joints were thoroughly washed with saline to remove excess blood and lipids. We selected explants with a relatively intact cartilage structure, carefully removing the cartilage from the joint while avoiding the subchondral bone. The explants were then cut into 3 mm × 3 mm sizes. Next, the explants were placed in 24-well plates and incubated in serum-free DMEM: F12 medium (Gibco) for 24 hours. Afterwards, the medium was replaced with 10% serum DMEM: F12 medium (Gibco) and cultured for 7 days. ICI-118551, at concentrations of 0, 1, or 10 μM, was added, and the medium was changed every 2 days. The supernatant was collected and mixed with 1,9-dimethylmethylene blue solution, and the release of glycosaminoglycans from the explants was detected at a wavelength of 535 nm. Additionally, the explants were fixed with 4% PFA and embedded in paraffin. After sectioning, histological analysis was performed using S.O. staining or immunofluorescence staining.

Statistical analysis

Statistical analyses were performed using GraphPad Prism (version 9.0), and data are expressed as mean ± SD unless otherwise indicated. For statistical comparisons, Student's t test (between 2 groups) or 1-way analysis of variance (ANOVA) (between multiple groups) with Tukey's analysis was used to compare normally distributed variables. Statistical significance was considered when $P < .05$ and is indicated as follows in the figures: $^{*}P < .05$, $^{**}P < .01$ and $^{***}P < .001$.

Competing interests

The authors declare no competing financial interests.

Contributors

JL designed the experiments and supervised the research. KH, XM, YX, LZ, FW, GW, YY, WJ, RW, YL, QS, XC, CW, KC, YW, MS, YS, XG, and ZG performed experiments. KH, XM, YX, LZ, HX, TY, YW, XP, ZG, KMS, and NW analysed and interpreted data. JL, KH, XM, YX, XP, KMS, and NW wrote or edited the manuscript with input from all coauthors. All authors approved the final version.

Funding

This work is supported by grants from the National Key Research and Development Program of China (2023YFB3810200 to JL, MS), the National Natural Science Foundation of China (92168204, 82225030 to JL; 81974326 to XP), the Shanghai Municipal Health Commission (2022XD034, 2025ZHYL018 to JL), the Shanghai Shenkang Hospital Development Center (SHDC12025116 to JL), the National Clinical Key Specialty Construction project of China (Z155080000004), the Shanghai Research Center of Rehabilitation Medicine (Top Priority Research Center of Shanghai) (2023ZZ02027), and the Shanghai Disabled Persons' Federation Key Laboratory of Intelligent Rehabilitation Assistive Appliance and Technology.

Data availability statement

Bulk RNA-seq data of induced primary chondrocytes are freely available within the NCBI GEO database GSE280035. The raw sequencing data of scRNA-seq are deposited in and can be accessed via the Genome Sequence Archive of the Beijing Institute of Genomics, Chinese Academy of Sciences (http://bigd.big.ac.cn/gsa/; Genome Sequence Archive [GSA]: PRJCA047023).

Declaration of generative AI and AI-assisted technologies in the writing process

During the preparation of this work, the authors used DeepSeek in order to improve language clarity and readability. After using this tool, the authors reviewed and edited the content as

needed and take full responsibility for the content of the published article.

Patient consent for publication

Not applicable. The study did not include identifiable patient information, images, or personal data.

Ethics approval

This study was approved by the Ethics Committee of Yangzhi Rehabilitation Hospital (Shanghai Sunshine Rehabilitation Center), Tongji University School of Medicine (approval number: 2022-022), and was conducted in accordance with the Declaration of Helsinki.

Provenance and peer review

Not commissioned; externally peer reviewed.

Supplementary materials

Supplementary material associated with this article can be found in the online version at doi:10.1016/j.ard.2025.12.004.

REFERENCES

[1] Tanaka EM. Regeneration: if they can do it, why can't we? Cell 2003;113:559–62. doi: 10.1016/s0092-8674(03)00395-7.

[2] Iismaa SE, Kaidonis X, Nicks AM, Bogush N, Kikuchi K, Naqvi N, et al. Comparative regenerative mechanisms across different mammalian tissues. NPJ Regen Med 2018;3:6. doi: 10.1038/s41536-018-0044-5.

[3] Baddour JA, Sousounis K, Tsonis PA. Organ repair and regeneration: an overview. Birth Defects Res C Embryo Today 2012;96:1–29. doi: 10.1002/bdrc.21006.

[4] Johnson VL, Hunter DJ. The epidemiology of osteoarthritis. Best Pract Res Clin Rheumatol 2014;28:5–15. doi: 10.1016/j.berh.2014.01.004.

[5] Huey DJ, Hu JC, Athanasiou KA. Unlike bone, cartilage regeneration remains elusive. Science 2012;338:917–21. doi: 10.1126/science.1222454.

[6] Makris EA, Gomoll AH, Malizos KN, Hu JC, Athanasiou KA. Repair and tissue engineering techniques for articular cartilage. Nat Rev Rheumatol 2015;11:21–34. doi: 10.1038/nrrheum.2014.157.

[7] Devitt BM, Bell SW, Webster KE, Feller JA, Whitehead TS. Surgical treatments of cartilage defects of the knee: systematic review of randomised controlled trials. Knee 2017;24:508–17. doi: 10.1016/j.knee.2016.12.002.

[8] Mithoefer K, McAdams T, Williams RJ, Kreuz PC, Mandelbaum BR. Clinical efficacy of the microfracture technique for articular cartilage repair in the knee: an evidence-based systematic analysis. Am J Sports Med 2009;37:2053–63. doi: 10.1177/0363546508328414.

[9] Jo CH, Lee YG, Shin WH, Kim H, Chai JW, Jeong EC, et al. Intra-articular injection of mesenchymal stem cells for the treatment of osteoarthritis of the knee: a proof-of-concept clinical trial. Stem Cells 2014;32:1254–66. doi: 10.1002/stem.1634.

[10] Yang W, Ma G, Li J, Guan T, He D, Yang D, et al. Anxiety and depression as potential risk factors for limited pain management in patients with elderly knee osteoarthritis: a cross-lagged study. BMC Musculoskelet Disord 2024;25:995. doi: 10.1186/s12891-024-08127-0.

[11] Chen YP, Huang YY, Wu Y, Kuo YJ, Lin CY. Depression negatively affects patient-reported knee functional outcome after intraarticular hyaluronic acid injection among geriatric patients with knee osteoarthritis. J Orthop Surg Res 2019;14:387. doi: 10.1186/s13018-019-1419-z.

[12] Silveira J, Oliveira D, Martins A, Costa L, Neto F, Ferreira-Gomes J, et al. The association between anxiety and depression symptoms and clinical and pain characteristics in patients with hip and knee osteoarthritis. ARP Rheumatol 2024;3:206–15. doi: 10.63032/sdvb2224.

[13] Zacková L, Jáni M, Brázdil M, Nikolova YS, Marečková K. Cognitive impairment and depression: meta-analysis of structural magnetic resonance imaging studies. Neuroimage Clin 2021;32:102830. doi: 10.1016/j.nicl.2021.102830.

[14] Swaab DF, Bao AM, Lucassen PJ. The stress system in the human brain in depression and neurodegeneration. Ageing Res Rev 2005;4:141–94. doi: 10.1016/j.arr.2005.03.003.

[15] Gong Q, He Y. Depression, neuroimaging and connectomics: a selective overview. Biol Psychiatry 2015;77:223–35. doi: 10.1016/j.biopsych.2014.08.009.

[16] Basser PJ, Mattiello J, LeBihan D. MR diffusion tensor spectroscopy and imaging. Biophys J 1994;66:259–67. doi: 10.1016/s0006-3495(94)80775-1.

[17] Pierpaoli C, Basser PJ. Toward a quantitative assessment of diffusion anisotropy. Magn Reson Med 1996;36:893–906. doi: 10.1002/mrm.1910360612.

[18] Mole JP, Subramanian L, Bracht T, Morris H, Metzler-Baddeley C, Linden DE. Increased fractional anisotropy in the motor tracts of Parkinson's disease suggests compensatory neuroplasticity or selective neurodegeneration. Eur Radiol 2016;26:3327–35. doi: 10.1007/s00330-015-4178-1.

[19] Wickersham IR, Finke S, Conzelmann KK, Callaway EM. Retrograde neuronal tracing with a deletion-mutant rabies virus. Nat Methods 2007;4:47–9. doi: 10.1038/nmeth999.

[20] Xiong SY, Wen HZ, Dai LM, Lou YX, Wang ZQ, Yi YL, et al. A brain-tumor neural circuit controls breast cancer progression in mice. J Clin Invest 2023;133:e167725. doi: 10.1172/jci167725.

[21] Cardoso F, Klein Wolterink RGJ, Godinho-Silva C, Domingues RG, Ribeiro H, da Silva JA, et al. Neuro-mesenchymal units control ILC2 and obesity via a brain-adipose circuit. Nature 2021;597:410–4. doi: 10.1038/s41586-021-03830-7.

[22] Jia F, Lv P, Miao H, Shi X, Mei H, Li L, et al. Optimization of the fluorescent protein expression level based on pseudorabies virus Bartha strain for neural circuit tracing. Front Neuroanat 2019;13:63. doi: 10.3389/fnana.2019.00063.

[23] Zhang X, Lei B, Yuan Y, Zhang L, Hu L, Jin S, et al. Brain control of humoral immune responses amenable to behavioural modulation. Nature 2020;581:204–8. doi: 10.1038/s41586-020-2235-7.

[24] Yao J, Zhang Q, Liao X, Li Q, Liang S, Li X, et al. A corticopontine circuit for initiation of urination. Nat Neurosci 2018;21:1541–50. doi: 10.1038/s41593-018-0256-4.

[25] Dong WY, Zhu X, Tang HD, Huang JY, Zhu MY, Cheng PK, et al. Brain regulation of gastric dysfunction induced by stress. Nat Metab 2023;5:1494–505. doi: 10.1038/s42255-023-00866-z.

[26] Milano G, Sanna Passino E, Deriu L, Careddu G, Manunta L, Manunta A, et al. The effect of platelet rich plasma combined with microfractures on the treatment of chondral defects: an experimental study in a sheep model. Osteoarthritis Cartilage 2010;18:971–80. doi: 10.1016/j.joca.2010.03.013.

[27] van den Borne MP, Raijmakers NJ, Vanlauwe J, Victor J, de Jong SN, Bellemans J, et al. International Cartilage Repair Society (ICRS) and Oswestry macroscopic cartilage evaluation scores validated for use in Autologous Chondrocyte Implantation (ACI) and microfracture. Osteoarthritis Cartilage 2007;15:1397–402. doi: 10.1016/j.joca.2007.05.005.

[28] Murphy MP, Koepke LS, Lopez MT, Tong X, Ambrosi TH, Gulati GS, et al. Articular cartilage regeneration by activated skeletal stem cells. Nat Med 2020;26:1583–92. doi: 10.1038/s41591-020-1013-2.

[29] Kozhemyakina E, Zhang M, Ionescu A, Ayturk UM, Ono N, Kobayashi A, et al. Identification of a Prg4-expressing articular cartilage progenitor cell population in mice. Arthritis Rheumatol 2015;67:1261–73. doi: 10.1002/art.39030.

[30] Glasson SS, Chambers MG, Van Den Berg WB, Little CB. The OARSI histopathology initiative—recommendations for histological assessments of osteoarthritis in the mouse. Osteoarthritis Cartilage 2010;18(Suppl 3):S17–23. doi: 10.1016/j.joca.2010.05.025.

[31] Yuan Y, Wu W, Chen M, Cai F, Fan C, Shen W, et al. Reward inhibits paraventricular CRH neurons to relieve stress. Curr Biol 2019;29:1243–1251.e4. doi: 10.1016/j.cub.2019.02.048.

[32] Reul JM, Holsboer F. On the role of corticotropin-releasing hormone receptors in anxiety and depression. Dialogues Clin Neurosci 2002;4:31–46. doi: 10.31887/DCNS.2002.4.1/jreul.

[33] Gold PW, Chrousos GP. Organization of the stress system and its dysregulation in melancholic and atypical depression: high vs low CRH/NE states. Mol Psychiatry 2002;7:254–75. doi: 10.1038/sj.mp.4001032.

[34] Eitner A, Pester J, Nietzsche S, Hofmann GO, Schaible HG. The innervation of synovium of human osteoarthritic joints in comparison with normal rat and sheep synovium. Osteoarthritis Cartilage 2013;21:1383–91. doi: 10.1016/j.joca.2013.06.018.

[35] Bennike T, Ayturk U, Haslauer CM, Froehlich JW, Proffen BL, Barnaby O, et al. A normative study of the synovial fluid proteome from healthy porcine knee joints. J Proteome Res 2014;13:4377–87. doi: 10.1021/pr500587x.

[36] Jay GD, Britt DE, Cha CJ. Lubricin is a product of megakaryocyte stimulating factor gene expression by human synovial fibroblasts. J Rheumatol 2000;27:594–600.

[37] Zhang B, Ma S, Rachmin I, He M, Baral P, Choi S, et al. Hyperactivation of sympathetic nerves drives depletion of melanocyte stem cells. Nature 2020;577:676–81. doi: 10.1038/s41586-020-1935-3.
[38] Feng J, Zhang C, Lischinsky JE, Jing M, Zhou J, Wang H, et al. A genetically encoded fluorescent sensor for rapid and specific in vivo detection of norepinephrine. Neuron 2019;102:745–761.e8. doi: 10.1016/j.neuron.2019.02.037.
[39] Feng J, Dong H, Lischinsky JE, Zhou J, Deng F, Zhuang C, et al. Monitoring norepinephrine release in vivo using next-generation GRABNE sensors. Neuron 2024;112:1930–1942.e6. doi: 10.1016/j.neuron.2024.03.001.
[40] Chen D, Qi Y, Zhang J, Yang Y. Deconstruction of a hypothalamic astrocyte-white adipocyte sympathetic axis that regulates lipolysis in mice. Nat Commun 2022;13:7536. doi: 10.1038/s41467-022-35258-6.
[41] Brown MR, Fisher LA, Spiess J, Rivier C, Rivier J, Vale W. Corticotropin-releasing factor: actions on the sympathetic nervous system and metabolism. Endocrinology 1982;111:928–31. doi: 10.1210/endo-111-3-928.
[42] Ignatyeva N, Gavrilov N, Timashev PS, Medvedeva EV. Prg4-expressing chondroprogenitor cells in the superficial zone of articular cartilage. Int J Mol Sci 2024;25:5605. doi: 10.3390/ijms25115605.
[43] Wang G, Chen S, Xie Z, Shen S, Xu W, Chen W, et al. TGFβ attenuates cartilage extracellular matrix degradation via enhancing FBXO6-mediated MMP14 ubiquitination. Ann Rheum Dis 2020;79:1111–20. doi: 10.1136/annrheumdis-2019-216911.
[44] Liu X, Jiang S, Jiang T, Lan Z, Zhang X, Zhong Z, et al. Bioenergetic-active exosomes for cartilage regeneration and homeostasis maintenance. Sci Adv 2024;10:eadp7872. doi: 10.1126/sciadv.adp7872.
[45] Huang SW, Wang WT, Lin LF, Liao CD, Liou TH, Lin HW. Association between psychiatric disorders and osteoarthritis: a nationwide longitudinal population-based study. Medicine (Baltimore) 2016;95:e4016. doi: 10.1097/md.0000000000004016.
[46] Osani MC, Bannuru RR. Efficacy and safety of duloxetine in osteoarthritis: a systematic review and meta-analysis. Korean J Intern Med 2019;34:966–73. doi: 10.3904/kjim.2018.460.
[47] Helminen EE, Sinikallio SH, Valjakka AL, Väisänen-Rouvali RH, Arokoski JP. Determinants of pain and functioning in knee osteoarthritis: a one-year prospective study. Clin Rehabil 2016;30:890–900. doi: 10.1177/0269215515619660.
[48] Jiao K, Niu LN, Li QH, Ren GT, Zhao CM, Liu YD, et al. β2-Adrenergic signal transduction plays a detrimental role in subchondral bone loss of temporomandibular joint in osteoarthritis. Sci Rep 2015;5:12593. doi: 10.1038/srep12593.
[49] Mitchell J, Lai LP, Peralta F, Xu Y, Sugamori K. β2-adrenergic receptors inhibit the expression of collagen type II in growth plate chondrocytes by stimulating the AP-1 factor Jun-B. Am J Physiol Endocrinol Metab 2011;300:E633–9. doi: 10.1152/ajpendo.00515.2010.
[50] Sohn R, Rösch G, Junker M, Meurer A, Zaucke F, Jenei-Lanzl Z. Adrenergic signalling in osteoarthritis. Cell Signal 2021;82:109948. doi: 10.1016/j.cellsig.2021.109948.
[51] Wei X, Qiu J, Lai R, Wei T, Lin Z, Huang S, et al. A human organoid drug screen identifies α2-adrenergic receptor signaling as a therapeutic target for cartilage regeneration. Cell Stem Cell 2024;31:1813–1830.e8. doi: 10.1016/j.stem.2024.09.001.
[52] Liu T, Yang L, Han X, Ding X, Li J, Yang J. Local sympathetic innervations modulate the lung innate immune responses. Sci Adv 2020;6:eaay1497. doi: 10.1126/sciadv.aay1497.
[53] Fu K, Robbins SR, McDougall JJ. Osteoarthritis: the genesis of pain. Rheumatology (Oxford) 2018;57 iv43-50. doi: 10.1093/rheumatology/kex419.
[54] Yu L, Zhu X, Peng K, Qin H, Yang K, Cai F, et al. Propofol alleviates anxiety-like behaviors associated with pain by inhibiting the hyperactivity of PVNCRH neurons via GABAA receptor β3 subunits. Adv Sci (Weinh) 2024;11:e2309059. doi: 10.1002/advs.202309059.
[55] Hallett M. Transcranial magnetic stimulation: a primer. Neuron 2007;55:187–99. doi: 10.1016/j.neuron.2007.06.026.
[56] Yang Y, Yuan J, Field RL, Ye D, Hu Z, Xu K, et al. Induction of a torpor-like hypothermic and hypometabolic state in rodents by ultrasound. Nat Metab 2023;5:789–803. doi: 10.1038/s42255-023-00804-z.
[57] Shivacharan RS, Rolle CE, Barbosa DAN, Cunningham TN, Feng A, Johnson ND, et al. Pilot study of responsive nucleus accumbens deep brain stimulation for loss-of-control eating. Nat Med 2022;28:1791–6. doi: 10.1038/s41591-022-01941-w.
[58] Chen Z, Chen X, Liu M, Ma L, Yu S. Volume of hypothalamus as a diagnostic biomarker of chronic migraine. Front Neurol 2019;10:606. doi: 10.3389/fneur.2019.00606.
[59] Rolls ET, Joliot M, Tzourio-Mazoyer N. Implementation of a new parcellation of the orbitofrontal cortex in the automated anatomical labeling atlas. Neuroimage 2015;122:1–5. doi: 10.1016/j.neuroimage.2015.07.075.
[60] Beynon RA, Alomar F, Saunders FR, Ebsim R, Faber BG, Jung M, et al. Use of dual-energy x-ray absorptiometry to evaluate variation in bone shape and alignment associated with radiographic knee osteoarthritis: findings from a study of 19,053 individuals in UK Biobank. Osteoarthr Cartil Open 2025;7:100667. doi: 10.1016/j.ocarto.2025.100667.
[61] Littlejohns TJ, Holliday J, Gibson LM, Garratt S, Oesingmann N, Alfaro-Almagro F, et al. The UK Biobank imaging enhancement of 100,000 participants: rationale, data collection, management and future directions. Nat Commun 2020;11:2624. doi: 10.1038/s41467-020-15948-9.
[62] Jin Y, Liu Q, Chen P, Zhao S, Jiang W, Wang F, et al. A novel prostaglandin E receptor 4 (EP4) small molecule antagonist induces articular cartilage regeneration. Cell Discov 2022;8:24. doi: 10.1038/s41421-022-00382-6.
[63] Lee EH, Park JY, Kwon HJ, Han PL. Repeated exposure with short-term behavioral stress resolves pre-existing stress-induced depressive-like behavior in mice. Nat Commun 2021;12:6682. doi: 10.1038/s41467-021-26968-4.
[64] Skehan P, Storeng R, Scudiero D, Monks A, McMahon J, Vistica D, et al. New colorimetric cytotoxicity assay for anticancer-drug screening. J Natl Cancer Inst 1990;82:1107–12. doi: 10.1093/jnci/82.13.1107.
[65] He L, Xu Z, Niu X, Li R, Wang F, You Y, et al. GPRC5B protects osteoarthritis by regulation of autophagy signaling. Acta Pharm Sin B 2023;13:2976–89. doi: 10.1016/j.apsb.2023.05.014.

Ann Rheum Dis 85 (2026) 761–770

Contents lists available at ScienceDirect

Annals of the Rheumatic Diseases

journal homepage: https://www.sciencedirect.com/journal/annals-of-the-rheumatic-diseases

Miscellaneous

Results of a 1-year randomised double-blind placebo-controlled trial with methotrexate 25 mg/week in recently diagnosed polymyalgia rheumatica

Thomas E. Bolhuis[1,2,†], Noortje E.S.E.P. Kooijman[1,2,†], Diane E. Marsman[1], Gijs F. Snijders[3], Alfons A. den Broeder[1,4], Nathan den Broeder[1,2], Aatke van der Maas[1,*]

[1] *Department of Rheumatology, Sint Maartenskliniek, Ubbergen, The Netherlands*
[2] *Radboudumc Graduate School, Radboud University Medical Center, Nijmegen, The Netherlands*
[3] *Department of Rheumatology, Gelre Ziekenhuizen, Apeldoorn and Zutphen, The Netherlands*
[4] *Department of Rheumatology, Radboud University Medical Center, Nijmegen, The Netherlands*

ARTICLE INFO

Article history:
Received 22 July 2025
Received in revised form 26 November 2025
Accepted 27 November 2025

ABSTRACT

Objectives: Methotrexate is recommended in current guidelines as a first-choice glucocorticoid (GC)-sparing agent for patients with polymyalgia rheumatica (PMR) prone to relapses or prolonged GC use. Previous randomised controlled trials (RCTs) have reported conflicting results but used low doses of methotrexate (7.5-10 mg/wk). More evidence on higher doses (25 mg/wk) is needed.

Methods: In this 52-week blinded, placebo-controlled RCT, patients with recently diagnosed PMR (per 2012 European League Against Rheumatism/American College of Rheumatology criteria) and <8 weeks of GC use were randomised 1:1 to methotrexate 25 mg/wk or placebo, alongside a 24-week GC-tapering protocol. The primary outcome was GC-free remission (Polymyalgia Rheumatica-Activity Score <10 and no GC use) at week 52, tested with a 1-sided Cochran-Mantel-Haenszel test stratified by sex and inflammatory markers.

Results: Sixty-four patients were recruited, of whom 58 were included in the final analysis. GC-free remission at 52 weeks was achieved in 80% of patients in the methotrexate group vs 46% in the placebo group (risk difference 34%, 1-sided 95% CI: 14%, 1-sided $P = .0042$).

Conclusions: This small but high-quality RCT demonstrated that methotrexate 25 mg/wk significantly increases the likelihood of achieving GC-free remission at 52 weeks in newly diagnosed PMR. These findings show a benefit of early introduction of methotrexate in PMR. Further research is needed to determine the optimal timing of methotrexate initiation.

*Correspondence to Dr Aatke van der Maas, Department of Rheumatology, Sint Maartenskliniek, Ubbergen, The Netherlands.
E-mail address: a.vandermaas@maartenskliniek.nl (A. van der Maas).
Handling editor Josef S. Smolen.
† These authors contributed equally to this work and share first authorship.

https://doi.org/10.1016/j.ard.2025.11.025

WHAT IS ALREADY KNOWN ON THIS TOPIC

- Three randomised controlled trials (RCTs) on methotrexate in polymyalgia rheumatica (PMR) showed inconsistent results regarding glucocorticoid (GC)-free remission and cumulative GC dose.
- These trials had methodologic limitations and used relatively low methotrexate doses (≤10 mg/wk).
- Higher doses (up to 25 mg/wk), as commonly used in rheumatoid arthritis, have not been studied in PMR.

WHAT THIS STUDY ADDS

- This RCT demonstrates the positive effect of methotrexate 25 mg/wk in recently diagnosed PMR on GC-free remission rates at 52 weeks compared with placebo.

HOW THIS STUDY MIGHT AFFECT RESEARCH, PRACTICE OR POLICY

- Initiating methotrexate early may improve outcomes in patients with newly diagnosed PMR.
- This approach may be especially beneficial for patients at risk of prolonged GC-therapy and associated adverse events.

INTRODUCTION

Polymyalgia rheumatica (PMR) is an inflammatory rheumatic disease affecting individuals older than 50 years. It is clinically characterised by pain and stiffness in neck, shoulders and/or hip girdle, leading to limitations in daily functioning and quality of life. Typically, these symptoms are accompanied by elevated acute-phase reactants. To this day, the pathophysiology of PMR remains unclear. Diagnosis of PMR is predominantly based on clinical features and laboratory findings, sometimes combined with imaging (ie, ultrasound, magnetic resonance imaging, and positron emission tomography-computed tomography) [1].

The cornerstone of treatment consists of glucocorticoids (GCs). Current European League Against Rheumatism (EULAR)/American College of Rheumatology (ACR) guidelines advise a starting dose of oral prednisone equivalent of 12.5 to 25 mg a day, followed by gradual tapering after reaching remission [2]. The minimum duration of treatment is 9 to 12 months, but can be substantially longer when relapses occur, posing a major difficulty in the treatment of PMR [1,3,4]. There are still 25% of patients with PMR taking GCs after more than 4 years [4]. Long-term GC treatment has several drawbacks, including increased risk of dose-dependent GC-related adverse events (ie, risk of infection, weight gain, osteoporosis, and diabetes mellitus) [1,5]. Therefore, it is important to investigate GC-sparing treatment options in PMR.

The optimal timing and role of GC-sparing agents in the treatment of PMR is not yet clear. In recent years, several GC-sparing agents, including conventional and biologic disease-modifying antirheumatic drugs (DMARDs), such as interleukin-6 (IL-6) and Janus kinase (JAK) inhibitors, have been studied [6].

The most frequently used DMARD in PMR is methotrexate [7]. However, evidence on methotrexate as a GC-sparing agent in PMR is conflicting. The efficacy of methotrexate has been investigated in 3 small randomised controlled trials (RCTs) [8–10] several retrospective studies [11–14] and 1 observational longitudinal cohort study [15], with inconsistent results. All previous RCTs used relatively low doses of methotrexate (7.5-10 mg/wk) and reported conflicting findings regarding treatment efficacy and GC-sparing potential.

In rheumatoid arthritis (RA), the optimal methotrexate dose has been shown to be around 20 to 25 mg/wk [16]. To this day, the effect of higher dosages of methotrexate in PMR has not yet been studied in an RCT.

Based on this limited data, current EULAR/ACR guidelines for the management of PMR recommend an early introduction of methotrexate, particularly in patients prone to relapses, prolonged GC-therapy or GC-related adverse events. In these recommendations, methotrexate is positioned as a first-choice GC-sparing agent. However, further research regarding methotrexate in the treatment of PMR is advised [2].

Given the limited and inconsistent evidence on methotrexate in PMR, we conducted this randomised, placebo-controlled trial to evaluate whether methotrexate 25 mg/wk is effective in achieving GC-free remission and reducing cumulative GC dose for patients with recently diagnosed PMR.

METHODS

Study design

We performed a double-blind, randomised placebo-controlled trial at the Rheumatology Department of Sint Maartenskliniek Nijmegen and Gelre Ziekenhuizen Apeldoorn and Zutphen, The Netherlands.

The original and amended study protocols can be found in appendices S1 and S2, respectively [17]. Changes to the protocol are summarized in appendix S3. Reporting was guided by the Consolidated Standards of Reporting Trials statement, with a checklist in appendix S4 appendix S14 [18]. In the study design, a local patient participation platform was asked to provide their input on the clinical relevance, the feasibility of the study and its measurements and readability of the patient information form.

Ethical approval

Medical ethical approval was obtained (NL69979.091.19; November 26, 2019), and the trial was registered in the Dutch trial registry (originally as NL8366 and later NL-OMON22681). All participants signed informed consent.

Participants

Patients were eligible for inclusion if they were recently diagnosed with PMR (ie, in the last 12 weeks), fulfilled the 2012 EULAR/ACR classification criteria [19] and were treated with GCs for less than 8 weeks before inclusion. PMR diagnosis was based on clinical grounds, and no standard protocolised imaging was used.

Exclusion criteria were a prednisolone daily dose equivalent above 30 mg, use of other immunomodulatory medication 3 months before inclusion, other concomitant inflammatory rheumatic diseases, and any comorbidities that can interfere with accurate assessment of PMR disease activity, for example, peripheral neuropathies, severe osteoarthritis of the shoulder or hip girdle, or other conditions that may substantially affect pain perception or movement, as judged by the physician. In addition, patients with previous hypersensitivity or other contraindications for prednisolone or methotrexate were excluded. During the study, if a different rheumatic diagnosis was deemed more likely than PMR (eg, RA), patients were pulled from the study due to the necessity of appropriate treatment.

Additional inclusion and exclusion criteria are detailed in appendix S5 appendix S4.

Randomisation and blinding

Sixty-four eligible patients were randomly allocated in a 1:1 ratio to receive either methotrexate 25 mg/wk or placebo in (5 mg) capsule format, with stratification based on sex and on the level of inflammatory markers at diagnosis before inclusion (low or high, cut-off erythrocyte sedimentation rate [ESR] ≥70 mm/h and/or C-reactive protein [CRP] ≥25 mg/L). Sex was documented as biological sex based on medical records. A computerised randomisation procedure with varying block size [4,6,8] was used. The randomisation sequence was generated by an independent pharmacist. All participating physicians and patients remained blinded during the study period, and investigators performing the analysis remained blinded until primary outcome analysis was completed. Study medication was produced by the pharmacy of Radboudumc, Nijmegen, The Netherlands, and distributed by the pharmacy of Sint Maartenskliniek, Nijmegen, The Netherlands. Methotrexate and placebo pills were identical in packaging. Furthermore, the capsules were identical to each other in appearance.

Procedures

Patients allocated to the intervention arm received methotrexate 15 mg/wk orally for the first 4 weeks, followed by 25 mg/wk for the remaining 48 weeks of the study period, taken in 2 doses throughout 1 day to improve bioavailability. Patients allocated to the placebo arm received matching placebo capsules. In addition, all patients received folic acid 5 mg twice weekly in compliance with local protocol for methotrexate treatment [20]. All patients received oral prednisolone, with an accelerated tapering protocol from 15 mg to 0 mg over 24 weeks as described previously and shown in appendix S6 appendix S5 [17]. In case of relapse, the prednisolone daily dose was raised to the last effective prerelapse dose and tapered again according to the accelerated tapering protocol. If a second relapse occurred, a local usual care tapering protocol using slow tapering was followed. Relapse was defined based on the clinical judgement of the treating physician.

Visits and assessment of outcomes took place at weeks 0, 4, 12, 24, 32, and 52. Due to the COVID-19 pandemic, we amended the study protocol so that visits other than weeks 0, 32, and 52 could be performed by telephone instead of face to face. Besides these assessments, laboratory safety monitoring was performed at weeks 8, 16, and 42, and participants were assessed between visits if deemed necessary. In case of adverse events, the number of pills could be lowered if necessary, with each capsule consisting of 5 mg of methotrexate (or placebo). Further elaboration on local treatment and follow-up can be found in appendix S2.

Outcomes

The primary outcome was GC-free remission at week 52, defined as a Polymyalgia Rheumatica-Activity Score (PMR-AS) of less than 10 and no current use of GCs. The PMR-AS is calculated as follows: CRP (mg/dL) + (duration of morning stiffness [in minutes] * 0.1) + elevation of upper limbs (ranging 0-3) + visual analogue score (VAS) for pain (ranging 0-10) + VAS physician's global (ranging 0-10) [21–24]. For telephone consultations, the physician VAS score was substituted by a numeric rating scale. Secondary outcomes were proportion of patients in GC-free remission at week 32 and proportion of patients in low-dose GC remission (defined as 5 mg a day or less), cumulative GC dose, total number of relapses and proportion of patients that relapsed at week 32 and week 52.

Other prespecified secondary outcomes include time to GC-free remission and first relapse, changes in PMR-AS, ESR, CRP, Patient Acceptable Symptom States (PASS) questions, health-related quality of life (EuroQol 5-dimension 5-level (EQ-5D-5L) questionnaire), Health Assessment Questionnaire (HAQ), and Patient Reported Outcome Measures Information System Physical Function (PROMIS-PF), as well as adverse events categorised following the Common Terminology Criteria for Adverse Events (CTCAE) version 5.0 [25]. Secondary outcomes are further elaborated upon in appendices S1 to S3. The questionnaires used in this study can be found in appendices S7 and S8.

Statistical analysis

The original intended sample size was 98 patients [17]. However, because of slower inclusion than intended due to the COVID-19 pandemic and consequent funding constraints that required stopping inclusion before the intended sample size was reached, the trial was amended to 1-sided testing for the primary outcome before the last patient ended the study, with a 1-tailed alpha of 0.05, based on the advice of the Data Safety Monitoring Board. This would result in a power of 78% for the prespecified effect size with the actual number of included patients as shown in appendices S1 and S2. This amendment was made before the trial was deblinded, and was approved by the Medical Ethics Review Committee Oost-Nederland.

Analyses were performed using Stata/IC version 13.1 for Windows. Distribution of data and missing values was examined, and descriptive statistics were applied as appropriate. A multiple imputation model was used to impute missing PMR-AS components for 20 datasets and is further elaborated upon in appendix S9 and S10. The primary outcome, GC-free remission after 52 weeks, was compared between the methotrexate and placebo group on an intention-to-treat (ITT) basis using a Cochran-Mantel-Haenszel test with stratification considered and reported using percentages and percentage differences. The primary outcome was further tested in a complete case analysis (only the cases with no missing values in the PMR-AS) and a per-protocol (PP) analysis (only the patients in whom the treatment protocol regarding the GC tapering was followed without protocol violations). In the PP analysis, participants were excluded if they either used less than 15 mg placebo or methotrexate, were treated for less than 24 weeks with placebo or methotrexate, were treated with GC >20 mg/d for at least 2 weeks (against protocol), or did not follow tapering advice for more than 8 weeks. Secondary outcomes were assessed using either Cochran-Mantel-Haenszel test, log-rank test, Mann-Whitney *U*-test, or Poisson regression as appropriate. All Poisson regression models were adjusted for stratification factors, as were all analyses of dichotomous outcomes. For the primary outcome, a 1-sided test and 1-sided 95% CI was used, and a P value <.05 was considered significant. For all other outcomes, 2-sided testing and 2-sided 95% CI were used. Details on protocol violations are provided in appendix S10.

Unfortunately, erroneous results of the study were presented at the ACR Convergence 2024 due to a coding error. This occurred before the initial analyses, resulting in some patients being analysed in the wrong allocation group. To address this issue, all the source data were audited by 2 researchers, and all analyses were repeated. This error was communicated to the

ACR, but unfortunately correction or retraction was not possible [26]. The corrected results were subsequently presented at the EULAR Congress 2025 [27].

RESULTS

A total of 64 patients were randomised, and 58 were included in the final analysis. Reasons for exclusion are described in Figure 1. The first patient was included on April 9, 2020 and the last visit was on February 8, 2024. Inclusion was ended as funding ran out before the intended 100 patients were included, due to the COVID-19 pandemic and consequent slower rate of inclusion. Patient characteristics are summarised in Table 1. No patients developed giant cell arteritis during the trial. Primary outcome values were imputed for 5 patients for whom the PMR-AS could not be calculated because of a missing component, as elaborated upon in appendix S9 and S10.

The proportion of patients in GC-free remission at 52 weeks in the ITT analysis (n = 58) was significantly higher in the methotrexate group compared with the placebo group, with proportions of patients in GC-free remission of 80% (24/30) vs 46% (13/28) for the methotrexate and placebo, respectively, with a risk difference of 34% (1-sided 95% CI: 14%, 1-sided $P = .0042$). The risk ratio was 1.7 (1-sided 95% CI: 1.2). In the complete case analysis, proportions of patients in GC-free remission for methotrexate (n = 29) and placebo (n = 26) were 79% vs 42%, respectively, with a risk difference of 37% (1-sided 95% CI: 17%, 1-sided $P = .006$). Result of the complete case analysis per stratum are also reported descriptively in appendix S11 and show no clear evidence of effect modification by stratum. In the PP analysis, methotrexate (n = 19) and placebo (n = 19) proportions of patients in GC-free remission were 84% vs 58%, respectively, with a risk difference of 26% (1-sided 95% CI: 3.2%, 1-sided $P = .034$), with patient flow and exclusion shown in Figure 1.

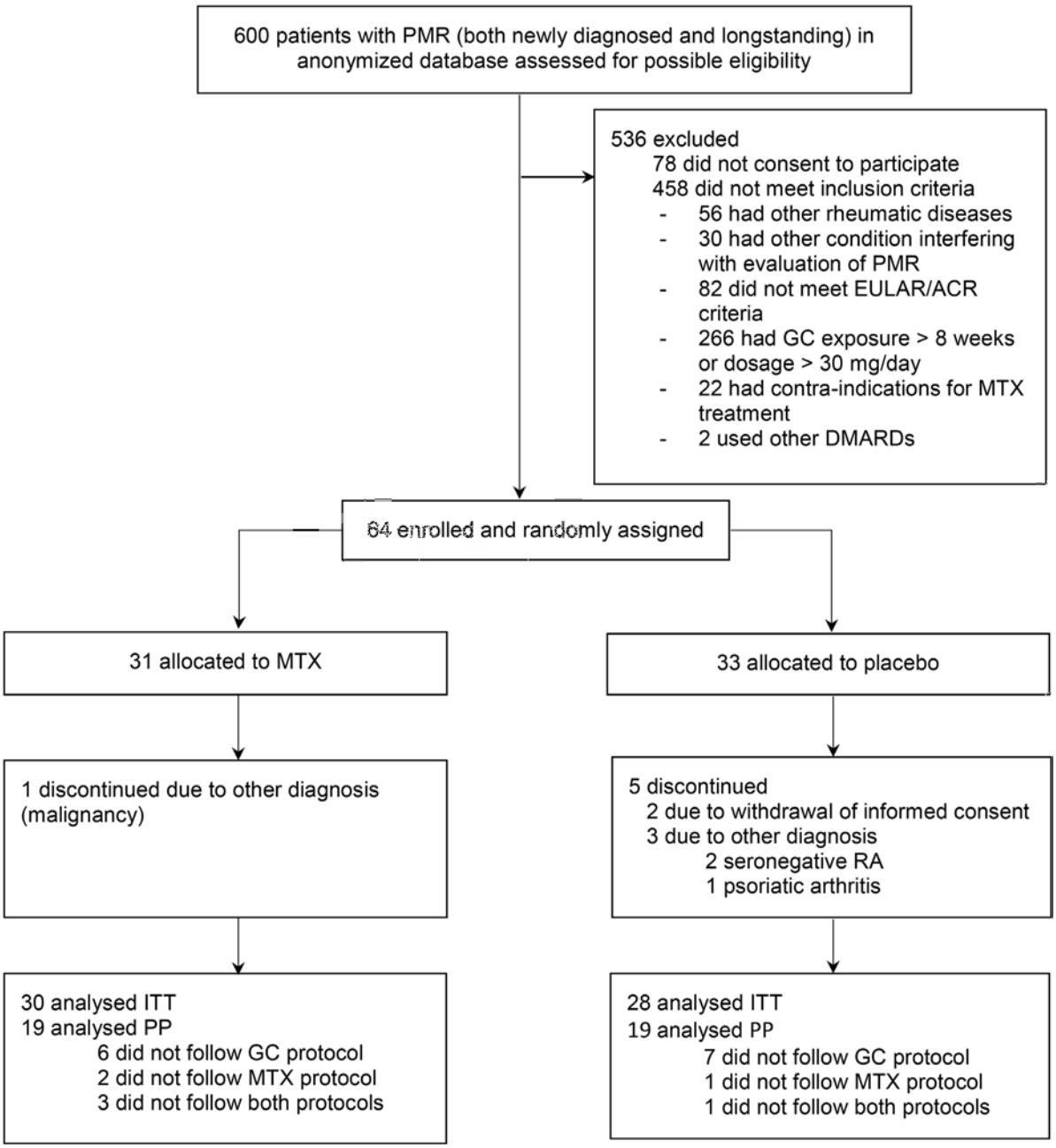

Figure 1. Flow diagram. ACR, American College of Rheumatology; DMARD, disease-modifying antirheumatic drug; EULAR, European League Against Rheumatism; GC, glucocorticoid; ITT, intention-to-treat; MTX, methotrexate; PMR, polymyalgia rheumatica; PP, per-protocol; RA, rheumatoid arthritis.

Table 1
Patient characteristics

Patient characteristic	Placebo (n = 28)	Methotrexate (n = 30)
Age (y)[a]	66 (7.5)	64 (9.0)
Sex		
Female, n (%)	14 (50)	14 (47)
Male, n (%)	14 (50)	16 (53)
Body mass index (kg/m^2)	28 (24-29)[b]	25 (23-28)
Smoking, n (%)		
Never	12 (43)	14 (47)
Former	15 (54)	13 (43)
Current	1 (4)	3 (10)
Alcohol use, n (%)		
Never	8 (26)	4 (13)
Former	2 (7)	3 (10)
Active	18 (64)	23 (77)
Comorbidity, n (%)		
Diabetes	3 (11)	1 (3)
Malignancy	2 (7)	3 (10)
Osteoporosis	4 (14)	1 (3)
Cardiovascular	14 (50)	8 (27)
Pre-treatment PMR symptom duration (wk)[c]	14 (7-19)	13 (8-20)
CRP at diagnosis (mg/L)[c]	23 (16-67)	26 (12-45)
ESR at diagnosis (mm/h)[c]	34 (27-45)[b]	32 (16-50)[d]
Rheumatoid factor positive, n (%)[e]	3 (11)[d]	5 (17)
ACPA positive, n (%)[e]	1 (4)	0 (0)
Peripheral arthritis	6 (22%)	2 (7%)
PMR-AS at baseline[c,f]	6 (3-10)[b]	7 (3-20)[b]
Prednisolone dose at baseline (mg/d)[c]	15 (15-17.5)	15 (13-15)
Cumulative GC dose before inclusion (mg)[c,g]	353 (165-466)	308 (150-600)

ACPA, anticitrullinated protein antibody; CRP, C-reactive protein; ESR, erythrocyte sedimentation rate; GC, glucocorticoid; PMR, polymyalgia rheumatica; PMR-AS, Polymyalgia Rheumatica Activity Score.
[a] Displayed as mean (SD).
[b] 2 missing.
[c] Displayed as median (IQR).
[d] 1 missing.
[e] Reference values: ≤14 U/mL and <16U/mL for rheumatoid factor and ACPA, respectively. Titre of ACPA positive patient was 25 E/mL, no peripheral synovitis was observed during the study in this patient. There were no patients positive for both ACPA and rheumatoid factor.
[f] The PMR-AS is calculated as follows: CRP (mg/dL) + (morning stiffness [in minutes] * 0.1) + elevation of upper limbs (ranging 0-3) + VAS for pain (ranging 0-10) + VAS physician's global (ranging 0-10).
[g] In prednisolone dose equivalent.

The secondary outcomes showed a significantly lower incidence rate of relapse and a faster time to GC-free remission in the methotrexate group. Time to GC-free remission in the methotrexate and placebo groups is shown in Figure 2. There was no significant difference in cumulative GC dose, number of relapsing patients, in PMR-AS, nor in number of adverse events between treatment groups as can be seen in Table 2 and Figures 3 and 4. Additional secondary outcomes, such as inflammatory parameters, HAQ, PASS, PROMIS per time point, are also detailed in appendix S12. Patient reported outcomes, including physical function (PROMIS-PF, HAQ), quality of life (EQ-5D-5L) and PASS, improved from baseline to week 52 in both groups. Descriptively, improvements in PROMIS-PF, HAQ, and PASS appeared somewhat greater in the methotrexate group, whereas EQ-5D-5L scores were largely comparable between groups. A tendency towards more patients having an adverse event ≥grade 2 was mainly caused by slightly elevated liver enzymes. In 8 patients dose adjustment was necessary due to adverse events, all of these patients were in the intervention group. Finally, there were no significant differences in safety related outcomes. Three serious adverse events occurred in the placebo group, consisting of a pulmonary embolism, ischaemic cerebrovascular event, and right humeral fracture. One serious adverse event occurred in the methotrexate group, consisting of a suspected methotrexate pneumonitis. Adverse events were graded according to CTCAE version 5.0 and are further elaborated upon in appendix S13 [25].

DISCUSSION

In this double-blind randomised, placebo-controlled trial, methotrexate showed a significant and clinically relevant effect in achieving GC-free disease remission in patients with recently diagnosed PMR. Patients who received methotrexate also had a significantly lower incidence rate of relapse and a faster time to GC-free remission. A significant GC-sparing effect was not observed in our trial, but may become evident with longer follow-up. Combined with pre-existing evidence, our results support the hypothesis that early introduction of methotrexate may be beneficial in PMR.

Earlier studies of methotrexate in PMR were conducted according to the research standards of that time and used relatively low doses of methotrexate. In this study, we used a comprehensive methodology, including a triple-blind design, preregistration and a higher dosage of methotrexate (comparable to the dose in patients with RA). The study by Caporali et al had a comparable study design except for the methotrexate dose, which was lower [8]. They also found a high percentage of GC-free patients after 76 weeks, with a similar risk difference of 34 % (95% CI: 11%-53%) between placebo and methotrexate as in this study. The follow-up however was longer and a cumulative GC-sparing effect could be demonstrated, leading to the hypothesis that extended monitoring is needed to answer the question whether a higher dose of methotrexate has a more profound GC-sparing effect. Notably, a substantial proportion (around ~32%) of patients in that trial presented with peripheral arthritis, possibly reflecting a PMR-RA overlap phenotype that may be more responsive to methotrexate, which could limit generalisability to a strict PMR population.

In our trial, the 52-week observation period, combined with a 24-week protocolised tapering regimen, may have been too short to detect between-group differences in cumulative GC exposure. Cumulative GC dose in the first year is largely determined by the initial higher dose phase, and the effects of methotrexate on GC use are revealed only later on during the study (as shown in Fig 3) when methotrexate is more likely to enable GC tapering and discontinuation without flare, resulting in a difference in GC-free remission at 52 weeks. This presumably means that the between-group difference in cumulative GC dose will continue to grow after 52 weeks, as more patients in the placebo group are still using GC at that time. Long-term follow-up of this trial is ongoing to evaluate whether a GC-sparing effect becomes evident over time. At the same time, it remains possible that methotrexate has only limited GC-sparing potential, particularly in comparison to IL-6 inhibitors, which have shown differences in cumulative GC dose within 1 year [28–30]. However, direct comparisons between GC-sparing agents are complicated by varying GC-tapering schemes and inclusion criteria.

These recent trials with IL-6 inhibitors, such as tocilizumab and sarilumab, have demonstrated efficacy in PMR, leading to approval by both the U.S. Food and Drug Administration (2023) and the European Medicines Agency (2024) of sarilumab for the treatment of refractory PMR [28–31]. Notably, although current ACR/EULAR guidelines recommend methotrexate as the first option GC-sparing treatment, these recommendations

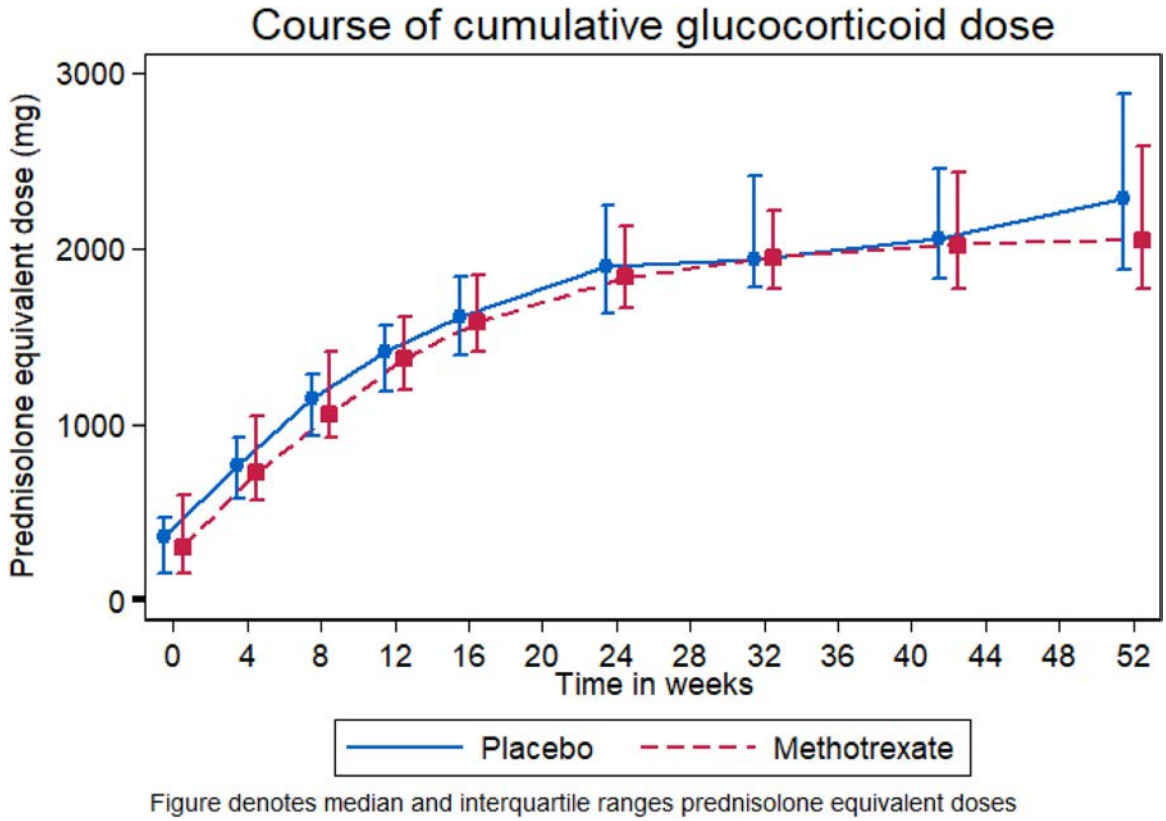

Figure 2. Cumulative glucocorticoid dose during the trial. In blue placebo and in red methotrexate. Lines display median cumulative glucocorticoid dose and bars display IQRs.

predate the IL-6 inhibitor studies. To define the relative position of methotrexate within the evolving treatment landscape, comparative studies between methotrexate and IL-6 inhibitors are needed. Future studies may extend this to other immunomodulatory drugs emerging for PMR.

The GC taper schedule used in this study can be debated, since it was faster than that commonly used in usual care. This may have caused relapses that would not have occurred in usual care. However, due to the close monitoring of patients, relapses were quickly recognised and subsequent increase in GC dose

Table 2
Primary and secondary outcomes for methotrexate vs placebo treatment

Outcome	Methotrexate (n = 30)	Placebo (n = 28)	Effect estimate	*P* value
GC free and remission week 52, n (%)[a]	24 (80%)	13 (46%)	34% (14%)[b]	.0042
Risk ratio			1.7 (1.2)[c]	
GC free and remission week 32, n (%)[a]	13 (46%)[d]	9 (33%)[e]	1.5 (0.79-2.98)[f]	.21
GC dose ≤5 mg week 52, n (%)	29 (97%)	22 (81%)[e]	1.2 (0.97-1.42)[f]	.084
GC dose ≤5 mg week 32, n (%)	27 (90%)	20 (74%)[e]	1.2 (0.93-1.56)[f]	.15
Median time to GC-free remission, week (95% CI)	28 (24-33)	39 (28-∞)	–	.013
Patients with ≥1 relapse wk 0-32, n (%)	18 (60%)	22 (81%)[e]	0.76 (0.55-1.05)[f]	.10
Patients with ≥1 relapse wk 0-52, n (%)	18 (60%)	22 (81%)[e]	0.76 (0.55-1.05)[f]	.10
Total number of relapses wk 0-52, n	31	45[e]	0.62 (0.39-0.99)[g]	.046
Patients with adverse event grade ≥2, n (%)	22 (73%)	15 (56%)	1.38 (0.95-2.01)[f]	.090
Total number of (any) adverse events	260[h]	240[i]	0.97 (0.82-1.16)[g]	.78
Total number of adverse events grade ≥2, n	46	42	1.03 (0.68-1.58)[g]	.86
Cumulative GC dose week 0-32 (mg)	1950 (1770-2218)	1940 (1783-2415)[e]	–	.65
Cumulative GC dose week 0-52 (mg)	2050 (1770-2583)	2288 (1880-2878)[e]	–	.17
Methotrexate/placebo dose adjustment, number of patients (%)	8 (27%)	0 (0%)	Not estimable[f]	
Methotrexate/placebo discontinued prematurely, n (%)	6 (20%)	7 (25%)	0.80 (0.30-2.15)[f]	

CRP, C-reactive protein; GC, glucocorticoid; PMR-AS, Polymyalgia Rheumatica Activity Score; VAS, visual analogue scale.
For continuous outcomes, medians (IQRs) are reported.
[a] Remission is based on the PMR-AS, which is calculated by CRP (mg/dL) + (morning stiffness (in minutes) * 0.1) + elevation of upper limbs (ranging 0-3) + VAS for pain (ranging 0-10) + VAS physician's global (ranging 0-10). A PMR-AS < 10 was considered in remission.
[b] Risk difference and 1-sided 95% CI.
[c] Risk ratio and 1-sided 95% CI.
[d] 2 missing.
[e] 1 missing.
[f] Risk ratio and 2-sided 95% CI.
[g] Incidence rate ratio and 2-sided 95% CI.
[h] From which 3 serious adverse events (pulmonary embolism, ischaemic cerebrovascular event, and right humeral fracture).
[i] From which 1 serious adverse event (suspected methotrexate pneumonitis).

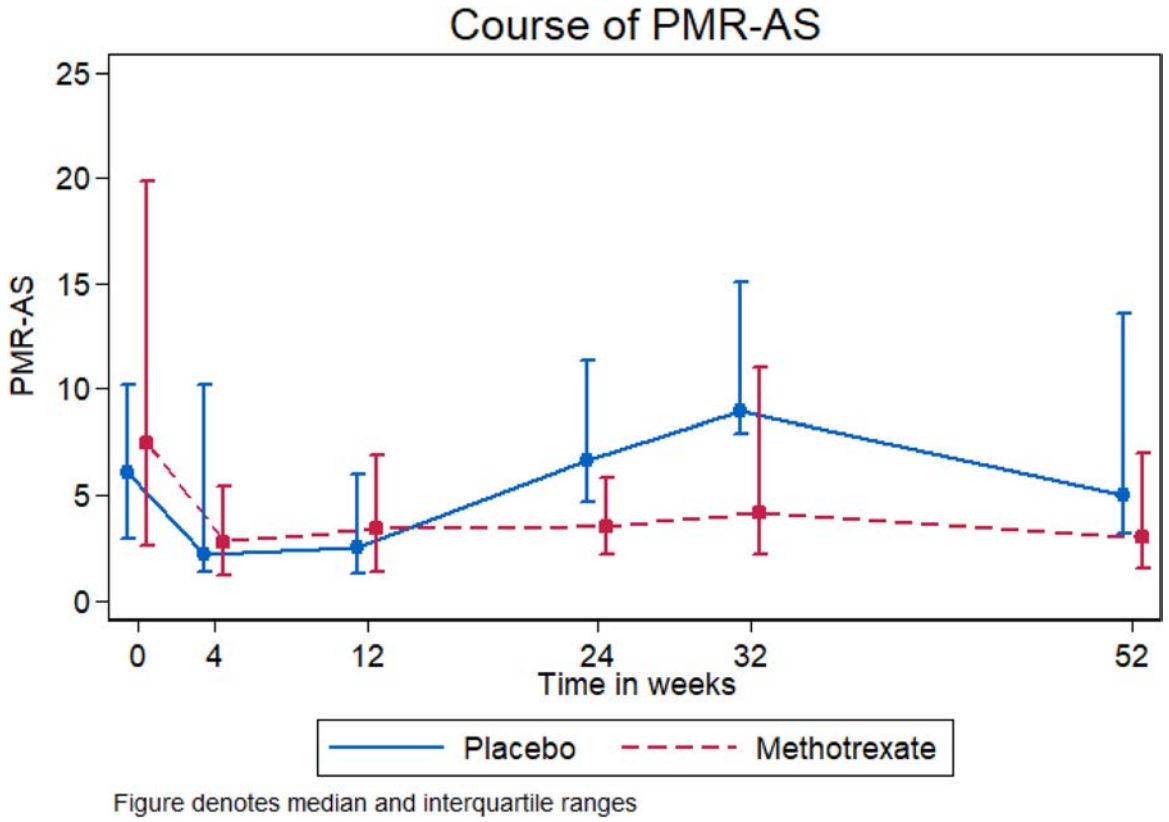

Figure 3. Disease activity during the trial. In blue placebo and in red methotrexate. Lines display median PMR-AS scores and bars display IQRs. PMR-AS, Polymyalgia Rheumatica Activity Score.

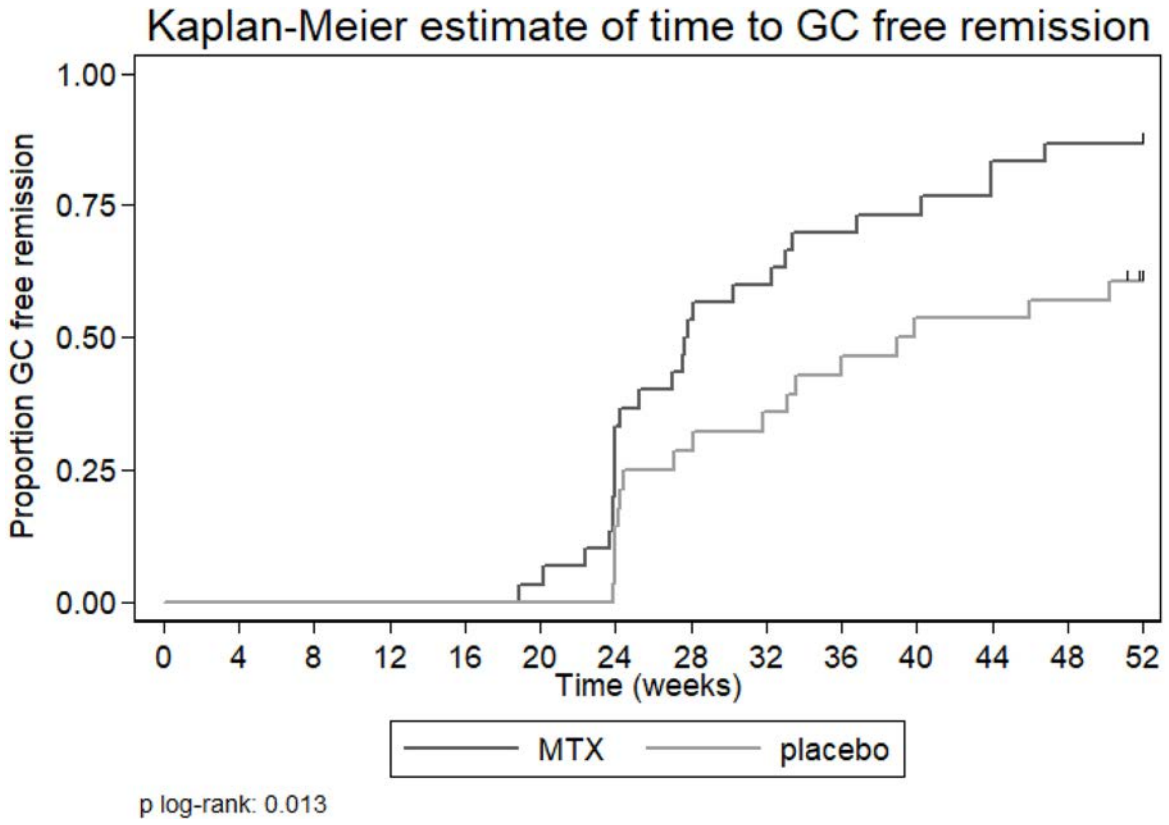

Figure 4. Kaplan-Meier estimate of time to GC-free remission in MTX vs placebo. In grey placebo and in black methotrexate. GC, glucocorticoid; MTX, methotrexate.

helped secure low disease activity as can be seen in the PMR-AS course over the 52 weeks, indicating no signs of substantial undertreatment. Another aspect regarding generalisability is our choice to include patients with newly diagnosed PMR in this trial. This choice was made to investigate the effects of early introduction of methotrexate (in line with the EULAR guidelines), but limits generalisability to patients with relapsing PMR.

However, there are limitations in this trial that require consideration. First, the anticipated sample size was unfortunately not met. However, although power was lower than intended, the larger-than-expected differences between the treatment arms still allowed significant differences to be detected. Second, 5 of the 6 dropouts occurred in the placebo group, including 3 with alternative diagnoses, suggesting that undiagnosed RA masked by methotrexate use could possibly contribute to an overestimation of the true effect. However, even when assuming a comparable number of dropouts would have occurred in the methotrexate group due to alternative diagnoses, the proportion of patients in GC-free remission would still remain higher in the methotrexate group compared with placebo (21/30 = 70% in the methotrexate group vs 13/28 = 46% in the placebo group), indicating that the observed difference is unlikely to be explained by differential dropout. Third, there are currently no validated criteria for defining relapse or remission in PMR, which may introduce variability and bias in outcome assessments [32]. However, this would bias between-group difference estimates towards 0 which is less worrisome given we still found significant differences in both the number of relapse and the proportion in GC-free remission. However, the lack of these criteria does complicate the comparison of results across studies. Lastly, due to the COVID-19 pandemic, a proportion of visits was performed digitally, which may have resulted in less precise measurements. During telephone consultations, the elevation upper limb score (a component of the PMR-AS) was assessed by patient report rather than direct observation, which may have introduced measurement variability at those visits. However, the outcomes at 32 and 52 weeks were uniformly assessed through in-person visits. Also, due to the study design, this is not expected to have resulted in biased difference estimates of outcomes between both groups.

Interestingly, in addition to the efficacy of methotrexate, patients in our placebo group tapered off prednisolone relatively well compared with patients with PMR in clinical practice. A recent systematic review showed that in clinical practice, on average, only 23% of patients with PMR are off of GC after 1 year of treatment [33]. In our trial, 46% of the placebo group were in GC-free remission after 1 year, despite following a faster initial tapering regime compared with standard care. This shows that faster GC tapering is possible in the right circumstances. One explanation for this finding could be the intensive tapering (potentially resulting in increased relapse percentage), tailored guidance, and monitoring provided to patients in our trial during GC tapering may have allowed tapering early enough to prevent prolonged GC use and associated GC-dependency. In addition, current guidelines recommend a tapering of at least 1 year in clinical practice, which by definition may prevent patients from achieving GC-free remission within this timeframe and may cause GC-dependency. Finally, the COVID-19 pandemic might have motivated patients extra to proceed with tapering to stop. However, our data might indicate that the initial GC tapering could potentially be accelerated, though a tapering protocol shorter than 24 weeks may not be optimal based on earlier trials [34].

In conclusion, this RCT showed a significant effect of methotrexate on reaching GC-free remission at 52 weeks in patients with recently diagnosed PMR. Additional research is needed to determine whether distinct patient subgroups with differential treatment response exist, and if so, to identify those most likely to benefit from early initiation of methotrexate, particularly in relation to risk of prolonged GC treatment. Moreover, studies are warranted to determine the optimal timing of methotrexate initiation, as well as how it can be best combined with tailored GC-tapering strategies. Given the outcomes in our placebo group, with a substantially shorter GC-tapering regimen than the recommended 9 to 12 months by the ACR/EULAR recommendations, further studies comparing different GC-tapering regimens could possibly help optimise long-term outcomes. Finally, comparative studies with other immunomodulatory agents (especially IL-6 inhibitors, JAK inhibitors, and rituximab) are needed to further clarify the position of methotrexate within the evolving treatment landscape in PMR.

Competing interests

All authors have completed the Unified Competing Interest form (available on request from the corresponding author) and declare: the Sint Maartenskliniek received a grant from the Dutch Arthritis Association (ReumaNederland) for the current study. No authors had financial relationships with any organisations that might have an interest in the submitted work in the previous 3 years. AAdB has received grants to the institution for quality-of-care projects and research outside the current study from AbbVie, Alfasigma, UCB, Galapagos, Pfizer, Novartis, Lilly, Sanofi, Gilead, and Celltrion. AvdM received travel and conference reimbursement from AbbVie in 2025.

Acknowledgements

We thank the investigators, research staff, health care providers, and especially the patients who participated in the PMR-MODE study. Results of this study were previously presented at ACR Convergence 2024 and EULAR Congress 2025.

Contributors

TEB contributed to the study design, study conduct, data collection, data analysis, data interpretation, drafting of figures and tables, and writing of the manuscript. NESEPK contributed to the study conduct, data collection, data analysis, data interpretation, drafting of figures and tables, and writing of the manuscript. GFS contributed to the study conduct, data collection, and writing of the manuscript. DEM contributed to the study design and writing of the manuscript. AAdB contributed to study design, data collection, data interpretation, and writing of the manuscript. NdB contributed to study design, data analysis, drafting of figures and tables, data interpretation, and writing of the manuscript. AvdM was principal investigator of this study and contributed to study design, data collection, study conduct, data interpretation, and writing of the manuscript. AvdM, as guarantor, accepts full responsibility for the work and the conduct of the study, had access to the data, and controlled the decision to publish. The corresponding author attests that all listed authors meet authorship criteria and that no others meeting the criteria have been omitted. All authors had full access to all the data in the study and had final responsibility for the decision to submit for publication.

Funding

This project was funded by Dutch Arthritis Association project 18-2-401. Dutch trial register NL-OMON22681, EudraCT 2019-002413-18.

Patient consent for publication

Not applicable.

Ethics approval

Medical ethical approval was obtained (NL69979.091.19; November 26, 2019), and the trial was registered in the Dutch trial registry (originally as NL8366 and later NL-OMON22681). All participants signed informed consent.

Provenance and peer review

Not commissioned; externally peer reviewed.

Supplementary materials

Supplementary material associated with this article can be found in the online version at doi:10.1016/j.ard.2025.11.025.

Orcid

Thomas E. Bolhuis: http://orcid.org/0000-0003-3911-3515
Noortje E.S.E.P. Kooijman: http://orcid.org/0000-0001-9125-1187
Diane E. Marsman: http://orcid.org/0000-0002-3103-1374
Gijs F. Snijders: http://orcid.org/0000-0002-2549-2713
Alfons A. den Broeder: http://orcid.org/0000-0002-9012-4079
Nathan den Broeder: http://orcid.org/0000-0001-7126-2209
Aatke van der Maas: http://orcid.org/0000-0002-3855-6763

REFERENCES

[1] Espígol-Frigolé G, Dejaco C, Mackie SL, Salvarani C, Matteson EL, Cid MC. Polymyalgia rheumatica. Lancet. 2023;402(10411):1459–72.
[2] Dejaco C, Singh YP, Perel P, Hutchings A, Camellino D, Mackie S, et al. 2015 recommendations for the management of polymyalgia rheumatica: a European League Against Rheumatism/American College of Rheumatology collaborative initiative. Ann Rheum Dis 2015;74(10):1799–807.
[3] Caporali R, Cimmino MA, Montecucco C, Cutolo M. Glucocorticoid treatment of polymyalgia rheumatica. Clin Exp Rheumatol 2011;29(5 suppl 68): S143–7.
[4] Partington RJ, Muller S, Helliwell T, Mallen CD, Abdul Sultan A. Incidence, prevalence and treatment burden of polymyalgia rheumatica in the UK over two decades: a population-based study. Ann Rheum Dis 2018;77(12):1750–6.
[5] Boers M, Hartman L, Opris-Belinski D, Bos R, Kok MR, Da Silva JA, et al. Low dose, add-on prednisolone in patients with rheumatoid arthritis aged 65+: the pragmatic randomised, double-blind placebo-controlled GLORIA trial. Ann Rheum Dis 2022;81(7):925–36.
[6] Kawka L, Chevet B, Arnaud L, Becker G, Carvajal Alegria G, Felten R. The pipeline of immunomodulatory therapies in polymyalgia rheumatica and giant cell arteritis: a systematic review of clinical trials. Autoimmun Rev 2024;23(7-8):103590.
[7] Albrecht K, Huscher D, Buttgereit F, Aringer M, Hoese G, Ochs W, et al. Long-term glucocorticoid treatment in patients with polymyalgia rheumatica, giant cell arteritis, or both diseases: results from a national rheumatology database. Rheumatol Int 2018;38(4):569–77.
[8] Caporali R, Cimmino MA, Ferraccioli G, Gerli R, Klersy C, Salvarani C, et al. Prednisone plus methotrexate for polymyalgia rheumatica: a randomized, double-blind, placebo-controlled trial. Ann Intern Med 2004;141(7):493–500.
[9] Ferraccioli G, Salaffi F, De Vita S, Casatta L, Bartoli E. Methotrexate in polymyalgia rheumatica: preliminary results of an open, randomized study. J Rheumatol 1996;23(4):624–8.
[10] van der Veen MJ, Dinant HJ, van Booma-Frankfort C, van Albada-Kuipers GA, Bijlsma JW. Can methotrexate be used as a steroid sparing agent in the treatment of polymyalgia rheumatica and giant cell arteritis? Ann Rheum Dis 1996;55(4):218–23.
[11] Feinberg HL, Sherman JD, Schrepferman CG, Dietzen CJ, Feinberg GD. The use of methotrexate in polymyalgia rheumatica. J Rheumatol 1996;23 (9):1550–2.
[12] Marsman D, Bolhuis T, Broeder ND, van den Hoogen F, den Broeder A, van der Maas A. Effect of add-on methotrexate in polymyalgia rheumatica patients flaring on glucocorticoids tapering: a retrospective study. Rheumatol Int 2021;41(3):611–6.
[13] Quartuccio L, Gregoraci G, Isola M, De Vita S. Retrospective analysis of the usefulness of a protocol with high-dose methotrexate in polymyalgia rheumatica: results of a single-center cohort of 100 patients. Geriatr Gerontol Int 2018;18(9):1410–4.
[14] Ruediger C, Nguyen L, Black R, Proudman S, Hill C. Efficacy of methotrexate in polymyalgia rheumatica in routine rheumatology clinical care. Intern Med J 2020;50(9):1067–72.
[15] de la Torre ML, Rodríguez AM, Pisoni CN. Usefulness of methotrexate in the reduction of relapses and recurrences in polymyalgia rheumatica: an observational study. J Clin Rheumatol 2020;26(7S suppl 2):S213–7.
[16] Smolen JS, Landewé R, Bijlsma J, Burmester G, Chatzidionysiou K, Dougados M, et al. EULAR recommendations for the management of rheumatoid arthritis with synthetic and biological disease-modifying antirheumatic drugs: 2016 update. Ann Rheum Dis 2017;76(6):960–77.
[17] Marsman DE, Bolhuis TE, den Broeder N, den Broeder AA, van der Maas A. PolyMyalgia rheumatica treatment with methotrexate in optimal dose in an early disease phase (PMR MODE): study protocol for a multicenter double-blind placebo controlled trial. Trials 2022;23(1):318.
[18] Moher D, Hopewell S, Schulz KF, Montori V, Gøtzsche PC, Devereaux PJ, et al. CONSORT 2010 explanation and elaboration: updated guidelines for reporting parallel group randomised trials. J Clin Epidemiol 2010;63(8):e1–37.
[19] Dasgupta B, Cimmino MA, Kremers HM, Schmidt WA, Schirmer M, Salvarani C, et al. 2012 provisional classification criteria for polymyalgia rheumatica: a European League Against Rheumatism/American College of Rheumatology collaborative initiative. Arthritis Rheum 2012;64 (4):943–54.
[20] van Ede AE, Laan RF, Rood MJ, Huizinga TW, van de Laar MA, van Denderen CJ, et al. Effect of folic or folinic acid supplementation on the toxicity and efficacy of methotrexate in rheumatoid arthritis: a forty-eight week, multicenter, randomized, double-blind, placebo-controlled study. Arthritis Rheum 2001;44(7):1515–24.
[21] Binard A, De Bandt M, Berthelot JM, Saraux A, Inflammatory Joint Disease Working Group CRI of the French Society for Rheumatology. Usefulness of the disease activity scores for polymyalgia rheumatica for predicting glucocorticoid dose changes: a study of 243 scenarios. Arthritis Rheum 2007;57 (3):481–6.
[22] Binard A, Lefebvre B, De Bandt M, Berthelot JM, Saraux A, Club "Rhumatismes et Inflammation". Validity of the polymyalgia rheumatica activity score in primary care practice. Ann Rheum Dis 2009;68(4):541–5.
[23] Leeb BF, Bird HA. A disease activity score for polymyalgia rheumatica. Ann Rheum Dis 2004;63(10):1279–83.
[24] Leeb BF, Rintelen B, Sautner J, Fassl C, Bird HA. The polymyalgia rheumatica activity score in daily use: proposal for a definition of remission. Arthritis Rheum 2007;57(5):810–5.
[25] US Department of Health and Human Services NIoH NCI. Common Terminology Criteria for Adverse Events (CTCAE) version 5.0. 2017. p.p 3462-3465 https://dctd.cancer.gov/research/ctep-trials/for-sites/adverse-events/ctcae-v5-5x7.pdf (Accessed July 22, 2025).
[26] Bolhuis T, Kooijman N, Marsman D, Snijders G, den Broeder A, den Broeder N, et al. Results of a one year randomized double-blind placebo-controlled trial with methotrexate 25 mg per week for recently diagnosed polymyalgia rheumatica. Arthritis Rheumatol 2024;76(suppl 9).
[27] Bolhuis TE, Kooijman N, Marsman D, Snijders GF, den Broeder AA, den Broeder N, et al. OP0064 randomized double-blind placebo-controlled trial of methotrexate 25mg weekly in newly diagnosed polymyalgia rheumatica. Ann Rheum Dis 2025;84:56–7.
[28] Bonelli M, Radner H, Kerschbaumer A, Mrak D, Durechova M, Stieger J, et al. Tocilizumab in patients with new onset polymyalgia rheumatica (PMR-SPARE): a phase 2/3 randomised controlled trial. Ann Rheum Dis 2022;81 (6):838–44.
[29] Devauchelle-Pensec V, Carvajal-Alegria G, Dernis E, Richez C, Truchetet ME, Wendling D, et al. Effect of tocilizumab on disease activity in patients with

active polymyalgia rheumatica receiving glucocorticoid therapy: a randomized clinical trial. JAMA 2022;328(11):1053–62.
[30] Spiera RF, Unizony S, Warrington KJ, Sloane J, Giannelou A, Nivens MC, et al. Sarilumab for relapse of polymyalgia rheumatica during glucocorticoid taper. N Engl J Med 2023;389(14):1263–72.
[31] Toussirot É, Martin A, Soubrier M, Rédeker S, Regent A. Rapid and sustained response to tocilizumab in patients with polymyalgia rheumatica resistant or intolerant to glucocorticoids: a multicenter open-label study. J Rheumatol 2016;43(1):249–50.
[32] Bolhuis TE, Bosch P, Falzon L, Owen CE, Yates M, Mackie SL, et al. Definitions of and instruments for disease activity, remission and relapse in polymyalgia rheumatica: a systematic literature review. Rheumatology (Oxford) 2025;64(2):455–69.
[33] Floris A, Piga M, Chessa E, Congia M, Erre GL, Angioni MM, et al. Long-term glucocorticoid treatment and high relapse rate remain unresolved issues in the real-life management of polymyalgia rheumatica: a systematic literature review and meta-analysis. Clin Rheumatol 2022;41(1):19–31.
[34] Marsman DE, den Broeder N, van den Hoogen FHJ, den Broeder AA, van der Maas A. Efficacy of rituximab in patients with polymyalgia rheumatica: a double-blind, randomised, placebo-controlled, proof-of-concept trial. Lancet Rheumatol 2021;3(11):e758–66.

Ann Rheum Dis 85 (2026) 771–772

Contents lists available at ScienceDirect

Annals of the Rheumatic Diseases

journal homepage: https://www.sciencedirect.com/journal/annals-of-the-rheumatic-diseases

Images in rheumatology

Asymmetric hand deformities with limited mobility

Yi Yang[1], Xiaoqin Yuan[1], Shanshan Zhang[1], Qian Luo[1], Yufeng Tang[1,*]

[1] *Department of Neurology, Mianyang Central Hospital, University of Electronic Science and Technology of China, Mianyang, China*

ARTICLE INFO

Article history:
Received 19 July 2025
Received in revised form 28 July 2025
Accepted 29 July 2025

ABSTRACT

A 52-year-old woman presented to the rheumatology department with a 6-year history of progressively limited hand mobility, bilateral joint pain, and worsening hand deformities. Examination revealed asymmetric deformities of both hands, more pronounced on the left (Fig, A), without joint tenderness, swelling, or Heberden's and Bouchard's nodes. Laboratory tests, including C-reactive protein, rheumatoid factor, anticyclic citrullinated peptide antibody, antinuclear antibody, antidouble-stranded DNA antibody, and anti-Smith antibody, revealed no abnormalities. Hand X-rays showed no evidence of inflammatory arthritis. Treatment with nonsteroidal anti-inflammatory drugs and corticosteroids was ineffective. She was referred to the neurology clinic, where neurological examination revealed bradykinesia and increased muscle tone in all 4 limbs, especially the left upper limb, without tremor or postural instability. Brain and cervical spine magnetic resonance imaging were unremarkable. Fluorine-18-L-dihydroxyphenylalanine (^{18}F-DOPA) positron emission tomography/computed tomography showed decreased dopamine metabolism in the bilateral striatum, which was more pronounced on the right (Fig, B). A diagnosis of striatal hand deformities (SHD) was made, and her symptoms improved with levodopa.

SHD, typically seen in advanced Parkinson disease, can present in early stages and is often misdiagnosed as rheumatoid arthritis, osteoarthritis, psoriatic arthritis, Dupuytren contracture, or other rheumatologic or orthopaedic conditions, especially when resting tremor, rigidity, or bradykinesia are absent [1]. It is characterised by flexion of the metacarpophalangeal joints, with or without hyperextension of the proximal interphalangeal joints; some patients may also show swan neck and Z-thumb deformities, finger cleft-ing, and abduction of the little finger [2]. The exact pathogenesis remains unclear, but striatal lesions causing rigidity and/or dystonia may underlie the condition. Levodopa is the first-line treatment, though some patients may benefit from botulinum toxin injections or subthalamic nucleus deep-brain stimulation [3]. SHD often begins unilaterally and progresses to asymmetric deformities with limited hand mobility, and the absence of clinical inflammatory findings helps distinguish it from other conditions.

*Correspondence to Dr Yufeng Tang, Department of Neurology, Mianyang Central Hospital, University of Electronic Science and Technology of China, Mianyang 621000, China.

E-mail address: dryufeng@126.com (Y. Tang).

Handling editor Josef S. Smolen.

https://doi.org/10.1016/j.ard.2025.07.025

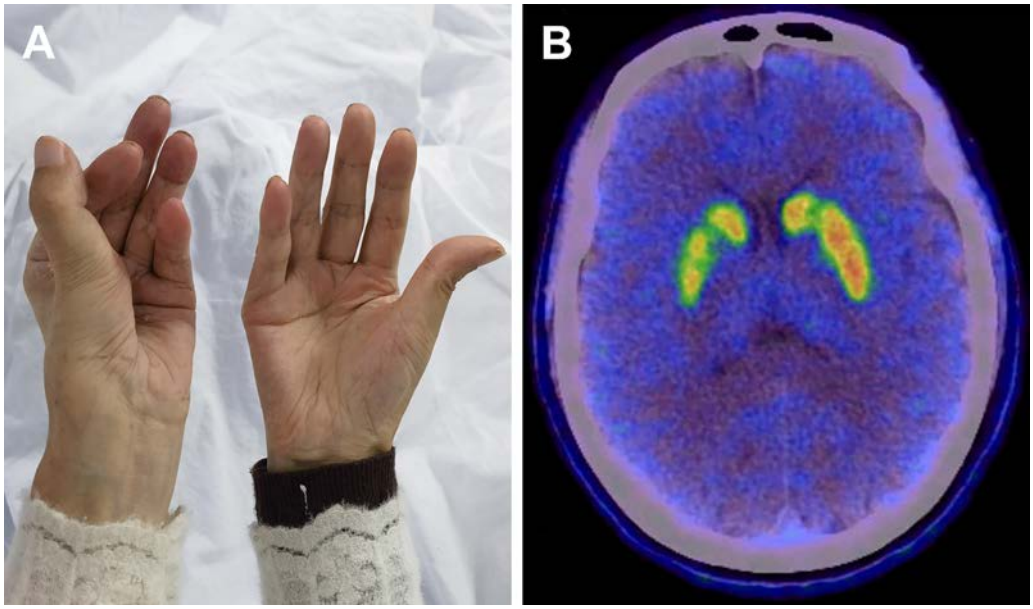

Figure. Striatal hand deformities in Parkinson disease. (A) Flexion of the left metacarpophalangeal joints, extension of the proximal interphalangeal joints, partial flexion of the distal interphalangeal joints, and flexion of the right metacarpophalangeal joints were observed. (B) ^{18}F-DOPA positron emission tomography/computed tomography showed reduced dopamine uptake in the bilateral striatum, which was more pronounced on the right. ^{18}F-DOPA, Fluorine-18-L-dihydroxyphenylalanine.

Competing interests

None.

CRediT authorship contribution statement

Yi Yang: Writing – original draft, Data curation, Conceptualization. **Xiaoqin Yuan:** Data curation. **Shanshan Zhang:** Resources, Formal analysis. **Qian Luo:** Resources, Investigation. **Yufeng Tang:** Writing – review & editing, Validation, Supervision.

Acknowledgements

We thank the patient for giving her consent for this publication.

Funding

None.

Patient consent for publication

Consent was obtained directly from the patient.

Ethics approval

This case report is exempt from formal ethics review. The patient had access to the manuscript and gave her written consent for the publication of images and/or information.

Provenance and peer review

Not commissioned; externally peer reviewed.

Data availability statement

All data underlying the results are available as part of the article and no additional source data are required.

Supplementary materials

Supplementary material associated with this article can be found in the online version at doi:10.1016/j.ard.2025.07.025.

Orcid

Yi Yang: http://orcid.org/0000-0002-8660-3501

REFERENCES

[1] Ashour R, Tintner R, Jankovic J. Striatal deformities of the hand and foot in Parkinson's disease. Lancet Neurol 2005;4(7):423–31.
[2] Brogren E, Dahlin LB, Franzen E, Lindholm B. Striatal hand deformities in Parkinson's disease: hand surgical perspectives. Mov Disord Clin Pract 2022;9(8):1047–54.
[3] Wijemanne S, Jankovic J. Hand, foot, and spine deformities in Parkinsonian disorders. J Neural Transm (Vienna) 2019;126(3):253–64.

Ann Rheum Dis 85 (2026) 773–774

Contents lists available at ScienceDirect

Annals of the Rheumatic Diseases

journal homepage: https://www.sciencedirect.com/journal/annals-of-the-rheumatic-diseases

Images in rheumatology

High-resolution imaging of giant cell arteritis with photon-counting computed tomography

Pranjal Rai[1,*], Norbert G. Campeau[1], Nikkole M. Weber[1], Matthew J. Koster[2], Kenneth J. Warrington[2], Girish Bathla[1]

[1] *Department of Radiology, Mayo Clinic, Rochester, Minnesota, USA*
[2] *Department of Rheumatology, Mayo Clinic, Rochester, Minnesota, USA*

A 77-year-old man presented with 5 months of headaches, jaw pain, dysphagia, dysphonia, weight loss, gait imbalance, and fatigue after returning from Africa. An initial evaluation for infectious aetiologies was unrevealing. Inflammatory markers were markedly elevated (erythrocyte sedimentation rate [ESR] 89 mm/h; C-reactive protein [CRP] 63.2 mg/L), raising suspicion for an inflammatory pathology. Brain magnetic resonance imaging (MRI) did not reveal any acute intracranial findings, but head computed tomography (CT) angiogram performed on a photon-counting computed tomography (PCCT) scanner showed multifocal narrowing and mural thickening of external and internal carotid artery branches (Fig), raising concern for giant cell arteritis (GCA). Targeted temporal artery ultrasound demonstrated a characteristic halo, and temporal artery biopsy confirmed GCA.

GCA, a systemic large vessel vasculitis, can involve multiple arterial vessels in the head and neck. Ultrasound is increasingly being used as a first-line test for suspected cranial GCA given the wider availability. However, its utility is operator dependent. Additionally, although the temporal and axillary arteries are consistently evaluated, the assessment of maxillary, lingual, and facial arteries is not routinely performed. Temporal artery biopsy sensitivity is also limited by skip lesions [1]. As corticosteroids rapidly suppress imaging findings, early assessment is pivotal. Contrast-enhanced MRI vessel-wall imaging adds complementary value for intracranial and orbital structures [2,3], but neither technique captures the full extent of the disease burden, given the limited assessment of other external carotid artery branches. Fluorine-18–labeled fluorodeoxyglucose positron emission tomography (^{18}F-FDG-PET) can help survey extracranial arterial inflammation. Although its availability is increasing, access and timeliness remain variable across institutions [4]. From a radiologic perspective, our institutional protocol for large vessel vasculitis involves CT angiography from the head through the pelvis to provide a comprehensive vascular survey that can mitigate diagnostic anchoring in nonspecific presentations, define the extent of vasculitis, evaluate for complications, and establish a baseline for longitudinal assessment of treatment response during treatment [5]. PCCT leverages the use of semiconductors which directly convert the x-ray photons into electrical signal. This enables higher spatial resolution (ultrathin slices of ~0.2 mm) and improved contrast, helping depict mural thickening and luminal narrowing of small- to medium-calibre arteries that are suboptimally evaluated by regular CT scanners [6]. By counting photons and minimising noise, it can also achieve potential dose reductions (by ~16%) in head CT angiograms relative to conventional CT [7]. Other advantages include rapid acquisition (whole-body imaging in seconds, compared with MRI examinations that may approach an hour), limited absolute or relative contraindications than MRI, and improved diagnostic confidence in cases where temporal artery involvement may be patchy or negligible. Limitations include its limited availability and high cost, increased data and workflow demands, and potential performance constraints at very high photon flux (pulse pile-up) with occasional novel artifacts [8].

*Correspondence to Dr Pranjal Rai.
E-mail address: raipranjal2@gmail.com (P. Rai).
Handling editor Josef Smolen.

https://doi.org/10.1016/j.ard.2025.12.017
Received 24 November 2025; Revised 15 December 2025; Accepted 29 December 2025

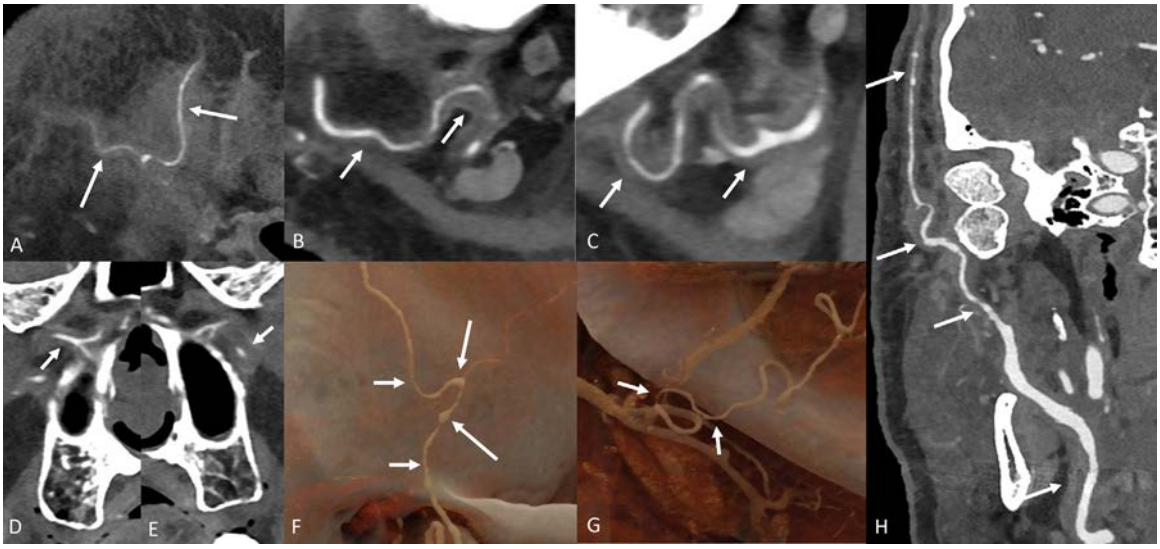

Figure. Sagittal (A-C) and coronal (D-E) multiplanar reformats from photon-counting CT angiogram source images show wall thickening and fat stranding (arrows) involving the right superficial temporal (A), bilateral facial (B, C), and maxillary arteries (D, E). Volume rendered images (F, G) show areas of luminal narrowing (short arrows) and pseudoaneurysms (long arrows) along the right STA (F) and right facial artery (G). Curved MPR (H) shows extensive involvement along the right ECA extending till the frontal branch of right STA (arrows).*ECA*, external carotid artery; *MPR*, multiplanar reconstruction; *STA*, superficial temporal artery.

Funding

None.

Competing interests

All authors declare they have no competing interests.

CRediT authorship contribution statement

Pranjal Rai: Writing – original draft, Software, Methodology, Conceptualization. **Norbert G. Campeau:** Writing – original draft, Data curation, Conceptualization. **Nikkole M. Weber:** Writing – review & editing, Visualization, Project administration. **Matthew J. Koster:** Writing – review & editing, Supervision, Investigation. **Kenneth J. Warrington:** Writing – review & editing, Investigation, Conceptualization. **Girish Bathla:** Writing – review & editing, Visualization, Supervision, Software.

Patient consent for publication

Not applicable.

Ethics approval

Not applicable.

Provenance and peer review

Not commissioned; externally peer reviewed.

Orcid

Pranjal Rai: http://orcid.org/0009-0008-3796-8273

REFERENCES

[1] Ponte C, Grayson PC, Robson JC, et al. 2022 American College of Rheumatology/EULAR classification criteria for giant cell arteritis. Ann Rheum Dis 2022;81(12):1647–53.
[2] Rai P, Soni N, Gopikonda SS, et al. Unilateral primary angiitis of the central nervous system: a rare and under-recognized entity. Am J Neuroradiol 2025 ajnr.A8970.
[3] Rai P, Bathla G. Multimodality imaging of giant cell arteritis. J Clin Neurosci 2025;142:111687.
[4] Prieto-Peña D, Castañeda S, Martínez-Rodríguez I, Atienza-Mateo B, Blanco R, González-Gay MA. Imaging tests in the early diagnosis of giant cell arteritis. J Clin Med 2021;10(16):3704.
[5] Stewart C, Asif RH, Dakkak T, Singh H, Javaid MA, Patel N. Diagnostic dilemmas in giant cell arteritis: overcoming anchoring bias. Case Rep Rheumatol 2025;2025:6632374.
[6] Shibata S, Urano M, Kitera N, et al. Giant-cell arteritis on photon-counting detector CT: a case report. Radiol Case Rep 2024;19(11):4721–4.
[7] Madhavan AA, Bathla G, Benson JC, Diehn FE, Nagelschneider AA, Lehman VT. High yield clinical applications for photon counting CT in neurovascular imaging. Br J Radiol 2024;97(1157):894–901.
[8] Diehn FE, Zhou Z, Thorne JE, et al. High-resolution head CTA: a prospective patient study comparing image quality of photon-counting detector CT and energy-integrating detector CT. AJNR Am J Neuroradiol 2024;45(10):1441–9.

Ann Rheum Dis 85 (2026) 775–777

Contents lists available at ScienceDirect

Annals of the Rheumatic Diseases

journal homepage: https://www.sciencedirect.com/journal/annals-of-the-rheumatic-diseases

Letter

Low-dose interleukin-2 in the treatment of refractory relapsing polychondritis

Relapsing polychondritis (RP) is a rare systemic disease characterised by recurrent inflammation and destruction of the cartilage followed by degeneration and deformation with poor prognosis [1,2]. Optimal treatment approaches for RP are still challenging. The disturbances of regulatory T cell (Treg) homeostasis are believed to play a crucial role in the pathogenesis of RP [3]. Low-dose interleukin-2 (Ld-IL2) restores Treg imbalance and has emerged as a promising therapy for autoimmune diseases [4]. We here reported the clinical efficacy of Ld-IL2 in patients with RP.

This study was conducted in the Department of Rheumatology and Immunology at Peking University People's Hospital between November 2019 to October 2023. Patients with RP who fulfilled the Michet criteria were recruited, who had an inadequate response to conventional glucocorticoids, immunosuppressants, or biologics treatments. Refractory RP was defined as inadequate disease control after 12 weeks of prior therapy or intolerance for any reason (Table). Ld-IL2 at a dose of 1 million IU was administered subcutaneously once daily for 5 consecutive days every week for 4 cycles and then once a week until week 12. Concomitant therapies included at least 4 weeks of stable background treatment with glucocorticoids at doses < 0.5 mg/kg/d and/or with immunosuppressants. Adjustments in dose or class of background therapy were not permitted except for glucocorticoids. Clinical and laboratory data were assessed every 4 weeks. Written informed consent was obtained from all subjects. Analyses were performed using SPSS version 22.0. *P* values were calculated using the Wilcoxon signed-rank test, and 2-sided $P < .05$ was considered significant.

Key clinical characteristics of the 10 patients with RP enrolled are shown in Table, including patient no. 9 who withdrew at week 4 due to nonmedical reasons. Nine patients completed the 12-week Ld-IL2 treatment period (9 females; median age, 39 years [range, 30-62 years]; median disease duration, 2 years [range, 0.5-4 years]). Relapsing polychondritis disease activity index (RPDAI) was decreased significantly from a median of 9 (range 9-23) at baseline to 0 (range 0-14) at week 12 ($P = .011$) (Fig A), particularly observing complete resolution of ear or nose chondritis in 7 patients. Representative photographs (Fig B) demonstrated the improvement in ear chondritis after 4 weeks of Ld-IL2 treatment. Furthermore, 6 of 9 (66.7%) patients achieved a complete RPDAI response (RPDAI = 0) at week 12. Four patients exhibited tracheobronchial involvement, with significant improvement in thickening of tracheal wall for patient no. 4 after 12 weeks (Fig C). Regarding the other 3 patients with tracheobronchial involvement, symptoms of coughing and expectoration were alleviated; however, no significant improvement in tracheobronchial stenosis was observed. No infections were reported in patients with tracheobronchial chondritis or stenosis during Ld-IL2 treatment. By week 12, 6/8 (75%) corticosteroid-treated patients with prednisone at a dose of 15 (range 10-22.5) mg achieved a ≥25% reduction. A significant increase in the absolute count and proportion of $CD4^+CD25^{hi}CD127^{lo}Foxp3^+$Tregs within CD4+ T cells was observed ($P < .05$), accompanied by a rise in Foxp3+Treg/Tcon ratio (Fig D-F). Ld-IL2 was well tolerated. The most common adverse events were injection-site reactions, requiring no intervention.

This was the first study to explore the effects and safety of Ld-IL2 treatment in patients with RP. We introduce promising evidence on the efficacy of Ld-IL2 in treating RP, a condition with limited therapeutic options.

After 12 weeks of treatment, RPDAI was significantly reduced, particularly with improvements in ear or nose chondritis and also tapering of glucocorticoids in this study, suggesting that the patients' outcomes were primarily attributable to Ld-IL2. Treg cells and Treg/Tcon ratio were significantly increased with Ld-IL2 treatment. Interestingly, no infections were observed in patients with tracheobronchial chondritis or stenosis during Ld-IL2 treatment [5].

Our findings suggest that Ld-IL2 is efficacious and safety for RP. The small sample size and absence of a control group restrict the generalisability of our findings and underscore the preliminary nature of this pilot investigation. Additionally, the open-label design might introduce bias, emphasising the need for caution in interpreting these results. Moreover, mechanistic studies elucidating the precise immunomodulatory pathways by which Ld-IL2 exerts its effects in RP could uncover new therapeutic targets and strategies.

CONTRIBUTORS

XZ had full access to all of the data in the study and takes responsibility for the integrity of the data and the accuracy of the data analysis. XZ, JH, and ZL were involved in concept and design. XZ and BH were involved in acquisition, analysis, or interpretation of data. XZ and RF were involved in drafting of the manuscript. BH, MS, XL, and RF were involved in administrative, technical, or material support. JH and ZL were involved in supervision.

XZ and BH equally contributed to this work.

https://doi.org/10.1016/j.ard.2025.10.005
Received 9 May 2025; Revised 30 September 2025; Accepted 5 October 2025

Table
Clinical characteristics of enrolled patients with RP at baseline

Patient no.	Sex	Age (y)	Disease duration (y)	Organ involvement of RP				Prior therapies[a]	Concomitant IS drugs	Pred dose (mg/d)	RPDAI
				Chondritis (ear or nose)	Arthritis	Ocular	Pulmonary				
1	F	47	2	Present	No history	No history	No history	GC, MTX, CsA	MTX, CsA	10	9
2	F	50	1	Present	No history	No history	History of	MTX	MTX	0	9
3	F	30	3	No history	No history	No history	Present[b]	GC, MMF, TNFi	LEF	15	14
4	F	62	1	Present	No history	History of	Present	GC, MTX	MTX	20	23
5	F	39	3	Present	No history	No history	Present	GC, CYC, tocilizumab	MMF, MTX	15	23
6	F	39	4	Present	No history	Present[c]	No history	GC, MMF, MTX, CsA, TNFi, tocilizumab, JAKi	MMF	22.5	9
7	F	38	2	Present	No history	No history	No history	GC, CYC, FK506, MTX	FK506, MTX	15	9
8	F	38	1	No history	History of	No history	Present	GC, CYC, tocilizumab	CsA	12.5	14
9	F	62	2	History of	Present	History of	No history	GC, CYC	CYC	15	1
10	F	56	0.5	Present	No history	No history	No history	GC	No	25	9

CsA, cyclosporin A; CYC, cyclophosphamide; FK506, tacrolimus; GC, glucocorticoids; IS, immunosuppressant; JAKi, Janus kinase inhibitors; LEF, leflunomide; MMF, mycophenolate mofetil; MTX, methotrexate; pred, prednisone; RP, relapsing polychondritis; RPDAI, Relapsing Polychondritis Disease Activity Index; TNFi, tumour necrosis factor inhibitors.

[a] Prior therapies were considered a failure if undertaken for 12 weeks without adequate disease control or not tolerated by the patient for any reason.

[b] With laryngeal stenosis and hoarseness.

[c] With right viral retinitis.

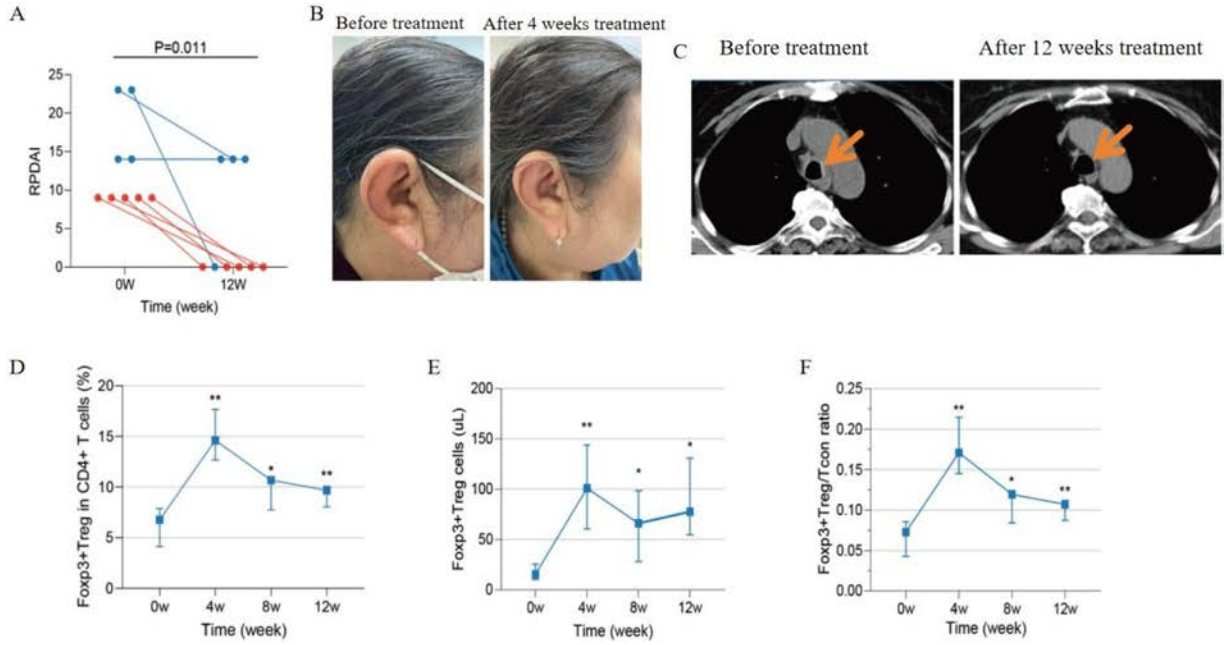

Figure. Clinical improvement and immunological response to Ld-IL2 therapy. (A) Significant decrease in relapsing polychondritis disease activity index (RPDAI) from baseline to week 12. The red circles indicate patients with only chondritis of the ear or nose, with blue circles indicating patients with other manifestations. (B) Representative photographs of patient no. 10 demonstrate improvement in ear chondritis after 4 weeks of treatment with Ld-IL2. (C) Representative photographs of patient no. 4 demonstrate improvement in circumferential thickening of tracheal wall after 12 weeks of treatment with Ld-IL2. (D-F) Changes of the proportion of $CD4^+CD25^{hi}CD127^{lo}Foxp3^+$Tregs within CD4 + T cells (D), $Foxp3^+$Treg absolute count (E) and $Foxp3^+$Treg/Tcon -ratio based on absolute count (F) in peripheral blood of patients with RP after the treatment of Ld-IL2. The conventional T (Tcon) cell population was defined as $CD4^+CD25^{lo}CD127^+$ cells. Data of flow cytometry are shown as median (IQR). $^*P < .05$; $^{**}P < .01$; compared to week 0.

FUNDING

This study was supported by Peking University People's Hospital Research and Development Funds (RDL2022-07), the National Natural Science Foundation of China (82171772, 32141004, 92374202, 82071813), the National Key R&D Program of China (2022YFE0131700 and 2022YFC3602000), and Peking University Clinical Scientist Training Program (BMU2023PYJH020).

Competing interests

All authors declare they have no competing interests.

CRediT authorship contribution statement

Xia Zhang: Writing – review & editing, Writing – original draft, Methodology, Funding acquisition, Formal analysis, Data curation. **Bo Huang:** Project administration, Methodology,

Investigation. **Ruiling Feng:** Writing – review & editing. **Miao Shao:** Resources. **Xue Li:** Resources, Project administration. **Zhanguo Li:** Supervision, Conceptualization. **Jing He:** Supervision, Conceptualization.

Patient consent for publication

Not applicable.

Ethics approval

Peking University People's Hospital Ethics Committee.

Provenance and peer review

Not commissioned; internally peer reviewed.

Orcid

Jing He: http://orcid.org/0000-0003-3904-8928

REFERENCES

[1] Mertz P, Sparks J, Kobrin D, Ogbonnaya SA, Sevim E, Michet C, et al. Relapsing polychondritis: Best practice & clinical rheumatology. Best Pract Res Clin Rheumatol 2023;37(1):101867. doi: 10.1016/j.berh.2023.101867.

[2] De Montmollin N, Dusser D, Lorut C, Dion J, Costedoat-Chalumeau N, Mouthon L, et al. Tracheobronchial involvement of relapsing polychondritis. Autoimmun Rev 2019;18(9):102353. doi: 10.1016/j.autrev.2019.102353.

[3] Hu FY, Wang J, Zhang SX, Su R, Yan N, Gao C, et al. Absolute reduction of peripheral regulatory T cell in patients with relapsing polychondritis. Clin Exp Rheumatol 2021;39(3):487–93. doi: 10.55563/clinexprheumatol/qndtvt.

[4] Kolios AGA, Tsokos GC, Klatzmann D. Interleukin-2 and regulatory T cells in rheumatic diseases. Nat Rev Rheumatol 2021;17(12):749–66. doi: 10.1038/s41584-021-00707-x.

[5] Zhou P, Chen J, He J, Zheng T, Yunis J, Makota V, et al. Low-dose IL-2 therapy invigorates CD8+ T cells for viral control in systemic lupus erythematosus. PLOS Pathog 2021;17(10):e1009858. doi: 10.1371/journal.ppat.1009858.

Xia Zhang[1], Bo Huang[1], Ruiling Feng[1], Miao Shao[1], Xue Li[1], Zhanguo Li[1,2,**], Jing He[1,*]

[1] *Department of Rheumatology and Immunology, Beijing Key Laboratory for Rheumatism Mechanism and Immune Diagnosis, Peking University People's Hospital, Beijing, China*

[2] *Peking-Tsinghua Center for Life Sciences,Peking University, Beijing, China*

*__Correspondence to__ Dr Jing He, Department of Rheumatology and Immunology, Peking University People's Hospital, Beijing, China.

**__Correspondence to__ Dr Zhanguo Li, Department of Rheumatology and Immunology, Peking University People's Hospital, Beijing, China.

E-mail addresses: li99@bjmu.edu.cn (Z. Li), hejing1105@126.com (J. He).

Ann Rheum Dis 85 (2026) 778–780

Contents lists available at ScienceDirect

Annals of the Rheumatic Diseases

journal homepage: https://www.sciencedirect.com/journal/annals-of-the-rheumatic-diseases

Letter

Work smarter, not harder: achieve expert-level diagnosis extraction from medical records with optimal prompting of large language models

The annotation of electronic health records (EHRs) has evolved from manual annotation to query-based algorithms to supervised machine learning (ML). Major consortia rely on supervised ML, which has persistent challenges: labour-intensive feature engineering and extensive manual annotation requirements due to the data-hungry nature of many ML models [1–3].

Large language models (LLMs) represent the next evolutionary step, showing promise for tackling this data annotation bottleneck by leveraging their inference capabilities developed through pretraining on large data volumes [3–5]. In our current study, we investigated an LLM's ability to serve as an annotation agent by providing instructions (prompts) rather than examples to extract diagnoses from EHRs with high accuracy.

We used a locally hosted (to ensure General Data Protection Regulation (GDPR) compliance and patient data security) DeepSeek R1 (32B parameters) LLM and supplied it with English prompts for Dutch data, leveraging its multilingual capabilities. The first target was to identify the diagnosis of rheumatoid arthritis (RA) in clinical notes. We applied zero-shot inference (ie, no training examples) and optimised the prompt using the rheumatologist's instructions and chain-of-thought (CoT) tokens (Supplementary Figure 1). Performance was evaluated according to datasets annotated by rheumatology clinicians.

We iteratively refined the prompt by checking the LLM's output against the same small data partition (n = 100) until reaching an accuracy >95%, after which we tested it on the next unseen partition (also n = 100). In case of low performance, we would have repeated this stepwise prompt refinement cycle. The final prompt was subsequently evaluated on 2 sets of data: (1) a held-out partition of the Leiden University Medical Center (LUMC) EHR (n = 500), and a partition of the Reumazorg Zuid West Nederland (RZWN) EHR (n = 100) to assess transferability. The datasets were independently annotated by 2 rheumatologists who established uniform annotation rules beforehand and remained blinded to the LLM outputs.

The LLM achieved 95% accuracy in the first data partition after 4 iterations (I1-I4) of prompt refinement (Fig). I1 was a basic diagnostic query; I2 added domain knowledge rules; and I3 and I4 were refined using CoT. The performance of I4 remained consistent in the second unseen batch, eliminating the need for further refinement. When used on the LUMC held-out data, I4 achieved 99% accuracy, while the external hospital RZWN data yielded 97% accuracy.

To test the generalizability to another disease, we changed the diagnosis to identify osteoarthritis instead, using 2 approaches: (1) the exact same prompt as RA, with only the target diagnosis changed (P1), and (2) a prompt enhanced with an added osteoarthritis-specific instruction (P2). We evaluated both versions on the LUMC held-out partition (n = 500). Interestingly, using the same prompt strategy already achieved 95% accuracy. When further refining the prompt with the clinicians' osteoarthritis-specific instruction, the accuracy improved to 98%.

Taken together, our study demonstrates that LLMs can extract diagnoses from EHRs with high accuracy. Annotation is required only for validation of the output and (if necessary) prompt refinement. Importantly, DeepSeek's CoT reasoning provides insights into model reasoning, enabling effective prompt engineering by identifying the areas of uncertainty for targeted refinements.

These findings have important implications for real-world EHR research, as LLMs can unlock information from large consortia with minimal effort. Beyond this research application, our results emphasise key principles for the clinical use of LLMs. As clinical adoption accelerates—for example, in clinical summarisation—understanding proper use and limitations becomes essential for clinicians [6]. Any LLM system requires carefully designed prompts, periodic re-evaluation, and robust fail-safes. Without these safeguards, inadequate prompting or hallucinations can generate incorrect conclusions that compromise patient care. Our study provides a template informed by expert-validated instructions that demonstrated generalizability across centres and diagnoses.

Competing interests

TDM reports financial support was provided by Horizon Europe. DS reports financial support was provided by Horizon Europe. NS reports financial support was provided by Horizon Europe. MJTR reports was provided by Horizon Europe. EBvdA reports financial support was provided by Horizon Europe. RK reports financial support was provided

Tjardo D. Maarseveen and Daniyal Selani contributed equally to this study.

https://doi.org/10.1016/j.ard.2025.11.001
Received 9 September 2025; Revised 28 October 2025; Accepted 1 November 2025

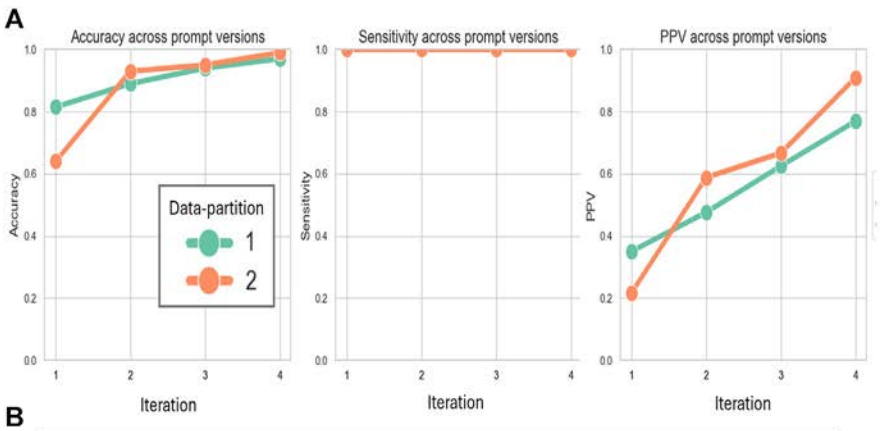

B

Phase	Accuracy	Sensitivity	Specificity	PPV	NPV
Rheumatoid arthritis					
Prompt engineering					
I1	0.64 [0.55-0.73]	1.00 [1.00-1.00]	0.60 [0.50-0.70]	0.22 [0.11-0.34]	1.00 [1.00-1.00]
I2	0.93 [0.88-0.98]	1.00 [1.00-1.00]	0.92 [0.87-0.98]	0.59 [0.35-0.82]	1.00 [1.00-1.00]
I3	0.95 [0.90-0.99]	1.00 [1.00-1.00]	0.94 [0.89-0.99]	0.67 [0.40-0.89]	1.00 [1.00-1.00]
I4	**0.99 [0.97-1.00]**	**1.00 [1.00-1.00]**	**0.99 [0.97-1.00]**	**0.91 [0.71-1.00]**	**1.00 [1.00-1.00]**
Validation					
Leiden (I4)	0.99 [0.98-1.00]	0.90 [0.71-1.00]	1.00 [0.99-1.00]	0.97 [0.93-1.00]	1.00 [0.98-1.00]
RZWN (I4)	0.97 [0.94-0.99]	0.91 [0.68-1.00]	0.98 [0.97-1.00]	0.83 [0.67-0.99]	0.99 [0.97-1.00]
Osteoarthritis					
Validation					
P1	0.95 [0.91-1.00]	0.90 [0.83-0.99]	0.96 [0.93-1.00]	0.86 [0.75-0.99]	0.97 [0.96-1.00]
P2	0.97 [0.94-1.00]	1.00 [1.00-1.00]	0.96 [0.93-1.00]	0.87 [0.78-0.99]	1.00 [1.00-1.00]

C

Best prompt iteration 4

System prompt: You are medical extraction expert

Query: Look for a confirmed diagnosis in the text & extract the exact words.

Instructions: Only focus on diagnoses from the list of interest (RA or OA)

A diagnosis counts as 'confirmed' if:
- the doctor explicitly states it as confirmed
- the doctor calls it a "working diagnosis"
- the patient had the diagnosis in the past

Do NOT count it as confirmed if:
- it's described as *probably, likely* or a *differential diagnosis (dd)*
- it's mentioned with another overlapping condition or as a mixed picture
- the doctor says a previous diagnosis is incorrect

Rate your confidence (0 to 10) based on how clear the text is.

Output: Diagnosis (yes or no)

Figure. Model performance overview. A, Performance improvement across 4 prompt engineering iterations (I1-I4) on optimisation (green line) and unseen test (orange line) partitions. I1: basic prompting; I2: domain knowledge; I3: refinement with chain-of-thought (CoT); and I4: final refinement. B, Performance metrics for rheumatoid arthritis (RA) identification in the unseen holdout datasets (Leiden University Medical Center [LUMC] and Reumazorg Zuid West Nederland [RZWN]) and for osteoarthritis identification (OA) using 2 prompt versions (P1: unchanged from the RA prompt; P2: domain-enhanced. C, Final optimised RA prompt summary). PPV: positive predictive value and NPV: negative predictive value

by Horizon Europe and ZonMW. The other authors declare they have no competing interests.

Acknowledgements

We thank David Steeman and Samantha Jurado-Zapata for their help in extracting and processing the Leiden University Medical Centre data. Additional thanks go to Bas van der Wal and Matthijs van Gijssel for preparing the Reumazorg Zuidwest Nederland data. Finally, we would like to thank Daniel Sukumar for proofreading the paper.

Contributors

TDM: Writing—review & editing, Writing—original draft, Visualisation, Validation, Software, Methodology, Investigation, Formal analysis, Data curation, Conceptualisation. DS: Writing—review & editing, Writing—original draft, Visualisation, Validation, Software, Methodology, Investigation, Formal analysis, Data curation, Conceptualisation. NS: Writing—review & editing, Validation, Software, Methodology, Investigation, Formal analysis, Data curation. RtB: Writing—review & editing, Validation, Methodology, Data curation. HKG: Writing—review & editing, Validation, Data curation. JV-vD: Writing—review & editing, Validation, Data curation. EBvdA: Writing—review & editing, Visualisation, Validation, Supervision, Methodology, Funding acquisition, Conceptualisation. MJTR: Writing—review & editing, Supervision, Resources, Funding acquisition. RK: Writing—review & editing, Writing—original draft, Visualisation, Validation, Supervision, Project administration, Methodology, Investigation, Funding acquisition, Formal analysis, Data curation, Conceptualisation.

Funding

This project was funded by the European Union via the Horizon grant for SPIDERR (activity number 101080711) and SQUEEZE (activity number 101095052). The study has further received funding from the ZonMW Klinische Fellow, number 40-00703-97-19069.

Patient consent for publication

Not applicable.

Ethics approval

We obtained ethical approval from the Medical Ethics Committee (METC) at Leiden University Medical Center according to study protocol B18.057.

Provenance and peer review

Not commissioned; externally peer reviewed.

Data availability statement

The study data are available upon reasonable request. We have made our prompts and code available in a public repository at: https://github.com/daniyal9538/LFA_LUMC.

Declaration of generative AI and AI-assisted technologies in the writing process

During the preparation of this work the authors used Claude.ai in order to improve the readability of the manuscript during preparation. After using this tool/service, the authors reviewed and edited the content as needed and take full responsibility for the content of the publication.

Patient and public involvement

Patients and/or the public were not involved in the design, or conduct, or reporting, or dissemination plans of this research.

Supplementary materials

Supplementary material associated with this article can be found in the online version at doi:10.1016/j.ard.2025.11.001.

Orcid

Tjardo D. Maarseveen: http://orcid.org/0000-0003-1701-1040

REFERENCES

[1] Yang S, Varghese P, Stephenson E, Tu K, Gronsbell J. Machine learning approaches for electronic health records phenotyping: a methodical review. J Am Med Inform Assoc 2023 Jan 18;30(2):367–81. doi: 10.1093/jamia/ocac216.

[2] Liao KP, Cai T, Gainer V, Goryachev S, Zeng-treitler Q, Raychaudhuri S, et al. Electronic medical records for discovery research in rheumatoid arthritis. Arthritis Care Res (Hoboken) 2010 Aug;62(8):1120–7. doi: 10.1002/acr.20184.

[3] Spasic I, Nenadic G. Clinical text data in machine learning: systematic review. JMIR Med Inform 2020;8(3):e17984. doi: 10.2196/17984.

[4] Sandmann S, Hegselmann S, Fujarski M, Bickmann L, Wild B, Eils R, et al. Benchmark evaluation of DeepSeek large language models in clinical decision-making. Nat Med 2025 Apr 23;31:2546–9. doi: 10.1038/s41591-025-03727-2.

[5] Grothey B, Odenkirchen J, Brkic A, Schömig-Markiefka B, Quaas A, Büttner R, et al. Comprehensive testing of large language models for extraction of structured data in pathology. Commun Med (Lond) 2025 Mar 31;5(1):96. doi: 10.1038/s43856-025-00808-8.

[6] Clusmann J, Kolbinger FR, Muti HS, Carrero ZI, Eckardt JN, Laleh NG, et al. The future landscape of large language models in medicine. Commun Med (Lond) 2023;3(1):141. doi: 10.1038/s43856-023-00370-1.

Tjardo D. Maarseveen[1], Daniyal Selani[2,3], Nils Steinz[1], Robin ten Brinck[1], Herman K. Glas[4], Josien Veris-van Dieren[4], Marcel J.T. Reinders[2,3], Erik B. van den Akker[2,3], Rachel Knevel[1,5,*]

[1] *Department of Rheumatology, Leiden University Medical Center, Leiden, Netherlands*

[2] *Leiden Computational Biology Centre, Leiden University Medical Center, Leiden, Zuid-Holland, Netherlands*

[3] *Delft Bioinformatics Lab, Delft University of Technology, Delft, Zuid-Holland, Netherlands*

[4] *Rheumatology Outpatient Clinics, Reumazorg Zuid West Nederland, Goes, Netherlands*

[5] *Rheumatology, Newcastle University Translational and Clinical Research Institute, Newcastle upon Tyne, UK*

*__Correspondence to__ Dr Rachel Knevel.
E-mail address: r.knevel@lumc.nl (R. Knevel).

Ann Rheum Dis 85 (2026) e43–e44

Contents lists available at ScienceDirect

Annals of the Rheumatic Diseases

journal homepage: https://www.sciencedirect.com/journal/annals-of-the-rheumatic-diseases

Correspondence

Correspondence on 'Deconstruction of tophi and synovium defines SPP1 $^{+}$ macrophages involved in extracellular matrix remodelling in gout' by Xu et al

The single-cell and spatial transcriptomic study by Xu et al [1] redefined gout pathogenesis by identifying *SPP1*$^{+}$ macrophages as key regulators of extracellular matrix (ECM) remodelling within tophaceous lesions. However, quantitative re-evaluation of their data suggests that the transition from intercritical to tophaceous gout arises not from higher systemic urate levels but from local immune-fibrotic reprogramming. The minimal difference in serum urate between groups indicates that urate burden alone does not determine tissue remodelling. Instead, *SPP1*-mediated macrophage plasticity, fibroblast interaction, and T-cell modulation collectively shape the chronic tophus architecture.

SPP1 coexpression with *MMP9, CHI3L1*, and *COL6A2* in macrophages defines a fibro-osteoclastic continuum bridging inflammation, fibrosis, and bone erosion. These hybrid cells likely perform dual roles in matrix production and degradation, reminiscent of the macrophage-myofibroblast transformation observed in systemic fibrotic diseases [2,3]. The presence of *SPP1-COL6A2* coexpression in the corona zone implies that macrophages directly contribute to the collagen scaffolding surrounding urate crystals [1], challenging the conventional notion that fibroblasts alone mediate fibrotic remodelling. This mechanism offers a biological basis for the coexistence of fibrosis and osteolysis in advanced gout, suggesting that targeting *SPP1-CD44* or *TGF-β-SMAD3* signalling could disrupt maladaptive repair before irreversible joint deformity occurs.

The immunologic milieu of tophaceous tissue further supports a transition from acute inflammation to regulatory tolerance. An increased proportion of *FOXP3*$^{+}$ *CTLA4*$^{+}$ regulatory T cells relative to cytotoxic T cells mirrors the immune suppression observed in fibrotic granulomatous diseases, such as sarcoidosis [1], in which tolerance prevents inflammation while allowing ECM accumulation [4]. This shift towards an anti-inflammatory yet profibrotic state aligns with the chronic reparative phenotype of gouty tophi. Modulation of this Treg-macrophage axis through metabolic reprogramming, such as *AMPK* activation, may restore immune balance without provoking acute flare-ups.

Despite its innovations, the study by Xu et al [1] may be subject to important methodological constraints. The spatial transcriptomic resolution of 55 μm inevitably captured mixed cellular populations [1], limiting precision in identifying true macrophage-fibroblast hybrids. Without single-molecule or lineage-tracing validation, the inferred transdifferentiation remains hypothetical. Furthermore, tissue dissociation using collagenase and hyaluronidase is known to induce stress-related transcripts, including *MMP9* and *CHI3L1,* thereby confounding the interpretation of ECM remodelling pathways [5]. These artefacts can exaggerate the prominence of fibrotic gene signatures. The small cohort (n = 6) further constrains generalizability and prevents adjustment for age-dependent macrophage reprogramming [1], which itself promotes fibrotic polarisation [3].

Collectively, these observations position gout as a disease of maladaptive tissue repair rather than persistent crystal-driven inflammation [1,6]. The limited urate gradient between clinical stages underscores that sustained *SPP1* signalling, not serum urate concentration, governs the persistence of tophus. Integrating transcriptomic insight with spatial validation will be essential to determine whether *SPP1*$^{+}$ macrophages represent true fibro-osteoclastic intermediates or an activated inflammatory subset. Clinically, targeting the *SPP1-CD44* or *TGF-β-SMAD3* axes, in concert with conventional urate-lowering therapy, may prevent the structural remodelling that underlies the progression of chronic gout.

Acknowledgements

None reported.

Contributors

TLT: Conceptualisation, Methodology, Investigation, Formal analysis, Validation, Writing—original draft, Writing—review and editing. S-CC: Conceptualisation, Methodology, Investigation, Formal analysis, Supervision, Validation, Writing—review and editing.

Funding

This work did not receive any specific grant from funding agencies in the public, commercial, or not-for-profit sectors.

Handling editor Josef S. Smolen.

https://doi.org/10.1016/j.ard.2025.10.030
Received 24 October 2025; Accepted 28 October 2025

Competing interests

The authors declare they have no competing interests for this work.

Patient consent for publication

Not applicable.

Ethics approval

Not applicable.

Provenance and peer review

Not applicable.

Data availability statement

Not applicable.

ORCID iDs

Shiuan-Chih Chen http://orcid.org/0000-0003-4301-0340

REFERENCES

[1] Xu H, Liu Z, Zhou X, Ji X, Liu X, Zhu X, et al. Deconstruction of tophi and synovium defines SPP1 + macrophages involved in extracellular matrix remodelling in gout. Ann Rheum Dis 2025 in press. doi: 10.1016/j.ard.2025.09.003.

[2] Ban JQ, Ao LH, He X, Zhao H, Li J. Advances in macrophage-myofibroblast transformation in fibrotic diseases. Front Immunol 2024;15:1461919. doi: 10.3389/fimmu.2024.1461919.

[3] Jiang Y, Cai R, Huang Y, Zhu L, Xiao L, Wang C, et al. Macrophages in organ fibrosis: from pathogenesis to therapeutic targets. Cell Death Discov 2024;10 (1):487. doi: 10.1038/s41420-024-02247-1.

[4] Zhang H, Jiang D, Zhu L, Zhou G, Xie B, Cui Y, et al. Imbalanced distribution of regulatory T cells and Th17.1 cells in the peripheral blood and BALF of sarcoidosis patients: relationship to disease activity and the fibrotic radiographic phenotype. Front Immunol 2023;14:1185443. doi: 10.3389/fimmu.2023.1185443.

[5] Machado L, Relaix F, Mourikis P. Stress relief: emerging methods to mitigate dissociation-induced artefacts. Trends Cell Biol 2021;31(11):888–97. doi: 10.1016/j.tcb.2021.05.004.

[6] Leask MP, Crișan TO, Ji A, Matsuo H, Köttgen A, Merriman TR. The pathogenesis of gout: molecular insights from genetic, epigenomic and transcriptomic studies. Nat Rev Rheumatol 2024;20(8):510–23. doi: 10.1038/s41584-024-01137-1.

Tsai Ling Ting[1,2,3], Shiuan-Chih Chen[1,4,5,*]

[1] *Institute of Medicine, College of Medicine, Chung Shan Medical University, Taichung, Taiwan*

[2] *Department of Nursing, Chung Shan Medical University Hospital, Taichung, Taiwan*

[3] *Division of Allergy, Immunology, and Rheumatology, Department of Internal Medicine, Chung Shan Medical University Hospital, Taichung, Taiwan*

[4] *School of Medicine, College of Medicine, Chung Shan Medical University, Taichung, Taiwan*

[5] *Department of Family and Community Medicine, Chung Shan Medical University Hospital, Taichung, Taiwan*

*__Correspondence to__ Prof Shiuan-Chih Chen, Institute of Medicine and School of Medicine, Chung Shan Medical University College of Medicine, Taichung, Taiwan.

E-mail address: sccy399@yahoo.com.tw (S.-C. Chen).

Ann Rheum Dis 85 (2026) e45–e46

Contents lists available at ScienceDirect

Annals of the Rheumatic Diseases

journal homepage: https://www.sciencedirect.com/journal/annals-of-the-rheumatic-diseases

Response

Response to correspondence on 'Deconstruction of tophi and synovium defines *SPP1* + macrophages involved in extracellular matrix remodelling in gout' by Xu et al

We thank Ting and Chen for their insightful correspondence on our article [1,2], in which they further develop the concept of gout as a disease of maladaptive tissue repair rather than simply persistent crystal-driven inflammation. Their emphasis on *SPP1*$^+$ macrophage plasticity and fibroblast interactions nicely complements our original interpretation of *SPP1*$^+$ tophaceous gout-associated macrophages as central organisers of extracellular matrix (ECM) remodelling in chronic gouty arthritis.

We agree that *SPP1* coexpression with *MMP9, CHI3L1*, and *COL6A2* serves to identify this cell subpopulation as occupying a fibro-osteogenic activation state that functionally links inflammation, fibrosis, and bone erosion. Moreover, they were enriched in the corona zone and exhibited strong integrin-mediated interactions with adjacent fibroblasts and osteoblasts, suggesting that inflammation, fibrosis, and bone erosion are coordinated by locally organised macrophage-fibroblast-osteoclast circuits within chronic gouty arthritis.

However, as Ting and Chen rightly point out, current evidence does not support definitive conclusions regarding cell transition. Our use of the term "fibroblast-like phenotype" intended to acknowledge this limitation without implying the occurrence of a confirmed macrophage-to-fibroblast transition [1]. Moreover, enzymatic digestion during single-cell RNA sequencing may induce stress-related expression of *MMP* family genes and *CHI3L1*, thereby exaggerating fibrotic signatures.

In this context, further lineage-tracing studies are warranted to clarify the origin and fate of *SPP1*$^+$ macrophages [3]. Fate-mapping approaches could help determine whether *SPP1*$^+$ macrophages in chronic gouty arthritis arise predominantly from recruited monocytes or from synovial resident macrophages [4]. Such experiments will be critical to explain the contributions of cell transition or niche-driven cell reprogramming to tophi formation, as well as their relationship with the emergence of specific *SPP1*$^+$ macrophage subsets.

Another key question that remains unanswered is how *SPP1*$^+$ macrophages remodel the ECM into tophi. Integrating an advanced optical platform, such as stimulated Raman scattering microscopy, is an ideal option, which enables noninvasive molecular profiling and high-resolution chemical imaging of monosodium urate crystals, collagen fibres, proteoglycans, lipids, and other ECM components, linking the chemical composition of the tophi to distinct *SPP1*$^+$ macrophage activation states [5,6].

Regarding spatial transcriptomics, as noted by Ting and Chen, the current spatial resolution remains insufficient to precisely define the niches where *SPP1*$^+$ macrophage-fibroblast crosstalk is most intense [2]. Next-generation high-resolution spatial transcriptomic platforms, combined with multimodal *in situ* validation, are essential for mapping *SPP1*$^+$ macrophage and synovial fibroblast subsets at near-single-cell resolution within tophi [7]. We expect these approaches to define a fundamental structural and functional unit, composed of *SPP1*$^+$ macrophages and fibroblasts together with surrounding remodeled extracellular matrix, which contributes to organization of the tophi.

Taken together, our findings demonstrate a niche-specific model of chronic gouty arthritis as a disorder of maladaptive tissue repair, wherein *SPP1*$^+$ macrophages and synovial fibroblasts jointly orchestrate tophi formation and osteochondral damage. We thank Ting and Chen for their thoughtful comments underscoring the importance of *SPP1*-centred macrophage plasticity and fibroblast interactions [2]. Looking ahead, we anticipate further integrative studies to inform more targeted therapeutic strategies for chronic gouty arthritis, grounded in a deeper understanding of the origin, function, and plasticity of *SPP1*$^+$ macrophages within their specific tissue niche.

Contributors

ZL reviewed the relevant literature and drafted the response. HX designed the overall response and contributed to writing, review, and editing.

Funding

This work was supported by the Natural Science Foundation of Shanghai (ref: 25ZR1402050 to HX) and the Shanghai Magnolia Program Pujiang Project (ref: 24PJD009 to HX).

Competing interests

The authors declare no competing interests for this work.

Patient consent for publication

Not applicable.

https://doi.org/10.1016/j.ard.2025.11.005
Received 3 November 2025; Accepted 6 November 2025

Ethics approval

Not applicable.

Provenance and peer review

Not applicable.

Orcid

Hanlin Xu: http://orcid.org/0000-0001-6828-620X

REFERENCES

[1] Xu H, Liu Z, Zhou X, Ji X, Liu X, Zhu X, et al. Deconstruction of tophi and synovium defines *SPP1*+ macrophages involved in extracellular matrix remodelling in gout. Ann Rheum Dis 2025 in press. doi: 10.1016/j.ard.2025.09.003.

[2] Ting TL, Chen S-C. Correspondence on 'Deconstruction of tophi and synovium defines *SPP1*+ macrophages involved in extracellular matrix remodelling in gout' by Xu et al. Ann Rheum Dis 2025. doi: 10.1016/j.ard.2025.10.030.

[3] Meng XM, Wang S, Huang XR, Yang C, Xiao J, Zhang Y, et al. Inflammatory macrophages can transdifferentiate into myofibroblasts during renal fibrosis. Cell Death Dis 2016;7(12):e2495. doi: 10.1038/cddis.2016.402.

[4] Yin W, Li Y, Song Y, Zhang J, Wu C, Chen Y, et al. CCRL2 promotes antitumor T-cell immunity via amplifying TLR4-mediated immunostimulatory macrophage activation. Proc Natl Acad Sci U S A 2021;118(16):e2024171118. doi: 10.1073/pnas.2024171118.

[5] Zhang B, Xu H, Chen J, Zhu X, Xue Y, Yang Y, et al. Highly specific and label-free histological identification of microcrystals in fresh human gout tissues with stimulated Raman scattering. Theranostics 2021;11(7):3074–88. doi: 10.7150/thno.53755.

[6] Xu H, Zhang B, Chen Y, Zeng F, Wang W, Chen Z, et al. Type II collagen facilitates gouty arthritis by regulating MSU crystallisation and inflammatory cell recruitment. Ann Rheum Dis 2023;82(3):416–27. doi: 10.1136/ard-2022-222764.

[7] Xiao Z, Cui L, Yuan Y, He N, Xie X, Lin S, et al. 3D reconstruction of a gastrulating human embryo. Cell 2024;187(11):2855–2874.e19. doi: 10.1016/j.cell.2024.03.041.

Zhechen Liu, Hanlin Xu*
Department of Sports Medicine, Huashan Hospital, Fudan University, Shanghai, China

***Correspondence to** Dr. Hanlin Xu, Department of Sports Medicine, Huashan Hospital, Fudan University, Shanghai, China
E-mail address: hanlinxu@fudan.edu.cn (H. Xu).